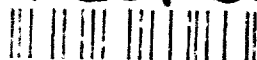


AD-A264 208



①



Scientific and Engineering Studies

Compiled 1989

Signal Processing Studies

A. H. Nuttall



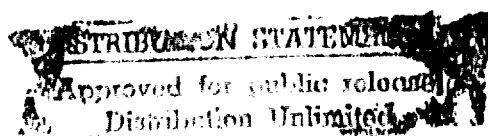
PUBLISHED BY

NAVAL UNDERWATER SYSTEMS CENTER

NEWPORT LABORATORY, NEWPORT, RHODE ISLAND

NEW LONDON LABORATORY, NEW LONDON, CONNECTICUT

93 4 20 018



93-08378



**BEST
AVAILABLE COPY**



Scientific and Engineering Studies

Compiled 1989

Signal Processing Studies

A. H. Nuttall



PUBLISHED BY

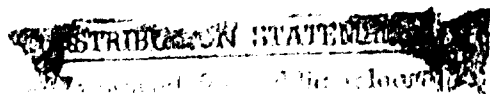
NAVAL UNDERWATER SYSTEMS CENTER

NEWPORT LABORATORY, NEWPORT, RHODE ISLAND

NEW LONDON LABORATORY, NEW LONDON, CONNECTICUT

93 4 20 018

93-08378



Foreword

This collection of technical reports addresses the following topics: evaluation of stability of the Wigner distribution function (WDF) in the presence of noise; determination of the WDF with minimum spread; computation of an alias-free WDF and complex ambiguity function from discrete-time samples; performance evaluation of a combiner with a dead zone in each channel; determination of the optimum memoryless nonlinear transformation for weak narrowband signals in noise; and estimation of the noise field directionality directly from the spatial correlation for linear, planar, and volumetric arrays.

Some of the material presented here is heavily based on the author's earlier work, which can be found in the following volumes in addition to the referenced technical reports:

Performance of Detection and Communication Systems,
NUSC Scientific and Engineering Studies, 1974;

Spectral Estimation,
NUSC Scientific and Engineering Studies, 1977;

Coherence Estimation,
NUSC Scientific and Engineering Studies, 1979;

Receiver Performance Evaluation and Spectral Analysis,
NUSC Scientific and Engineering Studies, 1981;

Signal Processing Studies,
NUSC Scientific and Engineering Studies, 1983;

Signal Processing Studies,
NUSC Scientific and Engineering Studies, 1985;

Signal Processing Studies,
NUSC Scientific and Engineering Studies, 1986;

Signal Processing Studies,
NUSC Scientific and Engineering Studies, 1987.

Dr. Daniel M. Viccione
Associate Technical Director
Research and Technology
NAVAL UNDERWATER SYSTEMS CENTER

Compiled 1989

TABLE OF CONTENTS

Foreword

- TR 8225 Wigner Distribution Function: Relation to Short-Term Spectral Estimation, Smoothing, and Performance in Noise
- TR 8317 The Wigner Distribution Function with Minimum Spread
- TR 8533 Alias-Free Wigner Distribution Function and Complex Ambiguity Function for Discrete-Time Samples
- TR 8595 Operating Characteristics for Combiner with a Dead Zone in Each Channel
- TR 8611 Optimum Memoryless Nonlinear Transformation for Weak Narrowband Signals in Noise
- TR 8631 Determination of Noise Field Directionality Directly from Spatial Correlation for Linear, Planar, and Volumetric Arrays
- TR 8599 Estimation of Noise Field Directionality; Comparison with Fourier Series Method

Subject Matter Index

Accession For	
NTIS CRA&I	<input checked="" type="checkbox"/>
DTIC TAB	<input type="checkbox"/>
Unannounced	<input type="checkbox"/>
Justification	
By	
Distribution /	
Availability Codes	
Dist	Avail and / or Special
A-1	

Technical Report 8225
16 February 1988

**Wigner Distribution Function: Relation to
Short-Term Spectral Estimation, Smoothing,
and Performance in Noise**

**A. H. Nuttall
ABSTRACT**

The properties and behavior of the Wigner Distribution Function (WDF) are investigated both analytically and by means of a number of simple informative examples. The lack of local temporal averaging when obtaining the instantaneous correlation function, and the lack of weighting the longer delay values when transforming to the instantaneous spectrum are shown to be the causes of the deleterious interference effects that are inherent to the WDF. The equivalence of short-term spectral estimation to the smoothed WDF offers an attractive alternative with guaranteed positive distribution values and no interference effects.

The performance of a processor which estimates the WDF of a signal waveform in the presence of additive noise is investigated in terms of the output mean, bias, and variance. Dependence on filtering the input and time-weighting is allowed and included in the analysis. Numerical application to a particular example is carried out.

Approved for public release; distribution is unlimited.

TABLE OF CONTENTS

	Page
LIST OF ILLUSTRATIONS	111
LIST OF SYMBOLS	iv
INTRODUCTION	1
BASIC PROPERTIES OF THE WDF	3
Definitions	3
Properties of WDF	6
Product and Convolution	8
Ambiguity Function	9
First Moments of W	12
Second Moments of W	15
Moments of W^2	16
Cross Wigner Distribution Function	19
Narrowband Real Waveform	22
Sampling Properties	23
EXAMPLES OF WDF	28
Gaussian Waveform	29
Gaussian-Modulated Tone	31
Multiple Modulated Tones	32
Linear Frequency Modulation	35
Gated Linear Frequency Modulation	40
SHORT-TERM SPECTRAL ESTIMATION	43
Weighted Spectral Estimate	43
Relation to WDFs	44
Marginals of Spectral Estimate	46
Moments of Spectral Estimate	47
Conditional Moment	49
EXAMPLES OF SHORT-TERM SPECTRAL ESTIMATION	51
Gaussian Waveform	51
Multiple Modulated Tones	53
Linear Frequency Modulation	55
More-General Weighting	57
SMOOTHING THE WDF	60
Philosophy and Approach	60
Alternative Averaging Procedures	63
Efficient Calculation of Short-Term Spectral Estimate	66
WDF With Minimum Spread	69

TABLE OF CONTENTS (Cont'd)

PERFORMANCE IN NOISE	70
Waveform Weighting	70
Mean Values	72
Variance of WDF Estimate	73
WDF Processor	77
SUMMARY	80
APPENDIX A. SLICES IN TIME OF THE WDF	A-1
APPENDIX B. OSCILLATING WDF FOR SEPARATED PULSES	B-1
APPENDIX C. AMBIGUITY FUNCTION OF (79)	C-1
APPENDIX D. ROTATION OF AXES	D-1
APPENDIX E. DISCRETE APPROXIMATION TO SHORT-TERM SPECTRAL ESTIMATE	E-1
APPENDIX F. SOME SMOOTHING CONSIDERATIONS	F-1
APPENDIX G. DERIVATION OF MINIMUM-SPREAD WDF	G-1
APPENDIX H. EXAMPLE OF WDF PROCESSOR	H-1
APPENDIX I. SMOOTHED WDF FOR $s(t) = t \exp(-t^2/2)$	I-1
APPENDIX J. DOUBLE CONVOLUTION OF TWO GAUSSIAN FUNCTIONS	J-1
REFERENCES	R-1

LIST OF ILLUSTRATIONS

Figure		Page
1	WDF for Narrowband Real Waveform	23
2	WDF for Sampled Version $\tilde{W}(t,f)$	25
3	$\tilde{W}(t,f)$ for Real Waveform $s(t)$	25
4	Contour of WDF (72) at $1/e$ Relative Level	30
5	Contour of (91) for $\Theta_0 = 1.5$	39
6	Contours of WDF for Gated Linear Frequency Modulation . . .	41
7	WDF Processor	77
8	Time and Frequency Characteristics of Figure 7	79
A-1	Low-Pass Spectrum $S(f)$	A-2
B-1	Waveform $s(t)$	B-1
D-1	Rotated Coordinate Axes	D-1
D-2	Triangle Interpretation of (D-5)	D-3
D-3	Ellipse in Rotated Coordinates	D-5
H-1	Plot of (H-40) or (H-41) for Fixed Θ_0	H-12
H-2	Plot for $\Theta_0 = 0$	H-12
H-3	Plot for $\Theta_0 = 1$	H-13
H-4	Plot for $\Theta_0 = 5$	H-13
H-5	Minimum MD Product	H-14
H-6	Quality Ratio for $\Theta_0 = 0$, $E_0/N_d = 20$	H-21
H-7	Quality Ratio for $\Theta_0 = 1$, $E_0/N_d = 20$	H-22
H-8	Quality Ratio for $\Theta_0 = 5$, $E_0/N_d = 20$	H-23

LIST OF SYMBOLS

WDF	Wigner Distribution Function
t	Time, (1)
$s(t)$	Waveform, function of time, (1)
τ	Time separation or lag variable, (1)
$R(t, \tau)$	Instantaneous correlation, (1)
f	Frequency, (3)
$W(t, f)$	WDF at time t and frequency f , (3), (10)
E	Waveform energy, (5), (14)
$S(f)$	Voltage density spectrum of $s(t)$, (9)
δ	Delta function, (13)
\otimes	Convolution, (19), (20)
ν	Frequency shift variable, (22)
$\chi(\nu, \tau)$	Ambiguity function, (22)
$A(\nu, f)$	Spectral function, (24)
Im	Imaginary part, (28)
δ'	Derivative of delta function, (29)
$\mu_f(t)$	Frequency center at time t , (30)
$M(t)$	Magnitude of $s(t)$, (31)
$\theta(t)$	Phase of $s(t)$, (31)
$\mu_t(f)$	Time center at frequency f , (33)
$A(f)$	Magnitude of $S(f)$, (34)
$\phi(f)$	Phase of $S(f)$, (34)
\bar{f}	Frequency center, (36)
\bar{t}	Time center, (37)

LIST OF SYMBOLS (Cont'd)

$\sigma_f^2(t)$	Instantaneous mean-square frequency spread, (42)
$W_{ab}(t,f)$	Cross WDF, (51)
$a(t), A(f)$	Fourier transform pair, (51)
$\chi_{ab}(\nu, \tau)$	Cross ambiguity function, (53)
$c(t)$	Complex envelope, (55)
f_0	Carrier frequency, (55)
Re	Real part, (55)
Δ_t	Sampling increment in time, (57)
\tilde{W}	Approximation to W , (57), (59)
m, n, N_f	Integers, (60)
T	Time spread, figure 2
B	Frequency spread, figure 3
f_H	Highest frequency in $s(t)$, (65)
t_0, f_0	Time and frequency shifts, (66)
Θ_0	Time-bandwidth product, (88)-(90)
$u(t)$	Weighting in time, (102)
$S_u(t,f)$	Voltage spectrum of s , relative to u , (102)
STSE	Short-term spectral estimate, (103)
E_s	Energy of waveform $s(t)$, (111)
E_u	Energy of weighting $u(t)$, (111)
σ_c	Effective duration of weighting, (146)
α_c	Linear frequency modulation parameter, (146)
Θ_c	Time-bandwidth product, (146)
$v_1(t)$	Time weighting, (148)
\hat{R}	Locally averaged correlation, (148), (150)

LIST OF SYMBOLS (Cont'd)

\hat{W}	Locally averaged WDF, (149)
$v_2(t, \tau)$	Time and lag weighting, (150)
$V_2(t, f)$	Transform (on τ) of v_2 , smoothing function, (151)
I	Spread measure, (163)
β_c	Specified slope in t, f plane, (163)
α_c	$2\pi\beta_c$, (163)
$s(t)$	Signal, (165)
$n(t)$	Additive noise, (165)
$x(t)$	Observed waveform, (165)
$C_n(\tau)$	Noise correlation, (166)
$G_n(f)$	Noise spectrum, (166)
$v(t)$	Weighting of x , (167)
$y(t)$	Weighted waveform, (167)
a, b, c, d	Components of W_{yy} , (168), (169)
overbar	Ensemble average, (172), (173)
$G_n^{(2)}(f)$	Modified noise spectral quantity, (178)
$B(t, f)$	Auxiliary function, (183)
Var	Variance of WDF estimate, (188)
$s_0(t)$	Input signal, figure 7
$n_0(t)$	Input noise, figure 7
$H(f)$	Filter, figure 7
N_d	Noise spectral level, (189)
B	Passband of filter H , figure 8
L	Duration of weighting v , figure 8
LFM	Linear Frequency Modulation
$\text{sgn}(x)$	1 for $x > 0$, -1 for $x < 0$

WIGNER DISTRIBUTION FUNCTION: RELATION TO SHORT-TERM SPECTRAL ESTIMATION, SMOOTHING, AND PERFORMANCE IN NOISE

INTRODUCTION

The potential of the Wigner Distribution Function (WDF) for characterizing the short-term local time and frequency content of a transient waveform has been amply demonstrated in a series of papers; for example, see the recent publications [1,2,3] and the extensive references listed therein. In particular, [1] contains numerical examples of the WDF for rectangularly gated linear frequency modulation and a version which has been smoothed with a square window in the time-frequency plane, in order to yield positive distribution values. Here, we will be concerned with smoothing so as to minimally spread the WDF, but will not presume all the information that is required for implementation via [2], nor do we limit consideration to a constant-magnitude function. We will then use the close connection between short-term spectral estimation and smoothed WDFs to suggest a possible analysis procedure and philosophy to extract information about a given waveform without an extensive search in waveform parameters. Finally, the performance of a particular WDF estimator in the presence of additive noise will be analyzed, both in terms of bias and variance.

This report summarizes and compiles many of the results in the publications noted above in a unified framework and notation. Also, numerous examples are presented in the various sections of this report to

illustrate and bring out some of the fundamental concepts and limitations of the WDF; these examples can be evaluated analytically in closed form, allowing for close investigation of the behavior of the WDF, and as control cases on any computer-written program for numerical evaluation of the WDF.

BASIC PROPERTIES OF THE WDF

DEFINITIONS

A natural definition of the time-varying correlation of a nonstationary complex stochastic process $s(t)$ is

$$R(t, \tau) = \overline{s(t + \frac{\tau}{2}) s^*(t - \frac{\tau}{2})} , \quad (1)$$

where the overbar denotes an ensemble average. The "center" time in (1) is t , while the "separation" time is τ . However, if an ensemble is not available, or if $s(t)$ is a deterministic waveform, the obvious extension of (1) is simply

$$R(t, \tau) = s(t + \frac{\tau}{2}) s^*(t - \frac{\tau}{2}) . \quad (2)$$

This quantity is interpreted as the instantaneous correlation of waveform $s(t)$ at time t , for separation (or lag) τ .

The associated "spectrum" at time t is then available, as usual, by Fourier transforming (2) on separation variable τ , to get at frequency f ,

$$\begin{aligned} W(t, f) &= \int d\tau \exp(-j2\pi f\tau) R(t, \tau) = \\ &= \int d\tau \exp(-j2\pi f\tau) s(t + \frac{\tau}{2}) s^*(t - \frac{\tau}{2}) . \end{aligned} \quad (3)$$

(Integrals without limits are over the range of nonzero integrand. Also, it is presumed that $s(t)$ and its derivatives decay fast enough to zero at $t = \pm\infty$ for all the integrals to converge.) This time-frequency function $W(t,f)$ is called the Wigner Distribution Function (WDF). It is a real function, even when $s(t)$ is complex, since

$$\begin{aligned} W^*(t,f) &= \int d\tau \exp(12\pi f\tau) s^*(t + \frac{\tau}{2}) s(t - \frac{\tau}{2}) = \\ &= \int du \exp(-12\pi fu) s^*(t - \frac{u}{2}) s(t + \frac{u}{2}) = W(t,f) . \end{aligned} \quad (4)$$

However, it is not necessarily positive, as the simple example of a rectangularly gated pulse quickly shows: for

$$s(t) = \begin{cases} a & \text{for } |t| < T/2 \\ 0 & \text{otherwise} \end{cases} ,$$

then

$$W(t,f) = 2E \frac{\sin[2\pi f(T - 2|t|)]}{2\pi fT} \quad \text{for } |t| < \frac{T}{2} , \text{ all } f ,$$

and zero otherwise, where E is the waveform energy:

$$E = \int dt |s(t)|^2 = |a|^2 T . \quad (5)$$

An even simpler example is furnished by waveforms with odd symmetry, $s(-t) = -s(t)$. Substitution in (3) immediately yields $W(0,0) = - \int d\tau |s(\tau/2)|^2 = -2E$. Thus the origin value of the WDF is always negative for an odd waveform.

More generally, when waveform $s(t)$ is expressed in terms of its even and odd parts according to

$$s(t) = e(t) + o(t) , \quad (6)$$

then the origin value of the WDF is

$$\begin{aligned} W(0,0) &= \int d\tau \, s(\tau/2) s^*(-\tau/2) = 2 \int dt \, s(t) s^*(-t) = \\ &= 2 \int dt [e(t) + o(t)] [e^*(t) - o^*(t)] = 2E_e - 2E_o , \end{aligned} \quad (7A)$$

where

$$E_e = \int dt |e(t)|^2 , \quad E_o = \int dt |o(t)|^2 \quad (7B)$$

are the energies of the even and odd parts respectively. For nonzero t, f , it can readily be shown that the magnitude of the WDF is upper bounded by $2E = 2(E_e + E_o)$.

PROPERTIES OF WDF

For $s(t)$ real, it readily follows from the definition of the WDF in (3) that

$$W(t, -f) = W(t, f) \quad \text{for } s(t) \text{ real .} \quad (8)$$

In this special case, it is only necessary to evaluate $W(t, f)$ for $f \geq 0$.

Define the voltage density spectrum of waveform $s(t)$ as

$$S(f) = \int dt \exp(-i2\pi ft) s(t) . \quad (9)$$

Then an alternative form for the WDF in (3) is

$$\begin{aligned} W(t, f) &= \int d\tau \exp(-i2\pi f\tau) s(t + \frac{\tau}{2}) s^*(t - \frac{\tau}{2}) = \\ &= \int dv \exp(i2\pi vt) S(f + \frac{v}{2}) S^*(f - \frac{v}{2}) , \end{aligned} \quad (10)$$

in terms of $S(f)$.

Integration on (10) immediately yields the marginals

$$\int dt W(t, f) = |S(f)|^2 , \quad (11)$$

and

$$\int df W(t, f) = |s(t)|^2 , \quad (12)$$

where we used the result

$$\int dx \exp(i2\pi xy) = \delta(y) . \quad (13)$$

The quantity in (11) is the energy density function, while that in (12) is the instantaneous power. If we complete the integrations on the remaining variables in (11) and (12), they both yield

$$\begin{aligned} \iint dt df W(t,f) &= E = \\ &= \int dt |s(t)|^2 = \int df |S(f)|^2 , \end{aligned} \quad (14)$$

where E is the total waveform energy.

If waveform $s(t)$ satisfies a time-limited restriction, namely

$$s(t) \neq 0 \quad \text{only for } t_1 < t < t_2 , \quad (15)$$

then (3) reduces to

$$W(t,f) = \int_{-T_m}^{T_m} d\tau \exp(-i2\pi f\tau) s(t + \frac{\tau}{2}) s^*(t - \frac{\tau}{2}) \quad \text{for } t_1 < t < t_2 , \quad (16)$$

and zero otherwise, where

$$T_m = 2 \min(t_2 - t, t - t_1) \quad \text{for } t_1 < t < t_2 . \quad (17)$$

Thus the WDF is time-limited if waveform $s(t)$ is time-limited; however, if there are gaps in $s(t)$, the behavior of the WDF is more complicated, as will be demonstrated later.

PRODUCT AND CONVOLUTION

If waveform $s(t)$ is the product of two other waveforms,

$$s(t) = a(t) b(t) , \quad (18)$$

then the WDF of $s(t)$ is (inserting subscripts as needed)

$$\begin{aligned} W_s(t, f) &= \int d\tau \exp(-i2\pi f\tau) R_s(t, \tau) = \\ &= \int d\tau \exp(-i2\pi f\tau) R_a(t, \tau) R_b(t, \tau) = \\ &= \int dv W_a(t, v) W_b(t, f - v) = \\ &= W_a(t, f) \otimes W_b(t, f) , \end{aligned} \quad (19)$$

which is a convolution on frequency f , for fixed t .

In a similar fashion, if $s(t)$ is the convolution in time, of two other waveforms,

$$s(t) = a(t) \otimes b(t) = \int d\tau a(\tau) b(t - \tau) , \quad (20)$$

then the WDF of $s(t)$ is

$$W_s(t, f) = W_a(t, f) \overset{t}{\otimes} W_b(t, f) = \int d\tau W_a(\tau, f) W_b(t - \tau, f) , \quad (21)$$

which is a convolution on time t , for fixed f .

AMBIGUITY FUNCTION

The WDF is closely related to the complex ambiguity function of $s(t)$, which is defined here as [4; section 7.2]

$$\begin{aligned} \chi(\nu, \tau) &= \int dt \exp(-i2\pi\nu t) s(t + \frac{\tau}{2}) s^*(t - \frac{\tau}{2}) = \\ &= \int dt \exp(-i2\pi\nu t) R(t, \tau) = \\ &= \int df \exp(i2\pi f \tau) S(f + \frac{\nu}{2}) S^*(f - \frac{\nu}{2}) . \end{aligned} \quad (22)$$

In fact, the two are double Fourier transforms of each other:

$$\begin{aligned} \iint dt df \exp(i2\pi f \tau - i2\pi\nu t) W(t, f) &= \\ = \iint dt df \exp(i2\pi f \tau - i2\pi\nu t) \int d\tau_1 \exp(-i2\pi f \tau_1) s(t + \frac{\tau_1}{2}) s^*(t - \frac{\tau_1}{2}) &= \\ = \iint dt d\tau_1 \exp(-i2\pi\nu t) s(t + \frac{\tau_1}{2}) s^*(t - \frac{\tau_1}{2}) \delta(\tau - \tau_1) &= \\ = \int dt \exp(-i2\pi\nu t) s(t + \frac{\tau}{2}) s^*(t - \frac{\tau}{2}) = \chi(\nu, \tau) . \end{aligned} \quad (23)$$

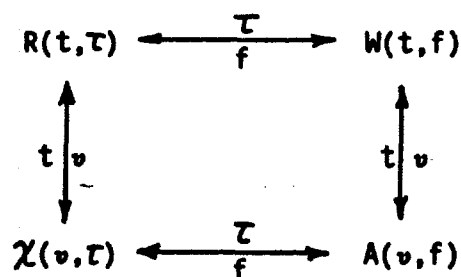
Here we used (3), (13), and (22).

In a similar fashion, the following (single) Fourier transform relationships on the WDF hold:

$$\int df \exp(i2\pi f\tau) W(t, f) = s(t + \frac{\tau}{2}) s^*(t - \frac{\tau}{2}) = R(t, \tau) ,$$

$$\int dt \exp(-i2\pi vt) W(t, f) = S(f + \frac{v}{2}) S^*(f - \frac{v}{2}) = A(v, f) . \quad (24)$$

These properties are summarized in the following diagram, where an arrow denotes a Fourier transform:



Not every function of t, f is a (legal) WDF; in fact, from (24) there follows

$$\int df \exp(i2\pi f(t_1 - t_2)) W\left(\frac{t_1 + t_2}{2}, f\right) = s(t_1) s^*(t_2) = R\left(\frac{t_1 + t_2}{2}, t_1 - t_2\right) . \quad (25)$$

Thus, in order for a candidate function $W(t,f)$ to be a WDF, the function resulting on the right-hand side of (25) must be separable in the variables t_1 and t_2 . When and only when that separability occurs, the waveform $s(t)$ can be recovered from correlation R or W (within a constant unknown phasor) as follows: let

$$s(t_0) = |s(t_0)| \exp(i\theta(t_0)) , \quad R(t_0, 0) = |s(t_0)|^2 , \quad (26)$$

where t_0 is arbitrary, except that $s(t_0) \neq 0$. Then, from the right-hand side of (25),

$$s(t) = \frac{R\left(\frac{t+t_0}{2}, t-t_0\right)}{s^*(t_0)} = \frac{R\left(\frac{t+t_0}{2}, t-t_0\right)}{\sqrt{R(t_0, 0)}} \exp(i\theta(t_0)) \quad \text{for all } t . \quad (27)$$

The special case of $t_0 = 0$ was given in [3; (17)]. The fact that the constant phase $\theta(t_0)$ is irretrievably lost in R and W can easily be seen by considering $s(t) = c g(t)$, for which $W_s(t,f) = |c|^2 W_g(t,f)$.

The box-like function $\text{rect}(t/T) \text{rect}(f/F) = 1$ for $|t| < T/2$ and $|f| < F/2$, zero otherwise, which was employed for smoothing in [1], is not a WDF, since the transform on the left-hand side of (25) yields $F \text{sinc}(Ft_1 - Ft_2)$ for $|t_1 + t_2| < T$, which is not separable in t_1 and t_2 . Also, the Gaussian function $\exp(-t^2/\sigma^2 - b^2 4\pi^2 f^2)$ is a legal WDF if and only if $b = \sigma$, in which case $s(t) = (4\pi\sigma^2)^{-1/4} \exp(-t^2/(2\sigma^2))$, with σ arbitrary.

FIRST MOMENTS OF W

The marginal integrals of W were given in (11) and (12). The (conditional) first moment of W, with respect to frequency, is

$$\begin{aligned}
 \int df f W(t, f) &= \int df f \int d\tau \exp(-i2\pi f\tau) s(t + \frac{\tau}{2}) s^*(t - \frac{\tau}{2}) = \\
 &= \int d\tau s(t + \frac{\tau}{2}) s^*(t - \frac{\tau}{2}) \int df f \exp(-i2\pi f\tau) = \\
 &= \frac{1}{2\pi} \int d\tau s(t + \frac{\tau}{2}) s^*(t - \frac{\tau}{2}) \delta'(\tau) = \frac{1}{2\pi} \text{Im}\{s'(t) s^*(t)\} . \quad (28)
 \end{aligned}$$

Here we used the result

$$i2\pi \int dx x \exp(i2\pi xy) = \delta'(y) , \quad (29)$$

obtainable directly from (13) by taking a derivative with respect to y.

Therefore the "frequency center at time t" of waveform s(t) is defined as

$$\nu_f(t) = \frac{\int df f W(t, f)}{\int df W(t, f)} = \frac{1}{2\pi} \frac{\text{Im}\{s'(t) s^*(t)\}}{|s(t)|^2} , \quad (30)$$

upon use of (28) and (12). If we let complex waveform s(t) be represented in terms of its amplitude and phase modulations according to

$$s(t) = M(t) \exp[i\theta(t)] , \quad (31)$$

then (30) yields simply

$$\nu_f(t) = \frac{1}{2\pi} \theta'(t) , \quad (32)$$

which is independent of amplitude modulation $M(t)$. (32) can also be interpreted as the instantaneous frequency at time t of waveform $s(t)$.

The "time center at frequency f " follows in an analogous fashion as

$$\nu_t(f) = \frac{\int dt \, t \, W(t, f)}{\int dt \, W(t, f)} = -\frac{1}{2\pi} \frac{\text{Im}\{S'(f) S^*(f)\}}{|S(f)|^2} . \quad (33)$$

If we represent the voltage density spectrum $S(f)$ in terms of its magnitude and phase,

$$S(f) = A(f) \exp[-i\theta(f)] , \quad (34)$$

then (33) reduces to

$$\nu_t(f) = \frac{1}{2\pi} \theta'(f) , \quad (35)$$

which is independent of $A(f)$. (35) can also be interpreted as the group delay at frequency f of waveform $s(t)$.

The unconditional first moments of W are frequency center

$$\bar{f} = \frac{\iint dt \, df \, f \, W(t, f)}{\iint dt \, df \, W(t, f)} = \frac{\int df \, f |S(f)|^2}{\int df |S(f)|^2} = \frac{\int df \, f A^2(f)}{\int df A^2(f)} \quad (36)$$

and time center

$$\bar{t} \equiv \frac{\iint dt df t W(t,f)}{\iint dt df W(t,f)} = \frac{\int dt t |s(t)|^2}{\int dt |s(t)|^2} = \frac{\int dt t M^2(t)}{\int dt M^2(t)} . \quad (37)$$

(36) follows directly from (11) and (34), while (37) follows directly from (12) and (31). Thus, \bar{f} is independent of $\theta(f)$, and \bar{t} is independent of $\theta(t)$.

Alternative forms to (36) and (37), in the complementary domains, are available:

$$\bar{f} = \frac{1}{2\pi} \frac{\int dt \operatorname{Im}\{s'(t) s^*(t)\}}{\int dt |s(t)|^2} = \frac{1}{2\pi} \frac{\int dt M^2(t) \theta'(t)}{\int dt M^2(t)} , \quad (38)$$

and

$$\bar{t} = -\frac{1}{2\pi} \frac{\int df \operatorname{Im}\{s'(f) s^*(f)\}}{\int df |s(f)|^2} = \frac{1}{2\pi} \frac{\int df A^2(f) \theta'(f)}{\int df A^2(f)} . \quad (39)$$

The result in (38) follows from the use of (28) and (12) in definition (36); a similar procedure yields (39). The frequency center \bar{f} in (38) is an average of the instantaneous frequency $\nu_f(t)$ in (32), weighted according to the magnitude-squared waveform, $M^2(t)$; similarly, time center \bar{t} in (39) is a weighted average of $\nu_t(f)$ in (35).

SECOND MOMENTS OF W

By taking two partial derivatives with respect to τ in (24), there follows

$$\int df f^2 W(t, f) = \frac{1}{8\pi^2} \left[[s'(t)]^2 - \operatorname{Re} \{ s''(t) s^*(t) \} \right]. \quad (40)$$

When we then employ (12) and (31), the (conditional) second moment with respect to f develops into the form

$$\frac{\int df f^2 W(t, f)}{\int df W(t, f)} = \frac{1}{8\pi^2} \left[\frac{M'^2(t)}{M^2(t)} - \frac{M''(t)}{M(t)} \right] + \left[\frac{\theta'(t)}{2\pi} \right]^2. \quad (41)$$

Therefore the instantaneous "mean-square frequency spread" is

$$\begin{aligned} \sigma_f^2(t) &= \frac{\int df [f - \nu_f(t)]^2 W(t, f)}{\int df W(t, f)} = \\ &= \frac{1}{8\pi^2} \left[\frac{M'^2(t)}{M^2(t)} - \frac{M''(t)}{M(t)} \right] = -\frac{1}{8\pi^2} \frac{d}{dt} \left\{ \frac{M'(t)}{M(t)} \right\}, \end{aligned} \quad (42)$$

where we employed (32) and (12). This result does not depend on phase modulation $\theta(t)$. However, it should be observed that this quantity can be negative; consider the example $M(t) = \exp(-t^\nu)$ for $t > 0$, with $0 < \nu < 1$. Thus (42) can not be interpreted as a true variance. This unfortunate feature of the WDF is due to the fact that $W(t, f)$ can go negative for some values of t, f .

The unconditional second moment with respect to f follows from (40) and (11), respectively, as

$$\iint dt df f^2 W(t, f) = \frac{1}{4\pi^2} \int dt |s'(t)|^2 = \int df f^2 |s(f)|^2. \quad (43)$$

Analogous relations for the second moments with respect to t can also be derived via a similar approach.

MOMENTS OF W^2

The marginal integral of the square of the WDF with respect to f is, via (3), (13), and (2),

$$\begin{aligned} \int df W^2(t, f) &= \int df \iint d\tau du \exp(-i2\pi f(\tau - u)) R(t, \tau) R^*(t, u) = \\ &= \int d\tau |R(t, \tau)|^2 = \int d\tau \left| s\left(t + \frac{\tau}{2}\right) \right|^2 \left| s\left(t - \frac{\tau}{2}\right) \right|^2 = \\ &= 2 \left\{ |s(\tau)|^2 \otimes |s(\tau)|^2 \right\}_{\tau=2t}, \end{aligned} \quad (44)$$

which is the convolution of $|s|^2$ with itself, at argument $2t$. The complementary result, integrating with respect to t , is

$$\begin{aligned} \int dt W^2(t, f) &= \int dv \left| s\left(f + \frac{v}{2}\right) \right|^2 \left| s\left(f - \frac{v}{2}\right) \right|^2 = \\ &= 2 \left\{ |s(v)|^2 \otimes |s(v)|^2 \right\}_{v=2f}. \end{aligned} \quad (45)$$

If we complete the integrations in (44) and (45) on the remaining variables, both yield the result

$$\iint dt df W^2(t, f) = E^2 ; \quad (46)$$

see (14). Also note, for comparison, that the double integral on W yielded E .

Although the results in (44) and (45) are not overly simple, continued integration does yield a surprisingly simple result; multiplying (44) by t , there follows

$$\begin{aligned} \iint dt df t W^2(t, f) &= \int dt t 2 \int dx |s(x)|^2 |s(2t - x)|^2 = \\ &= \int dx |s(x)|^2 2 \int dt t |s(2t - x)|^2 = \int dx |s(x)|^2 \int dy |s(y)|^2 (y + x)/2 = \\ &= \frac{1}{2} \int dx |s(x)|^2 [\bar{t}E + xE] = \frac{1}{2}[\bar{t}E^2 + \bar{t}E^2] = E^2 \bar{t} . \end{aligned} \quad (47)$$

Here we used (44), (37), and (14). Thus

$$\frac{\iint dt df t W^2(t, f)}{\iint dt df W^2(t, f)} = \bar{t} = \frac{\int dt t |s(t)|^2}{\int dt |s(t)|^2} \quad (48)$$

from (47), (46), and (37). This result in (48) is the same as (37), but now for W^2 rather than W .

Conditional first moments of W^2 with respect to f and t are also derivable; for example,

$$\begin{aligned}
 \int df f W^2(t, f) &= \frac{1}{12\pi} \int d\tau R''(t, \tau) \frac{\partial}{\partial \tau} R(t, \tau) = \\
 &= \frac{1}{2\pi} \int d\tau \left| s(t + \frac{\tau}{2}) \right|^2 \operatorname{Im} \left\{ s'(t - \frac{\tau}{2}) s^*(t - \frac{\tau}{2}) \right\} = \\
 &= \frac{1}{\pi} \int dx \left| s(2t - x) \right|^2 \operatorname{Im} \left\{ s'(x) s^*(x) \right\} = \\
 &= \frac{1}{\pi} \int dx M^2(2t - x) M^2(x) \Theta'(x) .
 \end{aligned} \tag{49}$$

Here we used (3), (29), (2), and (31). When normalized by the quantity in (44), the result is considerably more complicated than the corresponding result for W in (30) and (32); nevertheless, continued integrations simplify tremendously. In particular, there follows, from (49), (14), (38), (46), and (36),

$$\frac{\iint dt df f W^2(t, f)}{\iint dt df W^2(t, f)} = \bar{f} = \frac{\int df f |S(f)|^2}{\int df |S(f)|^2} . \tag{50}$$

This is the dual relation to (48), but derived by means of a different approach. Comparison of (50) with (36) reveals the same result for W as for W^2 .

CROSS WIGNER DISTRIBUTION FUNCTION

The cross WDF of two complex waveforms $a(t)$ and $b(t)$ is a generalization of (3) and (10) according to

$$\begin{aligned}
 W_{ab}(t, f) &= \int d\tau \exp(-i2\pi f\tau) R_{ab}(t, \tau) = \\
 &= \int d\tau \exp(-i2\pi f\tau) a(t + \frac{\tau}{2}) b^*(t - \frac{\tau}{2}) = \\
 &= \int dv \exp(i2\pi vt) A(f + \frac{v}{2}) B^*(f - \frac{v}{2}) , \quad (51)
 \end{aligned}$$

which is generally complex. If $a(t)$ and $b(t)$ are nonzero only for $a_1 < t < a_2$ and $b_1 < t < b_2$, respectively, then the integral limits on τ in (51) are explicitly τ_1, τ_2 , where

$$\tau_1 = 2 \max(a_1 - t, t - b_2) , \quad \tau_2 = 2 \min(a_2 - t, t - b_1) .$$

If $\tau_1 \geq \tau_2$, then W_{ab} is zero.

The following properties of the cross WDF result immediately:

$$W_{a^*b^*}(t, f) = W_{ab}^*(t, -f) ,$$

$$W_{ba}(t, f) = W_{ab}^*(t, f) ,$$

$$\int df W_{ab}(t, f) = a(t) b^*(t) ,$$

$$\int dt W_{ab}(t, f) = A(f) B^*(f) ,$$

$$\iint dt df W_{ab}(t, f) = \int dt a(t) b^*(t) = \int df A(f) B^*(f) ,$$

$$\iint dt df |W_{ab}(t, f)|^2 = E_a E_b .$$

$$\iint dt df W_{aa}(t, f) W_{bb}(t, f) = \left| \int dt a(t) b^*(t) \right|^2 = \left| \iint dt df W_{ab}(t, f) \right|^2 .$$

$$\iint dt df W_{ab}(t, f) W_{cd}^*(t, f) = \int dt a(t) c^*(t) * \int dt b^*(t) d(t) . \quad (52)$$

The last three relations follow upon substitution of (51), interchanging integrals, and the use of (13). Again, the double Fourier transform of the cross WDF yields the cross ambiguity function:

$$\begin{aligned} \iint dt df \exp(-i2\pi vt + i2\pi f\tau) W_{ab}(t, f) &= \\ &= \int dt \exp(-i2\pi vt) a(t + \frac{\tau}{2}) b^*(t - \frac{\tau}{2}) = \\ &= \int df \exp(i2\pi f\tau) A(f + \frac{v}{2}) B^*(f - \frac{v}{2}) = \\ &= \chi_{ab}(v, \tau) = \int dt \exp(-i2\pi vt) R_{ab}(t, \tau) . \end{aligned} \quad (53)$$

The magnitude-squared cross-WDF of waveforms a and b is also related to the auto-WDFs by means of a double convolution:

$$\begin{aligned}
 |W_{ab}(t, f)|^2 &= \iint d\tau_1 d\tau_2 \exp(-i2\pi f(\tau_1 - \tau_2)) * \\
 &* R_{aa}\left(t + \frac{\tau_1 + \tau_2}{4}, \frac{\tau_1 - \tau_2}{2}\right) R_{bb}\left(t - \frac{\tau_1 + \tau_2}{4}, \frac{\tau_1 - \tau_2}{2}\right) = \\
 &= \iint d\tau' d\tau \exp(-i2\pi f\tau') R_{aa}\left(t + \frac{\tau}{2}, \frac{\tau'}{2}\right) R_{bb}\left(t - \frac{\tau}{2}, \frac{\tau'}{2}\right) = \\
 &= \iint d\tau' d\tau \exp(-i2\pi f\tau') R_{aa}\left(t + \frac{\tau}{2}, \frac{\tau'}{2}\right) \int df' \exp\left(i2\pi f' \frac{\tau'}{2}\right) W_{bb}\left(t - \frac{\tau}{2}, f'\right) = \\
 &= \iint d\tau df' W_{bb}\left(t - \frac{\tau}{2}, f'\right) \int d\tau' \exp\left(-i2\pi(2f - f') \frac{\tau'}{2}\right) R_{aa}\left(t + \frac{\tau}{2}, \frac{\tau'}{2}\right) = \\
 &= 2 \iint d\tau df' W_{bb}\left(t - \frac{\tau}{2}, f'\right) W_{aa}\left(t + \frac{\tau}{2}, 2f - f'\right) = 4 \iint dt' df' W_{bb}(t', f') W_{aa}(2t - t', 2f - f') \\
 &= \iint d\tau dv W_{aa}\left(t + \frac{\tau}{2}, f + \frac{v}{2}\right) W_{bb}\left(t - \frac{\tau}{2}, f - \frac{v}{2}\right), \tag{54}
 \end{aligned}$$

where we let $\tau = (\tau_1 + \tau_2)/2$, $\tau' = \tau_1 - \tau_2$ in the third line.

Let $\bar{b}(t) = b(-t)$; then

$$W_{ab}(t, f) = 2 \chi_{a\bar{b}}(2f, 2t),$$

and

$$\text{convolution } W_{ab}(t, f) \overset{+}{\otimes} W_{cd}^*(t, f) = \chi_{a\bar{c}}(f, t) \chi_{b\bar{d}}^*(f, t) = \frac{1}{4} W_{ac}\left(\frac{t}{2}, \frac{f}{2}\right) W_{bd}^*\left(\frac{t}{2}, \frac{f}{2}\right),$$

$$\text{while cross correlation } \iint dt' df' W_{ab}(t, f) W_{cd}^*(t - \tau, f - \nu) = \chi_{ac}(\nu, t) \chi_{bd}^*(\nu, t) = \frac{1}{4} W_{ac}\left(\frac{\tau}{2}, \frac{\nu}{2}\right) W_{bd}^*\left(\frac{\tau}{2}, \frac{\nu}{2}\right).$$

NARROWBAND REAL WAVEFORM

When waveform $s(t)$ is narrowband and real, it can be expressed in terms of its low-pass complex envelope $c(t)$ according to

$$\begin{aligned} s(t) &= 2 \operatorname{Re}\{c(t) \exp(i2\pi f_0 t)\} = \\ &= c(t) \exp(i2\pi f_0 t) + c^*(t) \exp(-i2\pi f_0 t) , \end{aligned}$$

where f_0 is the carrier or center frequency of $s(t)$. The WDF of $s(t)$ is then expressible as

$$\begin{aligned} W_{ss}(t, f) &= \int d\tau \exp(-i2\pi f\tau) s(t + \frac{\tau}{2}) s^*(t - \frac{\tau}{2}) = \\ &= W_{cc}(t, f - f_0) + W_{cc}(t, -f - f_0) + \\ &+ 2 \operatorname{Re}\{W_{cc^*}(t, f) \exp(i4\pi f_0 t)\} . \end{aligned} \tag{55}$$

Here, we substituted for $s(t)$, and used (51) and (52). Since complex envelope $c(t)$ is low-pass, a representative contour plot of (55) appears as shown in figure 1. The wiggly lobe centered at $f = 0$ is subject to rapid oscillations in t , whereas those lobes centered at $\pm f_0$ are slowly varying with f and t . A small amount of averaging in time would wipe out the undesired oscillating lobe, but maintain the desired components at $f = \pm f_0$.

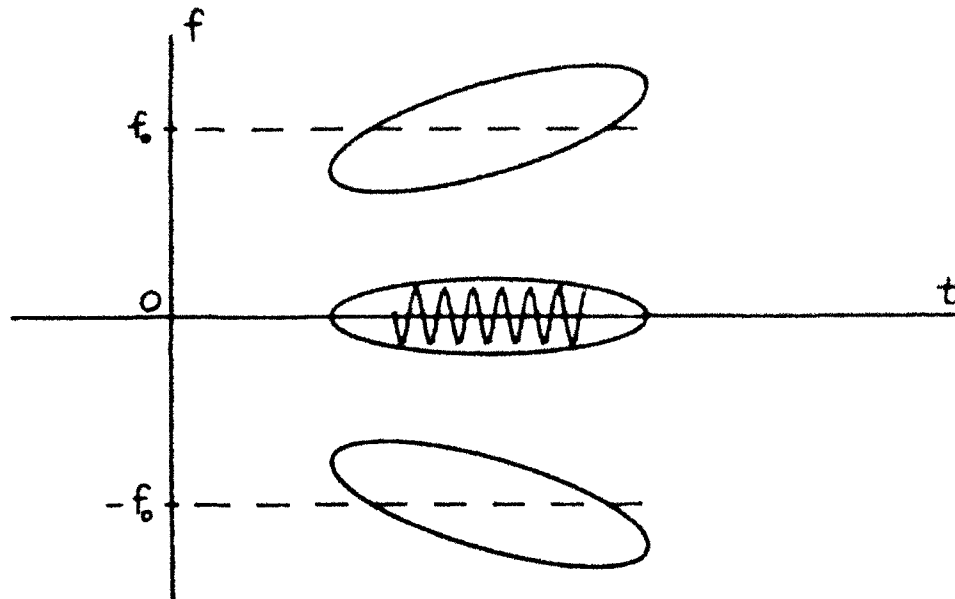


Figure 1. WDF for Narrowband Real Waveform

SAMPLING PROPERTIES

By letting $u = \tau/2$ in (3), the WDF becomes

$$W(t, f) = 2 \int du \exp(-i4\pi fu) s(t + u) s^*(t - u) , \quad (56)$$

where we again now allow general complex $s(t)$. If this integral is to be evaluated numerically on a computer, we will need to sample the integrand at some increment Δ_t , and apply some integration rule. In particular, if we use the Trapezoidal rule and carry out the summation over $-\infty, +\infty$, we have approximation

$$\tilde{W}(t, f) \approx 2\Delta_t \sum_k \exp(-i4\pi f k \Delta_t) s(t + k\Delta_t) s^*(t - k\Delta_t) \quad (57)$$

for all t, f . Since it is immediately seen from (57) that

$$\tilde{W}\left(t, f + \frac{1}{2\Delta_t}\right) = \tilde{W}(t, f) , \quad (58)$$

it follows that $\tilde{W}(t, f)$ has period $(2\Delta_t)^{-1}$ in f , when waveform $s(t)$ is sampled at increment Δ_t . In fact, it can be shown that \tilde{W} is the aliased version of W :

$$\tilde{W}(t, f) = \sum_n W(t, f - \frac{n}{2\Delta_t}) . \quad \text{See figure 2.} \quad (59)$$

Thus, $\tilde{W}(t, f)$ need be evaluated only over one period, say $(0, .5/\Delta_t)$.

Since (57) cannot be evaluated for all continuous values of t and f , we will limit its evaluation to

$$t = m\Delta_t , \quad f = \frac{n}{2N_f\Delta_t} , \quad (60)$$

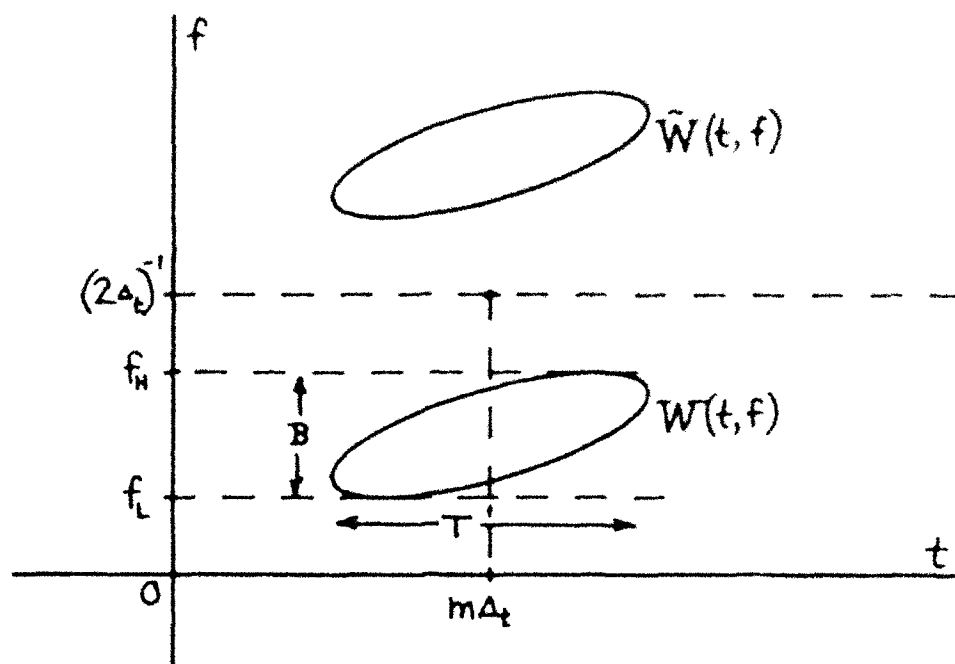
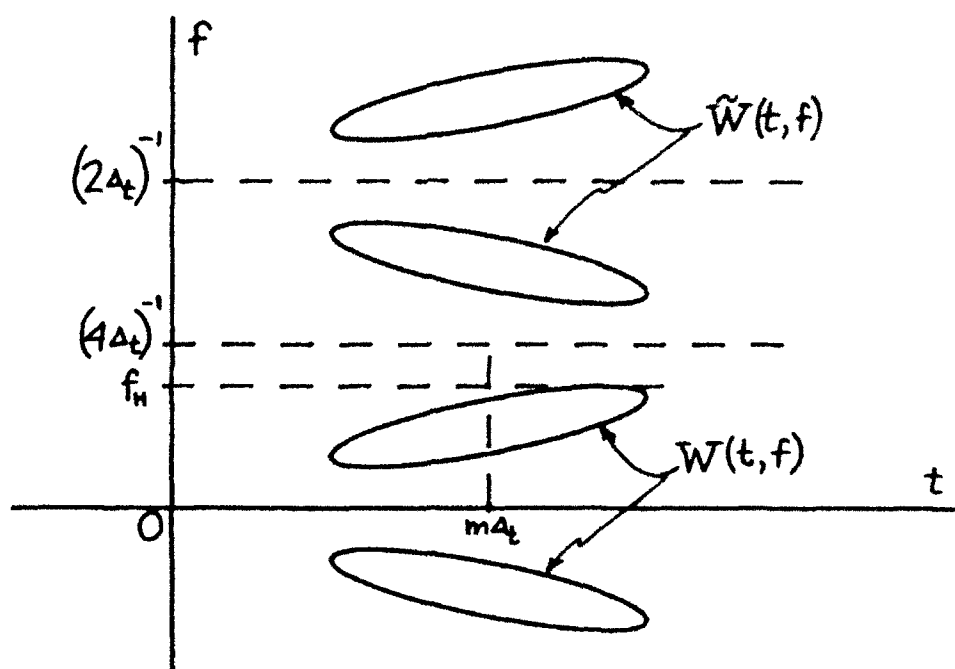
where m, n, N_f are integers. Then (57) becomes (exactly)

$$\tilde{W}\left(m\Delta_t, \frac{n}{2N_f\Delta_t}\right) = 2\Delta_t \sum_k \exp(-i2\pi nk/N_f) s((m+k)\Delta_t) s^*((m-k)\Delta_t) , \quad (61)$$

$\Delta_c = 2\Delta_t$ as in definition (57).

the right side of which is recognized as an N_f -point discrete Fourier transform. If the number of nonzero samples in k is greater than N_f , we simply collapse them mod N_f , without loss of accuracy; see [5; page 7]. Since the period of $\tilde{W}(t, f)$ is $(2\Delta_t)^{-1}$ in f , we only need consider $0 \leq n \leq N_f - 1$, that is, $0 \leq f < (2\Delta_t)^{-1}$. Values of m must be considered wherever the summand of (61) is nonzero.

A plot of two of the infinite number of lobes of $\tilde{W}(t, f)$ in (59) is depicted in figure 2 for a representative bandpass analytic waveform $s(t)$.


 Figure 2. WDF for Sampled Version $\tilde{W}(t, f)$

 Figure 3. $\tilde{W}(t, f)$ for Real Waveform $s(t)$

The spreads of the desired WDF term $\tilde{W}(t, f)$ are T and B in time and frequency, respectively. In order to guarantee that aliasing is insignificant in figure 2, we must choose

$$(2\Delta_t)^{-1} > B, \quad \text{that is, } \Delta_t < (2B)^{-1}. \quad (62)$$

For N_f equal to a power of 2 in (61), an FFT can be employed to evaluate \tilde{W} and will give the vertical slice in f indicated in figure 2 between $f = 0$ and $f = (2\Delta_t)^{-1}$, for the particular m value under consideration. Since the spacing of frequency values in (61) is $(2N_f\Delta_t)^{-1}$, then in order to keep track of the wiggles in $\tilde{W}(t, f)$ as a function of f , we must choose

$$(N_f\Delta_t)^{-1} < T^{-1}, \quad \text{that is, } N_f > T/\Delta_t > 2BT. \quad (63)$$

Thus the FFT size may have to be quite large for an extended WDF in t, f space.

If $s(t)$ is real, then (8) applies, meaning that \tilde{W} in (61) need only be computed for

$$0 \leq n \leq N_f/2, \quad \text{that is, } 0 \leq f \leq (4\Delta_t)^{-1}. \quad (64)$$

The pertinent approximate WDF \tilde{W} is depicted in figure 3. In order to avoid aliasing now, we must have

$$(4\Delta_t)^{-1} > f_H, \quad \text{that is, } \Delta_t < (4f_H)^{-1}, \quad (65)$$

where f_H is the highest frequency contained in $s(t)$. This sampling rate is twice as fast as the usual Nyquist rate for waveform $s(t)$, and is due to the unavoidable^{*} factors of $1/2$ in definition (3).

The procedure described above, in (61) et seq., realizes a slice in f , at fixed t , of the WDF; see figures 2 and 3. An alternative procedure for obtaining slices of the WDF in t , at fixed f , is described in appendix A; however, starting with time samples of $s(t)$, it requires an additional large-size FFT to start the calculations.

* But see (A-8) et seq.

EXAMPLES OF WDF

In this section, we present several examples of the WDF for waveforms that are likely to be encountered in practice, and that are amenable to simple closed form solution. A significant shortcut in the presentation is possible when it is observed from (3) that if

$$r(t) = s(t - t_0) \exp(i2\pi f_0 t + i\theta_0) , \quad (66)$$

which corresponds to a time delay and frequency shift, then

$$W_r(t, f) = W_s(t - t_0, f - f_0) . \quad (67)$$

Thus we can choose any convenient origin for the waveform s in time and frequency, without loss of generality, and then merely shift the WDF according to (67), as appropriate.

We will place heavy emphasis here on combinations of Gaussian pulses, both because of their analytic tractability and due to the fact that any waveform can be expanded into elementary waveforms consisting of Gaussian wavelets; see, for example, Gabor's original paper [6, part 1, section 5].

In the following, frequent use will be made of the following integral:

$$\int dx \exp(-\frac{1}{2} \alpha x^2 \pm \beta x) = \left(\frac{2\pi}{\alpha}\right)^{1/2} \exp\left(\frac{\beta^2}{2\alpha}\right) \quad \text{for } \alpha_r > 0 , \quad (68)$$

where α and β can be complex, with components

$$\alpha = \alpha_r + i\alpha_i, \quad \beta = \beta_r + i\beta_i. \quad (69)$$

Also, as a special case, there follows

$$\left| \int dx \exp\left(-\frac{1}{2} \alpha x^2 \pm \beta x\right) \right|^2 = \frac{2\pi}{(\alpha_r^2 + \alpha_i^2)^{1/2}} \exp\left[\frac{\alpha_r(\beta_r^2 - \beta_i^2) + 2\alpha_i\beta_r\beta_i}{\alpha_r^2 + \alpha_i^2} \right], \quad (70)$$

written out in terms of purely real quantities.

GAUSSIAN WAVEFORM

Let waveform

$$s(t) = a_0 \exp\left(-\frac{t^2}{2\sigma_0^2}\right); \quad a_0 \text{ complex}. \quad (71)$$

(Parameters will be real unless indicated otherwise.) Use of (3) and (68) yields WDF

$$W(t,f) = 2E \exp\left[-\frac{t^2}{\sigma_0^2} - (2\pi f\sigma_0)^2\right], \quad (72)$$

where E is the waveform energy:

$$E = \sqrt{\pi} |a_0|^2 \sigma_0. \quad (73)$$

The WDF consists of a single positive lobe in t, f space, centered at the origin.

Observe that $W(0,0)$ is equal to $2E$ for this example. In fact, from (3),

$$W(0,0) = \int dE s(E/2) s^*(-E/2) = 2E \quad \text{if } s(-t) = s(t) \quad (14)$$

Thus waveforms $s(t)$ with this even symmetry result in peak WDF values of $2E$ at the origin. However, if s has odd symmetry about zero, $s(-t) = -s(t)$, then $W(0,0) = -2E$.

The contours of equal height of the WDF in (72) are ellipses. The contour for the case where the levels are down to $\exp(-1)$ of their peak value is the ellipse indicated in figure 4. The area of this particular level ellipse is $1/2$ in the t, f plane. When this area is multiplied by the peak height of $2E$, the product is E , which is just the volume under the WDF, see (14). Thus the "effective extent" of the WDF in (72) is that given in figure 4, for relative level $1/e$ of the peak.

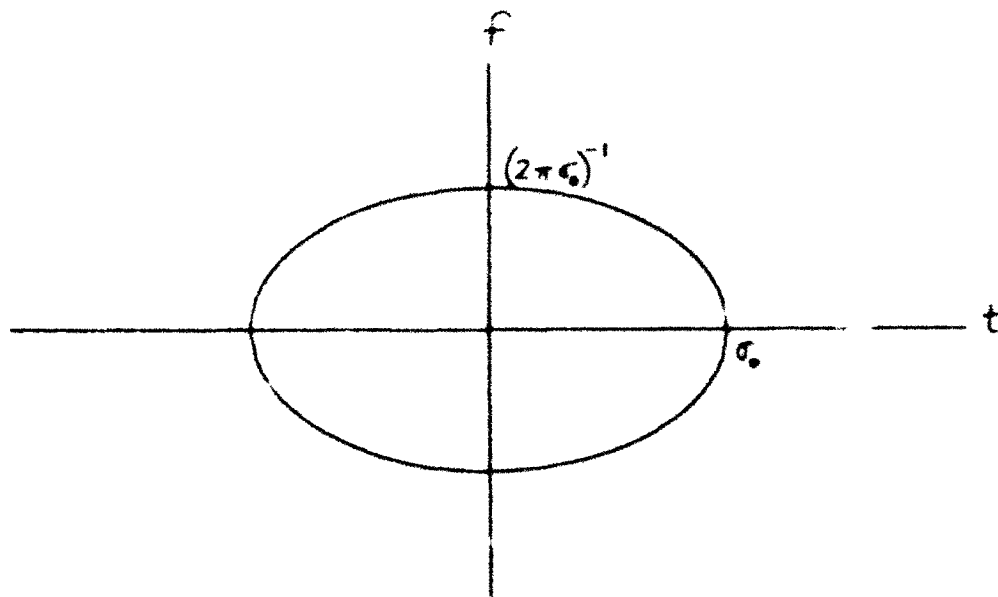


Figure 4. Contour of WDF (72) at $1/e$ Relative Level

GAUSSIAN-MODULATED TONE

$$s(t) = b_0 \cos(2\pi f_0 t + \theta_0) \exp\left(-\frac{t^2}{2\sigma_0^2}\right). \quad (75)$$

The energy of this waveform is

$$E = \frac{1}{2} \sqrt{\pi} b_0^2 \sigma_0 [1 + \cos(2\theta_0) \exp(-y_0^2)] . \quad (76)$$

and its WDF is

$$\begin{aligned} \left(\frac{1}{2} \sqrt{\pi} b_0^2 \sigma_0\right)^{-1} W(t, f) = & \exp[-x^2 - (y - y_0)^2] + \exp[-x^2 - (y + y_0)^2] + \\ & + 2 \cos(4\pi f_0 t + 2\theta_0) \exp[-x^2 - y^2] . \end{aligned} \quad (77)$$

where dimensionless variables

$$x = t/\sigma_0 , \quad y = 2\pi f \sigma_0 , \quad y_0 = 2\pi f_0 \sigma_0 . \quad (78)$$

There are two positive lobes centered at $(t, f) = (0, f_0)$ and $(0, -f_0)$, each of peak height approximately E (if y_0 is large). The contours of each of these lobes are circles in the x, y plane, or ellipses in the t, f plane, as indicated in figure 4. There is also an oscillating lobe centered at the origin; this is an example of the general situation depicted in figure 1.

It should also be observed from (77) that if a slice in frequency is taken of the WDF, at fixed time t , that there is no fast oscillation in any of the three lobes. Whatever value of the \cos is encountered, that value is maintained, and the only variation with y (frequency) is the Gaussian dependence. Thus if we locally averaged the WDF with respect to frequency alone, that would not eliminate the undesired oscillating lobe centered at $(0, 0)$.

MULTIPLE MODULATED TONES

Consider complex waveform

$$s(t) = \sum_k a_k \exp \left[i2\pi f_k t - \frac{(t - t_k)^2}{2\sigma_k^2} \right]; \quad \{a_k\} \text{ complex.} \quad (79)$$

This is a collection of tone bursts centered at $\{t_k, f_k\}$ in the t, f plane, with energy $E_k = \sqrt{\pi} |a_k|^2 \sigma_k$. The corresponding WDF follows from (3) and (68) as

$$\begin{aligned} W(t, f) = & 2 \sum_k E_k \exp \left[-\frac{(t - t_k)^2}{\sigma_k^2} - \sigma_k^2 4\pi^2 (f - f_k)^2 \right] + \\ & + 4\sqrt{\pi} \sum_{k < l} \tilde{\sigma}_{kl}^2 \exp \left[-\frac{(t - t_{kl})^2}{\tilde{\sigma}_{kl}^2} - \tilde{\sigma}_{kl}^2 4\pi^2 (f - f_{kl})^2 \right] * \\ & * \operatorname{Re} \left\{ a_k a_l^* \exp \left[i2\pi (f_k - f_l) t + i \tilde{\sigma}_{kl}^2 2\pi (f - f_{kl}) \left(\frac{t - t_k}{\sigma_k^2} - \frac{t - t_l}{\sigma_l^2} \right) \right] \right\}, \quad (80) \end{aligned}$$

where

$$\begin{aligned} t_{kl} &= \frac{1}{2} (t_k + t_l), \quad f_{kl} = \frac{1}{2} (f_k + f_l), \\ \tilde{\sigma}_{kl}^2 &= \frac{1}{2} (\sigma_k^2 + \sigma_l^2), \quad \frac{1}{\tilde{\sigma}_{kl}^2} = \frac{1}{2} \left(\frac{1}{\sigma_k^2} + \frac{1}{\sigma_l^2} \right). \quad (81) \end{aligned}$$

The first line of (80) represents the desired positive lobes centered at (t_k, f_k) , each scaled according to its energy. The remaining undesired lobes are centered at

$$\frac{t_k + t_l}{2}, \frac{f_k + f_l}{2} \quad \text{for all } k \neq l, \quad (82)$$

and oscillate with t and/or f . These locations in (82) are halfway between every possible pair of desired lobes; their amplitudes are proportional to the geometric means of the corresponding interacting lobes, and therefore constitute significant interference effects to interpretation of the computed WDF. Furthermore, the locations in (82) can occur in time where the waveform $s(t)$ is zero, and/or in frequency where the spectrum $S(f)$ is zero. This most undesirable feature of the WDF has been reported previously in [7,8]. The only saving feature, that should allow salvaging the WDF, is that the undesired lobes, $k \neq l$ in (80), oscillate positive-and-negative and can be averaged out by smoothing the WDF. Of course, via this smoothing procedure, the desired lobes will also be smeared somewhat, but this trade-off appears to be required in order to make a meaningful, useful interpretation of the WDF at all points of the t, f plane.

The envelope of the k, l lobe in (80) is proportional to an exponential of an elliptical function. When this exponential has decreased to $1/e$ of its peak value, the corresponding elliptical contour has area

$$\frac{\pi \sigma_{kl}}{2\pi \tilde{\sigma}_{kl}} = \frac{1}{4} \left(\frac{\sigma_k}{\sigma_l} + \frac{\sigma_l}{\sigma_k} \right) \geq \frac{1}{2} \quad (83)$$

in the t, f plane, the latter value of $1/2$ being the area of every desired lobe. Thus the undesired oscillating lobes are smeared out more than the desired positive lobes.

If we restrict (79) to two equal-duration bursts with the same time center, but different center frequencies, the undesired lobe oscillates only with t , not f . This is similar to example (75)-(77). On the other hand, if (79) is restricted to two equal-duration bursts with different time centers, but the same frequency center, the undesired lobe oscillates only with f , not t .

More generally, for two equal-duration bursts with different time and frequency centers, the undesired lobe has no fast oscillation along lines in the t, f plane which are parallel to the line joining the centers of the two positive lobes in the WDF. For two unequal-duration bursts, the situation is more complicated, and there is generally oscillation along all straight lines in the t, f plane.

What these simple examples demonstrate is that if we want to locally smooth (average) the WDF, in an effort to wipe out the undesired oscillating cross-terms, that smoothing must be applied in both t and f , not either one alone. Of course, such smoothing will also tend to smear the desired positive lobes; thus the minimum amount of smoothing to guarantee a nonnegative WDF is of interest.

Although these conclusions have been drawn from the particular example of Gaussian-modulated tone bursts in (79) (for analytic simplicity), they hold generally. Appendix B demonstrates the oscillating character of the interacting cross-terms of the WDF for a waveform with two separated energy bursts in time of general shape.

The ambiguity function of waveform $s(t)$ in (75) is considered in appendix C. It has some similar properties to the WDF and some significant differences, which make it much less desirable as a descriptor of a signal's concentration in time-frequency space.

LINEAR FREQUENCY MODULATION

Here, we consider waveform

$$s(t) = a_0 \exp \left[-\frac{t^2}{2\sigma_0^2} + i \frac{\alpha_0}{2} t^2 \right]; \quad \alpha_0 \geq 0, \quad a_0 \text{ complex}. \quad (84)$$

The instantaneous frequency, according to (31) and (32), is a linear function of time,

$$\nu_f(t) = \frac{\alpha_0}{2\pi} t, \quad (85)$$

while the envelope is Gaussian. When

$$t = t_0 = \pm \sigma_0 \sqrt{\pi/2}, \quad (86)$$

the magnitude of the waveform $s(t)$ is

$$|s(t_0)| = |a_0| \exp(-\pi/4) = .456 |s(0)|. \quad (87)$$

If we define the duration, Δt , of $s(t)$ as the time between these function values, then

$$\Delta t = \sigma_0 \sqrt{2\pi}. \quad (88)$$

During this time interval, the instantaneous frequency in (85) sweeps through a bandwidth

$$\Delta f = \frac{\alpha_0}{2\pi} \Delta t = \alpha_0 \sigma_0 \sqrt{2\pi}. \quad (89)$$

The time-bandwidth product of waveform $s(t)$ is therefore

$$\Delta t \Delta f = \alpha_0 \sigma_0^2 \equiv \theta_0 \quad (\geq 0), \quad (90)$$

when the time duration is defined as the interval between the function values in (87). This quantity, θ_0 , is an important parameter of the linear frequency modulation waveform (84).

The WDF of (84) follows, upon use of (3) and (68), as

$$\begin{aligned} W(t, f) &= 2E \exp \left[-\frac{t^2}{\sigma_0^2} - \sigma_0^2 (2\pi f - \alpha_0 t)^2 \right] = \\ &= 2E \exp \left[-x^2 - (y - x\theta_0)^2 \right] = \\ &= 2E \exp \left[-x^2 (1 + \theta_0^2) + 2xy \theta_0 - y^2 \right], \end{aligned} \quad (91)$$

where we employed (78) and (90). This is an everywhere-positive lobe centered at the origin of time-frequency space, with contours that are tilted ellipses. The peak value, $2E$, is independent of the amount of frequency modulation.

For a given value of time t , the frequency f that maximizes the WDF in (91) is

$$f = \frac{\alpha_0}{2\pi} t, \quad \text{that is, } y = x\theta_0, \quad (92)$$

which is just the instantaneous frequency in (85). However, this line, (92), in the t, f plane is not the major axis of the elliptical contours of the WDF. A similar observation regarding the ambiguity function $\chi(\nu, \tau)$, (23), of the linear frequency modulation waveform, namely

$$\chi(\nu, \tau) = E \exp \left[-\frac{1}{4} \{ x'^2 (1 + \theta_0^2) - 2x'y'\theta_0 + y'^2 \} \right], \quad (93)$$

where

$$x' = \frac{\tau}{\sigma_0}, \quad y' = 2\pi\nu\sigma_0, \quad (94)$$

has been made in [4; page 124].

What this means is that, if the WDF of a waveform is evaluated numerically from a given data sequence (via (61) for example), then the tilt of the major axis of the contours of the computed WDF is not directly the amount of linear frequency modulation in the waveform. Rather, the major axis of the ellipse in (91) lies along the line

$$y = x \tan \psi \quad (95)$$

in the x, y plane, where

$$\tan \psi = \frac{\sqrt{\theta_0^2 + 4} + \theta_0}{2} \geq \theta_0. \quad (96)$$

(See appendix D for detailed derivations on the rotation of coordinate axes.) Thus, the major axis (95) of the ellipse is more tilted than the instantaneous frequency line (92). Equation (96) can be inverted and solved for the linear frequency modulation parameter θ_0 according to

$$\theta_0 = \tan \psi - 1/\tan \psi, \quad (97)$$

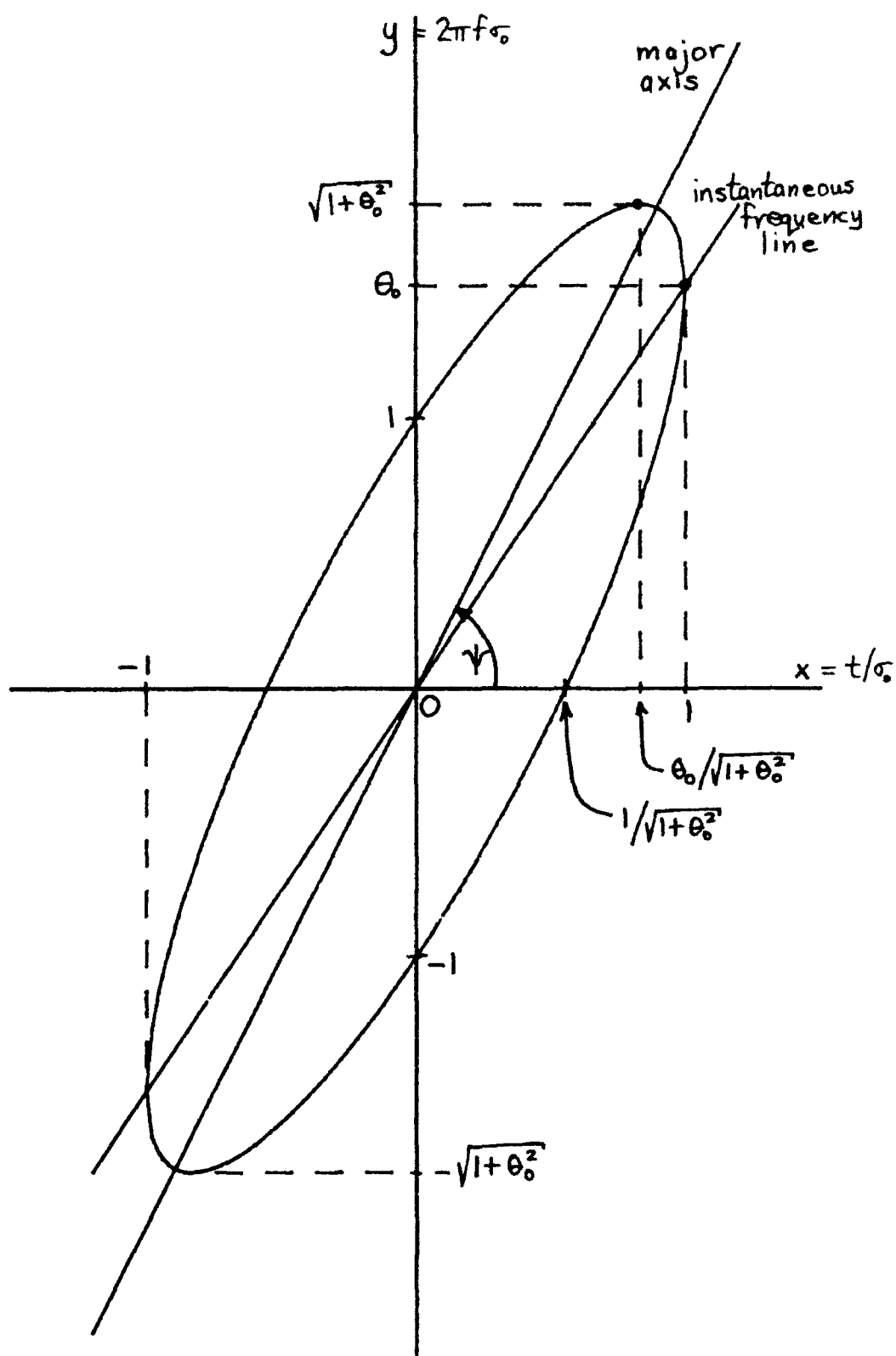
in terms of the measured or calculated major axis tilt, $\tan \psi$, in the x,y plane. The detailed procedure for solving for both σ_0 and α_0 , in terms of a computed WDF in the t,f plane, is discussed in the example in appendix D, especially (D-28) and (D-29).

When the exponential in (91) is down to 1/e of its peak value, the ellipse at that level has area π in the x,y plane. This may be seen by use of (D-1) and (D-20), with $A = 1 + \theta_0^2$, $B = -2\theta_0$, $C = 1$, $D = E = 0$, $F = -1$, for which $G = 1$ via (D-19). This corresponds to area 1/2 in the t,f plane, as seen by (78). Therefore, the peak height, $2E$, times the "effective" area is again E , as it was for the simple Gaussian pulse of (71) and figure 4. Thus, although the volume of the WDF in (91) has been redistributed in the t,f plane, by virtue of linear frequency modulation, the effective area is maintained, although now located as a tilted ellipse.

A plot of the ellipse of (91) at the 1/e level, namely

$$x^2 + (y - x\theta_0)^2 = x^2(1 + \theta_0^2) - 2xy\theta_0 + y^2 = 1, \quad (98)$$

is given in figure 5, when $\theta_0 = 1.5$. The instantaneous frequency line (92) as well as the major axis (95) are delineated, and are clearly seen not to overlie each other.

Figure 5. Contour of (91) for $\theta_0 = 1.5$

GATED LINEAR FREQUENCY MODULATION

All the previous examples in this section had Gaussian envelopes. We now consider a rectangularly gated waveform with linear frequency modulation:

$$s(t) = a_0 \exp\left[i \frac{\alpha_0}{2} t^2\right] \quad \text{for } |t| < \frac{T}{2}; \quad a_0 \text{ complex.} \quad (99)$$

Equation (3) yields directly WDF

$$W(t, f) = 2E \frac{\sin[(2\pi f - \alpha_0 t)(T - 2|t|)]}{(2\pi f - \alpha_0 t)T} \quad \text{for } |t| < \frac{T}{2}, \text{ all } f, \quad (100)$$

and zero otherwise. Along the instantaneous frequency line, (85), the WDF is $2E (1 - 2|t|/T)$ for $|t| < T/2$, which is nonoscillatory and positive. However, in other portions of the t, f plane, (100) does go negative, due to the sin term.

For a given value of t , the quantity W in (100) is maximized by choosing $f = \alpha_0 t/(2\pi)$, but, again, this is not the major axis of the contours of the WDF. In figure 6, these contours are plotted for $\alpha_0 T^2 = 1$ and $\alpha_0 T^2 = 10$. In fact, the contours are no longer ellipses, although they tend to resemble ellipses near the origin, when frequency modulation parameter $\alpha_0 T^2$ is large; see the bottom figure, where the instantaneous frequency line and the mountain ridge (curve of slowest descent) have been sketched.

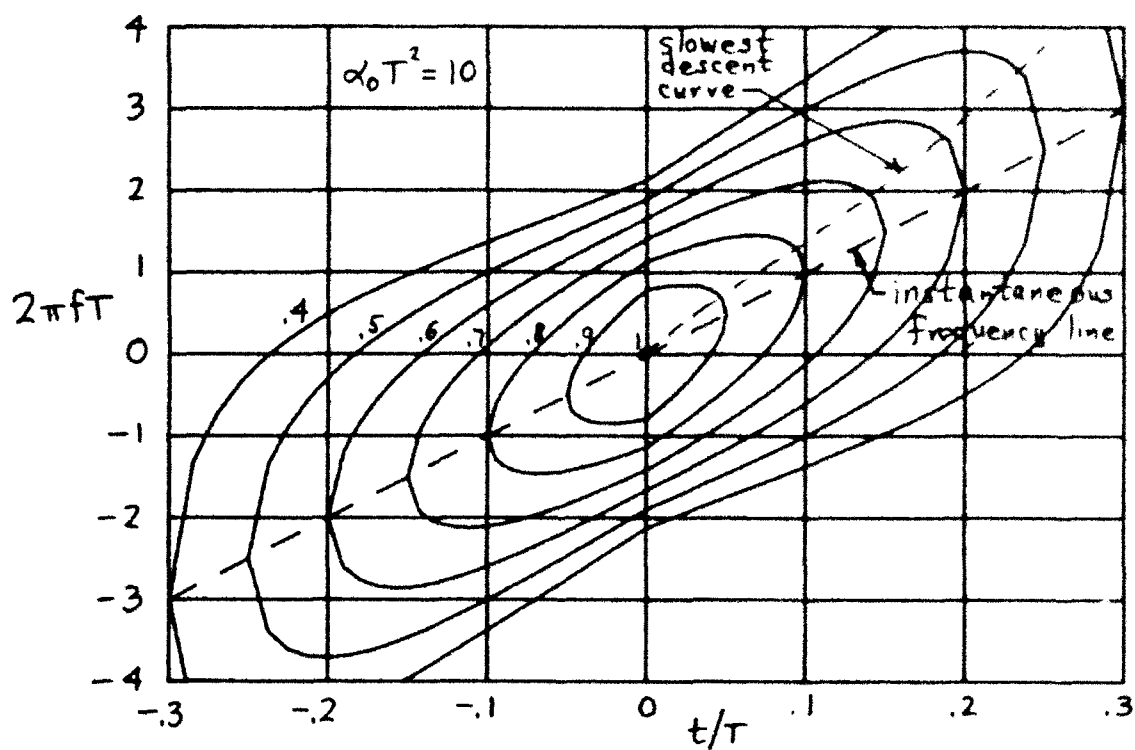
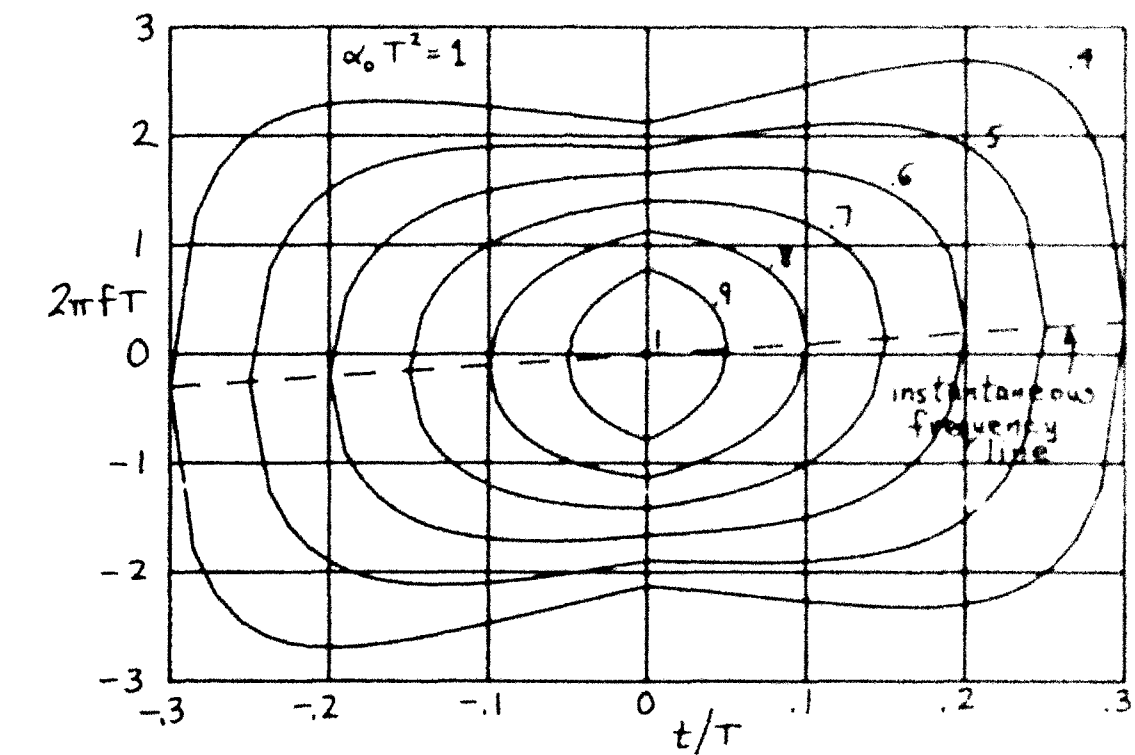


Figure 6. Contours of WDF for Gated LFM

The ambiguity function of waveform (99) is

$$\chi(\nu, \tau) = E \frac{\sin[\frac{1}{2}(2\nu\nu_0 - \omega_0^2\tau)(1 - |\tau|)]}{\frac{1}{2}(2\nu\nu_0 - \omega_0^2\tau)} \quad \text{for } |\tau| \leq 1, \text{ all } \nu, \quad (100)$$

and zero otherwise. It is similar to the WDF in (100), but is spread out more in the ν, τ plane.

SHORT-TERM SPECTRAL ESTIMATION

Some advantageous features of the WDF have been brought out by earlier examples, such as the concentrated positive lobes in the t, f plane about locations corresponding to obvious bursts of energy. However, the WDF also goes negative in surrounding regions, causing difficulty in interpretation; see figure 1, (80), appendix B, or [7,8]. What is needed is some form of smoothing of the WDF so as to eliminate or suppress the oscillating components; however, this averaging must be two-dimensional, carried out in both time and frequency, for the reasons presented in the sequel to (83). We now present one method of smoothing the WDF, which guarantees a non-negative distribution in time-frequency.

WEIGHTED SPECTRAL ESTIMATE

The voltage density spectrum $S(f)$, corresponding to waveform $s(t)$, was defined in (9) as the Fourier transform over all time. In order to bring out properties which are local in time, a weighting must be applied before transformation. In particular, we generalize (9) to

$$\begin{aligned} S_U(t, f) &= \int dt_1 \exp(-12\pi f t_1) s(t_1) u^*(t - t_1) = \\ &= \exp(-12\pi f t) \int df_1 \exp(12\pi t f_1) S(f_1) U^*(f - f_1) . \end{aligned} \quad (102)$$

where weighting u will tend to be a narrow function centered about its origin; thus the weighting in (102) will accent the behavior of waveform s in the neighborhood of time t . The function, U is the Fourier transform of u . The short-term power spectral estimate (at time t and frequency f) of waveform s , relative to weighting u , is then defined as

$$|S_u(t, f)|^2. \quad (103)$$

See also [2, p. 768].

The following symmetry properties of definition (102) follow:

$$S_u(t, f) = U_s^*(t, f) \exp(-i2\pi ft),$$

$$|S_u(t, f)|^2 = |U_s(t, f)|^2, \quad (104)$$

where U_s is the spectrum of waveform u relative to weighting s . That is, U_s is the dual of S_u . Also, by use of (53), we can express

$$S_u(t, f) = \chi_{s\bar{u}}(f, t) \exp(-i\pi ft) = \frac{1}{2} W_{su}\left(\frac{t}{2}, \frac{f}{2}\right) \exp(-i\pi ft), \quad (105)$$

in terms of the complex cross-ambiguity function of s and \bar{u} , where \bar{u} is the mirror image of u : $\bar{u}(t) = u(-t)$. Also, the same shifting property, given in (66) and (67) for the WDF, holds as well for quantity (103). In general,

$$\chi_{s\bar{u}}(f, t) = \frac{1}{2} W_{su}\left(\frac{t}{2}, \frac{f}{2}\right) \text{ for any } s, u.$$

RELATION TO WDFs

There is a very important relation between the short-term spectral estimate (STSE), (103), and the WDFs of s and u ; namely, by use of (102), (2), and (3), we have

$$\begin{aligned}
|S_U(t, f)|^2 &= \iint dt_1 dt_2 \exp(-i2\pi f(t_1 - t_2)) s(t_1) s^*(t_2) u^*(t - t_1) u(t - t_2) = \\
&= \iint d\tau dt' \exp(-i2\pi f\tau) s\left(t' + \frac{\tau}{2}\right) s^*\left(t' - \frac{\tau}{2}\right) u\left(t - t' + \frac{\tau}{2}\right) u^*\left(t - t' - \frac{\tau}{2}\right) = \\
&= \iint d\tau dt' \exp(-i2\pi f\tau) R_s(t', \tau) R_u(t - t', \tau) = \\
&= \iint dt' df' W_s(t', f') W_u(t - t', f - f') = \\
&= W_s(t, f) \underset{\text{via (105)}}{\circledast} W_u(t, f) = \left| \chi_{s, u}(f, t) \right|^2 = \frac{1}{4} \left| W_{s, u}\left(\frac{t}{2}, \frac{f}{2}\right) \right|^2, \quad (106)
\end{aligned}$$

This relation states that the STSE is a double convolution, in both t and f , of the WDFs of waveform s and weighting u . That is, the STSE $|S_U(t, f)|^2$ of waveform s , relative to weighting u , is a smoothed version of the WDF of waveform s , where the smoothing function is the WDF of weighting u . Furthermore, since the left-hand side of (106) can never be negative, and since s and u are arbitrary, (106) shows that the double convolution of any two WDFs is never negative for any values of t, f . This furnishes a possibility of accomplishing smoothing of a computed WDF of waveform s , with a guarantee of a nonnegative distribution resulting; of course, W_u must be a legal WDF, as discussed in (25) et seq., in order to guarantee this nonnegative property.

Since $|S_U|^2$ is a double convolution of WDFs W_s and W_u , it follows that the double Fourier transform of the STSE is given by

$$\iint dt df \exp(i2\pi f\tau - i2\pi t\nu) |S_u(t, f)|^2 = \chi_u(\nu, \tau) \chi_s(\nu, \tau) . \quad (107)$$

where χ_u and χ_s are the complex ambiguity functions of u and s , respectively; see (23). This leads to an alternative expression for the STSE as

$$|S_u(t, f)|^2 = \iint d\tau d\nu \exp(-i2\pi f\tau + i2\pi t\nu) \chi_u(\nu, \tau) \chi_s(\nu, \tau) . \quad (108)$$

Therefore, if the complex ambiguity function of s is computed, it can be multiplied by the ambiguity function of an arbitrary weighting function u , and followed by a two-dimensional Fourier transform. There is no need to calculate the WDF W_s via this route; also several different weighting functions could be utilized, each at the expense of a two-dimensional Fourier transform. The end result for the STSE is always nonnegative. Of course, the same result is obtainable directly by taking the magnitude-square of definition (102).

MARGINALS OF SPECTRAL ESTIMATE

There follows, from (106) and (12), the marginal relation

$$\int df |S_u(t, f)|^2 = \int dt' |s(t')|^2 |u(t - t')|^2 = |s(t)|^2 \overset{t}{\otimes} |u(t)|^2 . \quad (109)$$

Thus, the time marginal of $|S_u|^2$ is not directly $|s(t)|^2$, but is smeared by the weighting, according to $|u(t)|^2$. In a similar fashion, from (106) and (11), the frequency marginal is

$$\int dt |S_u(t, f)|^2 = |S(f)|^2 \overset{f}{\otimes} |U(f)|^2. \quad (110)$$

Again, $|S(f)|^2$ is smeared by window $|U(f)|^2$.

Finally, completing either of the integrations in (109) or (110), over the remaining variable, yields

$$\iint dt df |S_u(t, f)|^2 = E_s E_u, \quad (111)$$

where E_s and E_u are the energies of s and u , respectively; see (14).

Since weighting u is arbitrary and under our control, we can easily choose E_u to be 1, without loss of generality; then the volume under the STSE will be equal to the energy in waveform s being analyzed, just as for the WDF in (14).

MOMENTS OF SPECTRAL ESTIMATE

If we use (110) and (14), we find the following development:

$$\begin{aligned} \iint dt df f |S_u(t, f)|^2 &= \int df f \int dv |S(v)|^2 |U(f - v)|^2 = \\ &= \int dv |S(v)|^2 \int df (f - v + v) |U(f - v)|^2 = \\ &= \int dv |S(v)|^2 \left[\int df_1 f_1 |U(f_1)|^2 + v E_u \right] = \\ &= E_s \int df_1 f_1 |U(f_1)|^2 + E_u \int dv v |S(v)|^2. \end{aligned} \quad (112)$$

Combined with (111), there results

$$\frac{\iint dt df f |S_u(t, f)|^2}{\iint dt df |S_u(t, f)|^2} = \frac{\int df f |U(f)|^2}{\int df |U(f)|^2} + \frac{\int df f |S(f)|^2}{\int df |S(f)|^2} . \quad (113)$$

That is, the first moment in f of the STSE is the sum of the frequency centers of $|U|^2$ and $|S|^2$. This should be compared with the corresponding result in (36) for the WDF, where only the last term in (113) is present. The presence of weighting u in definition (102) adds an additional term to the frequency center unless $|U(f)|$ is even about $f = 0$; in this latter case, (113) reduces to (36).

In a similar fashion, the first moment in t of the STSE is found to be

$$\frac{\iint dt df t |S_u(t, f)|^2}{\iint dt df |S_u(t, f)|^2} = \frac{\int dt t |u(t)|^2}{\int dt |u(t)|^2} + \frac{\int dt t |s(t)|^2}{\int dt |s(t)|^2} . \quad (114)$$

Again, a sum of time centers results; but if weighting $|u(t)|$ is even about $t = 0$, then (114) reduces to the same result, (37), as for the WDF.

CONDITIONAL MOMENT

Just as in (28)-(35) for the WDF, conditional moments of the STSE can be defined. For example, directly from (105), we have

$$\int df f |S_u(t, f)|^2 = \int df f |\chi_{s\bar{u}}(f, t)|^2, \quad (115)$$

in terms of the cross-ambiguity function of s and \bar{u} , where $\bar{u}(t) = u(-t)$.

An alternative time-domain expression is possible for the frequency moment in (115): define

$$g(t, t_1) = s(t_1) u^*(t - t_1). \quad (116)$$

Then from (102) and (29),

$$\begin{aligned} \int df f |S_u(t, f)|^2 &= \int df f \iint dt_1 dt_2 \exp(-i2\pi f(t_1 - t_2)) g(t, t_1) g^*(t, t_2) = \\ &= \iint dt_1 dt_2 g(t, t_1) g^*(t, t_2) \frac{i}{2\pi} \delta'(t_1 - t_2) = \\ &= \frac{-i}{2\pi} \int dt_1 g'(t, t_1) g^*(t, t_1), \end{aligned} \quad (117)$$

where

$$g'(t, t_1) \equiv \frac{\partial}{\partial t_1} g(t, t_1) = \frac{\partial}{\partial t_1} \{s(t_1) u^*(t - t_1)\}. \quad (118)$$

If we represent waveform s in terms of its magnitude and phase according to (31), and do likewise for weighting u as

$$u(t) = E(t) \exp[iP(t)] , \quad (119)$$

then substitution in (117) results in the simplified form

$$\int df f |S_u(t, f)|^2 = \frac{1}{2\pi} \int dt_1 [\theta'(t_1) + P'(t - t_1)] M^2(t_1) E^2(t - t_1) . \quad (120)$$

When this result is combined with (109), the normalized conditional first moment is

$$\frac{\int df f |S_u(t, f)|^2}{\int df |S_u(t, f)|^2} = \frac{1}{2\pi} \frac{\int dt_1 [\theta'(t_1) + P'(t - t_1)] M^2(t_1) E^2(t - t_1)}{\int dt_1 M^2(t_1) E^2(t - t_1)} . \quad (121)$$

(This reduces to (38) when $E(t) = 1$, $P(t) = 0$, that is, $u(t) = 1$, in which case $S_u(t, f) = S(f)$.) Generally, (121) is an average of $\theta'(t_1) - P'(t - t_1)$, weighted according to the instantaneous powers of s and u .

EXAMPLES OF SHORT-TERM SPECTRAL ESTIMATION

Here we will reconsider many of the examples presented earlier for the WDF investigation. The particular example of weighting u adopted here in spectral definition (102) will be, for the time being,

$$u(t) = (\pi \sigma^2)^{-1/4} \exp\left(-\frac{t^2}{2\sigma^2}\right), \quad (122)$$

where duration measure σ is under our control. The energy E_u of this waveform is unity, in keeping with the discussion in (111) et seq., which guarantees that the volume under the STSE will be the energy $E_s = E$ of the waveform s being analyzed.

GAUSSIAN WAVEFORM

The waveform s was given in (71); its transform $S_u(t, f)$ is obtained by substituting (71) and (122) in (102) and using (68):

$$S_u(t, f) = \left(E \frac{\sigma_h}{\sigma_a}\right)^{1/2} \exp\left[-\frac{t^2}{4\sigma_a^2} - \pi^2 f^2 \sigma_h^2 - i\pi f t \frac{\sigma_0^2}{\sigma_a^2} + i \arg(a_0)\right], \quad (123)$$

where E is the energy of s and

$$\sigma_a^2 = \frac{1}{2}(\sigma^2 + \sigma_0^2), \quad \frac{1}{\sigma_h^2} = \frac{1}{2}\left(\frac{1}{\sigma^2} + \frac{1}{\sigma_0^2}\right), \quad \frac{\sigma_a}{\sigma_h} = \frac{1}{2}\left(\frac{\sigma}{\sigma_0} + \frac{\sigma_0}{\sigma}\right). \quad (124)$$

The quantity σ_a^2 is the arithmetic average of σ^2 and σ_0^2 , while σ_h^2 is the harmonic average. The STSE then follows immediately (or by use of (70) directly) as

$$|S_u(t,f)|^2 = E \frac{\sigma_h}{\sigma_a} \exp \left[-\frac{1}{2} \left(\frac{t^2}{\sigma_a^2} + 4\pi^2 f^2 \sigma_h^2 \right) \right]. \quad (125)$$

The volume under STSE (125) is readily verified to be E , as it must be. The half widths of the ellipse at the $1/e$ relative level are $\sqrt{2} \sigma_a$, $\sqrt{2} (2\pi \sigma_h)^{-1}$, respectively, in the t, f plane. The area of this ellipse in the t, f plane is

$$\frac{\sigma_a}{\sigma_h} = \frac{1}{2} \left(\frac{\sigma}{\sigma_0} + \frac{\sigma_0}{\sigma} \right) \geq 1. \quad (126)$$

This area is at least twice as great as that for the corresponding WDF in figure 4, and even then, only when the proper guess is used for the weighting u , namely $\sigma = \sigma_0$. Since waveform duration σ_0 will likely be unknown in practice, the mismatch factor in (126) will smear the concentration of the STSE somewhat. For example, if σ is off by a factor of 2 from σ_0 (either double or half), (126) is 1.25 instead of its minimum value of 1.

The area enlargement factor σ_a/σ_h in (126) is also the same factor by which the peak of the STSE in (125) is down from its best value of E . Thus, the STSE has a decreased peak and enlarged effective area relative to the WDF, the relative factor being at least 2, and being $\sigma/\sigma_0 + \sigma_0/\sigma$ in general. Both distributions contain volume E , independent of σ .

This example demonstrates the presence of "window effects" in the STSE that are not seen in the WDF. That is, whereas the effective ellipse in figure 4 depended only on waveform parameter σ_0 , the ellipse here depends additionally on weighting parameter σ , in such a fashion as to always smear the concentration of energy in the t, f plane by at least a factor of 2. In trade, we always have the guarantee that the STSE (103) will be nonnegative, and that it will not contain the large interference phenomena inherent in the WDF; see (80)-(81).

MULTIPLE MODULATED TONES

The waveform of interest is given in (79). The transform $S_u(t, f)$ is found by use of (122), (102), and (68):

$$S_u(t, f) = \sum_k \left(E_k \frac{\sigma_{hk}}{\sigma_{ak}} \right)^{1/2} \exp \left[- \frac{(t - t_k)^2}{4 \sigma_{ak}^2} - \pi^2 (f - f_k)^2 \sigma_{hk}^2 - \right. \\ \left. - i \pi (f - f_k) \frac{\sigma_k^2 t + \sigma^2 t_k}{\sigma_{ak}^2} + i \arg(a_k) \right], \quad (127)$$

where energy $E_k = \sqrt{\pi} |a_k|^2 \sigma_k$, and averages

$$\sigma_{ak}^2 = \frac{1}{2} (\sigma^2 + \sigma_k^2), \quad \frac{1}{\sigma_{hk}^2} = \frac{1}{2} \left(\frac{1}{\sigma^2} + \frac{1}{\sigma_k^2} \right). \quad (128)$$

The STSE is the magnitude squared value of (127); the resulting double sum has diagonal terms

$$\sum_k E_k \frac{\sigma_{hk}}{\sigma_{ak}} \exp \left[-\frac{1}{2} \left\{ \frac{(t - t_k)^2}{\sigma_{ak}^2} + 4\pi^2 (f - f_k)^2 \sigma_{hk}^2 \right\} \right], \quad (129)$$

which are identical to (125), except for the indexing by k and the shift to center t_k, f_k in the t, f plane, as expected. If one value of weighting parameter σ is used to evaluate the STSE for all t of interest, it cannot simultaneously match all the different possible values of $\{\sigma_k\}$ for the various pulses. This will cause some of the components in (129) to be more severely degraded than others, in terms of decreased peaks and spread effective areas; the pertinent factor is again

$$\frac{\sigma_{ak}}{\sigma_{hk}} = \frac{1}{2} \left(\frac{\sigma}{\sigma_k} + \frac{\sigma_k}{\sigma} \right) \quad (130)$$

for the k -th component lobe. If some apriori knowledge of the values of $\{\sigma_k\}$ is available, this suggests using different values of σ for those values of t near the corresponding values of $\{t_k\}$, in an effort to minimize the factors (130) for different k .

As for the off-diagonal terms of $|S_u(t, f)|^2$ in (127), the k, l term is proportional to

$$\exp \left[-\frac{(t - t_k)^2}{4 \sigma_{ak}^2} - \frac{(t - t_l)^2}{4 \sigma_{al}^2} - \pi^2 (f - f_k)^2 \sigma_{hk}^2 - \pi^2 (f - f_l)^2 \sigma_{hl}^2 \right]. \quad (131)$$

If t is not near one of the time centers $\{t_k\}$, or if f is not near one of the $\{f_k\}$, this term will be very small, due to the exponential decay. In particular, halfway between the dominant desired peaks of (129) at $\{t_k, f_k\}$, the quantity (131) will be essentially zero. This is in distinction to the WDF result in (80) et seq.

LINEAR FREQUENCY MODULATION

This waveform is specified in (84). Its STSE is, upon use of (70),

$$|S_u(t, f)|^2 = \frac{2E}{\sqrt{H_2}} \exp \left[-\frac{1}{H_2} \left\{ x^2(1 + r + r \theta_0^2) + y^2(1 + r)/r - 2xy \theta_0 \right\} \right], \quad (132)$$

where

$$\theta_0 = \alpha_0 \sigma_0^2, \quad r = \frac{\sigma^2}{\sigma_0^2}, \quad H_2 = \frac{1}{r} + 2 + r + r \theta_0^2. \quad (133)$$

and where we define, here,

$$x = \frac{t}{\sigma}, \quad y = 2\pi f \sigma. \quad (134)$$

By means of the results in appendix D, the area of the contour ellipse in (132), at the $1/e$ relative level, is found to be

$$\text{area} = \frac{1}{2} \sqrt{H_2} \quad \text{in the } t, f \text{ plane.} \quad (135)$$

Thus, the product of the peak height of the STSE in (132) and the effective area is again E , the volume under the STSE, regardless of the values of σ , σ_0 , θ_0 . (For $\theta_0 = 0$, (135) reduces to (126), as it must.)

To minimize the effective area and to maximize the peak value of the STSE, the common quantity H_2 in (133) should be minimized. This is accomplished by choosing the weighting parameter σ in (122) as

$$\sigma_{\text{opt}} = \frac{\sigma_0}{(1 + \theta_0^2)^{1/4}} \quad , \quad r_{\text{opt}} = \frac{1}{(1 + \theta_0^2)^{1/4}} \quad (136)$$

which would require knowledge of both the duration σ_0 and the amount of frequency modulation θ_0 in waveform s . Even if that information were available, the minimum area in (135) becomes

$$\text{minimum area} = \left(\frac{1 + \sqrt{1 + \theta_0^2}}{2} \right)^{1/2} \quad \text{in the t.f plane} \quad (137)$$

which still increases as $\sqrt{\theta_0}/2$ for large θ_0 . Thus, even the best choice of σ for the weighting results in considerable spreading of the concentration ellipse and in peak reduction of the STSE; searching in σ is not overly helpful because the simple weighting pulse (122) is a poor facsimile to the linear frequency modulation waveform (84), especially for large amounts of frequency modulation, as measured by parameter θ_0 .

MORE GENERAL WEIGHTING

There is no need to restrict the weighting u in STSE (102) and (103) to be the simple Gaussian pulse in (122). In this section, we generalize it to allow for some linear frequency modulation:

$$u(t) = (\pi \sigma^2)^{-1/4} \exp \left[-\frac{t^2}{2\sigma^2} + i \frac{a}{2} t^2 \right]; \quad E_u = 1. \quad (138)$$

The waveform of interest here is again the linear frequency modulation example

$$s(t) = a_0 \exp \left[-\frac{t^2}{2\sigma_0^2} + i \frac{a_0}{2} t^2 \right], \quad a_0 \geq 0. \quad (139)$$

as in (84).

The STSE follows from (102), (103), and (70), after a considerable amount of manipulations, as

$$\begin{aligned} |S_u(t, f)|^2 = \frac{2E}{\sqrt{H_3}} \exp \left[-\frac{1}{H_3} \left\{ x^2(1+r+r\theta_0^2+r^2q^2\theta_0^2) + \right. \right. \\ \left. \left. + y^2(1+r)/r - 2xy(1+rq)\theta_0 \right\} \right], \end{aligned} \quad (140)$$

where

$$r = \frac{\sigma^2}{\sigma_0^2}, \quad q = \frac{a}{a_0}, \quad H_3 = \frac{1}{r} + 2 + r + r(q-1)^2 \theta_0^2. \quad (141)$$

in addition to (134). The quantities r and q are mismatch factors, reflecting the lack of knowledge of weighting (138) about the waveform (139).

The area of the contour ellipse of (140) at the $1/e$ relative level is (by means of appendix D)

$$\text{area} = \frac{1}{2} \sqrt{H_3} \quad \text{in the } t, f \text{ plane} . \quad (142)$$

This is also the same factor by which the peak of (140) is down from E . Thus, a minimum value for H_3 is desired. This can be achieved by choosing $r = 1$, $q = 1$ in (141), for which the minimum $H_3 = 4$ and the minimum area = 1; however, this requires that we choose $\sigma = \sigma_0$ and $\alpha = \alpha_0$, which is not a likely situation in practice, without some apriori knowledge about the waveform s . If this fortuitous situation of perfect match of the parameters does occur, the STSE in (140) reduces to

$$|S_u(t, f)|^2 = E \exp \left[-\frac{1}{2} \{ x^2 (1 + \theta_0^2) - 2xy \theta_0 + y^2 \} \right] , \quad (143)$$

which is identical to the corresponding WDF in (91), except for a factor of 2 outside and inside the exponential. Thus, the effective area is doubled and the peak is halved.

As special cases of weighting (138), if $\alpha = 0$ (no frequency modulation in the weighting), then H_3 in (141) reduces to H_2 in (133). Alternatively, if $\alpha_0 \rightarrow 0$ (no frequency modulation in the waveform s), then $\theta_0(q-1) = \alpha_0 \sigma_0^2 (\alpha/\alpha_0 - 1) \sim \alpha \sigma_0^2$ and

$$H_3 \sim \frac{1}{r} + 2 + r + r \alpha^2 \sigma_0^4 = \left(\frac{\sigma}{\sigma_0} + \frac{\sigma_0}{\sigma} \right)^2 + (\alpha \sigma \sigma_0)^2. \quad (144)$$

This is minimized by choosing $\alpha = 0$ and $\sigma = \sigma_0$, giving value 4 as usual. Finally, for given q , H_3 in (141) is minimized by choosing $r = (1 + (q - 1)^2 \theta_0^2)^{-1/2}$, for which the minimum $H_3 = 2 + 2(1 + (q - 1)^2 \theta_0^2)^{1/2}$; however, again, this increases as $2|q - 1|\theta_0$ as θ_0 increases.

SMOOTHING THE WDF

It was demonstrated in (106) that the double convolution of any two WDFs is always nonnegative, and is in fact equal to the STSE of one waveform relative to the other:

$$W_s(t,f) \circledast^{tf} W_u(t,f) = |S_u(t,f)|^2. \quad (145)$$

This suggests that one should choose a (legal) WDF for weighting u which is as narrow as possible (least area or spread) in the t,f plane, in order to minimize the inherent spreading that (145) implies. The simple examples in the previous section demonstrated that, for the best choices of duration and linear frequency modulation parameters in the Gaussian weighting, an increase of .5 in the effective area in the t,f plane of the STSE, relative to the WDF, resulted.

PHILOSOPHY AND APPROACH

Since fine detail of the WDF $W_s(t,f)$ will likely vary in different portions of the t,f plane, this suggests the following possible procedure for analysis: For a given waveform $s(t)$, compute and plot the WDF $W_s(t,f)$ according to (3) or (61). Locate a t,f region of interest in the plane, where large (perhaps oscillatory) values of W_s occur; denote the center of the region as t_c, f_c . Estimate the duration, σ_c , and linear frequency

modulation index, α_c , of this particular region in the t, f plane. Perform the STSE of waveform $s(t)$ according to (102)-(103), with weighting

$$u(t) = (\pi \sigma_c^2)^{-1/4} \exp \left[-\frac{t^2}{2\sigma_c^2} + i \frac{\alpha_c}{2} t^2 \right], \quad \theta_c = \alpha_c \sigma_c^2, \quad (146)$$

(for reasons to be given below), but only for locations t, f in the plane near $t = t_c, f = f_c$.

The WDF of weighting (146) is (with $\alpha_c = 2\pi\beta_c$)

$$\begin{aligned} W_u(t, f) &= 2 \exp \left[-\frac{t^2}{\sigma_c^2} - 4\pi^2 \sigma_c^2 (f - \beta_c t)^2 \right] = \\ &= 2 \exp \left[-\frac{t^2}{\sigma_c^2} (1 + \theta_c^2) + 4\pi f t \theta_c - 4\pi^2 f^2 \sigma_c^2 \right], \end{aligned} \quad (147)$$

which has a contour ellipse, at the $1/e$ relative level, of area $1/2$ in the t, f plane, regardless of σ_c and α_c . This STSE procedure is equivalent to smoothing the WDF W_s of waveform s with the WDF in (147), for values near t_c, f_c in the t, f plane. Thus we have two alternative procedures for conducting the smoothing of a calculated WDF W_s , the first via direct evaluation of double convolution (145) for values of t, f near regions of interest, and the second via the STSE in (102) and (103). Which one to adopt will likely depend on the number of points that must be closely investigated in the t, f plane.

For other regions of interest in the t, f plane of the original WDF W_s , different values of t_c , f_c , σ_c , α_c must be extracted and the smoothing procedure repeated. Although tedious, this procedure will minimally spread the WDF W_s (by area .5) and it will guarantee a nonnegative distribution. This procedure is similar to that given in [2]; however, the information required to implement [2] is not easily available, and the current approach is not limited to constant-magnitude waveforms. A fine-grained analysis of a given general waveform s , for various t, f values and yielding nonnegative distribution values, is not going to be achieved without the expenditure of considerable effort and interaction between a user and preliminary analysis results.

This two-stage procedure, of observing the raw WDF and then computing different smoother versions in different regions, avoids the arbitrary pre-selection of time duration and frequency modulation content of the weighting in the STSE, which would overly smear the modified WDF for improper matches of parameter values. It also guarantees nonnegative estimates. In trade, there is approximately an increase of .5 in the effective area of the distribution in the t, f plane that must be accepted, in addition to a decreased peak value. For WDFs, W_s , with lobes which already occupy portions of the t, f plane with areas significantly greater than .5, this additional spreading (by area .5) is not very damaging, provided that σ_c and α_c are chosen correctly. Perhaps simultaneous plots of WDF $W_s(t, f)$ and STSE $|S_u(t, f)|^2$ would yield maximum information about waveform s .

In actual practice, where the integral definition in (102) is replaced by a numerical summation of samples taken at increment Δ , the quantity (145) is necessarily approximated. This problem is addressed in appendix E, where it is shown that the dominant term in the numerical approach is approximately the desired quantity (145). Furthermore, since the definition in (E-1) involves a magnitude-square, the approximation is guaranteed to be nonnegative. This need not be the case if the double convolution of WDFs W_s and W_u in (145) is approximated by sampling directly in the t, f plane and performing a double summation. However, for small enough increments in both t and f , this nonnegative aspect should be small and probably negligible; this latter approach was used in [1], although the smoothing function was not a legal WDF.

ALTERNATIVE AVERAGING PROCEDURES

Instead of using $R(t, \tau) = s(t + \frac{\tau}{2}) s^*(t - \frac{\tau}{2})$ in (2) as the instantaneous correlation at time t and separation τ , one could use a local average, in hopes of improving the correlation and distribution functions. That is, consider correlation definition

$$\hat{R}(t, \tau) = v_1(t) \circledast R(t, \tau) = \int dt' v_1(t - t') s(t' + \frac{\tau}{2}) s^*(t' - \frac{\tau}{2}) , \quad (148)$$

where v_1 is a fairly sharp, even, real function centered at the origin.

The corresponding "locally averaged" WDF is

$$\begin{aligned}\hat{W}(t, f) &= \int d\tau \exp(-i2\pi f\tau) \hat{R}(t, \tau) = \\ &= \int dt' v_1(t - t') W(t', f) = v_1(t) \overset{t}{\otimes} W(t, f) .\end{aligned}\quad (149)$$

This is a convolution, in time only, of the WDF of s with weighting v_1 . Reference to the discussion following (83) reveals that this form of averaging is inadequate, since it does not average additionally on frequency. Also, (149) need not remain positive, as would be desired of a smoothed WDF.

Furthermore, the Fourier transform in (149) (as well as (3)) is over all τ , thereby involving argument values of waveform s in (148) which are very distant from the time point, t , of interest. If $\hat{W}(t, f)$ or $W(t, f)$ is to be considered as the "spectrum at time t ," it is hard to justify why arbitrarily distant time points from location t should enter into their evaluations. Therefore, in addition to the local average in (148) for stability purposes, there should be a weighting in τ in (149) to better confine the Fourier transform to local values of waveform s about time instant t of interest.

To this aim, consider the more general form of average given by

$$\begin{aligned}\hat{R}(t, \tau) &= v_2(t, \tau) \overset{t}{\otimes} R(t, \tau) = \int dt' v_2(t - t', \tau) R(t', \tau) = \\ &= \int dt' v_2(t - t', \tau) \int df' \exp(i2\pi f'\tau) W(t', f') ,\end{aligned}\quad (150)$$

where weighting v_2 depends additionally on τ . Define its transform

$$V_2(t, f) = \int d\tau \exp(-i2\pi f\tau) v_2(t, \tau) . \quad (151)$$

Then the modified WDF corresponding to \hat{R} in (150) is

$$\begin{aligned} \hat{W}(t, f) &= \iint dt' df' W(t', f') V_2(t - t', f - f') = \\ &= W(t, f) \otimes V_2(t, f) , \end{aligned} \quad (152)$$

which is a double convolution of W with V_2 , on both t and f . However, since V_2 need not be a WDF, \hat{W} in (152) can become negative for some t, f values. This form of smoothing was considered previously in [9; (1.5)] and [10; (2.1)].

An additional justification of two-dimensional smoothing, from the frequency domain alternative viewpoint, is given in appendix F. Also, a generalization of the Gaussian WDF (147), with arbitrary area and linear frequency modulation content and which guarantees a positive distribution \hat{W} , is given in (F-7)-(F-19); this result generalizes that in [11] for no frequency modulation.

If we specialize weighting v_2 in (150) to the form

$$v_2(t, \tau) = u(t + \frac{\tau}{2}) u^*(t - \frac{\tau}{2}) , \quad (153)$$

then (151) yields

$$V_2(t, f) = W_u(t, f) , \quad (154)$$

and the general result in (152) specializes to (106), which is guaranteed positive. Thus the special case of weighting v_2 in (153) leads to the STSE of s , relative to u .

EFFICIENT CALCULATION OF SHORT-TERM SPECTRAL ESTIMATE

If we employ the weighting u in (146) with linear frequency modulation parameter α_c , the spectrum in (102) becomes

$$\begin{aligned}
 S_u(t, f) &= \int dt_1 \exp(-i2\pi ft_1) s(t_1) u^*(t - t_1) = \\
 &= \exp(-i2\pi ft) \int dt_2 \exp(-i2\pi ft_2) s(t + t_2) u^*(-t_2) = \\
 &= (\pi \sigma_c^2)^{-1/4} \exp(-i2\pi ft) \int dt_2 \exp(-i2\pi ft_2) s(t + t_2) \exp\left(-\frac{t_2^2}{2\sigma_c^2} - i\frac{\alpha_c}{2} t_2^2\right).
 \end{aligned}
 \tag{155}$$

The $\exp(-t_2^2/(2\sigma_c^2))$ term gates out the portion of $s(t + t_2)$ near the origin in t_2 , while the $\exp(-i\alpha_c t_2^2/2)$ term cancels linear frequency modulation in waveform s .

An approximation to (155) is obtained by sampling at increment Δ and using the Trapezoidal rule:

$$\begin{aligned} \tilde{S}_u(t, f) \equiv (\pi \sigma_c^2)^{-1/4} \exp(-i2\pi ft) \Delta \sum_k \exp(-i2\pi f \Delta k) * \\ * s(t + k\Delta) \exp\left[-\frac{1}{2} k^2 \Delta^2 \left(\frac{1}{\sigma_c^2} + i \alpha_c\right)\right], \end{aligned} \quad (156)$$

which has period $1/\Delta$ in f . In particular, the approximation to the STSE, at selected points, is

$$\begin{aligned} \left| \tilde{S}_u\left(m\Delta, \frac{n}{N\Delta}\right) \right|^2 = \frac{\Delta^2}{\sqrt{\pi} \sigma_c} \left| \sum_k \exp(-i2\pi nk/N) * \right. \\ * s(m\Delta + k\Delta) \exp\left[-\frac{1}{2} k^2 \Delta^2 \left(\frac{1}{\sigma_c^2} + i \alpha_c\right)\right] \left. \right|^2, \end{aligned} \quad (157)$$

which is an N -point discrete Fourier transform; m, n, N are integers.

The procedure for analysis is as follows: for a region of interest centered at t_c, f_c in the t, f plane, choose time values $m\Delta$ near t_c . Then for each m , sweep out n such that frequency $n/(N\Delta)$ is near f_c ; an FFT will give all f values in $(0, 1/\Delta)$. Plots of (157) give a fine-tuned STSE near t_c, f_c for the particular choices of σ_c, α_c . Additional estimates with different parameters will be required in other regions; there is no globally optimum smoothing that will yield high-quality positive spectral estimates for all t, f values.

The numerical evaluation of the exponential quantities

$$Q_2(k) \equiv \exp \left[-\frac{1}{2} k^2 \Delta^2 \left(\frac{1}{\sigma_c^2} + i \alpha_c \right) \right] = Q_2(-k) \quad (158)$$

in (157) can be effected very efficiently by the methods given in [12].

They are given by recurrences (which need to be evaluated only once for each σ_c, α_c)

$$\left. \begin{aligned} Q_1(k) &= Q_1(k-1) \exp(2c_2) \\ Q_2(k) &= Q_2(k-1) Q_1(k) \end{aligned} \right\} \text{ for } k \geq 1, \quad (159)$$

with starting values

$$Q_1(0) = \exp(-c_2), \quad Q_2(0) = 1,$$

$$c_2 = -\frac{1}{2} \Delta^2 \left(\frac{1}{\sigma_c^2} + i \alpha_c \right). \quad (160)$$

Only two complex multiplications per stage are required in (159).

Furthermore, since

$$\exp(-c_2) = \exp \left(\frac{\Delta^2}{2\sigma_c^2} \right) \exp \left(\frac{i \alpha \Delta^2}{2} \right) \equiv E (C + iS), \quad (161)$$

and

$$\exp(2c_2) = \frac{C^2 - S^2 - i2SC}{E^2}, \quad (162)$$

only one exp, cos, and sin must be evaluated to accomplish (159) for all k .

WDF WITH MINIMUM SPREAD

The virtues of smoothing WDF W_s of waveform s with the WDF W_u , (147), of weighting u , (146), were discussed earlier in this section. At that time, the selection of form (146) for the weighting was seemingly arbitrary. However, it is shown in appendix G that the weighting, u , which has a minimally spread WDF, is precisely that given in (146). The measure of spread is

$$I = \iint dt df W_u(t,f) (f - \beta_c t)^2, \quad (163)$$

where β_c is a specified (observed) slope of interest in the t, f plane, and $\alpha_c = 2\pi\beta_c$. This measure of spread concentrates the WDF about the specified slope; see (147). The actual minimum value of spread (163) is given in (G-24) as

$$\text{minimum } I = \frac{1}{8\pi^2 \sigma_c^2}, \quad (164A)$$

when weighting u is constrained to have mean square duration

$$\int dt t^2 |u(t)|^2 = \frac{\sigma_c^2}{2}, \quad (164B)$$

in addition to unit energy. Without these two constraints, the minimization of spread (163) is ill-posed; see appendix G.

PERFORMANCE IN NOISE

In this section, we investigate the bias and stability of a WDF estimate obtained from a noisy waveform. In particular, the given waveform x is

$$x(t) = s(t) + n(t) , \quad (165)$$

where s is a deterministic signal of interest, and n is an additive zero-mean stationary noise. In fact, we have

$$\overline{n(t)} = 0 , \quad \overline{n(t_1)n^*(t_2)} = C_n(t_1 - t_2) ,$$

$$G_n(f) = \int d\tau \exp(-i2\pi f\tau) C_n(\tau) , \quad (166)$$

where C_n and G_n are the noise covariance and power density spectrum, respectively.

WAVEFORM WEIGHTING

If the WDF of given waveform x in (165) were directly evaluated via definition (3), the result would be infinite, since the $N \times N$ (noise-cross-noise) terms do not decay for large arguments. Also, since the signal s will be assumed to be transient and decay to zero for large arguments, some gating or weighting of given waveform x is appropriate, in order to

concentrate on the time regions where signal s is largest. Accordingly, we consider the weighted waveform

$$y(t) = v(t) x(t) = v(t) [s(t) + n(t)] , \quad (167)$$

where $v(t)$ is a deterministic function under our control.

The WDF that will be calculated is therefore

$$\begin{aligned} W_{yy}(t, f) &= \int d\tau \exp(-i2\pi f\tau) y(t + \frac{\tau}{2}) y^*(t - \frac{\tau}{2}) = \\ &= a + b + c + d , \end{aligned} \quad (168)$$

where

$$\begin{aligned} a &= \int d\tau \exp(-i2\pi f\tau) R_{vv}(t, \tau) s(t + \frac{\tau}{2}) s^*(t - \frac{\tau}{2}) , \\ b &= \int d\tau \exp(-i2\pi f\tau) R_{vv}(t, \tau) n(t + \frac{\tau}{2}) n^*(t - \frac{\tau}{2}) , \\ c &= \int d\tau \exp(-i2\pi f\tau) R_{vv}(t, \tau) s(t + \frac{\tau}{2}) n^*(t - \frac{\tau}{2}) , \\ d &= \int d\tau \exp(-i2\pi f\tau) R_{vv}(t, \tau) n(t + \frac{\tau}{2}) s^*(t - \frac{\tau}{2}) , \end{aligned} \quad (169)$$

and

$$R_{vv}(t, \tau) = v(t + \frac{\tau}{2}) v^*(t - \frac{\tau}{2}) . \quad (170)$$

The first two quantities in (168) are, respectively, $S \times S$ and $N \times N$ terms, while the last two are $S \times N$ terms; here, S denotes signal, while N denotes noise. The $S \times S$ term, a , in (169) is real and non-random, while $N \times N$ term, b , is real and random. On the other hand, the $S \times N$ terms, c and d , are complex random, with $d^* = c$.

MEAN VALUES

An alternative expression for the $S \times S$ term in (169) is

$$\begin{aligned} a &= \int d\tau \exp(-i2\pi f\tau) R_{VV}(t, \tau) R_{SS}(t, \tau) = \\ &= W_{VV}(t, f) \odot^f W_{SS}(t, f) , \end{aligned} \quad (171)$$

in terms of the WDFs of weighting v and signal s .

The mean of the $N \times N$ term is

$$\begin{aligned} \bar{b} &= \int d\tau \exp(-i2\pi f\tau) R_{VV}(t, \tau) C_n(\tau) = \\ &= W_{VV}(t, f) \odot^f G_n(f) , \end{aligned} \quad (172)$$

where we made use of (166). And since noise n has zero mean, there follows, for the $S \times N$ terms, $\bar{c} = \bar{d} = 0$. Collecting these results together, the mean of WDF estimate (168) is

$$\overline{W_{yy}}(t, f) = W_{VV}(t, f) \odot^f [W_{SS}(t, f) + G_n(f)] . \quad (173)$$

No additional statistical properties on the noise n , such as a Gaussian process, are needed for result (173); this holds for an arbitrary stationary noise process. The difference in mean outputs, for signal present versus signal absent, is just a , as given by (171).

VARIANCE OF WDF ESTIMATE

In order to determine the variance of estimate (168), we need to assume that noise n is Gaussian. Furthermore, in addition to properties (166), we will presume that

$$\overline{n(t_1) n(t_2)} = 0, \quad (174)$$

as is true when n is an analytic process or a complex envelope [13, ch.2].

Then (168) yields

$$\begin{aligned} \overline{w_{yy}^2(t, f)} &= \overline{|w_{yy}(t, f)|^2} = \overline{a^2} + \overline{b^2} + \overline{|c|^2} + \overline{|d|^2} + \\ &+ 2 \overline{ab} + \overline{cd^*} + \overline{c^* d}, \end{aligned} \quad (175)$$

the other terms being zero due to n being zero-mean Gaussian noise.

The second term on the right-hand side of (175) can be developed from (169) as

$$\begin{aligned} \overline{b^2} &= \overline{|b|^2} = \iint d\tau_1 d\tau_2 \exp(-12\pi f(\tau_1 - \tau_2)) R_{VV}(t, \tau_1)^* \\ &\quad * R_{VV}^*(t, \tau_2) \left[c_n(\tau_1) c_n^*(\tau_2) + c_n^2\left(\frac{\tau_1 - \tau_2}{2}\right) \right], \end{aligned} \quad (176)$$

where we used (166) and (174). Referring to (172), we have

$$\overline{b^2} = \overline{b}^2 + \iint d\tau_1 d\tau_2 \exp(-i2\pi f(\tau_1 - \tau_2)) R_{VV}(t, \tau_1)^* \\ {}^*R_{VV}^*(t, \tau_2) C_n^2\left(\frac{\tau_1 - \tau_2}{2}\right). \quad (177)$$

At this point, it is convenient to define

$$G_n^{(2)}(f) = \int d\tau \exp(-i4\pi f\tau) C_n^2(\tau). \quad (178)$$

Then

$$G_n^{(2)}(f/2) = \int d\tau \exp(-i2\pi f\tau) C_n^2(\tau) = G_n(f) \otimes G_n(f) \quad (179)$$

and

$$C_n^2(\tau) = \int df \exp(i2\pi f\tau) G_n^{(2)}(f/2) = \\ = 2 \int dv \exp(i4\pi v\tau) G_n^{(2)}(v). \quad (180)$$

When this result is substituted in (177), there follows

$$\overline{b^2} = \overline{b}^2 + 2 \int dv W_{VV}^2(t, f - v) G_n^{(2)}(v) = \\ = \overline{b}^2 + 2 W_{VV}^2(t, f) \overset{f}{\otimes} G_n^{(2)}(f). \quad (181)$$

The third and fourth terms in (175) are

$$\begin{aligned} \overline{|d|}^2 &= \overline{|c|}^2 = \iint d\tau_1 d\tau_2 \exp(-i2\pi f(\tau_1 - \tau_2)) R_{VV}(t, \tau_1)^* \\ &\quad * R_{VV}^*(t, \tau_2) s\left(t + \frac{\tau_1}{2}\right) s^*\left(t + \frac{\tau_2}{2}\right) c_n\left(\frac{\tau_1 - \tau_2}{2}\right) = \\ &= \int dv G_n(v) \left| B\left(t, f - \frac{v}{2}\right) \right|^2. \end{aligned} \quad (182)$$

where

$$\begin{aligned} B(t, f) &\equiv \int d\tau \exp(-i2\pi f\tau) R_{VV}(t, \tau) s\left(t + \frac{\tau}{2}\right) = \\ &= \int dv \exp(i2\pi vt) W_{VV}\left(t, f - \frac{v}{2}\right) S(v). \end{aligned} \quad (183)$$

(As special cases, if weighting $v(t) = 1$ for all t , then $R_{VV}(t, \tau) = 1$ and

$$\overline{|c|}^2 = 4 \int dv G_n(v) |S(2f - v)|^2; \quad (184)$$

while, instead, if $G_n(f) = \hat{N}_d$ for all f , then $c_n(\tau) = \hat{N}_d \delta(\tau)$ and

$$\overline{|c|}^2 = 2 \hat{N}_d \int d\tau R_{VV}^2(t, \tau) \left| s\left(t + \frac{\tau}{2}\right) \right|^2. \quad (185)$$

If both conditions above hold, then

$$\overline{|c|}^2 = 4 \hat{N}_d E. \quad (186)$$

Returning to the general case again, the fifth term in (175) is given by combining (171) and (172), while the sixth term is

$$\begin{aligned} \overline{cd}^* &= \iint d\tau_1 d\tau_2 \exp(-i2\pi f(\tau_1 - \tau_2)) R_{vv}(t, \tau_1) * \\ &* R_{vv}^*(t, \tau_2) s\left(t + \frac{\tau_1}{2}\right) s^*\left(t - \frac{\tau_2}{2}\right) \overline{n^*\left(t - \frac{\tau_1}{2}\right) n^*\left(t + \frac{\tau_2}{2}\right)} = 0, \end{aligned} \quad (187)$$

by use of (174).

Combining the above results, we have, for the variance of the WDF estimate,

$$\begin{aligned} \text{Var}\{W_{yy}(t, f)\} &= a^2 + \overline{b^2} + 2\overline{|c|^2} + 2a\overline{b} - (a + \overline{b})^2 = \\ &= \overline{b^2} - \overline{b}^2 + 2\overline{|c|^2} = \\ &= 2 W_{vv}^2(t, f) \oplus G_n^{(2)}(f) + \quad (N \times N) \\ &+ 2 \int dv G_n(v) \left| B\left(t, f - \frac{v}{2}\right) \right|^2. \quad (S \times N) \end{aligned} \quad (188)$$

This result holds for arbitrary signal s , weighting v , and noise spectrum G_n . The quantities $G_n^{(2)}$ and B are defined in (178) and (183), respectively.

If we do not weight waveform $x(t)$, that is, choose $v(t) = 1$ for all t in (167), then $R_{VV}(t, \tau) = 1$, $W_{VV}(t, f) = \delta(f)$, and the $N \times N$ term in (188) becomes infinite; that is, the WDF estimate (168) has infinite variance if we do not weight in time, regardless of what the actual noise spectrum, G_n , is.

On the other hand, if the noise n is white, then $G_n(f) = \hat{N}_d$ for all f , $C_n(\tau) = \hat{N}_d \delta(\tau)$, and $G_n^{(2)}$ in (178) is infinite, which makes the $N \times N$ term in (188) infinite. Thus, if we do not filter out the noise which is out of the band of the signal, the WDF estimate has infinite variance, regardless of what time weighting v is employed.

WDF PROCESSOR

In view of the above observations, we now consider the general WDF processor depicted in figure 7. The only new element here is the

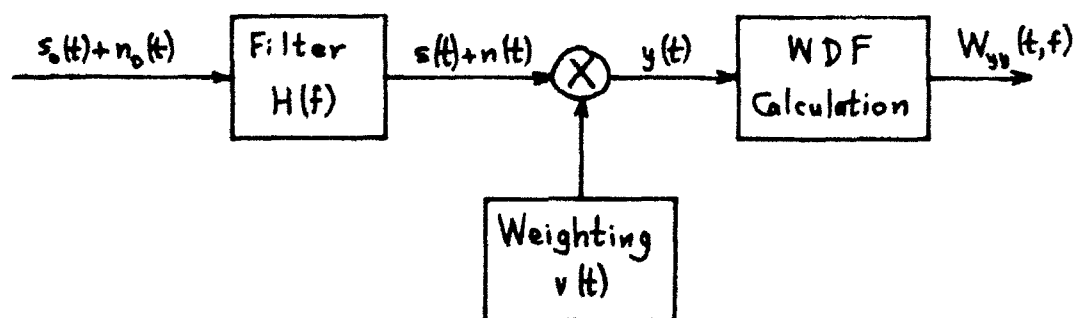


Figure 7. WDF Processor

time-invariant linear filter with transfer function H . The input noise n_o is presumed to be white over the band of the input signal s_o ; mathematically, this is handled by letting

$$G_{n_0}(f) = N_d \quad \text{for all } f, \quad (189)$$

where N_d is the double-sided noise spectral density level in watts/Hz. The linear filter $H(f)$ approximately matches the bandwidth of the input signal and passes $S_0(f)$ essentially unaltered, while filtering out undesired noise spectral components. The actual filter output signal s is given by

$$s(t) = h(t) \otimes s_0(t) = \int df \exp(i2\pi ft) H(f) S_0(f). \quad (190)$$

The weighting $v(t)$ approximately matches the duration of the signal and passes $s(t)$ essentially unaltered, while gating out undesired noise temporal components. Representative plots of the various quantities in figure 7 are given in figure 8.

A numerical example of the WDF processor in figure 7 is carried out in complete detail in appendix H, including the mean and variance results given earlier in this section. In particular, the input signal s_0 is a linear frequency modulation waveform with Gaussian amplitude modulation.

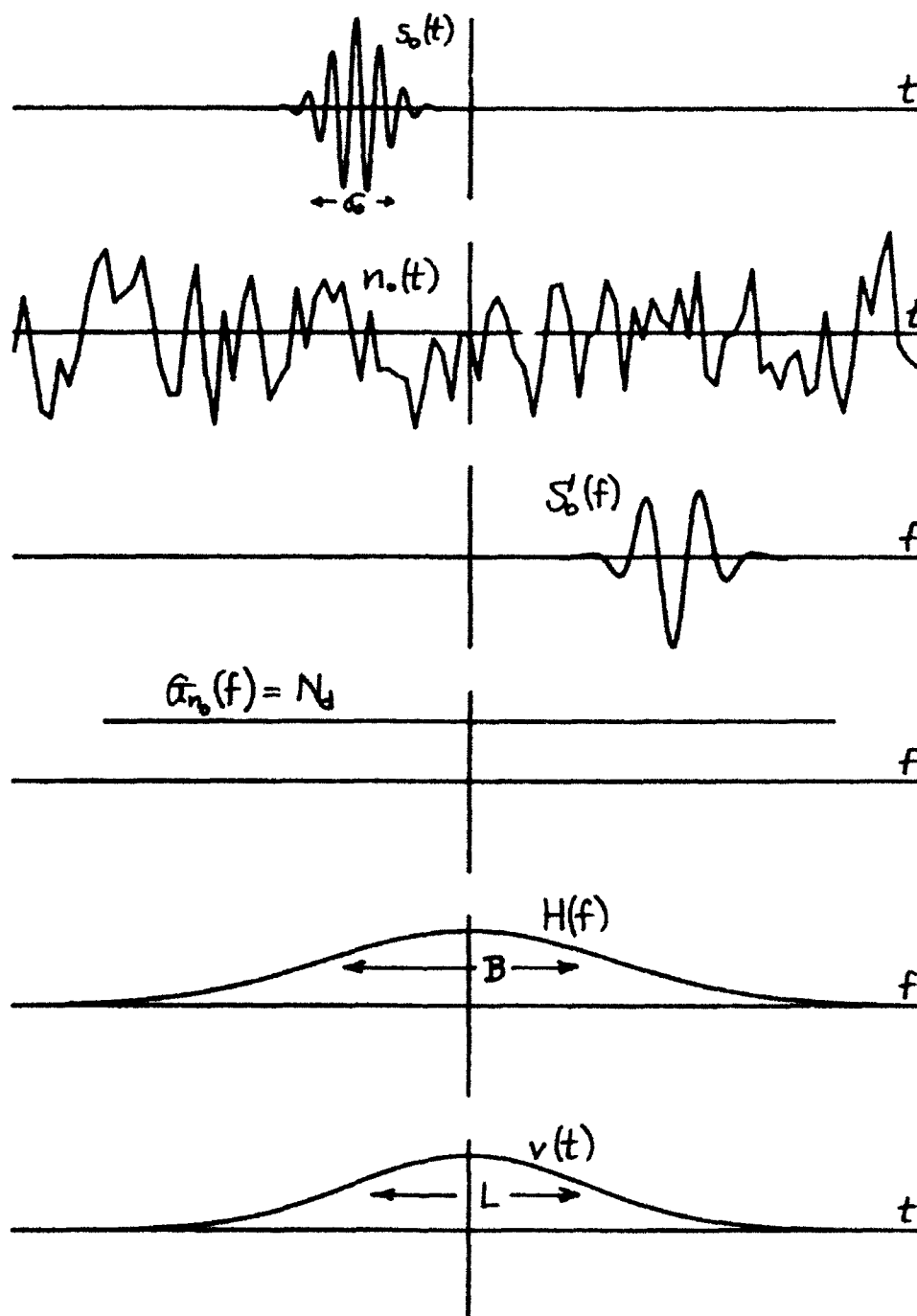


Figure 8. Time and Frequency Characteristics of Figure 7

SUMMARY

When a segment of a stationary random process is available, the method of Blackman and Tukey [14] tells us that, to estimate the correlation function at delay τ , we should average the product of waveform values separated in time by τ seconds, and that we should carry out this averaging over the total available data record, in order to reduce the effect of random fluctuations. For a nonstationary process, the averaging interval is further limited to that in which a significant change in statistics does not occur.

After obtaining the estimated correlation, the Blackman-Tukey method further directs us to weight the correlation values in the neighborhood of $\tau = 0$ more heavily than those for larger τ , and to Fourier transform the weighted correlation estimate. The weighting should taper off to zero for larger τ , so as to suppress these more noisy estimates, and the taper should be gradual so as not to create significant positive and negative sidelobes in the frequency domain.

These two operations, averaging in time and weighting in delay, are both totally absent in the WDF, as may be seen from (2) and (3). In fact, (2) and (3) might be viewed as the ultimate in greediness of a spectral estimate, since they include no averaging and no weighting. Viewed in this light, it is not surprising that the WDF has some very debilitating behavior in terms of negative distribution values and large interference terms.

The inclusion of averaging and weighting in the spectral estimate, as typified by (150)-(152) and (F-1), results in a modified distribution function which is a double convolution with a smoothing function in the t, f plane. Furthermore, the averaging and weighting in (F-1) takes place both in the f and ν domain (line 4) just as well as in the t and τ domain (line 3). Alternatively, line 2 indicates that the complex ambiguity function may be weighted in two dimensions and doubly Fourier transformed. However, the resultant modified WDF need not be positive.

The identity of this double convolution with a positive STSE, when the smoothing function is a legal WDF, allows for an alternative approach that is very attractive computationally and is easy to interpret. The preliminary calculation of the WDF serves to point out regions of interest in the t, f plane and to quantify the time and frequency extents, as well as the amount of linear frequency modulation, to utilize in weighting u in the STSE. This procedure is illustrated in appendix I for the waveform $s(t) = t \exp(-t^2/2)$ and shown to yield a physically meaningful smoothed distribution function, whereas the WDF is very difficult to justify and interpret on any physical grounds.

It was pointed out earlier that double convolution of a given WDF with a Gaussian WDF increases the spread of the smoothed function by area .5 in the t, f plane, since the effective area of a Gaussian WDF is .5. Strictly speaking, this is only true when the Gaussian WDF contour ellipse has the same tilt and the same ratio of major-to-minor axes as the given WDF (assumed Gaussian in the region of interest in the t, f plane). More

generally, if there is a mismatch in tilt or ratio of major-to-minor axes, the effective area is increased by more than .5, thereby leading to additional spreading in the t,f plane. The detailed derivations are presented in appendix J.

The performance of an estimator of the WDF of a signal in the presence of noise depends on the amount of filtering and weighting employed to suppress noise components in frequency and time. Exact relations for the mean output, the bias, and the variance of the WDF estimate are given.

APPENDIX A. SLICES IN TIME OF THE WDF

The voltage density spectrum of waveform $s(t)$ was given in (9). If $s(t)$ is sampled at increment Δ_t , an approximation is afforded according to

$$S(f) = \int dt \exp(-i2\pi ft) s(t) =$$

$$\approx \Delta_t \sum_k \exp(-i2\pi f k \Delta_t) s(k \Delta_t) \equiv \tilde{S}(f) \text{ for all } f. \quad (\text{A-1})$$

The summation on k runs over the range of nonzero summand. Since

$$\tilde{S}\left(f + \frac{1}{\Delta_t}\right) = \tilde{S}(f), \quad (\text{A-2})$$

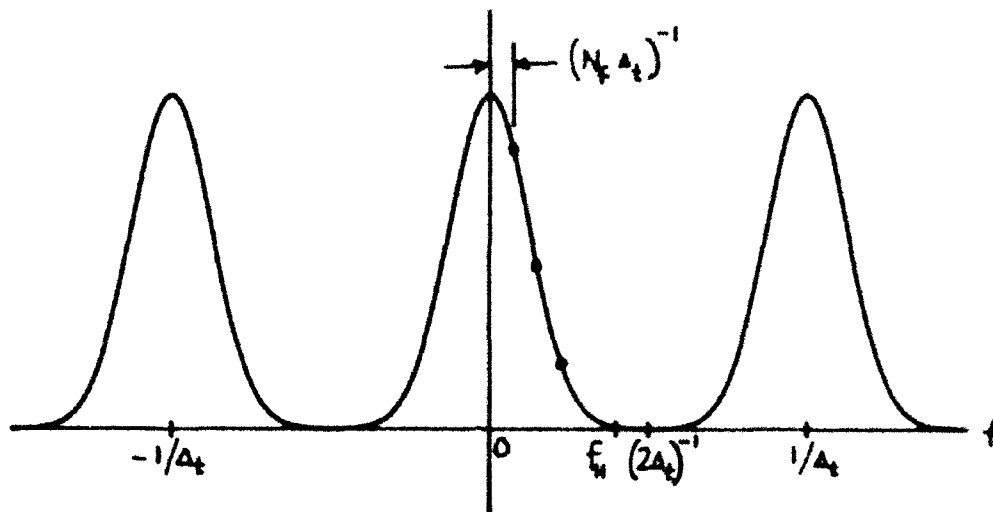
then $\tilde{S}(f)$ has period $1/\Delta_t$ in f . We limit the evaluation of $\tilde{S}(f)$ to the values

$$\tilde{S}\left(\frac{n}{N_f \Delta_t}\right) = \Delta_t \sum_k \exp(-i2\pi n k / N_f) s(k \Delta_t) \quad \text{for } 0 \leq n \leq N_f - 1, \quad (\text{A-3})$$

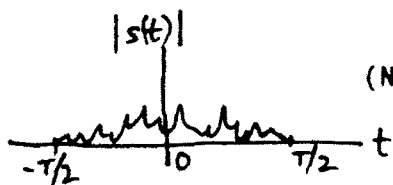
where n and N_f are integers, and thereby cover a full period of $\tilde{S}(f)$. A representative plot of $|\tilde{S}(f)|$ and its sampled values appears in figure A-1.

For the low-pass case of $\tilde{S}(f)$ depicted in figure A-1, it is necessary to choose

$$\Delta_t < (2f_H)^{-1} \quad (\text{A-4})$$

Figure A-1. Low-Pass Spectrum $\tilde{S}(f)$

in order to avoid aliasing ^{of $S(f)$.} We will also need frequency spacing



$$(N_f \Delta_t)^{-1} < (2T)^{-1}, \quad \text{that is, } N_f > 2T/\Delta_t \quad (\text{A-5})$$

in order to track the wiggles of $S(f)$ in frequency, where T is the effective time duration of $s(t)$. In fact, we may need frequency spacing $(N_f \Delta_t)^{-1}$ to be very small if we are to do further accurate integrations on $S(f)$. Thus we need

$$N_f > 4 f_H T, \quad (\text{A-6})$$

and perhaps much larger for further manipulations.

The WDF can be written in terms of the spectrum $S(f)$ according to (10):

$$\begin{aligned} W(t, f) &= \int dv \exp(i2\pi vt) S(f + \frac{v}{2}) S^*(f - \frac{v}{2}) = \\ &= 2 \int du \exp(i4\pi ut) S(f + u) S^*(f - u). \end{aligned} \quad (\text{A-7})$$

If we sample $S(f)$ at increment Δ_f in frequency, the Trapezoidal approximation to the WDF is

$$\hat{W}(t, f) \equiv 2\Delta_f \sum_l \exp(i4\pi t l \Delta_f) S(f + l\Delta_f) S^*(f - l\Delta_f) = \sum_l W\left(t - \frac{l}{2\Delta_f}, f\right) \quad (A-8)$$

for all t, f . Since

$$\hat{W}\left(t + \frac{1}{2\Delta_f}, f\right) = \hat{W}(t, f), \quad (A-9)$$

then $\hat{W}(t, f)$ has period $(2\Delta_f)^{-1}$ in t . Accordingly, we evaluate only

$$\hat{W}\left(\frac{m}{2N_t\Delta_f}, n\Delta_f\right) = 2\Delta_f \sum_l \exp(i2\pi m l / N_t) S((n+l)\Delta_f) S^*((n-l)\Delta_f) \quad (A-10)$$

for $0 \leq m \leq N_t - 1$, where m, n, N_t are integers. In this manner, we get a slice of $\hat{W}(t, f)$ in time t (m) for fixed frequency f (n). The operation in (A-10) can be efficiently realized as an N_t -point FFT of collapsed samples when N_t is a power of 2.

Now the only information on $S(f)$ that we have available are the samples of $\tilde{S}(f)$ given in (A-3). If we choose, without loss of generality,

$$\Delta_f = (N_f \Delta_t)^{-1}, \quad (A-11)$$

then (A-10) becomes (exactly)

$$\hat{W}\left(\frac{m\Delta_t}{2} \frac{N_f}{N_t}, \frac{n}{N_f\Delta_t}\right) = \frac{2}{N_f\Delta_t} \sum_l \exp(i2\pi m l / N_t) S\left(\frac{n+l}{N_f\Delta_t}\right) S^*\left(\frac{n-l}{N_f\Delta_t}\right) \quad (A-12)$$

for $0 \leq m \leq N_t - 1$. We then adopt as our approximation to \hat{W} , which itself is an approximation to W , the quantity

$$\tilde{W}\left(\frac{m\Delta_t}{2} \frac{N_f}{N_t}, \frac{n}{N_f\Delta_t}\right) \equiv \frac{2}{N_f\Delta_t} \sum_{\ell \in L_n} \exp(i2\pi m\ell/N_t) \tilde{S}\left(\frac{n+\ell}{N_f\Delta_t}\right) \tilde{S}^*\left(\frac{n-\ell}{N_f\Delta_t}\right) \quad (A-13)$$

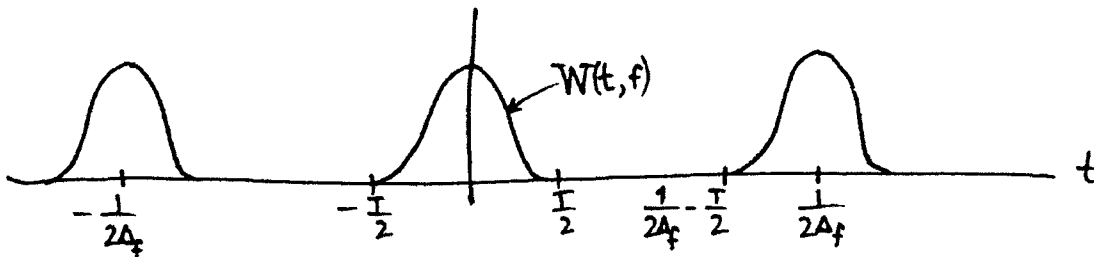
for $0 \leq m \leq N_t - 1$, where

$$\ell \in L_n \text{ denotes } |n \pm \ell| < N_f/2, \quad (A-14)$$

and we presume that $\tilde{S}(f)$ has been calculated for $|f| < (2\Delta_t)^{-1}$; see figure A-1.

The quantity $N_f\Delta_t$ may have to be large, in order to sample $\tilde{S}(f)$ finely enough for an accurate WDF. Then since the spacing in t , applied to $W(t, f)$, is $\frac{N_f\Delta_t}{2N_t}$, it may require a large value of N_t in order to keep track of the variations versus t . Also, n may not have to run through consecutive integer values, but may take on decimated values, so that $n/(N_f\Delta_t)$ tracks the f behavior adequately.

Addendum: $\hat{W}(t, f)$ in (A-8):



We are presuming that $s(t) \approx 0$ for $|t| > T/2$. So we need

$$\Delta_f < \frac{1}{2T}$$

in order to avoid aliasing of $W(t, f)$ in $\hat{W}(t, f)$. Then, when we choose (A-11), we must have $N_f > 2T/\Delta_t$ in order to avoid aliasing. This is identical to (A-5).

So we must satisfy (A-4), but need not satisfy (62) or (65). An alias-free WDF can be realized with the satisfaction of Nyquist criterion (A-4) only; the end result is (A-12) or (A-13).

APPENDIX B. OSCILLATING WDF FOR SEPARATED PULSES

Consider the waveform $s(t)$ in figure B-1 consisting of two separated energy bursts of general shape. Let t_1 and t_2 represent the "center" of each pulse, and let T_1 and T_2 be some measure of their durations. Define

$$t_c = \frac{1}{2}(t_1 + t_2) . \quad (B-1)$$

Let us investigate the WDF of $s(t)$ for t near t_c , that is, near the center of the two pulses. In particular, let time

$$t = t_c + \Delta , \quad (B-2)$$

where Δ is small. Then from (3),

$$\begin{aligned} W(t_c + \Delta, f) &= \int d\tau \exp(-i2\pi f\tau) s(t_c + \Delta + \frac{\tau}{2}) s^*(t_c + \Delta - \frac{\tau}{2}) = \\ &= \exp(-i2\pi f(t_1 - t_2)) \int dx \exp(-i2\pi fx) s(t_2 + \Delta + \frac{x}{2}) s^*(t_1 + \Delta - \frac{x}{2}), \end{aligned} \quad (B-3)$$

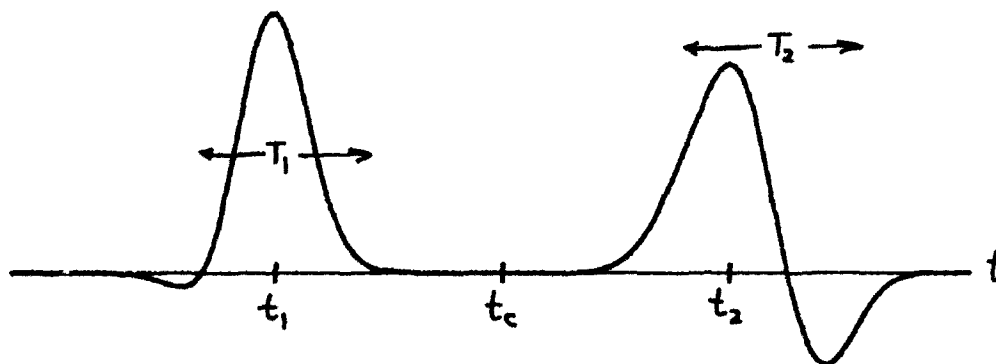


Figure B-1. Waveform $s(t)$

where we let $\tau = t_2 - t_1 + x$.

It can be seen from the integral expression in (B-3) and figure B-1, that for small Δ , only small values of x will contribute to the value of the WDF. In fact,

$$|x| < \min(T_1, T_2) \quad (B-4)$$

is the dominant range of contribution to the integral. Thus the variation with f of the integral component of (B-3) is slow. By contrast, the leading exponential term in (B-3) varies much faster with f , since

$$t_2 - t_1 > \max(T_1, T_2) > \min(T_1, T_2) . \quad (B-5)$$

Since these faster varying oscillations of the exponential term cannot be cancelled by the slower integral contribution of (B-3), the WDF will oscillate in f , for times t near $t_c = (t_1 + t_2)/2$. Thus separated time pulses will lead to oscillations (in f) of the WDF, near times midway between the pulses, regardless of their detailed shapes. An analogous argument can be presented for spectral components, based upon form (10) of the WDF.

Notice that as t_2 approaches t_1 , and the two pulses become one, the oscillating exponential term in (B-3) disappears, allowing for the possibility of a slowly varying (hopefully positive) lobe in the WDF.

APPENDIX C. AMBIGUITY FUNCTION OF (79)

The complex ambiguity function of waveform $s(t)$ in (79) is obtained by substitution into (22) and use of (68):

$$\chi(\nu, \tau) = \sqrt{\pi} \sum_{k\ell} a_k a_\ell^* \tilde{\sigma}_{k\ell} \exp \left[-\frac{1}{4} \frac{T_{k\ell}^2}{\tilde{\sigma}_{k\ell}^2} - \frac{1}{4} \tilde{\sigma}_{k\ell}^2 V_{k\ell}^2 + \right. \\ \left. + i \frac{1}{2} \frac{\sigma_\ell^2 - \sigma_k^2}{\sigma_\ell^2 + \sigma_k^2} T_{k\ell} V_{k\ell} + i 2\pi f_{k\ell} T_{k\ell} - i t_{k\ell} V_{k\ell} + i 2\pi f_{k\ell} (t_k - t_\ell) \right], \quad (C-1)$$

where

$$t_{k\ell} = \frac{1}{2}(t_k + t_\ell), \quad f_{k\ell} = \frac{1}{2}(f_k + f_\ell), \\ \tilde{\sigma}_{k\ell}^2 = \frac{1}{2}(\sigma_k^2 + \sigma_\ell^2), \quad \frac{1}{\tilde{\sigma}_{k\ell}^2} = \frac{1}{2} \left(\frac{1}{\sigma_k^2} + \frac{1}{\sigma_\ell^2} \right), \\ T_{k\ell} = \tau + t_\ell - t_k, \quad V_{k\ell} = 2\pi(\nu + f_\ell - f_k). \quad (C-2)$$

The diagonal terms of (C-1) are

$$\sum_k E_k \exp \left[-\frac{1}{4} \frac{\tau^2}{\sigma_k^2} - \frac{1}{4} \sigma_k^2 4\pi^2 \nu^2 + i 2\pi f_k \tau - i 2\pi t_k \nu \right], \quad (C-3)$$

which are complex and oscillate with τ and ν due to the imaginary terms.

The contour at the $1/e$ relative level, of the magnitude of the k -th term, is an ellipse with axes twice as large as those depicted in figure 4. In addition, the peak amplitude is decreased by a factor of 2 below that for

the WDF in (80). Thus the ambiguity function is a more smeared function of time-frequency than the WDF.

The ambiguity function has peaks of value

$$\sqrt{\pi} a_k a_l^* \tilde{\sigma}_{kl} \exp[i\pi(f_k + f_l)(t_k - t_l)] \quad (C-4)$$

centered at

$$(\tau, \nu) = (t_k - t_l, f_k - f_l) \quad (C-5)$$

for all k, l . The phases of (C-4) are virtually random relative to each other. A slice in ν , for fixed τ , varies (in addition to the Gaussian envelope) as

$$\exp\left[i2\pi\nu\left(\frac{1}{2} \frac{\sigma_l^2 - \sigma_k^2}{\sigma_l^2 + \sigma_k^2} T_{kl} - t_{kl}\right)\right], \quad (C-6)$$

which could be either a slow or fast variation, depending on the particular parameter values. All of these features make physical interpretation of the ambiguity function very difficult.

APPENDIX D. ROTATION OF AXES

Consider the general second-order curve described by

$$Ax^2 + Bxy + Cy^2 + Dx + Ey + F = 0 . \quad (D-1)$$

If we rotate the x, y coordinate axes according to figure D-1, we have

$$x = x' \cos(\beta) - y' \sin(\beta) , \quad (D-2)$$

$$y = x' \sin(\beta) + y' \cos(\beta) .$$

Substitution in (D-1) yields

$$A'x'^2 + B'x'y' + C'y'^2 + D'x' + E'y' + F = 0 , \quad (D-3)$$

where

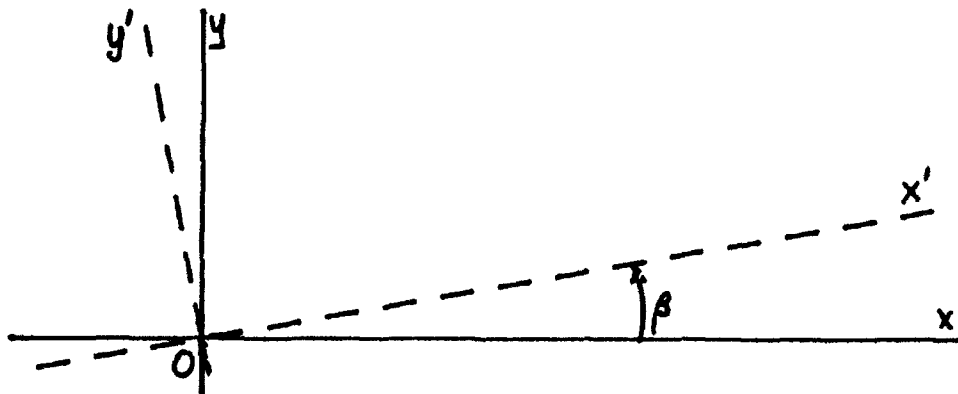


Figure D-1. Rotated Coordinate Axes

$$A' = \frac{1}{2}[A + C + (A - C) \cos(2B) + B \sin(2B)]$$

$$B' = B \cos(2B) + (C - A) \sin(2B)$$

$$C' = \frac{1}{2}[A + C - (A - C) \cos(2B) - B \sin(2B)]$$

$$D' = D \cos(B) + E \sin(B)$$

$$E' = -D \sin(B) + E \cos(B) . \quad (D-4)$$

If we want to eliminate the cross-product term in (D-3), we must make $B' = 0$, that is, take

$$\tan(2B) = \frac{B}{A - C} . \quad (D-5)$$

We will also choose $2B$ in the principal value range:

$$2B = \arctan \left(\frac{B}{A - C} \right) ; \quad (D-6)$$

that is

$$-\frac{\pi}{2} \leq 2B \leq \frac{\pi}{2} , \quad -\frac{\pi}{4} \leq B \leq \frac{\pi}{4} . \quad (D-7)$$

All other solutions for $2B$ differ by $n\pi$; that is, B differs by $n\pi/2$. These are the major and minor axes of the curve described by (D-1).

If we now define

$$R = \sqrt{(A - C)^2 + B^2} , \quad P = \operatorname{sgn}(A - C) , \quad (D-8)$$

where $\sqrt{}$ denotes the positive square root, we find

$$\cos(2\beta) = \frac{|A - C|}{R} = \frac{A - C}{R} P ; \quad (D-9)$$

see figure D-2. And since $\sin(2\beta)$ has the same polarity as $\tan(2\beta)$ in the principal value range,

$$\sin(2\beta) = \frac{|B|}{R} \operatorname{sgn}\left(\frac{B}{A - C}\right) = \frac{B}{R} P . \quad (D-10)$$

Also, since

$$\cos^2(\beta) = \frac{1}{2}(1 + \cos(2\beta)) = \frac{1}{2}\left(1 + \frac{|A - C|}{R}\right), \quad (D-11)$$

then

$$\begin{aligned} \cos(\beta) &= \sqrt{\frac{R + |A - C|}{2R}}, \\ \sin(\beta) &= \sqrt{\frac{R - |A - C|}{2R}} \operatorname{sgn}\left(\frac{B}{A - C}\right). \end{aligned} \quad (D-12)$$

It then follows that the coefficients in (D-4) simplify to

$$\begin{aligned} A' &= \frac{1}{2}(A + C + RP) \\ B' &= 0 \\ C' &= \frac{1}{2}(A + C - RP), \end{aligned} \quad (D-13)$$

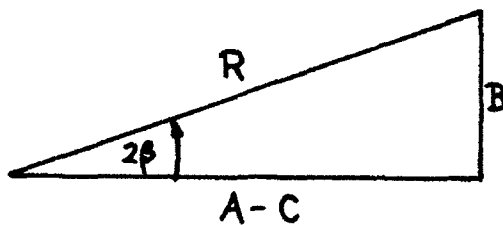


Figure D-2. Triangle Interpretation of (D-5)

from which there follows

$$A'C' = AC - \frac{1}{4} B^2 . \quad (D-14)$$

Additionally, we have

$$\begin{aligned} \tan(B) &= \frac{PR - (A - C)}{B} , \\ \cot(B) &= \frac{PR + (A - C)}{B} . \end{aligned} \quad (D-15)$$

As a result of the above, the general equation in (D-3) can be written as

$$A' \left(x' + \frac{D'}{2A'} \right)^2 + C' \left(y' + \frac{E'}{2C'} \right)^2 = \frac{D'^2}{4A'} + \frac{E'^2}{4C'} - F , \quad (D-16)$$

where

$$\frac{1}{2A'} = \frac{A + C - RP}{4AC - B^2} , \quad \frac{1}{2C'} = \frac{A + C + RP}{4AC - B^2} . \quad (D-17)$$

The simplest expressions for D' and E' appear to be those given in (D-4), in conjunction with (D-12). However, D'^2 and E'^2 can be simplified, resulting in expression

$$A' \left(x' + \frac{D'}{2A'} \right)^2 + C' \left(y' + \frac{E'}{2C'} \right)^2 = G , \quad (D-18)$$

where

$$G = \frac{AE^2 + CD^2 - BDE}{4AC - B^2} - F . \quad (D-19)$$

Now suppose that A and C in (D-1) are positive and that $4AC > B^2$. Then $A' > 0$ and $C' > 0$, meaning that (D-18) is an ellipse if $G > 0$.

Furthermore, if $A < C$, then $A' < C'$ and x' is the major axis. On the other hand, if $A > C$, then $A' > C'$ and x' is the minor axis. See figure D-3. The area of this ellipse is

$$Ax^2 + Bxy + Cy^2 + Dx + Ey + F = 0$$

$$\text{Area} = \frac{\pi G}{\sqrt{A'C'}} = \frac{2\pi G}{\sqrt{4AC - B^2}}, \quad (\text{D-20})$$

by use of (D-14), where G is given by (D-19).

It follows directly from (D-18) that the curve is a circle if and only if $A' = C'$, that is, $R = 0$ via (D-13), which in turn means $A = C$ and $B = 0$ from (D-8).

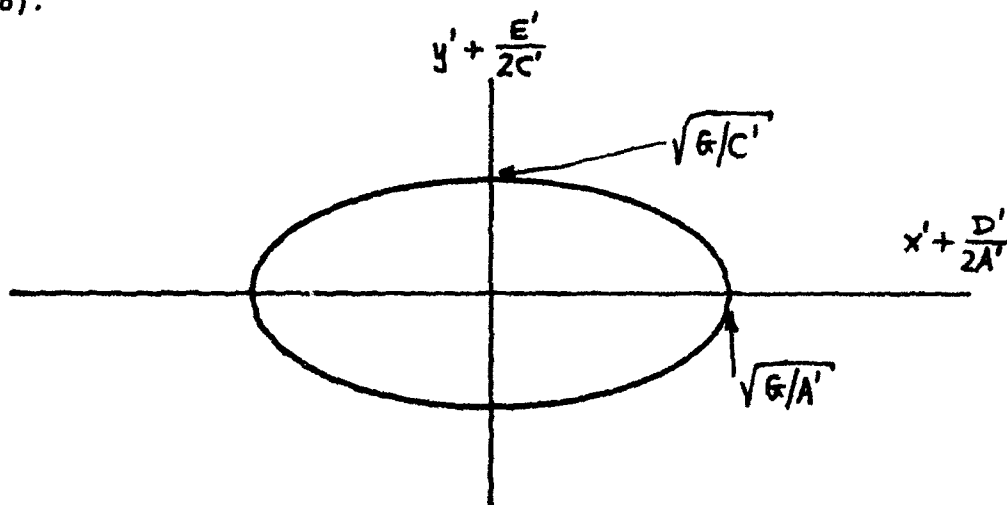


Figure D-3. Ellipse in Rotated Coordinates

EXAMPLE

Consider the ellipse in (91), for which

$$A = 1 + \theta_0^2, \quad B = -2\theta_0, \quad C = 1; \quad \theta_0 \geq 0. \quad (D-21)$$

Then (D-5) yields

$$\tan(2B) = -2/\theta_0, \quad (D-22)$$

from which there follows

$$\tan\left(2B + \frac{\pi}{2}\right) = -1/\tan(2B) = \theta_0/2, \quad (D-23)$$

$$B = \frac{1}{2} \arctan\left(\frac{\theta_0}{2}\right) - \frac{\pi}{4}.$$

As θ_0 varies from 0 to $+\infty$, B varies from $-\pi/4$ to 0; thus B always lies in the principal value range, as required by (D-7).

However, since $A > C$ in (D-21), then B is the angle in the x,y plane of the minor axis of ellipse (91). The major axis angle in the x,y plane is

$$\psi = B + \frac{\pi}{2}, \quad (D-24)$$

which varies from $\pi/4$ to $\pi/2$. There follows

$$\tan(2\psi) = \tan(2B + \pi) = \tan(2B) = -2/\theta_0 \quad (D-25)$$

from (D-22), whereupon the slope of the major axis in the x,y plane can be obtained as

$$\tan \psi = \frac{1}{2} \left(\theta_0 + \sqrt{\theta_0^2 + 4} \right). \quad (D-26)$$

This slope varies from 1 to $+\infty$ as θ_0 varies from 0 to $+\infty$. Conversely, given a measured slope, $\tan \psi$, of the major axis of a WDF contour in the x,y plane, the corresponding amount of linear frequency modulation can be determined from (D-25) or (D-26) as

$$\theta_0 = \tan \psi - 1/\tan \psi. \quad (D-27)$$

The final determination of frequency modulation parameter α_0 in (84) requires the additional knowledge of σ_0 in (90).

In practice, where both σ_0 and α_0 are unknown apriori, the WDF will likely be plotted directly on the t,f plane. According to (78) and (D-24), the major axis will then lie on the line

$$f = t \frac{\tan \psi}{2\pi\sigma_0^2}, \quad (D-28)$$

which can be observed and measured. But σ_0 can be determined separately from a slice in f (at fixed t) of the WDF, since the variation in f in (91) is proportional to

$$\exp \left[-\sigma_0^2 (2\pi f - \alpha_0 t)^2 \right]. \quad (D-29)$$

Thus the distance, between frequency values that are down by $1/e$ from the peak on this frequency slice, is $(\pi\sigma_0^2)^{-1}$, and can be used for direct calculation of σ_0 . Then (D-28) and (D-27) yield $\tan \psi$ and θ_0 , respectively.

APPENDIX E. DISCRETE APPROXIMATION TO SHORT-TERM SPECTRAL ESTIMATE

The STSE is given by (102) and (103). A discrete approximation, by means of the Trapezoidal rule, is furnished by

$$\begin{aligned}
 \mathcal{J}(t, f) &\equiv \left| \Delta \sum_k \exp(-i2\pi f \Delta k) s(k\Delta) u^*(t - k\Delta) \right|^2 = \\
 &= \Delta^2 \sum_{k, \ell} \exp(-i2\pi f \Delta(k - \ell)) s(k\Delta) s^*(\ell\Delta) u^*(t - k\Delta) u(t - \ell\Delta) = \\
 &= \Delta^2 \sum_{k, \ell} \exp(-i2\pi f \Delta(k - \ell)) R_s\left(\frac{k + \ell}{2} \Delta, k\Delta - \ell\Delta\right) R_u\left(t - \frac{k + \ell}{2} \Delta, k\Delta - \ell\Delta\right),
 \end{aligned} \tag{E-1}$$

where Δ is the sampling increment in time. Let

$$m = k - \ell, \quad n = k + \ell, \tag{E-2}$$

to get

$$\mathcal{J}(t, f) = \Delta^2 \sum_{\substack{m+n \\ \text{even}}} \exp(-i2\pi f \Delta m) R_s\left(\frac{n\Delta}{2}, m\Delta\right) R_u\left(t - \frac{n\Delta}{2}, m\Delta\right). \tag{E-3}$$

Define, for use below, the function

$$\begin{aligned}
 C(t_1, t, f) &= W_s(t_1, f) \overset{f}{\otimes} W_u(t - t_1, f) = \\
 &= \int df_1 W_s(t_1, f_1) W_u(t - t_1, f - f_1),
 \end{aligned} \tag{E-4}$$

which is the convolution, on f , of WDFs W_s and W_u . When the integral on t_1 is effected, it yields the desired double convolution:

$$\int dt_1 C(t_1, t, f) = W_s(t, f) \overset{tf}{\otimes} W_u(t, f) . \quad (E-5)$$

We now express R_s and R_u in (E-3) in terms of the inverse transforms of W_s and W_u , respectively, according to (24), interchange summations and integrations, and use the facts that [4, chapter 2]

$$\begin{aligned} \sum_{m \text{ even}} \exp(-i2\pi xm) &= \frac{1}{2} \sum_{\ell} \delta(x - \frac{1}{2}\ell) , \\ \sum_{m \text{ odd}} \exp(-i2\pi xm) &= \frac{1}{2} \sum_{\ell} (-1)^{\ell} \delta(x - \frac{1}{2}\ell) , \end{aligned} \quad (E-6)$$

to get approximation (E-1) in the form

$$\begin{aligned} g(t, f) &= \frac{\Delta}{2} \sum_{\ell} \sum_{n \text{ even}} c\left(\frac{n\Delta}{2}, t, f - \frac{\ell}{2\Delta}\right) + \\ &+ \frac{\Delta}{2} \sum_{\ell} (-1)^{\ell} \sum_{n \text{ odd}} c\left(\frac{n\Delta}{2}, t, f - \frac{\ell}{2\Delta}\right) . \end{aligned} \quad (E-7)$$

The $\ell = 0$ terms together give, where the sum is now over all n ,

$$\frac{\Delta}{2} \sum_n C(\frac{n\Delta}{2}, t, f) , \quad (E-8)$$

which is a discrete approximation to desired quantity (E-5).

The $\ell = 1$ terms in (E-7) yield

$$\frac{\Delta}{2} \sum_n (-1)^n C(\frac{n\Delta}{2}, t, f - \frac{1}{2\Delta}) , \quad (E-9)$$

which is approximately zero. A similar result holds for $\ell = -1$.

The $\ell = 2$ terms in (E-7) are

$$\frac{\Delta}{2} \sum_n C(\frac{n\Delta}{2}, t, f - \frac{1}{\Delta}) , \quad (E-10)$$

which is a discrete approximation to convolution (E-5), but shifted by frequency $1/\Delta$. For small sampling increment Δ in approximation (E-1), the quantity (E-10) will be small in the fundamental region centered at $f = 0$, and can be neglected. Thus (E-8) is the dominant term, giving

$$\begin{aligned} \mathcal{J}(t, f) &\cong \frac{\Delta}{2} \sum_n C(\frac{n\Delta}{2}, t, f) = \\ &\cong \int dt_1 C(t_1, t, f) = W_S(t, f) \odot_{tf} W_U(t, f) . \end{aligned} \quad (E-11)$$

APPENDIX F. SOME SMOOTHING CONSIDERATIONS

This discussion complements and extends that given in (148)-(152) regarding two-dimensional smoothing of the WDF. For easy reference, we repeat the diagram under (24) and furnish an additional one for the smoothing functions that will be employed here. An arrow denotes a Fourier transform.

WAVEFORM FUNCTIONS

$$\begin{array}{ccc}
 s\left(t + \frac{\tau}{2}\right) s^*\left(t - \frac{\tau}{2}\right) = R(t, \tau) & \xleftrightarrow[\tau]{f} & W(t, f) \\
 \updownarrow t, \nu & & \updownarrow t, \nu \\
 \chi(\nu, \tau) & \xleftrightarrow[\tau]{f} & A(\nu, f) = S\left(f + \frac{\nu}{2}\right) S^*\left(f - \frac{\nu}{2}\right)
 \end{array}$$

SMOOTHING FUNCTIONS

$$\begin{array}{ccc}
 v_2(t, \tau) & \xleftrightarrow[\tau]{f} & v_2(t, f) \\
 \updownarrow t, \nu & & \updownarrow t, \nu \\
 q_2(\nu, \tau) & \xleftrightarrow[\tau]{f} & q_2(\nu, f)
 \end{array}$$

By using the basic Fourier transform relations above, we may readily show that two-dimensional smoothing of WDF W with general function v_2 may be written in several alternative forms:

$$\begin{aligned}
D(t,f) &\equiv W(t,f) \otimes^{tf} V_2(t,f) = \\
&= \iint dv \, d\tau \exp[i2\pi(vt - f\tau)] \chi(v,\tau) q_2(v,\tau) = \\
&= \int d\tau \exp(-i2\pi f\tau) [R(t,\tau) \otimes^t v_2(t,\tau)] = \\
&= \int dv \exp(i2\pi vt) [A(v,f) \otimes^f Q_2(v,f)] . \tag{F-1}
\end{aligned}$$

The second line says that the ambiguity function χ of waveforms s should be weighted by q_2 and the product then double Fourier-transformed into the t, f plane. The third line indicates smoothing of R on t , followed by transformation of a weighted function of τ . The last line performs smoothing of A on f , followed by transformation of a weighted function of v . These relations extend those given in (150)-(152). The function V_2 above need not be a legal WDF. The volume under the smoothed distribution (F-1) is the product of the volumes under W and V_2 ; if the latter volume is unity, the energy of waveforms s results again, as is desired.

INADEQUACY OF TIME SMOOTHING ALONE

Consider the special case where smoothing function V_2 is a delta function of f ; then

$$\begin{aligned}
V_2(t,f) &= v_1(t) \delta(f) \\
v_2(t,\tau) &= v_1(t) \\
q_2(v,\tau) &= V_1(v) \\
Q_2(v,f) &= V_1(v) \delta(f) . \tag{F-2}
\end{aligned}$$

Equation (F-1) then simplifies to an averaging of the WDF solely in time:

$$\begin{aligned}
 W(t, f) \otimes^t v_1(t) &= \\
 &= \iint dv d\tau \exp[i2\pi(vt - f\tau)] \chi(v, \tau) v_1(v) = \\
 &= \int d\tau \exp(-i2\pi f\tau) [R(t, \tau) \otimes^t v_1(t)] = \\
 &= \int dv \exp(i2\pi vt) A(v, f) v_1(v) , \tag{F-3}
 \end{aligned}$$

which is an extension of (148)-(149).

The advantageous feature of locally averaging the instantaneous correlation R in time, indicated in line 3, is equivalent to weighting the "local spectrum"

$$A(v, f) = S(f + \frac{v}{2}) S^*(f - \frac{v}{2}) \tag{F-4}$$

in line 4 by function $v_1(v)$, prior to Fourier transforming back into the t domain. This weighting on v is sensible, since if WDF $W(t, f)$ or some modified version is to represent the spectrum at f , the transform on v in line 4 of (F-3) ought not to involve arbitrarily distant values of v ; otherwise, waveform spectrum S in (F-4) will then be utilized at argument values very different from the frequency f of interest and would be nonrepresentative. However, there is no weighting on τ in line 3 of (F-3), thereby allowing arbitrarily distant argument values of signal s , from the

time instant t of interest, to be considered; this unrealistic feature of the WDF is one of the reasons for its undesirable properties.

INADEQUACY OF FREQUENCY SMOOTHING ALONE

Now consider the alternative special case where V_2 in (F-1) is a delta function of t ; then

$$\begin{aligned} V_2(t, f) &= \delta(t) V_1(f) \\ v_2(t, \tau) &= \delta(t) v_1(\tau) \\ q_2(v, \tau) &= v_1(\tau) \\ Q_2(v, f) &= V_1(f) . \end{aligned} \tag{F-5}$$

Equation (F-1) then simplifies to an averaging of the WDF solely in frequency:

$$\begin{aligned} W(t, f) \otimes^f V_1(f) &= \\ &= \iint dv d\tau \exp[i2\pi(vt - f\tau)] \chi(v, \tau) v_1(\tau) = \\ &= \int d\tau \exp(-i2\pi f\tau) R(t, \tau) v_1(\tau) = \\ &= \int dv \exp(i2\pi vt) [A(v, f) \otimes^f V_1(f)] . \end{aligned} \tag{F-6}$$

The advantageous feature of averaging the "local spectrum" A in frequency, indicated in line 4, is equivalent to weighting the instantaneous correlation $R(t, \tau)$ in line 3 by function $v_1(\tau)$, prior to Fourier transforming back into the f domain. This weighting on τ is sensible, since if WDF $W(t, f)$ or some modified version is to represent the time behavior at t , the transform on τ in line 3 of (F-6) ought not to involve arbitrarily distant values of τ ; otherwise, waveform s will then be utilized at argument values very different from the time t of interest and would be non-representative. However, there is no weighting on ν in line 4 of (F-6), thereby allowing arbitrarily distant argument values of spectrum S , from the frequency f of interest, to be considered; this unrealistic feature of the WDF is an additional reason for its drawbacks.

SEPARABLE SMOOTHING

If smoothing function V_2 is separable, then

$$V_2(t, f) = v_a(t) v_b(f)$$

$$v_2(t, \tau) = v_a(t) v_b(\tau)$$

$$q_2(\nu, \tau) = v_a(\nu) v_b(\tau)$$

$$Q_2(\nu, f) = v_a(\nu) v_b(f) .$$

Then (F-1) gives, for example,

$$\begin{aligned}
 W(t,f) \otimes^t v_a(t) \otimes^f v_b(f) &= \\
 &= \int d\tau \exp(-i2\pi f\tau) v_b(\tau) \int dt' R(t - t', \tau) v_a(t') .
 \end{aligned}$$

This has both the desirable features of locally averaging the correlation and suppressing large- τ contributions. However, it restricts the form of averaging in the t, f plane and specifically disallows tilted smoothing regions which are not parallel to the t or f axes.

GENERAL GAUSSIAN TWO-DIMENSIONAL SMOOTHING

The inadequacies of smoothing in time alone or frequency alone suggest consideration of the general two-dimensional result in (F-1):

$$\begin{aligned}
 \hat{W}(t,f) &\equiv W(t,f) \otimes^{tf} v_2(t,f) = \\
 &= \int d\tau \exp(-i2\pi f\tau) \int dt' R(t - t', \tau) v_2(t', \tau) = \\
 &= \int d\tau \exp(-i2\pi f\tau) \int dt' s(t - t' + \frac{\tau}{2}) s^*(t - t' - \frac{\tau}{2}) v_2(t', \tau) . \quad (F-7)
 \end{aligned}$$

If we let $t_1 = t' + \frac{\tau}{2}$, $t_2 = t' - \frac{\tau}{2}$, this becomes

$$\hat{W}(t,f) = \iint dt_1 dt_2 \exp(-i2\pi f(t_1 - t_2)) s(t - t_2) s^*(t - t_1) v_2\left(\frac{t_1 + t_2}{2}, t_1 - t_2\right) . \quad (F-8)$$

Now let two-dimensional smoothing function V_2 have the general Gaussian form

$$V_2(t, f) = 2\sqrt{Q} \exp(-a^2 t^2 - 4\pi^2 b^2 f^2 - 4\pi c t f) , \quad (F-9)$$

where a, b, c are real constants and

$$Q = a^2 b^2 - c^2 . \quad (F-10)$$

The scale factor, $2\sqrt{Q}$, is chosen so that the volume under V_2 in the t, f plane is 1; this keeps the volume under the smoothed distribution in (F-1) or (F-7) at E , the energy of waveform s . In order that V_2 tend to zero at infinity in the t, f plane, we must have $Q > 0$. The area in the t, f plane of the contour ellipse of (F-9), at the $1/e$ relative level, is (appendix D)

$$\text{Area} = \frac{1/2}{\sqrt{a^2 b^2 - c^2}} = \frac{1/2}{\sqrt{Q}} . \quad (F-11)$$

The transform on f of V_2 in (F-9) is

$$v_2(t, \tau) = \frac{\sqrt{Q/\pi}}{b} \exp\left[-\frac{1}{b^2} \left\{ Q t^2 + \frac{\tau^2}{4} + i c t \tau \right\}\right] . \quad (F-12)$$

For completeness, the two remaining smoothing functions in (F-1) are

$$q_2(v, \tau) = \exp\left[-\frac{1}{4Q} \left(a^2 \tau^2 + 4\pi^2 b^2 v^2 + 4\pi c \tau v \right)\right] ,$$

$$Q_2(v, f) = \frac{2}{a} \sqrt{Q/\pi} \exp\left[-\frac{4\pi^2}{a^2} \left(Q f^2 + \frac{v^2}{4} - i c f v \right)\right] .$$

We can now determine the quantity necessary for evaluation of (F-8), namely

$$v_2\left(\frac{t_1 + t_2}{2}, t_1 - t_2\right) = \frac{\sqrt{Q/\pi}}{b} \exp\left[-\frac{1}{4b^2} \left\{ (Q + 1 + i2c) t_1^2 + (Q + 1 - i2c) t_2^2 + 2(Q - 1) t_1 t_2 \right\}\right]. \quad (F-13)$$

By the discussion in (25) et seq., this function in (F-13) is separable in t_1 and t_2 if and only if

$$Q = 1, \quad \text{that is, } a^2 b^2 - c^2 = 1. \quad (F-14)$$

Then V_2 in (F-9) is a legal WDF and the area ^{in the t, f plane} Λ in (F-11) becomes $1/2$. Also, smoothing V_2 in (F-9) is then exactly equivalent to the Gaussian smoothing considered previously in (147).

We are interested here, however, in the more general case of V_2 where Q is not necessarily 1, and therefore V_2 is not a legal WDF. If we substitute (F-13) in (F-8), the smoothed WDF becomes

$$\hat{W}(t, f) = \frac{\sqrt{Q/\pi}}{b} \iint dt_1 dt_2 x(t_1) x^*(t_2) \exp\left[-\frac{Q-1}{2b^2} t_1 t_2\right], \quad (F-15)$$

where

$$x(t_1) = s^*(t - t_1) \exp\left[-i2\pi f t_1 - (Q + 1 + i2c) \frac{t_1^2}{4b^2}\right]. \quad (F-16)$$

By expanding the exp in (F-15) in a power series, there follows

$$\hat{W}(t, f) = \frac{\sqrt{Q/\pi}}{b} \sum_{n=0}^{\infty} \frac{1}{n!} \left(\frac{1-Q}{2b^2}\right)^n \left|\int dt_1 x(t_1) t_1^n\right|^2. \quad (F-17)$$

It is obvious from (F-17) that a sufficient condition for smoothed WDF \hat{W} to be non-negative is $Q \leq 1$, that is

$$a^2b^2 - c^2 \leq 1. \quad (F-18)$$

(The special case of $c = 0$ was given in [11, (5)].) When this condition is used in (F-11), we see that the area of the concentration ellipse of (F-9) is

$$\text{Area} \geq 1/2 \text{ in the } t, f \text{ plane.} \quad (F-19)$$

Thus, smoothing with the Gaussian two-dimensional function V_2 in (F-9) always results in a non-negative distribution, provided that the ^{in the t, f plane}area of the ellipse at the $1/e$ relative level is greater than or equal to $1/2$. It is not necessary that V_2 in (F-9) be a legal WDF; that is, the area of the ellipse need not be precisely $1/2$. However, the most concentrated V_2 in (F-9), that guarantees nonnegative results, has area $1/2$. The only restrictions on parameters a, b, c are given by $0 < Q \leq 1$, that is, $0 < a^2b^2 - c^2 \leq 1$.

APPENDIX G. DERIVATION OF MINIMUM-SPREAD WDF

The short-term spectral estimate of waveform s , relative to weighting u , is given by the double convolution (106),

$$|S_u(t,f)|^2 = W_s(t,f) \otimes W_u(t,f) , \quad (G-1)$$

of the WDFs of s and u . It is therefore important to use, for weighting u , a function which has as narrow a WDF as possible, so that the smearing implied by (G-1) is minimized. In particular, since we are interested in analyzing waveforms with linear frequency modulation, we are interested in minimizing the spread of WDF W_u , as measured by the quadratic quantity

$$I = \iint dt df W_u(t,f) (f - \beta_c t)^2 , \quad (G-2)$$

where β_c is a specified (observed) slope in the t,f plane.

By expanding the quadratic in (G-2), we obtain spread

$$I = I_0 + I_1 + I_2 , \quad (G-3)$$

where

$$I_0 = \iint dt df f^2 W_u(t,f) ,$$

$$I_1 = -2\beta_c \iint dt df t f W_u(t,f) ,$$

$$I_2 = \beta_c^2 \iint dt df t^2 W_u(t,f) . \quad (G-4)$$

Reference to (43), (28), and (12), respectively, allows the terms in (G-4) to be simplified and expressed solely in the time domain as

$$\begin{aligned}
 I_0 &= \frac{1}{4\pi^2} \int dt |u'(t)|^2, \\
 I_1 &= -\frac{\beta_c}{\pi} \int dt t \operatorname{Im}\{u'(t) u^*(t)\}, \\
 I_2 &= \beta_c^2 \int dt t^2 |u(t)|^2.
 \end{aligned} \tag{G-5}$$

Adding these results together, the spread in (G-3) becomes

$$I = \frac{1}{4\pi^2} \int dt |u'(t) - i\alpha_c t u(t)|^2, \tag{G-6}$$

where we define

$$\alpha_c = 2\pi\beta_c. \tag{G-7}$$

Observe that the spread I in (G-6) is nonnegative, for all weightings u .

The function that minimizes I in (G-6) is

$$u(t) = a_0 \exp\left(i \frac{\alpha_c}{2} t^2\right), \quad a_0 \text{ complex}, \tag{G-8}$$

for which

$$I = 0, \quad W_u(t, f) = |a_0|^2 \delta(f - B_c t). \quad (G-9)$$

That is, the WDF is concentrated on the $f = B_c t$ line in the t, f plane.

However, the energy of (G-8) is

$$E_u = \infty, \quad (G-10)$$

which is unacceptable.

If we attempt to approximate (G-8) by unit energy weighting

$$u(t) = (\pi\sigma^2)^{-1/4} \exp\left(-\frac{t^2}{2\sigma^2} + i\frac{\alpha}{2}t^2\right), \quad (G-11)$$

the spread of u , as given by (G-6), turns out to be

$$I = \frac{1}{8\pi^2} \left[\frac{1}{\sigma^2} + \sigma^2(\alpha - \alpha_c)^2 \right]. \quad (G-12)$$

Now if $\alpha = \alpha_c$, that is, the linear frequency modulation parameter α in weighting u is exactly equal to given quantity α_c (from (G-7) and (G-2)), the spread is

$$I = \frac{1}{8\pi^2\sigma^2} > 0. \quad (G-13)$$

However, as duration σ of weighting (G-11) gets larger, the spread I tends to zero, even though the weighting has finite (unit) energy. Also, then (G-11) tends to a scaled version of (G-8) at each fixed t .

In order to eliminate these undesirable features of the weighting, it will not be sufficient to minimize spread I , subject only to a constraint on the energy of u . Rather, it will also be necessary to constrict the time duration of the weighting u . Accordingly, we will minimize spread I in (G-2)-(G-6), under the two constraints that

$$\int dt |u(t)|^2 = 1 = \iint dt df W_u(t, f) ,$$

$$\int dt t^2 |u(t)|^2 = \frac{\sigma_c^2}{2} = \iint dt df t^2 W_u(t, f) ; \quad (G-14)$$

see (14) and (12).

Thus consider

$$Q = \int dt |u'(t) - i\alpha_c t u(t)|^2 + \lambda \int dt |u(t)|^2 + \mu \int dt t^2 |u(t)|^2 , \quad (G-15)$$

where λ and μ are real Lagrange multipliers. Replacing $u(t)$ by $u(t) + \epsilon \eta(t)$, where $\eta(t)$ is an allowed variation, we have

$$Q + \delta Q = \int dt [u'(t) + \epsilon \eta'(t) - i\alpha_c t (u(t) + \epsilon \eta(t))] [u'^*(t) + \epsilon^* \eta'^*(t) +$$

$$+ i\alpha_c t (u^*(t) + \epsilon^* \eta^*(t))] + \int dt [u(t) + \epsilon \eta(t)] [u^*(t) + \epsilon^* \eta^*(t)] (\lambda + \mu t^2) . \quad (G-16)$$

Since the coefficient of ϵ^* must be zero, in order for $u(t)$ to be the optimum [15], we require the following:

$$\int dt \, n'^*(t) [u'(t) - i\alpha_c t u(t)] + \int dt \, n^*(t) [u'(t) - i\alpha_c t u(t)] i\alpha_c t + \\ + \int dt \, n^*(t) u(t) (\lambda + \mu t^2) = 0 \quad \text{for all } n(t) . \quad (G-17)$$

We now integrate by parts on the first term of (G-17), and presume that n, u, u' all decay to zero at $\pm\infty$. Since n is arbitrary, its coefficient under the integral must be zero; namely, we find that u must satisfy the following differential equation:

$$-u''(t) + i2\alpha_c t u'(t) + (i\alpha_c + \alpha_c^2 t^2 + \lambda + \mu t^2) u(t) = 0 \quad \text{for all } t . \quad (G-18)$$

If we try solution

$$u(t) = a \exp\left(\frac{1}{2} c t^2\right) , \quad a, c \text{ complex} , \quad (G-19)$$

in (G-18), we find that

$$t^2(-c^2 + i2\alpha_c c + \alpha_c^2 + \mu) - c + i\alpha_c + \lambda = 0 \quad \text{for all } t . \quad (G-20)$$

Then a solution of the form (G-19) exists with the choices

$$c = i\alpha_c \pm \sqrt{\mu} , \quad \lambda = \pm \sqrt{\mu} . \quad (G-21)$$

To determine $u(t)$ explicitly, we substitute (G-21) into (G-19) to get

$$u(t) = a \exp\left(i \frac{1}{2} \alpha_c t^2 \pm \frac{1}{2} \sqrt{\alpha_c} t^2\right). \quad (G-22)$$

When the two constraints in (G-14) are satisfied, there follows, for the optimum weighting,

$$u(t) = \left(\pi \sigma_c^2\right)^{-1/4} \exp\left(-\frac{t^2}{2\sigma_c^2} + i \frac{\alpha_c}{2} t^2\right). \quad (G-23)$$

This is linear frequency modulation with a Gaussian envelope.

The minimum value of the spread I in (G-6) for the optimum weighting (G-23) is

$$\text{minimum } I = \frac{1}{8\pi^2 \sigma_c^2}, \quad (G-24)$$

and the corresponding WDF is

$$\begin{aligned} W_u(t, f) &= 2 \exp\left[-\frac{t^2}{\sigma_c^2} - 4\pi^2 \sigma_c^2 (f - \beta_c t)^2\right] = \\ &= 2 \exp\left[-\frac{t^2}{\sigma_c^2} (1 + \theta_c^2) + 4\pi f t \theta_c - 4\pi^2 f^2 \sigma_c^2\right], \end{aligned} \quad (G-25)$$

where $\theta_c = \alpha_c \sigma_c^2$. The area of the contour ellipse at the $1/e$ relative level is $1/2$ in the t, f plane.

The mean-square time extent of the optimum weighting u in (G-23) is $\sigma_c^2/2$, as required by constraint (G-14). The mean-square frequency extent is obtained from voltage spectrum

$$U(f) = \pi^{1/4} \left(\frac{2\sigma_c}{1 - i\theta_c} \right)^{1/2} \exp \left(\frac{-2\pi^2 f^2 \sigma_c^2}{1 - i\theta_c} \right) \quad (G-26)$$

as

$$\int df f^2 |U(f)|^2 = \frac{1 + \theta_c^2}{8\pi^2 \sigma_c^2} . \quad (G-27)$$

APPENDIX H. EXAMPLE OF WDF PROCESSOR

The processor of interest here is depicted in figure 7, while representative characteristics of the waveforms and devices are sketched in figure 8. The mean output is given by (173) and the variance is given by (188). We will use the definitions and results in (165)-(189) freely in the following.

INPUT INFORMATION

The input signal waveform to figure 7 is Gaussian-modulated linear frequency modulation:

$$s_0(t) = a_0 \exp \left[-\frac{t^2}{2\sigma_0^2} + i \frac{\alpha_0}{2} t^2 \right], \quad E_0 = \sqrt{\pi} |a_0|^2 \sigma_0, \quad (\text{H-1})$$

where a_0 can be complex. The instantaneous input signal power,

$$|s_0(t)|^2 = |a_0|^2 \exp(-t^2/\sigma_0^2), \quad (\text{H-2})$$

peaks at $t = 0$ and has effective duration σ_0 .

The corresponding signal voltage density spectrum is

$$S_0(f) = a_0 \sigma_0 \left(\frac{2\pi}{1 - i\theta_0} \right)^{1/2} \exp \left(-\frac{2\pi^2 \sigma_0^2 f^2}{1 - i\theta_0} \right), \quad \theta_0 = \alpha_0 \sigma_0^2. \quad (\text{H-3})$$

The energy density spectrum is

$$|S_o(f)|^2 = \frac{2\pi |a_o|^2 \sigma_o^2}{\sqrt{1 + \theta_o^2}} \exp\left(-\frac{4\pi^2 \sigma_o^2 f^2}{1 + \theta_o^2}\right), \quad (H-4)$$

which peaks at $f = 0$. When

$$f = \pm f_o = \pm \frac{\sqrt{1 + \theta_o^2}}{2\pi \sigma_o}, \quad (H-5)$$

the energy density spectrum is reduced to $1/e$ of its peak value; hence f_o is a measure of the bandwidth of the linear frequency modulation waveform.

The input noise n_o to figure 7 has a white spectrum

$$G_{n_o}(f) = N_d \text{ for all } f. \quad (H-6)$$

The filter transfer function is

$$H(f) = \exp\left(-\frac{f^2}{2B^2}\right), \quad (H-7)$$

which peaks at $f = 0$; this coincides with the signal spectrum peak, which means that we are considering the most fortuitous situation. The weighting in figure 7 is taken to be

$$v(t) = \exp\left(-\frac{t^2}{2L^2}\right). \quad (H-8)$$

which peaks at $t = 0$; again, this coincides with the signal peak and is most favorable. The maximum values of H and v , being equal to 1, are chosen for convenience, without loss of generality; absolute level does not influence the performance of the processor in figure 7.

CALCULATIONS OF BASIC FUNCTIONS

We will make frequent use of (68)-(70) in evaluating the following quantities which are needed in (165)-(189); the choices for Gaussian functions for s_0, H, v , above, were made for analytic simplicity, since the various integrals can be conducted in closed form. More general cases would require numerical integrations.

The noise spectrum at the output of the filter is

$$G_n(f) = G_{n_0}(f) |H(f)|^2 = N_d \exp(-f^2/B^2) . \quad (H-9)$$

The corresponding noise correlation is

$$C_n(\tau) = \int df \exp(i2\pi f\tau) G_n(f) = \sqrt{\pi} N_d B \exp(-\pi^2 B^2 \tau^2) . \quad (H-10)$$

The auxiliary spectrum in (178) is

$$G_n^{(2)}(f) = \int d\tau \exp(-i4\pi f\tau) C_n^2(\tau) = \sqrt{\frac{\pi}{2}} N_d^2 B \exp(-2f^2/B^2) . \quad (H-11)$$

The instantaneous correlation of the weighting is

$$R_V(t, \tau) = v\left(t + \frac{\tau}{2}\right) v^*\left(t - \frac{\tau}{2}\right) = \exp\left(-\frac{t^2}{L^2} - \frac{\tau^2}{4L^2}\right), \quad (H-12)$$

and its corresponding WDF is

$$W_V(t, f) = \int d\tau \exp(-i2\pi f\tau) R_V(t, \tau) = 2\sqrt{\pi} L \exp\left(-\frac{t^2}{L^2} - 4\pi^2 L^2 f^2\right). \quad (H-13)$$

The filter impulse response is

$$h(\tau) = \int df \exp(i2\pi f\tau) H(f) = \sqrt{2\pi} B \exp(-2\pi^2 B^2 \tau^2), \quad (H-14)$$

leading to filter output signal

$$\begin{aligned} s(t) &= \int d\tau h(\tau) s_0(t - \tau) = \\ &= a_0 \left(\frac{D}{1 + D - i\theta_0} \right)^{1/2} \exp\left[-2\pi^2 B^2 \frac{1 - i\theta_0}{1 + D - i\theta_0} t^2 \right], \end{aligned} \quad (H-15)$$

where

$$\theta_0 = a_0 \sigma_0^2, \quad D = (2\pi B \sigma_0)^2. \quad (H-16)$$

This filter output signal is again a Gaussian-modulated linear frequency modulation waveform.

In general, for signal

$$s(t) = c_0 \exp(-ct^2/2), \quad c_0, c \text{ complex}, \quad E = \sqrt{\pi} |c_0|^2 / \sqrt{c_r}, \quad (H-17)$$

the WDF is

$$W_s(t, f) = 2\sqrt{\pi} \frac{|c_0|^2}{\sqrt{c_r}} \exp \left[-\frac{t^2 |c|^2 + 4\pi^2 f^2 + 4\pi f t c_i}{c_r} \right]. \quad (H-18)$$

When applied to example (H-15), we identify

$$c_0 = a_0 \left(\frac{D}{1 + D - i\theta_0} \right)^{1/2}, \quad c = 4\pi^2 B^2 \frac{1 - i\theta_0}{1 + D - i\theta_0}, \quad (H-19)$$

to obtain

$$|c_0|^2 = |a_0|^2 \frac{D}{\sqrt{D_1}}, \quad |c|^2 = (2\pi B)^4 \frac{1 + \theta_0^2}{D_2},$$

$$c_r = 4\pi^2 B^2 \frac{D_1}{D_2}, \quad c_i = -4\pi^2 B^2 \frac{D\theta_0}{D_2}, \quad (H-20)$$

where

$$D_1 = 1 + D + \theta_0^2, \quad D_2 = (1 + D)^2 + \theta_0^2. \quad (H-21)$$

When substituted in (H-18), there follows, for the WDF of s in (H-15),

$$W_s(t, f) = 2E_0 \left(\frac{D}{D_1} \right)^{1/2} \exp \left[-\frac{1}{D_1} \left\{ (1 + \theta_0^2) (2\pi B t)^2 + D_2 \left(\frac{f}{B} \right)^2 - 2D\theta_0 (2\pi B t) \left(\frac{f}{B} \right) \right\} \right]. \quad (H-22)$$

As bandwidth B of filter H in (H-7) tends to infinity, then $D \rightarrow \infty$,

$D_1 \rightarrow D$, $D_2 \rightarrow D^2$, and (H-22) yields

$$W_s(t, f) \rightarrow 2E_0 \exp \left[- (1 + \theta_0^2) \frac{t^2}{\sigma_0^2} - (2\pi \sigma_0 f)^2 + 4\pi \theta_0 f t \right] \text{ as } B \rightarrow \infty. \quad (H-23)$$

This agrees with (91) and (78). More generally, in order to keep the scale factor $(D/D_1)^{1/2}$ in (H-22) near 1, we need

$$D > 1 + \theta_0^2, \quad \text{that is, } B > \frac{\sqrt{1 + \theta_0^2}}{2\pi\sigma_0}. \quad (\text{H-24})$$

according to (H-21) and (H-16). But this latter quantity is just the bandwidth of signal s_0 ; see (H-5). Thus condition (H-24) yields the physically intuitive statement that the filter passband should be wider than the input signal bandwidth, in order not to decrease the peak value of the WDF of the filter output signal.

The area of the elliptical contour of the general WDF in (H-22), at the $1/e$ relative level, is $1/2$ in the t, f plane, regardless of the values of any of the parameters of the input signal and filter; this follows by the direct use of (D-1), (D-19), and (D-20). It is also consistent with the general fact that this is true for any signal of the form of (H-17), as may be seen by application of appendix D directly to (H-18), where c and c_0 are arbitrary complex constants.

The peak height of the signal WDF in (H-22) is $2E_0\sqrt{D/D_1}$; hence, the product of peak height and effective area is $E_0\sqrt{D/D_1}$, which is just the energy of s :

$$E = \int dt |s(t)|^2 = E_0 \sqrt{\frac{D}{D_1}} = \iint dt df W_s(t, f). \quad (\text{H-25})$$

This follows directly from (H-15) or (H-17).

The tilt of the major axis of the elliptical contours of (H-22) is given by B radians in the $(2\pi Bt, f/B)$ plane, where

$$\tan(2B) = \frac{\theta_0}{1 + D/2} , \quad (\text{H-26})$$

according to (D-5) and (H-21).

MEAN SIGNAL OUTPUT

The mean signal output of the WDF processor in figure 7 is given by (171) as

$$\begin{aligned} a &= \int d\tau \exp(-i2\pi f\tau) R_v(t, \tau) R_s(t, \tau) = \\ &= \int d\tau \exp(-i2\pi f\tau) R_{\tilde{s}}(t, \tau) = W_{\tilde{s}}(t, f) , \end{aligned} \quad (\text{H-27})$$

where

$$\tilde{s}(t) = v(t) s(t) = c_0 \exp(-\tilde{c} t^2/2) \quad (\text{H-28})$$

and

$$\tilde{c} = c + \frac{1}{L^2} \quad (\text{H-29})$$

according to (H-8) and (H-15)-(H-19). By analogy to (H-18), we have

$$\begin{aligned}
 a = W_{\tilde{z}}(t, f) &= 2 \sqrt{\pi} \frac{|c_0|^2}{\sqrt{\tilde{c}_r}} \exp \left[- \frac{t^2 |\tilde{c}|^2 + 4\pi^2 f^2 + 4\pi f t \tilde{c}_i}{\tilde{c}_r} \right] = \\
 &= 2E_0 \left(\frac{DR}{H_1} \right)^{1/2} \exp \left[- \frac{1}{H_1} \left\{ H_2 x^2 + D_2 y^2 - 2RD\theta_0 xy \right\} \right], \quad (H-30)
 \end{aligned}$$

where we defined

$$\begin{aligned}
 R &= (2\pi BL)^2, \quad x = t/L, \quad y = 2\pi fL, \\
 H_1 &= D_2 + RD_1 = (1 + D)(1 + D + R) + (1 + R)\theta_0^2, \\
 H_2 &= D_2 + 2RD_1 + R^2(1 + \theta_0^2) = (1 + D + R)^2 + (1 + R)^2\theta_0^2, \quad (H-31)
 \end{aligned}$$

and used

$$\tilde{c}_r = \frac{H_1}{L^2 D_2}, \quad \tilde{c}_i = - \frac{RD\theta_0}{L^2 D_2}, \quad |\tilde{c}|^2 = \frac{H_2}{L^4 D_2}. \quad (H-32)$$

The area of the concentration ellipse of $W_{\tilde{z}}$ in (H-30) at the $1/e$ relative level is $1/2$ in the t, f plane, regardless of the sizes of D and R ; so the signal WDF is not spread by the filtering and weighting operations in figure 7, at least for this example of (H-1) coupled with (H-7) and (H-8).

The peak height of WDF $W_{\tilde{z}}$ is given by the leading factor in (H-30). Since the effective area of this WDF is $1/2$, the product of peak height and effective area is $E_0 \sqrt{DR/H_1}$, which is just the energy of \tilde{z} :

$$\tilde{E} = \int dt |\tilde{z}(t)|^2 = E_0 \left(\frac{DR}{(1 + D)(1 + D + R) + (1 + R)\theta_0^2} \right)^{1/2}. \quad (H-33)$$

The parameters Θ_0, D, R are given in (H-16) and (H-31).

We now define

$$L_b = \frac{L}{\sqrt{1+R}} = \frac{L}{\sqrt{1+(2\pi BL)^2}}; \quad \frac{1}{L_b^2} = \frac{1}{L^2} + (2\pi B)^2. \quad (H-34)$$

Then (H-30) and (H-31) become

$$W_{\xi}(t, f) = 2E_c \left(\frac{DR}{H_1} \right)^{1/2} \exp \left[- \frac{1}{H_1} \left\{ \frac{H_2}{1+R} \left(\frac{t}{L_b} \right)^2 + D_2(1+R)(2\pi L_b f)^2 - 2RD\Theta_0(2\pi L_b f) \left(\frac{t}{L_b} \right) \right\} \right]. \quad (H-35)$$

The major axis of the elliptical contours is at angle $\tilde{\beta}$ radians in the $(t/L_b, 2\pi L_b f)$ plane, where

$$\tan(2\tilde{\beta}) = \frac{\Theta_0(1+R)}{1+R+D+RD/2}. \quad (H-36)$$

Given measurements or observations $\tilde{\beta}$ and σ_0 , this can be immediately solved for Θ_0 , where it is presumed that B and L are known since they are under our control.

As alternative fundamental parameter is more useful than the above; we introduce

$$M = (L/\sigma_0)^2, \quad (H-37)$$

which is the square of the ratio of weighting time to input signal duration.

Then (H-31) yields

$$R = DM, \quad (H-38)$$

where $D = (2\pi B\sigma_0)^2$ just as defined in (H-16). Eliminating R in favor of D and M , the peak height of W_s in (H-30) becomes

$$\text{Peak} = 2E_0 \left(\frac{D^2 M}{(1+D)(1+D+DM) + (1+DM)\theta_0^2} \right)^{1/2} . \quad (\text{H-39})$$

As checks on this quantity, observe that as $D \rightarrow \infty$, the factor of $2E_0$ in (H-39) approaches $(M/(M+1))^{1/2}$; in order to keep this latter quantity near 1, we need $M > 1$, that is, $L > \sigma_0$. This is consistent with physical reasoning on figure 7. Alternatively, as $M \rightarrow \infty$, the factor of $2E_0$ in (H-39) approaches $(D/(1+D+\theta_0^2))^{1/2}$; in order to keep this near 1, we need (H-24) to be observed, just as before.

More generally, in order to keep the signal factor in (H-39) near unity, we need to choose the combination of D and M large enough. For example, to keep the factor at value F , that is, maintain

$$\left(\frac{D^2 M}{(1+D)(1+D+DM) + (1+DM)\theta_0^2} \right)^{1/2} = F \quad (< 1) , \quad (\text{H-40})$$

we need to choose L in (H-37) such that

$$M = \frac{F^2[(1+D)^2 + \theta_0^2]}{D[D - F^2(1+D+\theta_0^2)]} . \quad (\text{H-41})$$

However, this relationship is useful only for

$$D > \frac{F^2}{1 - F^2}(1 + \theta_0^2) . \quad (\text{H-42})$$

A representative sketch of (H-40) is displayed in figure H-1. Small values of parameters M or D are not realizable without the other parameter tending to infinity, in order to maintain the factor in (H-40) at value F . Three numerical examples, for $\theta_0 = 0, 1, 5$ are given in figures H-2, H-3, and H-4, respectively. The larger F values can only be achieved through rather large D and/or M values.

There is, however, a minimum value of the product, MD , required to realize a specified value F for the factor in (H-40), when θ_0 is specified. In fact, we find from (H-41) that, for given F and θ_0 , the product MD is minimized by the choices

$$\begin{aligned} D_{\text{opt}} &= \frac{1 + \theta_0^2}{1 - F^2} \left[F^2 + \sqrt{\frac{1 + F^4 \theta_0^2}{1 + \theta_0^2}} \right], \\ M_{\text{opt}} &= \frac{2F^2}{1 - F^4} \left[1 + \sqrt{\frac{1 + F^4 \theta_0^2}{1 + \theta_0^2}} \right]. \end{aligned} \quad (\text{H-43})$$

The value M_{opt} is relatively insensitive to θ_0 ; in fact, it varies from $4F^2/(1 - F^4)$ to $2F^2(1 - F^2)$ as θ_0 varies from 0 to ∞ , which is less than a 2:1 variation.

The corresponding minimum product is

$$(MD)_{\text{min}} = \frac{2F^2}{(1 - F^2)^2} \left[1 + F^2 \theta_0^2 + \sqrt{(1 + \theta_0^2)(1 + F^4 \theta_0^2)} \right]. \quad (\text{H-44})$$

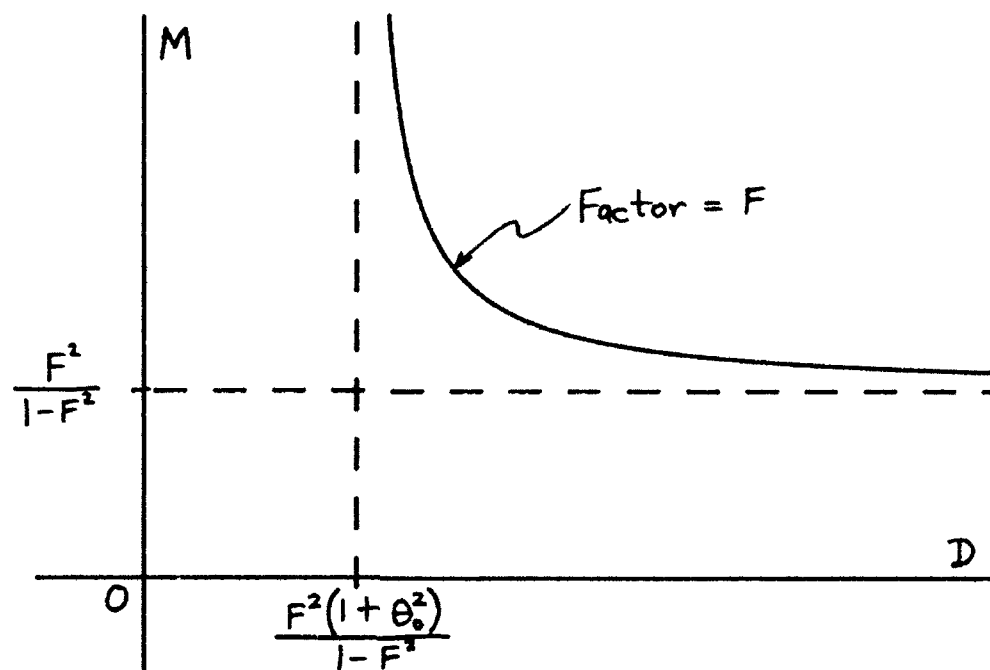


Figure H-1. Plot of (H-40) or (H-41) for Fixed θ_0 .

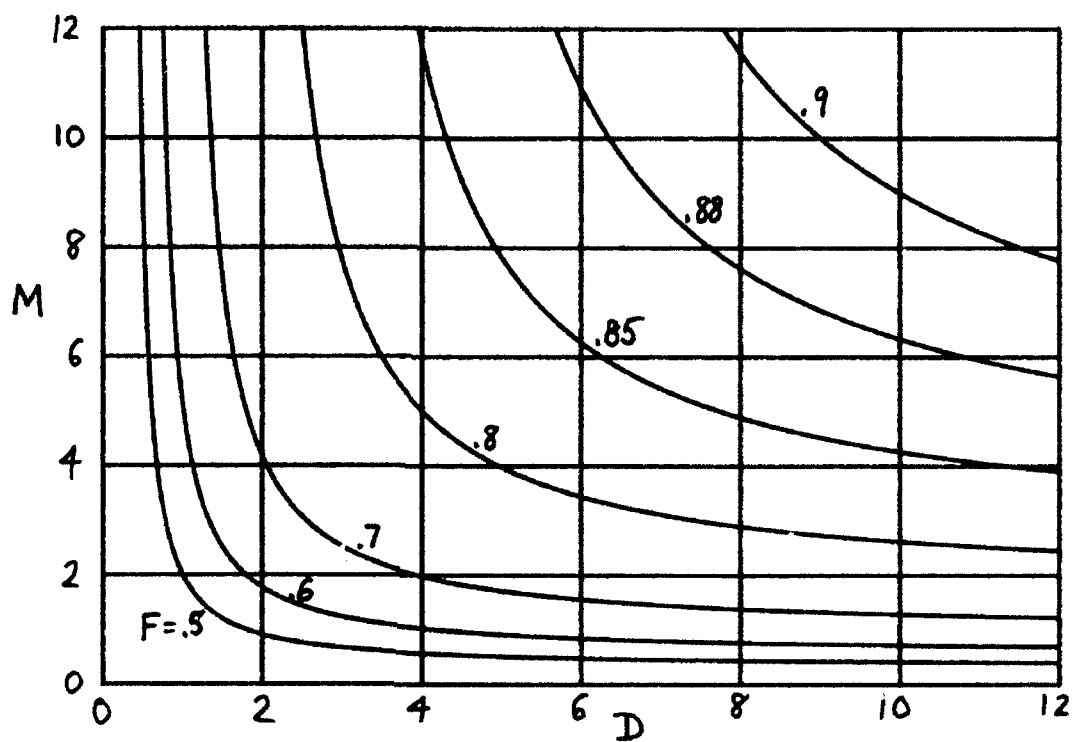
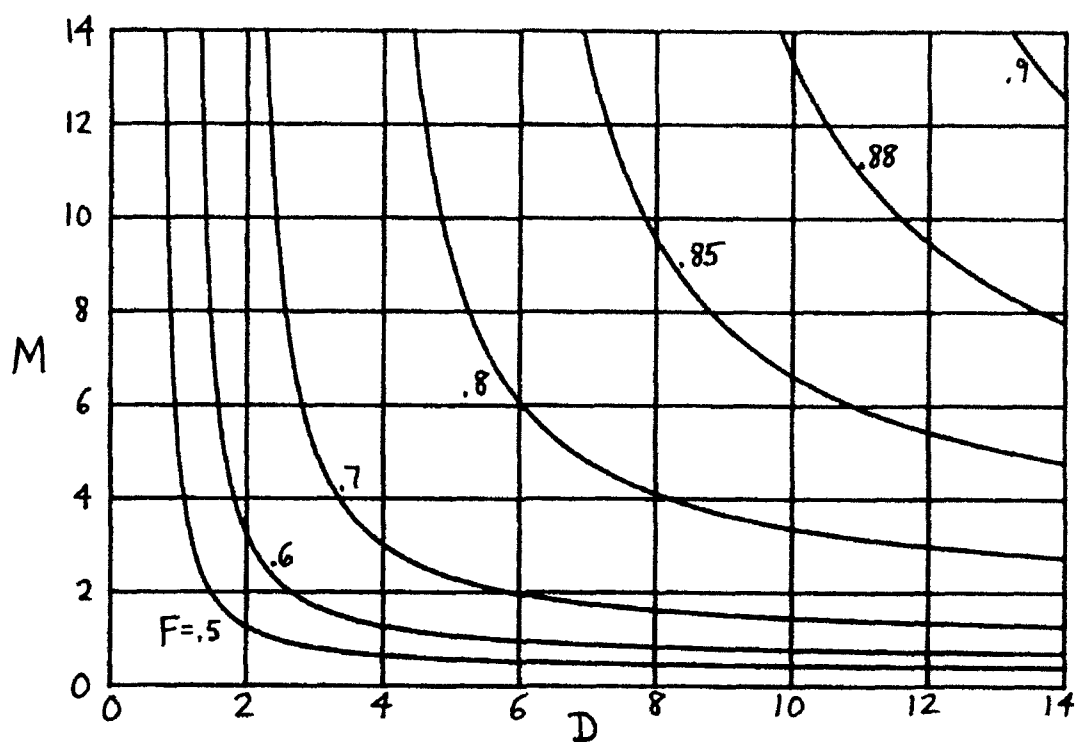
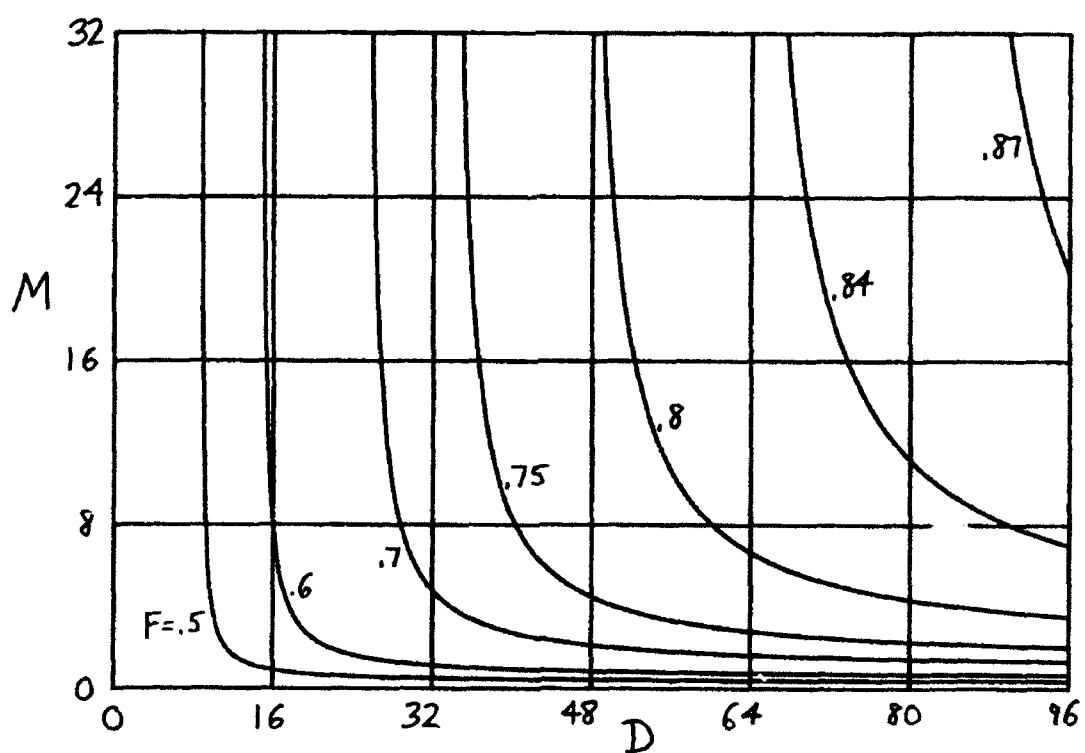


Figure H-2. Plot for $\theta_0 = 0$

Figure H-3. Plot for $\theta_0 = 1$ Figure H-4. Plot for $\theta_0 = 5$

In particular,

$$(MD)_{\min} \sim \frac{4F^2}{(1-F^2)^2} (1 + F^2 \theta_0^2) + 1 \text{ as } \theta_0 \rightarrow \infty; \quad (H-45)$$

in fact, this is a good approximation except near $\theta_0 = 0$. Thus, large amounts of linear frequency modulation, or values of F near 1, require very large MD.

At the other extreme,

$$(MD)_{\min} = \frac{4F^2}{(1-F^2)^2} \text{ for } \theta_0 = 0. \quad (H-46)$$

For example, if $F = 1/\sqrt{2}$, this product is 8; thus relatively large values of the product are required, even at the low end where there is no linear frequency modulation. A plot of (H-44) is given in figure H-5, for various specified values of factor F .

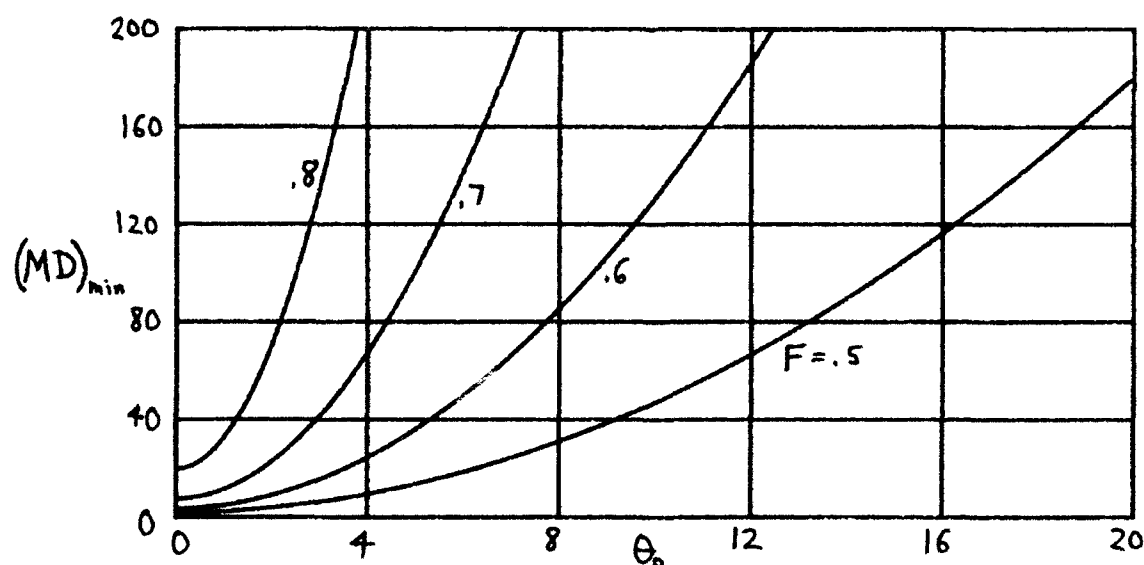


Figure H-5. Minimum MD Product

As a particular numerical example, for $\Theta_0 = 0$, $F = 1/\sqrt{2}$, we find

$$D_{\text{opt}} = 3, \quad M_{\text{opt}} = \frac{8}{3}, \quad (MD)_{\text{min}} = 8. \quad (\text{H-47})$$

So both D_{opt} and M_{opt} are somewhat larger than unity, even for F equal to $1/\sqrt{2}$. All these conclusions are drawn relative to the mean signal output alone; we now consider the noise output contributions.

MEAN NOISE OUTPUT

The mean noise output of the WDF processor in figure 7 is given by (172), (H-9), (H-13), and (H-31) as

$$\begin{aligned} \bar{b} &= W_V(t, f) \otimes^f G_n(f) = \\ &= N_d \left(\frac{R}{1+R} \right)^{1/2} \exp \left[-\frac{t^2}{L^2} - \frac{f^2}{B^2} \frac{R}{1+R} \right]. \end{aligned} \quad (\text{H-48})$$

(As $L \rightarrow \infty$, that is, no weighting, then $R \rightarrow \infty$, and $\bar{b} \rightarrow N_d \exp(-f^2/B^2) = G_n(f)$, as expected.)

The noise factor in (H-48), namely

$$\left(\frac{R}{1+R} \right)^{1/2} = \left(\frac{DM}{1+DM} \right)^{1/2}, \quad (\text{H-49})$$

is virtually unity when the mean signal degradation is small, according to the results of figure H-5. Thus the ratio of peak signal-to-noise means is approximately $2E_0/N_d$, according to (H-30) and (H-48). These latter

quantities, E_0 and N_d , are directly the input parameters to the WDF processor in figure 7; see (H-1) and (H-6).

VARIANCE OF NxN TERM

The variance of the NxN term at the WDF processor output is given by the third line of (188) as

$$\begin{aligned}
 V_{NN} &= 2 W_V^2(t, f) \otimes G_n^{(2)}(f) = \\
 &= N_d^2 \frac{R}{\sqrt{1+R}} \exp \left[-\frac{2t^2}{L^2} - \frac{2f^2}{B^2} \frac{R}{1+R} \right]. \quad (H-50)
 \end{aligned}$$

Here, we also used (H-11) and (H-13). As $L \rightarrow \infty$, then $M \rightarrow \infty$, $R \rightarrow \infty$, and $V_{NN} \rightarrow \infty$. Alternatively, as $B \rightarrow \infty$, then $D \rightarrow \infty$, $R \rightarrow \infty$, and $V_{NN} \rightarrow \infty$. These results for this particular example confirm the general observations in the sequel to (188).

The standard deviation of the NxN term, namely $\sqrt{V_{NN}}$, is precisely equal to the noise mean output in (H-48) for all t, f , except for a constant factor $(1+R)^{1/4} = (1+DM)^{1/4}$. Also, the axes of the elliptical contours of (H-48) and (H-50) are parallel to the t and f axes and are independent of Θ_0 , the amount of linear frequency modulation in the input signal.

VARIANCE OF $S \times N$ TERM

The variance of the $S \times N$ terms at the WDF processor output is given by the last line of (188) or by double the results in (182). Upon substitution of (H-10), (H-12), and (H-15) in (182) and an extreme amount of manipulations, there follows variance

$$V_{SN} = 4E_0 N_d \frac{R\sqrt{D}}{\sqrt{H_3}} \exp[-\xi(t,f)] , \quad (H-51)$$

where

$$H_3 = (1 + D + R/2)(1 + D + R + DR/2) + (1 + R)(1 + R/2) \theta_0^2 \quad (H-52)$$

and $\xi(t,f)$ is an elliptical function with minimum value at $t = f = 0$.

Namely,

$$\xi(t,f) = \frac{2t^2}{L^2} + c_r t^2 - \frac{\alpha^* \mu^2 + \alpha \mu^{*2} + 2\gamma |\mu|^2}{2(|\alpha|^2 - \gamma^2)} , \quad (H-53)$$

where

$$c = 4\pi^2 B^2 \frac{1 - i\theta_0}{1 + D - i\theta_0} ,$$

$$\alpha = \frac{1}{4} \left(c + \frac{2}{L^2} + 2\pi^2 B^2 \right) ,$$

$$\mu = - \left(\frac{c}{2} t + i2\pi f \right) ,$$

$$\gamma = \frac{1}{2} \pi^2 B^2 . \quad (H-54)$$

The quantity in the denominator of (H-53) can be simplified to

$$2(|\alpha|^2 - \gamma^2) = \frac{H_3}{2L^4 D_2} ; \quad (H-55)$$

however, $\xi(t,f)$ has not been reduced to its most compact form,

$$b_1 t^2 + b_2 f^2 + 2b_3 tf , \quad (H-56)$$

due to the excessive amount of labor required to simplify and obtain b_1, b_2, b_3 .

QUALITY MEASURE OF PERFORMANCE

We define a quality measure for the WDF processor output in figure 7 as

$$Q = \frac{\text{Difference of mean outputs}}{\text{Standard deviation of output}} = \frac{a}{(V_{SN} + V_{NN})^{1/2}} . \quad (H-57)$$

The relevant quantities are given by (171) and (188) generally. For the specific example in this appendix, the quality measure, at peak signal location $t = f = 0$, is obtained by combining (H-30), (H-50), and (H-51):

$$Q = \left(\frac{E_o}{N_d} \right)^{1/2} \left(\frac{\frac{4E_o}{N_d} \frac{D\sqrt{1+R}}{H_1}}{1 + \frac{4E_o}{N_d} \sqrt{\frac{D(1+R)}{H_3}}} \right)^{1/2} . \quad (H-58)$$

For convenience, we repeat the parameter definitions here:

$$\Theta_0 = \alpha_0 \sigma_0^2, \quad D = (2\pi B \sigma_0)^2, \quad M = (L/\sigma_0)^2,$$

$$R = DM,$$

$$H_1 = (1 + D)(1 + D + R) + (1 + R)\Theta_0^2,$$

$$H_3 = (1 + D + R/2)(1 + D + R + DR/2) + (1 + R)(1 + R/2)\Theta_0^2. \quad (H-59)$$

It has already been observed in (H-24) and in the sequel to (H-39) that $D > 1 + \Theta_0^2$ and $M > 1$ are desirable, in so far as the mean signal output is concerned. However, if filter bandwidth B (D) is made too large, then too much noise is allowed through; alternatively, if weighting duration L (M) is made too large, a noise degradation also results. Thus, it is expected that the quality ratio Q will peak for D in the neighborhood of $1 + \Theta_0^2$ and for M near 1.

It should be observed from (H-58) that even if input signal-to-noise measure E_0/N_d gets extremely large, the quality measure Q behaves according to $\sqrt{E_0/N_d}$, and not E_0/N_d . This is due to the saturation effects caused by the SxN term in the denominator of definition (H-57); it can also be seen directly from the quantitative result in (H-51), where variance V_{SN} is directly proportional to input signal energy E_0 as well as the noise density level N_d .

The quality ratio Q in (H-58) is plotted versus M in figures H-6, H-7, H-8 for $\theta_0 = 0, 1, 5$, respectively. The input ratio E_0/N_d is kept at value 20 in all cases; the only other fundamental parameter, D , is varied over a range wide enough to encompass the maximum of Q . However, for ease of plotting the results, the values of D which are less than the critical value, which leads to the peak Q , are separated from those that are greater than the critical value. For example, in figure H-6, $D = 1$ leads to the maximum value of Q that can be achieved for any value of M ; thus, the upper part of figure H-6 contains results for $D \leq 1$, while the lower part contains the remainder for $D \geq 1$. The corresponding critical values of D are 8 and 80 in figures H-7 and H-8, when $\theta_0 = 1$ and 5, respectively.

One important observation that is made apparent by these figures is that near the maximum, the quality ratio Q is not too sensitive to M and D ; that is, the maximum is broad in the neighborhood of the best parameter pair M, D . It should also be observed that as θ_0 increases, the peak value of Q decreases, although the decrease is not very significant, at least over the range $\theta_0 = 0, 1, 5$ used here. Finally, the values of the peaks in these figures are slightly less than $\sqrt{E_0/N_d}$, as anticipated above.

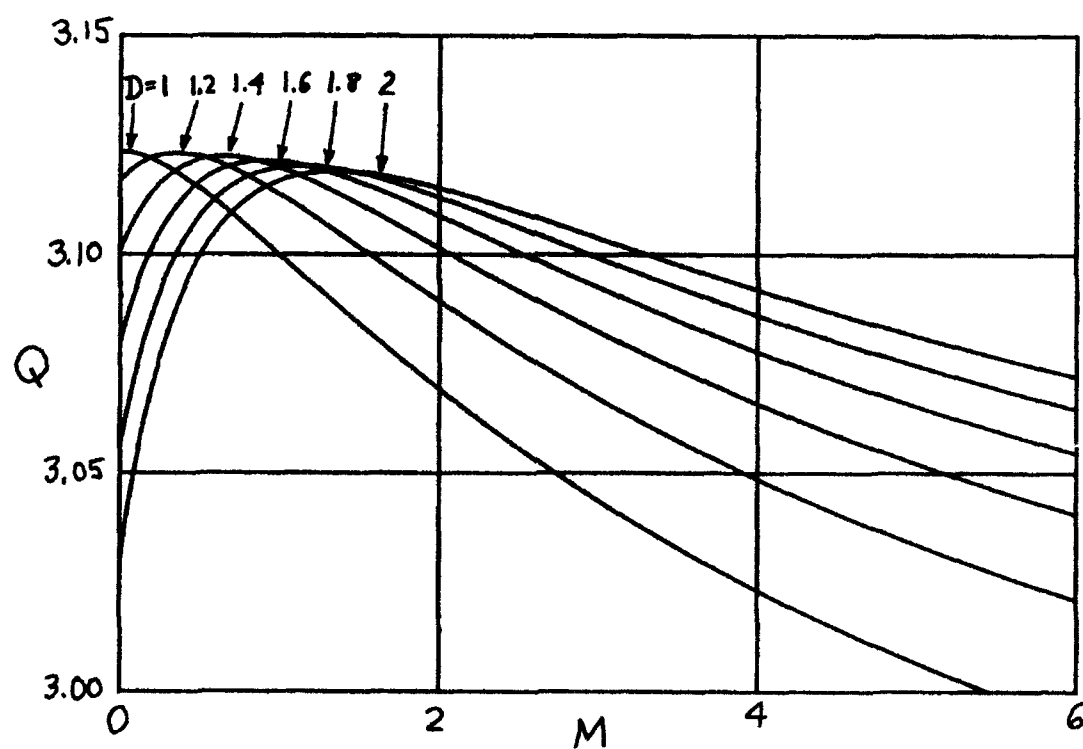
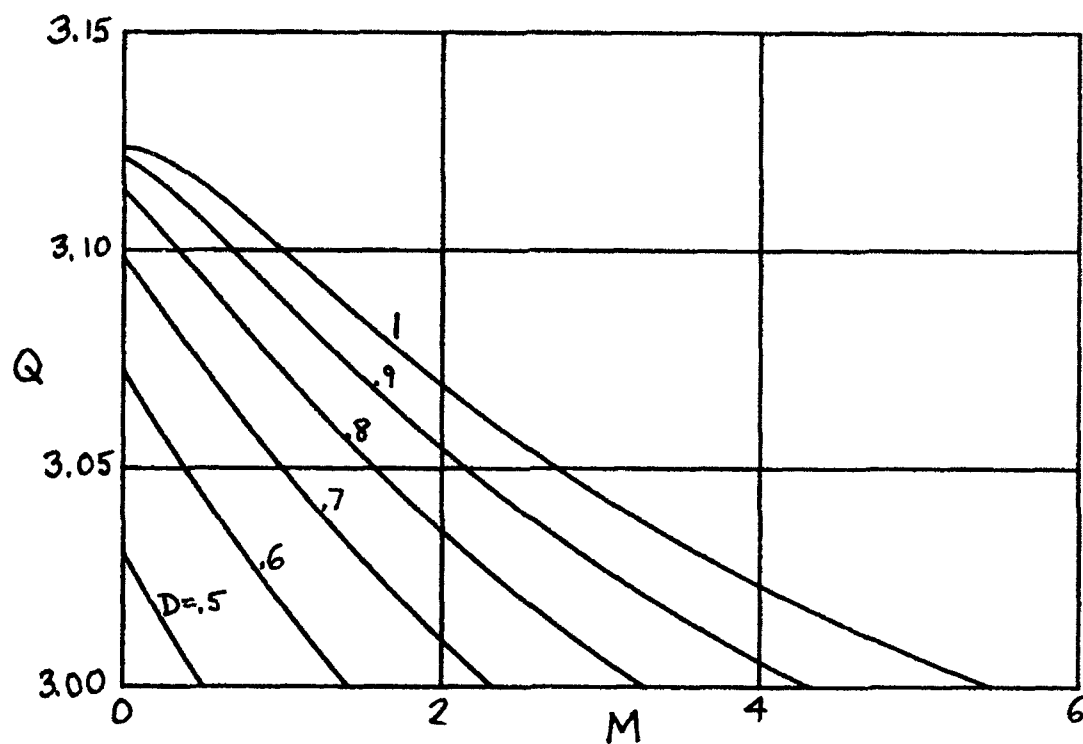


Figure H-6. Quality Ratio for $\theta_0 = 0$, $E_0/N_d = 20$

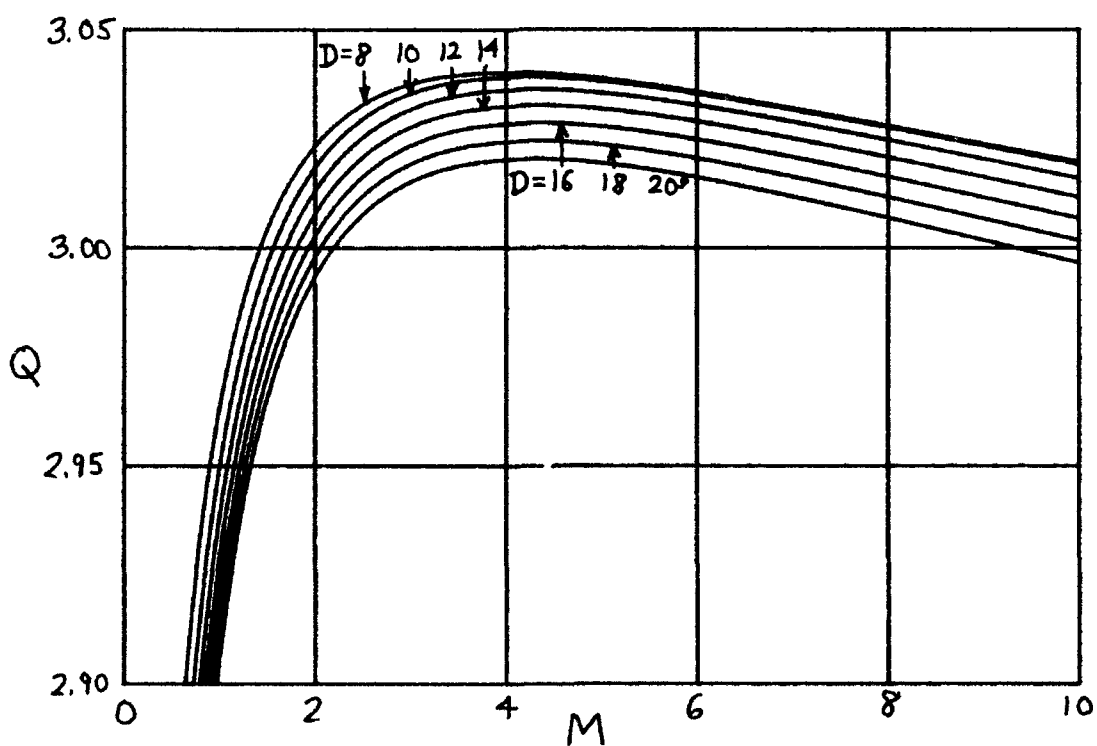
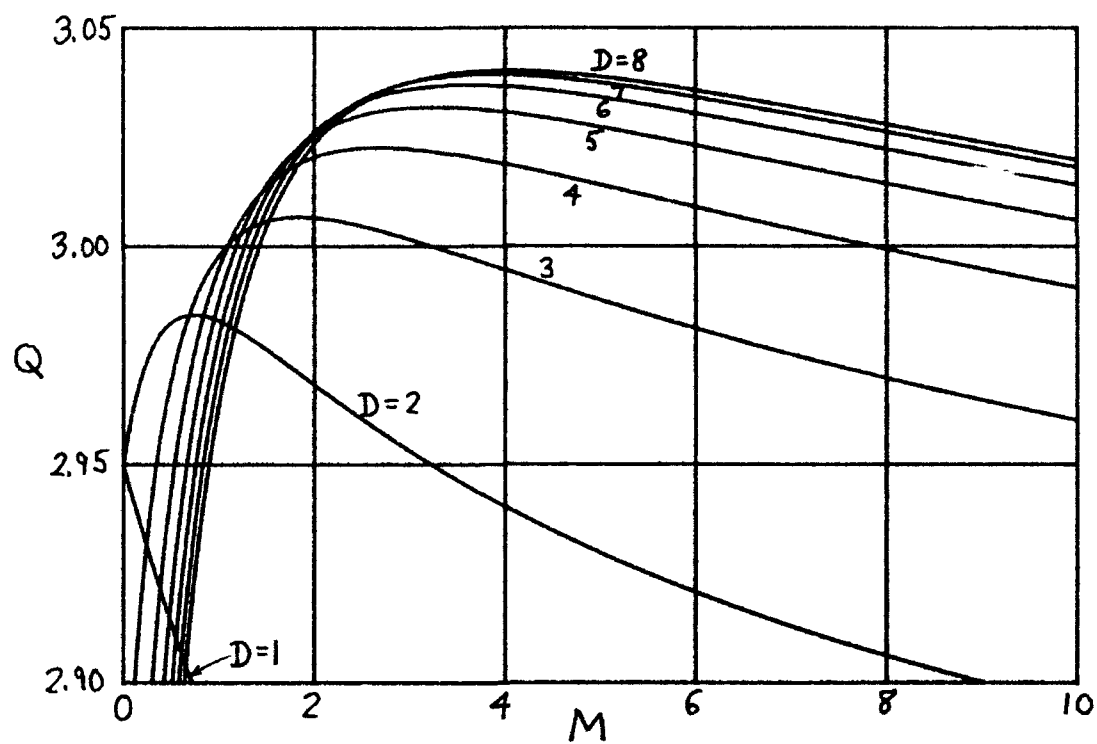


Figure H-7. Quality Ratio for $\theta_0 = 1$, $E_0/N_d = 20$

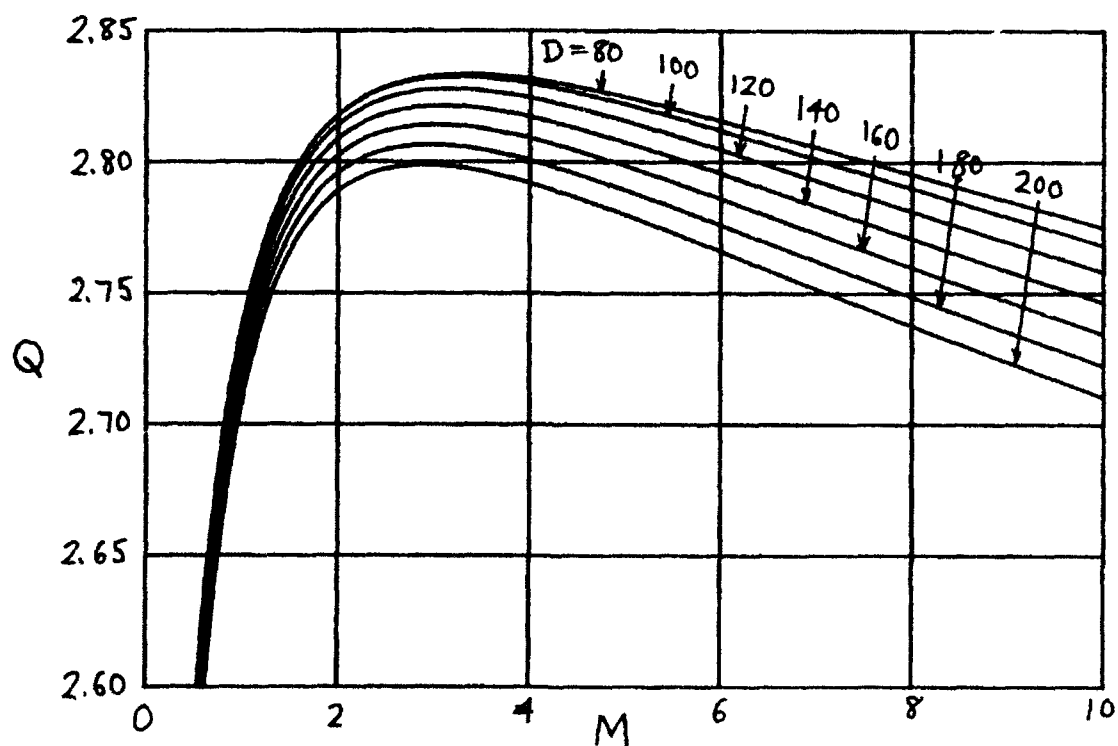
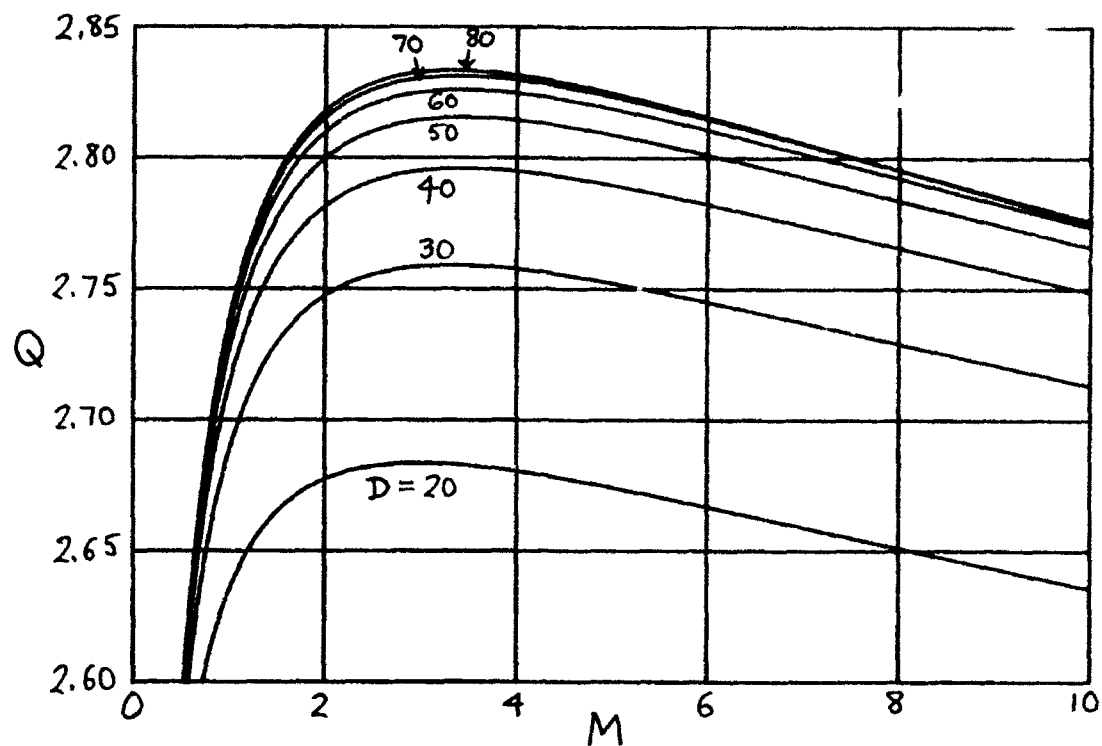


Figure H-8. Quality Ratio for $\theta_0 = 5$, $E_0/N_d = 20$

APPENDIX I. SMOOTHED WDF FOR $s(t) = t \exp(-t^2/2)$

For the waveform

$$s(t) = t \exp(-t^2/2) \quad \text{for all } t, \quad (\text{I-1})$$

the WDF is

$$W_s(t, f) = 2\sqrt{\pi} \exp(-t^2 - 4\pi^2 f^2)(t^2 + 4\pi^2 f^2 - \frac{1}{2}) = 2\sqrt{\pi} \exp(-r^2)(r^2 - \frac{1}{2}), \quad (\text{I-2})$$

with energy

$$E = \int dt |s(t)|^2 = \sqrt{\pi}/2. \quad (\text{I-3})$$

Contour plots of the WDF in (I-2) are concentric circles in the $(t, 2\pi f)$ plane; in fact, (I-2) is a function only of $r^2 = t^2 + (2\pi f)^2$. The origin value of W_s is $-2E = -\sqrt{\pi}$, and the WDF is negative for $r < 1/\sqrt{2}$, while it is positive for $r > 1/\sqrt{2}$.

Let us smooth this WDF with the most compact WDF; namely, use the Gaussian weighting function in (G-23) with WDF (G-25) with $\theta_c = 0$, $\sigma_c = 1$:

$$W_u(t, f) = 2 \exp(-t^2 - 4\pi^2 f^2) = 2 \exp(-r^2). \quad (\text{I-4})$$

The reason for these parameter choices of θ_c and σ_c is that the contours of (I-4) are also circles in the $(t, 2\pi f)$ plane and exactly match those of the waveform WDF in (I-2); this should lead to minimal spreading.

The result of smoothing (I-2) by (I-4) is

$$\begin{aligned} |S_U(t, f)|^2 &= W_S(t, f) \otimes W_U(t, f) = \\ &= \frac{1}{4} \sqrt{\pi} (t^2 + 4\pi^2 f^2) \exp\left(-\frac{1}{2}(t^2 + 4\pi^2 f^2)\right) = \frac{1}{4} \sqrt{\pi} r^2 \exp(-r^2/2), \end{aligned} \quad (I-5)$$

which has volume E as given by (I-3). Again, this is a function only of r^2 , but it is never negative. This smoothed distribution is zero at $r = 0$, and peaks at $r = \sqrt{2}$ with value .326. By contrast, the WDF in (I-2) is -1.77 at the origin, a large negative value. However, the waveform WDF in (I-2) does decay faster than the short-term spectral estimate in (I-5); this is an example of the tradeoffs that must be accepted when using short-term spectral estimation versus the WDF.

To lend credence to (I-5) as a better measure of the time-frequency content of $s(t)$, we observe that at $t = 0$, the center of gravity of (I-5) is

$$\bar{f}_0 = \frac{\int_{-\infty}^{\infty} df |S_U(0, f)|^2 f}{\int_{-\infty}^{\infty} df |S_U(0, f)|^2} = \frac{1}{\pi} \sqrt{\frac{2}{\pi}}. \quad (I-6)$$

Then we expect that

$$A \sin(2\pi \bar{f}_0 t) \quad (I-7)$$

ought to be a good fit to $s(t)$ of (I-1) for t near zero. In fact, plots of (I-1) and (I-7) for $A = \exp(-.5)$ overlap for $-1 < t < 1$.

If we attempt this same procedure for WDF W_s in (I-2), the denominator is

$$\int_0^{\infty} df W_s(0, f) = 0, \quad (I-8)$$

giving rise to $\bar{f}_0 = \infty$, which is useless.

With respect to $t = 1$ instead, we find center of gravity

$$\bar{f}_1 = \frac{\int_0^{\infty} df |S_u(1, f)|^2 f}{\int_0^{\infty} df |S_u(1, f)|^2} = \frac{1}{\pi} \sqrt{\frac{2}{\pi}} \frac{3}{4}. \quad (I-9)$$

Since $s(t)$ in (I-1) peaks at $t = 1$, we expect that

$$A \cos(2\pi \bar{f}_1(t - 1)) \quad (I-10)$$

ought to be a good fit to $s(t)$ for t near 1. In fact, plots of (I-1) and (I-10) for $A = \exp(-.5)$ show very good agreement for $.8 < t < 1.7$.

Thus, smoothing of the WDF W_s in (I-2) by means of WDF W_u in (I-4), for this example, results in a very meaningful distribution function.

APPENDIX J. DOUBLE CONVOLUTION OF TWO GAUSSIAN FUNCTIONS

By means of the double integral result

$$\iint dx dy \exp\left[-\frac{1}{2} \alpha x^2 - \frac{1}{2} \beta y^2 + \gamma xy + \mu x + \nu y\right] =$$

$$= \frac{2\pi}{(\alpha\beta - \gamma^2)^{1/2}} \exp\left[\frac{\beta\mu^2 + \alpha\nu^2 + 2\gamma\mu\nu}{2(\alpha\beta - \gamma^2)}\right] \quad (J-1)$$

for $\alpha_r > 0$, $\beta_r > 0$, $\alpha_r\beta_r > \gamma_r^2$, it is readily shown that the double convolution of two general Gaussian functions is given by

$$\exp\left[-\frac{1}{2} ax^2 - \frac{1}{2} by^2 - \sqrt{ab} \rho xy\right] \otimes^{xy} \exp\left[-\frac{1}{2} cx^2 - \frac{1}{2} dy^2 - \sqrt{cd} \lambda xy\right] = \quad (J-2)$$

$$= \frac{2\pi}{D^{1/2}} \exp\left[-\frac{N_1 x^2 + N_2 y^2 + 2N_3 xy}{2D}\right] \quad (J-3)$$

for $a, b, c, d > 0$, $|\rho| < 1$, $|\lambda| < 1$, where

$$D = ab(1 - \rho^2) + cd(1 - \lambda^2) + ad + bc - 2\sqrt{abcd} \rho \lambda$$

$$N_1 = ac[b(1 - \rho^2) + d(1 - \lambda^2)]$$

$$N_2 = bd[a(1 - \rho^2) + c(1 - \lambda^2)]$$

$$N_3 = \sqrt{abcd} [\sqrt{ab} \lambda(1 - \rho^2) + \sqrt{cd} \rho(1 - \lambda^2)] \quad (J-4)$$

Also, a useful auxiliary relation is

$$N_1 N_2 - N_3^2 = D abcd (1 - \rho^2)(1 - \lambda^2) . \quad (J-5)$$

Now let

$$\rho = \sin(\theta), \quad \text{where } -\frac{\pi}{2} < \theta < \frac{\pi}{2} ,$$

$$\lambda = \sin(\phi), \quad \text{where } -\frac{\pi}{2} < \phi < \frac{\pi}{2} . \quad (J-6)$$

Then the area of the contour ellipse at the $1/e$ relative level of the first exp in (J-2) is

$$A_1 = \frac{2\pi}{\sqrt{ab} \cos(\theta)} \quad (J-7)$$

in the x,y plane, where we used (D-1), (D-19), and (D-20). Similarly, the area of the second exp in (J-2) is

$$A_2 = \frac{2\pi}{\sqrt{cd} \cos(\phi)} . \quad (J-8)$$

The sum of these two effective areas is

$$A_1 + A_2 = 2\pi \frac{\sqrt{ab} \cos(\theta) + \sqrt{cd} \cos(\phi)}{\sqrt{abcd} \cos(\theta) \cos(\phi)} . \quad (J-9)$$

On the other hand, the area of the contour ellipse at the $1/e$ relative level of the smoothed exp in (J-3) is

$$A_3 = 2\pi \frac{\sqrt{D}}{\sqrt{abcd} \cos(\theta) \cos(\phi)} \quad (J-10)$$

in the x,y plane, where we can express D from (J-4) as

$$\begin{aligned} D &= ab \cos^2(\theta) + cd \cos^2(\phi) + ad + bc - 2\sqrt{abcd} \sin(\theta)\sin(\phi) = \\ &= [\sqrt{ab} \cos(\theta) + \sqrt{cd} \cos(\phi)]^2 + |\sqrt{ad} \exp(i\theta) - \sqrt{bc} \exp(i\phi)|^2. \end{aligned} \quad (J-11)$$

Comparison of the square root of (J-11) with the numerator of (J-9) reveals that

$$A_3 \geq A_1 + A_2, \quad (J-12)$$

with equality occurring if and only if

$$\sqrt{ad} = \sqrt{bc} \quad \text{and} \quad \theta = \phi. \quad (J-13)$$

That is, in order for $A_3 = A_1 + A_2$, we must have

$$\frac{d}{c} = \frac{b}{a} \quad \text{and} \quad \lambda = \rho. \quad (J-14)$$

Physically, this requirement states that the contour ellipses of the two exp terms in (J-2) must have the same ratio of major-to-minor axes and they must have the same tilt. If either condition is violated, then $A_3 > A_1 + A_2$, the exact amount depending on the second term in (J-11).

EFFICIENT CALCULATION OF GAUSSIAN FUNCTION

If the general two-dimensional Gaussian function in (J-2) is sampled on an equi-spaced grid, for purposes of convolution, it will be necessary to compute the quantity

$$Q_2(m,n) = \exp(-am^2 - bn^2 - cmn) \quad (J-15)$$

for integers $-M \leq m \leq M$, $-N \leq n \leq N$. The following efficient procedure is based upon the general method given in [12].

We observe first that

$$Q_2(-m, -n) = Q_2(m, n) , \quad (J-16)$$

which cuts the effort by one-half. There also follows

$$Q_2(m, n) = Q_2(m, n-1) Q_1(m, n) , \quad (J-17)$$

where

$$Q_1(m, n) = \exp[-b(2n-1) - cm] = Q_1(m, n-1) \exp(-2b) . \quad (J-18)$$

These recurrences can be started with

$$Q_1(m, 0) = \exp(b - cm) ,$$

$$Q_2(m, 0) = \exp(-am^2) = Q_2(-m, 0) . \quad (J-19)$$

Furthermore, these latter two quantities are available through the recurrence

$$\left. \begin{aligned} Q_1(m, 0) &= Q_1(m-1, 0) \exp(-c) \\ Q_1(m-1, 0) &= Q_1(m, 0) \exp(+c) \end{aligned} \right\} \text{ for } m \geq 1 , \quad (J-20)$$

with

$$Q_1(0,0) = \exp(b) , \quad (J-21)$$

and the recurrence

$$\left. \begin{aligned} Q_2(m,0) &= Q_2(m-1,0) E(m) \\ E(m) &= E(m-1) \exp(-2a) \end{aligned} \right\} \text{ for } m \geq 1 , \quad (J-22)$$

with

$$Q_2(0,0) = 1, \quad E(0) = \exp(a) . \quad (J-23)$$

The only case not covered by the above recurrences is for $m = 0$; then

$$\left. \begin{aligned} Q_2(0,n) &= Q_2(0,n-1) F(n) \\ F(n) &= F(n-1) \exp(-2b) \end{aligned} \right\} \text{ for } n \geq 1 , \quad (J-24)$$

with

$$F(0) = \exp(b) . \quad (J-25)$$

A program for the evaluation of (J-15) is given below. Only three exponentials, in lines 90-110, need to be evaluated. Also, the only storage required is for the final quantity $Q_2(m,n)$ in lines 60-70. The auxiliary variables $Q_1(m,n)$, $E(m)$, $F(n)$ introduced above need never be stored. The check on accuracy in lines 390-470 would be discarded, of course, in any

practical application; it is appended as a check on any typographical errors in entering the program into another computer.

```

10      A=.037                                ! exp(-A m^2 - B n^2 - C m n)
20      B=.051                                ! for -M<=m<=M, -N<=n<=N
30      C=.044
40      M=5
50      N=7
60      REDIM Q2(-M:M,-N:N)
70      DIM Q2(50,50)
80      DOUBLE M,N,Ms,Ns                      ! INTEGERS
90      Ea=EXP(A)
100     Eb=EXP(B)
110     Ec=EXP(C)
120     Q2(0,0)=1.
130     E=Eb
140     E2b=Eb*Eb
150     FOR Ns=1 TO N
160     E=E/E2b
170     Q2(0,Ns)=Q2(0,Ns-1)*E
180     NEXT Ns
190     E=Ea
200     E2a=Ea*Ea
210     Q1po=Q1mo=Eb
220     FOR Ms=1 TO M
230     Q1p=Q1po=Q1po/Ec
240     Q1m=Q1mo=Q1mo*Ec
250     E=E/E2a
260     Q2(-Ms,0)=Q2(Ms,0)=Q2(Ms-1,0)*E
270     FOR Ns=1 TO N
280     Q1p=Q1p/E2b
290     Q1m=Q1m/E2b
300     Q2(Ms,Ns)=Q2(Ms,Ns-1)*Q1p
310     Q2(-Ms,Ns)=Q2(-Ms,Ns-1)*Q1m
320     NEXT Ns
330     NEXT Ms
340     FOR Ms=-M TO M
350     FOR Ns=1 TO N
360     Q2(-Ms,-Ns)=Q2(Ms,Ns)
370     NEXT Ns
380     NEXT Ms
390     Big=0.                                ! MAXIMUM ERROR CHECK
400     FOR Ms=-M TO M
410     FOR Ns=-N TO N
420     E=EXP(-A*Ms*Ms-B*Ns*Ns-C*Ms*Ns)
430     Error=E-Q2(Ms,Ns)
440     Big=MAX(Big,ABS(Error))
450     NEXT Ns
460     NEXT Ms
470     PRINT Big
480     END

```

REFERENCES

1. N. Yen, "Time and Frequency Representation of Acoustic Signals by Means of the Wigner Distribution Function: Implementation and Interpretation," Journal of Acoustical Society of America, vol. 81, no. 6, pp. 1841-1850, June 1987.
2. J. C. Andrieux et al, "Optimum Smoothing of the Wigner-Ville Distribution," IEEE Transactions on Acoustics, Speech, and Signal Processing, vol. ASSP-35, no. 6, pp. 764-768, June 1987.
3. Kai-Bor Yu and S. Cheng, "Signal Synthesis from Pseudo-Wigner Distribution and Applications," IEEE Transactions on Acoustics, Speech, and Signal Processing, vol. ASSP-35, no. 9, pp. 1289-1301, September 1987.
4. P. M. Woodward, Probability and Information Theory, With Applications to Radar, Pergamon Press, New York, NY, 1957.
5. A. H. Nuttall, Accurate Efficient Evaluation of Cumulative or Exceedance Probability Distributions Directly From Characteristic Functions, NUSC Technical Report 7023, Naval Underwater Systems Center, New London, CT, 1 October 1983.
6. D. Gabor, "Theory of Communication," Journal of Institute of Electrical Engineers, vol. 93, part III, pp. 429-457, 1946.
7. L. Cohen, "On a Fundamental Property of the Wigner Distribution Function," IEEE Transactions on Acoustics, Speech, and Signal Processing, vol. ASSP-35, no. 4, pp. 559-561, April 1987.

REFERENCES (Cont'd)

8. L. Cohen and C. A. Pickover, "A Comparison of Joint Time-Frequency Distributions for Speech Signals," IEEE International Symposium on Circuits and Systems, pp. 42-45, August 1986.
9. L. Cohen and T. E. Posch, "Positive Time-Frequency Distribution Functions," IEEE Transactions on Acoustics, Speech, and Signal Processing, vol. ASSP-33, no. 1, pp. 31-38, February 1985.
10. L. Cohen and T. E. Posch, "Generalized Ambiguity Functions," IEEE International Conference on Acoustics, Speech, and Signal Processing, March 26-29, 1985.
11. N. D. Cartwright, "A Non-Negative Wigner-Type Distribution," Physics, vol. 83A, pp. 210-212, 1976.
12. A. H. Nuttall, Efficient Evaluation of Polynomials and Exponentials of Polynomials for Equi-Spaced Arguments, NUSC Technical Report 7995, Naval Underwater Systems Center, New London, CT, 1 April 1987. Also IEEE Transactions on Acoustics, Speech, and Signal Processing, vol. ASSP-35, no. 10, pp. 1486-1487, October 1987.
13. C. W. Helstrom, Statistical Theory of Signal Detection, Second Edition, Pergamon Press, New York, NY, 1968.
14. R. B. Blackman and J. W. Tukey, The Measurement of Power Spectra, Dover Publications, New York, NY, 1959.
15. A. H. Nuttall, A Shortcut in Calculus of Variations for Complex Functions, NUSC Technical Memorandum 2020-179-70, Naval Underwater Systems Center, New London, CT, 21 September 1970.

Technical Report 8317
1 June 1988

**The Wigner Distribution Function
With Minimum Spread**

**A. H. Nuttall
ABSTRACT**

The Wigner distribution function (WDF) with minimum quadratic spread corresponds to a Gaussian amplitude-modulated waveform with linear frequency modulation. The optimum WDF is two-dimensional Gaussian and has contours of equal height which are identical to the penalty contours of the quadratic spread measure employed. An alternative measure of spread, involving an exponential reward for concentration, leads to identically the same optimum waveform and WDF. A generalization to a certain class of smoothed WDFs is also possible and is presented.

The sensitivity of the effective area of a smoothed WDF, to mismatch in shape factor and tilt in the time-frequency plane, is evaluated quantitatively.

Approved for public release; distribution is unlimited.

TABLE OF CONTENTS

	Page
LIST OF ILLUSTRATIONS	ii
LIST OF SYMBOLS	ii
INTRODUCTION	1
MINIMUM QUADRATIC SPREAD	2
Penalty Measure and Spread	3
Derivation of Spread	4
Optimum Weighting	6
Optimum WDF	7
ALTERNATIVE REWARD MEASURE	8
GENERALIZATION TO SMOOTHED WDF	9
SENSITIVITY TO MISMATCH	12
SUMMARY	17
APPENDIX A. MAXIMIZATION OF REWARD VALUE	18
APPENDIX B. MOMENTS OF DISTRIBUTION D	27
APPENDIX C. GENERAL TILTED ELLIPSE	31
APPENDIX D. KERNEL APPROACH TO PENALTY FUNCTION	36
REFERENCES	40

LIST OF ILLUSTRATIONS

Figure		Page
1	Contour Ellipses for Mismatched Tilt	15
2	Area Ratio (34) for $F_1 = 2$, $F_2 = 2$, $A_2 = 2$, $\beta_1 = \pi/4$	15
3	Contour Ellipses for Mismatched Shape Factor	16
4	Area Ratio (34) for $F_1 = 2$, $A_2 = 2$, $\beta_1 = \pi/4$, $\beta_2 = \pi/4$	16
C-1	Rotated Coordinate Axes	31

LIST OF SYMBOLS

WDF	Wigner distribution function
t	time
f	frequency
s(t)	waveform analyzed, (1)
u(t)	weighting function, (1)
S_u	short-term spectral estimate, (1)
W_s	WDF of s(t), (1)
W_u	WDF of u(t), (1), (2)
\otimes	convolution, (1)
δ	delta function
P(t,f)	penalty measure, (3)
a,b,c	parameters of P, (3)
I	spread of WDF W_u , (4)

LIST OF SYMBOLS (Cont'd)

Q	real constant, (5)
$u'(t)$	derivative of $u(t)$ with respect to t , (10)
B	complex constant, (11)
$T(t)$	temporary auxiliary function, (13)
$u_0(t)$	optimum weighting, (20)
I_0	minimum spread, (21)
W_0	optimum WDF, (22)
D	generalized smoothing distribution, (23)
V_2	smoothing function, (23)
v	frequency separation variable, (23), (24)
τ	time separation variable, (23), (24)
χ_u	complex ambiguity function of u , (24)
q_2	double Fourier transform of V_2 , (25)
superscript v	partial derivative with respect to v , (27)
superscript τ	partial derivative with respect to τ , (27)
I_D	spread of distribution D , (30)
$R(t,f)$	reward function, (22A), (A-1)
V	reward value, (22B), (A-5)
$K(x,y)$	Hermitian kernel, (A-11), (A-12)
λ_n	eigenvalue, (A-12)
$\phi_n(x)$	eigenfunction, (A-12)
$He_n(x)$	Hermite polynomial, (A-27)
A	area of ellipse, figure C-1
B	tilt of ellipse, figure C-1
F	shape factor of ellipse, (C-4)

THE WIGNER DISTRIBUTION FUNCTION WITH MINIMUM SPREAD

INTRODUCTION

A number of advantageous features associated with smoothing a Wigner distribution function (WDF) were discussed in a recent report [1]. At that time, it was shown that the WDF with minimum quadratic spread, about the line $f = B_c t$ in the time-frequency plane, was a two-dimensional Gaussian function, when constraints of finite energy and mean-square duration were imposed [1, app. G]. However, a more appropriate measure of spread about the origin in the t, f plane is adopted here and minimized, yielding a unique waveform and corresponding WDF. Additionally, a reward measure for concentration is shown to yield identically the same optimum WDF.

An additional property of smoothing two-dimensional WDFs was also demonstrated; namely, if two Gaussian mountains are doubly-convolved with each other, the effective area of the result is greater than the sum of the two effective areas, unless the contours of both WDFs have the same tilt and ratio of major-to-minor axes [1, app. J]. A quantitative investigation of the effect of mismatch in these parameters on the effective area is conducted herein.

It is assumed that the reader is familiar with the content and approach of the earlier report; accordingly, this follow-on effort will be briefer and will not review the considerable history and background of the WDF.

MINIMUM QUADRATIC SPREAD

It was shown in [1, (102) and (106)] that the short-term spectral estimate is equal to the double convolution of the WDF of the waveform $s(t)$ being analyzed with the WDF of the weighting $u(t)$ employed. That is,

$$\begin{aligned} |S_u(t, f)|^2 &\equiv \left| \int dt_1 \exp(-i2\pi f t_1) s(t_1) u^*(t - t_1) \right|^2 = \\ &= \iint dt_1 df_1 W_s(t_1, f_1) W_u(t - t_1, f - f_1) = W_s(t, f) \stackrel{tf}{\otimes} W_u(t, f), \end{aligned} \quad (1)$$

where \otimes denotes convolution. Here,

$$W_u(t, f) = \int d\tau \exp(-i2\pi f \tau) u(t + \frac{\tau}{2}) u^*(t - \frac{\tau}{2}) \quad (2)$$

is the WDF of complex weighting $u(t)$; a similar definition holds for WDF W_s . (Generalizations to non-Wigner smoothing functions for W_u are given in [1, app. F].)

Since the WDF W_s of waveform $s(t)$ has some good energy localization properties (and some deleterious negative oscillations), it is desired that the smearing in the t, f plane, implied by convolution (1), be minimized. That is, we would like WDF W_u of weighting $u(t)$ to be as concentrated as possible about the origin of the t, f plane. The ideal of an impulse, $\delta(t)\delta(f)$, is not a legal WDF, and must be discarded. Since the left-hand side of (1) can never be negative, we can be assured, by this smoothing procedure of two WDFs, that we will always get a physically-meaningful distribution in the t, f plane; that is, the smoothed distribution will always be non-negative for all t, f and have a volume equal to the energy of waveform $s(t)$, ^{when $u(t)$ has unit energy.} For example, see [1, (111) et seq.].

PENALTY MEASURE AND SPREAD

In order to confine WDF W_u near the origin, we define a penalty measure which is zero at $t, f = 0, 0$ and which increases quadratically with t and f . Namely, the penalty measure is

$$P(t, f) = a^2 t^2 + 4\pi^2 b^2 f^2 + 4\pi c t f, \quad a, b, c \text{ real}, \quad (3)$$

and the corresponding spread of the WDF W_u is defined as

$$I = \iint dt df W_u(t, f) P(t, f). \quad (4)$$

Contours of equal penalty in (3) are tilted ellipses in the t, f plane; these would be selected upon observation of a calculated WDF W_s of waveform $s(t)$ in regions of interest, i.e., high activity.

Therefore, real constants a, b, c are presumed known. Define quantity

$$Q = a^2 b^2 - c^2. \quad (5)$$

Then, in order that penalty

$$P(t, f) > 0 \quad \text{for} \quad t, f \neq 0, 0, \quad (6)$$

it is necessary that

$$Q > 0. \quad (7)$$

The property (6) was not satisfied by penalty function $(f - \beta_c t)^2$ in [1, app. G]; that function was zero all along the line $f = \beta_c t$, allowing the WDF to become impulsive there.

We also want WDF W_u in (1) and (4) to have unit volume, for two reasons. First of all, this will guarantee that the short-term spectral estimate on the left-hand side of (1) will have a volume equal to the signal energy, regardless of weighting $u(t)$ employed. Secondly, without this volume constraint, $u(t)$ and W_u would collapse to zero, giving a meaningless spread value of $I = 0$ in (4). Thus we require that

$$1 = \iint dt df W_u(t, f) = \int dt |u(t)|^2. \quad (8)$$

Subject to this integral constraint, we want to minimize spread I in (4), and find the particular weighting $u(t)$ and corresponding optimum WDF W_u . Notice that we are imposing no constraint of positivity on W_u .

DERIVATION OF SPREAD

Substitute (3) into (4) to get spread

$$I = \iint dt df W_u(t, f) (a^2 t^2 + 4\pi^2 b^2 f^2 + 4\pi c t f), \quad (9)$$

where WDF W_u is given in terms of $u(t)$ according to (2). By using the results in [1, (G-4) and (G-5)], we can express (9) solely in the time domain as

$$\begin{aligned} I &= a^2 \int dt t^2 |u(t)|^2 + b^2 \int dt |u'(t)|^2 + 2c \int dt t \operatorname{Im}\{u'(t) u^*(t)\} = \\ &= \int dt [a^2 t^2 |u(t)|^2 + b^2 |u'(t)|^2 + ict u(t) u'^*(t) - ict u^*(t) u'(t)]. \end{aligned} \quad (10)$$

For reasons to become apparent shortly, define complex constant

$$B = \frac{\sqrt{Q} + ic}{b^2}; \quad (11)$$

then, by using (5), we find

$$b^2 |B|^2 = a^2 . \quad (12)$$

Now consider the quantity

$$\begin{aligned} T(t) &\equiv b^2 |u'(t) + Bt u(t)|^2 = \\ &= b^2 |u'(t)|^2 + b^2 |B|^2 t^2 |u(t)|^2 + b^2 Bt u(t) u'^*(t) + b^2 B^* t u^*(t) u'(t) = \\ &= b^2 |u'(t)|^2 + a^2 t^2 |u(t)|^2 + (\sqrt{Q} + ic)t u(t) u'^*(t) + \\ &\quad + (\sqrt{Q} - ic)t u^*(t) u'(t) . \end{aligned} \quad (13)$$

Comparison of (10) and (13) immediately reveals that

$$\int dt T(t) = I + \sqrt{Q} \int dt t [u(t) u'^*(t) + u^*(t) u'(t)] . \quad (14)$$

We now integrate by parts, letting

$$U = t u(t), \quad dV = dt u'^*(t) , \quad (15)$$

to find that

$$\begin{aligned} \int dt t u(t) u'^*(t) &= - \int dt [u(t) + t u'(t)] u^*(t) = \\ &= - \int dt |u(t)|^2 - \int dt t u'(t) u^*(t) . \end{aligned} \quad (16)$$

We presume that $u(t)$ goes to zero at $t = \pm\infty$, consistent with energy constraint (8).

When (16) is employed in (14), there follows

$$\int dt T(t) = I - \sqrt{Q} \int dt |u(t)|^2 . \quad (17)$$

Thus the desired expression for spread I is given by (17) and (13) as

$$I = b^2 \int dt |u'(t) + Bt u(t)|^2 + \sqrt{Q} \int dt |u(t)|^2. \quad (18)$$

This general result holds for any weighting $u(t)$; it is obviously positive in all cases, since $Q > 0$.

OPTIMUM WEIGHTING

The last term in (18) cannot be altered; it is equal to \sqrt{Q} , as seen by reference to constraint (8). Furthermore, the minimum value for the remaining term in (18) is zero and is obtained for weighting $u(t)$ which satisfies the differential equation

$$u'(t) + Bt u(t) = 0 \quad \text{for all } t. \quad (19)$$

The only solution to (19) is

$$u_0(t) = A \exp\left(-\frac{1}{2} Bt^2\right) \quad \text{for all } t, \quad (20)$$

where complex constant A is chosen for unit energy, and B is given by (11). That is, $u_0(t)$ has Gaussian amplitude-modulation and linear frequency-modulation. The phase of A is ambiguous.

The resultant minimum value of spread I in (18) is obviously

$$I_0 = \sqrt{Q} = \sqrt{a^2 b^2 - c^2}, \quad (21)$$

where we employed (5). It is always positive, as seen by reference to requirements (6) and (7).

OPTIMUM WDF

The WDF corresponding to optimum weighting (20) is obtained by substitution in (2), and use of [1, (H-17) and (H-18)], as

$$W_0(t,f) = 2 \exp \left[- \frac{a^2 t^2 + 4\pi^2 b^2 f^2 + 4\pi c t f}{\sqrt{Q}} \right]. \quad (22)$$

The area of the contour ellipse at the $1/e$ relative level is $1/2$ in the t, f plane, as expected.

Observe that the numerator of the exp in (22) is identically the quadratic penalty function $P(t,f)$ imposed in (3). That is, the contours of optimum WDF (22) are identical to the contours of equal penalty of $P(t,f)$ in (3). This result is intuitively satisfying: the optimum WDF packs as much volume inside a given penalty contour as possible, to the extent that the resultant WDF values are equal all along that given penalty contour.

Observe also, that although positivity of the WDF W_u was not imposed as a constraint in the minimization of spread I in (4) or (9), the resultant optimum WDF in (22) is, in fact, everywhere positive. Although the optimum weighting (20) has an ambiguous phase, the optimum WDF has no ambiguity; there is a unique optimum WDF, namely (22).

ALTERNATIVE REWARD MEASURE

Instead of penalizing the spread of WDF W_u about the origin in t, f space, we could alternatively utilize a measure which rewards concentration about $t, f = 0, 0$. In particular, consider reward function

$$R(t, f) = \exp[-a^2 t^2 - 4\pi^2 b^2 f^2 - 4\pi c t f] \quad (22a)$$

and reward value

$$V = \iint dt df R(t, f) W_u(t, f) \quad (22b)$$

for WDF W_u . The origin value of $R(t, f)$ is 1; in order for $R(t, f)$ to decay to zero as t and/or f tend to infinity, we must have condition (7) satisfied again. Notice that the contours of equal reward are ellipses in the t, f plane.

The maximization of reward value V , subject to volume constraint (8) on W_u , is conducted in appendix A. It is shown there that the optimum weighting is again (20), and that the optimum WDF is (22). The maximum value of reward V is

$$V_{\max} = \frac{1}{1 + \sqrt{Q}} = \frac{1}{1 + \sqrt{a^2 b^2 - c^2}}. \quad (22c)$$

More general results, for arbitrary reward functions $R(t, f)$ in (22b), are presented in appendix A.

GENERALIZATION TO SMOOTHED WDF

A general class of distributions* has been presented in [2, (1.7) and (1.8)]. In current notation, that class is given by [1, (F-1)] as

$$D(t,f) \equiv W_u(t,f) \overset{tf}{\otimes} V_2(t,f) = \iint dv d\tau \exp(i2\pi vt - i2\pi f\tau) \chi_u(v,\tau) q_2(v,\tau) , \quad (23)$$

where WDF W_u is given by (2), and $V_2(t,f)$ is a general two-dimensional smoothing function. The complex ambiguity function of $u(t)$ is

$$\chi_u(v,\tau) = \int dt \exp(-i2\pi vt) u(t + \frac{\tau}{2}) u^*(t - \frac{\tau}{2}) , \quad (24)$$

while

$$q_2(v,\tau) = \iint dt df \exp(-i2\pi vt + i2\pi f\tau) V_2(t,f) \quad (25)$$

is a double Fourier transform of the smoothing function V_2 . Observe that if there is no smoothing, then

$$V_2(t,f) = \delta(t) \delta(f)$$

$$q_2(v,\tau) = 1 \text{ for all } v,\tau$$

$$D(t,f) = W_u(t,f) . \quad (26)$$

*This section is based upon a suggestion by Leon Cohen, Hunter College, New York, NY, that the optimum WDF results here actually apply to a wider class of distributions.

Now it is shown in appendix B that the following second moments of generalized smoothing distribution D can be expressed in terms of derivatives of χ_u and q_2 at the origin:

$$\begin{aligned} \iint dt df t^2 D(t,f) &= -\frac{1}{4\pi^2} [\chi_u^{vv}(0,0) q_2(0,0) + 2\chi_u^v(0,0) q_2^v(0,0) + \\ &\quad + \chi_u(0,0) q_2^{vv}(0,0)] , \\ \iint dt df t f D(t,f) &= \frac{1}{4\pi^2} [\chi_u^{\tau v}(0,0) q_2(0,0) + \chi_u^{\tau}(0,0) q_2^v(0,0) + \\ &\quad + \chi_u^v(0,0) q_2^{\tau}(0,0) + \chi_u(0,0) q_2^{v\tau}(0,0)] , \\ \iint dt df f^2 D(t,f) &= -\frac{1}{4\pi^2} [\chi_u^{\tau\tau}(0,0) q_2(0,0) + 2\chi_u^{\tau}(0,0) q_2^{\tau}(0,0) + \\ &\quad + \chi_u(0,0) q_2^{\tau\tau}(0,0)] . \end{aligned} \quad (27)$$

Here, for example, superscript v denotes a partial derivative with respect to v , which is then evaluated at the origin, $v, \tau = 0, 0$.

It follows immediately that if origin value

$$q_2(0,0) = 1 , \quad (28)$$

and if the five origin derivatives

$$q_2^v(0,0) = q_2^{\tau}(0,0) = q_2^{vv}(0,0) = q_2^{v\tau}(0,0) = q_2^{\tau\tau}(0,0) = 0 , \quad (29)$$

then (27) reduces to the moments that would have resulted from employing the no-smoothing result (26) in (27). Thus, distributions $D(t,f)$ resulting from (23), with properties (28) and (29) for q_2 , have the same second moments

as the WDF $W_u(t,f)$. Hence, the spread I_D of distribution $D(t,f)$ is given by (see (9))

$$\begin{aligned} I_D &= \iint dt df D(t,f) (a^2 t^2 + 4\pi^2 b^2 f^2 + 4\pi c t f) = \\ &= \iint dt df W_u(t,f) (a^2 t^2 + 4\pi^2 b^2 f^2 + 4\pi c t f) = I, \end{aligned} \quad (30)$$

which is exactly the spread I of WDF $W_u(t,f)$. That is, smoothed distribution $D(t,f)$ in (23) has the same spread as WDF $W_u(t,f)$, when smoothing function $V_2(t,f)$ (actually transform q_2) satisfies the properties in (28) and (29). Notice that these properties are considerably less restrictive than requiring

$$q_2(v,0) = q_2(0,\tau) = 1 \quad \text{for all } v, \tau, \quad (31)$$

which arises when one is interested in maintaining the marginals [2, (1.6)].

We must also observe from (23) that the volume under generalized smoothing distribution D is equal to the product of the volume under W_u and the volume under V_2 . But the latter quantity is unity, by virtue of (28). What all this means is, that if we minimize spread I_D in (30), subject to a unit volume constraint on D , the end result is precisely (18) and (20), and the optimum WDF W_u is again given by (22). The corresponding distribution D is obtained by substitution of (22) into (23) and specification of the complete V_2 or q_2 functions. The properties in (28) and (29) are not sufficient to completely specify q_2 or D ; all that is specified by (28) and (29) are the second order moments of D in (27). It should also be noted that all the conditions in (29) cannot be met by the general tilted Gaussian q_2 function employed in [1, (F-9) and sequel to (F-12)].

SENSITIVITY TO MISMATCH

In [1, app. J], it was shown that if two Gaussian mountains are doubly-convolved in x, y space, the effective area A_3 of the resultant is greater than the sum of the individual areas, except when the two elliptical contours have the same tilt and the same ratio of major-to-minor axis (shape factor). Here, we wish to investigate, quantitatively, the increase in effective area above the minimum value, when the tilt and shape factors are not at their optimum values. This situation can arise when observation of WDF W_s of waveform $s(t)$ is contaminated, in a particular region of interest in the t, f plane, by interference effects, thereby making estimation of the tilt and the shape factor of the elliptical contours somewhat inaccurate.

The general situation is considered mathematically in appendix C. Ellipse 1 has

$$\text{area } A_1, \text{ tilt } \beta_1, \text{ shape factor } F_1, \quad (32)$$

while ellipse 2 has

$$\text{area } A_2, \text{ tilt } \beta_2, \text{ shape factor } F_2. \quad (33)$$

The ratio

$$\frac{A_3}{A_1 + A_2} \quad (34)$$

is presented in (C-13) in terms of a number of auxiliary quantities.

The initial example we consider is where ellipse 1 has seven different areas, namely

$$A_1 = .5, 1, 2, 3, 4, 5, 6 \quad \beta_1 = \frac{\pi}{4} \quad F_1 = 2. \quad (35)$$

The tilt is fixed at $\pi/4$ radians and the shape factor at 2. On the other hand, ellipse 2 has

$$A_2 = 2 \quad \beta_2 = -\frac{\pi}{4} \text{ to } \frac{\pi}{4} \quad F_2 = 2. \quad (36)$$

That is, the shape factor is perfect at $F_2 = F_1 = 2$, but the tilt is swept over a $\pi/2$ range (greater discrepancies than $\pi/2$ lead to obvious periodicities and symmetries centered about $\beta_2 = \beta_1$ as well as about $\beta_2 = \beta_1 \pm \pi/2$ and about $\beta_2 = \beta_1 + \pi$). The situation under investigation is depicted in figure 1, where ellipse 2 is dotted.

The effect of mismatch in tilt is presented quantitatively in figure 2. As expected, ratio (34) is 1 at $\beta_2 = \beta_1 = \pi/4$, regardless of area A_1 . The most degradation (upper-most curve) is realized for $A_1 = 2$, i.e., when the areas of the two ellipses are equal. The maximum increase in area is only 25 percent, when β_2 is off by $\pi/2$ radians; however, if the shape factor is significantly larger than 1, the sensitivity to the tilt would be much greater, as figure 1 shows.

The final example utilizes the exact same parameter values as (35) for ellipse 1, while ellipse 2 has

$$A_2 = 2 \quad \beta_2 = \frac{\pi}{4} \quad F_2 = 2 \text{ to } 6. \quad (37)$$

Now the tilt is perfect at $\beta_2 = \beta_1 = \pi/4$, but the shape factor F_2 varies above the best value of 2. The situation is depicted in figure 3, where ellipse 2 is again dotted.

Ratio (34) is plotted in figure 4 versus the shape factor F_2 . Again, the upper-most curve corresponds to the case where $A_1 = A_2 = 2$. There is no need to compute ratio (34) for $F_2 < F_1 = 2$, because the values for $F_2 = F_1 r$ are the same as those for $F_2 = F_1/r$. Additional cases of interest can be investigated by use of the program listed in appendix C.

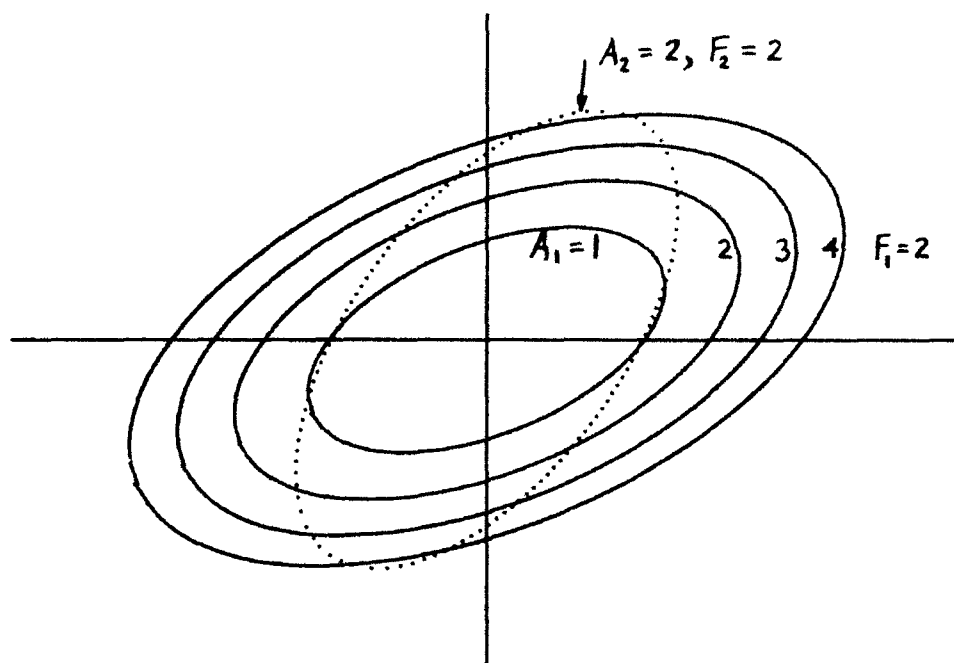
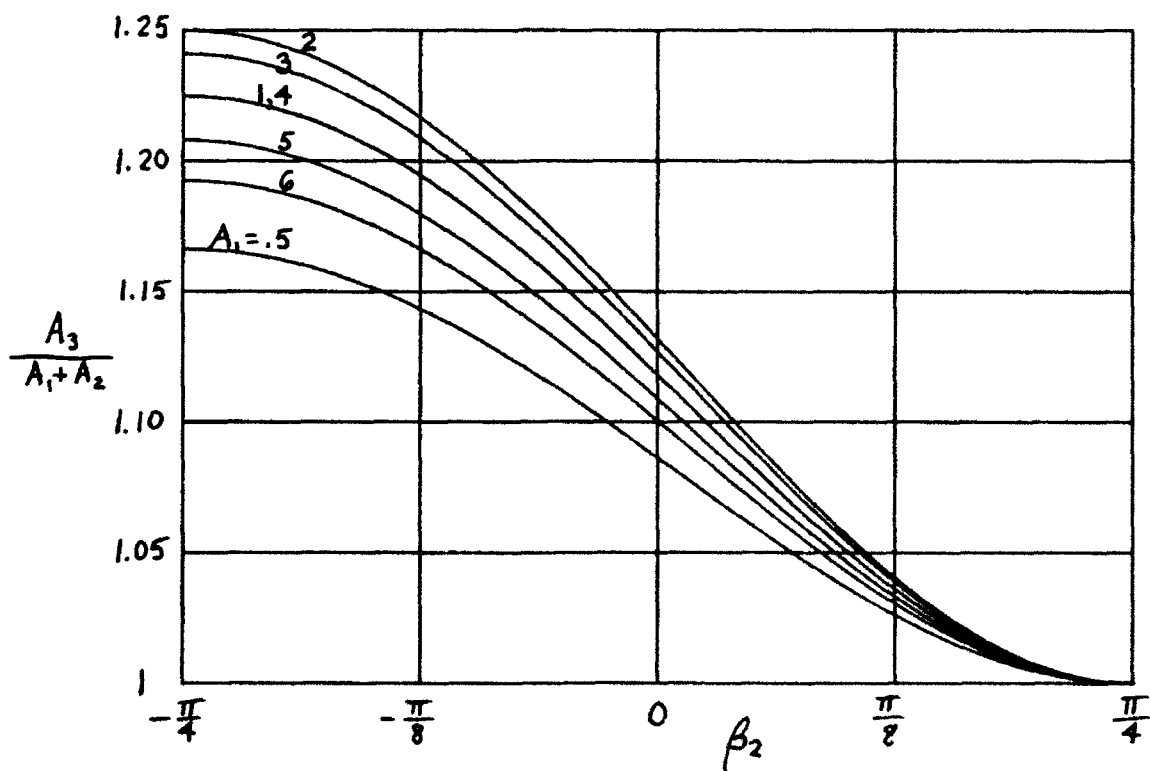


Figure 1. Contour Ellipses for Mismatched Tilt

Figure 2. Area Ratio (34) for $F_1 = 2$, $F_2 = 2$, $A_2 = 2$, $\beta_1 = \pi/4$

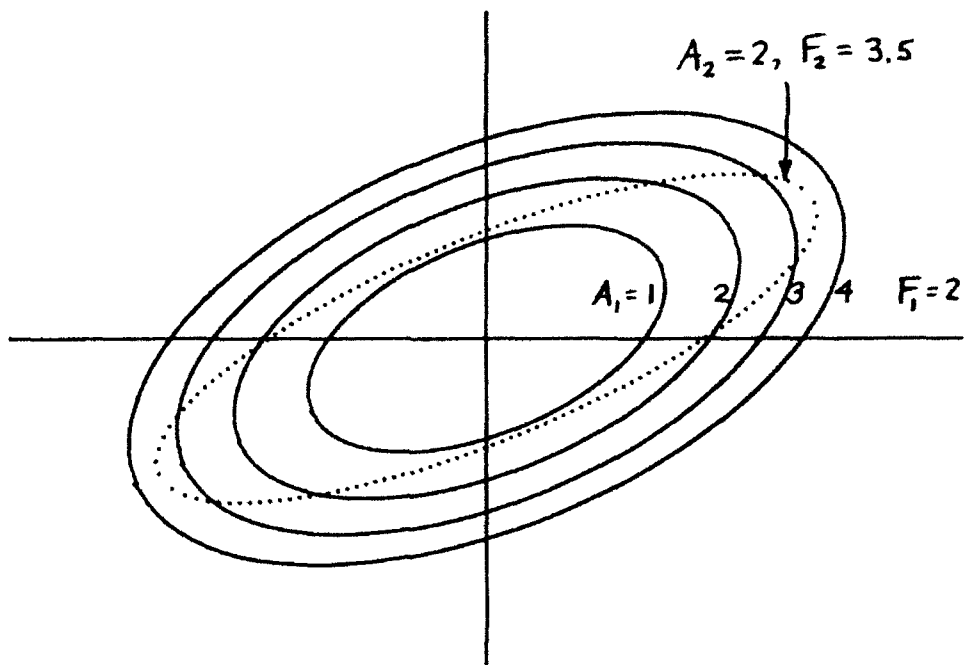


Figure 3. Contour Ellipses for Mismatched Shape Factor

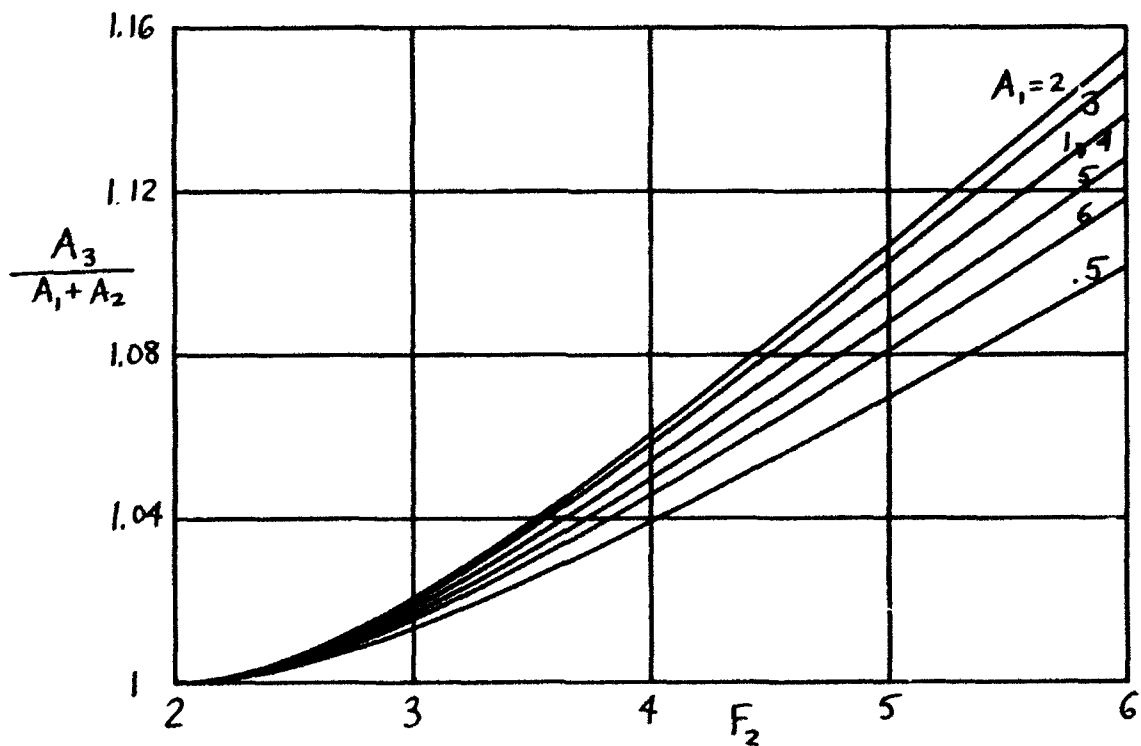


Figure 4. Area Ratio (34) for $F_1 = 2$, $A_2 = 2$, $\beta_1 = \pi/4$, $\beta_2 = \pi/4$

SUMMARY

The most compact WDF W_u that can be used for two-dimensional smoothing of a measured WDF W_s is a Gaussian function in two variables, when the measure of spread is quadratic in the time and frequency variables t and f , or the reward measure is exponential. Furthermore, this two-dimensional convolution guarantees a non-negative modified distribution, since the result is equivalent to a short-term spectral estimate. Extensions to a particular class of generalized distributions yields the same optimum WDF. The corresponding waveform has Gaussian amplitude modulation and linear frequency-modulation.

The additional smearing caused by mismatched smoothing functions to the true parameters of a measured WDF has been investigated numerically for a few examples, and found not to be overly sensitive to the exact values. However, the multitude of parameters has prevented simplification of the area spread factor; accordingly, a program allowing calculation of particular cases is included to allow for further investigation.

The WDFs for the Hermite functions of order n are given in closed form, in terms of a Laguerre polynomial of order n . This result is extended to cross-WDFs in appendix A; in this manner, we can investigate the WDF of an arbitrary waveform when expanded in a weighted sum of Hermite functions, including linear frequency-modulation.

APPENDIX A. MAXIMIZATION OF REWARD VALUE

We want to find that WDF, $W_u(t,f)$, which is maximally concentrated about the origin in t,f space, where the measure of reward for concentration is

$$R(t,f) = \exp[-a^2 t^2 - 4\pi^2 b^2 f^2 - 4\pi c t f] , \quad a,b,c \text{ real} . \quad (\text{A-1})$$

Thus, the maximum reward occurs at the origin,

$$R(0,0) = 1 , \quad (\text{A-2})$$

and the contours of equal reward are ellipses in the t,f plane. In order for $R(t,f)$ to decay to zero as t and/or f tend to infinity, we must have

$$Q > 0 , \quad (\text{A-3})$$

where

$$Q = a^2 b^2 - c^2 . \quad (\text{A-4})$$

The reward value associated with WDF W_u is the real quantity

$$V = \iint dt df R(t,f) W_u(t,f) , \quad (\text{A-5})$$

which we wish to maximize, where

$$W_u(t,f) = \int d\tau \exp(-i2\pi f\tau) u(t + \frac{\tau}{2}) u^*(t - \frac{\tau}{2}) \quad (\text{A-6})$$

in terms of weighting $u(t)$. We must constrain the volume of W_u , in order that V in (A-5) not tend to infinity as $u(t)$ is simply increased in level. Thus, we have integral constraint

$$1 = \iint dt df W_u(t,f) = \int dt |u(t)|^2 . \quad (\text{A-7})$$

ALTERNATIVE FORM FOR V

If we substitute (A-6) in (A-5), there follows

$$V = \iint dt d\tau r(t, \tau) u(t + \frac{\tau}{2}) u^*(t - \frac{\tau}{2}) , \quad (A-8)$$

where

$$r(t, \tau) = \int df \exp(-i2\pi f\tau) R(t, f) . \quad (A-9)$$

A more useful alternative form for (A-8) is

$$V = \iint dx dy K(x, y) u(x) u^*(y) , \quad (A-10)$$

where kernel

$$K(x, y) = r\left(\frac{x+y}{2} , x-y\right) . \quad (A-11)$$

EIGENFUNCTIONS OF K

In this and the following subsection, kernel K is Hermitian, but otherwise arbitrary; it is not limited to form (A-11) with (A-9) and (A-1). Suppose $\{\lambda_n\}$ and $\{\phi_n\}$ are the eigenvalues and eigenfunctions of kernel K; i.e.,

$$\int dx K(x, y) \phi_n(x) = \lambda_n \phi_n(y) \quad \text{for } n = 0, 1, 2, \dots , \quad (A-12)$$

where $\lambda_0 \geq \lambda_1 \geq \lambda_2 \dots$, and

$$\int dx \phi_n^*(x) \phi_m(x) = \delta_{nm} . \quad (A-13)$$

Then the kernel can be expanded according to

$$K(x,y) = \sum_{n=0}^{\infty} \lambda_n \phi_n^*(x) \phi_n(y) . \quad (A-14)$$

Also, there follows immediately

$$\iint dx dy K(x,y) \phi_n(x) \phi_n^*(y) = \lambda_n . \quad (A-15)$$

EXPANSION OF u

Suppose we expand weighting u in a series of eigenfunctions of Hermitian kernel K :

$$u(x) = \sum_{n=0}^{\infty} g_n \phi_n(x) , \quad \text{where } g_n = \int dx u(x) \phi_n^*(x) . \quad (A-16)$$

Then general reward expression V in (A-10) becomes

$$\begin{aligned} V &= \int dy u^*(y) \int dx K(x,y) \sum_{n=0}^{\infty} g_n \phi_n(x) = \\ &= \sum_{n=0}^{\infty} g_n \int dy u^*(y) \lambda_n \phi_n(y) = \sum_{n=0}^{\infty} |g_n|^2 \lambda_n , \end{aligned} \quad (A-17)$$

where we used (A-12) and (A-16). At the same time, the energy of u in (A-16) is

$$E_u = \int dx |u(x)|^2 = \sum_{n=0}^{\infty} |g_n|^2 . \quad (A-18)$$

Now if the energy E_u of u is constrained at 1, as in (A-7), then the best choice of coefficients $\{g_n\}$ to maximize V in (A-17) is, since $\lambda_0 \geq \lambda_1 \geq \lambda_2 \dots$, obviously

$$|g_0| = 1 \quad \text{and} \quad g_n = 0 \quad \text{for} \quad n \geq 1. \quad (\text{A-19})$$

That is, the optimum weighting is

$$u_0(x) = \phi_0(x) \exp(i\theta), \quad (\text{A-20})$$

where constant θ is arbitrary, while the maximum reward is

$$V_{\max} = \lambda_0. \quad (\text{A-21})$$

That is, the zero-th order eigenvalue and eigenfunction of general Hermitian kernel K in (A-12) are the solutions to the problem of interest here, namely maximization of reward value V in (A-10) by choice of weighting u . For a general kernel, a recursive numerical procedure could be employed on (A-12) to determine λ_0 and ϕ_0 , if desired.

The formulation in these last two subsections is actually general enough to cover the earlier penalty function considered in (3) et seq. The only difference is that the eigenvalues $\{\lambda_n\}$ now increase with n , and we must select the eigenfunction corresponding to the minimum eigenvalue, in order to realize the least penalty. This approach is the subject of appendix D.

SPECIAL CASE OF EXPONENTIAL REWARD

We now specialize the general results of the previous two subsections to the reward function (A-1). Substitution in (A-9) and use of (A-4) yields

$$r(t, \tau) = \frac{1}{2\sqrt{\pi} b} \exp \left[-\frac{Qt^2 + \frac{1}{4}\tau^2 - ict\tau}{b^2} \right]; \quad (\text{A-22})$$

compare [1, (F-9) and (F-12)]. Then (A-11) immediately gives Hermitian kernel

$$K(x, y) = \frac{1}{2\sqrt{\pi} b} \exp \left[-\frac{x^2 D^* + y^2 D + 2xy(Q-1)}{4b^2} \right], \quad (\text{A-23})$$

where

$$D = Q + 1 + i2c. \quad (\text{A-24})$$

At this point, we refer to Mehler's expansion [3, (67)] to obtain (after some labor)

$$K(x, y) = \sum_{n=0}^{\infty} \lambda_n \phi_n^*(x) \phi_n(y), \quad (\text{A-25})$$

where

$$\lambda_n = \frac{(1 - \sqrt{Q})^n}{(1 + \sqrt{Q})^{n+1}}, \quad (\text{A-26})$$

$$\phi_n(x) = A \exp \left[-\frac{x^2}{2} \frac{\sqrt{Q} + ic}{b^2} \right] \frac{1}{\sqrt{n!}} \text{He}_n \left(2^{1/2} Q^{1/4} x/b \right), \quad (\text{A-27})$$

and

$$|A|^2 = \frac{Q^{1/4}}{\sqrt{\pi} b}. \quad (\text{A-28})$$

The function $He_n(x)$ is the Hermite polynomial [4, 22.2.15]. It is easily verified that (A-27) satisfies orthonormality relation (A-13).

OPTIMUM WEIGHTING

Since $Q > 0$ by (A-3), the eigenvalues in (A-26) satisfy $\lambda_0 > \lambda_1 > \lambda_2 \dots$. Therefore, the maximum reward is

$$V_{\max} = \lambda_0 = \frac{1}{1 + \sqrt{Q}} = \frac{1}{1 + \sqrt{a^2 b^2 - c^2}}, \quad (\text{A-29})$$

and the corresponding weighting is

$$u_0(t) = \phi_0(t) = A \exp \left[-\frac{t^2}{2} \frac{\sqrt{Q} + ic}{b^2} \right] \quad (\text{A-30})$$

from (A-27) and (A-28). This is identical to (20) combined with (11). Therefore the optimum WDF is again (22) for reward measure (A-1), as well as penalty measure (3). The waveform in (A-30) has Gaussian amplitude modulation and linear frequency-modulation.

HIGHER-ORDER HERMITE FUNCTIONS

For $n > 0$, the reward values $\{\lambda_n\}$ in (A-26) are all less than optimum value λ_0 . We have succeeded in obtaining these explicit values without having to evaluate the WDFs of the corresponding Hermite waveforms in (A-27). We now rectify this situation. The WDF of $\phi_n(t)$ in (A-27) is given by integral

$$\begin{aligned}
W_n(t, f) &= \int d\tau \exp(-i2\pi f\tau) \phi_n(t + \frac{\tau}{2}) \phi_n^*(t - \frac{\tau}{2}) = \\
&= \frac{|A|^2}{n!} \int d\tau \exp \left[-i2\pi f\tau - \frac{1}{2} B \left(t + \frac{\tau}{2} \right)^2 - \frac{1}{2} B^* \left(t - \frac{\tau}{2} \right)^2 \right] * \\
&\quad * \text{He}_n \left(F \left(t + \frac{\tau}{2} \right) \right) \text{He}_n \left(F \left(t - \frac{\tau}{2} \right) \right), \tag{A-31}
\end{aligned}$$

where

$$B = \frac{\sqrt{Q} + ic}{b^2}, \quad F = \frac{2^{1/2} Q^{1/4}}{b}, \quad |A|^2 = \frac{Q^{1/4}}{\sqrt{\pi} b}. \tag{A-32}$$

Now a more general integral result already exists in closed form; from [5, p. 292, (30)], we have, in a form more useful for present purposes,

$$\begin{aligned}
&\int dx \exp \left(-\frac{1}{2} x^2 + ax \right) \text{He}_m(b+x) \text{He}_n(b-x) = \\
&= \sqrt{2\pi} (-1)^m m! (b-a)^{n-m} L_m^{(n-m)}(b^2 - a^2) \exp(a^2/2) \quad \text{for } m \leq n, \tag{A-33}
\end{aligned}$$

where $L_m^{(\alpha)}(x)$ is the generalized Laguerre polynomial [4, 22.2.12]. When (A-33) is used on (A-32), there follows, for the WDF of waveform $\phi_n(t)$ in (A-27), the compact result

$$W_n(t, f) = (-1)^n 2 L_n(2U) \exp(-U), \tag{A-34}$$

where

$$U = \frac{a^2 t^2 + 4\pi^2 b^2 f^2 + 4\pi c t f}{\sqrt{Q}}. \tag{A-35}$$

This result reduces to (22) for $n = 0$. Again, contours of equal values of the WDF are ellipses in the t, f plane.

CROSS-WDFs

Suppose a general waveform $u(t)$ is expanded in a set of orthonormal Hermite functions with linear frequency-modulation (α positive real, β real)

$$\phi_n(t) = \left(\frac{\alpha}{\pi}\right)^{1/4} \exp\left[-\frac{1}{2}(\alpha + i\beta)t^2\right] \text{He}_n(\sqrt{2\alpha}t)/\sqrt{n!}, \quad (\text{A-36})$$

according to

$$u(t) = \sum_{n=0}^{\infty} u_n \phi_n(t). \quad (\text{A-37})$$

Then the WDF of $u(t)$ becomes

$$\begin{aligned} W_u(t, f) &= \int d\tau \exp(-i2\pi f\tau) u\left(t + \frac{\tau}{2}\right) u^*\left(t - \frac{\tau}{2}\right) = \\ &= \sum_{m, n=0}^{\infty} u_m u_n^* W_{mn}(t, f), \end{aligned} \quad (\text{A-38})$$

where cross-WDF

$$W_{mn}(t, f) = \int d\tau \exp(-i2\pi f\tau) \phi_m\left(t + \frac{\tau}{2}\right) \phi_n^*\left(t - \frac{\tau}{2}\right). \quad (\text{A-39})$$

When (A-36) is substituted in (A-39), and (A-33) is utilized, the cross-WDF can be expressed as

$$W_{mn}(t, f) = 2(-1)^m \sqrt{\frac{m!}{n!}} z^{n-m} L_m^{(n-m)}(|z|^2) \exp(-|z|^2/2) \text{ for } m \leq n, \quad (\text{A-40})$$

where

$$\begin{aligned} z &= \sqrt{\frac{2}{\alpha}} [\alpha t + i(2\pi f + \beta t)], \\ |z|^2 &= \frac{2}{\alpha} [(\alpha^2 + \beta^2)t^2 + 4\pi^2 f^2 + 4\pi\beta t f]. \end{aligned} \quad (\text{A-41})$$

These results generalize [6, pp. 456-7] and [7, p. 547].

The origin value of (A-40) is

$$W_{mn}(0,0) = 2(-1)^m \delta_{mn} , \quad (A-42)$$

consistent with unit energy of $\phi_n(t)$ and their even or odd character. The cross-WDF in (A-40) is a function only of the three variables m, n, z , where z is the complex combination in (A-41). The parameters α and β in (A-36) are perfectly general; when they are specialized to match (A-27), and when we set $m = n$, then (A-40) reduces to (A-34). Equations (A-38) and (A-40) afford a direct calculation of the WDF of a general waveform $u(t)$, once the coefficients are determined by

$$u_n = \int dt u(t) \phi_n^*(t) . \quad (A-43)$$

APPENDIX B. MOMENTS OF DISTRIBUTION D

The generalized smoothing distribution D is given by (23) in terms of a double Fourier transform of product

$$P(v, \tau) = \chi_u(v, \tau) q_2(v, \tau) . \quad (B-1)$$

Therefore, the inverse relation is

$$P(v, \tau) = \iint dt df \exp(-i2\pi vt + i2\pi f\tau) D(t, f) . \quad (B-2)$$

If we let superscript ν denote a partial derivative with respect to v , there immediately follows from (B-2),

$$\begin{aligned} P(0,0) &= \iint dt df D(t, f) \\ P^\nu(0,0) &= -i2\pi \iint dt df t D(t, f) \\ P^\tau(0,0) &= i2\pi \iint dt df f D(t, f) \\ P^{\nu\nu}(0,0) &= -4\pi^2 \iint dt df t^2 D(t, f) \\ P^{\nu\tau}(0,0) &= 4\pi^2 \iint dt df t f D(t, f) \\ P^{\tau\tau}(0,0) &= -4\pi^2 \iint dt df f^2 D(t, f) . \end{aligned} \quad (B-3)$$

When these relations are written out explicitly in terms of χ_u and

q_2 , according to (B-1), we find that the moments of D are

$$\begin{aligned}
 \iint dt \, df \, D(t, f) &= \chi_i(0, 0) \, q_2(0, 0) \\
 \iint dt \, df \, t \, D(t, f) &= \frac{1}{2\pi} [\chi_u^v(0, 0) \, q_2(0, 0) + \chi_u(0, 0) \, q_2^v(0, 0)] \\
 \iint dt \, df \, f \, D(t, f) &= \frac{-1}{2\pi} [\chi_u^f(0, 0) \, q_2(0, 0) + \chi_u(0, 0) \, q_2^f(0, 0)] \\
 \iint dt \, df \, t^2 \, D(t, f) &= -\frac{1}{4\pi^2} [\chi_u^{vv}(0, 0) \, q_2(0, 0) + 2\chi_u^v(0, 0) \, q_2^v(0, 0) + \\
 &\quad + \chi_u(0, 0) \, q_2^{vv}(0, 0)] \\
 \iint dt \, df \, t \, f \, D(t, f) &= \frac{1}{4\pi^2} [\chi_u^{vf}(0, 0) \, q_2(0, 0) + \chi_u^f(0, 0) \, q_2^v(0, 0) + \\
 &\quad + \chi_u^v(0, 0) \, q_2^f(0, 0) + \chi_u(0, 0) \, q_2^{vf}(0, 0)] \\
 \iint dt \, df \, f^2 \, D(t, f) &= -\frac{1}{4\pi^2} [\chi_u^{ff}(0, 0) \, q_2(0, 0) + 2\chi_u^f(0, 0) \, q_2^f(0, 0) + \\
 &\quad + \chi_u(0, 0) \, q_2^{ff}(0, 0)] .
 \end{aligned} \tag{B-4}$$

Since q_2 is a double Fourier transform of V_2 , of exactly the same form as (B-2), it follows immediately, by similarity to (B-3), that the required derivatives of q_2 in (B-4) can be found from smoothing function V_2 as

$$\begin{aligned}
q_2(0,0) &= \iint dt \, df \, v_2(t,f) \\
q_2^v(0,0) &= -i2\pi \iint dt \, df \, t \, v_2(t,f) \\
q_2^f(0,0) &= i2\pi \iint dt \, df \, f \, v_2(t,f) \\
q_2^{vv}(0,0) &= -4\pi^2 \iint dt \, df \, t^2 \, v_2(t,f) \\
q_2^{vf}(0,0) &= 4\pi^2 \iint dt \, df \, t \, f \, v_2(t,f) \\
q_2^{ff}(0,0) &= -4\pi^2 \iint dt \, df \, f^2 \, v_2(t,f) .
\end{aligned} \tag{B-5}$$

COMPLEX AMBIGUITY FUNCTION PROPERTIES

The required derivatives of χ_u in (B-4) can be determined from definition (24). We list them here for completeness and future reference:

$$\begin{aligned}
\chi_u(0,0) &= \int dt \, |u(t)|^2 \\
\chi_u^v(0,0) &= -i2\pi \int dt \, t \, |u(t)|^2 \\
\chi_u^f(0,0) &= i \int dt \, \text{Im} \{u'(t) \, u^*(t)\} \\
\chi_u^{vv}(0,0) &= -4\pi^2 \int dt \, t^2 \, |u(t)|^2 \\
\chi_u^{vf}(0,0) &= 2\pi \int dt \, t \, \text{Im} \{u'(t) \, u^*(t)\} \\
\chi_u^{ff}(0,0) &= - \int dt \, |u'(t)|^2 .
\end{aligned} \tag{B-6}$$

These quantities are all real, with the exception of the two single derivatives, both of which are purely imaginary. These second-order derivative values of χ_u can be expressed solely in terms of $u(t)$ and $u'(t)$.

Since we can express complex ambiguity function χ_u in terms of the WDF W_u according to

$$\chi_u(v, \tau) = \iint dt df \exp(-i2\pi v t + i2\pi f \tau) W_u(t, f) , \quad (B-7)$$

it readily follows from (B-6) that

$$\begin{aligned} \iint dt df W_u(t, f) &= \int dt |u(t)|^2 \\ \iint dt df t W_u(t, f) &= \int dt t |u(t)|^2 \\ \iint dt df f W_u(t, f) &= \frac{1}{2\pi} \int dt \operatorname{Im}\{u'(t) u^*(t)\} \\ \iint dt df t^2 W_u(t, f) &= \int dt t^2 |u(t)|^2 \\ \iint dt df t f W_u(t, f) &= \frac{1}{2\pi} \int dt t \operatorname{Im}\{u'(t) u^*(t)\} \\ \iint dt df f^2 W_u(t, f) &= \frac{1}{4\pi^2} \int dt |u'(t)|^2 . \end{aligned} \quad (B-8)$$

APPENDIX C. GENERAL TILTED ELLIPSE

It will be convenient to be able to specify the area, tilt, and shape factor of an ellipse directly, instead of trying to solve for these quantities from the general form

$$\frac{1}{2} ax^2 + \frac{1}{2} by^2 + \sqrt{ab} \rho xy = 1 \quad (C-1)$$

employed in [1, (J-2)]. Accordingly, as done in [1, app. D], we employ the rotated coordinates depicted in figure C-1 below. The equation of the ellipse in x', y' space is

$$\left(\frac{x'}{x'_0}\right)^2 + \left(\frac{y'}{y'_0}\right)^2 = 1. \quad (C-2)$$

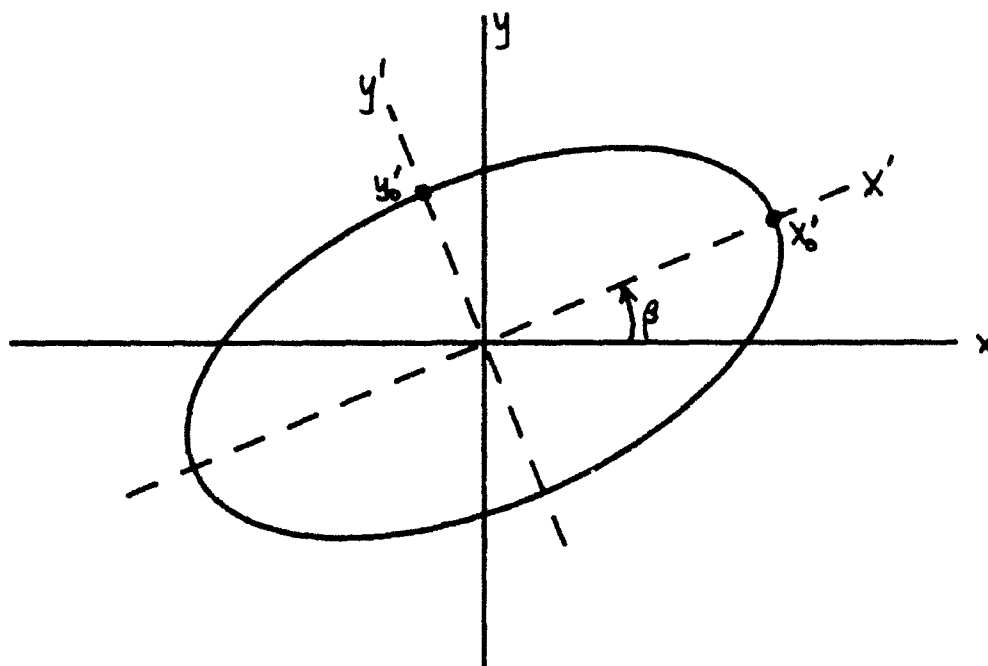


Figure C-1. Rotated Coordinate Axes

But since the area of this ellipse is

$$A = \pi x'_0 y'_0 , \quad (C-3)$$

while its shape factor is

$$F = \frac{x'_0}{y'_0} , \quad (C-4)$$

it is a simple matter to find that

$$A F = \pi x'^2_0 , \quad A/F = \pi y'^2_0 , \quad (C-5)$$

leading to the desirable form

$$\frac{x'^2}{F} + F y'^2 = \frac{A}{\pi} . \quad (C-6)$$

Furthermore, the coordinate axes in figure C-1 are related according to

$$\left. \begin{aligned} x' &= xC + yS \\ y' &= -xS + yC \end{aligned} \right\} \quad C = \cos(\beta) , \quad S = \sin(\beta) . \quad (C-7)$$

Substitution in (C-6) yields

$$\frac{1}{2} x^2 \left(\frac{C^2}{F} + FS^2 \right) + \frac{1}{2} y^2 \left(\frac{S^2}{F} + FC^2 \right) + xy SC \left(\frac{1}{F} - F \right) = \frac{A}{2\pi} , \quad (C-8)$$

which is of the form (C-1) under identifications

$$\begin{aligned} a &= \frac{2\pi}{A} \left(\frac{C^2}{F} + FS^2 \right) , \quad b = \frac{2\pi}{A} \left(\frac{S^2}{F} + FC^2 \right) , \\ \rho &= \frac{\gamma}{\sqrt{1 + \gamma^2}} \quad \text{with} \quad \gamma = SC \left(\frac{1}{F} - F \right) . \end{aligned} \quad (C-9)$$

Once area A , tilt β , and shape factor F are specified, (C-9) affords a ready calculation of a, b, ρ ; quantities C and S are given by (C-7). Since

$\rho = \sin(\theta)$ in [1, (J-6)], we have

$$\sin(\theta) = \frac{\gamma}{\sqrt{1 + \gamma^2}}, \quad \cos(\theta) = \frac{1}{\sqrt{1 + \gamma^2}}, \quad (C-10)$$

which are needed below.

In order to distinguish the two Gaussian mountains being doubly convolved in [1, (J-2)], we label them with subscripts 1 and 2, respectively, thereby obtaining

$$c = \frac{2\pi}{A_1} \left(\frac{C_1^2}{F_1} + F_1 S_1^2 \right), \quad b = \frac{2\pi}{A_1} \left(\frac{S_1^2}{F_1} + F_1 C_1^2 \right), \quad S_1 = \sin(B_1), \quad C_1 = \cos(B_1),$$

$$\gamma_1 = S_1 C_1 \left(\frac{1}{F_1} - F_1 \right), \quad \sin(\theta) = \frac{\gamma_1}{\sqrt{1 + \gamma_1^2}}, \quad \cos(\theta) = \frac{1}{\sqrt{1 + \gamma_1^2}}, \quad (C-11)$$

and

$$c = \frac{2\pi}{A_2} \left(\frac{C_2^2}{F_2} + F_2 S_2^2 \right), \quad d = \frac{2\pi}{A_2} \left(\frac{S_2^2}{F_2} + F_2 C_2^2 \right), \quad S_2 = \sin(B_2), \quad C_2 = \cos(B_2),$$

$$\gamma_2 = S_2 C_2 \left(\frac{1}{F_2} - F_2 \right), \quad \sin(\theta) = \frac{\gamma_2}{\sqrt{1 + \gamma_2^2}}, \quad \cos(\theta) = \frac{1}{\sqrt{1 + \gamma_2^2}}. \quad (C-12)$$

We are now in a position to evaluate the effective area A_3 of the resultant convolution; namely from [1, (J-9)-(J-11)], we have

$$\frac{A_3}{A_1 + A_2} = \frac{\sqrt{D}}{\sqrt{ab} \cos(\theta) + \sqrt{cd} \cos(\theta)}, \quad (C-13)$$

where

$$D = ab \cos^2(\theta) + cd \cos^2(\phi) + ad + bc - 2\sqrt{abcd} \sin(\theta) \sin(\phi) . \quad (C-14)$$

The minimum value of (C-13) is 1, attained when shape factors $F_1 = F_2$ and tilts $\beta_1 = \beta_2$. More generally, when we specify

A_1, β_1, F_1 for ellipse 1 ,

A_2, β_2, F_2 for ellipse 2 , (C-15)

equations (C-11) and (C-12) allow for evaluation of all the parameters needed in (C-13) and (C-14). A sample program in BASIC is attached.

Subroutine E computes $a, b, \sin(\theta), \cos(\theta)$ as given by (C-9) and (C-10) in terms of given area A , shape factor F , and tilt β ($=B$).

```

10  GINIT
20  PLOTTER IS "GRAPHICS"
30  GRAPHICS ON
40  WINDOW -PI/4,PI/4,1,1.25
50  GRID PI/8,.05
60  F1=2                                ! SHAPE FACTOR
70  B1=PI/4                            ! TILT
80  A2=2                                ! AREA
90  F2=2
100 DATA .5,1,2,3,4,5,6
110 DIM A1(1:7)
120 READ A1(*)
130 FOR I=1 TO 7
140  A1=A1(I)
150  CALL E(A1,F1,B1,As,Bs,St,Ct)
160  Ab=As*Bs
170  FOR B2=-PI/4 TO PI/4 STEP PI/100
180  CALL E(A2,F2,B2,Cs,Ds,Sp,Cp)
190  Cd=Cs*Ds
200  D=Ab*Ct*Ct+Cd*Cp*Cp+As*Ds+B*Cs-2.*SQR(Ab*Cd)*St*Sp
210  A312=SQR(D)*A1*A2/(2.*PI*(A1+A2))
220  PLOT B2,A312
230  NEXT B2
240  PENUP
250  NEXT I
260  PAUSE
270  END
280  !
290  SUB E(A,F,B,As,Bs,St,Ct)
300  S=SIN(B)
310  C=COS(B)
320  G=S*C*(1./F-F)
330  Sq=SQR(1.+G*G)
340  St=G/Sq
350  Ct=1./Sq
360  C2=C*C
370  S2=S*S
380  T=2.*PI/A
390  As=T*(C2/F+S2*F)
400  Bs=T*(S2/F+C2*F)
410  SUBEND

```

APPENDIX D. KERNEL APPROACH TO PENALTY FUNCTION

The general formulation in (A-11) through (A-21) will be applied in this appendix to the penalty function (3):

$$P(t,f) = a^2 t^2 + 4\pi^2 b^2 f^2 + 4\pi c t f . \quad (D-1)$$

Substitution in (A-9) (in place of reward R) yields

$$\begin{aligned} r(t,\tau) &= \int df \exp(-i2\pi f\tau) P(t,f) = \\ &= \int df \exp(-i2\pi f\tau) (a^2 t^2 + 4\pi^2 b^2 f^2 + 4\pi c t f) = \\ &= a^2 t^2 \delta(\tau) - b^2 \delta''(\tau) + i2c t \delta'(\tau) . \end{aligned} \quad (D-2)$$

Then kernel K follows from (A-11) as

$$\begin{aligned} K(x,y) &= r\left(\frac{x+y}{2}, x-y\right) = \\ &= \frac{a^2}{4} (x+y)^2 \delta(x-y) - b^2 \delta''(x-y) + ic (x+y) \delta'(x-y) , \end{aligned} \quad (D-3)$$

which is Hermitian.

The integral equation (A-12), that must be solved, can be simplified by use of the facts that

$$\begin{aligned} \frac{1}{4} a^2 \int dx (x+y)^2 \delta(x-y) \phi_n(x) &= a^2 y^2 \phi_n(y) , \\ -b^2 \int dx \delta''(x-y) \phi_n(x) &= -b^2 \phi_n''(y) , \\ ic \int dx (x+y) \delta'(x-y) \phi_n(x) &= -ic [2y \phi_n'(y) + \phi_n(y)] , \end{aligned} \quad (D-4)$$

where the last two results are obtained by integration by parts. Then (A-12) yields differential equation

$$b^2 \phi_n''(y) + i2cy \phi_n'(y) + (\lambda_n + ic - a^2 y^2) \phi_n(y) = 0 . \quad (D-5)$$

If we try solution

$$\phi_0(y) = A \exp\left(-\frac{1}{2} B y^2\right) \quad (D-6)$$

in (D-5), we find it to be acceptable if we take

$$B = \frac{\sqrt{Q} + ic}{b^2} , \quad \lambda_0 = \sqrt{Q} . \quad (D-7)$$

These results agree with (11) and (20), as expected. To find the general solution of (D-5), we try solution form

$$\phi(y) = \exp\left(-\frac{1}{2} B y^2\right) H(y) , \quad (D-8)$$

with B still given by (D-7). This form in (D-8) is no loss of generality since H is still arbitrary. Use of (D-8) in (D-5) results in

$$\begin{aligned} & b^2 H''(y) + 2y H'(y) (-b^2 B + ic) + \\ & + H(y) (-b^2 B + b^2 B^2 y^2 - i2cBy^2 + \lambda + ic - a^2 y^2) = 0 . \end{aligned} \quad (D-9)$$

When the value for B in (D-7) is utilized, (D-9) simplifies to

$$b^2 H''(y) - 2\sqrt{Q} y H'(y) + (\lambda - \sqrt{Q}) H(y) = 0 . \quad (D-10)$$

(As a partial check, if $H(y) = A$, then $\lambda = \sqrt{Q}$, as in (D-7).)

Now, in (D-9), let

$$H(y) = G(Fy) , \quad H'(y) = F G'(Fy) , \quad H''(y) = F^2 G''(Fy) , \quad (D-11)$$

where F is arbitrary for the moment, thereby obtaining

$$b^2 F^2 G''(Fy) - 2\sqrt{Q} y F G'(Fy) + (\lambda - \sqrt{Q}) G(Fy) = 0. \quad (D-12)$$

Now let $x = Fy$ to get

$$G''(x) - \frac{2\sqrt{Q}}{b^2 F^2} x G'(x) + \frac{\lambda - \sqrt{Q}}{b^2 F^2} G(x) = 0. \quad (D-13)$$

If we now let (without loss of generality)

$$F = \frac{2^{1/2} Q^{1/4}}{b}, \quad (D-14)$$

then (D-13) simplifies further to

$$G''(x) - x G'(x) + \frac{\lambda - \sqrt{Q}}{2\sqrt{Q}} G(x) = 0. \quad (D-15)$$

We now appeal to [4, 22.6.21] and observe that if

$$\frac{\lambda - \sqrt{Q}}{2\sqrt{Q}} = n = \text{integer}, \quad (D-16)$$

then a solution of (D-15) is

$$G(x) = \text{He}_n(x), \quad \lambda_n = \sqrt{Q}(1 + 2n). \quad (D-17)$$

Also, (D-11) yields

$$H(y) = G(Fy) = \text{He}_n(Fy), \quad (D-18)$$

while (D-8) gives

$$\phi_n(y) = A \exp\left(-\frac{1}{2} B y^2\right) \text{He}_n(Fy) / \sqrt{n!}, \quad (D-19)$$

with

$$B = \frac{\sqrt{Q} + ic}{b^2}, \quad F = \frac{2^{1/2} Q^{1/4}}{b}, \quad |A|^2 = \frac{Q^{1/4}}{\sqrt{\pi} b}, \quad (D-20)$$

where the unit energy normalization of ϕ_n has been imposed. The corresponding eigenvalue follows from (D-17) as

$$\lambda_n = \sqrt{Q}(1 + 2n) = \sqrt{a^2 b^2 - c^2}(1 + 2n) . \quad (D-21)$$

The minimum obviously occurs for $n = 0$.

Result (D-19) agrees with (A-27). However, the λ_n given here by (D-21) differs from that given by (A-26), because we are solving for the minimum penalty here versus the maximum reward there.

REFERENCES

1. A. H. Nuttall, Wigner Distribution Function: Relation to Short-Term Spectral Estimation, Smoothing, and Performance in Noise, NUSC Technical Report 8225, Nav 1 Underwater Systems Center, New London, CT, 16 February 1988.
2. L. Cohen and T. E. Posch, "Positive Time-Frequency Distribution Functions," IEEE Transactions on Acoustics, Speech, and Signal Processing, vol. ASSP-33, no. 1, pp. 31-38, February 1985.
3. J. F. Barrett and D. G. Lampard, "An Expansion for Some Second-Order Probability Distributions and its Application to Noise Problems," IRE Transactions on Information Theory, volume IT-1, number 1, pp. 10-15, March 1955.
4. Handbook of Mathematical Functions, National Bureau of Standards, Applied Mathematics Series, number 55, U.S. Department of Commerce, U.S. Government Printing Office, Washington, D.C., June 1964.
5. A. Erdélyi et al, Tables of Integral Transforms, volume II, McGraw-Hill Book Company, NY, 1954.
6. H. J. Groenewold, "On the Principles of Elementary Quantum Mechanics," Physica, vol. XII, no. 7, pp. 405-460, October 1946.
7. M. S. Bartlett and J. E. Moyal, "The Exact Transition Probabilities of Quantum-Mechanical Oscillators, Calculated by the Phase-Space Method," Proc. of Cambridge Phil. Soc., vol. 45, pp. 545-553, 1949.

Technical Report 8533
14 April 1989

**Alias-Free Wigner Distribution Function
and Complex Ambiguity Function for Discrete-
Time Samples**

A. H. Nuttall
ABSTRACT

If an arbitrary complex continuous waveform $s(t)$ with finite overall frequency extent F Hertz is sampled with time increment $\Delta < 1/F$, the aliasing can be controlled and the continuous time waveform $s(t)$ reconstructed exactly at any desired time instant from waveform samples $\{s(k\Delta)\}$. On the other hand, it is commonly believed that aliasing of the corresponding Wigner distribution function (WDF) can only be avoided by sampling twice as fast; i.e., $\Delta < (2F)^{-1}$ is thought to be required. Alternatively, interpolation of the time data has been suggested as a means of circumventing aliasing of the WDF; however, the computational burden has proven excessive if done by sinc function interpolation.

It is demonstrated here that this conjecture is false and that the usual sampling criterion, $\Delta < 1/F$, suffices for exact reconstruction of the original continuous WDF as well as the complex ambiguity function (CAF) at all time/frequency locations without an excessive amount of computational effort. The inadequacy of earlier investigations was due to incomplete processing of all the information available in data samples $\{s(k\Delta)\}$. Correct processing eliminates the troublesome close-in aliasing lobes, leaving only the standard aliasing lobes that can be suppressed if sampling increment $\Delta < 1/F$. The new feature is a diamond-shaped gating function in the two-frequency domain where interspersed aliasing lobes occur.

The required data processing for an alias-free WDF and CAF is strikingly simple. It requires that the available time data be immediately transformed to the frequency domain and that the frequency domain versions of the WDF and CAF integrals be employed rather than the time domain forms. Discretization of the reconstructed alias-free WDF and CAF in both time and frequency is then investigated and the required FFT sizes and ranges of variables are determined. Interpolation of samples $\{s(k\Delta)\}$ or reconstruction of $s(t)$ from these samples is neither necessary nor utilized.

Approved for public release; distribution is unlimited.

TABLE OF CONTENTS

	Page
LIST OF ILLUSTRATIONS	ii
LIST OF SYMBOLS	iii
INTRODUCTION	1
NOTATION	3
WAVEFORM CHARACTERIZATION AND RATE OF VARIATION	6
Spectrum of Sampled Waveform	8
Examples	11
TWO-DIMENSIONAL CONTINUOUS FUNCTIONS	14
TWO-DIMENSIONAL FUNCTIONS FOR DISCRETE-TIME SAMPLES	17
Sampled Temporal Correlation Function	17
Approximate Wigner Distribution Function	18
Approximate Spectral Correlation Function via WDF	23
Approximate Complex Ambiguity Function	28
Approximate Spectral Correlation Function via CAF	31
Summary Status in All Four Domains	34
RECOVERY OF ORIGINAL CONTINUOUS TWO-DIMENSIONAL FUNCTIONS	36
Simplification of SCF $A_a(v, f)$	36
Recovery of Original WDF and CAF	39
Recovery of Original TCF	39
Direct Time Domain Recovery of Continuous WDF	40
Discussion	41
DISCRETE PROCESSING IN FREQUENCY DOMAIN	44
Evaluation of WDF	44
Discretization in Time and Frequency	47
Increments in t and f	48
Summary of WDF Equations	49
Evaluation of CAF	50
INTERPOLATION OF TIME WAVEFORM	51
DISCUSSION/SUMMARY	54
Time Domain Approach	54
Frequency Domain Approach	55
Comparison	55
APPENDIX A. EXTENTS AND RATES OF VARIATION OF TCF, WDF, CAF, SCF	A-1
APPENDIX B. IMPULSIVE SAMPLING APPROACH	B-1
APPENDIX C. RECOVERY VIA DIRECT CONVOLUTION	C-1
APPENDIX D. EVALUATION OF CAF	D-1
APPENDIX E. TCF OF IMPULSIVELY SAMPLED WAVEFORM	E-1
REFERENCES	R-1

LIST OF ILLUSTRATIONS

Figure		Page
1	Bandlimited Waveform Spectrum $S(f)$	7
2	Spectrum $\tilde{S}(f)$ of Sampled Waveform	7
3	Extent of Spectral Correlation Function $A(v, f)$	16
4	Available Values of TCF $R(t, \tau)$	18
5	WDF Approximations	21
6	Approximate SCF $A_a(v, f)$	26
7	CAF Approximations	30
8	Locations of Available Information	35
9	Waveform $s(t)$	43
10	Time-Aliased WDF	45
11	Time-Aliased Waveform $\hat{s}(t)$	52
A-1	Extents of the Two-Dimensional Functions	A-3
A-2	Spectrum of Real Waveform	A-6
C-1	Sample Values of $\Delta^2 \mathcal{D}(t, \tau)$	C-5
D-1	Delay-Aliased CAF	D-3
E-1	Impulse Locations for $r_i(t, \tau)$ in (E-9)	E-4
E-2	Impulse Locations for $a_i(v, f)$ in (E-11)	E-4

LIST OF SYMBOLS

t	time
$s(t)$	complex waveform
f	frequency
$S(f)$	voltage-density spectrum of $s(t)$, (13)
F	total bandwidth of $S(f)$, (14) and figure 1
Δ	time sampling increment, (15)
$\tilde{S}(f)$	approximation to $S(f)$, (16)
$W(t, f)$	WDF, (26), (33)
τ	time separation, (26), (32)
ν	frequency separation, (26), (35)
$R(t, \tau)$	TCF, (32)
$\chi(\nu, \tau)$	CAF, (34)
$A(\nu, f)$	SCF, (35)
$W_a(t, f)$	approximate WDF, (40) and (41)
$A_a(\nu, f)$	approximate SCF, (46) and (58)
$D(\nu, f)$	diamond gating function, (53)
$\chi_a(\nu, \tau)$	approximate CAF, (56) and (57)
$\bar{S}(f)$	spectrum computed from time samples, (69)
T	overall effective duration of $s(t)$, (84) and figure 9
N	FFT size, (86)
$\tilde{W}(t, f)$	frequency domain WDF approximation, (91)
M	size of FFT, (99), (113)
$\hat{s}(t)$	time aliased waveform, (114) and figure 11
$\hat{W}(t, f)$	time domain WDF approximation, (123)

LIST OF SYMBOLS (Cont'd)

sub i	impulsive approximations, (B-1),(B-2)
$d(t,f)$	interpolation function in time t, (C-3)
$d(v,\tau)$	interpolation function in delay τ , (C-6)
$D(t,\tau)$	two-dimensional interpolation function, (C-9)

ABBREVIATIONS

FFT	Fast Fourier Transform, (12)
WDF	Wigner Distribution Function, (26),(33)
TCF	Temporal Correlation Function, (32)
CAF	Complex Ambiguity Function, (34)
SCF	Spectral Correlation Function, (35)

ALIAS-FREE WIGNER DISTRIBUTION FUNCTION AND
COMPLEX AMBIGUITY FUNCTION FOR DISCRETE-TIME SAMPLES

INTRODUCTION

The attributes of the Wigner distribution function (WDF) have come under close scrutiny in recent years; see, for example, [1,2,3] and the references listed therein. However, the numerical calculation of the WDF from discrete time data still suffers from the belief that the sampling rate of a given time waveform must be twice as large for computation of an alias-free WDF, as the rate required for reconstruction of the original continuous waveform. If true, this would double the number of data points that must be collected to cover a given time interval, and greatly increase the number of subsequent computations. This contention applies to the complex analytic waveform as well as to a real waveform.

It is the purpose of this report to establish the fact that the sampling rate need not be doubled, and that an alias-free WDF, as well as complex ambiguity function (CAF), can still be quickly and efficiently obtained, provided that all the information in the available data stream is extracted and properly processed. Some recent effort on this topic [4,5,6] did not discover the particular complete set of processing required, leading to the conjecture [5, page 1068] that it was not possible to accomplish the desired goal for the WDF.

We will show not only that the desired goal can be achieved, but that the required data processing for an alias-free WDF and CAF is strikingly simple. Our approach to the solution initially involves the four time/frequency domains associated with the WDF and its various Fourier transforms. However, in hindsight, an extremely simple and direct method of obtaining the WDF and CAF will be presented, which requires only FFTs (fast Fourier transforms) for its implementation.

An alias-free discrete WDF and CAF have been achieved in [7] and [8], by means of interpolating either the waveform time samples or the spectrum frequency samples. Also, the ranges and required increment sizes in time and frequency of the various two-dimensional functions have been carefully scrutinized in [7], by discrete Fourier transform techniques. However, that approach does not illuminate how the various aliasing lobes interact and can be controlled. Furthermore, we utilize a continuous approximation approach (rather than a discrete Fourier technique), which lends tremendous insight into the shortcomings of current processing methods and brings out the fundamental properties of the various two-dimensional functions and their domains of definition. The final discretization in time and frequency is only done with deference to practical computer evaluation.

In fact, we will not define a discrete WDF or CAF here. Instead, we attempt to recover the WDF and CAF of the original continuous time waveform, by developing approximations and then controlling or eliminating the errors in these approximations. Only after this is accomplished, do we then address discretization of the time and frequency arguments of the two-dimensional functions of interest.

NOTATION

For economy of presentation, a number of notational and manipulative shortcuts are employed here. We have collected them all together at this point, and will employ them freely later, with minimal comment. We define

$$\text{rect}(x) = \begin{cases} 1 & \text{for } |x| < 1/2 \\ 0 & \text{otherwise} \end{cases}, \quad (1)$$

$$\text{sinc}(x) = \frac{\sin(\pi x)}{\pi x} \quad \text{for all } x. \quad (2)$$

The symbols \int and \sum without limits denote that integration and summation are to be conducted over the complete range of nonzero integrand and summand, respectively.

The convolution of two functions $g(x)$ and $h(x)$ is denoted by

$$g(x) \otimes h(x) = \int du \, g(u) \, h(x - u). \quad (3)$$

The two-dimensional convolution of two functions is

$$g(x,y) \otimes_{xy} h(x,y) = \iint du \, dv \, g(u,v) \, h(x - u, y - v). \quad (4)$$

The Fourier transform of a time domain function $s(t)$ into its spectrum in the frequency domain f is according to the pair of relations

$$S(f) = \int dt \, \exp(-i2\pi ft) \, s(t),$$

$$s(t) = \int df \, \exp(i2\pi ft) \, S(f). \quad (5)$$

Then the Fourier transform of a product of time functions is equal to the convolution of the two spectra:

$$\int dt \exp(-i2\pi ft) a(t) b(t) = A(f) \otimes B(f) . \quad (6)$$

The infinite impulse train in time t , with spacing Δ , is

$$\Delta \sum_n \delta(t - n\Delta) , \quad n \text{ integer} . \quad (7)$$

Its Fourier transform is another infinite impulse train in frequency f , with reciprocal spacing:

$$\int dt \exp(-i2\pi ft) \Delta \sum_n \delta(t - n\Delta) = \sum_n \delta(f - \frac{n}{\Delta}) . \quad (8)$$

Combination of (6) and (8) leads to a very useful relation that is employed frequently in the following:

$$\begin{aligned} \int dt \exp(-i2\pi ft) a(t) \Delta \sum_n \delta(t - n\Delta) &= \\ &= A(f) \otimes \sum_n \delta(f - \frac{n}{\Delta}) = \sum_n A(f - \frac{n}{\Delta}) . \end{aligned} \quad (9)$$

The discrete Fourier transform operation arises frequently; consider

$$Z(n) \equiv \sum_k \exp(-i2\pi kn/N) z(k) \quad \text{for all } n . \quad (10)$$

The periodicity of $Z(n)$ means that it only need be computed for one period, namely $0 \leq n \leq N - 1$. The absence of limits on the sum in (10) means that it goes from $k = -\infty$ to $+\infty$. However, since $z(k)$, $z(k \pm N)$, $z(k \pm 2N)$, ... all receive the same weight in (10), regardless of the value of n , the values of $\{z(k)\}$ can be "collapsed" according to

$$\tilde{z}(k) \equiv \begin{cases} \sum_j z(k + jN) & \text{for } 0 \leq k \leq N - 1 \\ 0 & \text{otherwise} \end{cases} \quad (11)$$

and (10) becomes identically

$$Z(n) = \sum_{k=0}^{N-1} \exp(-i2\pi kn/N) \tilde{z}(k) \quad \text{for all } n. \quad (12)$$

For N highly composite, FFT routines can be employed for efficient evaluation of (12) for $0 \leq n \leq N - 1$. The manipulation of (10) into (12) is called collapsing (or prealiasing), and the operation in (11) is modulo N addition. The nonzero values of $\{z_k\}$ in (10) can occur anywhere on the k -axis, and there can be an arbitrary number of them; nevertheless, (12) is an identity with (10). The value of $Z(n)$ for any n can be obtained immediately from the FFT output, by looking up the value in location n modulo N .

WAVEFORM CHARACTERIZATION AND RATE OF VARIATION

The continuous complex waveform of interest is $s(t)$, with Fourier spectrum

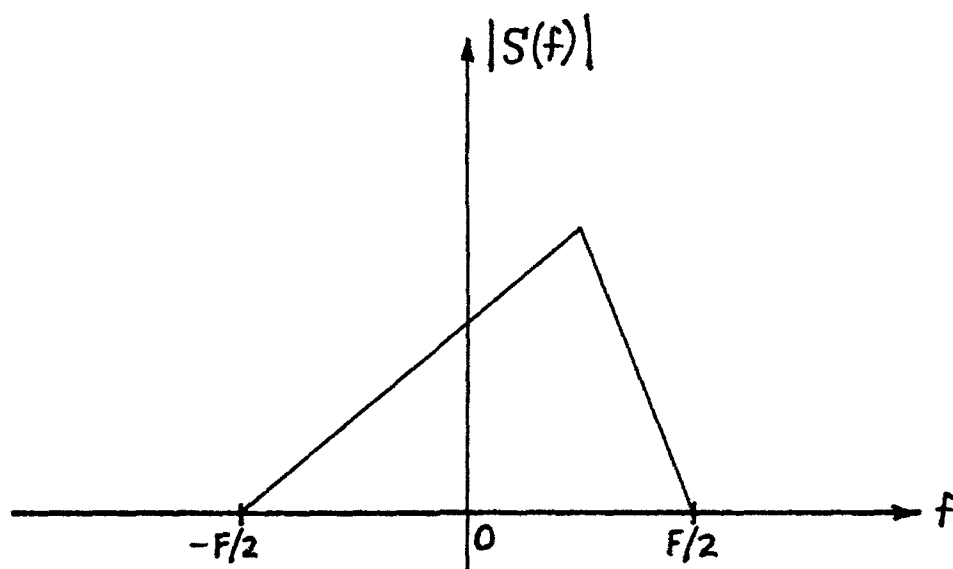
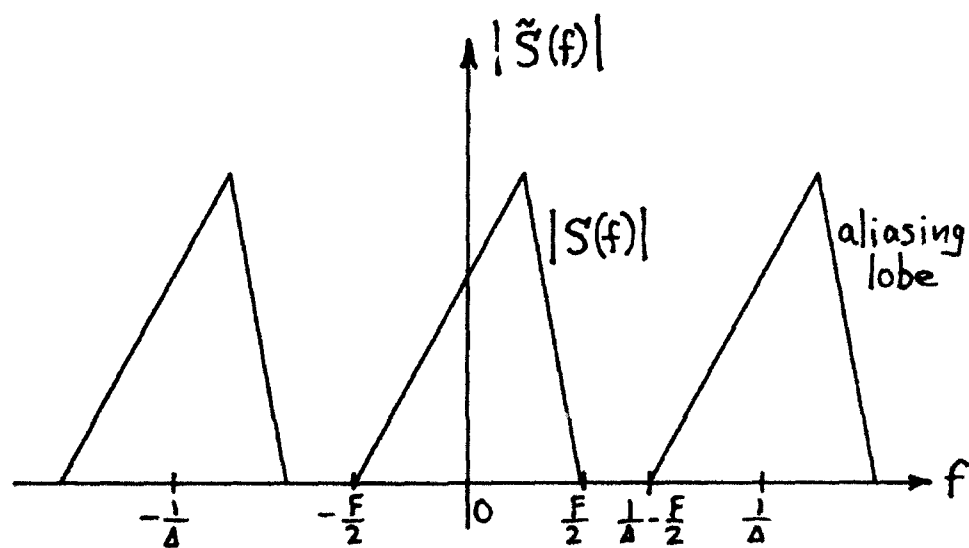
$$S(f) = \int dt \exp(-i2\pi ft) s(t) \quad \text{for all } f. \quad (13)$$

We presume here that spectrum $S(f)$ is bandlimited, with total extent F Hz; i.e.,

$$S(f) = 0 \quad \text{for } |f| > F/2. \quad (14)$$

Notice in figure 1 that spectrum $S(f)$ is centered at $f = 0$, without loss of generality, since waveform $s(t)$ could be multiplied by $\exp(-i2\pi f_0 t)$ to downshift it by f_0 Hz, to any convenient center frequency, as desired.

If we were given a real waveform, we would replace it by its analytic waveform or complex envelope, thereby allowing the minimal possible time-sampling rate that can still exactly represent and recover the complex waveform. This sampling rate is half that required for sampling the corresponding real lowpass waveform, without loss of information. Nevertheless, the decreased sampling rate applied to the complex waveform is still sufficient to get an alias-free WDF and CAF. (Of course, the samples are now complex, whereas they were formerly real for the real waveform case.)

Figure 1. Bandlimited Waveform Spectrum $S(f)$ Figure 2. Spectrum $\tilde{S}(f)$ of Sampled Waveform

SPECTRUM OF SAMPLED WAVEFORM

Waveform $s(t)$ is sampled at time increment Δ seconds, yielding samples

$$\{s(k\Delta)\} \quad \text{for all integer } k. \quad (15)$$

The spectrum of this sampled waveform is defined by means of a Trapezoidal approximation to defining integral (13):

$$\begin{aligned} \tilde{S}(f) &\equiv \Delta \sum_k \exp(-i2\pi f \Delta k) s(k\Delta) = \\ &= \int dt \exp(-i2\pi f t) s(t) \Delta \sum_k \delta(t - k\Delta) = \\ &= S(f) \otimes \sum_k \delta(f - \frac{k}{\Delta}) = \sum_k S(f - \frac{k}{\Delta}) \quad \text{for all } f, \end{aligned} \quad (16)$$

where we used (6)-(9). The approximating spectrum $\tilde{S}(f)$ has period $1/\Delta$ in f and is depicted in figure 2. It will have nonoverlapping aliasing lobes if

$$\Delta < \frac{1}{F}. \quad (17)$$

This fundamental sampling rate condition will be presumed to be true, henceforth. In fact, in order to keep the number of samples $\{s(k\Delta)\}$ small, (17) will be presumed to be closely met. It is very important to minimize the number of samples that must be manipulated, so that the computational burden in evaluating the WDF is not overwhelming.

Another interpretation of approximation $\tilde{S}(f)$ is afforded by line 2 of (16): $\tilde{S}(f)$ is the spectrum (Fourier transform) of the signal $s(t)$ sampled (multiplied) by the infinite impulse train at spacing Δ . This alternative interpretation will also arise later, when we investigate sampling relative to the WDF and its various two-dimensional transform domains.

Since sampling rate condition (17) is presumed to be met, then spectrum $\tilde{S}(f)$ in figure 2 can be gated with a rectangular function, and $S(f)$ can be recovered; i.e.,

$$S(f) = \tilde{S}(f) \text{ rect}(f\Delta) \quad \text{for all } f. \quad (18)$$

Therefore, the time waveform $s(t)$ can also be recovered exactly, for all t , by means of inverse transform (5):

$$\begin{aligned} s(t) &= \int df \exp(i2\pi ft) \tilde{S}(f) \text{ rect}(f\Delta) = \\ &= \tilde{s}(t) \otimes \frac{1}{\Delta} \text{ sinc}\left(\frac{t}{\Delta}\right). \end{aligned} \quad (19)$$

However, since from line 2 of (16), product waveform

$$\tilde{s}(t) = s(t) \Delta \sum_k \delta(t - k\Delta) = \Delta \sum_k s(k\Delta) \delta(t - k\Delta), \quad (20)$$

then (19) becomes

$$s(t) = \sum_k s(k\Delta) \text{ sinc}\left(\frac{t}{\Delta} - k\right) \quad \text{for all } t, \quad (21)$$

which is the standard interpolation formula for a bandlimited waveform.

It should be pointed out here that (21) is not an attractive computational procedure, and that an excellent alternative is available. Namely, from (16), compute from the available samples,

$$\tilde{S}(f) = \Delta \sum_k \exp(-i2\pi f\Delta k) s(k\Delta) \quad \text{for } |f| < \frac{1}{2\Delta}, \quad (22)$$

and then use the top line of (19) to recover waveform

$$s(t) = \int_{-\frac{1}{2\Delta}}^{\frac{1}{2\Delta}} df \exp(i2\pi ft) \tilde{S}(f) \quad \text{for all } t. \quad (23)$$

The reason this gating procedure is attractive is that (22) and (23) can both be done by FFT procedures.* Also, this seemingly trivial sidelight will reoccur in WDF and CAF reconstruction, where it will have a significant impact.

Notice that we have not defined a discrete spectrum, per se. Rather, we have concentrated on getting an approximation $\tilde{S}(f)$ to the original continuous spectrum $S(f)$, both defined for all f . If sampling condition (17) is met, $\Delta < 1/F$, the approximation affords the possibility of exact recovery of $S(f)$ at any f . This philosophy, namely avoiding arbitrary definitions of discrete functions, in favor of direct approximations to the desired continuous functions, is pursued throughout this report. It is believed that this clarifies the fundamental limitations and processing that must be performed in order to achieve the desired quantities. Finally, after demonstrating the viability of this approach, in order to reduce the mathematical equations to practical calculations, we discretize the time and/or frequency arguments of the approximations, as appropriate, and manipulate the equations into attractive FFT forms. We end up, of course, with discrete data processing forms that are suitable for efficient computer realization, but the

*Actually, termination of the sum in (22) at finite k limits will yield an approximation to $\tilde{S}(f)$; the error can be controlled to any desired degree by taking enough terms. Also, the integral in (23) will have to be approximated, say, by the Trapezoidal rule; the attendant time-aliasing can be minimized by choosing the frequency increment small enough. These details will be investigated later.

discretization in time/frequency is deferred to the latest possible location, since it is not fundamental to the ideas of controlling or eliminating aliasing.

The sampling increment Δ will not be set equal to 1 in this report, for several reasons. It is easier to keep track of dimensions, and dimensional checks on the equations are accomplished more readily. It is also easier to obtain physical interpretation of time instants and increments, as well as frequency limits and bandwidths. Finally, it will be seen to eliminate confusion and ambiguity as to precisely where time and frequency samples of the temporal correlation function, WDF, and CAF are being taken; the importance of this last point can not be overemphasized.

EXAMPLES

It is very informative at this point to consider a couple of continuous waveforms and their corresponding WDFs, in terms of their rates of variation. Consider first, spectrum

$$S(f) = \frac{1}{F} \text{rect}\left(\frac{f}{F}\right) = \begin{cases} 1/F & \text{for } |f| < F/2 \\ 0 & \text{otherwise} \end{cases}, \quad (24)$$

for which the waveform is

$$s(t) = \text{sinc}(Ft) = \frac{\sin(\pi Ft)}{\pi Ft} \quad \text{for all } t. \quad (25)$$

The corresponding WDF, at time t and frequency f , is [9, (10)]

$$\begin{aligned}
W(t, f) &= \int d\tau \exp(-i2\pi f\tau) s(t + \frac{\tau}{2}) s^*(t - \frac{\tau}{2}) = \\
&= \int dv \exp(i2\pi vt) S(f + \frac{v}{2}) S^*(f - \frac{v}{2}) = \\
&= \left\{ \begin{array}{ll} \frac{\sin[2\pi Ft(1 - 2|f|/F)]}{\pi F^2 t} & \text{for } |f| < \frac{F}{2} \\ 0 & \text{for } |f| > \frac{F}{2} \end{array} \right\} \text{ for all } t \\
&= \frac{2}{F} \left(1 - 2 \frac{|f|}{F}\right) \text{sinc} [2Ft(1 - 2\frac{|f|}{F})] \text{rect}(\frac{f}{F}) . \quad (26)
\end{aligned}$$

Then, for instance, the slice of the WDF at zero frequency,

$$W(t, 0) = \frac{2}{F} \text{sinc}(2Ft) , \quad (27)$$

varies twice as fast as waveform $s(t)$ in (25). Therefore, although sampling $s(t)$ in (25) with time increment $\Delta < 1/F$ is sufficient to reconstruct $s(t)$, we need a time increment half as large in order to adequately sample slice (27) of the WDF at $f = 0$. In fact, $W(t, f)$ in (26) varies faster with t than $s(t)$ does, whenever $|f| < F/4$.

This example points out that the WDF must be computed twice as finely as the waveform samples, lest important information about the energy distribution of $s(t)$ in t, f space be lost. In fact, if (27) were computed at time points

$$t_n = (n + \frac{1}{2}) \frac{1}{F} \quad \text{for all } n , \quad (28)$$

which have time increment $\Delta_t = 1/F$, then the WDF values obtained would be

$$W\left(\left(n + \frac{1}{2}\right) \frac{1}{F}, 0\right) = \frac{2}{F} \text{sinc}(2n + 1) = 0 \quad \text{for all } n. \quad (29)$$

We would be led to believe from samples (29) that there is no energy along the $f = 0$ line in t, f space, whereas continuous version (27) indicates a considerable contribution.

A second example is

$$s(t) = \exp\left(-\frac{t^2}{2\sigma^2}\right),$$

$$S(f) = \sqrt{2\pi} \sigma \exp(-2\pi^2 \sigma^2 f^2), \quad (30)$$

for which the WDF is

$$W(t, f) = 2\sqrt{\pi} \sigma \exp\left(-\frac{t^2}{\sigma^2} - 4\pi^2 \sigma^2 f^2\right). \quad (31)$$

This WDF varies faster with t than $s(t)$ does, and faster with f than $S(f)$ does. In fact, the rates of variation of $W(t, f)$ and $|s(t)|^2$ are the same with t , while those of $W(t, f)$ and $|S(f)|^2$ are the same in f .

Both of the examples above illustrate the need to compute the WDF at finer increments than are adequate for the time waveform or spectrum. However, this does not mean that the time waveform need be sampled more frequently than requirement (17). Rate (17) is fine for sampling waveform $s(t)$, but the corresponding WDF can and must then be computed at finer increments.

TWO-DIMENSIONAL CONTINUOUS FUNCTIONS

For a continuous waveform $s(t)$ with spectrum $S(f)$, there are four useful two-dimensional characterizations. The first is the continuous temporal correlation function (TCF)

$$R(t, \tau) = s(t + \frac{\tau}{2}) s^*(t - \frac{\tau}{2}) \quad \text{for all } t, \tau. \quad (32)$$

Variable t is absolute time in seconds, while τ is relative time or time separation. The corresponding Wigner distribution function (WDF) is a Fourier transform on τ :

$$W(t, f) = \int d\tau \exp(-i2\pi f\tau) R(t, \tau) \quad \text{for all } t, f. \quad (33)$$

The alternative Fourier transform on t yields the complex ambiguity function (CAF):

$$\chi(v, \tau) = \int dt \exp(-i2\pi vt) R(t, \tau) \quad \text{for all } v, \tau. \quad (34)$$

Functions W and χ are two-dimensional Fourier transforms of each other.

Finally, completing both routes (by t or by τ), we have the spectral correlation function (SCF) as another Fourier transform, according to several equivalent forms

$$\begin{aligned}
A(v, f) &= \int dt \exp(-i2\pi vt) W(t, f) = \\
&= \int d\tau \exp(-i2\pi f\tau) \chi(v, \tau) = \\
&= \iint dt d\tau \exp(-i2\pi vt - i2\pi f\tau) R(t, \tau) = \\
&= S(f + \frac{v}{2}) S^*(f - \frac{v}{2}) \quad \text{for all } v, f. \quad (35)
\end{aligned}$$

This last relation in terms of the spectrum $S(f)$ of waveform $s(t)$ will turn out to be extremely important and useful. It also enables interpretation of f as absolute frequency in Hz, while v is relative frequency or frequency separation.

The names for the TCF and SCF have been drawn from the similarity of their forms in (32) and (35), respectively, to correlation operations. The latter name is also used in [10, (5)-(7)] for a similar quantity.

Recalling the bandlimited character of $S(f)$ in (14) and figure 1, we see that SCF $A(v, f)$ in (35) can be nonzero only when

$$\left| f \pm \frac{v}{2} \right| < \frac{F}{2}. \quad (36)$$

This region in the two-frequency domain (v, f plane) is depicted in figure 3. It is a diamond-shaped region centered at the origin of the v, f plane. Outside this diamond, SCF $A(v, f)$ is identically zero. Thus, a bandlimited spectrum $S(f)$ is reflected in the v, f domain as a diamond-limited SCF $A(v, f)$.

Since (35) can be inverted to give

$$\begin{aligned} W(t, f) &= \int dv \exp(i2\pi vt) A(v, f) , \\ x(v, \tau) &= \int df \exp(i2\pi f\tau) A(v, f) , \end{aligned} \quad (37)$$

it follows from figure 3 that

$$\begin{aligned} W(t, f) &= 0 \quad \text{for } |f| > F/2 , \\ x(v, \tau) &= 0 \quad \text{for } |v| > F . \end{aligned} \quad (38)$$

Thus the WDF and CAF are bandlimited in their respective frequency variables. These properties will be useful later when we study the effects of aliasing in the various domains. More generally, the extents and rates of variation of the TCF, WDF, CAF, and SCF are summarized in appendix A.

The following symmetry properties on the TCF and SCF reduce computational effort by a factor of two:

$$R(t, -\tau) = R^*(t, \tau) ,$$

$$A(-v, f) = A^*(v, f) .$$

These follow immediately from (32) and (35), respectively.

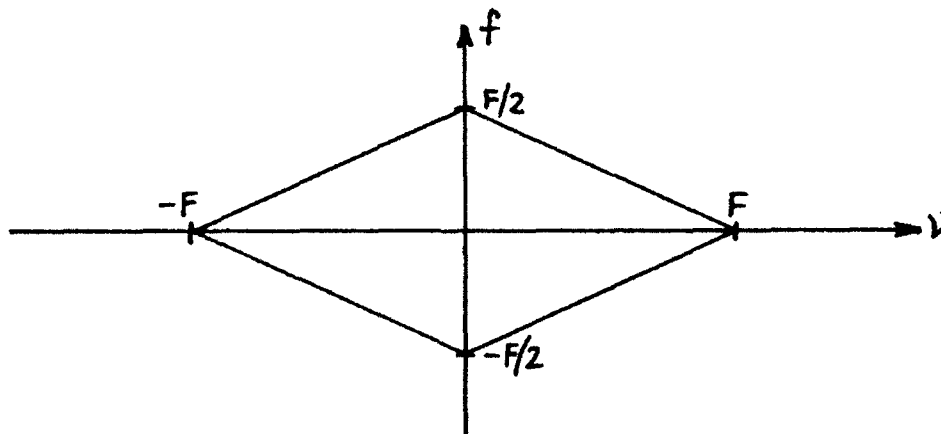


Figure 3. Extent of Spectral Correlation Function $A(v, f)$

TWO-DIMENSIONAL FUNCTIONS FOR DISCRETE-TIME SAMPLES

The available data samples of waveform $s(t)$ are, as given in (15),

$$\{s(k\Delta)\} \quad \text{for integer } k.$$

SAMPLED TEMPORAL CORRELATION FUNCTION

From these values, the totality of information, that can be computed regarding the continuous TCF $R(t, \tau)$ in (32), are the two sets of discrete values

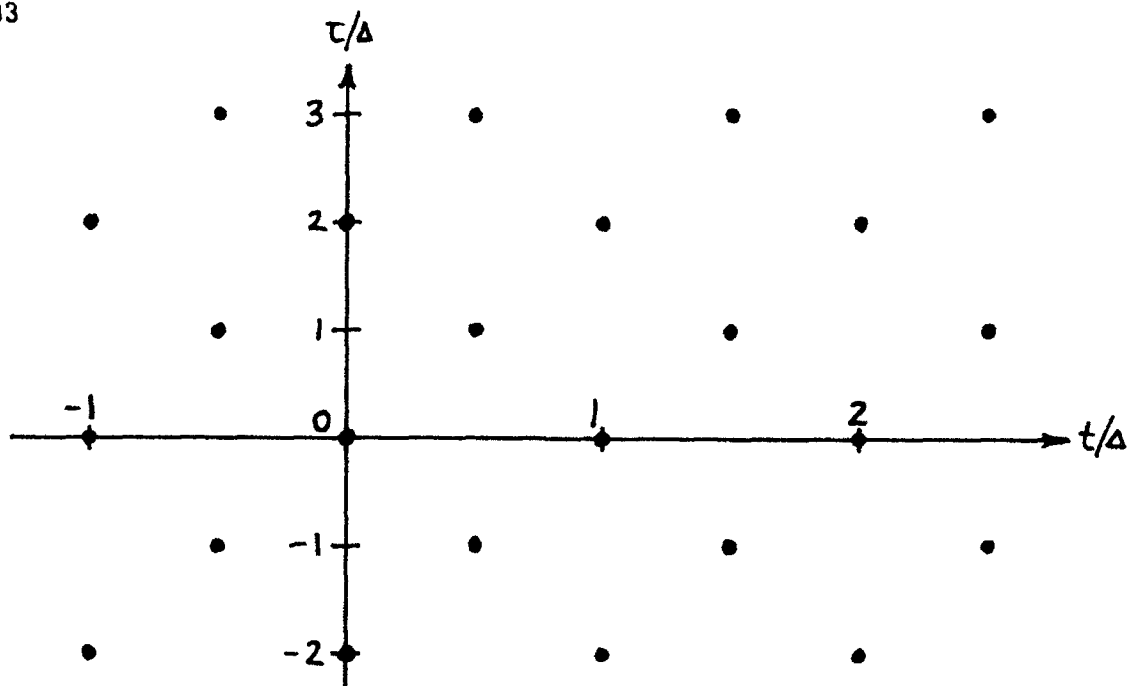
$$R(m\Delta, 2q\Delta) = s(m\Delta + q\Delta) s^*(m\Delta - q\Delta) \quad (39a)$$

and

$$R\left(\left(m + \frac{1}{2}\right)\Delta, (2q + 1)\Delta\right) = s(m\Delta + q\Delta + \Delta) s^*(m\Delta - q\Delta) \quad (39b)$$

} for integers
m and q.

Thus both the t and τ variables in $R(t, \tau)$ are discretized, as indicated in figure 4. However, observe that the available information is interspersed in the t, τ plane. Thus, for fixed t , the separation in available τ values is 2Δ , not Δ , whether t/Δ is integer or half-integer. Similarly, for fixed τ , the separation in available t values is Δ , not $\Delta/2$, whether τ/Δ is an even or odd integer. This lack of intermediate values in both slices is what has led (in the past) to incomplete processing of the available information. What is needed to solve the aliasing problem is a combination of all the interspersed information in figure 4 into a single unified two-dimensional description. That solution will be found to reside in the SCF domain, ν, f .

Figure 4. Available Values of TCF $R(t, \tau)$

APPROXIMATE WIGNER DISTRIBUTION FUNCTION

Guided by definition (33), we adopt the following Trapezoidal approximation to the continuous WDF $W(t, f)$ at time $t = m\Delta$, m integer:

$$W_a(m\Delta, f) \equiv 2\Delta \sum_q \exp(-i2\pi f 2q\Delta) R(m\Delta, 2q\Delta) \quad \text{for all } f. \quad (40)$$

Subscript a on W_a denotes that it is only an approximation to the true continuous W . Notice that the τ increment in (40) is 2Δ , as it must be, according to (39a) and figure 4; we are taking a vertical slice at $t = m\Delta$ in figure 4. The approximation in (40) is always real. It utilizes only the upper line of information available in (39). Notice also that this function is defined for all f .

However, there is an additional approximation to $W(t, f)$ available at time $t = (m + \frac{1}{2})\Delta$, by use of the bottom line of (39); namely, guided again

by definition (33), we have Trapezoidal approximation

$$W_a\left(\left(m + \frac{1}{2}\right)\Delta, f\right) \cong 2\Delta \sum_q \exp[-i2\pi f(2q + 1)\Delta] R\left(\left(m + \frac{1}{2}\right)\Delta, (2q + 1)\Delta\right) \text{ for all } f. \quad (41)$$

m is still an integer. Again, the τ increment is 2Δ , but it is shifted by Δ , as (39b) and figure 4 dictate. We are now taking a vertical slice at $t = \left(m + \frac{1}{2}\right)\Delta$ in figure 4; this is in keeping with the philosophy developed earlier in (24)-(31). Approximation (41) is also real.

Equations (40) and (41) can be developed into some informative forms; from (40) and (9), approximation

$$\begin{aligned} W_a(m\Delta, f) &= \int d\tau \exp(-i2\pi f\tau) R(m\Delta, \tau) 2\Delta \sum_q \delta(\tau - 2q\Delta) = \\ &= W(m\Delta, f) \otimes \sum_q \delta\left(f - \frac{q}{2\Delta}\right) = \\ &= \sum_q W(m\Delta, f - \frac{q}{2\Delta}) \quad \text{for all } f. \end{aligned} \quad (42)$$

Similarly, (41) yields

$$\begin{aligned} W_a\left(\left(m + \frac{1}{2}\right)\Delta, f\right) &= \int d\tau \exp(-i2\pi f\tau) R\left(\left(m + \frac{1}{2}\right)\Delta, \tau\right) 2\Delta \sum_q \delta(\tau - 2q\Delta - \Delta) = \\ &= W\left(\left(m + \frac{1}{2}\right)\Delta, f\right) \otimes \sum_q (-1)^q \delta\left(f - \frac{q}{2\Delta}\right) = \\ &= \sum_q (-1)^q W\left(\left(m + \frac{1}{2}\right)\Delta, f - \frac{q}{2\Delta}\right) \quad \text{for all } f. \end{aligned} \quad (43)$$

The $(-1)^q$ factor is due to the time delay of Δ seconds in the impulse train; more generally, for delay τ_0 ,

$$\begin{aligned}
 \int d\tau \exp(-i2\pi f\tau) 2\Delta \sum_q \delta(\tau - 2q\Delta - \tau_0) &= \\
 = \exp(-i2\pi f\tau_0) \sum_q \delta(f - \frac{q}{2\Delta}) &= \\
 = \sum_q \exp(-i\pi q \tau_0/\Delta) \delta(f - \frac{q}{2\Delta}) . & \quad (44)
 \end{aligned}$$

The two relations, (42) and (43), are equivalent to those given in [4, (9)] and [6, (14)]. Observe that the aliasing lobes are separated by only $(2\Delta)^{-1}$ in the frequency domain, not $1/\Delta$ as was the case for the signal aliasing lobes in figure 2. These approximations, W_a , are illustrated in figure 5, for two adjacent time instants at $m\Delta$ and $(m + \frac{1}{2})\Delta$. We have used property (38) in drawing figure 5.

In order for either approximation, by itself, to be free of aliasing, we would need

$$\frac{F}{2} < \frac{1}{2\Delta} - \frac{F}{2} , \quad \text{i.e., } \Delta < \frac{1}{2F} . \quad (45)$$

This relation, obtained directly from both plots in figure 5, is the usual one quoted^{*} regarding an alias-free WDF. It is seen to require a sampling rate twice as fine as (17). If we satisfy (17), but not (45), then the approximations in figure 5 are significantly aliased.

* The case where $s(t)$ is a real waveform is treated in appendix A.

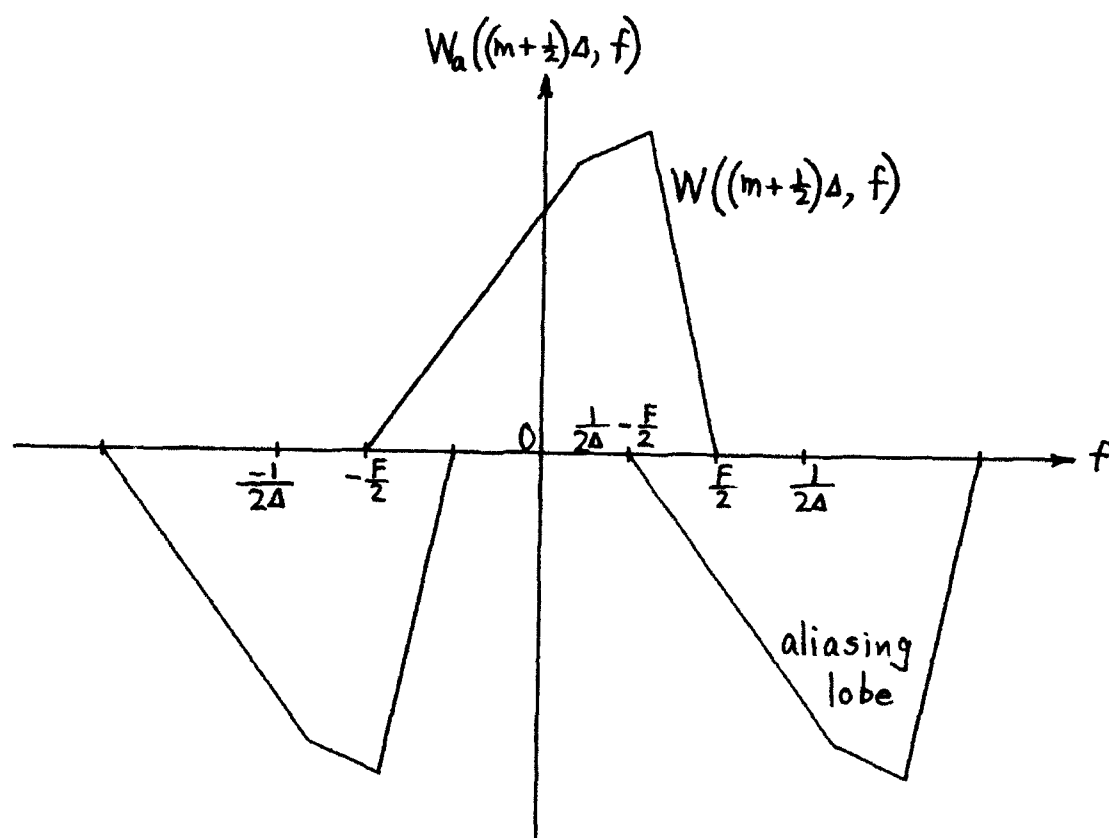
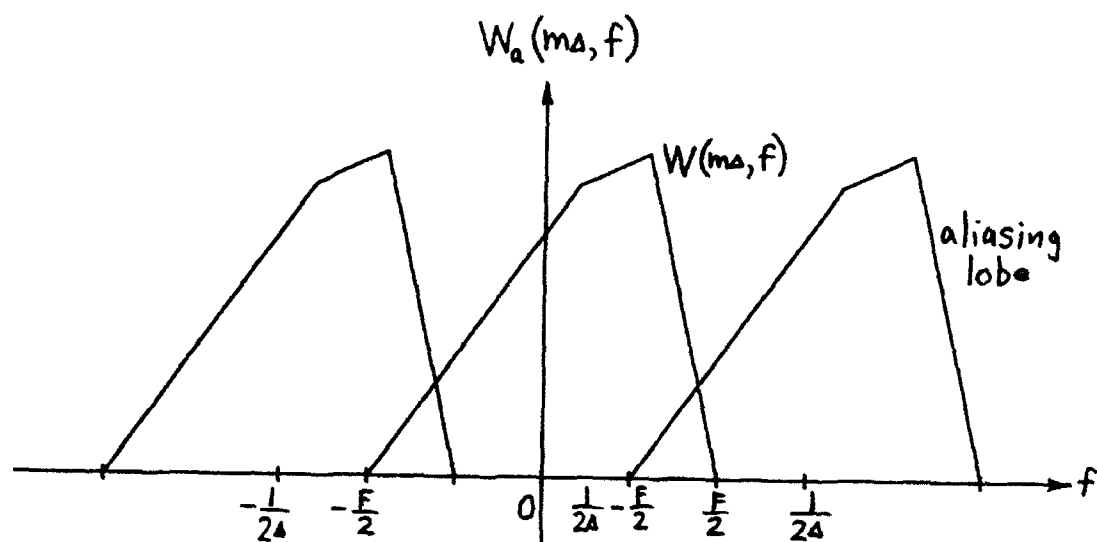


Figure 5. WDF Approximations

The two approximations, (40) and (41), use all the available information (39) about the TCF $R(t, \tau)$ in the t, τ plane. However, we cannot average these two WDF approximations, in hopes of cancelling out the close-in lobes centered at $f = \pm(2\Delta)^{-1}$, because the two times, $m\Delta$ and $(m + \frac{1}{2})\Delta$, are not identical. (This timing observation is one reason for keeping Δ itself in all the equations, rather than setting Δ equal to 1 and losing track of the meaning of m vs. $m + \frac{1}{2}$). Nor can we discard either one of approximations (42) and (43), especially if criterion $\Delta < 1/F$ is closely met; the examples in (24)-(27) amply demonstrate the rapid variation of the WDF with time t .

We see from (40) and (41) that approximations to the continuous WDF are available at discrete time values with separation $\Delta_t = \Delta/2$ and at a continuum of f values. Thus we have succeeded in eliminating the discrete nature of one of the two initial time variables in the TCF, namely τ .

APPROXIMATE SPECTRAL CORRELATION FUNCTION VIA WDF

Guided by line 1 of definition (35), we adopt the following Trapezoidal approximation to the original SCF $A(v, f)$:

$$A_a^{(w)}(v, f) \equiv \frac{\Delta}{2} \sum_n \exp\left(-i2\pi v \frac{n\Delta}{2}\right) W_a\left(\frac{n\Delta}{2}, f\right) =$$

$$= \frac{\Delta}{2} \left\{ \sum_{n \text{ even}} + \sum_{n \text{ odd}} \right\} \exp\left(-i2\pi v \frac{n\Delta}{2}\right) W_a\left(\frac{n\Delta}{2}, f\right) \quad \text{for all } v, f. \quad (46)$$

Notice that this function is defined on a continuum in v, f space. The superscript w on approximation A_a denotes the fact that we have used the WDF route to get into the v, f plane. The increment on t in (46) is $\Delta_t = \Delta/2$, in keeping with the available WDF values in (40) and (41) together. This approximation satisfies the symmetry rule, $A_a^{(w)}(-v, f) = A_a^{(w)}(v, f)^*$, just as for the original SCF $A(v, f)$.

We let $n = 2m$ in the first sum in (46), and let $n = 2m + 1$ in the second sum. There follows, upon use of (42) and (43),

$$A_a^{(w)}(v, f) = \frac{\Delta}{2} \sum_m \exp(-i2\pi v \Delta m) W_a(m\Delta, f) +$$

$$+ \frac{\Delta}{2} \sum_m \exp\left(-i2\pi v \Delta \left(m + \frac{1}{2}\right)\right) W_a\left(\left(m + \frac{1}{2}\right)\Delta, f\right) =$$

$$= \frac{1}{2} \sum_q \Delta \sum_m \exp(-i2\pi v \Delta m) W(m\Delta, f - \frac{q}{2\Delta}) +$$

$$+ \frac{1}{2} \sum_q (-1)^q \Delta \sum_m \exp[-i2\pi v \Delta (m + \frac{1}{2})] W\left(\left(m + \frac{1}{2}\right)\Delta, f - \frac{q}{2\Delta}\right). \quad (47)$$

But

$$\begin{aligned}
 & \Delta \sum_m \exp(-i2\pi v \Delta m) W(m\Delta, f') = \\
 & = \int dt \exp(-i2\pi v t) W(t, f') \Delta \sum_m \delta(t - m\Delta) = \\
 & = A(v, f') \bigoplus^v \sum_m \delta(v - \frac{m}{\Delta}) = \\
 & = \sum_m A(v - \frac{m}{\Delta}, f') , \tag{48}
 \end{aligned}$$

while

$$\begin{aligned}
 & \Delta \sum_m \exp[-i2\pi v \Delta(m + \frac{1}{2})] W((m + \frac{1}{2})\Delta, f') = \\
 & = \int dt \exp(-i2\pi v t) W(t, f') \Delta \sum_m \delta(t - (m + \frac{1}{2})\Delta) = \\
 & = A(v, f') \bigoplus^v \sum_m (-1)^m \delta(v - \frac{m}{\Delta}) = \\
 & = \sum_m (-1)^m A(v - \frac{m}{\Delta}, f') . \tag{49}
 \end{aligned}$$

The use of these two relations in (47) yields the approximate SCF

$$A_a^{(w)}(v, f) = \frac{1}{2} \sum_q \sum_m A(v - \frac{m}{\Delta}, f - \frac{q}{2\Delta}) + \quad (50a)$$

$$+ \frac{1}{2} \sum_q \sum_m (-1)^{q+m} A(v - \frac{m}{\Delta}, f - \frac{q}{2\Delta}) = \quad (50b)$$

$$= \sum_q \sum_{\substack{m \\ q+m \text{ even}}} A(v - \frac{m}{\Delta}, f - \frac{q}{2\Delta}) \quad \text{for all } v, f. \quad (51)$$

We now have a function defined on a two-dimensional continuum in the two-frequency domain, v, f .

At this point, the reason for pursuing the use of all the available information becomes obvious. All the close-in lobes that caused problems have precisely cancelled in the SCF domain! Figure 6 depicts the regions in the v, f plane where approximation $A_a^{(w)}(v, f)$ in (51) can be nonzero; see also figure 3.

The SCF term in (50a) corresponds to use of only the information about the TCF given in (39a), within a factor of 2, whereas (50b) arises from (39b). Term (50a) by itself contains all the aliasing lobes centered at $v = \frac{m}{\Delta}, f = \frac{q}{2\Delta}$, with separations $\Delta_v = 1/\Delta, \Delta_f = (2\Delta)^{-1}$; condition (17) is then insufficient to prevent overlap, and (50a) is seriously aliased. A similar situation exists for (50b) by itself. It is only the average of these two pieces of information that succeeds in elimination of the troublesome close-in aliasing lobes in v, f space. And it is only in this last domain, where the functions are continuous in both variables, that this average can be conducted.

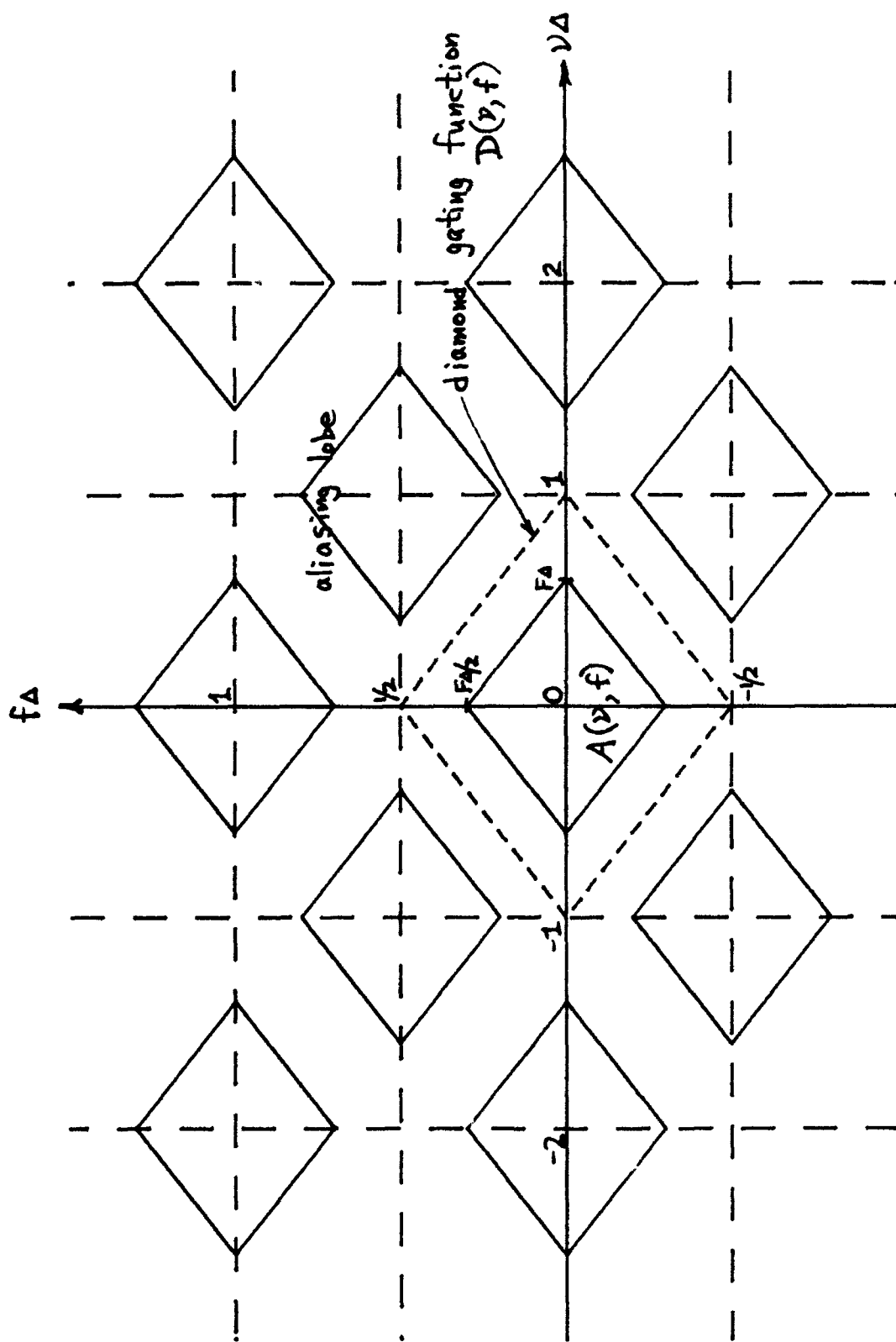


Figure 6. Approximate SCF $A_a(v, f)$

There will be no overlap of any of the remaining aliasing lobes in figure 6 if we choose, as in (17),

$$\Delta < \frac{1}{F} . \quad (52)$$

Notice that we do not have to require $\Delta < (2F)^{-1}$, in order to avoid the overlap. Furthermore, if we define the diamond gating function (see figure 6)

$$D(v, f) = \begin{cases} 1 & \text{for } \left| f \pm \frac{v}{2} \right| < \frac{1}{2\Delta} \\ 0 & \text{otherwise} \end{cases} , \quad (53)$$

then we can recover exactly the original SCF from approximation (51) according to

$$A_a^{(w)}(v, f) D(v, f) = A(v, f) \quad \text{for all } v, f . \quad (54)$$

But recovery of $A(v, f)$ is tantamount to recovering the exact continuous WDF, since

$$W(t, f) = \int dv \exp(i2\pi vt) A(v, f) \quad \text{for all } t, f . \quad (55)$$

Thus, criterion (52) is sufficient to guarantee the possibility of getting an alias-free WDF from discrete-time data.

Additional interpretations of (54) and a simple method of computing approximation $A_a^{(w)}(v, f)$ are addressed in the next section, after we have also looked at the route to the v, f plane by way of the CAF.

APPROXIMATE COMPLEX AMBIGUITY FUNCTION

Based on definition (34), we utilize the Trapezoidal approximation to the continuous CAF $x(v, \tau)$ at delay $\tau = 2q\Delta$, q integer:

$$\begin{aligned}
 x_a(v, 2q\Delta) &\equiv \Delta \sum_m \exp(-i2\pi v \Delta m) R(m\Delta, 2q\Delta) = \\
 &= \int dt \exp(-i2\pi vt) R(t, 2q\Delta) \Delta \sum_m \delta(t - m\Delta) = \\
 &= x(v, 2q\Delta) \otimes \sum_m \delta(v - \frac{m}{\Delta}) = \\
 &= \sum_m x(v - \frac{m}{\Delta}, 2q\Delta) \quad \text{for all } v. \quad (56)
 \end{aligned}$$

Notice that the t increment is Δ , as it must be, according to (39a) and figure 4; we are taking a horizontal slice at $\tau = 2q\Delta$ in figure 4.

However, there is an additional approximation available to the CAF, at delay $\tau = (2q + 1)\Delta$; again, referring to (34),

$$\begin{aligned}
 x_a(v, (2q + 1)\Delta) &\equiv \Delta \sum_m \exp[-i2\pi v \Delta(m + \frac{1}{2})] R_a((m + \frac{1}{2})\Delta, (2q + 1)\Delta) = \\
 &= \int dt \exp(-i2\pi vt) R(t, (2q + 1)\Delta) \Delta \sum_m \delta(t - (m + \frac{1}{2})\Delta) = \\
 &= x(v, (2q + 1)\Delta) \otimes \sum_m (-1)^m \delta(v - \frac{m}{\Delta}) = \\
 &= \sum_m (-1)^m x(v - \frac{m}{\Delta}, (2q + 1)\Delta) \quad \text{for all } v. \quad (57)
 \end{aligned}$$

The t increment is again Δ , but it is shifted by $\Delta/2$, in keeping with (39b) and figure 4. We are now taking a horizontal slice at $\tau = (2q + 1)\Delta$ in figure 4. The $(-1)^m$ factor is explained by (44).

The aliasing lobes in (56) and (57) are separated only by $\Delta_\nu = 1/\Delta$ and will overlap on the ν axis unless $\Delta < (2F)^{-1}$; see (38) and figure 7. Thus, the approximate CAF, $\chi_a(\nu, n\Delta)$ for n integer, suffers overlap due to aliasing, just as the WDF, $W_a(\frac{n}{2}\Delta, f)$ for n integer, does; elimination of overlap is achieved only if the stringent requirement $\Delta < (2F)^{-1}$ is met. Furthermore, again, we cannot directly average the two results in figure 7, in hopes of canceling the close-in lobes centered at $\nu = \pm 1/\Delta$, because the two delays, $2q\Delta$ and $(2q + 1)\Delta$, are not identical.

Equations (56) and (57), together, illustrate that approximations to the continuous CAF are available at discrete delay values with separation $\Delta_\tau = \Delta$ and at a continuum of ν values. Now we have succeeded in eliminating the discrete nature of the other of the two initial time variables in the TCF, namely t . The remaining Fourier transform into the SCF domain will eliminate the other discrete variable.

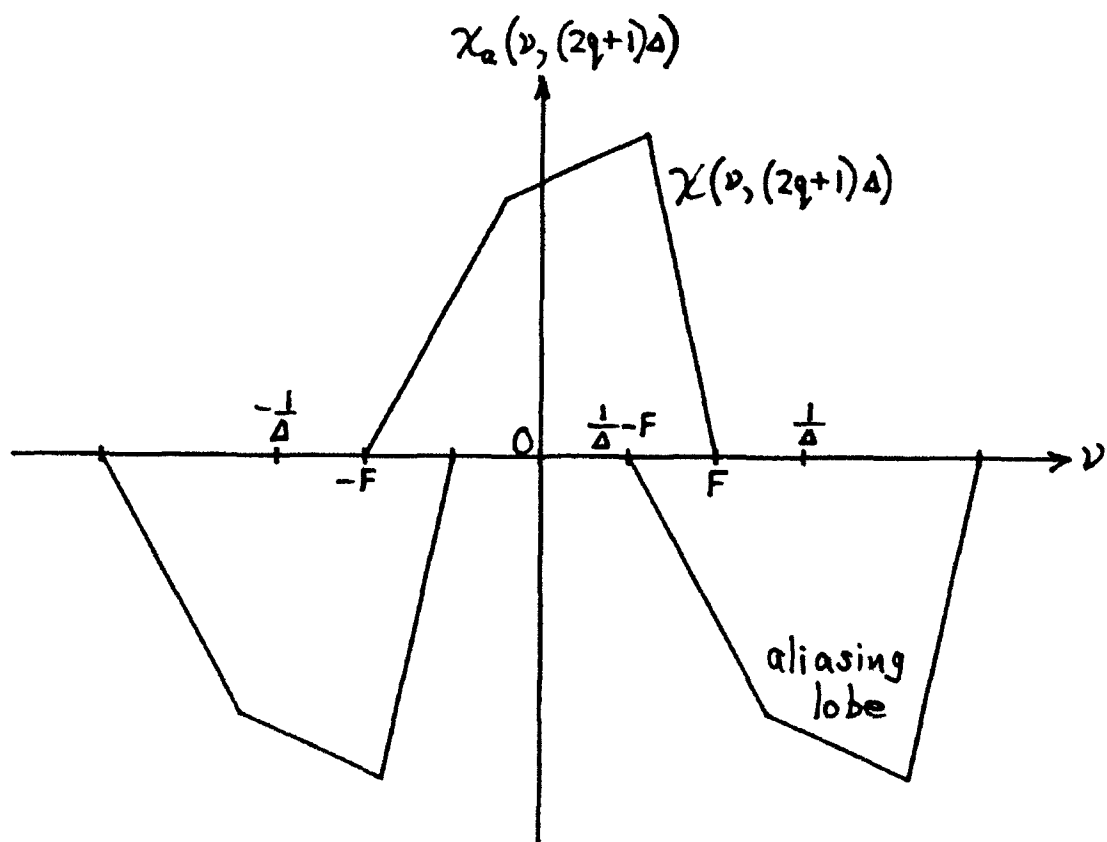
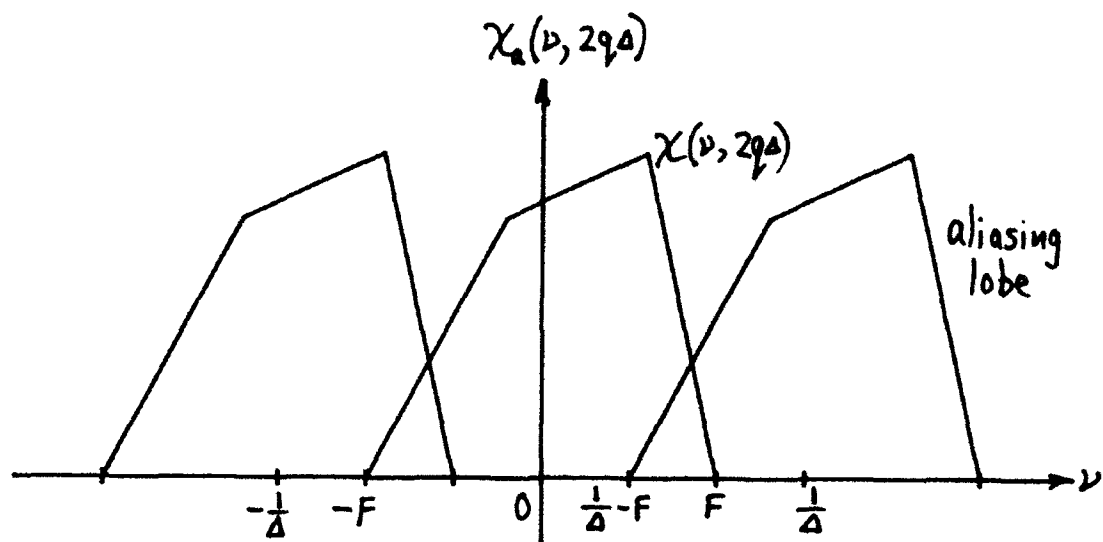


Figure 7. CAF Approximations

APPROXIMATE SPECTRAL CORRELATION FUNCTION VIA CAF

Guided by line 2 of definition (35), we obtain the following approximation to the original SCF $A(v, f)$:

$$\begin{aligned}
 A_a^{(c)}(v, f) &\equiv \Delta \sum_n \exp(-i2\pi f n \Delta) x_a(v, n\Delta) = \\
 &= \Delta \left\{ \sum_{n \text{ even}} + \sum_{n \text{ odd}} \right\} \exp(-i2\pi f n \Delta) x_a(v, n\Delta) \quad \text{for all } v, f. \quad (58)
 \end{aligned}$$

The superscript c on approximation A_a denotes that we are obtaining this result by way of the CAF. The increment on τ in (58) is $\Delta_\tau = \Delta$, in keeping with the available CAF values in (56) and (57) together.

Let $n = 2q$ in the first sum in (58), and let $n = 2q + 1$ in the second sum. There follows, upon use of (56) and (57),

$$\begin{aligned}
 A_a^{(c)}(v, f) &= \Delta \sum_q \exp(-i2\pi f \Delta 2q) x_a(v, 2q\Delta) + \\
 &+ \Delta \sum_q \exp[-i2\pi f \Delta (2q + 1)] x_a(v, (2q + 1)\Delta) = \\
 &= \sum_m \Delta \sum_q \exp(-i2\pi f \Delta 2q) x\left(v - \frac{m}{\Delta}, 2q\Delta\right) + \\
 &+ \sum_m (-1)^m \Delta \sum_q \exp[-i2\pi f \Delta (2q + 1)] x\left(v - \frac{m}{\Delta}, (2q + 1)\Delta\right). \quad (59)
 \end{aligned}$$

But

$$\begin{aligned}
 & \Delta \sum_q \exp(-i2\pi f \Delta 2q) \chi(v', 2q\Delta) = \\
 & = \int d\tau \exp(-i2\pi f \tau) \chi(v', \tau) \Delta \sum_q \delta(\tau - 2q\Delta) = \\
 & = A(v', f) \otimes \frac{1}{2} \sum_q \delta(f - \frac{q}{2\Delta}) = \\
 & = \frac{1}{2} \sum_q A(v', f - \frac{q}{2\Delta}) , \tag{60}
 \end{aligned}$$

while

$$\begin{aligned}
 & \Delta \sum_q \exp[-i2\pi f \Delta (2q + 1)] \chi(v', (2q + 1)\Delta) = \\
 & = \int d\tau \exp(-i2\pi f \tau) \chi(v', \tau) \Delta \sum_q \delta(\tau - (2q + 1)\Delta) = \\
 & = A(v', f) \otimes \frac{1}{2} \sum_q (-1)^q \delta(f - \frac{q}{2\Delta}) = \\
 & = \frac{1}{2} \sum_q (-1)^q A(v', f - \frac{q}{2\Delta}) . \tag{61}
 \end{aligned}$$

The use of these two relations in (59) yields the approximate SCF

$$\begin{aligned}
A_a^{(c)}(v, f) &= \frac{1}{2} \sum_m \sum_q A(v - \frac{m}{\Delta}, f - \frac{q}{2\Delta}) + \\
&+ \frac{1}{2} \sum_m \sum_q (-1)^{m+q} A(v - \frac{m}{\Delta}, f - \frac{q}{2\Delta}) = \\
&= \sum_{\substack{m \\ m+q \text{ even}}} \sum_q A(v - \frac{m}{\Delta}, f - \frac{q}{2\Delta}) \quad \text{for all } v, f. \quad (62)
\end{aligned}$$

But this result is identical to the approximate SCF $A_a^{(w)}(v, f)$ given in (51) and figure 6. That is, we obtain the same continuous approximation in the v, f domain, whether we approach it via the WDF or the CAF. This apparently fortuitous result is due to the fact that we used all the available information about the TCF when we started with (39), and kept all of it in passage through the WDF or CAF domains.

Figure 6 is again applicable, and we now see that we can drop superscripts w and c from (51) and (62), respectively, since there is only one approximation in the SCF domain. (The comments following (51) are also directly applicable here.)

A rigorous proof of the equality of the two approximations available for the SCF is given in appendix B. It utilizes an impulsive sampling approach, similar to (9) but in two dimensions, and can be considered as an alternative to the approximation approach developed in this section. Of course, the end result for the SCF in the v, f domain is again (51) or (62) or figure 6.

SUMMARY STATUS IN ALL FOUR DOMAINS

The results for the approximations to the TCF, WDF, CAF, and SCF are sketched in figure 8. These plots are a condensation of the exact analytical results given by (39), (42) & (43), (56) & (57), and (51) & (62), respectively. For example, the approximate WDF in the lower left of figure 8 is available only along the slices where $t = n\Delta/2$, n integer. Along these slices, the aliasing lobes (in frequency) alternate in polarity if n is odd, but remain positive for n even. (Positive lobes are drawn toward the right side in the figure).

Horizontal movement from one diagram to another in figure 8 is accomplished by a Fourier transform from t to ν (or vice versa). Vertical movement is according to a Fourier pair relating τ and f . Finally, the diagonal connection between R_a and A_a , or between W_a and x_a , is by means of a double Fourier transform.

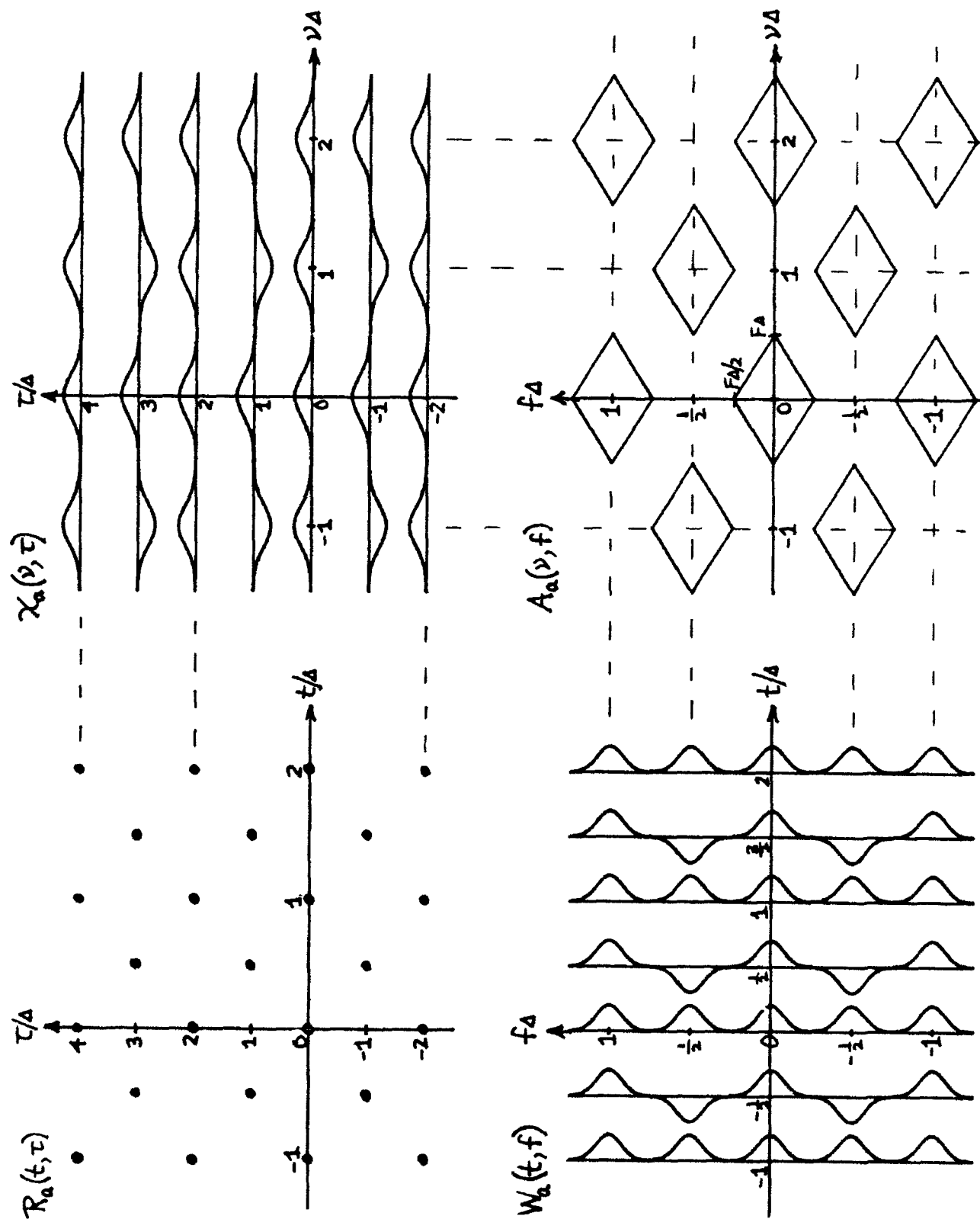


Figure 8. Locations of Available Information

RECOVERY OF ORIGINAL CONTINUOUS TWO-DIMENSIONAL FUNCTIONS

We have seen, by means of (52)-(54) and figure 6, that the original SCF can be recovered from the approximate SCF

$$A_a(v, f) = \sum_q \sum_{\substack{m \\ q+m \text{ even}}} A(v - \frac{m}{\Delta}, f - \frac{q}{2\Delta}) \quad \text{for all } v, f, \quad (63)$$

by means of the diamond gating function $D(v, f)$ in (53), provided that $\Delta < 1/F$. We have used (51) and (62) here, and dropped the superscripts in accordance with the discussion following (62). This means that we have the possibility of evaluating the original continuous TCF $R(t, \tau)$, WDF $W(t, f)$, and CAF $\chi(v, \tau)$ at any argument values we please.

SIMPLIFICATION OF SCF $A_a(v, f)$

It would be an extremely tedious task to evaluate the approximate SCF A_a directly by its definition (46) coupled with (40) and (41), which, in turn, are based upon starting information (39). In fact, there is a startlingly simple way of computing A_a .

Recall from (16) that spectrum

$$\begin{aligned} \tilde{S}(f) &= \Delta \sum_k \exp(-i2\pi f \Delta k) s(k\Delta) = \\ &= \sum_k S(f - \frac{k}{\Delta}) \quad \text{for all } f. \end{aligned} \quad (64)$$

Therefore

$$\begin{aligned}\tilde{S}(f + \frac{v}{2}) \tilde{S}^*(f - \frac{v}{2}) &= \sum_k \sum_l S(f + \frac{v}{2} - \frac{k}{\Delta}) S^*(f - \frac{v}{2} - \frac{l}{\Delta}) = \\ &= \sum_k \sum_l A(v - \frac{k-l}{\Delta}, f - \frac{k+l}{2\Delta}) \quad \text{for all } v, f, \end{aligned} \quad (65)$$

where we used (35). Now let $m = k - l$ and $q = k + l$; then

$\frac{m+q}{2} = k$, $\frac{q-m}{2} = l$, meaning that $m \pm q$ must always be even. Therefore, (65) can be expressed as

$$\tilde{S}(f + \frac{v}{2}) \tilde{S}^*(f - \frac{v}{2}) = \sum_{\substack{q \\ q+m \text{ even}}} \sum_m A(v - \frac{m}{\Delta}, f - \frac{q}{2\Delta}) \quad \text{for all } v, f. \quad (66)$$

But (66) is identical with (63)! Thus we have the compact result for the approximate SCF

$$A_a(v, f) = \tilde{S}(f + \frac{v}{2}) \tilde{S}^*(f - \frac{v}{2}) \quad \text{for all } v, f, \quad (67)$$

where

$$\tilde{S}(f) = \Delta \sum_k \exp(-i2\pi f \Delta k) s(k\Delta) \quad \text{for all } f, \quad (68)$$

in terms of the original time samples $\{s(k\Delta)\}$.

It is convenient at this point to define, for all f , the function

$$\bar{S}(f) = \tilde{S}(f) \text{rect}(\Delta f) = \begin{cases} \Delta \sum_k \exp(-i2\pi f \Delta k) s(k\Delta) & \text{for } |f| < \frac{1}{2\Delta} \\ 0 & \text{otherwise} \end{cases}, \quad (69)$$

which can be computed directly from the samples $\{s(k\Delta)\}$. Then since $\Delta < 1/F$, reference to figure 2 and (18) reveals that

$$\bar{S}(f) = S(f) \quad \text{for all } f. \quad (70)$$

The only reason for distinguishing between \bar{S} and S is that we think of \bar{S} as being computed directly from samples $\{s(k\Delta)\}$ via (69), whereas we think of S as being computed from $s(t)$ via Fourier transform (13). Strictly, since $S(f)$ is bandlimited to $\pm F/2$, $\bar{S}(f)$ in (69) only needs to be computed in that somewhat smaller range of f .

At this point, we refer back to (52)-(54) and figure 6 to find that

$$A(v, f) = A_a(v, f) \quad D(v, f) = \bar{S}(f + \frac{v}{2}) \bar{S}^*(f - \frac{v}{2}) \quad \text{for all } v, f, \quad (71)$$

since only the origin lobe in figure 6 can contribute, and there is no overlap. Thus we have a very direct way of recovering the original SCF from the time data samples: compute $\bar{S}(f)$ from (69), and then $A(v, f)$ from (71). All these results are predicated on sampling rate condition $\Delta < 1/F$; they do not require $\Delta < (2F)^{-1}$.

If we substitute (70) in (71), we have original definition (35). Thus we have come full circle on the SCF, returning with an obvious relation. This indicates that a shortcut could have been taken with regard to getting the key result (67). We have pursued the longer route because it indicates what the complete set of fundamental processing equations are, and it clarifies a number of points that have been under contention in the literature.

RECOVERY OF ORIGINAL WDF AND CAF

From (37) and (71), we obtain the original continuous WDF as

$$W(t, f) = \int dv \exp(i2\pi vt) \bar{S}(f + \frac{v}{2}) \bar{S}^*(f - \frac{v}{2}) \quad \text{for all } t, f, \quad (72)$$

where $\bar{S}(f)$ is given by (69) in terms of samples $\{s(k\Delta)\}$. The truncation of $\bar{S}(f)$ at $f = \pm (2\Delta)^{-1}$ in (69) is what prevents all the distant sidelobes of $A_a(v, f)$ from contributing. We could hardly have expected a simpler result.

From (37) and (71), we also obtain the original CAF according to

$$\chi(v, \tau) = \int df \exp(i2\pi f\tau) \bar{S}(f + \frac{v}{2}) \bar{S}^*(f - \frac{v}{2}) \quad \text{for all } v, \tau. \quad (73)$$

Thus, both the WDF and the CAF can be recovered by single Fourier transforms of the same product function, but on complementary variables v and f , respectively.

RECOVERY OF ORIGINAL TCF

Probably the best way to recover the original TCF $R(t, \tau)$ is by means of a combination of (32), (5), and (70):

$$R(t, \tau) = s(t + \frac{\tau}{2}) s^*(t - \frac{\tau}{2}), \quad (74)$$

with

$$s(t) = \int df \exp(i2\pi ft) \bar{S}(f). \quad (75)$$

All the above procedures employ $\bar{S}(f)$ and a Fourier transform in some fashion. The quantity $\bar{S}(f)$ can be computed at any f of interest, directly from samples $\{s(k\Delta)\}$, by means of (69).

DIRECT TIME DOMAIN RECOVERY OF CONTINUOUS WDF

We have given two alternatives for the recovery of continuous time waveform $s(t)$ from samples $\{s(k\Delta)\}$. They are (21) or (75) & (69). If we employ the former in the time definition of the original WDF (line 1 of (26)), we find, for all t, f ,

$$\begin{aligned}
 W(t, f) &= \int d\tau \exp(-i2\pi f\tau) s(t + \frac{\tau}{2}) s^*(t - \frac{\tau}{2}) = \\
 &= \Delta \sum_k \sum_l \exp[-i2\pi f\Delta(k - l)] s(k\Delta) s^*(l\Delta) W_0(t - \frac{k+l}{2}\Delta, f), \quad (76)
 \end{aligned}$$

where

$$W_0(t, f) = \begin{cases} \frac{\sin[2\pi(1 - 2|f|\Delta) t/\Delta]}{\pi t/\Delta} & \text{for } |f| < \frac{1}{2\Delta} \\ 0 & \text{for } |f| > \frac{1}{2\Delta} \end{cases} \quad \text{for all } t. \quad (77)$$

This result is equivalent to [5, (5)&(6)]. However, as noted there, this alternative for the WDF is not computationally attractive, although (76) is certainly alias-free because it is restoring $W(t, f)$ itself, and not some approximation to it.

As an aside, if the frequency domain version of the WDF is used instead (line 2 of (26)), and if (21) is immediately transformed into the frequency domain, we get directly

$$S(f) = \tilde{S}(f) \text{ rect}(\Delta f) = \bar{S}(f) , \quad (78)$$

in complete agreement with (72).

In the sequel to (62), it was mentioned that an alternative approach involving impulsive sampling could be used to get various impulsive two-dimensional functions from samples $\{s(k\Delta)\}$. In a similar vein, the continuous two-dimensional functions can be recovered by direct convolution (interpolation) in the domain(s) of interest. These alternative forms are not as numerically useful as the ones presented above, and so are deferred to appendix C. However, some useful insight into the inadequacy of some past attempts at interpolation is gained by this alternative viewpoint, and the readers attention is directed to these results.

DISCUSSION

In retrospect, (72) and (69) are an obvious result. We know that the original continuous WDF is given by (line 2 of (26))

$$W(t, f) = \int dv \exp(i2\pi vt) S(f + \frac{v}{2}) S^*(f - \frac{v}{2}) \quad \text{for all } t, f . \quad (79)$$

So if we can get $S(f)$ exactly from samples $\{s(k\Delta)\}$, in some (any) fashion, we can get W via (79). But, in fact, $\tilde{S}(f)$ in (69) is identically equal to $S(f)$ for all f , when $\Delta < 1/F$. Condition $\Delta < (2F)^{-1}$ is patently unnecessary and too restrictive. A similar comment holds with regard to the CAF.

Given samples $\{s(k\Delta)\}$, the function $\bar{S}(f)$ in (69) can be computed at any desired f values of interest. Therefore the product

$$\bar{S}(f + \frac{v}{2}) \bar{S}^*(f - \frac{v}{2}) \quad (80)$$

required in (72) and (73) can be computed at any v, f values needed, and the integrals for $W(t, f)$ and $\chi(v, \tau)$ evaluated very accurately at any arguments of interest.

This is the major difference relative to the TCF $R(t, \tau)$, (74), which could only be calculated at interspersed points in the t, τ plane from the available data; see (39) and figure 4. Strictly, waveform $s(t)$ could be interpolated, and then TCF $R(t, \tau)$ filled in at the intermediate points of interest in figure 4. This viable alternative requires just slightly more calculations than the frequency domain approach given above; we will discuss and compare both alternatives in a later section.

In practice, $\bar{S}(f)$ will only be calculated at a discrete set of frequencies, in order to economize on computational effort. We then find that the product function (80) is available at interspersed points in the v, f plane in an identical manner to that for TCF $R(t, \tau)$ in figure 4. In fact, if $\bar{S}(f)$ is computed only for $f/\Delta_f = \text{integer}$, then (80) is available only at

$$f/\Delta_f = \text{integer} , \quad v/\Delta_f = \text{even integer} \quad (81)$$

and at

$$f/\Delta_f = \text{odd integer}/2 , \quad v/\Delta_f = \text{odd integer} . \quad (82)$$

Just as this type of interspersed sampling required a finer sampling interval in the time domain (see figure 5 and (45)), so also is a finer increment required here in the frequency domain. Namely, we must have

$$\Delta_f < \frac{1}{2T}, \quad (83)$$

in order to avoid aliasing in the t domain of the reconstructed WDF via Fourier transform (72). The same requirement holds for aliasing control in the τ domain of the reconstructed CAF via (73). Here, T is the overall effective duration of waveform $s(t)$:

$$|s(t)| \approx 0 \quad \text{for } |t| > T/2. \quad (84)$$

See figure 9. (The waveform can be centered at $t = 0$ without loss of generality, merely by time delaying it.) However, there is a very convenient and efficient way to meet requirement (83), as will be shown shortly, whereas requirement (45), $\Delta < (2F)^{-1}$, is very unattractive, at least through direct sampling of time domain waveform $s(t)$.

Since the total extent of the spectrum $S(f)$ is F Hz (see (14) and figure 1), waveform $s(t)$ cannot be strictly time-limited. However, we assume that a finite T value can be found for figure 9 such that approximation (84) is a good one. Strictly, (84) should read

$$\frac{|s(t)|}{\max |s(t)|} \ll 1 \quad \text{for } |t| > T/2. \quad (85)$$

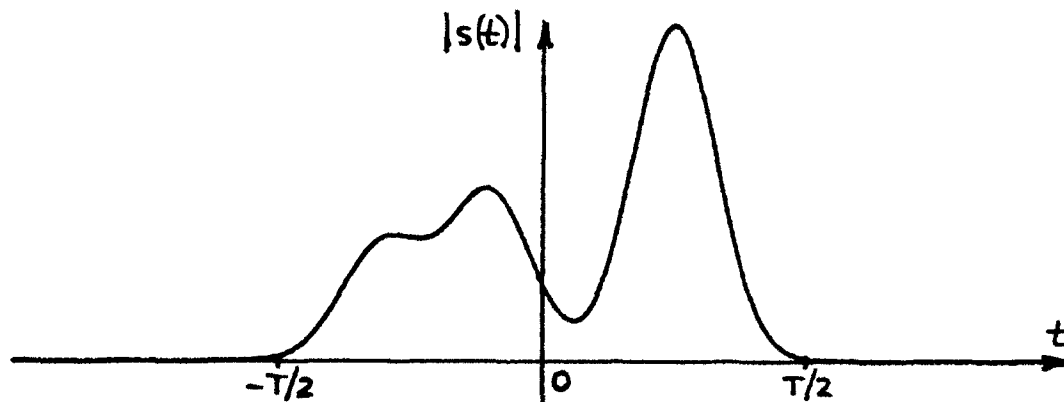


Figure 9. Waveform $s(t)$

DISCRETE PROCESSING IN FREQUENCY DOMAIN

Thus far, we have not discretized in the frequency domain; both ν and f have been allowed to take on continuous values. So we have, from (69),

$$\bar{S}(f) = \Delta \sum_k \exp(-i2\pi f \Delta k) s(k\Delta) \quad \text{for } |f| < \frac{1}{2\Delta}. \quad (86)$$

Now, suppose that we only evaluate $\bar{S}(f)$ at a set of discrete frequencies, according to

$$\bar{S}\left(\frac{n}{N\Delta}\right) = \Delta \sum_k \exp(-i2\pi nk/N) s(k\Delta) \quad \text{for } |n| < \frac{N}{2}. \quad (87)$$

Since the sum on the right-hand side of (87) has period N in n , we can evaluate it quickly via a collapsed N -point FFT; see (10)-(12). The negative n values desired in (87) are easily accommodated by means of a modulo N look-up in the FFT output.

EVALUATION OF WDF

The increment in argument f of $\bar{S}(f)$ in (87) is

$$\Delta_f = \frac{1}{N\Delta}. \quad (88)$$

In order to use these results in approximating integral (72) for the WDF,

$$W(t, f) = \int d\nu \exp(i2\pi \nu t) \bar{S}\left(f + \frac{\nu}{2}\right) \bar{S}^*\left(f - \frac{\nu}{2}\right), \quad (89)$$

we need to have the increment in ν satisfy (due to the $\nu/2$ arguments)

$$\frac{1}{2} \Delta_v = \frac{1}{N\Delta}, \quad \text{i.e.,} \quad \Delta_v = \frac{2}{N\Delta}. \quad (90)$$

So if we limit v in (89) to the values $\frac{2\ell}{N\Delta}$, one possible Trapezoidal approximation to W is

$$\tilde{W}(t, f) \equiv \frac{2}{N\Delta} \sum_{\ell} \exp(i2\pi \frac{2\ell}{N\Delta} t) \bar{S}(f + \frac{\ell}{N\Delta}) \bar{S}^*(f - \frac{\ell}{N\Delta}) \quad \text{for all } t, f. \quad (91)$$

This function is defined on a continuum in time, frequency space. But this can be developed according to

$$\begin{aligned} \tilde{W}(t, f) &= \int dv \exp(i2\pi vt) \bar{S}(f + \frac{v}{2}) \bar{S}^*(f - \frac{v}{2}) \frac{2}{N\Delta} \sum_{\ell} \delta(v - \frac{2\ell}{N\Delta}) = \\ &= W(t, f) \otimes \sum_{\ell} \delta(t - \ell \frac{N\Delta}{2}) = \\ &= \sum_{\ell} W(t - \ell \frac{N\Delta}{2}, f) \quad \text{for all } t, f, \end{aligned} \quad (92)$$

where we used (72).

Since waveform $s(t)$ is approximately limited to $|t| < T/2$ (see (84) and figure 9), then WDF $W(t, f)$ is also approximately limited to $|t| < T/2$, as may be seen from line 1 of (26). The approximation (92) then appears as in figure 10.

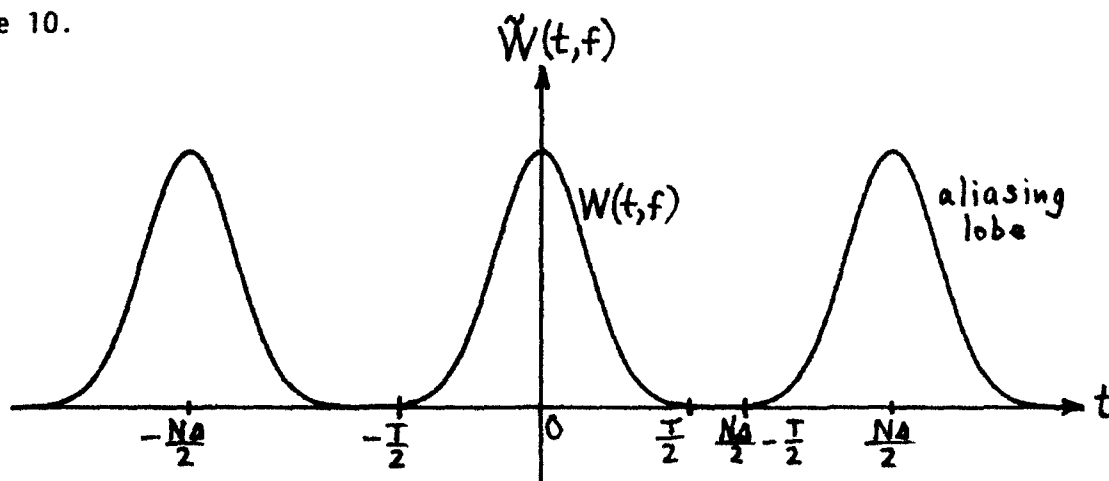


Figure 10. Time-Aliased WDF

In order that approximate WDF \tilde{W} not suffer significant overlap in time, we see that we need

$$\frac{T}{2} < \frac{N\Delta}{2} - \frac{T}{2}, \quad \text{i.e., } N > \frac{2T}{\Delta}. \quad (93)$$

The FFT size, N , in (87) must be at least twice as large as the number of samples, T/Δ , taken of waveform $s(t)$. Recalling (88), this inequality becomes

$$\Delta_f = \frac{1}{N\Delta} < \frac{1}{2T}, \quad (94)$$

consistent with (83), as predicted. Thus, approximation $\tilde{W}(t, f)$ is an extremely good approximation to $W(t, f)$ for $|t| < T/2$ if FFT size N satisfies (93). The goodness of \tilde{W} depends critically on the degree of satisfaction of (85).

More generally, we could limit the ν values in (89) to

$$\nu = \nu_0 + \frac{2\ell}{N\Delta}, \quad \nu_0 \text{ arbitrary} \quad (\Delta_\nu = \frac{2}{N\Delta}), \quad (95)$$

getting alternative approximation

$$\begin{aligned} \tilde{W}_a(t, f) &\equiv \int d\nu \exp(i2\pi t\nu) \bar{S}(f + \frac{\nu}{2}) \bar{S}^*(f - \frac{\nu}{2}) \frac{2}{N\Delta} \sum_{\ell} \delta(\nu - \nu_0 - \frac{2\ell}{N\Delta}) = \\ &= W(t, f) \otimes \left\{ \exp(i2\pi t\nu_0) \sum_{\ell} \delta\left(t - \ell \frac{N\Delta}{2}\right) \right\} = \\ &= \sum_{\ell} W\left(t - \ell \frac{N\Delta}{2}, f\right) \exp(i\pi\nu_0 N\Delta\ell) \quad \text{for all } t, f. \end{aligned} \quad (96)$$

The plot for $|\tilde{W}_a(t, f)|$ is identical to that of $|\tilde{W}(t, f)|$ in figure 10, since the magnitude of phase factor $\exp(i\pi\nu_0 N\Delta\ell)$ is 1 for all ℓ . The main lobe, $\ell = 0$, is unaffected by the choice of ν_0 . So criterion (93) is again sufficient to avoid time-aliasing in \tilde{W}_a , regardless of shift ν_0 .

DISCRETIZATION IN TIME AND FREQUENCY

For convenience, we therefore return to \tilde{W} in (91) and get, in particular, the values

$$\tilde{W}(t, \frac{n}{N\Delta}) = \frac{2}{N\Delta} \sum_l \exp(i2\pi \frac{2l}{N\Delta} t) \bar{S}(\frac{n+l}{N\Delta}) \bar{S}^*(\frac{n-l}{N\Delta}) \quad \text{for all } t, \quad (97)$$

where we must choose frequency $f = \frac{n}{N\Delta}$, in order to use the available samples of \bar{S} in (87). We now further choose time

$$t = \frac{m\Delta}{2} \frac{N}{M} \quad (98)$$

and get the approximation in the form

$$\tilde{W}(\frac{m\Delta}{2} \frac{N}{M}, \frac{n}{N\Delta}) = \frac{2}{N\Delta} \sum_l \exp(i2\pi m l / M) \bar{S}(\frac{n+l}{N\Delta}) \bar{S}^*(\frac{n-l}{N\Delta}) . \quad (99)$$

The reason for this choice of t values is that this sum can be accomplished as a collapsed M -point FFT as described in (10)-(12). The range of values that must be covered is

$$\frac{|m|\Delta}{2} \frac{N}{M} < \frac{T}{2}, \quad \text{i.e., } |m| < \frac{T}{\Delta} \frac{M}{N} \quad (100)$$

and

$$\frac{|n|}{N\Delta} < \frac{F}{2}, \quad \text{i.e., } |n| < F\Delta \frac{N}{2}. \quad (101)$$

Coincidentally, this identical procedure above has already been derived by the author in [9, (A-13)&(A-14)]. However, it was done, at that time, to generate slices in time of the WDF, without realizing that the procedure also had an alias-elimination feature. Requirement (93) was [9, (A-5)&(A-6)].

INCREMENTS IN t AND f

The increments in t and f in approximation $\tilde{W}(t,f)$ in (99) are

$$\Delta_t = \frac{\Delta}{2} \frac{N}{M} \quad \text{and} \quad \Delta_f = \frac{1}{N\Delta} . \quad (102)$$

Since the original WDF is given by

$$W(t,f) = \int d\tau \exp(-i2\pi f\tau) R(t,\tau) , \quad (103)$$

and the effective extent of $R(t,\tau)$ in τ is $\pm T$ for the waveform $s(t)$ satisfying (84), then we must require

$$\Delta_f < \frac{1}{2T} , \quad \text{i.e., } N > \frac{2T}{\Delta} , \quad (104)$$

in order to track the variation of $W(t,f)$ in f . (See appendix A.) However, this was a condition already encountered in (93).

Furthermore, since we have the alternative Fourier transform

$$W(t,f) = \int dv \exp(i2\pi vt) A(v,f) , \quad (105)$$

and the extent of $A(v,f)$ in v is $\pm F$, then we must also have

$$\Delta_t < \frac{1}{2F} , \quad \text{i.e., } \Delta < \frac{1}{F} \frac{M}{N} , \quad (106)$$

in order to track $W(t,f)$ variations in t . Now if we choose M smaller than N , say $M = N/2$, then we obtain condition $\Delta < (2F)^{-1}$. But this is a finer time sampling increment than required. Also (102) gives $\Delta_t = \Delta$, which does not track $W(t,f)$ adequately in time; see (24)-(31). Conversely, if we choose M larger than N , say $M = 2N$, then we get $\Delta < 2/F$, which is already accommodated by the earlier requirement

$\Delta < 1/F$. And $\Delta_t = \Delta/4$, which is overly fine in time. So, in order to minimize the range of m values needed for investigation, we choose

$$M = N . \quad (107)$$

Notice that the time increment Δ_t in (102) for $\tilde{W}(t,f)$ is then $\Delta_t = \Delta/2$, not the Δ that was sufficient for sampling $s(t)$. This is consistent with the fact that $W(t,f)$ can be sharper in t than $s(t)$.

SUMMARY OF WDF EQUATIONS

Here we summarize the major assumptions and requirements and list the major equations by which the approximate WDF \tilde{W} can be computed.

Assumptions:

$$\begin{aligned} S(f) &= 0 & \text{for } |f| > F/2 , \\ |s(t)| &\approx 0 & \text{for } |t| > T/2 . \end{aligned} \quad (108)$$

This is no loss of generality, since the waveform can be time delayed and frequency shifted as desired.

Requirements:

$$\begin{aligned} \Delta &< \frac{1}{F} , \\ N &> \frac{2T}{\Delta} \quad (> 2TF) . \end{aligned} \quad (109)$$

Equations:

$$\tilde{S}\left(\frac{n}{N\Delta}\right) = \left\{ \begin{array}{ll} \Delta \sum_k \exp(-i2\pi nk/N) s(k\Delta) & \text{for } |n| < \frac{N}{2} \\ 0 & \text{otherwise} \end{array} \right\} . \quad (110)$$

$$\tilde{W}(\frac{m\Delta}{2}, \frac{n}{N\Delta}) = \frac{2}{N\Delta} \sum_l \exp(i2\pi m l / N) \bar{S}(\frac{n+l}{N\Delta}) \bar{S}^*(\frac{n-l}{N\Delta})$$

$$\text{for } |m| < \frac{T}{\Delta}, \quad |n| < \frac{N}{2} F\Delta. \quad (111)$$

Operation (110) can be accomplished by a single N-point FFT with collapsing, while (111) requires an N-point FFT for each n value of interest. The latter N-point FFT (for a given n) will sweep out N values of integer m; this will cover a total time range of $N \frac{\Delta}{2} > T$, as desired. The total number of n (frequency) values to be searched is $NF\Delta$. Values of \tilde{W} for negative values of m are available in location m modulo N of the FFT output.

For the most advantageous choices of

$$\Delta = \frac{1}{F}, \quad N = \frac{2T}{\Delta} = 2TF, \quad (112)$$

we have ranges

$$|m| < TF, \quad |n| < TF.$$

EVALUATION OF CAF

The equations for calculation of the CAF, from discretized frequency samples of $\bar{S}(f)$, are very similar to those given above for the WDF. Accordingly, they are deferred to appendix D.

INTERPOLATION OF TIME WAVEFORM

It was mentioned in the sequel to (80) that available data samples $\{s(k\Delta)\}$ could be interpolated in time, to fill in the vacant spots of TCF $R(t, \tau)$ in figure 4. One procedure to accomplish this is by direct use of sinc-function interpolation in (21). However, a more efficient procedure is by use of FFTs.

From (22), we can get samples of the approximate spectrum according to

$$\tilde{S}\left(\frac{m}{M\Delta}\right) = \Delta \sum_k \exp(-i2\pi mk/M) s(k\Delta) \quad \text{for } |m| \leq \frac{M}{2}. \quad (113)$$

which can be accomplished by an M -point FFT. The frequency increment is $\Delta_f = (M\Delta)^{-1}$. The original continuous time waveform is

$$\begin{aligned} s(t) &= \int df \exp(i2\pi ft) S(f) = \\ &= \int_{-(2\Delta)^{-1}}^{(2\Delta)^{-1}} df \exp(i2\pi ft) \tilde{S}(f) = \\ &\approx \frac{1}{M\Delta} \sum_{m=-M/2}^{M/2} \exp(i2\pi \frac{m}{M\Delta} t) \tilde{S}\left(\frac{m}{M\Delta}\right) = \\ &\equiv \hat{S}(t) \quad \text{for all } t, \end{aligned} \quad (114)$$

where we have utilized the fact that $\Delta < 1/F$. (The tic mark on the summation symbol indicates that the summand values at $m = \pm M/2$ must be scaled by $1/2$.)

But approximation $\hat{s}(t)$ can be developed in the form

$$\hat{s}(t) = \int_{-\frac{1}{2\Delta}}^{\frac{1}{2\Delta}} df \exp(i2\pi ft) \tilde{S}(f) \frac{1}{M\Delta} \sum_{m=-M/2}^{M/2} \delta(f - \frac{m}{M\Delta}) =$$

$$= \int df \exp(i2\pi ft) S(f) \frac{1}{M\Delta} \sum_m \delta(f - \frac{m}{M\Delta}) =$$

$$s(t) \otimes \sum_m \delta(t - mM\Delta) = \sum_m s(t - mM\Delta) \quad \text{for all } t. \quad (115)$$

This aliased function is illustrated in figure 11.

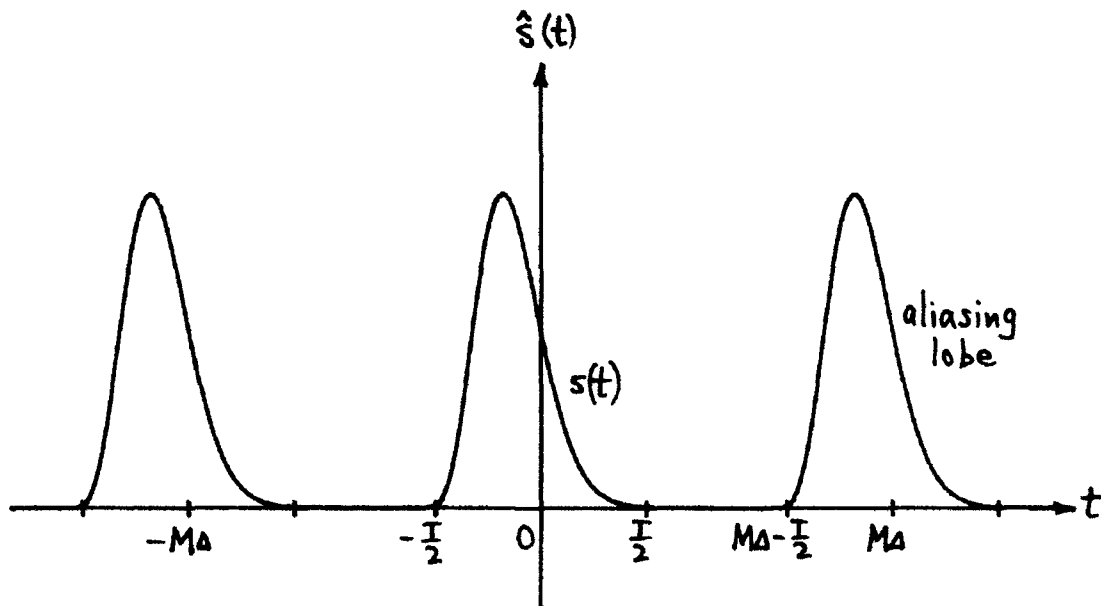


Figure 11. Time-Aliased Waveform $\hat{s}(t)$

In order to avoid time overlap in figure 11, we must have

$$M > \frac{T}{\Delta} \quad (> TF) . \quad (116)$$

If this FFT size requirement for (113) is met, then figure 11 reveals that

$$\hat{s}(t) \approx s(t) \quad \text{for } |t| < \frac{M\Delta}{2} ; \quad (117)$$

that is, we can expect that $\hat{s}(t)$ is a good approximation to $s(t)$.

In particular, if we want to interpolate samples $\{s(k\Delta)\}$ by a factor of 2, we have, from (117) and (114),

$$s\left(\frac{n\Delta}{2}\right) \approx \hat{s}\left(\frac{n\Delta}{2}\right) = \frac{1}{M\Delta} \sum_{m=-M/2}^{M/2} \exp(i2\pi \frac{mn}{2M}) \tilde{S}\left(\frac{m}{M\Delta}\right) \quad \text{for } |n| < M . \quad (118)$$

This can be done by a $2M$ -point FFT with zero-fill, and $\left\{\tilde{S}\left(\frac{m}{M\Delta}\right)\right\}_{-M/2}^{M/2}$ are made available by the M -point FFT in (113). The two requirements that must be met are

$$\Delta < \frac{1}{F}, \quad 2M > \frac{2T}{\Delta} \quad (> 2TF) . \quad (119)$$

This is the procedure utilized in [8].

DISCUSSION/SUMMARY

We have two alternatives for computing an alias-free WDF and CAF. The requirements that must be met are

$$\Delta < \frac{1}{F}, \quad M > \frac{T}{\Delta}, \quad N = 2M > \frac{2T}{\Delta}. \quad (120)$$

The processing equations are summarized below.

TIME DOMAIN APPROACH

$$\tilde{S}\left(\frac{m}{M\Delta}\right) = \Delta \sum_k \exp(-i2\pi mk/M) s(k\Delta) \quad \text{for } |m| \leq \frac{M}{2}, \quad (121)$$

$$\hat{S}\left(\frac{n\Delta}{2}\right) = \left\{ \begin{array}{ll} \frac{1}{M\Delta} \sum_{m=-M/2}^{M/2} \exp(i2\pi mn/N) \tilde{S}\left(\frac{m}{M\Delta}\right) & \text{for } |n| < M \\ 0 & \text{otherwise} \end{array} \right\}, \quad (122)$$

$$\hat{W}\left(\frac{m\Delta}{2}, \frac{n}{N\Delta}\right) = \Delta \sum_l \exp(-i2\pi nl/N) \hat{S}\left(\frac{m+l}{2} \Delta\right) \hat{S}^*\left(\frac{m-l}{2} \Delta\right) \\ \text{for } |m| < \frac{T}{\Delta}, \quad |n| < \frac{N}{2} F\Delta < \frac{N}{2}. \quad (123)$$

In the last equation, we obtain slices of the WDF in frequency (n) at fixed time (m). (This result is in essential agreement with [7, (77) and (74)]; however, we are not restricted here to $T = M\Delta$.)

FREQUENCY DOMAIN APPROACH

$$\bar{S}\left(\frac{n}{N\Delta}\right) = \begin{cases} \Delta \sum_k \exp(-i2\pi nk/N) s(k\Delta) & \text{for } |n| < \frac{N}{2}, \\ 0 & \text{otherwise} \end{cases}, \quad (124)$$

$$\begin{aligned} \tilde{W}\left(\frac{m\Delta}{2}, \frac{n}{N\Delta}\right) &= \frac{2}{N\Delta} \sum_l \exp(i2\pi ml/N) \bar{S}\left(\frac{n+l}{N\Delta}\right) \bar{S}^*\left(\frac{n-l}{N\Delta}\right) \\ &\text{for } |m| < \frac{T}{\Delta} < \frac{N}{2}, \quad |n| < \frac{N}{2} F\Delta. \end{aligned} \quad (125)$$

Here, we obtain slices of the WDF in time (m) at fixed frequency (n). (This result is in essential agreement with [7, (81)]; however, we are not restricted here to $2T = N\Delta$.)

COMPARISON

Since waveform $s(t) \approx 0$ for $|t| > T/2$, the sum on k in (121) can be confined to $|k| < \frac{T}{2\Delta} < \frac{M}{2} = \frac{N}{4}$, while the sum on k in (124) can similarly be confined to $|k| < \frac{T}{2\Delta} < \frac{N}{4}$.

The time domain approach requires one M -point ($M = N/2$) FFT, one N -point FFT, and then an N -point FFT for each time index m of interest. The frequency domain approach requires one N -point FFT and then an N -point FFT for each frequency index n of interest. Thus, the time domain approach requires one additional $M = \frac{N}{2}$ -point FFT, which is a negligible difference, compared with the multiple FFTs that must be performed for (123) or (125). The major difference between the two approaches appears to be whether one wants slices in frequency, or slices in time, of the WDF.

It should be emphasized that the procedure here reconstructs the original WDF of the continuous waveform $s(t)$, at any time, frequency (t, f) arguments of interest, from the samples $\{s(k\Delta)\}$. There is no need to define or set up some arbitrary discrete form of the WDF. The discretization of the t, f arguments of the WDFs is undertaken only after this reconstruction procedure has been delineated (via the ν, f plane) and the sufficiency of sampling requirement $\Delta < 1/F$ established. Of course, this eventual discretization in time/frequency is necessary in order to reduce the general procedure to a practical efficient algorithm. A similar set of arguments applies equally well to the reconstruction of the CAF.

An alternative philosophy, to developing Trapezoidal approximations for the various two-dimensional functions, is given in appendix B in terms of a pair of interspersed impulsive trains in the t, τ plane. The end result for the approximate SCF in the ν, f plane is shown to be identical to that obtained earlier.

The connection of this two-dimensional impulse train with direct time domain sampling of the waveform $s(t)$ is considered in appendix E. Again, the two approaches, time domain sampling versus t, τ domain sampling, are shown to yield the same result. Finally, the fundamental rules and patterns relating two-dimensional interspersed infinite sampling trains are displayed at the end of appendix E.

APPENDIX A. EXTENTS AND RATES OF VARIATION
OF TCF, WDF, CAF, SCF

From (5), we have Fourier pair

$$S(f) = \int dt \exp(-i2\pi ft) s(t) ,$$

$$s(t) = \int df \exp(i2\pi ft) S(f) ; \quad (A-1)$$

and from figures 1 and 2, we know that if

$$S(f) = 0 \quad \text{for } |f| > F/2 , \quad (A-2)$$

then samples $\{s(k\Delta_t)\}$ are sufficient for reconstruction of $s(t)$ if $\Delta_t < 1/F$. That is, if a spectrum is bandlimited in the frequency domain to total extent F Hz, samples of the corresponding time function must be taken with time increment $\Delta_t < 1/F$, in order not to lose any significant information.

In a similar vein, the duality of the equations in (A-1) indicates that if, instead,

$$s(t) = 0 \quad \text{for } |t| > T/2 , \quad (A-3)$$

then spectrum samples $\{S(n\Delta_f)\}$ are sufficient for reconstruction of $S(f)$ if frequency increment $\Delta_f < 1/T$.

The general rule, here, is that if a function in one domain is essentially limited to overall extent E , samples in its Fourier transform domain must be taken finer than $1/E$, in order not to lose any information. This rule will be used frequently below.

EXTENTS OF TCF, WDF, CAF, AND SCF

Henceforth, we assume that

$$S(f) \approx 0 \quad \text{for } |f| > F/2$$

and

$$s(t) \approx 0 \quad \text{for } |t| > T/2. \quad (\text{A-4})$$

Thus, the overall frequency and time extents are approximately F Hz and T seconds, respectively. It then readily follows from (32)-(38), namely,

$$R(t, \tau) = s(t + \frac{\tau}{2}) s^*(t - \frac{\tau}{2}), \quad (\text{A-5})$$

$$A(v, f) = S(f + \frac{v}{2}) S^*(f - \frac{v}{2}), \quad (\text{A-6})$$

$$W(t, f) = \int d\tau \exp(-i2\pi f\tau) R(t, \tau) = \quad (\text{A-7})$$

$$= \int dv \exp(i2\pi vt) A(v, f), \quad (\text{A-8})$$

$$\chi(v, \tau) = \int dt \exp(-i2\pi vt) R(t, \tau) = \quad (\text{A-9})$$

$$= \int df \exp(i2\pi f\tau) A(v, f), \quad (\text{A-10})$$

that the extents of these functions are as depicted in figure A-1. The solid curves depict the contour level within which the function is essentially

concentrated. In fact, for Gaussian waveform $s(t) = a \exp(-\frac{t^2}{2\sigma^2})$, the

choices $T = 4\sigma$, $F = \frac{2}{\pi\sigma}$, for example, give these exact results in figure A-1,

at the $\exp(-4) = .018$ level.

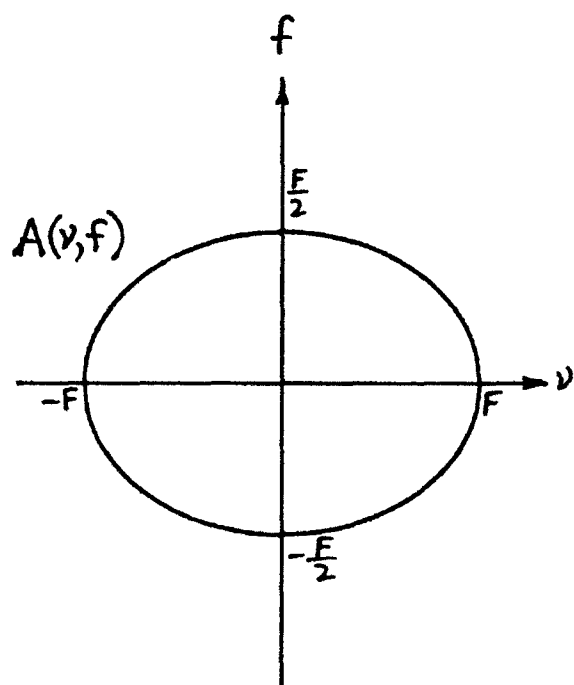
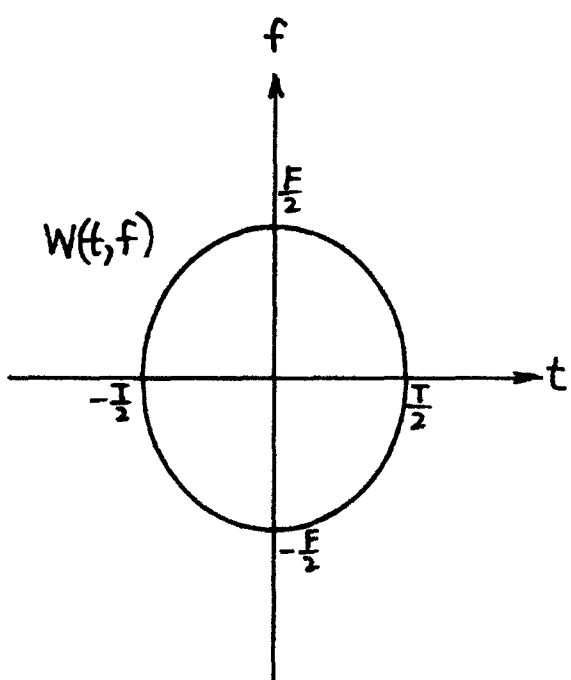
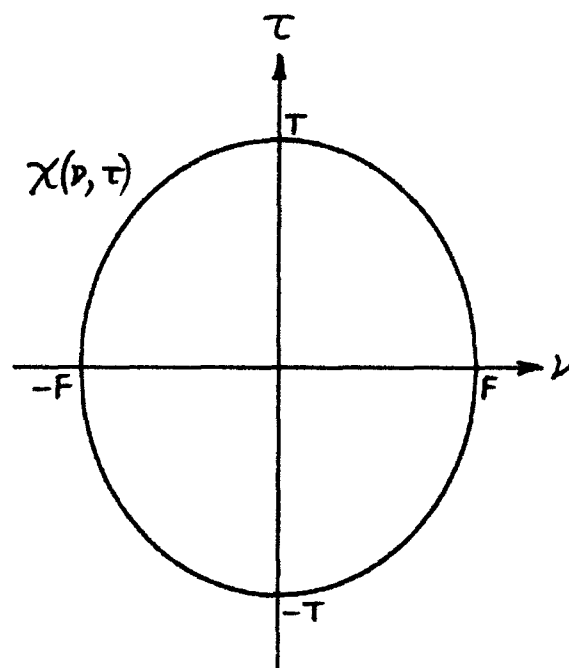
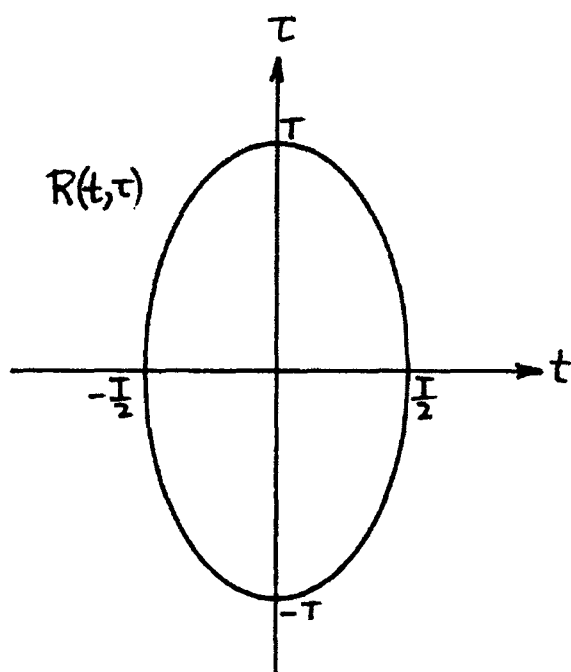


Figure A-1. Extents of the Two-Dimensional Functions

RATES OF VARIATION

We now combine the sampling rule deduced under (A-3) with the extents in figure A-1. From (A-7) and (A-8), we must have sampling increments (i.e., spacings of argument values on left-hand side) satisfy

$$\left. \begin{array}{l} \Delta_f < \frac{1}{2T} \\ \Delta_t < \frac{1}{2F} \end{array} \right\} \text{ to adequately track WDF .} \quad (\text{A-11})$$

From (A-9) and (A-10), we need

$$\left. \begin{array}{l} \Delta_v < \frac{1}{T} \\ \Delta_\tau < \frac{1}{F} \end{array} \right\} \text{ to track CAF .} \quad (\text{A-12})$$

By inverting (A-7)-(A-10), we express

$$R(t, \tau) = \int df \exp(i2\pi f\tau) W(t, f) = \quad (\text{A-13})$$

$$= \int dv \exp(i2\pi vt) x(v, \tau) , \quad (\text{A-14})$$

$$A(v, f) = \int dt \exp(-i2\pi vt) W(t, f) = \quad (\text{A-15})$$

$$= \int d\tau \exp(-i2\pi f\tau) x(v, \tau) . \quad (\text{A-16})$$

There follows from (A-13) and (A-14), that we need

$$\left. \begin{array}{l} \Delta_\tau < \frac{1}{F} \\ \Delta_t < \frac{1}{2F} \end{array} \right\} \text{ to track TCF ,} \quad (\text{A-17})$$

while from (A-15) and (A-16),

$$\left. \begin{array}{l} \Delta_v < \frac{1}{T} \\ \Delta_f < \frac{1}{2T} \end{array} \right\} \text{ to track SCF .} \quad (\text{A-18})$$

These last four restrictions are identical to those given in (A-11) and (A-12). The total number of samples required to completely describe any one of the four two-dimensional characterizations is $T^2 F^2$.

SAMPLING RATE FOR REAL WAVEFORM

Requirement (17) on the time sampling increment, $\Delta < 1/F$, for recovery of the time waveform $s(t)$, is based upon figures 1 and 2 for a complex envelope waveform $s(t)$. If $s(t)$ were, instead, a real waveform $s_1(t)$, the earlier development covers this case as well, but with a change in notation. The spectrum $S_1(f)$ of waveform $s_1(t)$ is symmetric about $f = 0$, as depicted in figure A-2. F is now the total frequency extent of the positive-frequency components of $s_1(t)$.

We now have frequency limit

$$\frac{F_1}{2} = f_c + \frac{F}{2} , \quad (\text{A-19})$$

and the stringent requirement (45), for an unaliased WDF, becomes

$$\Delta < \frac{1}{2F_1} = \frac{1}{4f_c + 2F} . \quad (\text{A-20})$$

For a narrowband waveform, $f_c \gg F$, this requires an unnecessarily high sampling rate, compared to what would be required for the waveform

corresponding to single-sided bandwidth F . Extraction of the complex envelope (or analytic function) of $s_1(t)$ would return us to WDF requirement

$\Delta < \frac{1}{2F}$, as in (45). This pre-processing feature is recommended for all real waveforms. However, we also want to avoid this more stringent WDF requirement and be subject only to the $\Delta < 1/F$ limitation.

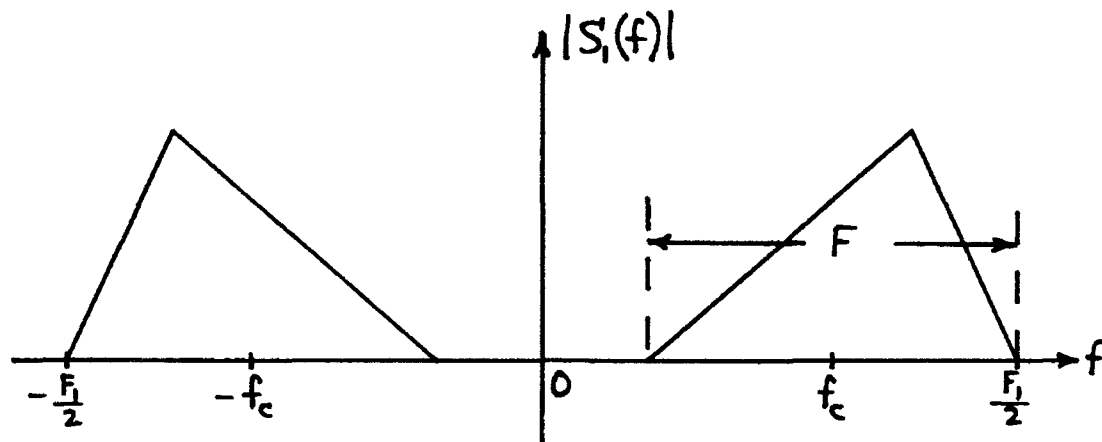


Figure A-2. Spectrum of Real Waveform

APPENDIX B. IMPULSIVE SAMPLING APPROACH

Instead of trying to develop Trapezoidal approximations to the WDF, CAF, and SCF integrals from the available information about the TCF in (39), we adopt here the philosophy that continuous TCF $R(t, \tau)$ has had a pair of impulsive trains applied to it, yielding the impulsive approximation

$$\begin{aligned}
 R_i(t, \tau) &\equiv \Delta^2 R(t, \tau) \left[\sum_m \delta(t - m\Delta) \sum_q \delta(\tau - 2q\Delta) + \right. \\
 &\quad \left. + \sum_m \delta\left(t - \left(m + \frac{1}{2}\right)\Delta\right) \sum_q \delta\left(\tau - (2q + 1)\Delta\right) \right] = \\
 &= \Delta^2 R(t, \tau) \sum_{\substack{n \\ n+1 \text{ even}}} \sum_{\substack{l \\ l \text{ even}}} \delta\left(t - \frac{n\Delta}{2}\right) \delta(\tau - l\Delta) = \\
 &= \Delta^2 \sum_{\substack{n \\ n+1 \text{ even}}} \sum_{\substack{l \\ l \text{ even}}} R\left(\frac{n\Delta}{2}, l\Delta\right) \delta\left(t - \frac{n\Delta}{2}\right) \delta(\tau - l\Delta) . \tag{B-1}
 \end{aligned}$$

That is, a couple of two-dimensional impulse trains, interspersed in the t, τ plane, have been applied, so as to use all the available information in (39). This is identical to the result for the TCF of impulsive time waveform $s_i(t)$, obtained by multiplying $s(t)$ by a sampling train; see appendix E.

We now define the corresponding WDF, CAF, and SCF as rigorous Fourier transforms of (B-1), using the standard forms, for all argument values,

$$\begin{aligned}
W_i(t, f) &= \int d\tau \exp(-i2\pi f\tau) R_i(t, \tau) , \\
x_i(v, \tau) &= \int dt \exp(-i2\pi v t) R_i(t, \tau) , \\
A_i(v, f) &= \int dt \exp(-i2\pi v t) W_i(t, f) = \\
&= \int d\tau \exp(-i2\pi f\tau) x_i(v, \tau) = \\
&= \iint dt d\tau \exp(-i2\pi v t - i2\pi f\tau) R_i(t, \tau) . \quad (B-2)
\end{aligned}$$

These exact interrelationships indicate that the same SCF A_i will result from TCF R_i , whether we proceed by way of the WDF or the CAF.

We have, in detail, WDF

$$\begin{aligned}
W_i(t, f) &= \int d\tau \exp(-i2\pi f\tau) R_i(t, \tau) = \\
&= \frac{1}{2} \Delta \sum_m \delta(t - m\Delta) \int d\tau \exp(-i2\pi f\tau) R(t, \tau) 2\Delta \sum_q \delta(\tau - 2q\Delta) + \\
&+ \frac{1}{2} \Delta \sum_m \delta\left(t - \left(m + \frac{1}{2}\right)\Delta\right) \int d\tau \exp(-i2\pi f\tau) R(t, \tau) 2\Delta \sum_q \delta\left(\tau - (2q + 1)\Delta\right) = \\
&= \frac{1}{2} \Delta \sum_m \delta(t - m\Delta) W(t, f) \bigotimes \sum_q^f \delta\left(f - \frac{q}{2\Delta}\right) + \\
&+ \frac{1}{2} \Delta \sum_m \delta\left(t - \left(m + \frac{1}{2}\right)\Delta\right) W(t, f) \bigotimes \sum_q^f (-1)^q \delta\left(f - \frac{q}{2\Delta}\right) = \\
&= \frac{1}{2} \Delta \sum_m \delta(t - m\Delta) \sum_q W(t, f - \frac{q}{2\Delta}) + \\
&+ \frac{1}{2} \Delta \sum_m \delta\left(t - \left(m + \frac{1}{2}\right)\Delta\right) \sum_q (-1)^q W(t, f - \frac{q}{2\Delta}) = \quad (B-3)
\end{aligned}$$

$$\begin{aligned}
&= \frac{1}{2} \Delta \sum_m \delta(t - m\Delta) \sum_q W(m\Delta, f - \frac{q}{2\Delta}) + \\
&+ \frac{1}{2} \Delta \sum_m \delta(t - (m + \frac{1}{2})\Delta) \sum_q (-1)^q W((m + \frac{1}{2})\Delta, f - \frac{q}{2\Delta}) = \\
&= \frac{1}{2} \Delta \sum_m \delta(t - m\Delta) W_a(m\Delta, f) + \frac{1}{2} \Delta \sum_m \delta(t - (m + \frac{1}{2})\Delta) W_a((m + \frac{1}{2})\Delta, f) = \\
&= \frac{\Delta}{2} \sum_n \delta(t - \frac{n\Delta}{2}) W_a(\frac{n\Delta}{2}, f), \tag{B-4}
\end{aligned}$$

using (42) and (43). Thus, the areas of the impulses in W_i are equal to the approximations W_a developed in (42) and (43), within a scale factor of $\Delta/2$.

Continuing on, from (B-3), the SCF is

$$\begin{aligned}
A_i(v, f) &= \int dt \exp(-i2\pi vt) W_i(t, f) = \\
&= \frac{1}{2} \sum_q \int dt \exp(-i2\pi vt) W(t, f - \frac{q}{2\Delta}) \Delta \sum_m \delta(t - m\Delta) + \\
&+ \frac{1}{2} \sum_q (-1)^q \int dt \exp(-i2\pi vt) W(t, f - \frac{q}{2\Delta}) \Delta \sum_m \delta(t - (m + \frac{1}{2})\Delta) =
\end{aligned}$$

$$\begin{aligned}
&= \frac{1}{2} \sum_q A(v, f - \frac{q}{2\Delta}) \otimes \sum_m^v \delta(v - \frac{m}{\Delta}) + \\
&+ \frac{1}{2} \sum_q (-1)^q A(v, f - \frac{q}{2\Delta}) \otimes \sum_m^v (-1)^m \delta(v - \frac{m}{\Delta}) = \\
&= \frac{1}{2} \sum_q \sum_m A(v - \frac{m}{\Delta}, f - \frac{q}{2\Delta}) + \\
&+ \frac{1}{2} \sum_q \sum_m (-1)^{q+m} A(v - \frac{m}{\Delta}, f - \frac{q}{2\Delta}) = \\
&= \sum_{\substack{q \\ q+m \text{ even}}} \sum_m A(v - \frac{m}{\Delta}, f - \frac{q}{2\Delta}) \quad \text{for all } v, f. \quad (8-5)
\end{aligned}$$

Thus, the SCF A_i , resulting from the impulsive sampling approach applied to the TCF, is not impulsive at all in the v, f plane, and is identical with the approximations A_a developed in (51) and (62).

Proceeding instead via the CAF, we have

$$\begin{aligned}
x_i(v, \tau) &= \int dt \exp(-i2\pi vt) R_i(t, \tau) = \\
&= \Delta \sum_q \delta(\tau - 2q\Delta) \int dt \exp(-i2\pi vt) R(t, \tau) \Delta \sum_m \delta(t - m\Delta) + \\
&+ \Delta \sum_q \delta(\tau - (2q + 1)\Delta) \int dt \exp(-i2\pi vt) R(t, \tau) \Delta \sum_m \delta(t - (m + \frac{1}{2})\Delta) =
\end{aligned}$$

$$\begin{aligned}
&= \Delta \sum_q \delta(\tau - 2q\Delta) \chi(v, \tau) \otimes \sum_m \delta(v - \frac{m}{\Delta}) + \\
&+ \Delta \sum_q \delta(\tau - (2q + 1)\Delta) \chi(v, \tau) \otimes \sum_m (-1)^m \delta(v - \frac{m}{\Delta}) = \\
&= \Delta \sum_q \delta(\tau - 2q\Delta) \sum_m \chi(v - \frac{m}{\Delta}, \tau) + \\
&+ \Delta \sum_q \delta(\tau - (2q + 1)\Delta) \sum_m (-1)^m \chi(v - \frac{m}{\Delta}, \tau) = \tag{B-6} \\
&= \Delta \sum_q \delta(\tau - 2q\Delta) \sum_m \chi(v - \frac{m}{\Delta}, 2q\Delta) + \\
&+ \Delta \sum_q \delta(\tau - (2q + 1)\Delta) \sum_m (-1)^m \chi(v - \frac{m}{\Delta}, (2q + 1)\Delta) = \\
&= \Delta \sum_q \delta(\tau - 2q\Delta) \chi_a(v, 2q\Delta) + \Delta \sum_q \delta(\tau - (2q + 1)\Delta) \chi_a(v, (2q + 1)\Delta) = \\
&= \Delta \sum_n \delta(\tau - n\Delta) \chi_a(v, n\Delta) , \tag{B-7}
\end{aligned}$$

via (56) and (57). Thus, the areas of the impulses in χ_i are equal to the approximations χ_a in (56) and (57), within a scale factor of Δ .

Now strictly speaking, there is no need to proceed to SCF A_i via the CAF x_i , since (B-2) shows that there is only one A_i function, regardless of how reached. Nevertheless, for completeness, we also present the last route. We have, using (B-6),

$$\begin{aligned}
 A_i(v, f) &= \int d\tau \exp(-i2\pi f\tau) x_i(v, \tau) = \\
 &= \frac{1}{2} \sum_m \int d\tau \exp(-i2\pi f\tau) x(v - \frac{m}{\Delta}, \tau) 2\Delta \sum_q \delta(\tau - 2q\Delta) + \\
 &+ \frac{1}{2} \sum_m (-1)^m \int d\tau \exp(-i2\pi f\tau) x(v - \frac{m}{\Delta}, \tau) 2\Delta \sum_q \delta(\tau - (2q + 1)\Delta) = \\
 &= \frac{1}{2} \sum_m A(v - \frac{m}{\Delta}, f) \sum_q^f \delta(f - \frac{q}{2\Delta}) + \\
 &+ \frac{1}{2} \sum_m (-1)^m A(v - \frac{m}{\Delta}, f) \sum_q^f (-1)^q \delta(f - \frac{q}{2\Delta}) = \\
 &= \frac{1}{2} \sum_m \sum_q A(v - \frac{m}{\Delta}, f - \frac{q}{2\Delta}) + \frac{1}{2} \sum_m \sum_q (-1)^{m+q} A(v - \frac{m}{\Delta}, f - \frac{q}{2\Delta}) = \\
 &= \sum_{m+q \text{ even}} \sum_q A(v - \frac{m}{\Delta}, f - \frac{q}{2\Delta}) \quad \text{for all } v, f. \quad (B-8)
 \end{aligned}$$

As anticipated, this is identical with (B-5). Thus we get a unique SCF in the v, f plane.

APPENDIX C. RECOVERY VIA DIRECT CONVOLUTION

This appendix is closely coupled with the previous one; it shows how to recover the original continuous two-dimensional TCF, CAF, and WDF from their impulsive counterparts. From (B-5), (B-8), (51), (62), (53), (54), and figure 6, the original SCF is

$$A(v, f) = A_i(v, f) D(v, f) . \quad (C-1)$$

WDF RECOVERY

We have, using (B-4),

$$\begin{aligned} W(t, f) &= \int dv \exp(i2\pi vt) A_i(v, f) D(v, f) = \\ &= W_i(t, f) \overset{t}{\otimes} d(t, f) = \\ &= \sum_n W_a\left(\frac{n\Delta}{2}, f\right) \frac{\Delta}{2} d\left(t - \frac{n\Delta}{2}, f\right) \quad \text{for all } t, f , \end{aligned} \quad (C-2)$$

where

$$\begin{aligned} \frac{\Delta}{2} d(t, f) &= \frac{\Delta}{2} \int dv \exp(i2\pi vt) D(v, f) = \\ &= \left\{ \begin{array}{l} \frac{\sin[2\pi \frac{t}{\Delta}(1 - 2\Delta|f|)]}{2\pi \frac{t}{\Delta}} \quad \text{for } |f| < \frac{1}{2\Delta} \\ 0 \quad \text{for } |f| > \frac{1}{2\Delta} \end{array} \right\} \quad \text{for all } t \\ &= (1 - 2\Delta|f|) \operatorname{sinc}\left[2 \frac{t}{\Delta}(1 - 2\Delta|f|)\right] \operatorname{rect}(\Delta f) . \end{aligned} \quad (C-3)$$

These results agree with [6, (27) & (28)]. Interpolation rule (C-2) uses the available slices of information in the t, f plane of figure 8. A particular case of (C-3) is

$$\frac{\Delta}{2} d(0, f) = (1 - 2\Delta |f|) \text{rect}(\Delta f) . \quad (\text{C-4})$$

CAF RECOVERY

From (C-1) and (B-7), there follows

$$\begin{aligned} x(v, \tau) &= \int df \exp(i2\pi f\tau) A_i(v, f) D(v, f) = \\ &= x_i(v, \tau) \otimes d(v, \tau) = \\ &= \sum_n x_a(v, n\Delta) \Delta d(v, \tau - n\Delta) \quad \text{for all } v, \tau , \end{aligned} \quad (\text{C-5})$$

where

$$\begin{aligned} \Delta d(v, \tau) &= \Delta \int df \exp(i2\pi f\tau) D(v, f) = \\ &= \left\{ \begin{array}{ll} \frac{\sin[\pi \frac{\tau}{\Delta}(1 - \Delta |v|)]}{\pi \tau / \Delta} & \text{for } |v| < \frac{1}{\Delta} \\ 0 & \text{for } |v| > \frac{1}{\Delta} \end{array} \right\} \quad \text{for all } \tau \\ &= (1 - \Delta |v|) \text{sinc} \left[\frac{\tau}{\Delta}(1 - \Delta |v|) \right] \text{rect}(\frac{1}{2} \Delta v) . \end{aligned} \quad (\text{C-6})$$

Interpolation rule (C-5) uses the available slices of information in the v, τ plane of figure 8. A special case of (C-6) is

$$\Delta d(v, 0) = (1 - \Delta |v|) \text{rect}(\frac{1}{2} \Delta v) . \quad (\text{C-7})$$

TCF RECOVERY

From (C-1) and (B-1),

$$\begin{aligned}
 R(t, \tau) &= \iint dv df \exp(i2\pi vt + i2\pi f\tau) A_i(v, f) D(v, f) = \\
 &= R_i(t, \tau) \overset{t\tau}{\otimes} \mathcal{J}(t, \tau) = \\
 &= \sum_n \sum_{\substack{l \\ n+l \text{ even}}} R\left(\frac{n\Delta}{2}, l\Delta\right) \Delta^2 \mathcal{J}\left(t - \frac{n\Delta}{2}, \tau - l\Delta\right) \quad \text{for all } t, \tau, \quad (C-8)
 \end{aligned}$$

where

$$\begin{aligned}
 \Delta^2 \mathcal{J}(t, \tau) &= \Delta^2 \iint dv df \exp(i2\pi vt + i2\pi f\tau) D(v, f) = \\
 &= \frac{\sin^2(\pi t/\Delta) - \sin^2(\frac{\pi \tau}{2\Delta})}{\frac{\pi^2}{\Delta^2} (t^2 - \frac{\tau^2}{4})} = \\
 &= \frac{\sin(\frac{\pi t}{\Delta}) + \sin(\frac{\pi \tau}{2\Delta})}{\frac{\pi}{\Delta}(t + \frac{\tau}{2})} \frac{\sin(\frac{\pi t}{\Delta}) - \sin(\frac{\pi \tau}{2\Delta})}{\frac{\pi}{\Delta}(t - \frac{\tau}{2})} \quad \text{for all } t, \tau. \quad (C-9)
 \end{aligned}$$

Particular values are

$$\Delta^2 \mathcal{J}\left(\pm \frac{\tau}{2}, \tau\right) = \text{sinc}\left(\frac{\tau}{\Delta}\right). \quad (C-10)$$

It should be observed that (C-8) dictates two-dimensional interpolation in the t, τ plane of figure 8. Attempts at simpler one-dimensional interpolation in t or τ alone are bound to fail.

PROPERTIES OF $\mathcal{D}(t, \tau)$

The two-dimensional function $\mathcal{D}(t, \tau)$ is unlike any proposed previously for interpolation of TCF $R(t, \tau)$. Some of its properties are listed here.

$$\mathcal{D}(-t, \tau) = \mathcal{D}(t, -\tau) = \mathcal{D}(t, \tau) . \quad (C-11)$$

$$\Delta^2 \mathcal{D}(m\Delta, 2q\Delta) = \frac{\sin^2(\pi m) - \sin^2(\pi q)}{\pi^2(m^2 - q^2)} . \quad (C-12)$$

If $m \neq q$ or $m \neq -q$, then $\mathcal{D} = 0$. If $m = q$, then $t = \tau/2$, while if $m = -q$, then $t = -\tau/2$, giving

$$\Delta^2 \mathcal{D}(\pm q\Delta, 2q\Delta) = \text{sinc}(2q) . \quad (C-13)$$

Therefore $\mathcal{D}(m\Delta, 2q\Delta) = 0$ for all m, q , except that $\Delta^2 \mathcal{D}(0, 0) = 1$. Similarly,

$$\mathcal{D}\left((m + \frac{1}{2})\Delta, (2q + 1)\Delta\right) = 0 \quad \text{for all } m, q . \quad (C-14)$$

If we define

$$\mathcal{J}(t, \tau) = \mathcal{D}(t, 2\tau) = \frac{\sin^2(\pi t/\Delta) - \sin^2(\pi \tau/\Delta)}{\pi^2(t^2 - \tau^2)} , \quad (C-15)$$

then

$$\mathcal{J}(\tau, t) = \mathcal{J}(t, \tau) , \quad (C-16)$$

meaning that $\mathcal{J}(t, \tau)$ is symmetric about the 45° line in the t, τ plane. Figure C-1 depicts some sample values of \mathcal{D} in the first quadrant. In particular,

$$\Delta^2 \mathcal{D}(m\Delta, (2q+1)\Delta) = \frac{-1}{\pi^2 [m^2 - (q + \frac{1}{2})^2]},$$

$$\Delta^2 \mathcal{D}((m + \frac{1}{2})\Delta, 2q\Delta) = \frac{1}{\pi^2 [(m + \frac{1}{2})^2 - q^2]}. \quad (C-17)$$

Interpolation function $\mathcal{D}(t, \tau)$ decays slowest along the $t = \pm\tau/2$ lines in the t, τ plane, and fastest along the $t = 0$ and $\tau = 0$ lines. So direct interpolation of the TCF is not best approximated by horizontal or vertical slices, but in fact, by points between these slices.

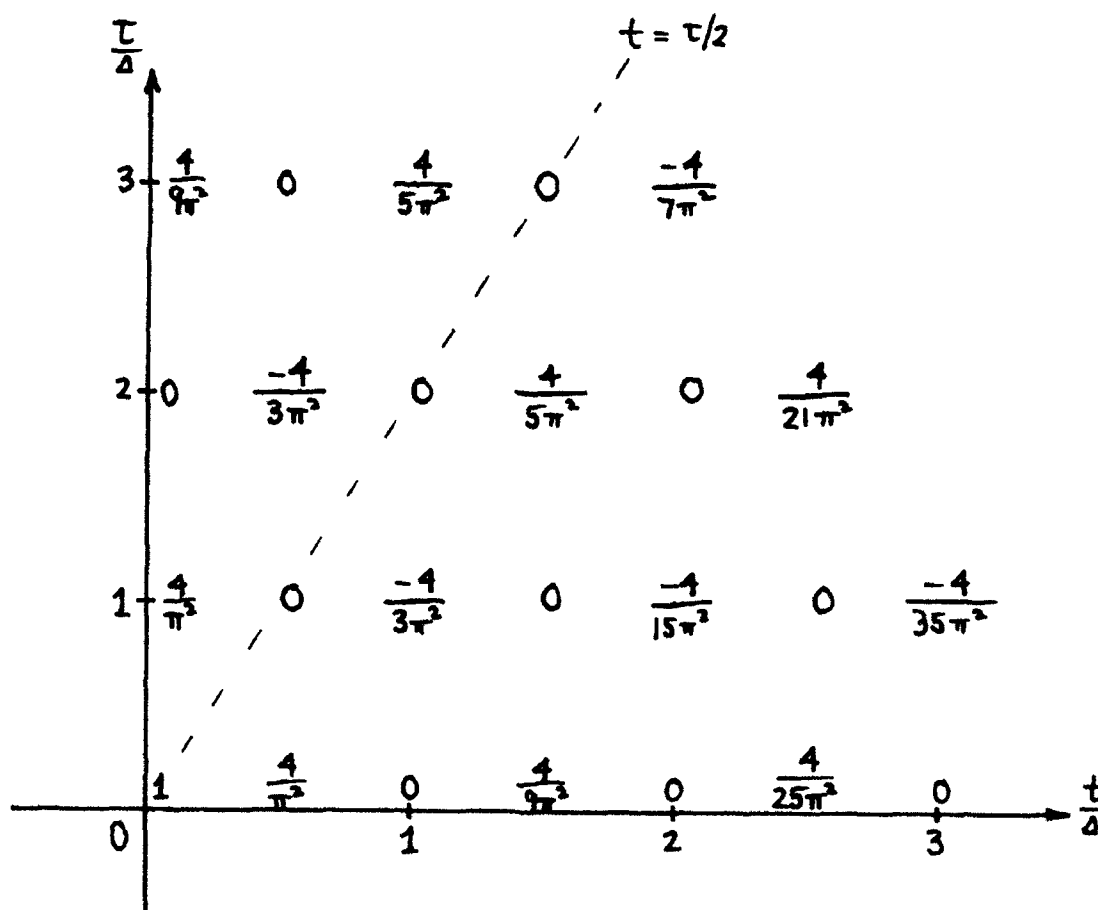


Figure C-1. Sample Values of $\Delta^2 \mathcal{D}(t, \tau)$

APPENDIX D. EVALUATION OF CAF

The original CAF of waveform $s(t)$ is given by (73), in terms of spectrum $\bar{S}(f)$ defined in (69). As in (87), we again presume that only the discrete frequency calculations

$$\bar{S}\left(\frac{n}{N\Delta}\right) = \Delta \sum_k \exp(-i2\pi nk/N) s(k\Delta) \quad \text{for } |n| < \frac{N}{2} \quad (D-1)$$

are available. Since the frequency increment is $\Delta_f = (N\Delta)^{-1}$, we approximate CAF (73) according to

$$\begin{aligned} \tilde{x}(v, \tau) &\equiv \frac{1}{N\Delta} \sum_n \exp(i2\pi \frac{n}{N\Delta} \tau) \bar{S}\left(\frac{n}{N\Delta} + \frac{v}{2}\right) \bar{S}^*\left(\frac{n}{N\Delta} - \frac{v}{2}\right) = \\ &= \int df \exp(i2\pi f \tau) \bar{S}\left(f + \frac{v}{2}\right) \bar{S}^*\left(f - \frac{v}{2}\right) \frac{1}{N\Delta} \sum_n \delta\left(f - \frac{n}{N\Delta}\right) = \\ &= x(v, \tau) \bigotimes \sum_n \delta(\tau - n N\Delta) = \\ &= \sum_n x(v, \tau - n N\Delta) \quad \text{for all } v, \tau. \end{aligned} \quad (D-2)$$

Since waveform $s(t)$ is approximately limited to $|t| < T/2$ (see (84) and figure 9), then CAF $x(v, \tau)$ is approximately limited to $|\tau| < T$, as may be seen by substituting (32) into (34):

$$x(v, \tau) = \int dt \exp(-i2\pi vt) s(t + \frac{\tau}{2}) s^*(t - \frac{\tau}{2}) . \quad (D-3)$$

Therefore, the approximate CAF \tilde{x} takes the appearance shown in figure D-1.

It is seen that overlap is negligible if we take

$$T < N\Delta - T, \quad \text{i.e.,} \quad N > \frac{2T}{\Delta} . \quad (D-4)$$

This requirement on the FFT size in (D-1) is the same as that established in (93) for the approximate WDF \tilde{W} .

DISCRETIZATION IN v and τ

In order to utilize available samples (D-1) in the evaluation of approximation (D-2), we restrict the evaluation of the approximate CAF to frequency-shift values

$$\tilde{x}(\frac{2m}{N\Delta}, \tau) = \frac{1}{N\Delta} \sum_n \exp(i2\pi \frac{n}{N\Delta} \tau) \bar{S}(\frac{n+m}{N\Delta}) \bar{S}^*(\frac{n-m}{N\Delta}) \quad \text{for all } \tau . \quad (D-5)$$

Furthermore, we consider only the particular values of time delay given by

$$\tilde{x}(\frac{2m}{N\Delta}, q\Delta) = \frac{1}{N\Delta} \sum_n \exp(i2\pi nq/N) \bar{S}(\frac{n+m}{N\Delta}) \bar{S}^*(\frac{n-m}{N\Delta}) , \quad (D-6)$$

since the right-hand side is now an N -point FFT for each m value of interest.

N values of q are swept out by each FFT. Compare (D-6) with (111).

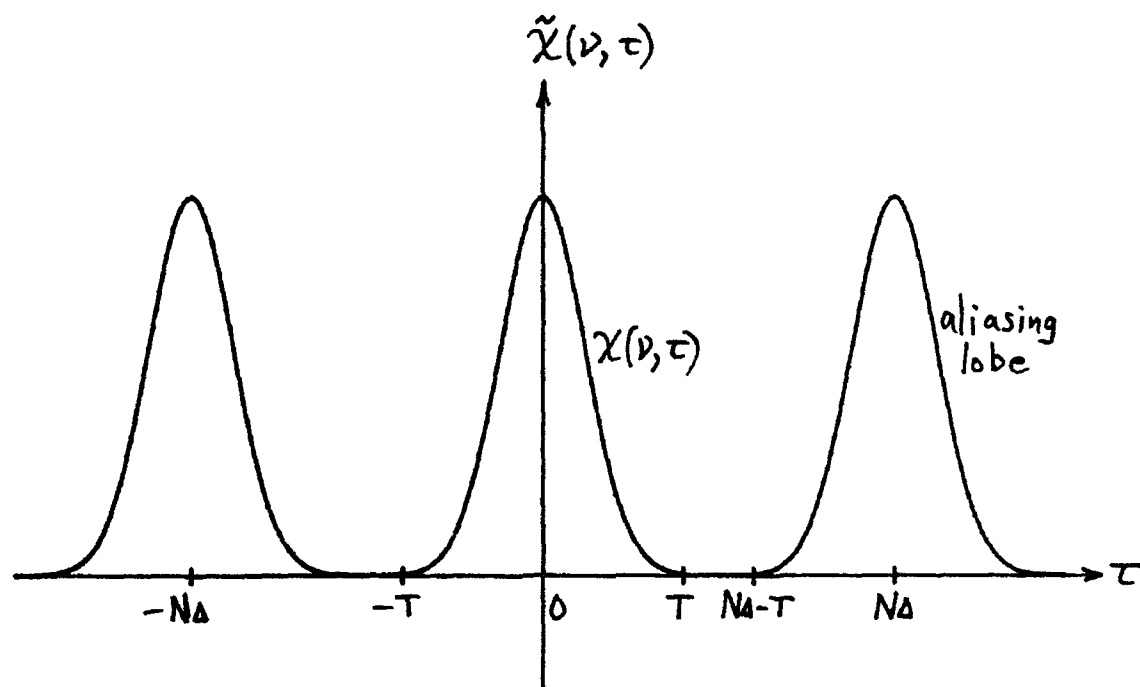


Figure D-1. Delay-Aliased CAF

APPENDIX E. TCF OF IMPULSIVELY-SAMPLED WAVEFORM

Suppose continuous waveform $s(t)$ is sampled with an infinite impulse train (with delay t_0) yielding impulsive waveform

$$s_i(t) = s(t) \Delta \sum_k \delta(t - t_0 - k\Delta) . \quad (E-1)$$

The corresponding TCF is

$$\begin{aligned} R_i(t, \tau) &\equiv s_i(t + \frac{\tau}{2}) s_i^*(t - \frac{\tau}{2}) = \\ &= R(t, \tau) \Delta^2 \sum_k \sum_m \delta(t - t_0 + \frac{\tau}{2} - k\Delta) \delta(t - t_0 - \frac{\tau}{2} - m\Delta) . \end{aligned} \quad (E-2)$$

This function has impulses in the t, τ plane at

$$\left. \begin{aligned} t - t_0 + \frac{\tau}{2} &= k\Delta \\ t - t_0 - \frac{\tau}{2} &= m\Delta \end{aligned} \right\} , \quad \text{i.e., at } \begin{cases} t = t_0 + \frac{k+m}{2} \Delta \\ \tau = (k-m)\Delta . \end{cases} \quad (E-3)$$

Furthermore, the area of each of these impulses is 1:

$$\iint dt d\tau \delta(t - t_0 + \frac{\tau}{2} - k\Delta) \delta(t - t_0 - \frac{\tau}{2} - m\Delta) = \int d\tau \delta(\tau + m\Delta - k\Delta) = 1 . \quad (E-4)$$

So (E-2) can be expressed alternatively as

$$R_i(t, \tau) = R(t, \tau) \Delta^2 \sum_k \sum_m \delta(t - t_0 - \frac{k+m}{2} \Delta) \delta(\tau - (k-m)\Delta) . \quad (E-5)$$

Now let

$$n = k + m, \quad l = k - m. \quad (E-6)$$

Then $n \pm l$ must be even, giving

$$\begin{aligned} R_i(t, \tau) &= R(t, \tau) \Delta^2 \sum_n \sum_{\substack{l \\ n+l \text{ even}}} \delta(t - t_0 - \frac{n}{2} \Delta) \delta(\tau - l\Delta) = \\ &= \Delta^2 \sum_n \sum_{\substack{l \\ n+l \text{ even}}} R(t_0 + \frac{n}{2} \Delta, l\Delta) \delta(t - t_0 - \frac{n}{2} \Delta) \delta(\tau - l\Delta). \end{aligned} \quad (E-7)$$

This is a slight generalization of (B-1), to allow for delayed sampling.

Thus, the two approaches, (B-1) and (E-1), yield identical results.

FUNDAMENTAL TWO-DIMENSIONAL SAMPLING PATTERNS

Suppose, in (B-1), that we let

$$R(t, \tau) = 1 \quad \text{for all } t, \tau. \quad (E-8)$$

Then $R_i(t, \tau)$ there approaches

$$r_i(t, \tau) \equiv \Delta^2 \sum_n \sum_{\substack{l \\ n+l \text{ even}}} \delta(t - \frac{n\Delta}{2}) \delta(\tau - l\Delta). \quad (E-9)$$

But, at the same time, use of (E-8) in SCF (35) yields

$$A(v, f) = \delta(v) \delta(f), \quad (E-10)$$

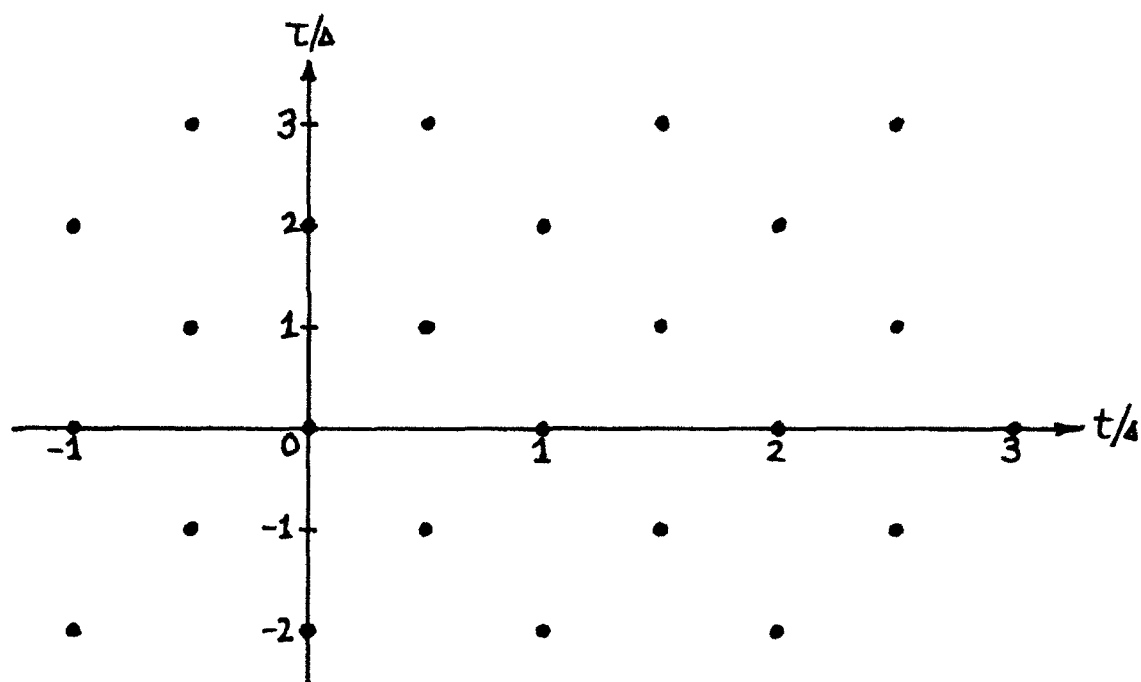
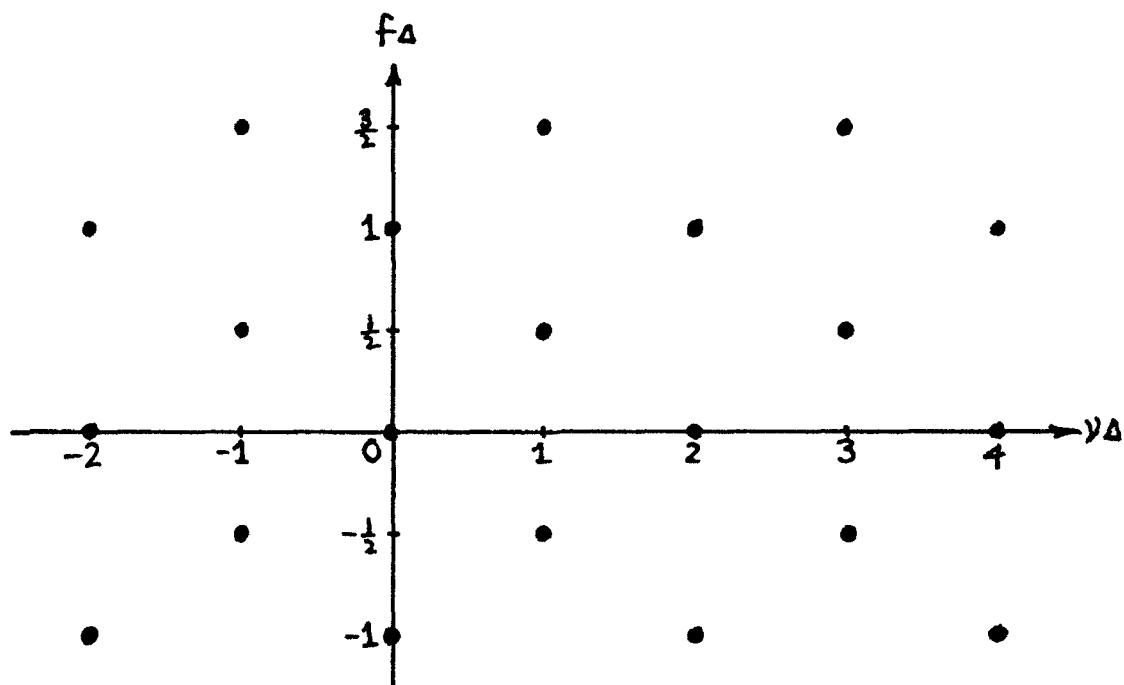
while (B-5) and (B-8) approach

$$a_i(v, f) = \sum_{\substack{q \\ q+m}} \sum_{\substack{m \\ \text{even}}} \delta\left(v - \frac{m}{\Delta}\right) \delta\left(f - \frac{q}{2\Delta}\right). \quad (\text{E-11})$$

Thus, (E-9) and (E-11) are a double Fourier transform pair:

$$a_i(v, f) = \iint dt \, d\tau \exp(-i2\pi vt - i2\pi f\tau) r_i(t, \tau). \quad (\text{E-12})$$

They generalize one-dimensional result (7)&(8) to two dimensions with interspersed sampling. The impulse patterns of $r_i(t, \tau)$ and $a_i(v, f)$ in their respective domains are displayed in figures E-1 and E-2.

Figure E-1. Impulse Locations for $r_i(t, \tau)$ in (E-9)Figure E-2. Impulse Locations for $a_i(\nu, f)$ in (E-11).

REFERENCES

1. N. Yen, "Time and Frequency Representation of Acoustic Signals by Means of the Wigner Distribution Function: Implementation and Interpretation," Journal of Acoustical Society of America, vol. 81, no. 6, pp. 1841-1850, June 1987.
2. J. C. Andrieux et al., "Optimum Smoothing of the Wigner-Ville Distribution," IEEE Transactions on Acoustics, Speech, and Signal Processing, vol. ASSP-35, no. 6, pp. 764-768, June 1987.
3. Kai-Bor Yu and S. Cheng, "Signal Synthesis from Pseudo-Wigner Distribution and Applications," IEEE Transactions on Acoustics, Speech, and Signal Processing, vol. ASSP-35, no. 9, pp. 1289-1301, September 1987.
4. D. S. K. Chan, "A Non-Aliased Discrete-Time Wigner Distribution for Time-Frequency Signal Analysis," Proc. ICASSP, Paris, France, pp. 1333-1336, May 1982.
5. T. A. C. M. Claasen and W. F. G. Mecklenbräuer, "The Aliasing Problem in Discrete-Time Wigner Distributions," IEEE Transactions on Acoustics, Speech, and Signal Processing, vol. ASSP-31, no. 5, pp. 1067-1072, October 1983.

REFERENCES (Cont'd)

6. F. Peyrin and Rémy Prost, "A Unified Definition for the Discrete-Time, Discrete-Frequency, and Discrete-Time/Frequency Wigner Distributions," IEEE Transactions on Acoustics, Speech, and Signal Processing, vol. ASSP-34, no. 4, pp. 858-867, August 1986.
7. M. A. Poletti, "The Development of a Discrete Transform for the Wigner Distribution and Ambiguity Function," Journal of Acoustical Society of America, vol. 84, no. 1, pp. 238-252, July 1988.
8. H. R. E. Van Maanen, "Duplication of the Sampling Frequency of Periodically Sampled Signals for the Calculation of the Discrete Wigner Distribution," Journal of Audio Engineering Society, vol. 33, no. 11, pp. 892-894, November 1985.
9. A. H. Nuttall, Wigner Distribution Function: Relation to Short-Term Spectral Estimation, Smoothing, and Performance in Noise, NUSC Technical Report 8225, Naval Underwater Systems Center, New London, CT, 16 February 1988.
10. W. A. Gardner, "Signal Interception: A Unifying Theoretical Framework for Feature Detection," IEEE Transactions on Communications, vol. 36, no. 8, pp. 897-906, August 1988.

Technical Report 8595
10 August 1989

Operating Characteristics for Combiner
With a Dead Zone in Each Channel

A. H. Nuttall
ABSTRACT

The receiver operating characteristics, namely detection probability versus false alarm probability for a combiner which employs nonlinearities with dead zones in each of its channels, are derived in closed form as a function of N , the number of channels; F , the fraction of data passed by the nonlinearity in each channel; R , the signal-to-noise ratio in each channel; and T , the system output threshold. Plots of these results for $N = 1, 2, 4, 6, 8, 16, 32, 64$ and $F = 1, .1, .01, .001$ reveal that inclusion of the dead zone does not significantly degrade performance, the typical loss being of the order of 1 dB for small N , and 3 dB for larger N , in the important operating ranges. The only limitation is that certain ranges of false alarm probabilities are unachievable; however, since these ranges generally correspond to undesirable operating conditions, the limitation is not too relevant.

Approved for public release; distribution is unlimited.

TABLE OF CONTENTS

	Page
LIST OF ILLUSTRATIONS	ii
LIST OF TABLES	iii
LIST OF SYMBOLS	iv
INTRODUCTION	1
PROCESSOR DESCRIPTION	3
ANALYSIS OF PERFORMANCE	5
EXPONENTIAL EXAMPLE	9
Statistics of Detector Output	9
Characteristic Function of Output z	11
Auxiliary Functions	12
Exceedance Distribution Function of Output z	13
Detection and False Alarm Probabilities	14
Special Cases	15
GRAPHICAL RESULTS	17
Achievable False Alarm Values	18
Erratic Behavior of Receiver Operating Characteristics	19
Observations	20
SUMMARY	51
APPENDIX. Program for Receiver Operating Characteristics	53
REFERENCES	59

LIST OF ILLUSTRATIONS

Figure		Page
1.	Processor Block Diagram	4
2.	Nonlinear Device Characteristics	4
3.	ROC for $N = 1$, $F = 1$.	22
4.	ROC for $N = 2$, $F = 1$.	23
5.	ROC for $N = 2$, $F = .1$	24
6.	ROC for $N = 2$, $F = .01$	25
7.	ROC for $N = 2$, $F = .001$	26
8.	ROC for $N = 4$, $F = 1$.	27
9.	ROC for $N = 4$, $F = .1$	28
10.	ROC for $N = 4$, $F = .01$	29
11.	ROC for $N = 4$, $F = .001$	30
12.	ROC for $N = 6$, $F = 1$.	31
13.	ROC for $N = 6$, $F = .1$	32
14.	ROC for $N = 6$, $F = .01$	33
15.	ROC for $N = 6$, $F = .001$	34
16.	ROC for $N = 8$, $F = 1$.	35
17.	ROC for $N = 8$, $F = .1$	36
18.	ROC for $N = 8$, $F = .01$	37
19.	ROC for $N = 8$, $F = .001$	38
20.	ROC for $N = 16$, $F = 1$.	39
21.	ROC for $N = 16$, $F = .1$	40
22.	ROC for $N = 16$, $F = .01$	41
23.	ROC for $N = 16$, $F = .001$	42
24.	ROC for $N = 32$, $F = 1$.	43

LIST OF ILLUSTRATIONS (cont'd)

Figure		Page
25.	ROC for $N = 32$, $F = .1$	44
26.	ROC for $N = 32$, $F = .01$	45
27.	ROC for $N = 32$, $F = .001$	46
28.	ROC for $N = 64$, $F = 1.$	47
29.	ROC for $N = 64$, $F = .1$	48
30.	ROC for $N = 64$, $F = .01$	49
31.	ROC for $N = 64$, $F = .001$	50

LIST OF TABLES

Table		Page
1.	Required Signal-to-Noise Ratio for $P_F = 1E-6$, $P_D = .5$	21
2.	Required Signal-to-Noise Ratio for $P_F = 1E-8$, $P_D = .9$	21

LIST OF SYMBOLS

N	number of channels, figure 1
F	fraction of data passed by nonlinearity, (3),(27)
R	signal-to-noise power ratio in each channel
T	system output threshold, figure 1
r_n	n -th input to system, figure 1
x_n	squared-envelope filter output, figure 1
L	breakpoint (threshold) of nonlinearity, figure 2,(28)
y_n	output of nonlinearity, figure 1
z	system output, figure 1
$p_x(u)$	probability density function of random variable x
$P_x(u)$	cumulative distribution function of x , (1),(13)
$Q_x(u)$	exceedance distribution function of x , (1),(13)
$p_y(u)$	probability density function of random variable y , (4)
$f_y(\xi)$	characteristic function of random variable y , (5),(14)
z	summer output, (6)
$f_z(\xi)$	characteristic function of random variable z , (7),(16)
P_F	false alarm probability, (8),(26),(32)
P_D	detection probability, (8),(25),(32)
a	auxiliary parameter, (12)
B	auxiliary parameter, (15)
$E(u,n)$	auxiliary function, (17)
$p_n(u)$	normalized probability density function, (18)
$f_n(\xi)$	normalized characteristic function, (19)
$Q_n(u)$	normalized exceedance distribution function, (20)

LIST OF SYMBOLS (cont'd)

$p_z(u)$	probability density function of output z , (22)
$Q_z(u)$	exceedance distribution function of z , (23)
$R(\text{dB})$	signal-to-noise ratio R in decibels, (33)
ROC	receiver operating characteristic

OPERATING CHARACTERISTICS FOR COMBINER
WITH A DEAD ZONE IN EACH CHANNEL

INTRODUCTION

Some data processing shortcuts are often required in order to keep the computational burden in today's detection and tracking systems within manageable limits. One strategem to accomplish this goal is to quantize the signal levels at various points in the receiver processing chain. Another is to reject low-level quantities, and retain only the larger terms, in the belief that only the latter will lead to statistically meaningful decisions on signal presence versus absence.

Here, we investigate one such technique, where all levels below a breakpoint or threshold value are rejected, that is, set to zero, while those signal levels above the breakpoint are retained in their full accuracy. In particular, this approach is employed in each branch of a combiner, as encountered in diversity or multiple ping transmission. The question to be addressed is the cost of this data reduction procedure, in terms of the additional signal-to-noise ratio required to maintain a desired level of performance, as measured by the false alarm and detection probabilities.

PROCESSOR DESCRIPTION

The processor of interest is depicted in figure 1. Received inputs r_1, \dots, r_N are either composed of noise-only or they all contain signal plus noise. An example of this situation is afforded by a multiple ping transmission, with search on the range of a possible target. The received signal in each channel (if present) is match-filtered and square-law envelope-detected at the candidate time instant of suspected or hypothesized peak output.

At this point, instead of simply summing up these multiple outputs, and in an effort to reduce the amount of information sent on for further data processing, the squared envelope x_n in the n -th channel is subjected to the nonlinear operation depicted in figure 2. Namely, all input levels to the nonlinearity below breakpoint (threshold) value L are replaced by zero, whereas those levels above the breakpoint are kept as is. The breakpoint value L is chosen so that a specified fraction F of the input data to the nonlinearity is passed, when noise-alone is present at the inputs; the hope is that F can be chosen very small, without significant degradation in performance. Finally, the output of the summer in figure 1 is compared with output threshold T for purposes of deciding on signal presence versus absence.

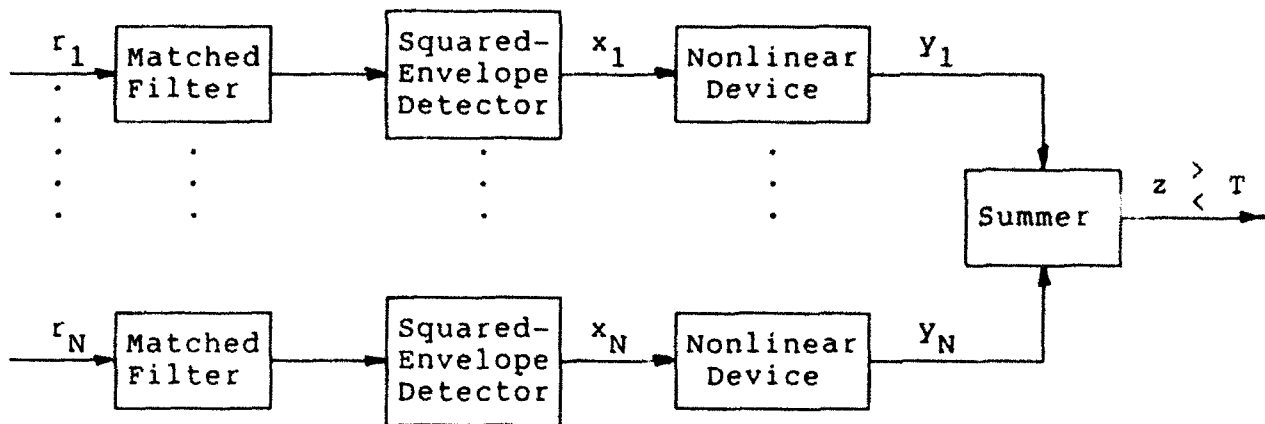


Figure 1. Processor Block Diagram

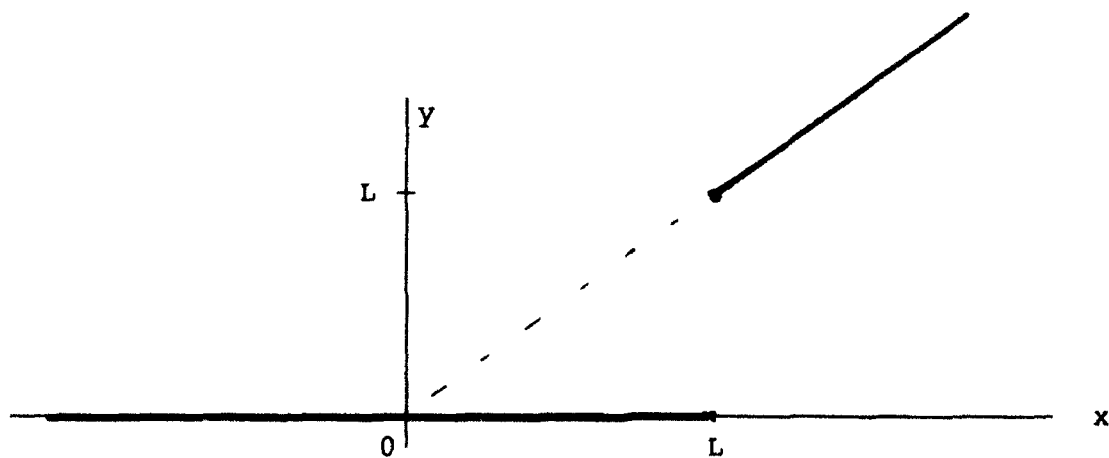


Figure 2. Nonlinear Device Characteristic

ANALYSIS OF PERFORMANCE

The inputs $\{r_n\}$ to figure 1 are presumed to be statistically independent of each other, whether signal is present or not. The squared-envelope outputs $\{x_n\}$ are, therefore, also statistically independent of each other, with probability density function $p_x(u)$, which is presumed known for both cases of signal present as well as signal absent. The corresponding cumulative distribution function and exceedance distribution function are, respectively,

$$P_x(u) = \int_{-\infty}^u dt p_x(t) = \text{Prob}(x \leq u) ,$$

$$Q_x(u) = \int_{u+}^{\infty} dt p_x(t) = \text{Prob}(x > u) . \quad (1)$$

The nonlinear device in figures 1 and 2 is characterized mathematically by

$$y = \begin{cases} 0 & \text{for } x < L \\ x & \text{for } x \geq L \end{cases} ; \quad L \geq 0 . \quad (2)$$

Breakpoint L is presumed nonnegative, since the output of the squared-envelope detector in figure 1 can never be negative. The fraction of data passed by the nonlinearity is

$$F = \text{Prob}(x > L) = Q_x(L) . \quad (3)$$

Since exceedance distribution function Q_x is known, this equation can be solved for the required breakpoint value L , once fraction

F is specified. This calculation is done for the noise-only case, since the breakpoint is desired to be set for this condition.

Inspection of figure 2 immediately reveals that the probability density function of random variable y_n is given by

$$p_y(u) = P_x(L) \delta(u) + p_x(u) U(u - L) , \quad (4)$$

where δ and U are the delta function and the unit step function, respectively. Therefore, the characteristic function of random variable y_n is

$$\begin{aligned} f_y(\xi) &= \int_{-\infty}^{\infty} du \exp(i\xi u) p_y(u) = \\ &= P_x(L) + \int_L^{\infty} du \exp(i\xi u) p_x(u) . \end{aligned} \quad (5)$$

Finally, using the statistical independence of the system inputs, the summer output,

$$z = \sum_{n=1}^N y_n , \quad (6)$$

has characteristic function

$$f_z(\xi) = [f_y(\xi)]^N = \left[P_x(L) + \int_L^{\infty} du \exp(i\xi u) p_x(u) \right]^N . \quad (7)$$

For general given probability density function $p_x(u)$, the integral on u in (7) can be done efficiently by means of a fast Fourier transform. Then the numerical evaluation of the exceedance distribution function of z , namely $Q_z(u)$, can be

accomplished by the techniques utilized in [1, 2, 3]. This numerical approach would have to be carried out for both cases of signal absent and signal present, in order to get the false alarm probability P_F as well as the detection probability P_D . Specifically,

$$P_F = Q_z(T; \text{noise-only}) ,$$

$$P_D = Q_z(T; \text{signal-plus-noise}) . \quad (8)$$

In essence, (7) characterizes the performance of the processor in figures 1 and 2. The remaining effort is the analytical and numerical manipulation of (7) into useful computer forms and evaluation.

EXPONENTIAL EXAMPLE

STATISTICS OF DETECTOR OUTPUT

If the inputs $\{r_n\}$ to the processor of figure 1 are Gaussian, then the squared-envelope detector outputs $\{x_n\}$ are exponentially distributed. We take the probability density function of x_n to be

$$p_x(u) = \begin{cases} 0 & \text{for } u < 0 \\ \exp(-u) & \text{for } u \geq 0 \end{cases} \quad \text{for noise-only.} \quad (9)$$

This corresponds to a mean value of

$$\bar{x} = \int_{-\infty}^{\infty} du \, u \, p_x(u) = 1 \quad \text{for noise-only.} \quad (10)$$

This choice of scaling at the detector output does not constitute any loss of generality, since absolute level obviously has no effect upon the receiver operating characteristics of the processor in figure 1.

For Gaussian signal also present at the system input, the probability density function of x_n is

$$p_x(u) = \begin{cases} 0 & \text{for } u < 0 \\ a \exp(-au) & \text{for } u \geq 0 \end{cases} \quad \text{for signal-present.} \quad (11)$$

Here,

$$a = \frac{1}{1 + R}, \quad (12)$$

where R is the signal-to-noise power ratio at the matched filter output. (If $R = 0$, then $a = 1$, and (11) reduces to (9).) Thus,

any signal processing gains associated with the filtering process are incorporated in the value of R . Observe that R is the signal-to-noise power ratio per channel or per ping, not the "total signal-to-noise ratio" at the system output.

Another signal model, which also leads to probability density function (11) for the detector output, is slow Rayleigh fading in the medium through which the transmitted pings traveled. That is, during a single ping duration, the medium attenuation is constant, but from ping to ping, the attenuation is statistically independent and governed by a Rayleigh probability density function on the received signal envelope.

CHARACTERISTIC FUNCTION OF OUTPUT z

We will determine the statistics of output z of figure 1 for the signal-present probability density function of x , as given by (11). The case for noise-only will then follow immediately by setting $a = 1$.

The cumulative distribution and exceedance distribution functions of x_n are given by substitution of (11) in (1), that is

$$\begin{aligned} P_x(u) &= \begin{cases} 0 & \text{for } u < 0 \\ 1 - \exp(-au) & \text{for } u \geq 0 \end{cases}, \\ Q_x(u) &= \begin{cases} 1 & \text{for } u < 0 \\ \exp(-au) & \text{for } u \geq 0 \end{cases}. \end{aligned} \quad (13)$$

The characteristic function of random variable y is obtained by substituting (11) and (13) in (5); thus

$$\begin{aligned} f_y(\xi) &= 1 - \exp(-aL) + \int_L^{\infty} du \, a \exp(i\xi u - au) = \\ &= 1 - B + B \frac{a \exp(i\xi L)}{a - i\xi}, \end{aligned} \quad (14)$$

where we define

$$B = \exp(-aL); \quad L \geq 0. \quad (15)$$

The characteristic function of output z is given by (7) as

$$\begin{aligned} f_z(\xi) &= \left[1 - B + B \frac{a \exp(i\xi L)}{a - i\xi} \right]^N = \\ &= \sum_{n=0}^N \binom{N}{n} (1-B)^{N-n} B^n \frac{\exp(i\xi Ln)}{(1-i\xi/a)^n}. \end{aligned} \quad (16)$$

AUXILIARY FUNCTIONS

Define the set of functions

$$E(u, n) = \left\{ \begin{array}{ll} 1 & \text{for } u < 0, \\ \int_u^\infty dt \frac{t^n \exp(-t)}{n!} = \exp(-u) e_n(u) = \exp(-u) \sum_{k=0}^n \frac{u^k}{k!} & \text{for } u \geq 0, \end{array} \right\} \quad (17)$$

for $n \geq 0$. Here, we used the partial-exponential notation $e_n(u)$ given in [4; 6.5.11]. The expansion of the integral in (17) may be verified by repeated integrations by parts.

Also, define the set of normalized probability density functions

$$p_n(u) = \left\{ \begin{array}{ll} 0 & \text{for } u < 0 \\ \frac{u^{n-1} \exp(-u)}{(n-1)!} & \text{for } u \geq 0 \end{array} \right\} \quad \text{for } n \geq 1,$$

$$p_0(u) = \delta(u) \quad \text{for all } u. \quad (18)$$

The corresponding characteristic functions are

$$f_n(\xi) = \frac{1}{(1-i\xi)^n} \quad \text{for } n \geq 0, \quad (19)$$

while the exceedance distribution functions are

$$Q_n(u) = E(u, n-1) \quad \text{for all } u, \quad n \geq 1,$$

$$Q_0(u) = \left\{ \begin{array}{ll} 1 & \text{for } u < 0 \\ 0 & \text{for } u \geq 0 \end{array} \right\}. \quad (20)$$

EXCEEDANCE DISTRIBUTION FUNCTION OF OUTPUT z

Since $p_n(u)$ and $f_n(\xi)$ are a Fourier transform pair for $n \geq 0$, it follows that

$$\frac{1}{(1-i\xi/a)^n} \quad \text{and} \quad a p_n(au) \quad (21)$$

are a Fourier transform pair. Then (16) allows us to determine the probability density function of output random variable z as

$$p_z(u) = \sum_{n=0}^N \binom{N}{n} (1-B)^{N-n} B^n a p_n(a(u - Ln)) \quad \text{for all } u, \quad (22)$$

where the "shift factor" $u - Ln$ is due to the $\exp(i\xi Ln)$ term. This is a useful expansion, even for large N , since all the terms are positive or zero; there is no cancellation, as there would be for an alternating series.

The exceedance distribution function of z follows immediately from (22) as

$$Q_z(u) = \sum_{n=0}^N \binom{N}{n} (1-B)^{N-n} B^n Q_n(a(u - Ln)) \quad \text{for all } u. \quad (23)$$

Again, this series has no negative terms. Also, the Q_n terms are sums of positive quantities, as may be seen by referring to (20) and (17). We will be interested only in $u \geq 0$ in the following; then the $n = 0$ term in (23) is, by use of (20),

$$(1 - B)^N Q_0(au) = 0 \quad \text{for } u \geq 0. \quad (24)$$

DETECTION AND FALSE ALARM PROBABILITIES

We now utilize (8), (23), (24), and (20) to obtain the detection probability as

$$P_D = \sum_{n=1}^N \binom{N}{n} (1-B)^{N-n} B^n E(a(T - Ln), n-1) . \quad (25)$$

Here, B is given by (15), and a is given by (12).

The false alarm probability is obtained by setting $R = 0$, that is, $a = 1$:

$$P_F = \sum_{n=1}^N \binom{N}{n} (1-F)^{N-n} F^n E(T - Ln, n-1) . \quad (26)$$

Here, we have utilized (3) and the sequel, (13), and the fact that B in (15) reduces, for $a = 1$, to

$$\exp(-L) = Q_x(L; \text{noise-only}) = F , \quad (27)$$

which is the fraction of data passed by the nonlinearity in figure 1, for noise-only. In fact, (27) allows us to explicitly solve for the required breakpoint value L, for this exponential example, as

$$L = -\ln(F) . \quad (28)$$

To summarize, (25) and (26) give the detection and false alarm probabilities in terms of fundamental quantities

- N, number of channels,
 - F, fraction of data passed,
 - R, signal-to-noise power ratio per channel,
 - T, output threshold.
- (29)

The remaining variables in (25) and (26) are given by (28), (12), and (15) as

$$L = -\ln(F) , \quad a = \frac{1}{1+R} , \quad B = \exp(-aL) = F^{\frac{1}{1+R}} . \quad (30)$$

SPECIAL CASES

For $N = 1$, one channel, (25) and (26) reduce to

$$P_F = F Q_1(T-L) = \begin{cases} F & \text{for } 0 \leq T < L \\ \exp(-T) & \text{for } L \leq T \end{cases} ,$$

$$P_D = B Q_1(a(T-L)) = \begin{cases} F^a & \text{for } 0 \leq T < L \\ \exp(-aT) & \text{for } L \leq T \end{cases} . \quad (31)$$

That is, $P_D = P_F^a$ for $N = 1$, independent of the value of fraction F . This is obvious from (13) in this case.

Instead, if fraction $F = 1$, that is, no nonlinearity, then (28) and (15) yield $L = 0$, $B = 1$, and we find

$$\left. \begin{aligned} P_F &= E(T, N-1) \\ P_D &= E(aT, N-1) \end{aligned} \right\} \quad \text{for } F = 1 . \quad (32)$$

These results agree with [5; (7) and (8)]. A program for the evaluation of general results (25) and (26), as well as the special case (32), is presented in the appendix.

GRAPHICAL RESULTS

In figure 3*, the receiver operating characteristic (ROC) is given for $N = 1$, $F = 1$. That is, there is one channel and the nonlinearity is not active. There is no need to consider values of F less than 1, according to the comment under (31); however, see the subsection below on achievable false alarm values. The curves in figure 3 are parameterized according to

$$R(\text{dB}) = 10 \log_{10} R. \quad (33)$$

The remaining fundamental quantity, threshold T in (29), has been eliminated, and P_D is plotted versus P_F on normal probability paper.

In figures 4, 5, 6, 7, the number of channels is kept at $N = 2$, while fraction

$$F = 1, .1, .01, .001, \quad (34)$$

respectively. Additional cases for

$$N = 4, 6, 8, 16, 32, 64, \quad (35)$$

in figures 8 through 31, complete the coverage in a similar fashion.

*Figures 3 through 31 are grouped at the end of this section.

ACHIEVABLE FALSE ALARM VALUES

Not all values of false alarm probability can be reached by the processing system of figure 1. Since the nonlinear device output y_n can only take on the values $y_n = 0$ and $y_n \geq L$, the sum z can only assume the values $z = 0$ and $z \geq L$. Also, since the probability of $z = 0$ is $(1 - F)^N$ for noise-only, where F is the fraction of data passed by the nonlinearity in each channel, then the probability of getting $z \geq L$ is $1 - (1 - F)^N$. Thus, the range of reachable false alarm probabilities is

$$P_F \leq 1 - (1 - F)^N . \quad (36)$$

This bound holds regardless of the form of the probability density for random variables $\{x_n\}$ in figure 1.

For the special case of $N = 1$, this rule yields $P_F \leq F$. Thus, the plot in figure 3 for $N = 1$, $F = 1$ must be modified for $F < 1$, to the extent that only the values for $P_F \leq F$ are achievable.

For $N > 1$, the rule in (36) first becomes obvious in figure 6 for $N = 2$, $F = .01$. Namely, (36) yields

$$P_F \leq 1 - (1 - .01)^2 = .0199 . \quad (37)$$

Thus, the curves in figure 6 are terminated to the right of this value of the false alarm probability. This termination feature occurs in numerous other figures, always governed by (36).

ERRATIC BEHAVIOR OF RECEIVER OPERATING CHARACTERISTICS

Some of the curves develop significant kinks for larger values of the false alarm probability; see figure 31 for the most pronounced example in this set of results. This behavior is not due to computer round-off error; rather, it is due to the shifted components of probability density function (22) "kicking in" when the output threshold reaches various multiples of breakpoint L . Equivalently, the shifted E-function components of the detection probability and false alarm probability in (25) and (26) are activated at different threshold levels, reflecting the inherent abrupt change of behavior of these functions at zero argument. For example,

$$\begin{aligned}
 E(u,0) &= \begin{cases} 1 & \text{for } u < 0 \\ \exp(-u) & \text{for } u \geq 0 \end{cases}, \\
 E(u,1) &= \begin{cases} 1 & \text{for } u < 0 \\ \exp(-u)(1+u) & \text{for } u \geq 0 \end{cases}. \quad (38)
 \end{aligned}$$

Thus, $E(u,0)$ has a discontinuous slope at $u = 0$, while $E(u,1)$ has a discontinuous second derivative at $u = 0$.

OBSERVATIONS

The required signal-to-noise ratios for various values of N and F are presented in tables 1 and 2 for two different levels of performance, as read directly from figures 3 through 31. The overriding impression is that the degradation in performance is not severe, even for small values of F , the fraction of data passed by the nonlinearity. For example, from table 1, the decibel difference at $F = .001$ versus $F = 1$ is, for $N = 1, 2, 4, 6, 8, 16, 32, 64$, respectively, just

0, 0.3, 0.8, 1.0, 1.2, 1.7, 2.2, 2.7 dB.

For table 2, these differences are substantially the same:

0, 0.2, 0.5, 0.8, 1.0, 1.5, 2.0, 2.5 dB.

Thus, the losses increase from 0 dB at $N = 1$ channel, to less than 3 dB for $N = 64$ channels.

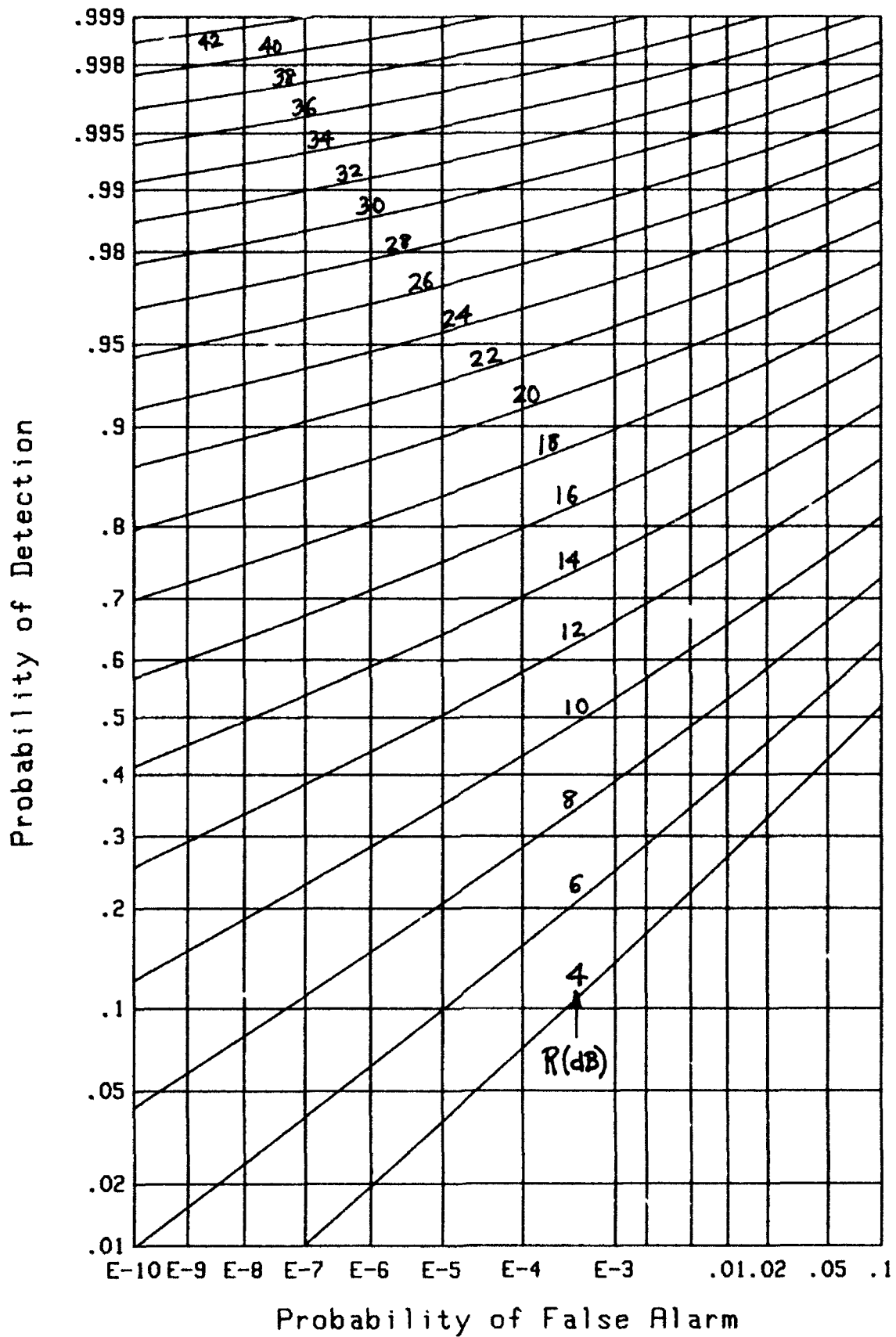
The situation is slightly worse for the lower-quality case of $P_F = 1E-3$, $P_D = .5$. Namely, as F is changed from 1 to .001, the required increment in signal-to-noise ratio is 0 dB for $N = 1$, whereas it is 3.4 dB for $N = 64$.

N	Required R(dB) for F =			
	1	.1	.01	.001
1	12.8	12.8	12.8	12.8
2	9.5	9.6	9.7	9.8
4	6.8	6.9	7.2	7.6
6	5.4	5.5	5.9	6.4
8	4.5	4.6	5.1	5.7
16	2.3	2.6	3.2	4.0
32	0.4	0.7	1.6	2.6
64	-1.4	-1.0	0.1	1.3

Table 1. Required Signal-to-Noise Ratio for $P_F = 1E-6$, $P_D = .5$

N	Required R(dB) for F =			
	1	.1	.01	.001
1	22.4	22.4	22.4	22.4
2	16.0	16.0	16.1	16.2
4	11.6	11.6	11.8	12.1
6	9.4	9.6	9.9	10.2
8	8.1	8.2	8.6	9.1
16	5.3	5.6	6.1	6.8
32	2.9	3.3	4.0	4.9
64	0.8	1.2	2.2	3.3

Table 2. Required Signal-to-Noise Ratio for $P_F = 1E-8$, $P_D = .9$

Figure 3. ROC for $N=1$, $F=1$.

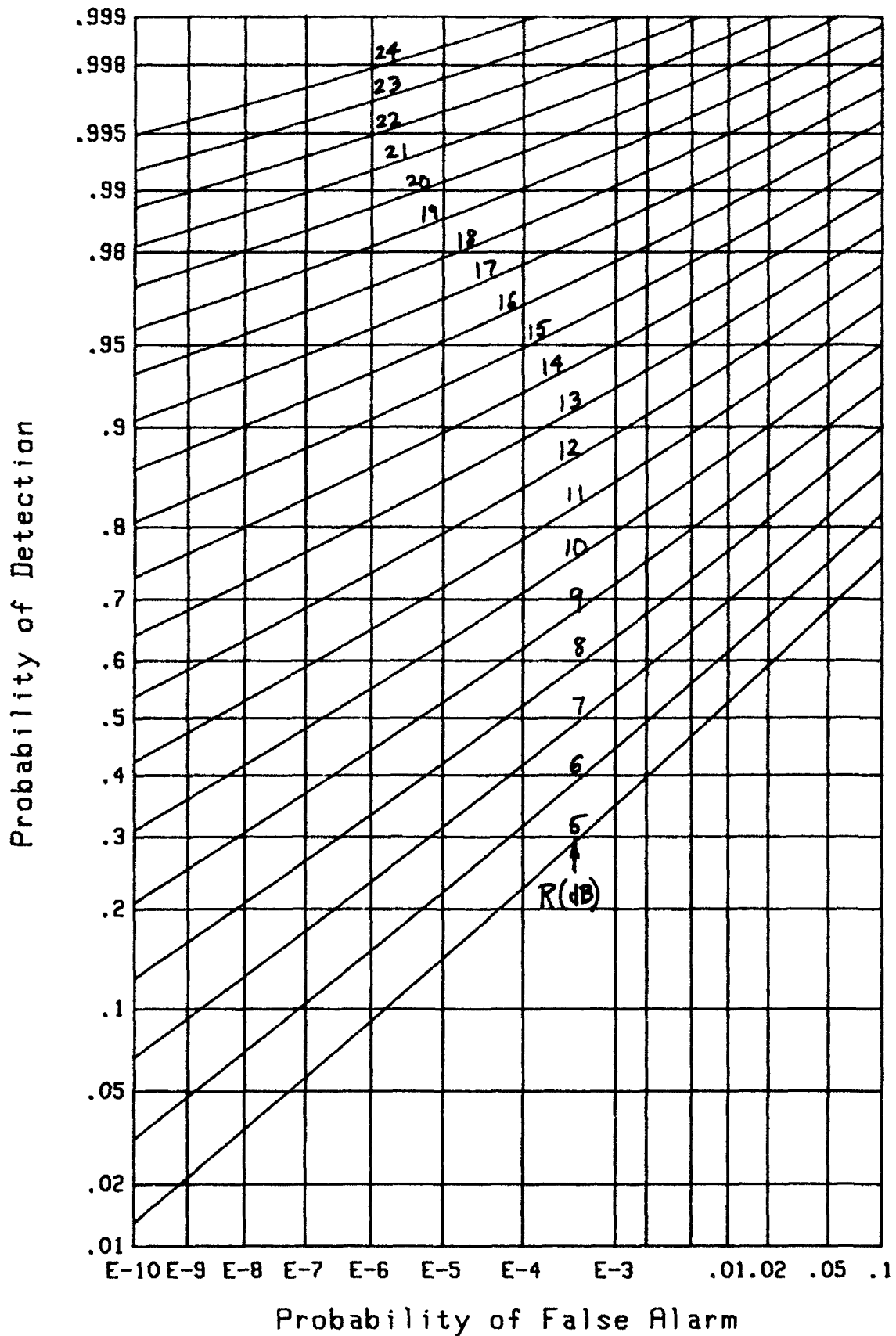


Figure 4. ROC for $N=2$, $F=1$.

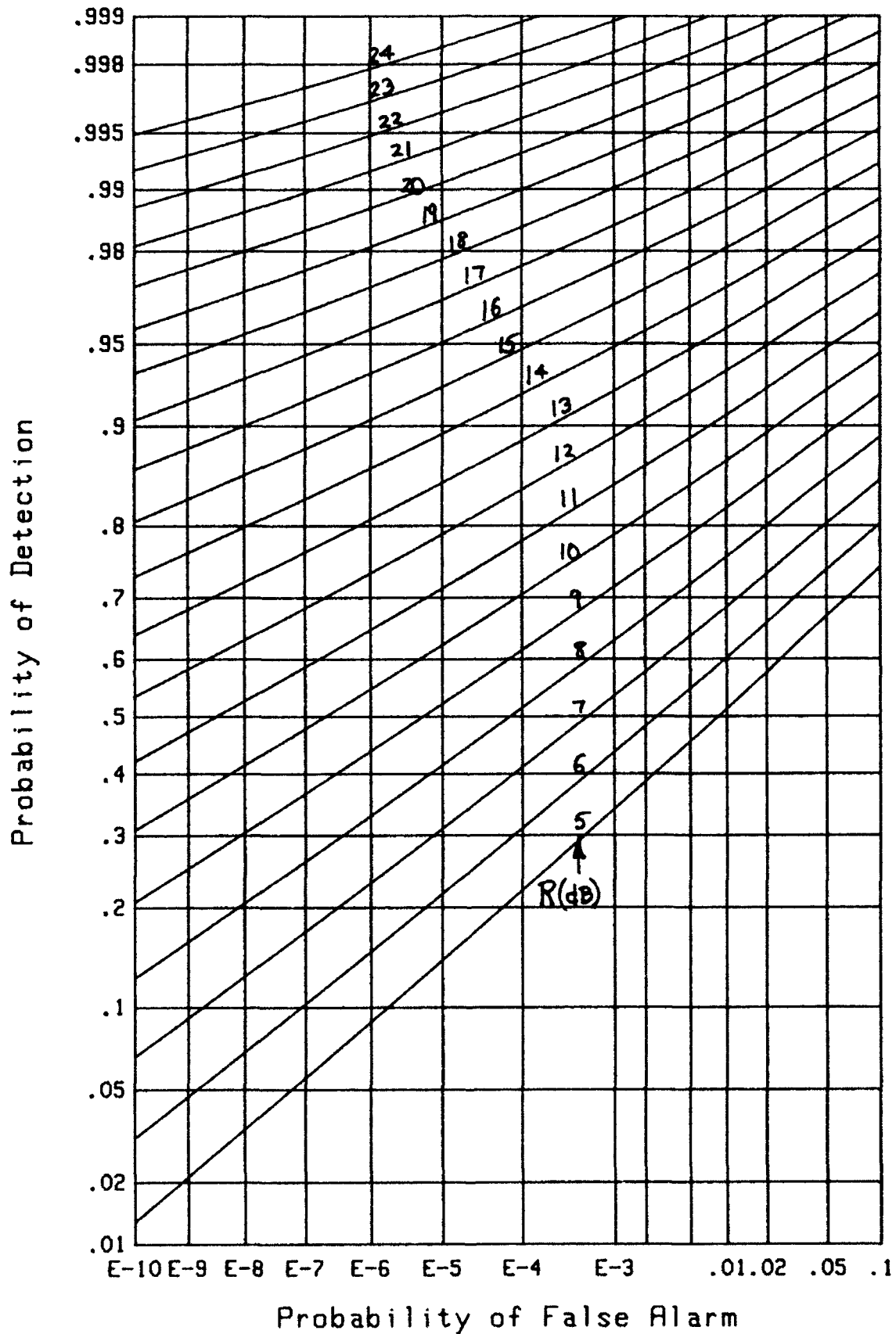


Figure 5. ROC for $N=2$, $F=.1$

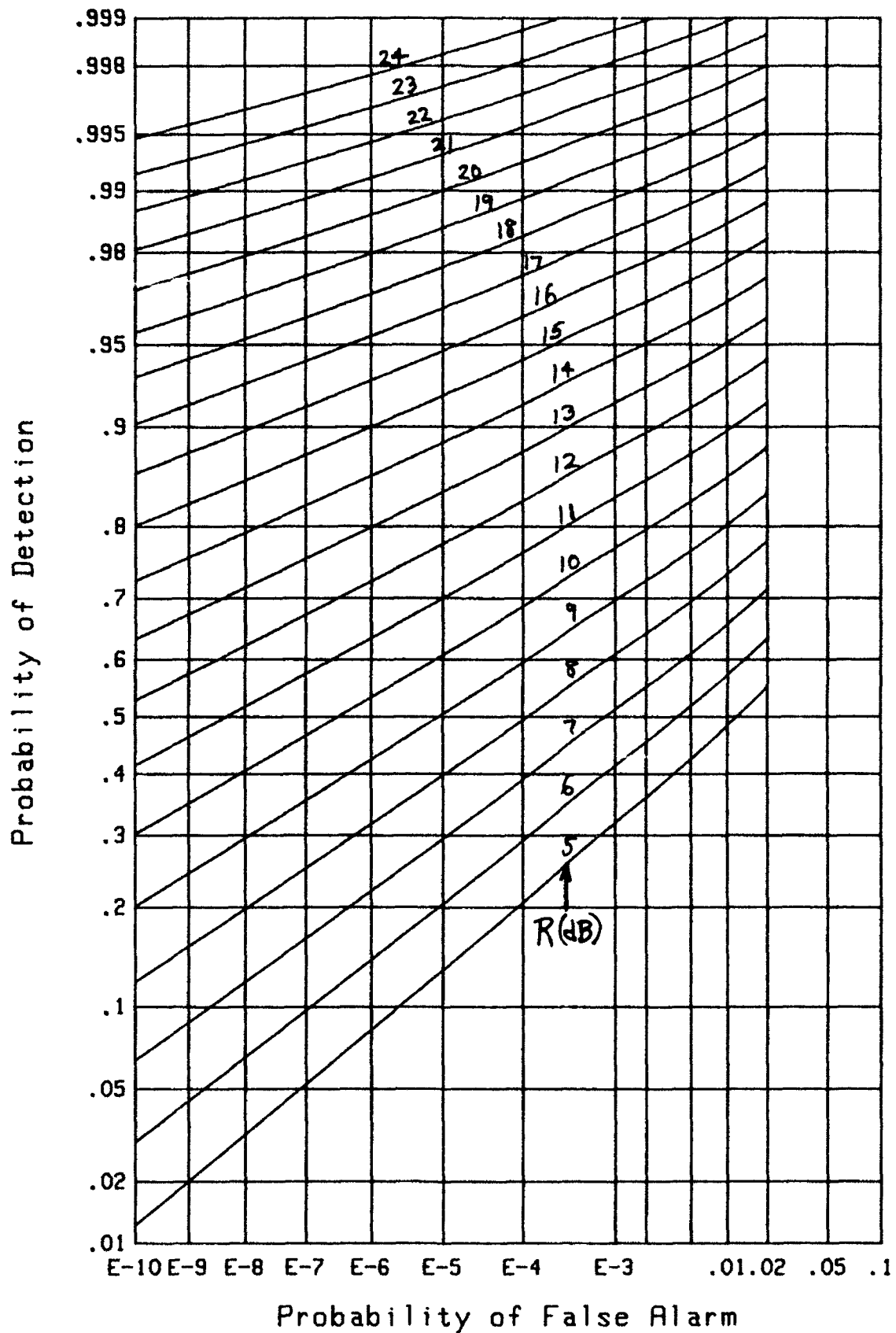
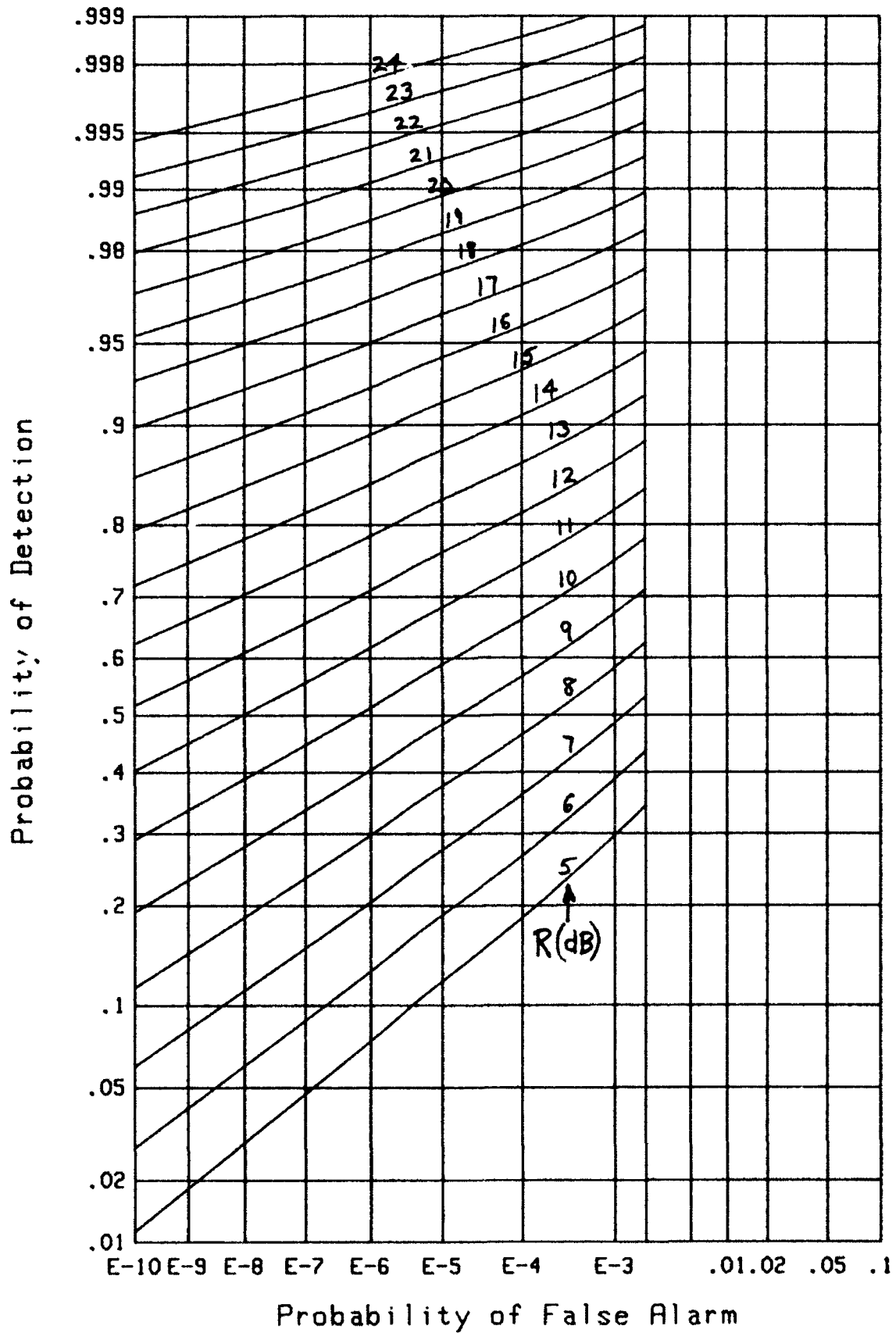


Figure 6. ROC for $N=2$, $F=.01$

Figure 7. ROC for $N=2$, $F=.001$

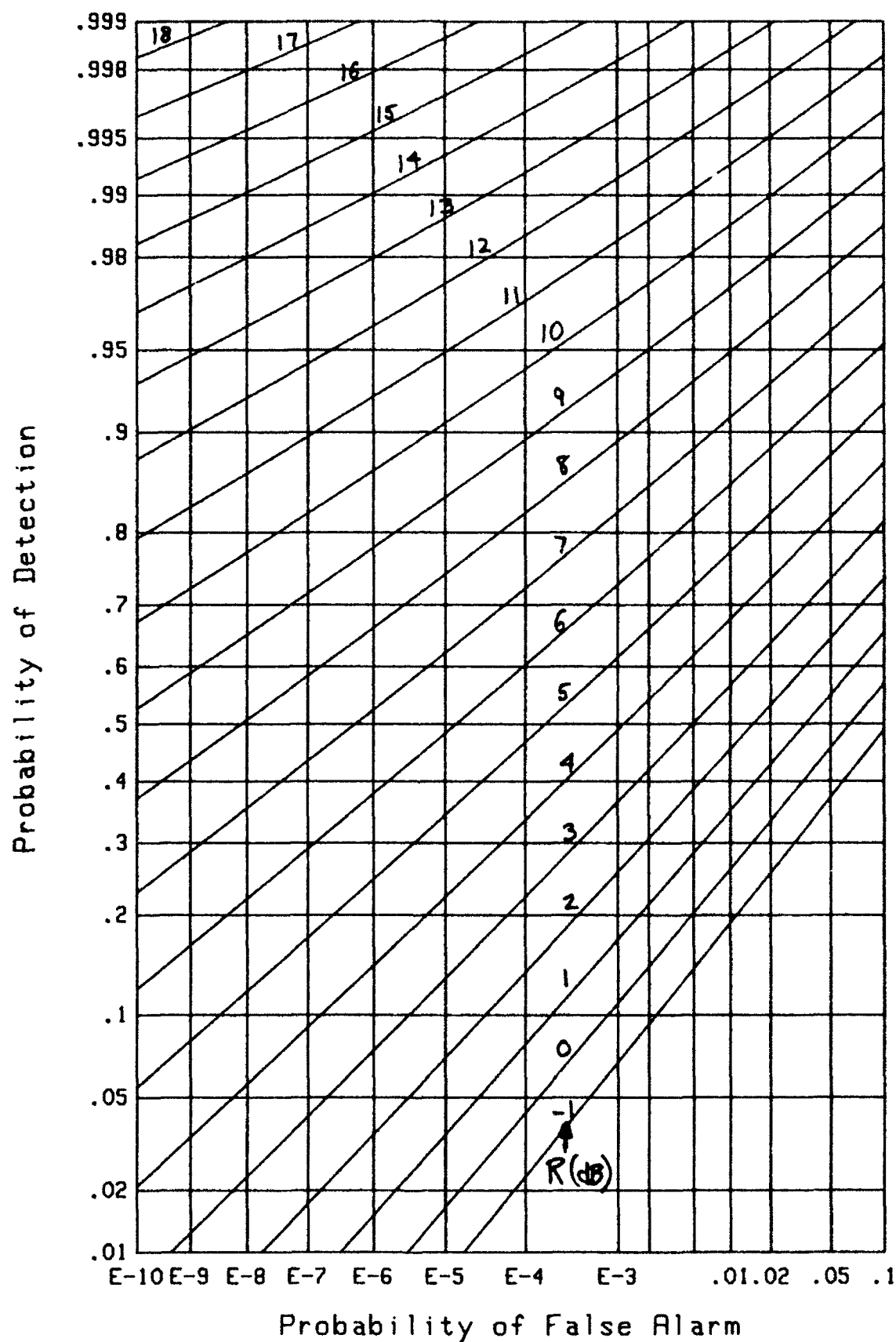
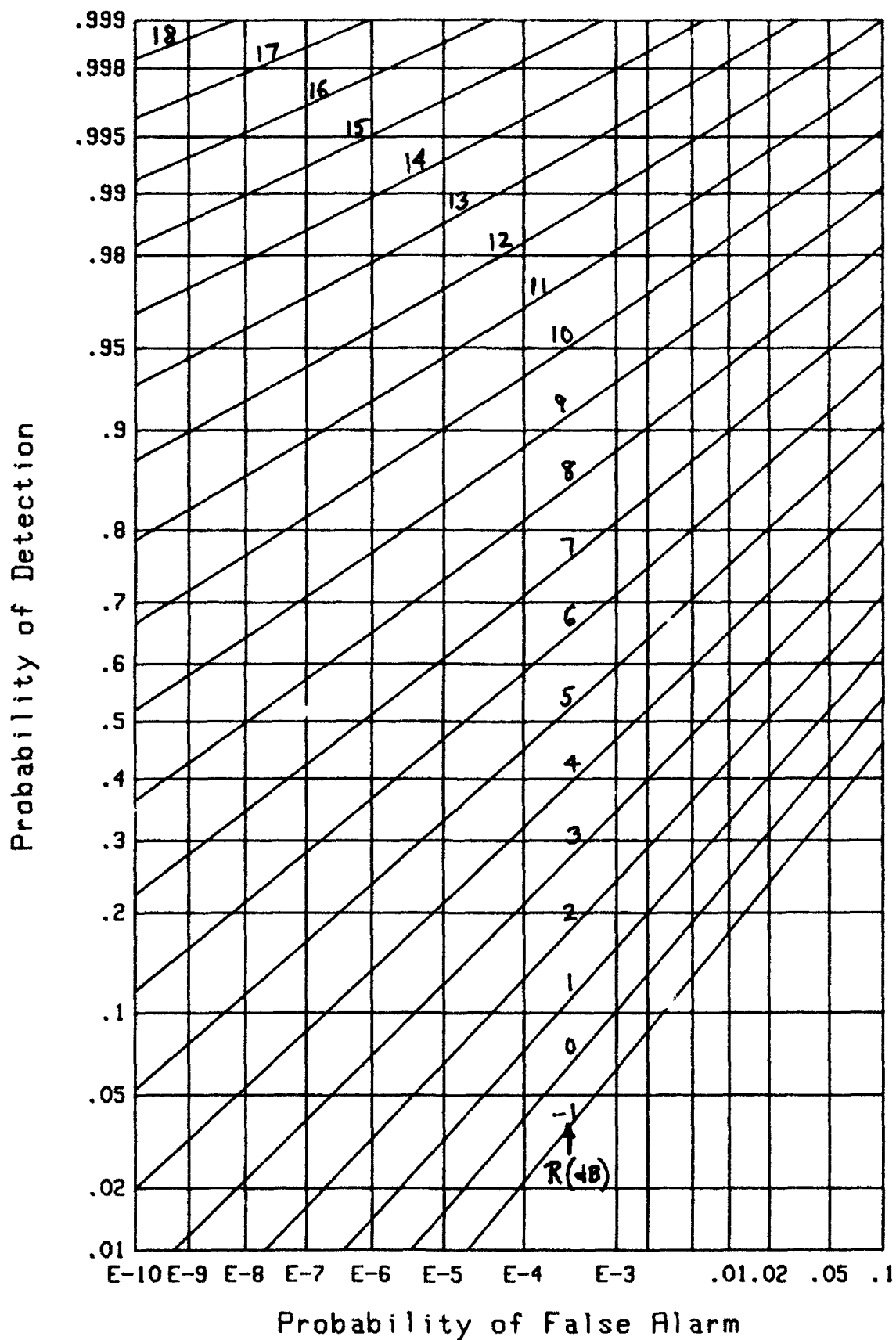
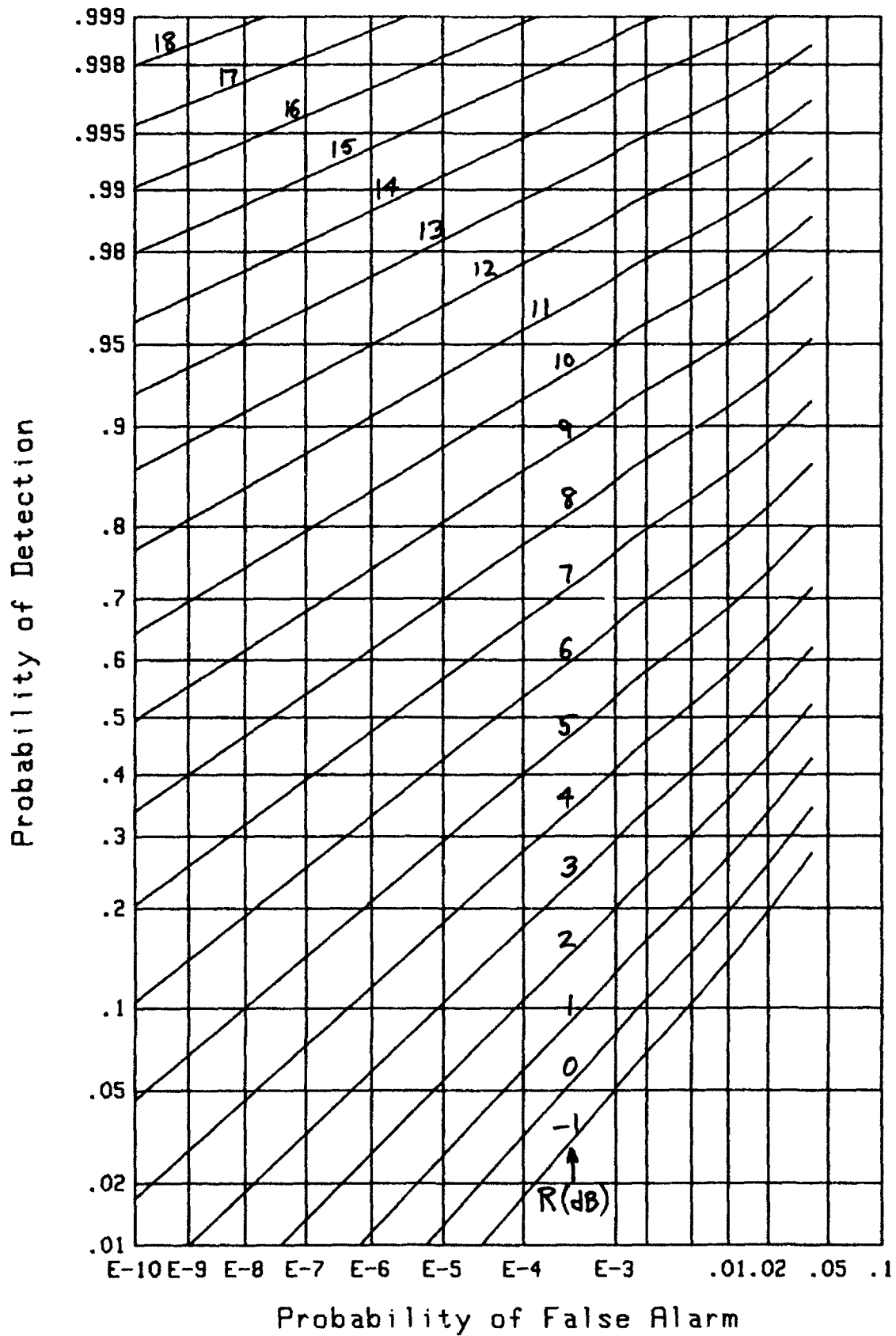
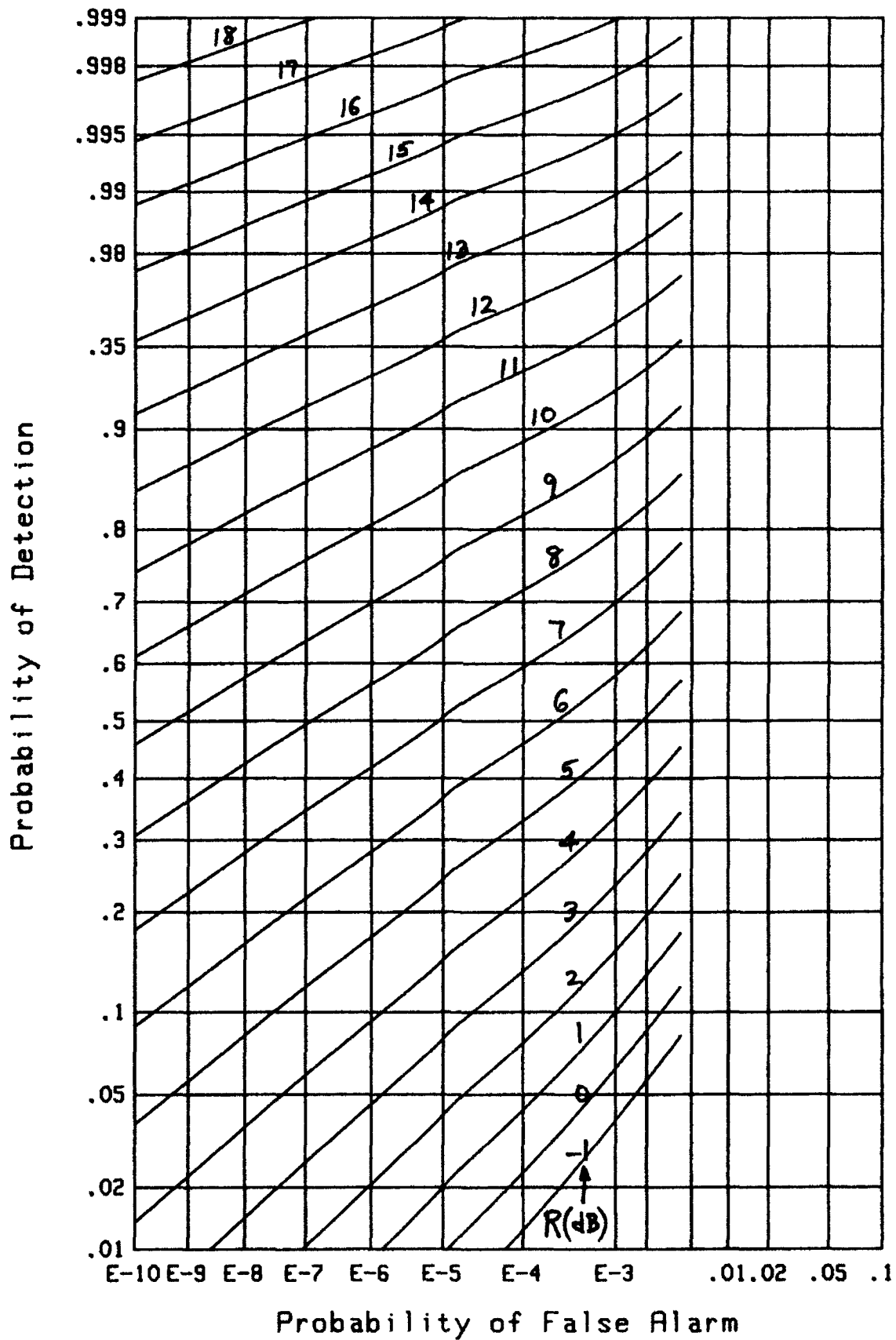
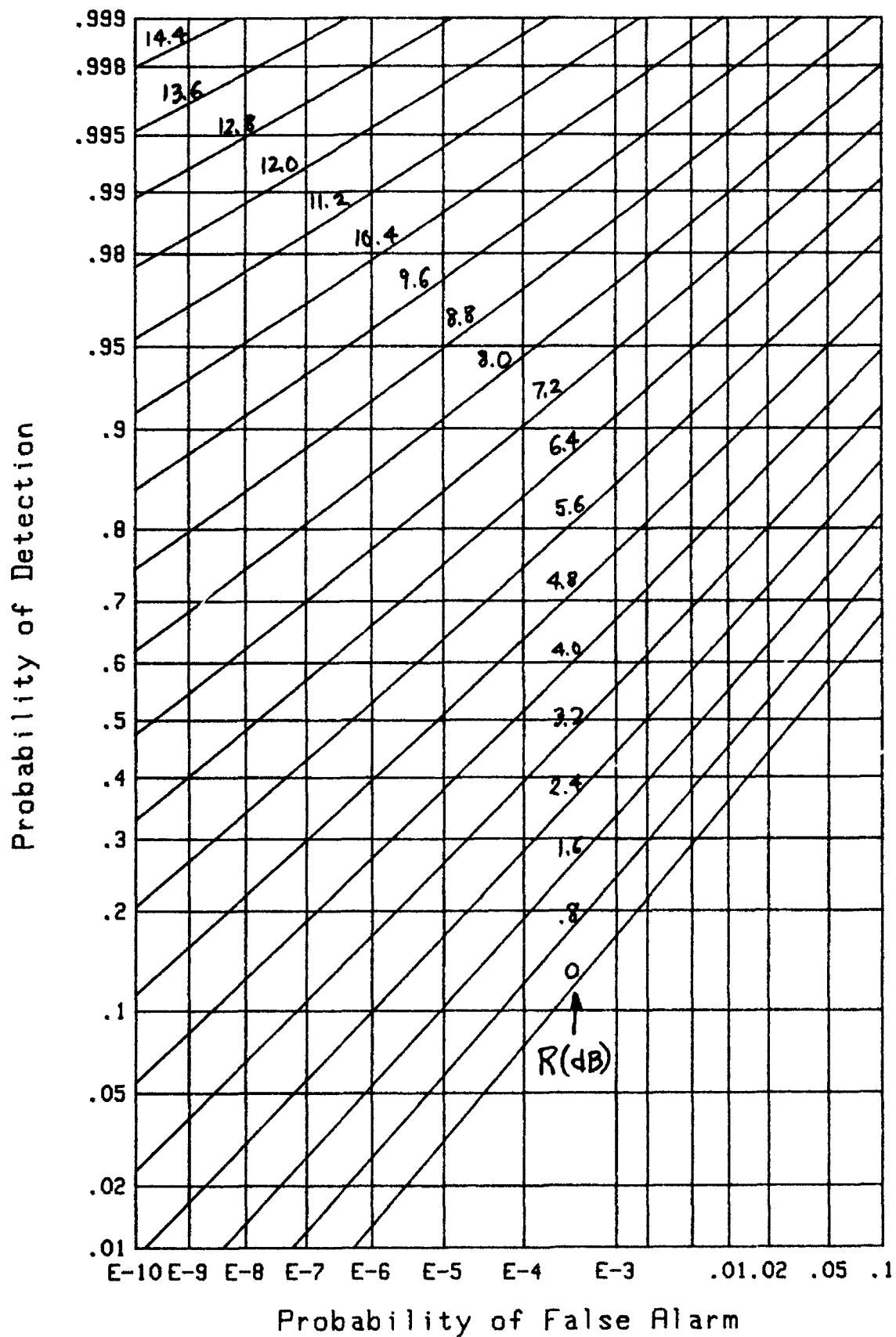


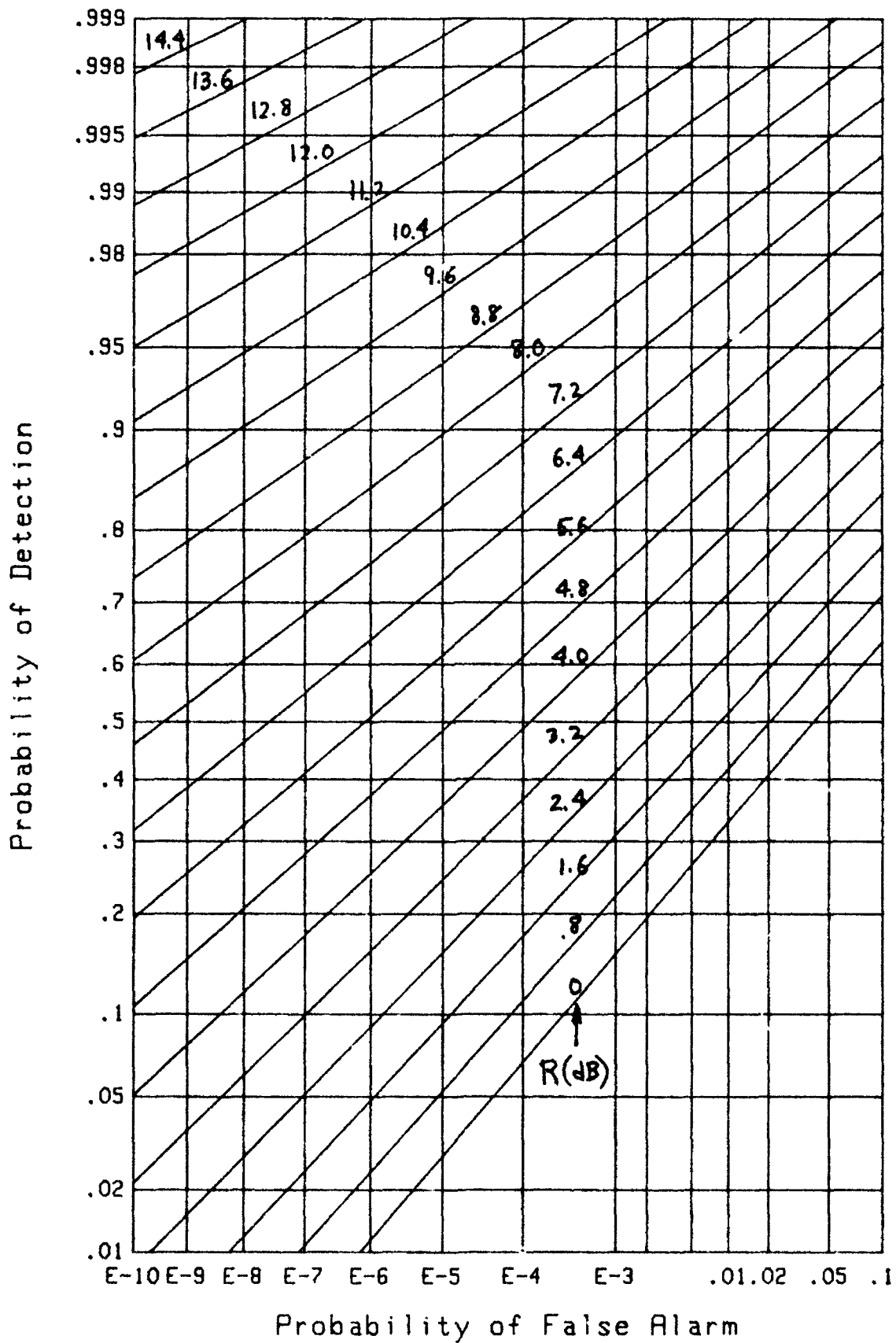
Figure 8. ROC for $N=4$, $F=1$.

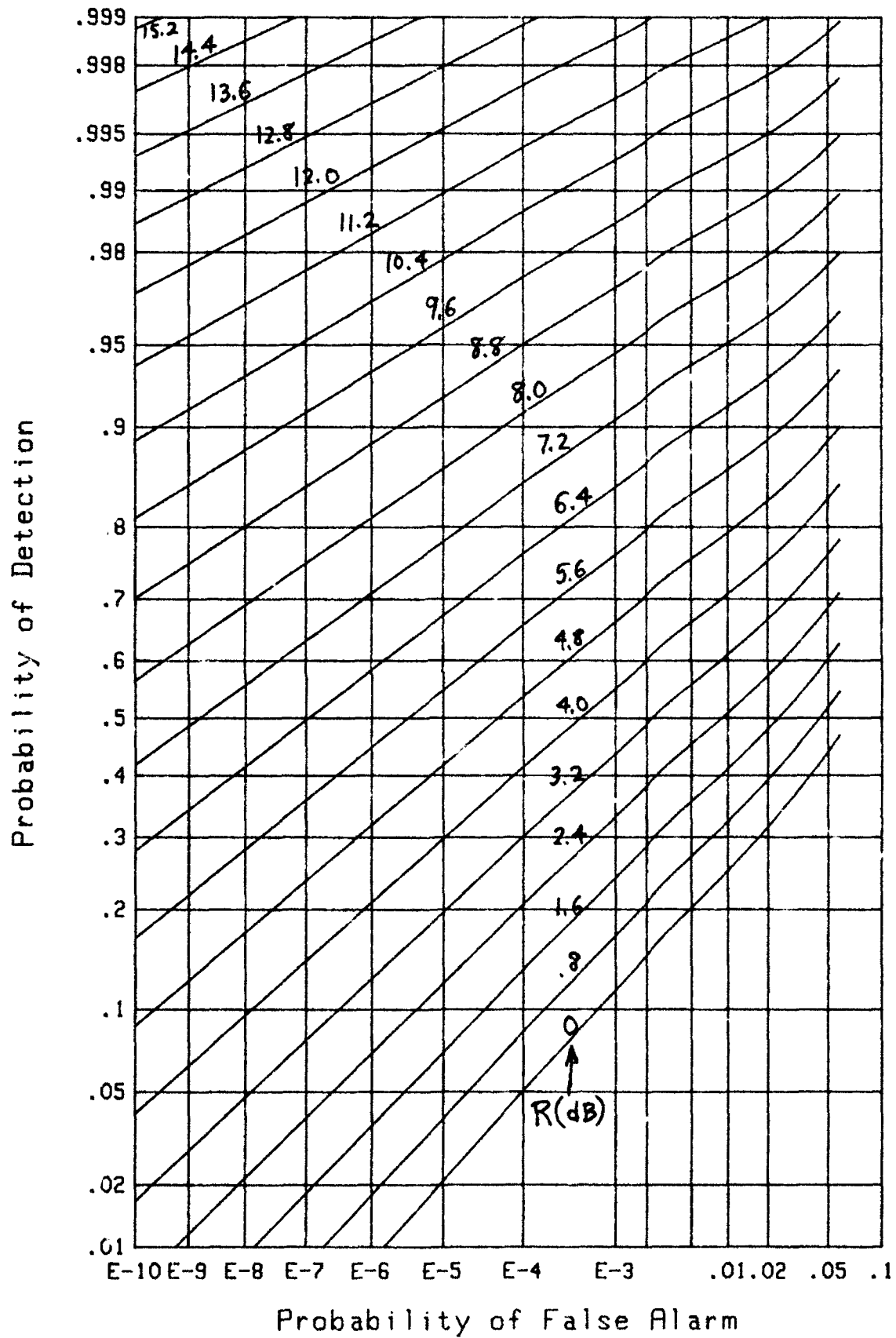
Figure 9. ROC for $N=4$, $F=.1$

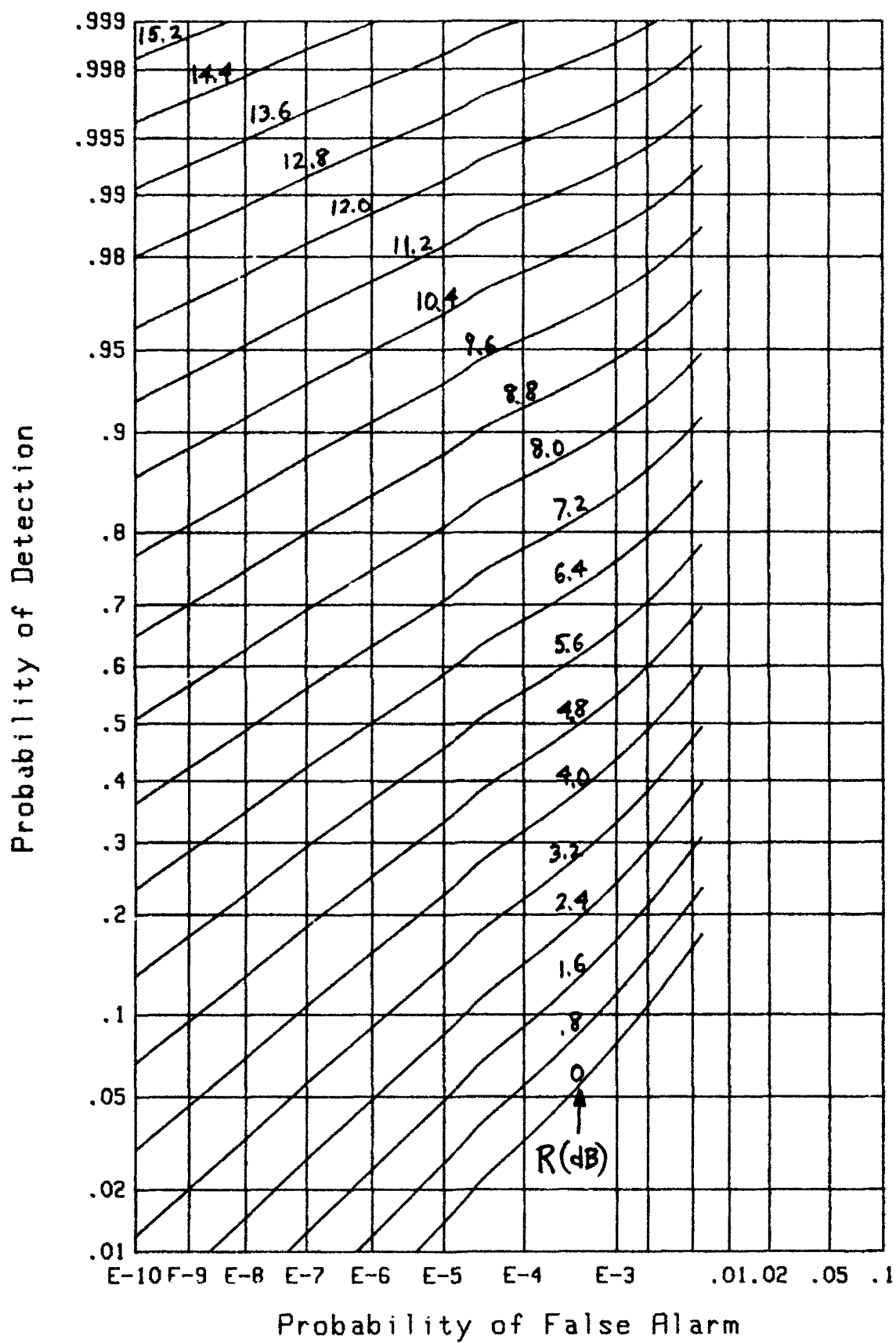
Figure 10. ROC for $N=4$, $F=.01$

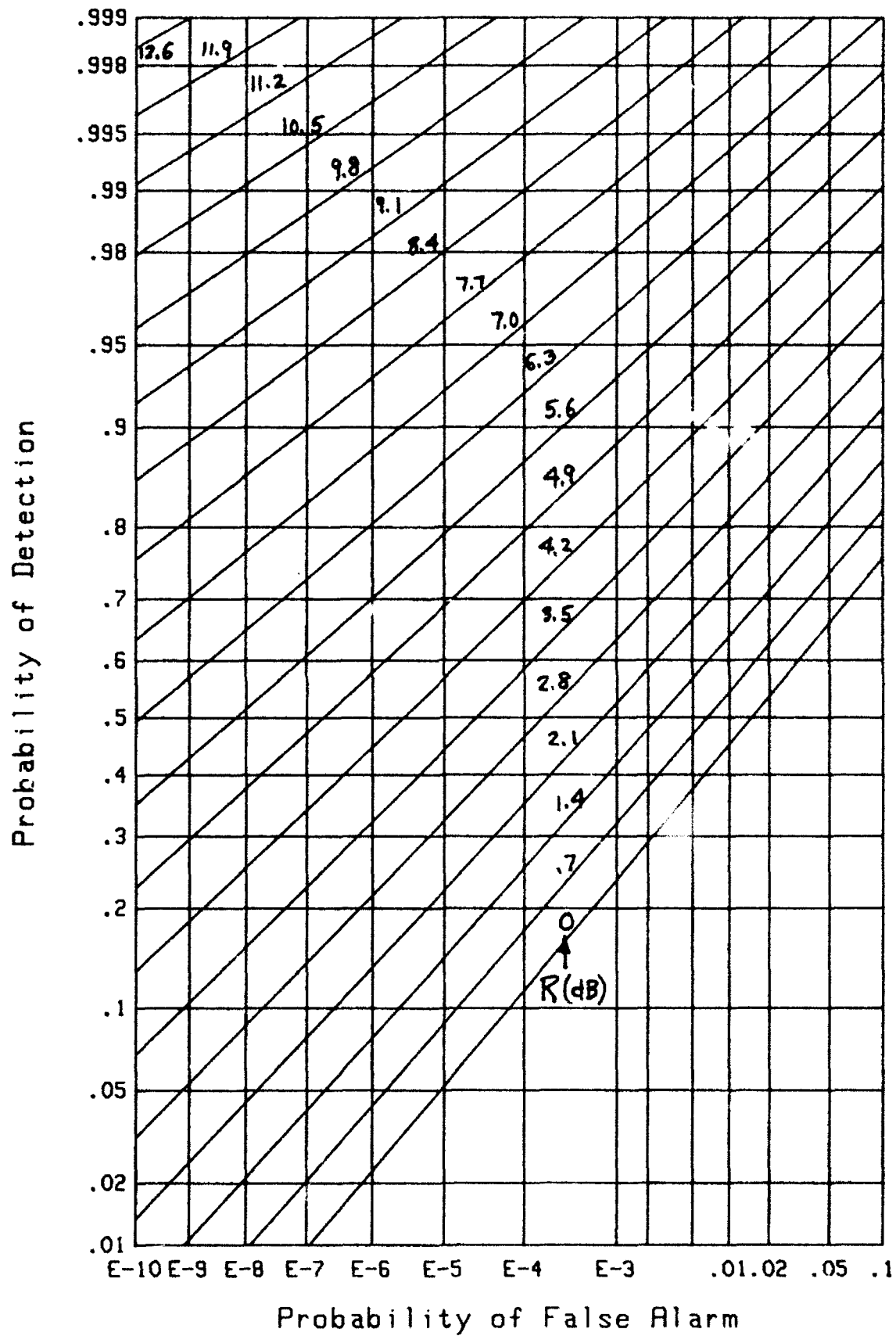
Figure 11. ROC for $N=4$, $F=.001$

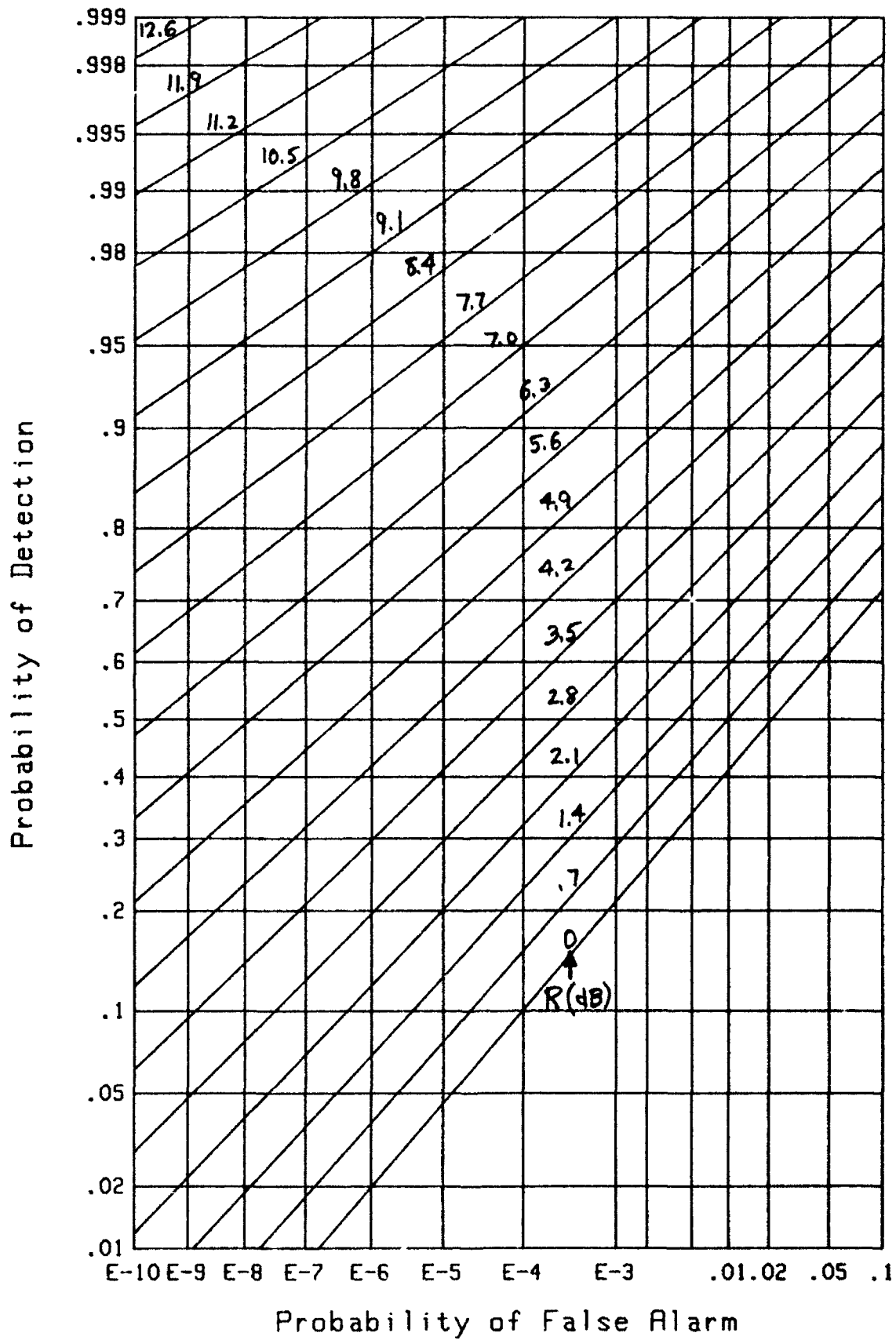
Figure 12. ROC for $N=6$, $F=1$.

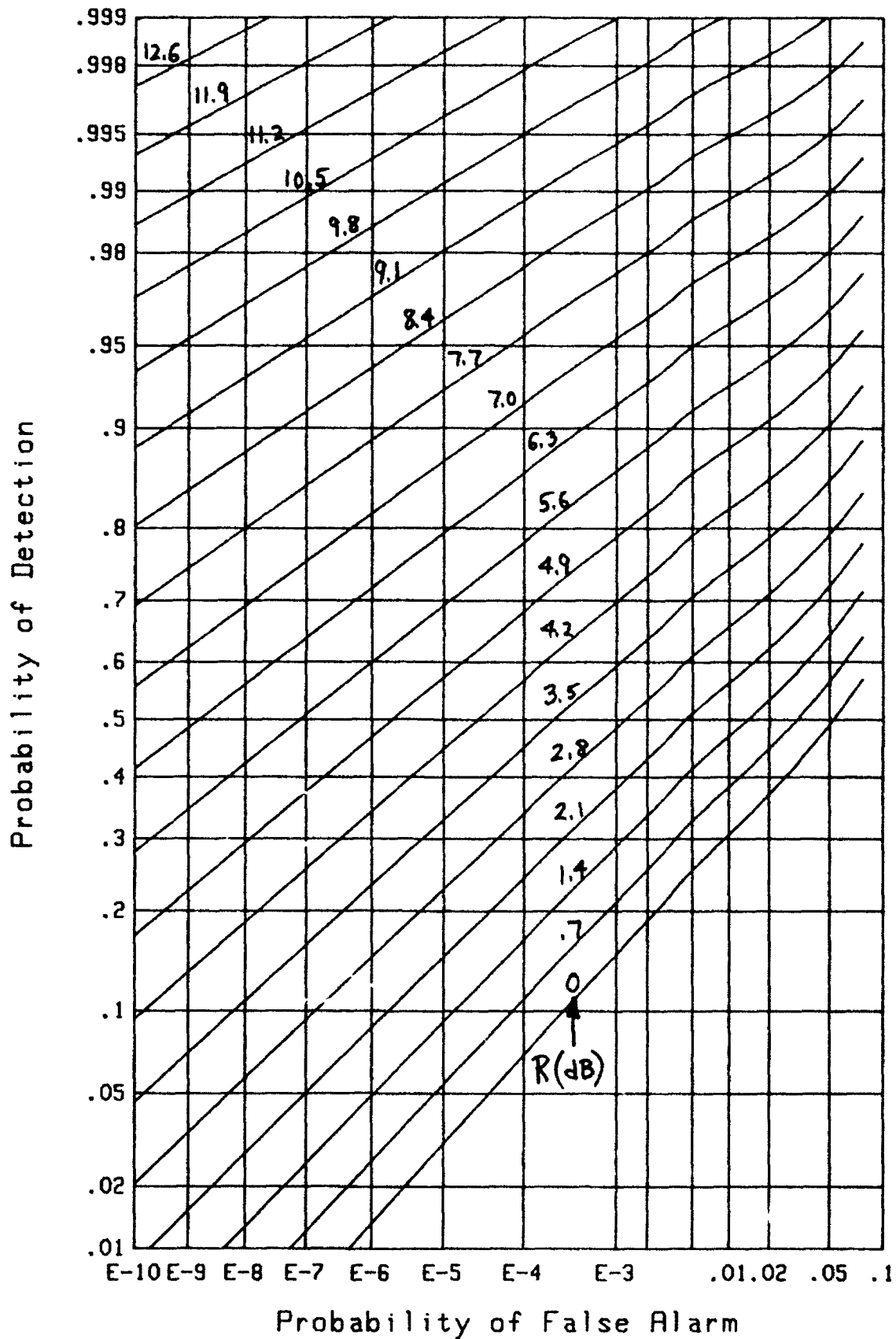
Figure 13. ROC for $N=6$, $F=.1$

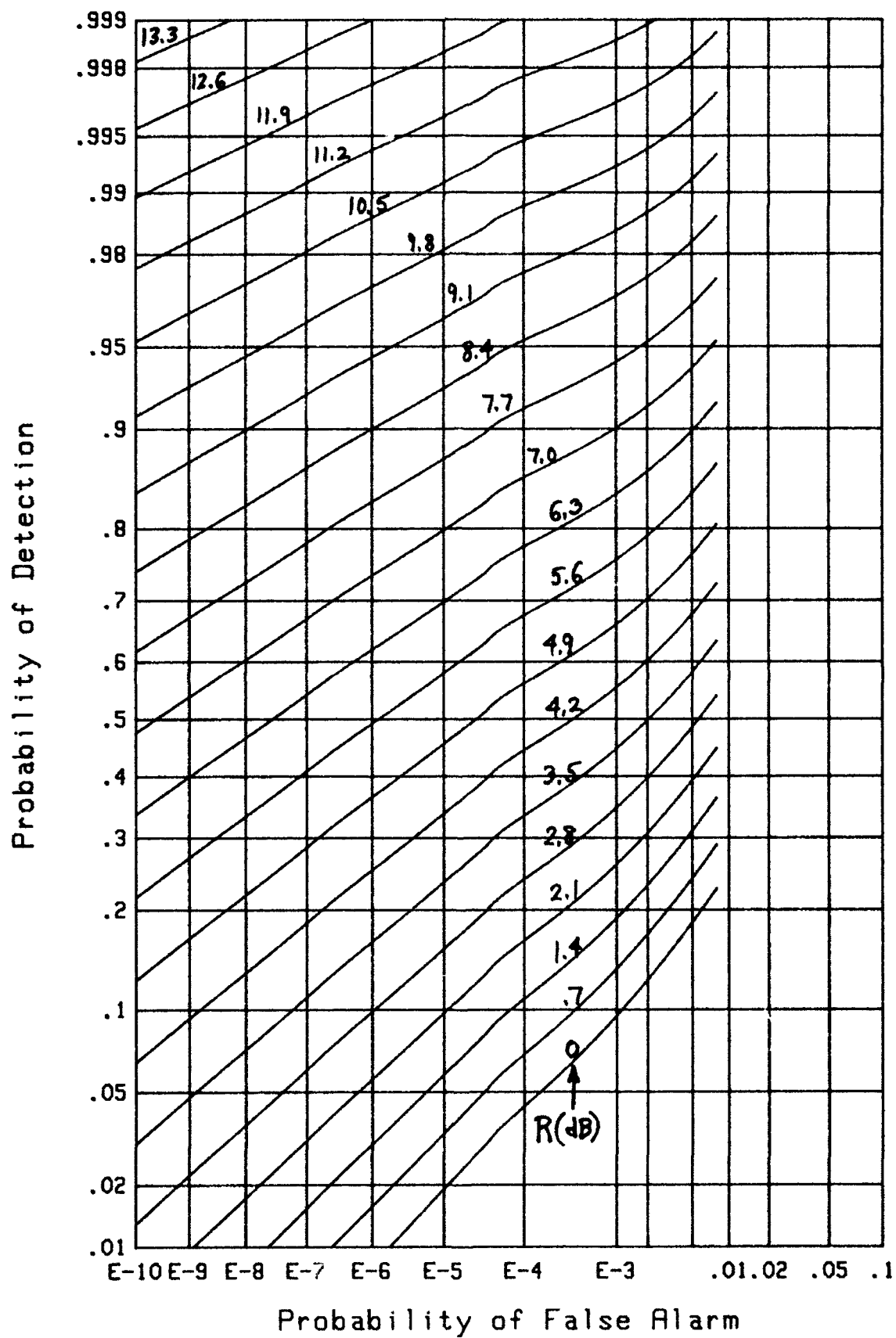
Figure 14. ROC for $N=6$, $F=.01$

Figure 15. ROC for $N=6$, $F=.001$

Figure 16. ROC for $N=8$, $F=1$.

Figure 17. ROC for $N=8$, $F=.1$

Figure 18. ROC for $N=8$, $F=.01$

Figure 19. ROC for $N=8$, $F=.001$

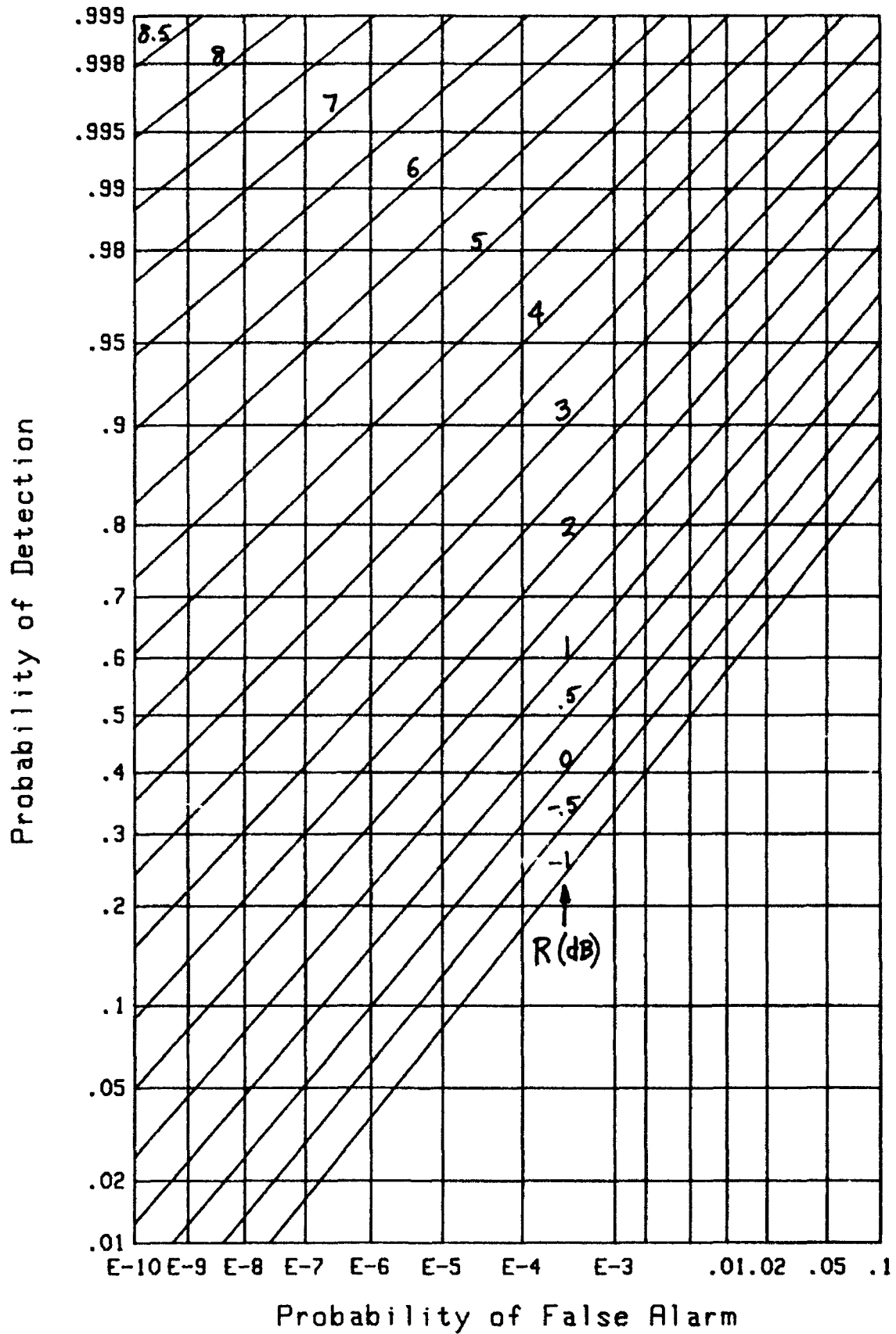


Figure 20. ROC for $N=16$, $F=1$.

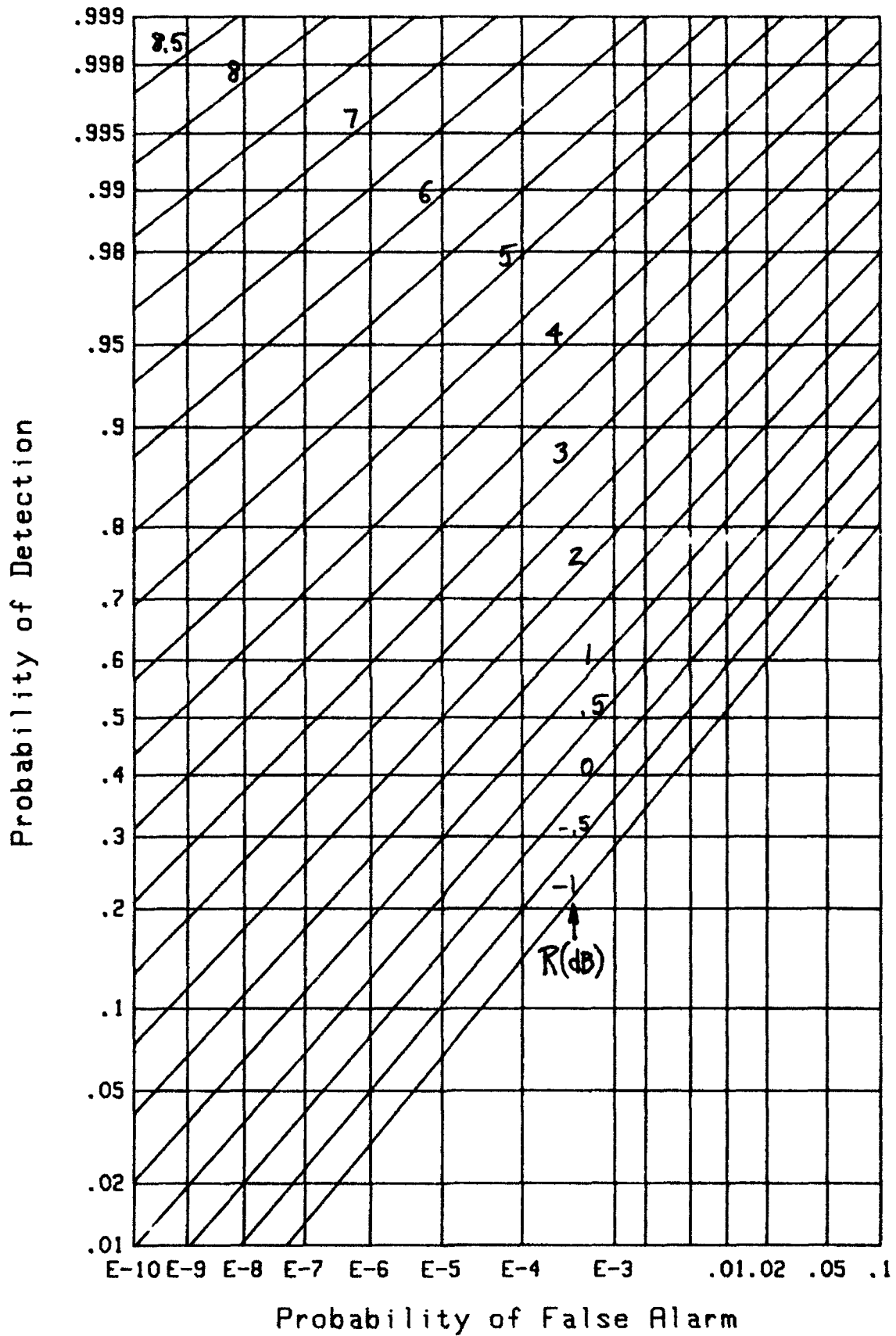
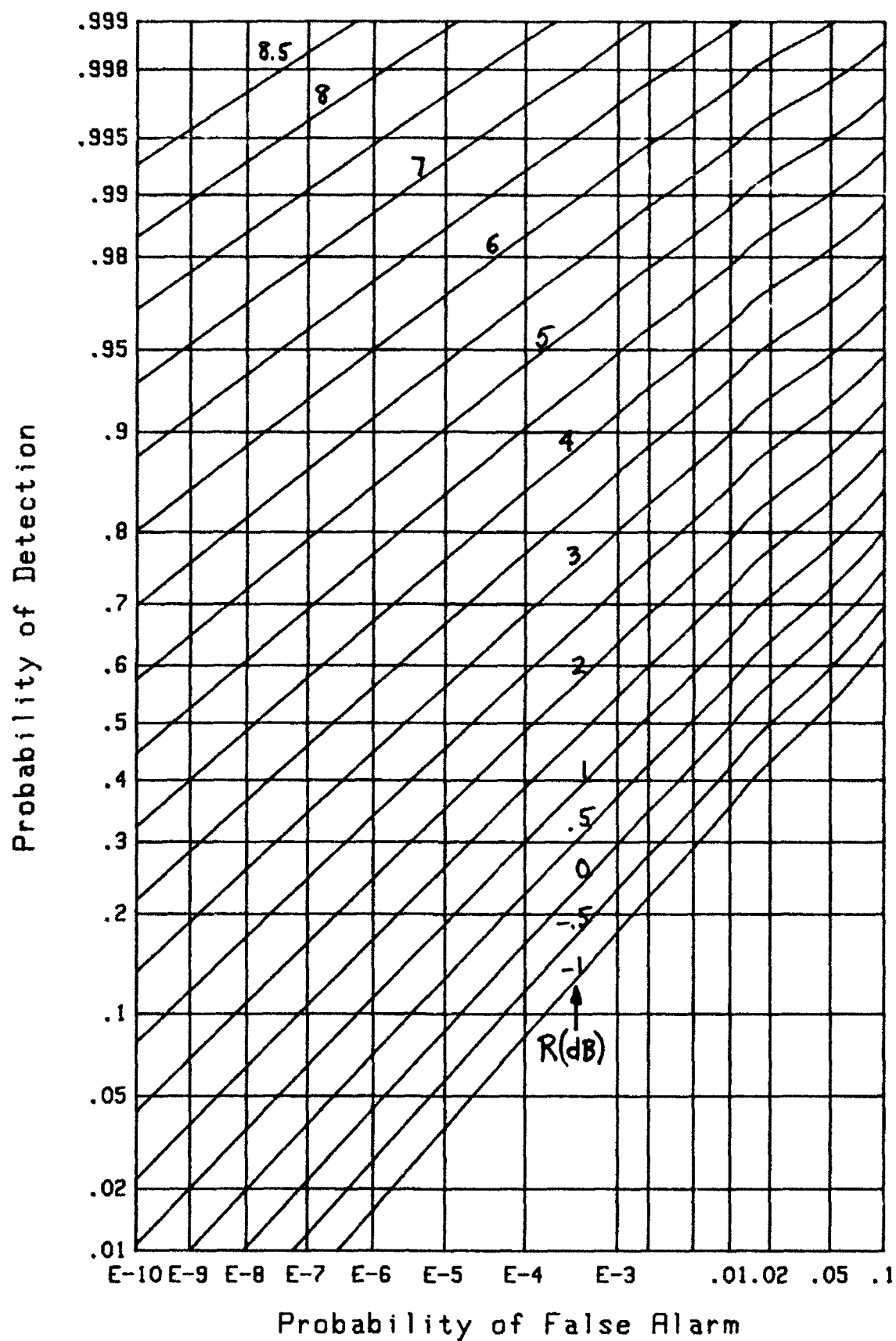
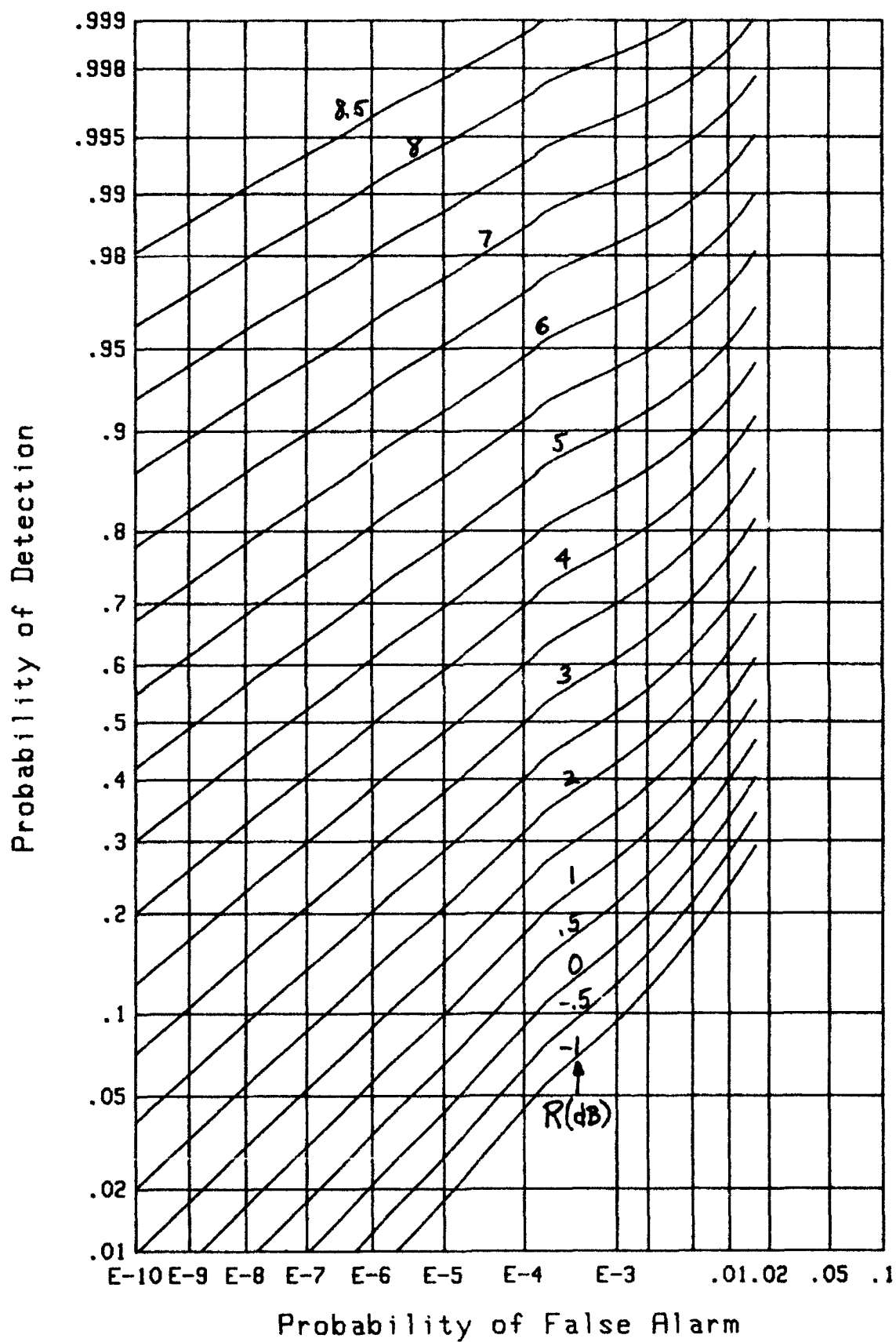
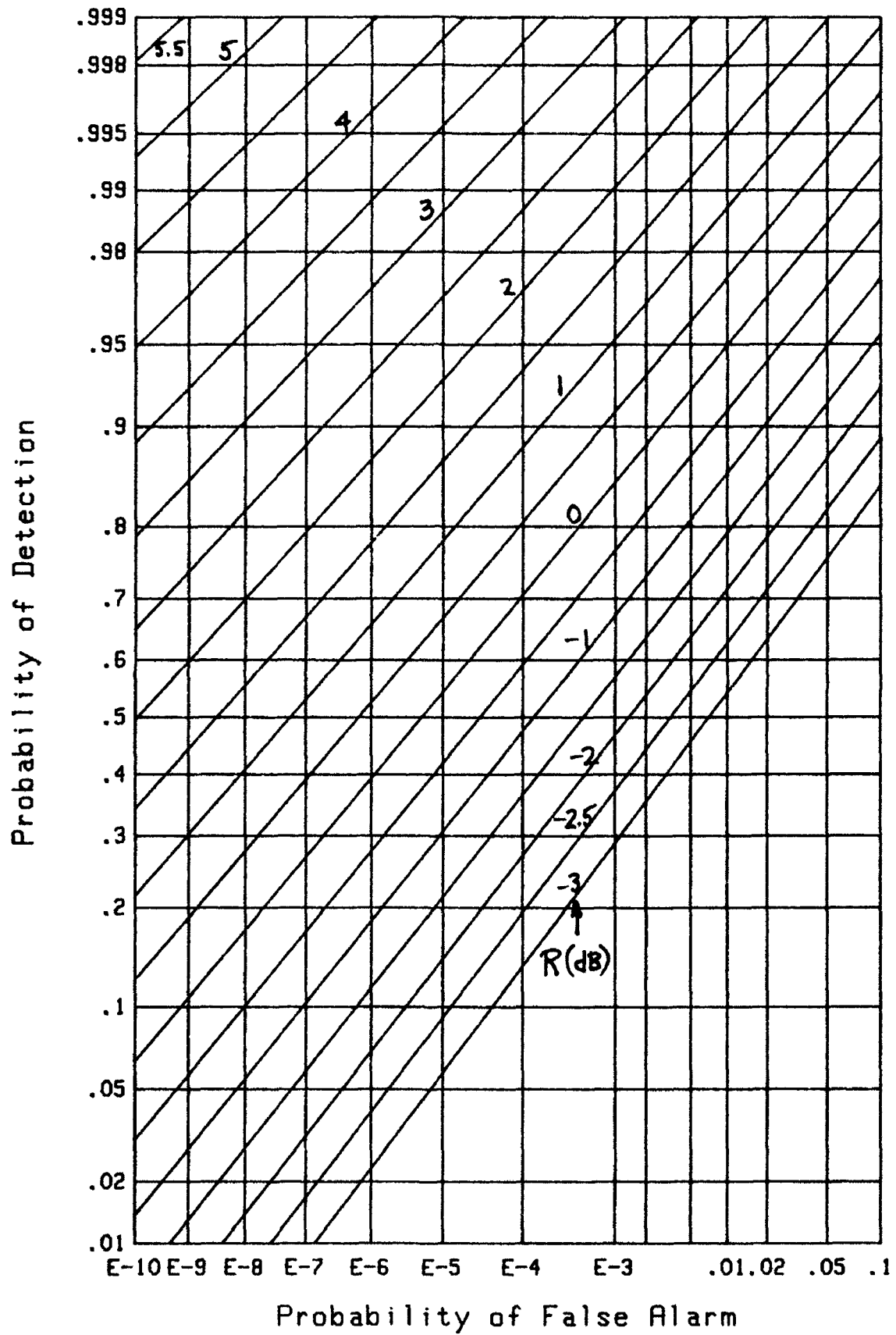


Figure 21. ROC for $N=16$, $F=.1$

Figure 22. ROC for $N=16$, $F=.01$

Figure 23. ROC for $N=16$, $F=.001$

Figure 24. ROC for $N=32$, $F=1$.

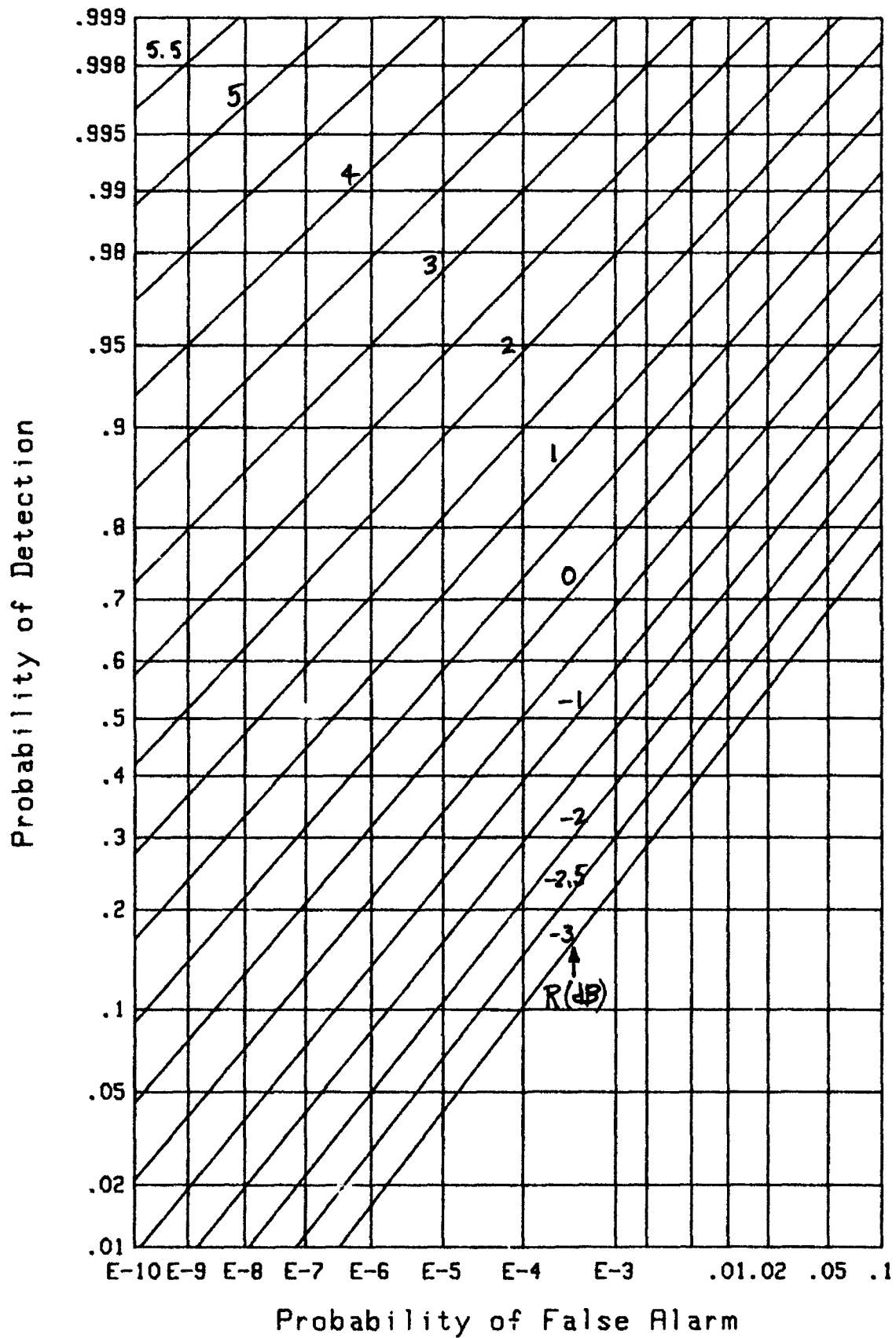


Figure 25. ROC for $N=32$, $F=.1$

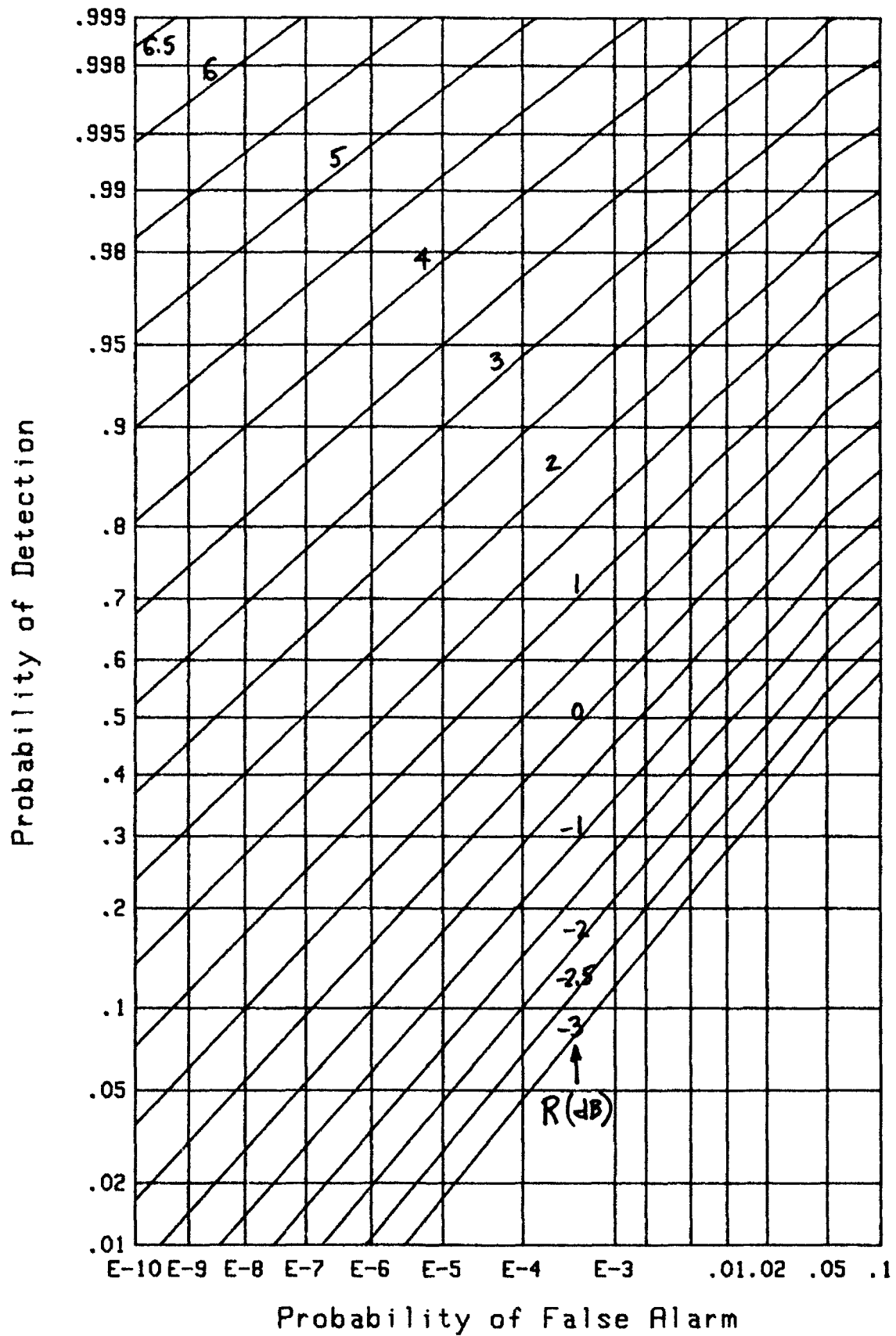
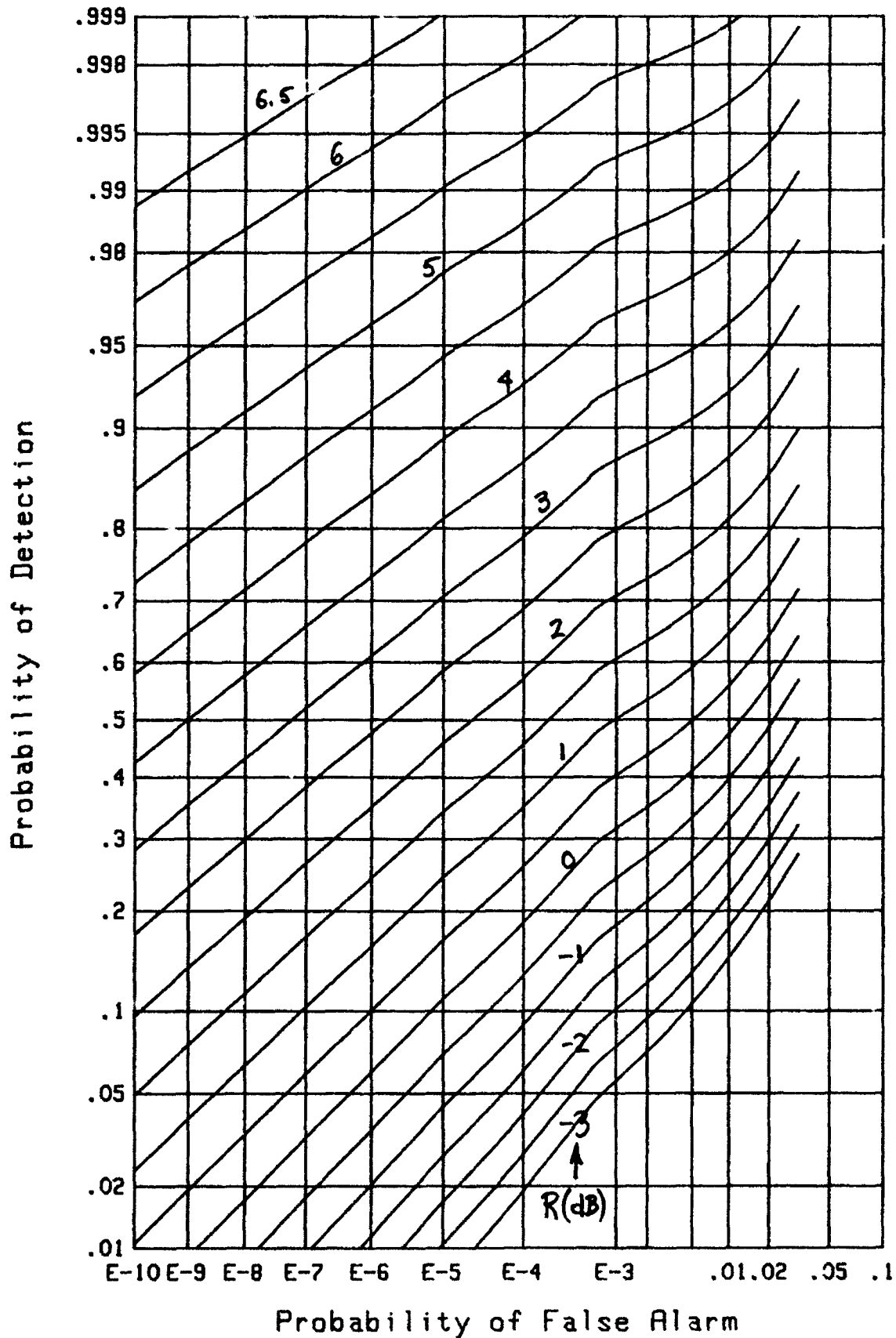
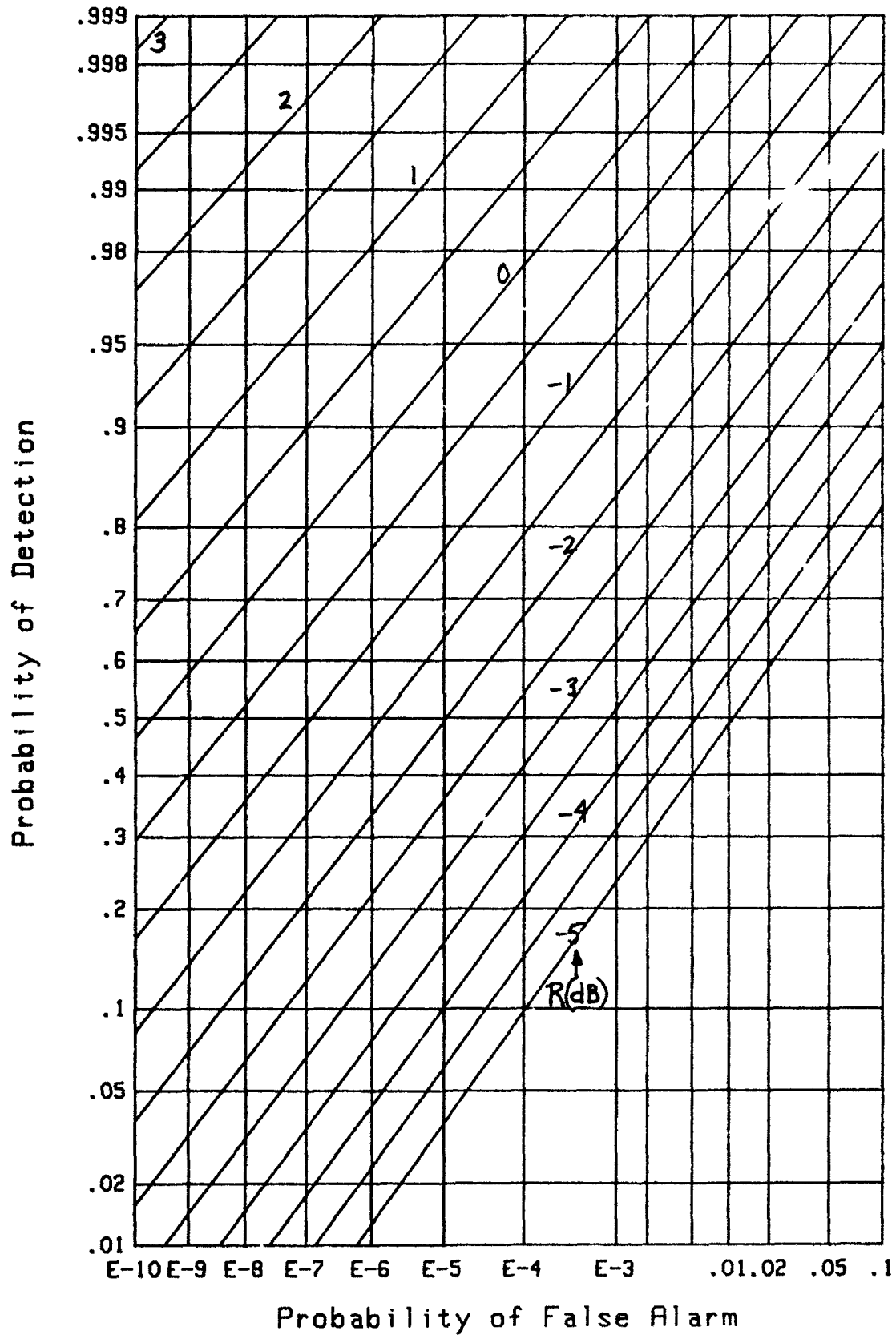
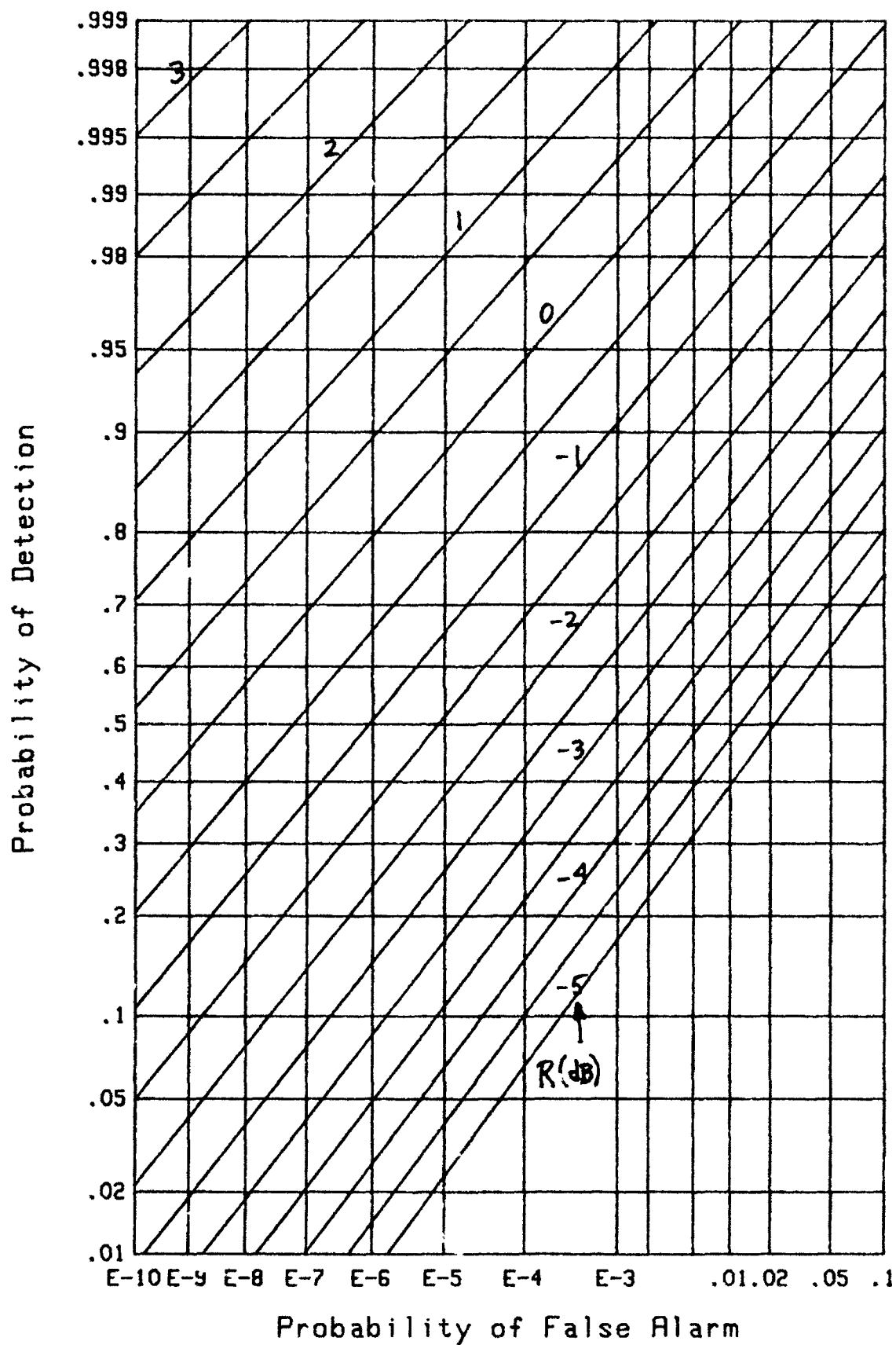


Figure 26. ROC for $N=32$, $F=.01$

Figure 27. ROC for $N=32$, $F=.001$

Figure 28. ROC for $N=64$, $F=1$.

Figure 29. ROC for $N=64$, $F=.1$

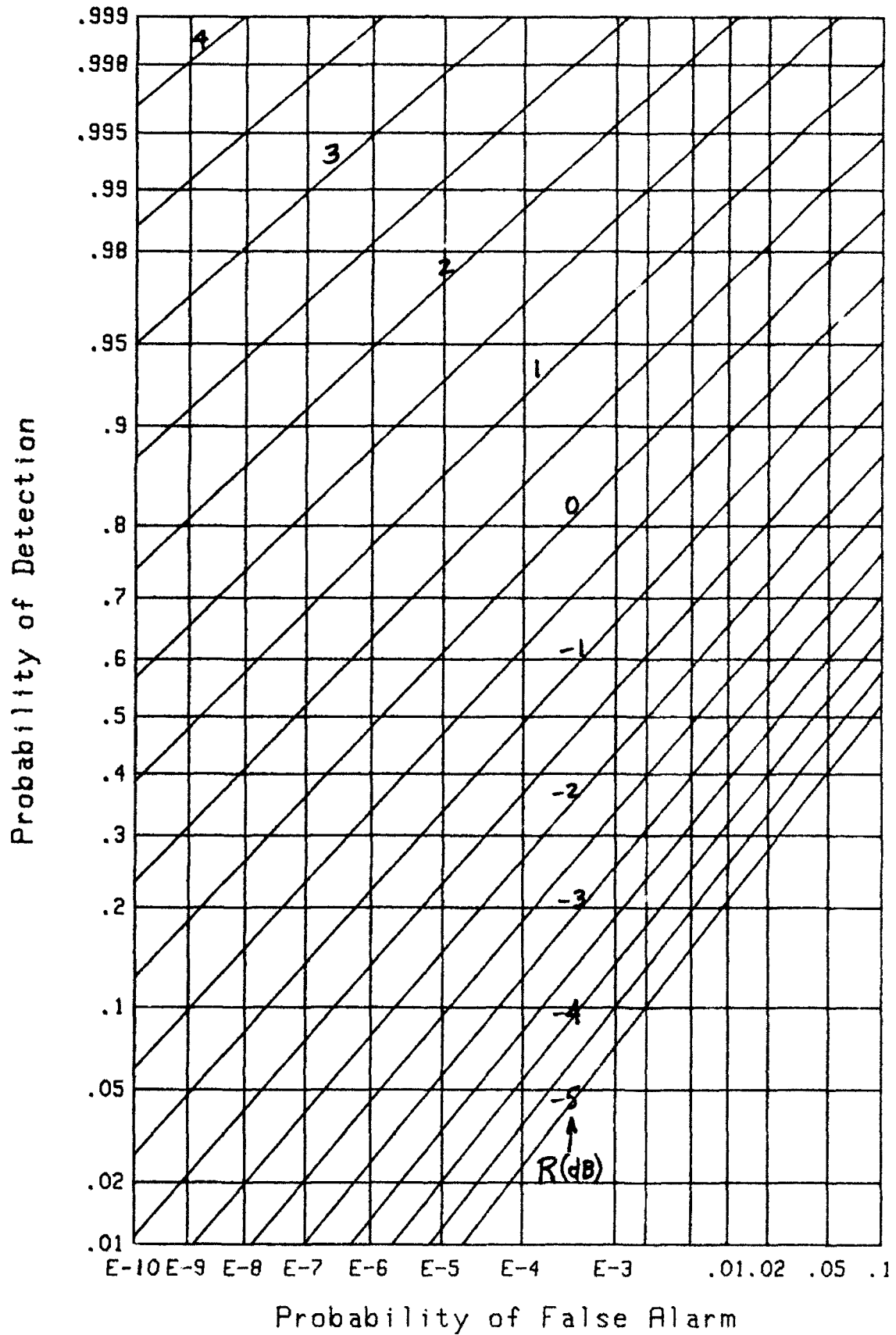
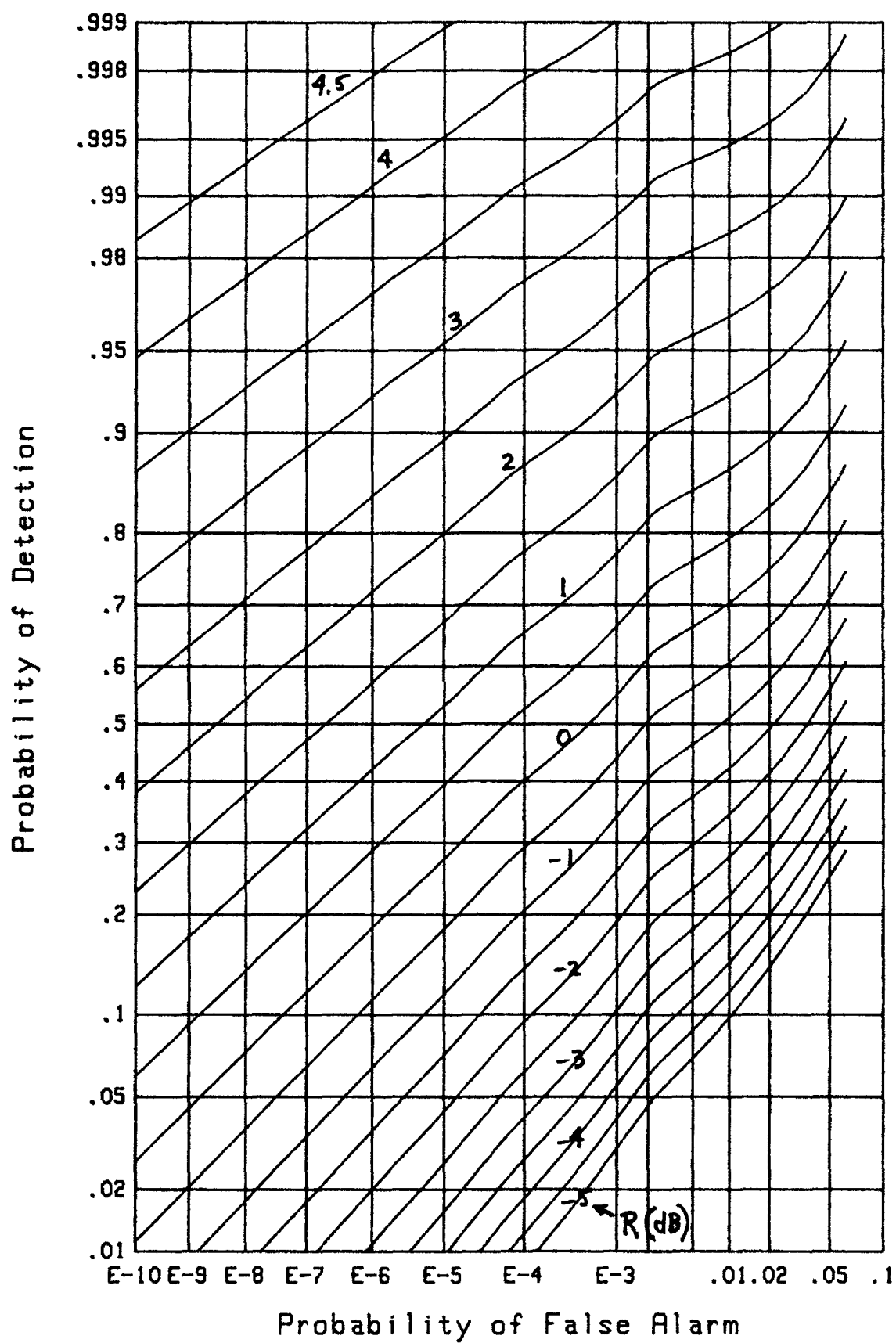


Figure 30. ROC for $N=64$, $F=.01$

Figure 31. ROC for $N=64$, $F=.001$

SUMMARY

The cost of suppressing the low-level outputs of the detected squared-envelopes is generally minimal, unless the number of channels becomes very large. This conclusion has been drawn only for the example where these squared-envelopes have an exponential probability density function for both the noise-only as well as the signal-plus-noise cases. It should also be checked out for other candidate forms of probability density functions besides exponential.

One line of reasoning that makes this conclusion more acceptable is that it is only the larger outputs from the detectors that are going to lead to positive statements about signal presence. Thus, suppression of the smaller outputs should be inconsequential, at least for few channels. However, for a large number of channels, the sum of many nonzero low-level quantities may add up to a significant value and affect an occasional detection decision.

APPENDIX A. PROGRAM FOR RECEIVER OPERATING CHARACTERISTICS

```

10  ! GENERATE PD VS PF; COMBINER WITH DEAD ZONE IN EACH CHANNEL, TR8595
20  N=64                      ! NUMBER OF CHANNELS; N>=1
30  F=.001                    ! FRACTION OF DATA PASSED; 0.<F<=1.
40  DIM T(100)                ! THRESHOLD VALUES
50  COM Pf(100),Pd1(100),Pd2(100),Pd3(100),Pd4(100),Pd5(100)
60  COM Pd6(100),Pd7(100),Pd8(100),Pd9(100),Pd10(100),Pd11(100)
70  COM Pd12(100),Pd13(100),Pd14(100),Pd15(100),Pd16(100),Pd17(100)
80  COM Pd18(100),Pd19(100),Pd20(100)
90  DOUBLE N,I,J              ! INTEGERS
100 T=.01
110 T=T+.01
120 Pf=FNPf(T,F,N)
130   IF Pf>.1 THEN 110
140 T1=MAX(T-.01,.01)
150 T=T+.01
160 Pf=FNPf(T,F,N)
170   IF Pf>1E-10 THEN 150
180 T2=T
190 DelT=(T2-T1)/100.
200 FOR I=0 TO 100
210 T=T1+DelT*I
220 T(I)=T                    ! THRESHOLD VALUES
230 Pf(I)=FNPf(T,F,N)        ! FALSE ALARM PROBABILITIES
240 NEXT I
250   Rldb=-5                  ! STARTING SIGNAL-TO-NOISE RATIO (dB)
260   Delr=.5                  ! INCREMENT IN SHR (dB)
270   FOR J=1 TO 20
280     Rdb=Rldb+(J-1)*Delr    ! SIGNAL-TO-NOISE RATIO PER CHANNEL (dB)
290     R=10.^(.1*Rdb)         ! POWER RATIO
300     FOR I=0 TO 100
310       T=T(I)
320       Pd=FNPd(R,T,F,N)    ! DETECTION PROBABILITIES
330       IF J=1 THEN Pd1(I)=Pd
340       IF J=2 THEN Pd2(I)=Pd
350       IF J=3 THEN Pd3(I)=Pd
360       IF J=4 THEN Pd4(I)=Pd
370       IF J=5 THEN Pd5(I)=Pd
380       IF J=6 THEN Pd6(I)=Pd
390       IF J=7 THEN Pd7(I)=Pd
400       IF J=8 THEN Pd8(I)=Pd
410       IF J=9 THEN Pd9(I)=Pd
420       IF J=10 THEN Pd10(I)=Pd
430       IF J=11 THEN Pd11(I)=Pd
440       IF J=12 THEN Pd12(I)=Pd
450       IF J=13 THEN Pd13(I)=Pd
460       IF J=14 THEN Pd14(I)=Pd
470       IF J=15 THEN Pd15(I)=Pd
480       IF J=16 THEN Pd16(I)=Pd
490       IF J=17 THEN Pd17(I)=Pd
500       IF J=18 THEN Pd18(I)=Pd
510       IF J=19 THEN Pd19(I)=Pd
520       IF J=20 THEN Pd20(I)=Pd
530     NEXT I
540   NEXT J

```

```

550   FOR I=0 TO 100
560   Pf(I)=FNInvphi(Pf(I))
570   Pd1(I)=FNInvphi(Pd1(I))
580   Pd2(I)=FNInvphi(Pd2(I))
590   Pd3(I)=FNInvphi(Pd3(I))
600   Pd4(I)=FNInvphi(Pd4(I))
610   Pd5(I)=FNInvphi(Pd5(I))
620   Pd6(I)=FNInvphi(Pd6(I))
630   Pd7(I)=FNInvphi(Pd7(I))
640   Pd8(I)=FNInvphi(Pd8(I))
650   Pd9(I)=FNInvphi(Pd9(I))
660   Pd10(I)=FNInvphi(Pd10(I))
670   Pd11(I)=FNInvphi(Pd11(I))
680   Pd12(I)=FNInvphi(Pd12(I))
690   Pd13(I)=FNInvphi(Pd13(I))
700   Pd14(I)=FNInvphi(Pd14(I))
710   Pd15(I)=FNInvphi(Pd15(I))
720   Pd16(I)=FNInvphi(Pd16(I))
730   Pd17(I)=FNInvphi(Pd17(I))
740   Pd18(I)=FNInvphi(Pd18(I))
750   Pd19(I)=FNInvphi(Pd19(I))
760   Pd20(I)=FNInvphi(Pd20(I))
770   NEXT I
780   CALL Plot
790   END
800   !
810   DEF FNInvphi(X)      ! AMS 55, 26.2.23
820   IF X=.5 THEN RETURN 0.
830   P=MIN(X,1.-X)
840   T=-LOG(P)
850   T=SQR(T+T)
860   P=1.+T*(1.432788+T*(.189269+T*.001308))
870   P=T-(2.515517+T*(.802853+T*.010328))/P
880   IF X<.5 THEN P=-P
890   RETURN P
900   FNEND
910   !
920   DEF FNE(U,DOUBLE N)  ! N>=0
930   DOUBLE K             ! INTEGER
940   IF U<=0. THEN RETURN 1.
950   S=T=EXP(-U)
960   IF N=0 THEN RETURN S
970   FOR K=1 TO N
980   T=T*U/K
990   S=S+T
1000  NEXT K
1010  RETURN S
1020  FNEND
1030  !

```

```

1040 DEF FNPf(T,F,DOUBLE N) ! FALSE ALARM PROB. T>=0,0<F<=1,N>=1
1050 DOUBLE Ns,N1 ! INTEGERS
1060 IF F<1. THEN 1090
1070 Pf=FNE(T,N-1)
1080 RETURN Pf
1090 L=-LOG(F)
1100 N1=N+1
1110 F1=1.-F
1120 A=F/F1
1130 Tn=F1^N
1140 C=T
1150 Pf=0.
1160 FOR Ns=1 TO N
1170 C=C-L
1180 Tn=Tn*A*(N1-Ns)/Ns
1190 Pf=Pf+Tn*FNE(C,Ns-1)
1200 NEXT Ns
1210 RETURN Pf
1220 FNEND
1230 !
1240 DEF FNPd(R,T,F,DOUBLE N) ! DETECTION PROB. R>=0,T>=0,0<F<=1,N>=1
1250 DOUBLE Ns,N1 ! INTEGERS
1260 As=1./(1.+R) ! a
1270 IF F<1. THEN 1300
1280 Pd=FNE(As*T,N-1)
1290 RETURN Pd
1300 L=-LOG(F)
1310 N1=N+1
1320 B=EXP(-As*L)
1330 B1=1.-B
1340 A=B/B1
1350 Tn=B1^N
1360 C=T
1370 Pd=0.
1380 FOR Ns=1 TO N
1390 C=C-L
1400 Tn=Tn*A*(N1-Ns)/Ns
1410 Pd=Pd+Tn*FNE(As*C,Ns-1)
1420 NEXT Ns
1430 RETURN Pd
1440 FNEND
1450 !

```

```

1460 SUB Plot ! PLOT PD VS PF ON NORMAL PROBABILITY PAPER
1470 COM Pf(*),Pd1(*),Pd2(*),Pd3(*),Pd4(*),Pd5(*)
1480 COM Pd6(*),Pd7(*),Pd8(*),Pd9(*),Pd10(*),Pd11(*)
1490 COM Pd12(*),Pd13(*),Pd14(*),Pd15(*),Pd16(*),Pd17(*)
1500 COM Pd18(*),Pd19(*),Pd20(*)
1510 DIM A#[30],B#[30],C#[31]
1520 DIM Xlabel$(1:30),Ylabel$(1:30)
1530 DIM Xcoord(1:30),Ycoord(1:30)
1540 DIM Xgrid(1:30),Ygrid(1:30)
1550 DOUBLE N,Lx,Ly,Nx,Ny,I ! INTEGERS
1560 !
1570 A#="Probability of False Alarm"
1580 B#="Probability of Detection"
1590 C#="Figure ROC for N=64, F=.001"
1600 !
1610 Lx=12
1620 REDIM Xlabel$(1:Lx),Xcoord(1:Lx)
1630 DATA E-10,E-9,E-8,E-7,E-6,E-5,E-4,E-3,.01,.02,.05,.1
1640 READ Xlabel$(*)
1650 DATA 1E-10,1E-9,1E-8,1E-7,1E-6,1E-5,1E-4,.001,.01,.02,.05,.1
1660 READ Xcoord(*)
1670 !
1680 Ly=18
1690 REDIM Ylabel$(1:Ly),Ycoord(1:Ly)
1700 DATA .01,.02,.05,.1,.2,.3,.4,.5,.6,.7,.8,.9
1710 DATA .95,.98,.99,.995,.998,.999
1720 READ Ylabel$(*)
1730 DATA .01,.02,.05,.1,.2,.3,.4,.5,.6,.7,.8,.9
1740 DATA .95,.98,.99,.995,.998,.999
1750 READ Ycoord(*)
1760 !
1770 Nx=14
1780 REDIM Xgrid(1:Nx)
1790 DATA 1E-10,1E-9,1E-8,1E-7,1E-6,1E-5,1E-4
1800 DATA .001,.002,.005,.01,.02,.05,.1
1810 READ Xgrid(*)
1820 !
1830 Ny=18
1840 REDIM Ygrid(1:Ny)
1850 DATA .01,.02,.05,.1,.2,.3,.4,.5,.6,.7,.8,.9
1860 DATA .95,.98,.99,.995,.998,.999
1870 READ Ygrid(*)
1880 !
1890 FOR I=1 TO Lx
1900 Xcoord(I)=FNInvphi(Xcoord(I))
1910 NEXT I
1920 FOR I=1 TO Ly
1930 Ycoord(I)=FNInvphi(Ycoord(I))
1940 NEXT I
1950 FOR I=1 TO Nx
1960 Xgrid(I)=FNInvphi(Xgrid(I))
1970 NEXT I
1980 FOR I=1 TO Ny
1990 Ygrid(I)=FNInvphi(Ygrid(I))
2000 NEXT I

```

```

2010  X1=Xgrid(1)
2020  X2=Xgrid(Nx)
2030  Y1=Ygrid(1)
2040  Y2=Ygrid(Ny)
2050  GINIT 200./260.                                !  VERTICAL PAPER
2060  PLOTTER IS 505,"HPGL"
2070  PRINTER IS 505
2080  PRINT "VS2"
2090  LIMIT PLOTTER 505,0.,200.,0.,260.                !  1 GDU = 2 mm
2100  VIEWPORT 22.,85.,19.,122.
2110  WINDOW X1,X2,Y1,Y2
2120  FOR I=1 TO Nx
2130  MOVE Xgrid(I),Y1
2140  DRAW Xgrid(I),Y2
2150  NEXT I
2160  FOR I=1 TO Ny
2170  MOVE X1,Ygrid(I)
2180  DRAW X2,Ygrid(I)
2190  NEXT I
2200  LDIR 0
2210  CSIZE 2.3,.5
2220  LORG 5
2230  Y=Y1-(Y2-Y1)*.02
2240  FOR I=1 TO Lx
2250  MOVE Xcoord(I),Y
2260  LABEL Xlabel$(I)
2270  NEXT I
2280  CSIZE 3.,.5
2290  MOVE .5*(X1+X2),Y1-.06*(Y2-Y1)
2300  LABEL A$
2310  MOVE .5*(X1+X2),Y1-.1*(Y2-Y1)
2320  LABEL C$
2330  CSIZE 2.3,.5
2340  LORG 8
2350  X=X1-(X2-X1)*.01
2360  FOR I=1 TO Ly
2370  MOVE X,Ycoord(I)
2380  LABEL Ylabel$(I)
2390  NEXT I
2400  LDIR PI/2.
2410  CSIZE 3.,.5
2420  LORG 5
2430  MOVE X1-.15*(X2-X1),.5*(Y1+Y2)
2440  LABEL B$
2450  PENUP

```

```
2460 PLOT Pf(*),Pd1(*)
2470 PENUP
2480 PLOT Pf(*),Pd2(*)
2490 PENUP
2500 PLOT Pf(*),Pd3(*)
2510 PENUP
2520 PLOT Pf(*),Pd4(*)
2530 PENUP
2540 PLOT Pf(*),Pd5(*)
2550 PENUP
2560 PLOT Pf(*),Pd6(*)
2570 PENUP
2580 PLOT Pf(*),Pd7(*)
2590 PENUP
2600 PLOT Pf(*),Pd8(*)
2610 PENUP
2620 PLOT Pf(*),Pd9(*)
2630 PENUP
2640 PLOT Pf(*),Pd10(*)
2650 PENUP
2660 PLOT Pf(*),Pd11(*)
2670 PENUP
2680 PLOT Pf(*),Pd12(*)
2690 PENUP
2700 PLOT Pf(*),Pd13(*)
2710 PENUP
2720 PLOT Pf(*),Pd14(*)
2730 PENUP
2740 PLOT Pf(*),Pd15(*)
2750 PENUP
2760 PLOT Pf(*),Pd16(*)
2770 PENUP
2780 PLOT Pf(*),Pd17(*)
2790 PENUP
2800 PLOT Pf(*),Pd18(*)
2810 PENUP
2820 PLOT Pf(*),Pd19(*)
2830 PENUP
2840 PLOT Pf(*),Pd20(*)
2850 PENUP
2860 BEEP 500,2
2870 PAUSE
2880 PRINTER IS CRT
2890 PLOTTER 505 IS TERMINATED
2900 SUBEND
```

REFERENCES

1. A. H. Nuttall, **Accurate Efficient Evaluation of Cumulative or Exceedance Probability Distributions Directly From Characteristic Functions**, NUSC Technical Report 7023, Naval Underwater Systems Center, New London, CT, 1 October 1983.
2. A. H. Nuttall, **Operating Characteristics of Cross-Correlator With or Without Sample Mean Removal**, NUSC Technical Report 7045, Naval Underwater Systems Center, New London, CT, 14 August 1984.
3. A. H. Nuttall, **Evaluation of Densities and Distributions via Hermite and Generalized Laguerre Series Employing High-Order Expansion Coefficients Determined Recursively via Moments or Cumulants**, NUSC Technical Report 7377, Naval Underwater Systems Center, New London, CT, 28 February 1985.
4. **Handbook of Mathematical Functions**, U. S. Department of Commerce, National Bureau of Standards, Applied Mathematics Series No. 55, U. S. Government Printing Office, Washington, DC, June 1964.
5. A. H. Nuttall and A. F. Magaraci, **Signal-to-Noise Ratios Required for Short-Term Narrowband Detection of Gaussian Processes**, NUSC Technical Report 4417, Naval Underwater Systems Center, New London, CT, 20 October 1972.

Technical Report 8611
1 October 1989

**Optimum Memoryless Nonlinear Transformation
For Weak Narrowband Signals in Noise**

**A. H. Nuttall
ABSTRACT**

The optimum memoryless nonlinear transformation for weak narrowband signals in narrowband noise is derived in terms of the joint probability density function of the noise amplitude and phase modulations. The optimization is in terms of maximizing the magnitude of the deflection of the complex envelope at the nonlinearity output for small signal inputs of arbitrary characteristics. The optimum nonlinearity is complex, in general, meaning that a phase modulation, in addition to that present at the input to the nonlinearity, is superimposed. A problem with the behavior of the optimum nonlinearity is traced back to a shortcoming in the approximate analysis, and a method for circumventing the problem is presented. Two methods of treating the spurious weak signal component at the nonlinearity output are considered and compared quantitatively. Finally, the optimum nonlinearity for processing phase differences is derived for a particular model of noise statistics and shown to be closely related to an earlier processor.

Approved for public release; distribution is unlimited.

TABLE OF CONTENTS

	Page
LIST OF ILLUSTRATIONS	ii
LIST OF SYMBOLS	ii
INTRODUCTION	1
LOWPASS REAL WAVEFORM	3
Mean Outputs	3
Output Deflection	5
Maximum Deflection	6
Example	7
Physical Interpretation	9
NARROWBAND WAVEFORM	15
Mean Outputs	16
Small Input Signal-to-Noise Ratio	18
Difference in Mean Outputs	21
Variance of Output	24
Output Deflection	25
Maximum Deflection	25
Physical Interpretation	28
Examples	30
Discussion of Imaginary Term	32
Size of Neglected Term	33
OPTIMUM NONLINEARITY FOR PHASE CHANGES	35
Nonlinear Processing	35
Input Noise Statistics	36
Mean Output	37
Small Input Signal-to-Noise Ratio	38
Variance of Output	41
Optimum Nonlinearity	42
Example	44
SUMMARY	45
APPENDIX A. JACOBIAN OF TRANSFORMATION	47
APPENDIX B. INDEPENDENCE OF ADDITIVE CONSTANT	49
APPENDIX C. BEHAVIOR OF OPTIMUM NONLINEARITY	51
APPENDIX D. ALTERNATIVE FORMS IN RECTANGULAR COORDINATES	59
APPENDIX E. CONSTRAINED MAXIMIZATION OF DEFLECTION	63
REFERENCES	73

LIST OF ILLUSTRATIONS

Figure	Page
1. Outputs from General Nonlinearity g	10
2. Outputs from Optimum Nonlinearity g_m	10
3. Outputs from Modified Optimum Nonlinearity \tilde{g}_m	10
4. Outputs from General Nonlinearity g	29
5. Outputs from Optimum Nonlinearity g_m	29
6. Outputs from Modified Optimum Nonlinearity \tilde{g}_m	29

LIST OF SYMBOLS

t	time
$x(t)$	input waveform, (1),(14)
$s(t)$	input signal waveform, (1)
$n(t)$	input noise waveform, (1)
$g\{x\}$	nonlinearity characteristic, (2),(15)
$y(t)$	nonlinearity output, (2),(15)
$y_1(t)$	signal-plus-noise output, (2),(16)
$y_o(t)$	noise-only output, (2)
overbar	mean value, averaged over noise statistics, (3)
$p(u)$	probability density function of input noise, (3)
var	variance, (8A),(40),(42)
d^2	deflection, (9),(10),(43),(44)
$g_m\{x\}$	optimum nonlinearity, (11),(45)
d_m^2	maximum deflection, (12),(46)

$\tilde{g}_m\{x\}$	modified nonlinearity
$A_x(t)$	input amplitude modulation, (13)
$\phi_x(t)$	input phase modulation, (13)
$h\{A,\phi\}$	nonlinear transformation, (15),(22)
arg	argument of complex number, (15)
$A_s(t)$	signal amplitude modulation, (16)
$\phi_s(t)$	signal phase modulation, (16)
$A_n(t)$	noise amplitude modulation, (16)
$\phi_n(t)$	noise phase modulation, (16)
$p(A,\phi)$	noise joint probability density function, (18)
$p_1(A,\phi)$	partial derivative of p , (25)
$p_2(A,\phi)$	partial derivative of p , (25)
q_1, q_2	auxiliary functions, (31),(47)
z_a, z_b	complex numbers, (33),(35),(36),(57),(58)
Δ	time between samples, (62)
$h\{A,\phi,\bar{A},\bar{\phi}\}$	nonlinear transformation, (63)-(65)

OPTIMUM MEMORYLESS NONLINEAR TRANSFORMATION
FOR WEAK NARROWBAND SIGNALS IN NOISE

INTRODUCTION

For strong additive noise that is not Gaussian, a nonlinear transformation that suppresses the noise, but passes the signal, is useful in aiding in the detection of weak signals. Here, we will first review the standard memoryless nonlinear transformation of a lowpass real waveform composed of signal-plus-noise or noise-alone and maximize the deflection. A problem arises for the "optimum" nonlinearity, which indicates the possibility of infinite deflection; this behavior is traced to a shortcoming of the approximate analysis, and a method for circumventing it is presented.

Then, we extend these ideas to a narrowband waveform containing both amplitude and phase modulation on the signal as well as the noise. In both cases, a deflection measure, for small input signals with arbitrary characteristics, will be maximized by choice of the arbitrary memoryless nonlinearity characteristic. The presence of a spurious weak signal component at the nonlinearity output will be fully discussed and treated in two different ways. Also, the apparent infinity of the "optimum" nonlinearity and its corresponding deflection will be thoroughly investigated, and a method will be presented for ameliorating the shortcomings of the approximate analysis.

Some of the results of this investigation confirm those in [1,2]. However, we give a full derivation of the method and elaborate at length on how to handle the spurious signal component and anomalous behavior. Additionally, the loss of detectability, caused by the desire to completely suppress the spurious signal component, is evaluated quantitatively.

A complete derivation of the optimum nonlinearity operating in the presence of noise with phase dependence of a particular kind is also presented. The corresponding maximum deflection is derived in terms of the amplitude and phase difference probability density functions. The anomaly for small noise amplitudes is discussed and illustrated by examples.

LOWPASS REAL WAVEFORM

Received real waveform $x(t)$ is composed of signal-plus-noise or noise-alone, where the additive noise $n(t)$ is considerably stronger than the signal and can be non-Gaussian. That is, input

$$x(t) = \left\{ \begin{array}{c} s(t) + n(t) \\ \text{or} \\ n(t) \end{array} \right\}, \quad (1)$$

where $s(t)$ is the signal waveform with arbitrary characteristics. This waveform is passed through arbitrary memoryless nonlinearity g giving output

$$y(t) = g\{x(t)\} = \left\{ \begin{array}{c} g\{s(t) + n(t)\} \\ \text{or} \\ g\{n(t)\} \end{array} \right\} \equiv \left\{ \begin{array}{c} y_1(t) \\ \text{or} \\ y_0(t) \end{array} \right\}. \quad (2)$$

Transformation g need not be analytic.

MEAN OUTPUTS

For a given signal amplitude $s(t)$ at time t , the mean output of the nonlinearity is given by averaging over the noise statistics:^{*}

$$\overline{y_1(t)} = \overline{g\{s(t) + n(t)\}} = \int du \, p(u) \, g\{s(t) + u\}, \quad (3)$$

^{*}Integrals without limits are over the range of nonzero integrand.

where p is the known probability density function of noise $n(t)$ at time t . (We have suppressed any t dependence of p , but this analysis allows for nonstationary additive noise, if need be.) Now let the change of variable, $x = s(t) + u$, be made in (3) to get

$$\overline{y_1(t)} = \int dx p(x - s(t)) g\{x\} = \quad (4)$$

$$\approx \int dx [p(x) - s(t) p'(x)] g\{x\} , \quad (5)$$

where we expanded the noise probability density function p about the point x , through linear terms in (weak) signal amplitude $s(t)$.

A note of caution is in order regarding expansion (5). Since x can range over $(-\infty, +\infty)$, we are presuming that probability density function $p(x)$ has a local tangent for all x ; that is, $p(x)$ has no discontinuities in slope. If we attempt to employ the following results on a density $p(x)$ that violates this condition, the conclusions may be incorrect and a closer investigation is warranted.

For noise-alone, we set $s(t) = 0$ in (4) to get mean output

$$\overline{y_0(t)} = \int dx p(x) g\{x\} . \quad (6)$$

The difference in mean outputs, that is, signal-present versus signal absent, follows from (5) and (6) as the approximation

$$\overline{y_1(t)} - \overline{y_0(t)} \approx - s(t) \int dx p'(x) g\{x\} . \quad (7)$$

OUTPUT DEFLECTION

At the same time, the variance of the output of the non-linearity for noise-alone is

$$\text{var}(y_o(t)) = \overline{y_o^2(t)} - \overline{y_o(t)}^2, \quad (8A)$$

where mean-square value

$$\overline{y_o^2(t)} = \overline{g^2\{n(t)\}} = \int dx \, p(x) \, g^2\{x\}. \quad (8B)$$

Combining (6)-(8), we define an output deflection from the nonlinearity g as

$$\begin{aligned} d^2 &= \frac{[\overline{y_1(t)} - \overline{y_o(t)}]^2}{\text{var}(y_o(t))} = \\ &= s^2(t) \frac{\left[\int dx \, p'(x) \, g\{x\} \right]^2}{\int dx \, p(x) \, g^2\{x\} - \left[\int dx \, p(x) \, g\{x\} \right]^2}. \end{aligned} \quad (9)$$

This is an approximation to the deflection since it utilizes (5). Therefore, the following results based on (9) are also approximations.

MAXIMUM DEFLECTION

We would like to maximize this small-signal deflection at the nonlinearity output by choice of the nonlinearity characteristic g . However, two observations should be made. First, the absolute scale of g is immaterial to the deflection; that is, a $g\{x\}$ obviously gives the same deflection d^2 as does $g\{x\}$. Second, an additive constant to g does not affect the deflection; that is, $g\{x\} + b$ gives the same value of d^2 as does $g\{x\}$. This is easily verified by direct substitution of $g\{x\} + b$ for $g\{x\}$ in (9), whereupon b is seen to cancel out everywhere. More generally, nonlinearity $a g\{x\} + b$ gives the same deflection as $g\{x\}$.

What this means is that, without loss of generality, we can set the nonlinearity mean output for noise-alone, $\overline{y_0(t)}$, equal to zero, and not detract from the attainable values of deflection criterion (9). So, setting (6) to zero, (9) becomes

$$d^2 = s^2(t) \frac{\left[\int dx p'(x) g\{x\} \right]^2}{\int dx p(x) g^2\{x\}} . \quad (10)$$

But now, by use of Schwartz's inequality, this ratio is maximized by the optimum memoryless nonlinearity

$$g_m\{x\} = - \frac{p'(x)}{p(x)} = - \frac{d}{dx} \ln p(x) . \quad (11)$$

Here, we have taken advantage of the scaling independence in order to supply the factor -1 for convenience. The resulting maximum deflection is

$$d_m^2 = s^2(t) \int dx \frac{p'^2(x)}{p(x)} . \quad (12)$$

Substitution of optimum nonlinearity (11) into noise-alone mean output (6) immediately yields zero, consistent with the assumption utilized in reducing (9) to (10). We should also notice that signal value $s(t)$ appears as a multiplicative term in general deflections (9) and (10); thus, the optimum nonlinearity g_m can be selected, as in (11), without regard to the particular signal amplitude. It also allows $s(t)$ to be deterministic or random, as the case may be. These approximations are all predicated on the small-signal assumption utilized in (5).

EXAMPLE

As an example of (11) and (12), consider Gaussian noise for which

$$p(x) = \frac{1}{\sqrt{2\pi} \sigma_n} \exp \left[-\frac{(x - \mu_n)^2}{2\sigma_n^2} \right] \quad \text{for all } x .$$

As noted under (5), this probability density function has no discontinuities in slope. Substitution in (11) and (12) gives

$$g_m\{x\} = \frac{x - \mu_n}{\sigma_n^2} \quad \text{for all } x$$

and

$$d_m^2 = \frac{s^2(t)}{\sigma_n^2} .$$

Thus the (approximate) optimum nonlinearity is, in fact, linear, and the maximum deflection is the instantaneous signal-to-noise power ratio at the input to the nonlinearity.

By the arguments given in the sequel to (9), we could equally well use nonlinearity

$$\tilde{g}_m\{x\} = x$$

and realize the same maximum deflection d_m^2 . This latter nonlinearity, \tilde{g}_m , would have a nonzero noise-only mean output, namely μ_n ; however, this is not a problem since it is known and could be subtracted from the output of \tilde{g}_m , if desired.

In the general case, we can always use (modified) optimum nonlinearity

$$\tilde{g}_m\{x\} = a g_m\{x\} + b$$

instead of (11) and still get maximum deflection d_m^2 in (12), where a and b can be chosen for convenience. The major difference is that the noise-only mean output is then b , not zero; however, since b is known, this constitutes no limitation or problem.

PHYSICAL INTERPRETATION

The general situation is depicted in the series of plots in figures 1 - 3. The noise-only output $y_0(t)$ is given on the left side of each plot, while the signal-plus-noise output $y_1(t)$ is given on the right side. The mean of each waveform is indicated by a horizontal dashed line. Figure 1 represents the starting point of the analysis, namely (2). Figure 2 indicates the output waveforms for the case of the optimum nonlinearity g_m in (11), that is, $y_0(t)$ now has zero mean. The nonlinearity g_m maximizes the ratio of the mean of $y_1(t)$ to the standard deviation σ_0 of $y_0(t)$. Finally, figure 3 biases both $y_0(t)$ and $y_1(t)$ by constant b and scales both by factor a ; it represents the outputs of nonlinearity \tilde{g}_m .

Another note of caution is in order relative to approximations (11) and (12). If $p(x)$ is zero at any value of x , the optimum nonlinearity g_m approaches infinity at that point, and the maximum deflection d_m^2 may become infinite as well. This is physically unrealistic and indicates that certain forms of the noise probability density function p are disallowed or that the approximations have gone awry. For example, if p approaches zero at an isolated point, it must do so faster than linearly in order that integral (12) remain finite from the contribution in the neighborhood of that point. However, integral (12) is itself an approximation and must also be investigated more closely.

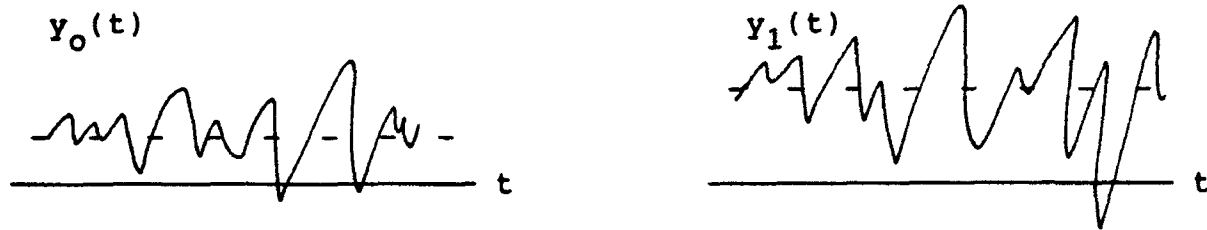


Figure 1. Outputs from General Nonlinearity g

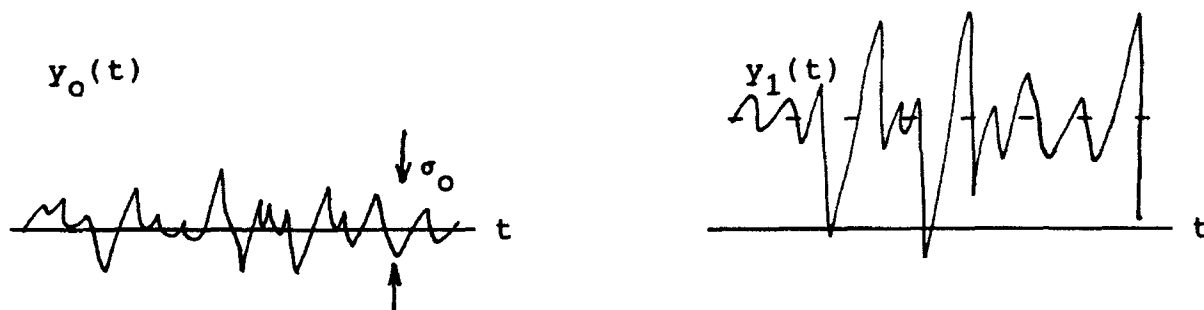


Figure 2. Outputs from Optimum Nonlinearity g_m

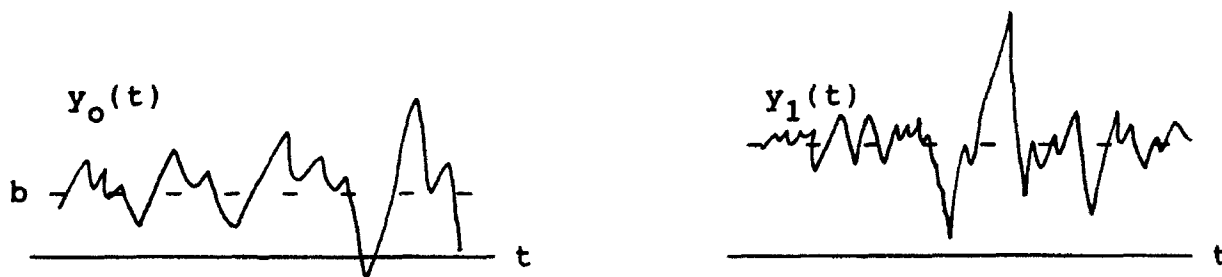


Figure 3. Outputs from Modified Optimum Nonlinearity \tilde{g}_m

This possibility of infinite deflection is not entirely due to inadequacy of the approximation utilized in (5) and the sequel. In general, if we use (4), (6), (8), and the upper line of (9), we have, for any g , exact deflection

$$\bar{d}^2(s) = \frac{\left[\int dx [p(x-s) - p(x)] g(x) \right]^2}{\int dx p(x) g^2(x)},$$

where we have replaced $s(t)$ by s for notational brevity. Now suppose that we consider signal value s known and that non-linearity g can be chosen with this knowledge. The optimum nonlinearity is then (with no approximations)

$$\bar{g}_e(x;s) = \frac{p(x-s) - p(x)}{p(x)} = \frac{p(x-s)}{p(x)} - 1.$$

Although it is physically unrealistic to presume signal value s known, this approach is informative in that it pinpoints the source and rate of approach of the infinities. It is immediately seen that if $p(x)$ approaches zero somewhere, then $\bar{g}_e(x;s)$ approaches infinity at that x value (unless $s = 0$). The corresponding maximum deflection for nonlinearity $\bar{g}_e(x;s)$ is

$$\bar{d}_e^2(s) = \int dx \frac{[p(x-s) - p(x)]^2}{p(x)} = \int dx \frac{p^2(x-s)}{p(x)} - 1,$$

and will remain finite only if p approaches zero less fast than linearly. Thus, the condition on the rate of approach of p to zero, in order to maintain finite deflection, is reversed from the conclusion above based on approximation (5). This reversal

is very important to know about, but the possibility of infinite deflection still remains.

If we now make the small-signal assumptions on the exact results above, we find

$$\bar{g}_e\{x;s\} \sim -s \frac{p'(x)}{p(x)} = s g_m\{x\} ,$$

$$\bar{d}_e^2(s) \sim s^2 \int dx \frac{p'^2(x)}{p(x)} = d_m^2 ,$$

consistent with (11) and (12), respectively. (The multiplicative factor of s in $\bar{g}_e\{x;s\}$ is merely an irrelevant scale factor, as far as the deflection is concerned.) No nonlinearity can outperform $\bar{d}_e^2(s)$ for any signal value s , since the latter result allows for use of knowledge of $p(x)$ as well as value s . So if d_m^2 in (12) gives a result larger than $\bar{d}_e^2(s)$, it means that the approximation giving rise to (12) was faulty. In that case, we should revert to exact deflection $\bar{d}^2(s)$ and substitute the particular nonlinearity g being employed. For example, if approximate optimum nonlinearity g_m in (11) is utilized, the corresponding deflection is found to be

$$\bar{d}_m^2(s) = \frac{\left[\int dx p(x-s) p'(x)/p(x) \right]^2}{\int dx p'^2(x)/p(x)} .$$

Of course, $\bar{d}_m^2(s) \leq \bar{d}_e^2(s)$ in all cases.

Some examples are useful at this point. For Gaussian noise, we have

$$p(x) = (2\pi)^{-1/2} \exp(-x^2/2) \quad \text{for all } x ,$$

$$g_m\{x\} = - \frac{p'(x)}{p(x)} = x ,$$

$$d_m^2 = s^2 \int dx \frac{p'^2(x)}{p(x)} = s^2 ,$$

$$\bar{d}_m^2(s) = s^2 ,$$

$$\bar{g}_e\{x;s\} = \exp\left(sx - \frac{1}{2}s^2\right) - 1 \sim sx = s g_m\{x\} ,$$

$$\bar{d}_e^2(s) = \exp(s^2) - 1 \sim s^2 = d_m^2 .$$

The quantity $\bar{d}_e^2(s)$ is larger than d_m^2 for all s (except $s = 0$).

All of these results are self consistent.

For exponential noise,

$$p(x) = \frac{1}{2} \exp(-|x|) \quad \text{for all } x ,$$

$$g_m\{x\} = - \frac{p'(x)}{p(x)} = \text{sgn}(x) ,$$

$$d_m^2 = s^2 \int dx \frac{p'^2(x)}{p(x)} = s^2 ,$$

$$\bar{d}_m^2(s) = [1 - \exp(-|s|)]^2 \sim s^2 - |s|^3 ,$$

$$\bar{g}_e\{x;s\} = \exp(-|x-s| + |x|) - 1 ,$$

$$\bar{d}_e^2(s) = \frac{2}{3} \exp(|s|) + \frac{1}{3} \exp(-2|s|) - 1 \sim s^2 - \frac{1}{3} |s|^3 .$$

Now, $\bar{d}_e^2(s)$ is less than d_m^2 for $0 < |s| < 2.07$; thus the approximation d_m^2 is somewhat optimistic and $\bar{d}_m^2(s)$ should be used instead. A sketch of nonlinearity $\bar{g}_e\{x;s\}$ reveals that it

resembles $s \operatorname{sgn}(x)$, especially for small s . This example is consistent except for d_m^2 , despite the fact that $p'(x)$ is discontinuous at the one point $x = 0$.

For a noise probability density function with a zero (at the origin for convenience), we have, for example,

$$p(x) = a |x|^\nu \exp(-|x|^\mu), \quad \nu > 0, \quad \mu > 0,$$

$$g_m\{x\} = - \frac{p'(x)}{p(x)} \sim - \frac{\nu}{x} \quad \text{as } x \rightarrow 0,$$

$$d_m^2 = s^2 \int dx \frac{p'^2(x)}{p(x)} < \infty \quad \text{if } \nu > 1,$$

$$\bar{d}_m^2(s) = 0 \quad \text{if } \nu < 1,$$

$$\bar{g}_e\{x;s\} = \frac{p(x-s)}{p(x)} - 1 \sim \frac{p(-s)}{a |x|^\nu} \quad \text{as } x \rightarrow 0,$$

$$\bar{d}_e^2(s) < \infty \quad \text{if } \nu < 1.$$

As anticipated, the condition for finite deflection is reversed in the exact result ($\nu < 1$) versus the approximation ($\nu > 1$). In addition, the rate of growth of the optimum nonlinearity near $x = 0$ is milder for the exact result and of a very different character. The reason that $\bar{d}_m^2(s)$ is zero for $\nu < 1$ is that $p'(x)/p(x) \sim 1/x$, whereas $p'^2(x)/p(x) \sim x^{\nu-2}$ as $x \rightarrow 0+$; thus, the integrand of the denominator of $\bar{d}_m^2(s)$ has a higher-order singularity at $x = 0$ and approaches infinity at a faster rate than the numerator. This example exemplifies the need for close scrutiny of a noise probability density function which has a zero value anywhere in its range.

NARROWBAND WAVEFORM

The available input waveform of interest in this section has the form

$$A_x(t) \cos[2\pi f_0 t + \phi_x(t)] , \quad (13)$$

where f_0 is the known center frequency, and $A_x(t)$ and $\phi_x(t)$ are the lowpass amplitude and phase modulations, respectively. The complex envelope of this waveform, which can be easily extracted from (13), is

$$x(t) = A_x(t) \exp[i\phi_x(t)] . \quad (14)$$

We will allow an arbitrary complex memoryless nonlinear transformation h of $A_x(t)$ and $\phi_x(t)$; that is, the output is modified complex envelope

$$y(t) = h\{A_x(t), \phi_x(t)\} = h\{|x(t)|, \arg(x(t))\} = g\{x(t)\} , \quad (15)$$

where g is an arbitrary complex function of complex argument $x(t)$. Transformation g need not be analytic.

The input $x(t)$ to nonlinearity g is composed of signal-plus-noise (or noise-alone); thus, we can express the signal-plus-noise output as

$$y_1(t) = g\{A_s(t) \exp[i\phi_s(t)] + A_n(t) \exp[i\phi_n(t)]\} , \quad (16)$$

where $A_s(t)$ and $\phi_s(t)$ are the arbitrary input signal amplitude and phase modulations, while $A_n(t)$ and $\phi_n(t)$ are the input noise amplitude and phase modulations, respectively. We presume a low

input signal-to-noise ratio; that is,

$$A_s^2(t) \ll \overline{A_n^2(t)} . \quad (17)$$

However, there are no limitations on the sizes of phase modulations $\phi_s(t)$ and $\phi_n(t)$, nor on the signal characteristics. The joint probability density function of the noise amplitude and phase modulations is presumed known; that is, $p(A_n, \phi_n)$ is given. (Again, although we suppress any t dependence of p , the following analysis allows for nonstationary noise simply by reinstating any t dependence in p .)

MEAN OUTPUTS

For given signal amplitude and phase modulations $A_s(t)$ and $\phi_s(t)$, the complex mean output from the nonlinearity g is, from (16),

$$\overline{y_1(t)} = \iint dA_n d\phi_n g\{A_s(t)\exp[i\phi_s(t)] + A_n \exp[i\phi_n]\} p(A_n, \phi_n). \quad (18)$$

We now make the change of variables

$$A \exp[i\phi] = A_s(t) \exp[i\phi_s(t)] + A_n \exp[i\phi_n] \quad (19)$$

in (18). The Jacobian of this two-dimensional transformation is derived in appendix A; it is

$$\frac{\partial(A_n, \phi_n)}{\partial(A, \phi)} = \frac{A}{A_n} = \frac{A}{|A \exp[i\phi] - A_s(t) \exp[i\phi_s(t)]|} . \quad (20)$$

At this point, for notational convenience, we will suppress the t dependence of A_s and ϕ_s ; this time dependence will be reestablished after all the following mathematical manipulations have been completed. The use of (19) and (20) converts (18) into the following exact result for the complex mean output

$$\overline{y_1(t)} = \iint dA d\phi \frac{A}{|A \exp(i\phi) - A_s \exp(i\phi_s)|} g\{A \exp(i\phi)\} \times \\ \times p(|A \exp(i\phi) - A_s \exp(i\phi_s)|, \arg\{A \exp(i\phi) - A_s \exp(i\phi_s)\}). \quad (21)$$

This expression could be written in an entirely equivalent form by replacing $g\{A \exp(i\phi)\}$ with $h\{A, \phi\}$; that is, from (14) and (15),

$$h\{A, \phi\} = g\{A \exp(i\phi)\} \quad \text{for all } A, \phi. \quad (22)$$

This latter form, in terms of h , more clearly accents that a completely arbitrary transformation of A and ϕ is allowed; however, since g is arbitrary, the same is true of the form $g\{A \exp(i\phi)\}$, which is used henceforth.

SMALL INPUT SIGNAL-TO-NOISE RATIO

We now make use of the low input signal-to-noise ratio assumption, (17), by expanding (21) through first-order terms in the signal amplitude modulation A_s . Since

$$|1 - \epsilon - i\delta| = \sqrt{(1 - \epsilon)^2 + \delta^2} \sim 1 - \epsilon ,$$

and

$$\arg(1 - \epsilon - i\delta) \sim -\delta ,$$

through linear terms in real variables ϵ and δ , then

$$|A \exp(i\phi) - A_s \exp(i\phi_s)| \sim A - A_s \cos(\phi_s - \phi) \quad \text{for } A_s \ll A , \quad (23)$$

$$\arg\{A \exp(i\phi) - A_s \exp(i\phi_s)\} \sim \phi - \frac{A_s}{A} \sin(\phi_s - \phi) \quad \text{for } A_s \ll A .$$

Substitution in (21) yields

$$\begin{aligned} \overline{Y_1(t)} \sim & \iint dA \, d\phi \frac{A}{A - A_s \cos(\phi_s - \phi)} g\{A \exp(i\phi)\} \times \\ & \times p\left(A - A_s \cos(\phi_s - \phi), \phi - \frac{A_s}{A} \sin(\phi_s - \phi)\right) . \end{aligned} \quad (24)$$

Define

$$p_1(A, \phi) = \frac{\partial}{\partial A} p(A, \phi) , \quad p_2(A, \phi) = \frac{\partial}{\partial \phi} p(A, \phi) , \quad (25)$$

where it is presumed that these derivatives of p exist. Then the term in (24) involving joint probability density function p can be expanded as

$$p(A, \phi) - A_S \cos(\phi_S - \phi) p_1(A, \phi) - \frac{A_S}{A} \sin(\phi_S - \phi) p_2(A, \phi) , \quad (26)$$

to linear terms in A_S . Coupled with

$$\frac{A}{A - A_S \cos(\phi_S - \phi)} \sim 1 + \frac{A_S}{A} \cos(\phi_S - \phi) \quad \text{for } A_S \ll A , \quad (27)$$

(24) develops into

$$\begin{aligned} \overline{y_1(t)} &\sim \iint dA d\phi \left[1 + \frac{A_S}{A} \cos(\phi_S - \phi) \right] g\{A \exp(i\phi)\} \times \\ &\times \left[p(A, \phi) - A_S \cos(\phi_S - \phi) p_1(A, \phi) - \frac{A_S}{A} \sin(\phi_S - \phi) p_2(A, \phi) \right] = \\ &\sim \iint dA d\phi g\{A \exp(i\phi)\} \left[p(A, \phi) + \frac{A_S}{A} \cos(\phi_S - \phi) p(A, \phi) - \right. \\ &\quad \left. - A_S \cos(\phi_S - \phi) p_1(A, \phi) - \frac{A_S}{A} \sin(\phi_S - \phi) p_2(A, \phi) \right] , \quad (28) \end{aligned}$$

through linear terms in A_S . There is no presumption about the form of nonlinearity g in these expressions.

There is a fundamental flaw in the use of approximations (23) and (27) in integral (21). The approximations specifically require that $A > A_S$, yet they are used in end result (28) all the way down to $A = 0$. The results in (23) should be augmented with

$$\left. \begin{aligned} |A \exp(i\phi) - A_S \exp(i\phi_S)| &\sim A_S \\ \arg\{A \exp(i\phi) - A_S \exp(i\phi_S)\} &\sim \phi_S + \pi \end{aligned} \right\} \quad \text{for } A \ll A_S .$$

This would not only eliminate the troublesome $1/A$ dependencies for small A in (23)-(28), but in fact convert the Jacobian to a linear A dependence for small A , a very marked change.

The reason we do not incorporate this behavior is that it would greatly complicate (28), and the intermediate range, $A \approx A_s$, would still not be covered. What this means is that we can anticipate some problems with approximation (28) and further results based on (28), for small A ; in fact, we must be willing to modify or discard the $1/A$ dependency in some cases and ranges, since it is based upon an invalid approximation. We will return to this point later and elaborate in more detail.

The mean output from complex nonlinearity g , for noise-only, is available directly from exact result (21) by setting $A_s = 0$:

$$\overline{y_0(t)} = \iint dA d\phi g\{A \exp(i\phi)\} p(A, \phi) . \quad (29)$$

DIFFERENCE IN MEAN OUTPUTS

The difference in complex mean outputs from nonlinearity g , for signal-present versus signal-absent, is then available from (28) and (29) as

$$\begin{aligned} \overline{y_1(t)} - \overline{y_0(t)} = & -A_s \iint dA d\phi g\{A \exp(i\phi)\} \times \\ & \times [\cos(\phi_s - \phi) q_1(A, \phi) + \sin(\phi_s - \phi) q_2(A, \phi)] , \end{aligned} \quad (30)$$

where, using (25), the real quantities

$$q_1(A, \phi) = A \frac{\partial}{\partial A} \left(\frac{p(A, \phi)}{A} \right) , \quad q_2(A, \phi) = \frac{\partial}{\partial \phi} \left(\frac{p(A, \phi)}{A} \right) . \quad (31)$$

The approximate result in (30) is similar to that in (7) for the lowpass real case in that signal amplitude A_s appears multiplicatively as a linear factor. However, (30) is still complicated by the appearance of signal phase ϕ_s inside the integrals. If we expand the cos and sin terms in (30), we find

$$\overline{y_1(t)} - \overline{y_0(t)} = -A_s (\cos \phi_s z_a + \sin \phi_s z_b) , \quad (32)$$

where complex numbers (due to the allowed complexity of g)

$$\begin{aligned} z_a = & \iint dA d\phi g\{A \exp(i\phi)\} [\cos \phi q_1(A, \phi) - \sin \phi q_2(A, \phi)] , \\ z_b = & \iint dA d\phi g\{A \exp(i\phi)\} [\sin \phi q_1(A, \phi) + \cos \phi q_2(A, \phi)] . \end{aligned} \quad (33)$$

An alternative form of (32) is more useful; specifically, the difference of mean outputs can be expressed as

$$\begin{aligned}\overline{y_1(t)} - \overline{y_0(t)} &= -\frac{1}{2} A_s \exp(i\phi_s) (z_a - iz_b) - \frac{1}{2} A_s \exp(-i\phi_s) (z_a + iz_b) = \\ &= -\frac{1}{2} A_s(t) \exp[i\phi_s(t)] (z_a - iz_b) - \frac{1}{2} A_s(t) \exp[-i\phi_s(t)] (z_a + iz_b),\end{aligned}\quad (34)$$

where we have reestablished the time dependence of the signal amplitude and phase modulations $A_s(t)$ and $\phi_s(t)$, respectively. The two complex numbers in (34) can be written as

$$z_a - iz_b = \iint dA d\phi g\{A \exp(i\phi)\} \exp(-i\phi) [q_1(A, \phi) - iq_2(A, \phi)], \quad (35)$$

$$z_a + iz_b = \iint dA d\phi g\{A \exp(i\phi)\} \exp(+i\phi) [q_1(A, \phi) + iq_2(A, \phi)]. \quad (36)$$

The leading term in (34) contains a replica of the input signal to the nonlinearity g , namely,

$$A_s(t) \exp[i\phi_s(t)] , \quad (37)$$

and will be called the desired signal component in the difference of mean outputs. The remaining signal-dependent term in (34), namely,

$$A_s(t) \exp[-i\phi_s(t)] , \quad (38)$$

is of no interest since it has a distorted phase modulation. That is, (38) will not correlate with the local reference, since the latter has exactly the same form (38). Henceforth, we simply

ignore the extra term (38) in difference (34). Thus, for the desired signal component, we have

$$\left(\overline{y_1(t)} - \overline{y_0(t)}\right)_{\text{desired}} = -\frac{1}{2} A_s(t) \exp[i\phi_s(t)] (z_a - iz_b) , \quad (39)$$

where the complex number $z_a - iz_b$ is given by (35).

The simplest example of this behavior is furnished by the nonanalytic nonlinearity

$$g\{z\} = |z|^2 ,$$

for which the output is

$$\begin{aligned} y_1(t) &= |A_s(t) \exp[i\phi_s(t)] + A_n(t) \exp[i\phi_n(t)]|^2 = \\ &= A_n^2(t) + A_n(t) \exp[-i\phi_n(t)] A_s(t) \exp[i\phi_s(t)] + \\ &+ A_n(t) \exp[i\phi_n(t)] A_s(t) \exp[-i\phi_s(t)] + A_s^2(t) . \end{aligned}$$

Both types of signal terms, (37) and (38), are exhibited here.

VARIANCE OF OUTPUT

At the same time, the variance of the output of the nonlinearity, for noise-alone, is

$$\begin{aligned} \text{var}(y_o(t)) &= \overline{|y_o(t) - \overline{y_o(t)}|^2} = \\ &= \overline{|y_o(t)|^2} - |\overline{y_o(t)}|^2, \end{aligned} \quad (40)$$

where $y_o(t)$ is available from (16) by setting $A_s(t) = 0$:

$$y_o(t) = g\{A_n(t) \exp[i\phi_n(t)]\}. \quad (41)$$

There follows immediately the exact result

$$\begin{aligned} \text{var}(y_o(t)) &= \overline{|g\{A_n(t) \exp[i\phi_n(t)]\}|^2} - \left| \overline{g\{A_n(t) \exp[i\phi_n(t)]\}} \right|^2 = \\ &= \iint dA d\phi |g\{A \exp(i\phi)\}|^2 p(A, \phi) - \\ &= \left| \iint dA d\phi g\{A \exp(i\phi)\} p(A, \phi) \right|^2, \end{aligned} \quad (42)$$

where $p(A, \phi)$ is again the joint probability density function of the noise amplitude and phase modulations.

OUTPUT DEFLECTION

We are now prepared to define an output deflection from nonlinearity g (analogous to (9)) as

$$d^2 = \frac{|\overline{y_1(t)} - \overline{y_0(t)}|_{\text{desired}}^2}{\text{var}(\overline{y_0(t)})}$$

$$= \frac{1}{4} A_s^2(t) \frac{\left| \iint dA d\phi g\{A \exp(i\phi)\} \exp(-i\phi) [q_1(A, \phi) - iq_2(A, \phi)] \right|^2}{\iint dA d\phi |g\{ \}|^2 p(A, \phi) - \left| \iint dA d\phi g\{ \} p(A, \phi) \right|^2},$$

(43)

where we used (39), (35), and (42). Since (30)-(39) are based on approximation (28), deflection (43) is likewise an approximation.

MAXIMUM DEFLECTION

We would like to maximize this small-signal deflection (43) at the nonlinearity output, by choice of the nonlinearity characteristic g . However, as in the sequel to (9), two important observations must be made. First, the absolute scale of g is obviously immaterial to the value of d^2 . Second, an additive complex constant to g does not affect d^2 ; this last property is derived in appendix B. Thus, nonlinearity $a g\{A \exp(i\phi)\} + b$ gives the same deflection as $g\{A \exp(i\phi)\}$, where a and b are arbitrary complex constants.

What this means is that, without loss of generality, we can set the complex nonlinearity mean output for noise-alone, $\overline{y_0(t)}$,

equal to zero, and not detract from the attainable values of deflection criterion (43). So, setting (29) to zero, (43) becomes

$$d^2 = \frac{A_s^2(t)}{4} \frac{\left| \iint dA d\phi g\{A \exp(i\phi)\} \exp(-i\phi) [q_1(A, \phi) - iq_2(A, \phi)] \right|^2}{\iint dA d\phi |g\{A \exp(i\phi)\}|^2 p(A, \phi)} \quad (44)$$

But now, since g is completely arbitrary, this ratio is maximized (according to Schwartz's inequality) by the (approximate) optimum memoryless nonlinearity

$$\begin{aligned} g_m\{A \exp(i\phi)\} &= h_m\{A, \phi\} = - \frac{\exp(i\phi) (q_1(A, \phi) + iq_2(A, \phi))}{p(A, \phi)} = \\ &= - \frac{\exp(i\phi)}{p(A, \phi)} \left[A \frac{\partial (p(A, \phi))}{\partial A} + i \frac{\partial (p(A, \phi))}{\partial \phi} \right] = \\ &= - \exp(i\phi) \left[\frac{\partial}{\partial A} \ln \left(\frac{p(A, \phi)}{A} \right) + \frac{i}{A} \frac{\partial}{\partial \phi} \ln\{p(A, \phi)\} \right], \quad (45) \end{aligned}$$

where we used (22) and (31). Here, we also have taken advantage of the scaling independence in order to supply the factor -1 for convenience. This result agrees with [1; (9)].

The resulting maximum deflection is

$$\begin{aligned} d_m^2 &= \frac{1}{4} A_s^2(t) \iint dA d\phi \frac{|q_1(A, \phi) + iq_2(A, \phi)|^2}{p(A, \phi)} = \\ &= \frac{1}{4} A_s^2(t) \iint dA d\phi \frac{q_1^2(A, \phi) + q_2^2(A, \phi)}{p(A, \phi)}, \quad (46) \end{aligned}$$

where q_1 and q_2 are available from (31) as

$$q_1(A, \phi) = A \frac{\partial}{\partial A} \left(\frac{p(A, \phi)}{A} \right) , \quad q_2(A, \phi) = \frac{\partial}{\partial \phi} \left(\frac{p(A, \phi)}{A} \right) . \quad (47)$$

Whether the phase term, $q_2(A, \phi)/p(A, \phi)$, in optimum nonlinearity (45) is important or not can be ascertained from (46) by evaluating it with and without the q_2^2/p term present. Some limitations of approximations (45) and (46) concerning the $1/A$ dependencies are given in appendix C, as well as an alternative approach.

Substitution of optimum nonlinearity (45) into noise-alone mean output (29) immediately yields the conjugate of the integral in (B-1), which is shown to be identically zero in (B-4). This is consistent with the nonrestrictive assumption utilized in reducing (43) to (44). It should also be noted that signal amplitude $A_s(t)$ appears as a multiplicative term in general deflections (43) and (44); thus, the optimum nonlinearity g_m can be selected, as in (45), without regard to the particular signal amplitude. It also allows $A_s(t) \exp[i\phi_s(t)]$ to be deterministic or random, as the case may be. This is all predicated on the small signal assumption utilized in (22)–(28). The actual output time waveform from the optimum nonlinearity g_m in (45) is obtained by replacing argument $A \exp(i\phi)$ with $A_s(t) \exp[i\phi_s(t)] + A_n(t) \exp[i\phi_n(t)]$; see (16).

PHYSICAL INTERPRETATION

A physical interpretation of what is taking place in this complex envelope case is given in figures 4 - 6. The noise-only output $y_0(t)$ is plotted on the left side of each figure as a complex point in the plane, which moves as time progresses. The noise-only mean output for arbitrary nonlinearity g is indicated by a dashed arrow in figure 4 to the complex point $\overline{y_0(t)}$ given by (29). For any nonlinearity g selected, this is a known point since joint probability density function $p(A, \phi)$ is known.

When signal is also present, the situation for output $y_1(t)$ is depicted on the right side of each figure. The mean output for arbitrary nonlinearity g is indicated by a dashed arrow in figure 4 to the complex point $\overline{y_1(t)}$ given by (21) or (28). This, too, is a known point for specified g, A_s, ϕ_s .

When we choose the class of nonlinearities g that have zero-mean noise-only output $\overline{y_0(t)}$, as done in (43)-(44), we are taking advantage of knowledge of these locations and the situation is as shown in figure 5. The mean location of complex waveform $y_0(t)$ is now at the origin of coordinates and its standard deviation from the origin is indicated by σ_0 . Then the plot of $y_1(t)$ appears on the right side of figure 5, where the dashed arrow is drawn to the point $\overline{y_1(t)}$. When we maximize the deflection criterion d^2 in (44), we are maximizing the ratio of the length of the arrow on the right side to the standard deviation σ_0 on the left side. Physically, we are trying to make

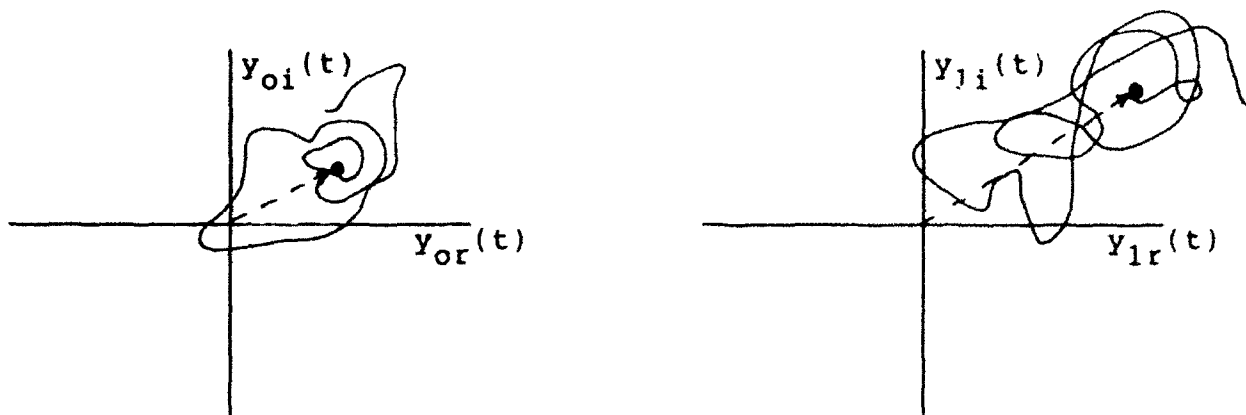


Figure 4. Outputs from General Nonlinearity g

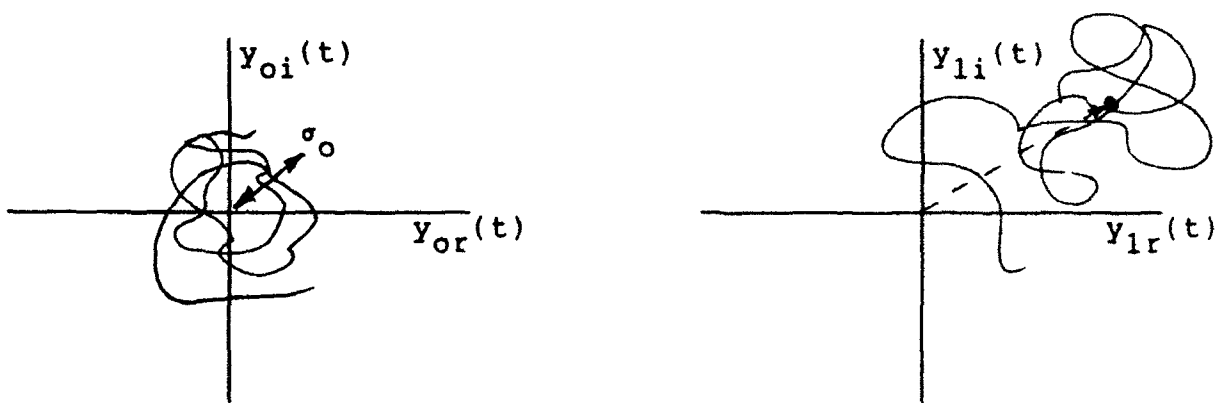


Figure 5. Outputs from Optimum Nonlinearity g_m

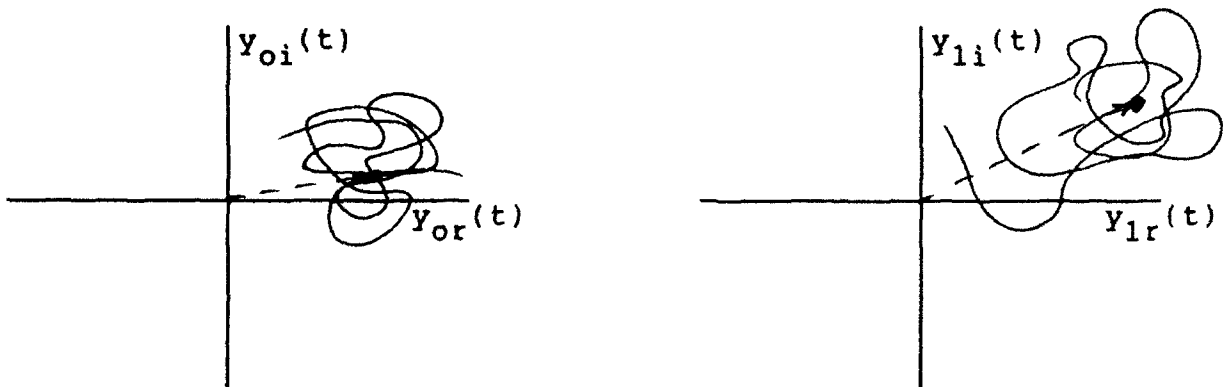


Figure 6. Outputs from Modified Optimum Nonlinearity \tilde{g}_m

the signal-present average distance from the origin as large as possible relative to the signal-absent deviations from the origin.

Finally, figure 6 represents the outputs when the optimum nonlinearity is scaled and biased by an arbitrary factor and additive constant. Both $y_0(t)$ and $y_1(t)$ are similarly scaled and shifted, but the maximum deflection is unchanged.

EXAMPLES

As an example of (45) and (46), suppose the narrowband noise is zero-mean Gaussian; then

$$p(A, \phi) = \frac{A}{2\pi\sigma_n^2} \exp\left(-\frac{A^2}{2\sigma_n^2}\right) \quad \text{for } A > 0, |\phi| < \pi, \quad (48)$$

giving

$$g_m\{A \exp(i\phi)\} = \frac{1}{2\sigma_n^2} A \exp(i\phi) \quad (49)$$

and

$$d_m^2 = \frac{A_s^2(t)/2}{\sigma_n^2}. \quad (50)$$

Thus, the optimum nonlinearity in (49) is linear and the maximum deflection is the signal-to-noise power ratio at the input to the nonlinearity. A more thorough analysis of this example is given in appendix C.

By the arguments given in the sequel to (43), we could equally well use nonlinearity

$$\tilde{g}_m\{A \exp(i\phi)\} = A \exp(i\phi)$$

and realize the same maximum deflection d_m^2 in (50). In the general case, we can always use (modified) optimum nonlinearity

$$\tilde{g}_m\{A \exp(i\phi)\} = a g_m\{A \exp(i\phi)\} + b$$

instead of (45), and still realize maximum deflection d_m^2 in (46), where complex constants a and b can be chosen for convenience. The major difference is that the noise-only mean output is then b , not zero; however, since b is known, this constitutes no limitation or problem. This case is depicted in figure 6.

As a second (more general) example, if the noise amplitude and phase modulations are statistically independent, then

$$p(A, \phi) = p_a(A) p_b(\phi) , \quad (51)$$

and (45) reduces to

$$g_m\{A \exp(i\phi)\} = h_m\{A, \phi\} = - \exp(i\phi) \left[\frac{d}{dA} \ln \left(\frac{p_a(A)}{A} \right) + i \frac{1}{A} \frac{p'_b(\phi)}{p_b(\phi)} \right] . \quad (52)$$

This result agrees with [1; (10) and (16)]. The maximum deflection, (46), is

$$d_m^2 = \frac{1}{4} A_s^2(t) \left\{ \int dA \frac{[p'_a(A) - p_a(A)/A]^2}{p_a(A)} + \right. \\ \left. + \int dA \frac{p_a(A)}{A^2} \int d\phi \frac{p_b'^2(\phi)}{p_b(\phi)} \right\}. \quad (53)$$

The relative importance of the $p'_b(\phi)$ term can be easily ascertained from here. The $1/A$ dependencies are thoroughly discussed in appendix C.

DISCUSSION OF IMAGINARY TERM

In general, for the optimum nonlinearity in (45), the $\exp(i\phi)$ factor indicates a replication of the phase-modulation at its input; that is, from (16),

$$\arg\{A_s(t) \exp[i\phi_s(t)] + A_n(t) \exp[i\phi_n(t)]\} \quad (54)$$

is reproduced at the output of g_m . And if the imaginary term inside the bracket of (45) were zero, that is, $q_2 = 0$, this would be the totality of phase modulation at the output of the optimum nonlinearity. Since $q_2 = 0$ corresponds to $p(A, \phi)$ being independent of ϕ , the modification of the amplitude modulation at the nonlinearity input would then be according to

$$- \frac{\partial}{\partial A} \ln \left\{ \frac{p_a(A)}{A} \right\}, \quad (55)$$

and the maximum deflection is

$$d_m^2 = \frac{1}{4} A_s^2(t) \int dA \frac{[p'_a(A) - p_a(A)/A]^2}{p_a(A)}. \quad (56)$$

However, the presence of the extra imaginary term in (45) means that additional amplitude and phase modulations to those given in (55) and (54), respectively, are superposed on the output. Whether this is significant, in practice, will depend on a quantitative investigation of the relative sizes of q_1^2 and q_2^2 in maximum deflection (46).

SIZE OF NEGLECTED TERM

When we expressed the difference of mean outputs from nonlinearity g in the form (34), we discarded the second term as being of an undesirable form. To see how this neglected term compares with the retained term, in terms of magnitude, we need to compare $|z_a - iz_b|$ with $|z_a + iz_b|$. For the optimum nonlinearity g_m in (45), we have, from (35) and (36),

$$|z_a - iz_b|_m = \iint dA d\phi \frac{q_1^2(A, \phi) + q_2^2(A, \phi)}{p(A, \phi)}, \quad (57)$$

$$\begin{aligned} |z_a + iz_b|_m &= \left| \iint dA d\phi \exp(i2\phi) \frac{[q_1(A, \phi) + iq_2(A, \phi)]^2}{p(A, \phi)} \right| = \\ &= \left| \iint dA d\phi \exp(i2\phi) \frac{q_1^2(A, \phi) - q_2^2(A, \phi) + i2 q_1(A, \phi) q_2(A, \phi)}{p(A, \phi)} \right|. \quad (58) \end{aligned}$$

Thus, the $\exp(i2\phi)$ term chops up the ϕ integral, since 2ϕ ranges

over 4π , leading to a small value for (58). In addition, the q_1^2 and q_2^2 terms cancel each other in (58), whereas they add in (57). It can also be observed that (57) is identical with the maximum deflection (46), except for factor $A_s^2(t)/4$. Some alternative forms to (57) and (58) in rectangular coordinates are given in appendix D.

Of course, in all cases,

$$\begin{aligned} |z_a + iz_b|_m &\leq \iint dA d\phi |\exp(i2\phi)| \frac{|q_1(A, \phi) + iq_2(A, \phi)|^2}{p(A, \phi)} = \\ &= |z_a - iz_b|_m ; \end{aligned} \quad (59)$$

however, it is expected that we will have

$$|z_a + iz_b|_m \ll |z_a - iz_b|_m \quad (60)$$

in most practical cases. As an example, the Gaussian noise considered in (48)-(50) yields

$$\begin{aligned} |z_a - iz_b|_m &= \frac{2}{\sigma_n^2} , \\ |z_a + iz_b|_m &= \left| \int_0^{+\infty} dA \int_{-\pi}^{\pi} d\phi \exp(i2\phi) \frac{A^3 \exp[-A^2/(2\sigma_n^2)]}{2\pi\sigma_n^6} \right| = 0. \end{aligned} \quad (61)$$

Thus, neglecting the second term in (34) is justified, both in terms of physical interpretation and in terms of magnitude of contribution.

OPTIMUM NONLINEARITY FOR PHASE CHANGES

It is hard to conceive of an independent physical narrowband noise process for which the phase $\phi_n(t)$ would not be uniformly distributed over a 2π interval. In that case, (51) is relevant, with $p_b(\phi)$ constant of value $(2\pi)^{-1}$. Then the second term in optimum nonlinearity (52) is absent, as is the additive term in (53); see also (55) and (56).

NONLINEAR PROCESSING

In this situation, it may be advantageous to resort to additional processing of the phase changes between adjacent time samples of input $x(t)$; regular phase changes would occur for a frequency-shifted narrowband process, such as encountered in FSK communication. In particular, we consider nonlinear processing of adjacent time samples of the received waveform, namely,

$$A_x(t), \phi_x(t), A_x(t-\Delta), \phi_x(t-\Delta), \quad (62)$$

where Δ is the time between samples; see also (13) and (14).

Thus, the output of the nonlinearity is generalized from (15) to

$$y(t) = h\{A_x(t), \phi_x(t), A_x(t-\Delta), \phi_x(t-\Delta)\}, \quad (63)$$

where h is an arbitrary complex nonlinear transformation of four real variables.

INPUT NOISE STATISTICS

The required statistical information about the input noise process is now the joint probability density function of noise quantities

$$A_n(t), \phi_n(t), A_n(t-\Delta), \phi_n(t-\Delta) . \quad (64)$$

We denote these random variables by

$$A_n, \phi_n, \bar{A}_n, \bar{\phi}_n, \quad (65)$$

respectively, and presume that their joint probability density function has the form

$$p_a(\bar{A}_n) p_b(\bar{\phi}_n) p_a(A_n) p_c(\phi_n - \bar{\phi}_n) . \quad (66)$$

That is, all the random variables (65) are statistically independent except that $\phi_n = \phi_n(t)$ depends on $\bar{\phi}_n = \phi_n(t-\Delta)$; thus, probability density function p_c can be expected to peak at a point(s) related to the frequency shift(s) of the noise carrier.

MEAN OUTPUT

The mean output from the general nonlinearity, for signal present, is

$$\begin{aligned} \overline{y_1(t)} &= \overline{h\{A_x(t), \phi_x(t), A_x(t-\Delta), \phi_x(t-\Delta)\}} = \\ &= \iiint dA_n d\phi_n d\bar{A}_n d\bar{\phi}_n p_a(\bar{A}_n) p_b(\bar{\phi}_n) p_a(A_n) p_c(\phi_n - \bar{\phi}_n) \times \\ &\times h\{|A_n \exp(i\phi_n) + A_s \exp(i\phi_s)|, \arg\{A_n \exp(i\phi_n) + A_s \exp(i\phi_s)\}, \\ &|\bar{A}_n \exp(i\bar{\phi}_n) + \bar{A}_s \exp(i\bar{\phi}_s)|, \arg\{\bar{A}_n \exp(i\bar{\phi}_n) + \bar{A}_s \exp(i\bar{\phi}_s)\}\}, \end{aligned} \quad (67)$$

where we suppressed the time dependence of the signal terms (for now) by using the notation

$$A_s = A_s(t), \phi_s = \phi_s(t), \bar{A}_s = A_s(t-\Delta), \bar{\phi}_s = \phi_s(t-\Delta). \quad (68)$$

Now make the changes of variables (using appendix A)

$$\begin{aligned} A \exp(i\phi) &= A_n \exp(i\phi_n) + A_s \exp(i\phi_s), \\ \bar{A} \exp(i\bar{\phi}) &= \bar{A}_n \exp(i\bar{\phi}_n) + \bar{A}_s \exp(i\bar{\phi}_s), \end{aligned} \quad (69)$$

to obtain mean output

$$\begin{aligned} \overline{y_1(t)} &= \iiint dA d\phi d\bar{A} d\bar{\phi} \frac{A}{\mu} \frac{\bar{A}}{\bar{\mu}} p_a(\bar{\mu}) p_b(\bar{\theta}) \times \\ &\times p_a(\mu) p_c(\theta - \bar{\theta}) h\{A, \phi, \bar{A}, \bar{\phi}\}, \end{aligned} \quad (70)$$

where

$$\begin{aligned}
 \mu &= \mu(A, \phi) = |A \exp(i\phi) - A_s \exp(i\phi_s)| , \\
 \bar{\mu} &= \bar{\mu}(\bar{A}, \bar{\phi}) = |\bar{A} \exp(i\bar{\phi}) - \bar{A}_s \exp(i\bar{\phi}_s)| , \\
 \theta &= \theta(A, \phi) = \arg\{A \exp(i\phi) - A_s \exp(i\phi_s)\} , \\
 \bar{\theta} &= \bar{\theta}(\bar{A}, \bar{\phi}) = \arg\{\bar{A} \exp(i\bar{\phi}) - \bar{A}_s \exp(i\bar{\phi}_s)\} . \quad (71)
 \end{aligned}$$

This result, (70), is exact.

SMALL INPUT SIGNAL-TO-NOISE RATIO

For small signal-to-noise ratios, we can now expand the quantities in (71) in power series in A_s and \bar{A}_s through linear terms. Reference to (23) yields

$$\left. \begin{aligned}
 \mu &\sim A - A_s \cos(\phi_s - \phi) \\
 \bar{\mu} &\sim \bar{A} - \bar{A}_s \cos(\bar{\phi}_s - \bar{\phi}) \\
 \theta &\sim \phi - \frac{A_s}{A} \sin(\phi_s - \phi) \\
 \bar{\theta} &\sim \bar{\phi} - \frac{\bar{A}_s}{\bar{A}} \sin(\bar{\phi}_s - \bar{\phi})
 \end{aligned} \right\} \begin{array}{l} \text{for } A_s \ll A \\ \text{and } \bar{A}_s \ll \bar{A} . \end{array} \quad (72)$$

Therefore

$$\frac{A}{\mu} \sim \frac{A}{A - A_S \cos(\phi_S - \phi)} \sim 1 + \frac{A_S}{A} \cos(\phi_S - \phi) ,$$

$$\frac{\bar{A}}{\bar{\mu}} \sim 1 + \frac{\bar{A}_S}{\bar{A}} \cos(\bar{\phi}_S - \bar{\phi}) , \quad (73)$$

where we used (72) and (27). Substitution in (70) gives approximation

$$\begin{aligned} \overline{y_1(t)} &= \iiint dA \, d\phi \, d\bar{A} \, d\bar{\phi} \left[1 + \frac{A_S}{A} \cos(\phi_S - \phi) \right] \left[1 + \frac{\bar{A}_S}{\bar{A}} \cos(\bar{\phi}_S - \bar{\phi}) \right] \times \\ &\times p_a(\bar{A} - \bar{A}_S \cos(\bar{\phi}_S - \bar{\phi})) p_b\left(\bar{\phi} - \frac{\bar{A}_S}{\bar{A}} \sin(\bar{\phi}_S - \bar{\phi})\right) p_a(A - A_S \cos(\phi_S - \\ &- \phi)) p_c\left(\phi - \bar{\phi} - \frac{A_S}{A} \sin(\phi_S - \phi) + \frac{\bar{A}_S}{\bar{A}} \sin(\bar{\phi}_S - \bar{\phi})\right) h\{A, \phi, \bar{A}, \bar{\phi}\}. \quad (74) \end{aligned}$$

Again, however, as noted below (28), the $1/A$ and $1/\bar{A}$ dependencies are incorrect for small A or \bar{A} ; we must be prepared to modify or discard the $1/A$ dependency in some cases where infinities in behavior arise. The discussion in appendix C is again very relevant.

Now we could expand mean output (74) through linear terms in A_S and \bar{A}_S . However, since we have only one nonlinearity $h\{\}$ to choose, we will not be able to simultaneously maximize the coefficients of both A_S and \bar{A}_S . Instead, we concentrate solely on $A_S = A_S(t)$ and maximize its coefficient; this is consistent with the observation that the output of nonlinearity (63) at time $t-\Delta$ will already have maximized the coefficient of $\bar{A}_S = A_S(t-\Delta)$

when it was the current output. Then, to linear terms in A_s , (74) becomes

$$\begin{aligned} \overline{y_1(t)} \sim & \iiint dA \, d\phi \, d\bar{A} \, d\bar{\phi} \left\{ p_a(\bar{A}) \, p_b(\bar{\phi}) \, p_a(A) \, p_c(\phi - \bar{\phi}) + \right. \\ & + \frac{A_s}{A} \cos(\phi_s - \phi) \, p_a(\bar{A}) \, p_b(\bar{\phi}) \, p_a(A) \, p_c(\phi - \bar{\phi}) - \\ & - A_s \cos(\phi_s - \phi) \, p_a(\bar{A}) \, p_b(\bar{\phi}) \, p'_a(A) \, p_c(\phi - \bar{\phi}) - \\ & \left. - \frac{A_s}{A} \sin(\phi_s - \phi) \, p_a(\bar{A}) \, p_b(\bar{\phi}) \, p_a(A) \, p'_c(\phi - \bar{\phi}) \right\} h\{A, \phi, \bar{A}, \bar{\phi}\} . \quad (75) \end{aligned}$$

The leading term in (75) is $\overline{y_0(t)}$, the noise-only mean output. The remaining terms contain A_s linearly and a combination of $\exp(i\phi_s)$ and $\exp(-i\phi_s)$ terms. As explained in (34) and the sequel, the desired signal term is that containing just $\exp(i\phi_s)$. It is, from (75),

$$\begin{aligned} \frac{1}{2} A_s \exp(i\phi_s) \iiint dA \, d\phi \, d\bar{A} \, d\bar{\phi} \, h\{A, \phi, \bar{A}, \bar{\phi}\} \exp(-i\phi) \, p_a(\bar{A}) \, p_b(\bar{\phi}) \times \\ \times \left\{ \frac{p_a(A)}{A} \, p_c(\phi - \bar{\phi}) - p'_a(A) \, p'_c(\phi - \bar{\phi}) + i \frac{p_a(A)}{A} \, p'_c(\phi - \bar{\phi}) \right\} . \quad (76) \end{aligned}$$

VARIANCE OF OUTPUT

At the same time, the variance of the nonlinearity output (63) for noise-only is exactly

$$\text{var}(y_o(t)) = \iiint dA d\phi d\bar{A} d\bar{\phi} \left| h\{A, \phi, \bar{A}, \bar{\phi}\} \right|^2 p_a(\bar{A}) p_b(\bar{\phi}) p_a(A) p_c(\phi - \bar{\phi}) \quad (77)$$

where we have set $\overline{y_o(t)} = 0$ as usual. The deflection is equal to the magnitude-squared value of (76) divided by (77). This deflection is maximized by the optimum nonlinearity

$$\begin{aligned} h_m\{A, \phi, \bar{A}, \bar{\phi}\} &= \exp(i\phi) \left[\frac{1}{A} - \frac{p'_a(A)}{p_a(A)} - i \frac{1}{A} \frac{p'_c(\phi - \bar{\phi})}{p_c(\phi - \bar{\phi})} \right] = \\ &= - \exp(i\phi) \left[\frac{d}{dA} \ln \left(\frac{p_a(A)}{A} \right) + i \frac{1}{A} \frac{p'_c(\phi - \bar{\phi})}{p_c(\phi - \bar{\phi})} \right], \end{aligned} \quad (78)$$

where we have canceled out common terms involving $p_a(\bar{A})$ and $p_b(\bar{\phi})$. We must again take note that (78) is only an approximation and is not accurate for small A .

OPTIMUM NONLINEARITY

Nonlinearity (78) is identical to (52) except for the replacement of $p_b(\phi)$ by $p_c(\phi - \bar{\phi})$; this agrees with the comment in [1; second paragraph under (10)]. Thus, the optimum nonlinearity h_m is independent of amplitude variable \bar{A} and depends only on difference, $\phi - \bar{\phi}$, of phase variables, except for leading factor $\exp(i\phi)$, which reproduces the phase of the input; see the second argument $\phi_x(t)$ in (63). In order to employ (78), the probability density function p_a of noise amplitude, and the probability density function p_c of noise phase changes between samples, must be determined.

If we define auxiliary functions

$$\begin{aligned} h_a\{A\} &= - \frac{d}{dA} \ln \left(\frac{p_a(A)}{A} \right) , \\ h_c\{\theta\} &= - \frac{d}{d\theta} \ln p_c(\theta) , \end{aligned} \quad (79)$$

then (78) can be expressed as

$$h_m\{A, \phi, \bar{A}, \bar{\phi}\} = \exp(i\phi) \left[h_a\{A\} + i \frac{1}{A} h_c\{\phi - \bar{\phi}\} \right] , \quad (80)$$

and the optimum nonlinearity output is, by use of (63), explicitly

$$y(t) = \exp[i\phi_x(t)] \left[h_a\{A_x(t)\} + i \frac{h_c\{\phi_x(t) - \phi_x(t-\Delta)\}}{A_x(t)} \right] . \quad (81)$$

All of these results are predicated on the particular model of

noise statistics as given by (66). Another model for the noise joint probability density function would lead to a different optimum nonlinearity.

When the optimum nonlinearity, (80), is substituted into the deflection, which is the magnitude-squared value of (76) divided by variance (77), the maximum deflection is found to be

$$d_m^2 = \frac{1}{4} A_s^2(t) \left[\int dA p_a(A) h_a^2(A) + \int dA \frac{p_a(A)}{A^2} \int d\theta p_c(\theta) h_c^2(\theta) \right] . \quad (82)$$

This quantity depends only on the probability density functions p_a and p_c ; see (64)-(66) and (79). The presence of the $p_a(A)/A^2$ term has been discussed earlier and is not valid for small A ; see also appendix C.

EXAMPLE

Suppose that probability density functions

$$p_a(A) = \frac{A}{\sigma_a^2} \exp\left(\frac{-A^2}{2\sigma_a^2}\right) \quad \text{for } A > 0 ,$$

$$p_c(\theta) = (2\pi\sigma_c^2)^{-1/2} \exp\left(\frac{-\theta^2}{2\sigma_c^2}\right) \quad \text{for all } \theta . \quad (83)$$

Then (79) yields

$$h_a\{A\} = \frac{A}{\sigma_a^2} \quad \text{for } A > 0 , \quad h_c\{\theta\} = \frac{\theta}{\sigma_c^2} , \quad (84)$$

and optimum nonlinearity (80) becomes

$$h_m\{A, \phi, \bar{A}, \bar{\phi}\} = \exp(i\phi) \left[\frac{A}{\sigma_a^2} + i \frac{1}{A} \frac{\phi - \bar{\phi}}{\sigma_c^2} \right] . \quad (85)$$

The maximum deflection follows from (82) as

$$d_m^2 = \frac{A_s^2(t)/2}{\sigma_a^2} + \frac{A_s^2(t)}{4\sigma_c^2} \int_0^{+\infty} \frac{dA}{A^2} \frac{A}{\sigma_a^2} \exp\left(\frac{-A^2}{2\sigma_a^2}\right) . \quad (86)$$

However, the last integral on A does not converge at $A = 0$; this is an example where the inadequacies of the small-signal approximations in (72) and (73) cannot be ignored, and (86) is useless. The $1/A$ dependency in (85) and the $1/A^2$ term in (86) are incorrect for small A and must be eliminated in that range.

SUMMARY

The transformation of coordinates in (19) and the sequel was performed so that the series expansion of $\overline{y_1(t)}$ could be done in terms of derivatives of noise joint probability density function p , rather than derivatives of nonlinearity g . This allows g to be discontinuous, but presumes that probability density function p is differentiable. An alternative approach based upon an analytic transformation g is given in (E-20) and the sequel.

The deflection criterion has been based upon a difference of complex mean outputs for arbitrary signal waveform, as given by (30). This philosophy has been explained in figure 5; it takes full advantage of the fact that noise-only mean output $\overline{y_0(t)}$ is a known complex quantity and can be subtracted out. Equivalently, restricting the nonlinear transformation to the class with zero-mean noise-only outputs does not detract from the attainable deflection values.

Even for small input signal amplitudes, the difference in mean outputs, (34), contains a spurious term in addition to the desirable term, for a general nonlinearity g . We have chosen to ignore the undesired term and to concentrate on maximization of the desired one. After pursuing this approach, we returned to a quantitative measure of the size of the undesired term and found that it was generally quite small; see (57)-(61). Thus, our approach was confirmed to be a consistent one. An alternative viewpoint is given in appendix E, where it is shown that

deliberate suppression of this spurious term causes a degradation in the maximum deflection attainable.

In equations (45), (52), (78), and (80), there is a $1/A$ term in the imaginary part of the "optimum" nonlinearity. This would appear to indicate that the imaginary component is very important for small inputs; see (81) for example. However, we have then violated the assumptions under which these results were derived, such as in (23), (26), (27), (72), (73), and (75). For example, (23) presumes that A is much larger than A_s . What this means is that the true optimum nonlinearity does not really have a $1/A$ dependence for small A ; however, we do not know what the exact dependence is for small A , because our presumptions preclude investigation in that region. In practice, this means that, for small inputs, we must somehow limit the size of the imaginary part of the nonlinearity output, but the exact transition value and behavior is unknown. A discussion of this problem is presented in appendix C, along with an example of its application and illustration of the basic principles.

APPENDIX A. JACOBIAN OF TRANSFORMATION

Suppose we want to make the two-dimensional transformation between polar coordinates r, θ and ρ, ϕ , according to

$$r \exp(i\theta) = \rho \exp(i\phi) + a \exp(ib) , \quad (A-1)$$

where a and b are arbitrary real constants. The Jacobian of this transformation is

$$\frac{\partial(r, \theta)}{\partial(\rho, \phi)} = \begin{vmatrix} \frac{\partial r}{\partial \rho} & \frac{\partial r}{\partial \phi} \\ \frac{\partial \theta}{\partial \rho} & \frac{\partial \theta}{\partial \phi} \end{vmatrix} . \quad (A-2)$$

From (A-1), there follows directly

$$\frac{\partial r}{\partial \rho} \exp(i\theta) + r i \exp(i\theta) \frac{\partial \theta}{\partial \rho} = \exp(i\phi) ,$$

$$\frac{\partial r}{\partial \phi} \exp(i\theta) + r i \exp(i\theta) \frac{\partial \theta}{\partial \phi} = \rho i \exp(i\phi) . \quad (A-3)$$

Equating real and imaginary parts of these two equations, we have

$$\frac{\partial r}{\partial \rho} = \cos(\phi - \theta) , \quad r \frac{\partial \theta}{\partial \rho} = \sin(\phi - \theta) ,$$

$$\frac{\partial r}{\partial \phi} = - \rho \sin(\phi - \theta) , \quad r \frac{\partial \theta}{\partial \phi} = \rho \cos(\phi - \theta) . \quad (A-4)$$

Substituting in (A-2), there follows the desired result

$$\begin{aligned}\frac{\partial(r, \theta)}{\partial(\rho, \phi)} &= \frac{\rho}{r} = \frac{\rho}{|\rho \exp(i\phi) + a \exp(ib)|} = \\ &= \frac{\rho}{(\rho^2 + a^2 + 2a\rho \cos(\phi-b))^{1/2}},\end{aligned}\quad (A-5)$$

where we used (A-1).

If there were a need to solve for the individual terms in (A-2), they can be obtained from (A-4), by using the real and imaginary parts of (A-1) to eliminate $\cos\theta$ and $\sin\theta$, with the end results

$$\begin{aligned}\frac{\partial r}{\partial \rho} &= \frac{1}{r} [\rho + a \cos(\phi-b)], \\ \frac{\partial r}{\partial \phi} &= -\frac{a\rho}{r} \sin(\phi-b), \\ \frac{\partial \theta}{\partial \rho} &= \frac{a}{r^2} \sin(\phi-b), \\ \frac{\partial \theta}{\partial \phi} &= \frac{\rho}{r^2} [\rho + a \cos(\phi-b)],\end{aligned}\quad (A-6)$$

with

$$r = (\rho^2 + a^2 + 2a\rho \cos(\phi-b))^{1/2}. \quad (A-7)$$

APPENDIX B. INDEPENDENCE OF ADDITIVE CONSTANT

We will show here that the deflection (43) is unchanged if $g\{A \exp(i\phi)\}$ is replaced by $g\{A \exp(i\phi)\} + b$, where b is a complex constant. This is a simple exercise for the denominator of (43), as a direct substitution and expansion immediately reveals that b cancels out everywhere.

For the numerator of (43), we have an additive term (inside the magnitude-squared) of value

$$b \iint dA d\phi \exp(-i\phi) \left[A \frac{\partial}{\partial A} \left(\frac{p(A, \phi)}{A} \right) - i \frac{\partial}{\partial \phi} \left(\frac{p(A, \phi)}{A} \right) \right] . \quad (B-1)$$

However, integration by parts yields*

$$\int dA A \frac{\partial}{\partial A} \left(\frac{p(A, \phi)}{A} \right) = - \int dA \frac{p(A, \phi)}{A} \quad (B-2)$$

as well as**

$$\int d\phi \exp(-i\phi) \frac{\partial}{\partial \phi} \left(\frac{p(A, \phi)}{A} \right) = i \int d\phi \exp(-i\phi) \frac{p(A, \phi)}{A} . \quad (B-3)$$

Substitution of these two results in (B-1) yields

$$b \left[\int d\phi \exp(-i\phi) (-1) \int dA \frac{p(A, \phi)}{A} - i \int dA i \int d\phi \exp(-i\phi) \frac{p(A, \phi)}{A} \right] \quad (B-4)$$

which is identically zero. Thus, the additive term dependent on b is zero.

*Result (B-2) is true if $p(0, \phi) = 0$.

**The 2π periodicity of $p(A, \phi)$ in ϕ is utilized in getting (B-3).

APPENDIX C. BEHAVIOR OF OPTIMUM NONLINEARITY

Some problems with the approximations utilized in (23)-(27), in order to simplify the mean output $\overline{y_1(t)}$, were pointed out in the sequel to (28) and were manifested in the example in (53) by means of the $1/A$ dependencies for small A . To circumvent these limitations, we will adopt the procedure used just after figure 3 for the lowpass case, namely, investigation of the exact deflection and corresponding optimum nonlinearity with knowledge of signal amplitude $A_s(t)$ and phase $\phi_s(t)$. Again, although physically unrealistic, this approach is informative and does furnish an absolute upper bound on performance.

The starting point is the exact result (21) for the non-linearity mean output,

$$\overline{y_1(t)} = \iint dA d\phi \frac{A}{|z|} g\{A \exp(i\phi)\} p(|z|, \arg(z)) , \quad (C-1)$$

where (dropping explicit signal t dependence)

$$z = A \exp(i\phi) - A_s \exp(i\phi_s). \quad (C-2)$$

The noise-only mean output is obtained by setting $A_s = 0$:

$$\overline{y_0(t)} = \iint dA d\phi g\{A \exp(i\phi)\} p(A, \phi) . \quad (C-3)$$

The variance of $y_0(t)$ is given by (42).

We now define exact deflection

$$\bar{d}^2(A_s, \phi_s) = \frac{|\overline{y_1(t)} - \overline{y_0(t)}|^2}{\text{var}(y_0(t))}, \quad (C-4)$$

where the dependence on signal parameters is made explicit. Since the absolute scale of nonlinearity g and an additive constant to g do not affect the deflection, we can simplify (C-4) to

$$\bar{d}^2(A_s, \phi_s) = \frac{\left| \iint dA d\phi g\{A \exp(i\phi)\} \left[\frac{A}{|z|} p(|z|, \arg(z)) - p(A, \phi) \right] \right|^2}{\iint dA d\phi |g\{A \exp(i\phi)\}|^2 p(A, \phi)}. \quad (C-5)$$

By Schwartz's inequality, the optimum nonlinearity (with no approximations, but with assumed knowledge of A_s and ϕ_s) is

$$\bar{g}_e(A, \phi; A_s, \phi_s) = \frac{A}{|z|} \frac{p(|z|, \arg(z))}{p(A, \phi)} - 1, \quad (C-6)$$

where z is given by (C-2). The corresponding maximum deflection follows from (C-5) as

$$\begin{aligned} \bar{d}_e^2(A_s, \phi_s) &= \iint dA d\phi \left[\frac{A}{|z|} p(|z|, \arg(z)) - p(A, \phi) \right]^2 / p(A, \phi) = \\ &= \iint dA d\phi \frac{A^2}{|z|^2} \frac{p^2(|z|, \arg(z))}{p(A, \phi)} - 1. \end{aligned} \quad (C-7)$$

From (C-2), since

$$|z| = \left[A^2 + A_s^2 - 2 A A_s \cos(\phi_s - \phi) \right]^{1/2}, \quad (C-8)$$

it follows that

$$|z| \sim A_s \text{ as } A \rightarrow 0+ \text{ (if } A_s \neq 0) \quad (C-9)$$

and, therefore, exact optimum nonlinearity \bar{g}_e in (C-6) has no $1/A$ dependency for small A (unless probability density function $p(A, \phi)$ approaches zero rapidly for small A), but in fact has a linear dependence on A . That is,

$$\bar{g}_e(A, \phi; A_s, \phi_s) \sim \frac{A}{p(A, \phi)} \frac{p(A_s, \phi_s + \pi)}{A_s} - 1 \text{ as } A \rightarrow 0+ . \quad (C-10)$$

Similarly, the integrand of maximum deflection \bar{d}_e^2 in (C-7) has no $1/A^2$ dependence, but in fact, an A^2 dependence for small A :

$$\frac{A^2}{p(A, \phi)} \frac{p^2(A_s, \phi_s + \pi)}{A_s^2} \text{ as } A \rightarrow 0+ . \quad (C-11)$$

These are marked differences in behavior from the approximate results of (45)-(47).

It should also be noted that optimum nonlinearity \bar{g}_e in (C-6) is real. (More precisely, one of the possible optimum nonlinearities is real since complex multiplicative constants can be dropped.) The reason this disagrees with the complex solution in (45) is that A_s and ϕ_s are presumed known in (C-6). When ϕ_s is unknown, then even if (C-6) is developed in a power series in A_s , it is not possible to extract a nonlinearity that is independent of ϕ_s ; this information is too deeply embedded in optimum form (C-6). Thus, (C-6) should only be regarded as a guide to good

processing, especially for small A, but otherwise it is not overly useful. The corresponding maximum deflection in (C-7) is probably more useful since it furnishes an absolute upper bound on performance for any nonlinearity. If an approximate result, like (46) or (50) or (53), outperforms (C-7), it is in error and must be modified or discarded. The apparent infinity in (53) at $A = 0$, for example, is conspicuously wrong; reference to (C-11) indicates that the true near-origin behavior is significantly different.

The philosophy in this appendix is very different from that utilized in (34)-(39). There, a desired type of signal term was identified up front, while the nonlinearity characteristic g was still arbitrary; then, that particular type of term was maximized by choice of g . Here, the entire nonlinearity output difference of means was maximized without any type of term being designated as desired. Thus, we should expect to be able to realize a larger deflection in this latter case since no terms have been suppressed or ignored. The only problem with this approach is that, after the maximization, it is not generally possible to extract a meaningful nonlinear device that is independent of the input signal values of amplitude and phase.

An example to illustrate these points is furnished by Gaussian narrowband noise as in (48):

$$p(A, \phi) = \frac{A}{2\pi\sigma_n^2} \exp\left(-\frac{A^2}{2\sigma_n^2}\right) \quad \text{for } A > 0, |\phi| < \pi. \quad (\text{C-12})$$

Then, (C-6) and (C-8) immediately yield optimum nonlinearity

$$\bar{g}_e(A, \phi; A_s, \phi_s) = \exp \left[\frac{A A_s}{2 \sigma_n^2} \cos(\phi_s - \phi) - \frac{A_s^2}{2 \sigma_n^2} \right] - 1 \quad (C-13)$$

For small A_s , this behaves according to

$$\bar{g}_e(A, \phi; A_s, \phi_s) \sim \frac{A A_s}{2 \sigma_n^2} \cos(\phi_s - \phi) \quad \text{as } A_s \rightarrow 0 \quad (C-14)$$

Even though there is a linear term in A_s , which could be factored out, the remaining nonlinearity, namely $\frac{A}{2 \sigma_n^2} \cos(\phi_s - \phi)$, depends on ϕ_s . It is now too late to express

$$\begin{aligned} & \frac{A A_s}{2 \sigma_n^2} \cos(\phi_s - \phi) = \\ & = \frac{1}{2 \sigma_n^2} \left[A \exp(-i\phi) A_s \exp(i\phi_s) + A \exp(i\phi) A_s \exp(-i\phi_s) \right] \quad (C-15) \end{aligned}$$

and to drop the $A_s \exp(-i\phi_s)$ term as being undesired since this component has been an integral part of the maximization of deflection (C-5). In fact, if we drop that term in (C-15), we are left with nonlinearity

$$A \exp(-i\phi) \frac{A_s}{2 \sigma_n^2} \exp(i\phi_s) \quad (C-16)$$

which can be modified to $A \exp(-i\phi)$ since complex multiplicative factors on the nonlinearity are irrelevant. However, $A \exp(-i\phi)$

manifestly has the wrong phase behavior; see (49). Thus, this series of (late) approximations and replacements can lead to a nonsense processor and must be avoided.

The maximum deflection for this example is obtained by substituting (C-12) in (C-7):

$$\begin{aligned} \bar{d}_e^2(A_s, \phi_s) &= \int_0^{+\infty} dA \int_{-\pi}^{\pi} d\phi \frac{A}{2\pi\sigma_n^2} \exp\left[-\frac{1}{\sigma_n^2}\left(\frac{1}{2}A^2 + A_s^2 - 2AA_s \cos(\phi_s - \phi)\right)\right] - 1 \\ &= \frac{1}{2} \int_0^{+\infty} dA A \exp\left[-\frac{A^2}{2\sigma_n^2} - \frac{A_s^2}{\sigma_n^2}\right] I_0\left(\frac{2AA_s}{\sigma_n^2}\right) - 1 = \exp\left(\frac{A_s^2}{\sigma_n^2}\right) - 1, \quad (C-17) \end{aligned}$$

where we used [3; 6.631 4]. Observe that this quantity is independent of signal phase ϕ_s . For small input signal-to-noise ratio, this becomes

$$\bar{d}_e^2(A_s, \phi_s) \sim \frac{A_s^2}{\sigma_n^2} \quad \text{as} \quad \frac{A_s}{\sigma_n} \rightarrow 0. \quad (C-18)$$

This latter approximation is twice as large as (50) and is due to the fact that, here, we have retained all the signal terms at the nonlinearity output, whereas the method leading to (50) discarded one of the two possible terms. See the discussion immediately after (C-11).

For some purposes, it may be more useful to express the above relations in terms of the joint probability density function of the in-phase and quadrature components of the narrowband noise rather than the amplitude and phase. Thus, if we let $w(u,v)$ be

the joint probability density function of

$$u_n + i v_n = A_n \exp(i \phi_n) , \quad (C-19)$$

then the joint probability density function p of amplitude and phase is given by

$$p(A, \phi) = A w(A \cos \phi, A \sin \phi) . \quad (C-20)$$

APPENDIX D. ALTERNATIVE FORMS IN RECTANGULAR COORDINATES

In (C-19) and (C-20), the joint probability density function $w(u,v)$ of the in-phase and quadrature components of the input noise,

$$u_n + iv_n = A_n \exp(i\phi_n) , \quad (D-1)$$

was introduced; it is related to the joint probability density function p of amplitude and phase by

$$p(A, \phi) = A w(A \cos \phi, A \sin \phi) . \quad (D-2)$$

When we employ this result in (31), there follows

$$q_1(A, \phi) = A[\cos \phi w_1(A \cos \phi, A \sin \phi) + \sin \phi w_2(A \cos \phi, A \sin \phi)] , \quad (D-3)$$

$$q_2(A, \phi) = A[-\sin \phi w_1(A \cos \phi, A \sin \phi) + \cos \phi w_2(A \cos \phi, A \sin \phi)] ,$$

and therefore

$$q_1(A, \phi) + iq_2(A, \phi) = A \exp(-i\phi) W(A \cos \phi, A \sin \phi) ,$$

$$q_1(A, \phi) - iq_2(A, \phi) = A \exp(i\phi) W^*(A \cos \phi, A \sin \phi) , \quad (D-4)$$

where

$$W(u, v) = w_1(u, v) + iw_2(u, v) = \left(\frac{\partial}{\partial u} + i \frac{\partial}{\partial v} \right) w(u, v) . \quad (D-5)$$

When (D-4) is employed in (35) and (36), there follows

$$\begin{aligned}
z_a - iz_b &= \iint dA d\phi A g\{A \exp(i\phi)\} W^*(A \cos\phi, A \sin\phi) = \\
&= \iint du dv g\{u + iv\} W^*(u, v) \quad (D-6)
\end{aligned}$$

and

$$\begin{aligned}
z_a + iz_b &= \iint dA d\phi A g\{A \exp(i\phi)\} W(A \cos\phi, A \sin\phi) = \\
&= \iint du dv g\{u + iv\} W(u, v) . \quad (D-7)
\end{aligned}$$

When the optimum nonlinearity, (45), is expressed in the notation of (D-2)-(D-5), we have

$$g_m\{A \exp(i\phi)\} = - \frac{W(A \cos\phi, A \sin\phi)}{w(A \cos\phi, A \sin\phi)} , \quad (D-8)$$

or

$$g_m\{u + iv\} = - \frac{W(u, v)}{w(u, v)} . \quad (D-9)$$

When this is utilized in (D-6) and (D-7), the following alternatives to (57)-(59) result:

$$\begin{aligned}
(z_a - iz_b)_m &= - \iint du dv \frac{|W(u, v)|^2}{w(u, v)} = - \iint du dv \frac{w_1^2(u, v) + w_2^2(u, v)}{w(u, v)} , \\
(z_a + iz_b)_m &= - \iint du dv \frac{w^2(u, v)}{w(u, v)} = - \iint du dv \frac{[w_1(u, v) + iw_2(u, v)]^2}{w(u, v)} \\
&= - \iint du dv \frac{w_1^2(u, v) - w_2^2(u, v) + i2 w_1(u, v) w_2(u, v)}{w(u, v)} . \quad (D-10)
\end{aligned}$$

As an example of these results, suppose that joint probability density function

$$w(u,v) = f(u^2 + v^2); \quad \text{that is, } p(A,\phi) = A f(A^2) . \quad (\text{D-11})$$

The noise joint probability density function is independent of angle. Then

$$\begin{aligned} w_1(u,v) &= 2 u f'(u^2 + v^2) , \\ w_2(u,v) &= 2 v f'(u^2 + v^2) , \end{aligned} \quad (\text{D-12})$$

and (D-10) yields

$$\begin{aligned} (z_a - iz_b)_m &= -4 \iint du dv (u^2 + v^2) \frac{f'^2(u^2 + v^2)}{f(u^2 + v^2)} = \\ &= -8\pi \int_0^{+\infty} dA A^3 \frac{f'^2(A^2)}{f(A^2)} , \end{aligned} \quad (\text{D-13})$$

$$\begin{aligned} (z_a + iz_b)_m &= -4 \iint du dv (u + iv)^2 \frac{f'^2(u^2 + v^2)}{f(u^2 + v^2)} = \\ &= -4 \int_{-\pi}^{\pi} d\phi \exp(i2\phi) \int_0^{+\infty} dA A^3 \frac{f'^2(A^2)}{f(A^2)} = 0 . \end{aligned} \quad (\text{D-14})$$

Example (D-11) is a generalization of Gaussian probability density function (48) and (D-14) generalizes (61).

APPENDIX E. CONSTRAINED MAXIMIZATION OF DEFLECTION

When the difference of mean outputs was expanded through linear terms in signal amplitude $A_s(t)$, the end result for arbitrary nonlinearity g was (34):

$$\begin{aligned} \overline{y_1(t)} - \overline{y_0(t)} = & -\frac{1}{2} A_s(t) \exp[i\phi_s(t)] (z_a - iz_b) - \\ & -\frac{1}{2} A_s(t) \exp[-i\phi_s(t)] (z_a + iz_b) . \quad (E-1) \end{aligned}$$

At that time, we ignored the second term as being of no interest and maximized the first (desired) term; see (39) and (43). Then, we later returned to investigate the relative sizes of these terms in (57)-(61) and appendix D.

Here, we adopt a different viewpoint: we force the second term in (E-1) to be zero and then we maximize the magnitude of the first term by choice of nonlinearity g . More precisely, we maximize deflection (43), subject to integral constraint

$$\iint du \, dv \, g\{u + iv\} W(u,v) = 0 ; \quad (E-2)$$

this last equation comes from (D-7) and (D-5).

The first point to observe is that the absolute scale of g does not affect (43) or (E-2). The second is that the same independence is true for an additive complex constant, b , to g . This was proven in appendix B for (43) and follows for (E-2) since

$$\begin{aligned}
\iint du dv b w(u,v) &= b \iint du dv \left(\frac{\partial}{\partial u} + i \frac{\partial}{\partial v} \right) w(u,v) = \\
&= b \int dv \int du \frac{\partial}{\partial u} w(u,v) + ib \int du \int dv \frac{\partial}{\partial v} w(u,v) = 0, \quad (E-3)
\end{aligned}$$

where we used (D-5) and the facts that

$$\begin{aligned}
\int du \frac{\partial}{\partial u} w(u,v) &= \left[w(u,v) + c_1(v) \right]_{u=-\infty}^{u=+\infty} = 0, \\
\int dv \frac{\partial}{\partial v} w(u,v) &= \left[w(u,v) + c_2(u) \right]_{v=-\infty}^{v=+\infty} = 0. \quad (E-4)
\end{aligned}$$

What this means is that, without loss of generality, we can set the complex nonlinearity mean output for noise-alone, $\overline{y_0(t)}$, equal to zero. This results in deflection (44), which can be expressed in the form

$$d^2 = \frac{1}{4} A_s^2(t) \frac{\left| \iint du dv g\{u + iv\} W^*(u,v) \right|^2}{\iint du dv |g\{u + iv\}|^2 w(u,v)}, \quad (E-5)$$

where we used (D-4), (D-1), and (D-2). The problem of interest here is to maximize (E-5), subject to constraint (E-2), by choice of nonlinearity g .

Since (E-2) is really two constraints on the real and imaginary parts, we need two real Lagrange multipliers; letting I denote the integral in (E-2), we must add to (E-5) the two real terms

$$\lambda_r I_r + \lambda_i I_i = \lambda_r \frac{I + I^*}{2} + \lambda_i \frac{I - I^*}{i2} = \frac{1}{2} (I \lambda^* + I^* \lambda) , \quad (E-6)$$

where λ is a complex Lagrange multiplier. Then, the essential quantity we must maximize is

$$Q = \frac{\left| \iiint g W^* \right|^2}{\iiint |g|^2 w} - \lambda^* \iiint g W - \lambda \iiint g^* W^* , \quad (E-7)$$

where we have dropped irrelevant scale factors and adopted an extremely abbreviated notation for the time being.

If we replace

$$g(u + iv) \quad \text{by} \quad g_m(u + iv) + \epsilon \eta(u + iv) , \quad (E-8)$$

where $g_m\{ \}$ is the optimum nonlinearity, $\eta\{ \}$ is any perturbation, and ϵ is an arbitrary complex constant, the new value of Q is

$$\begin{aligned} Q_m + \delta Q &= \frac{\iiint (g_m + \epsilon \eta) W^* \iiint (g_m + \epsilon \eta)^* W}{\iiint (g_m + \epsilon \eta) (g_m + \epsilon \eta)^* w} - \\ &- \lambda^* \iiint (g_m + \epsilon \eta) W - \lambda \iiint (g_m + \epsilon \eta)^* W^* . \end{aligned} \quad (E-9)$$

Let constants

$$N = \iiint g_m W^* , \quad D = \iiint |g_m|^2 w ; \quad (E-10)$$

N is complex, while D is real. If we set the partial derivative of $Q_m + \delta Q$ with respect to ϵ^* (for fixed ϵ) equal to zero, and then set $\epsilon = 0$, $\epsilon^* = 0$, we find that we must satisfy

$$\frac{D N \iint \eta^* W - |N|^2 \iint g_m \eta^* W}{D^2} - \lambda \iint \eta^* W^* = 0 \quad (E-11)$$

for all perturbations $\eta = \eta\{u + iv\}$. That is,

$$\iint \eta^* \left[\frac{N}{D} W - \frac{|N|^2}{D^2} W g_m - \lambda W^* \right] = 0 \quad \text{for all } \eta. \quad (E-12)$$

The solution for the optimum nonlinearity is therefore (dropping irrelevant scale factors)

$$g_m = - \frac{W - \frac{D\lambda}{N} W^*}{W}. \quad (E-13)$$

In order to solve for the unknown constants, we must substitute (E-13) into the constraint (E-2). But, first, we define the two additional quantities

$$M = \iint \frac{|W|^2}{W}, \quad C = \iint \frac{W^2}{W}; \quad (E-14)$$

M is real, while C is complex. Then the substitution yields

$$0 = \iint g_m W = -C + \frac{D\lambda}{N} M. \quad (E-15)$$

Equation (E-15) can be solved for

$$\frac{D\lambda}{N} = \frac{C}{M}. \quad (E-16)$$

Use of this result in (E-13) gives the optimum constrained nonlinearity

$$g_m(u + iv) = - \frac{W(u,v) - \frac{C}{M} W^*(u,v)}{w(u,v)}, \quad (E-17)$$

where constants M and C are given by (E-14). By comparison, the unconstrained optimum nonlinearity did not have the W^* term; see (D-9).

The corresponding maximum deflection is obtained by the use of (E-17) and (E-14) in (E-5):

$$d_m^2 = \frac{1}{4} A_s^2(t) M \left(1 - \frac{|C|^2}{M^2} \right). \quad (E-19)$$

The factor

$$1 - \frac{|C|^2}{M^2} = 1 - \left| \frac{\iint du dv W^2(u,v)/w(u,v)}{\iint du dv |W(u,v)|^2/w(u,v)} \right|^2 \quad (E-19)$$

is the amount by which the constraint (E-2) degrades the attainable deflection; see (46) and (D-4).

ALTERNATIVE APPROACH

If we return to exact mean output $\overline{y_1(t)}$ in (18) and presume now that nonlinearity g is analytic, then a series expansion in $A_s(t)$ yields directly

$$\overline{y_1(t)} - \overline{y_0(t)} = \sim A_s(t) \exp[i\phi_s(t)] \iint dA_n d\phi_n p(A_n, \phi_n) g'_a[A_n \exp[i\phi_n]]. \quad (E-20)$$

The subscript a on g denotes that nonlinearity g is now required to be analytic. We immediately see that the second term in (34), of the form $A_s(t) \exp[-i\phi_s(t)]$, is absent. Now use (D-2) and (D-1) to obtain

$$\overline{y_1(t)} - \overline{y_0(t)} = A_s(t) \exp[i\phi_s(t)] \iint du dv w(u, v) g'_a\{u + iv\}. \quad (E-21)$$

The double integral in (E-21), denoted by I , can be put in two different forms: first, since

$$\frac{\partial}{\partial u} (w(u, v) g_a\{u + iv\}) = w_1(u, v) g_a\{u + iv\} + w(u, v) g'_a\{u + iv\}, \quad (E-22)$$

then

$$\begin{aligned} \int du w(u, v) g'_a\{u + iv\} &= \\ &= \int du \frac{\partial}{\partial u} (w(u, v) g_a\{u + iv\}) - \int du w_1(u, v) g_a\{u + iv\}. \quad (E-23) \end{aligned}$$

The first term is

$$\left[w(u,v) g_a\{u + iv\} + c(v) \right]_{u=-\infty}^{u=+\infty} = 0 , \quad (E-24)$$

since we presume that probability density function $w(u,v)$ goes to zero fast enough at $u = \pm\infty$. Therefore, integrating (E-23) on v ,

$$I = \iint du dv w(u,v) g'_a\{u+iv\} = - \iint du dv w(u,v) g_a\{u+iv\}. \quad (E-25)$$

A similar approach to (E-22), but involving $\partial/\partial v$ instead, yields the alternative expression

$$I = i \iint du dv w_2(u,v) g_a\{u + iv\} . \quad (E-26)$$

Since (E-25) and (E-26) are equal, we obtain

$$\iint du dv W(u,v) g_a\{u + iv\} = 0 , \quad (E-27)$$

where we used (D-5):

$$W(u,v) = w_1(u,v) + iw_2(u,v) = \left(\frac{\partial}{\partial u} + i \frac{\partial}{\partial v} \right) w(u,v) . \quad (E-28)$$

But (E-27) is identical to the constraint (E-2) that we adopted earlier in this appendix. Thus, the assumption of analyticity of nonlinearity g_a automatically realizes the constraint that eliminates the second (undesired) term in (E-1). This is also obvious directly from expansion (E-20).

Since I is given by both (E-25) and (E-26), it is also given by the linear combination

$$\begin{aligned}
I &= -\rho \iint du dv w_1(u,v) g_a\{u+iv\} + (1-\rho)i \iint du dv w_2(u,v) g_a\{u+iv\} = \\
&= - \iint du dv g_a\{u+iv\} [\rho w_1(u,v) - i(1-\rho) w_2(u,v)] , \quad (E-29)
\end{aligned}$$

where ρ is any complex constant. Notice that an additive constant to g_a does not affect I , since

$$\int du w_1(u,v) = \int du \frac{\partial}{\partial u} w(u,v) = \left[w(u,v) + c(v) \right]_{u=-\infty}^{u=+\infty} = 0 , \quad (E-30)$$

and similarly,

$$\int dv w_2(u,v) = 0 . \quad (E-31)$$

Then, by reference to (42) and the upper line of (43), the deflection can be expressed as

$$d^2 = A_s^2(t) \frac{\left| \iint du dv g_a\{u+iv\} [\rho w_1(u,v) - i(1-\rho) w_2(u,v)] \right|^2}{\iint du dv |g_a\{u+iv\}|^2 w(u,v)} , \quad (E-32)$$

where we used (E-21), (E-29), (D-2), and (D-1). Now if g_a were unrestricted, the optimum nonlinearity is now

$$\begin{aligned}
g_{am}\{u+iv\} &= -2 \frac{\rho^* w_1(u,v) + i(1-\rho^*) w_2(u,v)}{w(u,v)} = \\
&= - \frac{\rho^* (W + W^*) + (1-\rho^*) (W - W^*)}{W} = \\
&= - \frac{W(u,v) - (1-2\rho^*) W^*(u,v)}{W(u,v)} , \quad (E-33)
\end{aligned}$$

where we used (E-28). But since (E-27) must be satisfied by this candidate nonlinearity g_{am} , we find that

$$1 - 2\rho^* = \frac{C}{M}, \quad (E-34)$$

where C and M are given by (E-14), and (E-33) becomes identically (E-17).

The only thing wrong with this latter alternative approach in (E-20) and the sequel is that there is no guarantee that (E-33) yields an analytic nonlinearity g for any ρ . Thus, (E-33) may not be a valid solution. Furthermore, it is unnecessarily restrictive to limit g to being analytic, and the identical optimum nonlinearity, obtained earlier in (E-17), was not restricted to being analytic. In summary, (E-17) is the optimum constrained nonlinearity which eliminates the $A_s(t) \exp[-i\phi_s(t)]$ term, while (D-9) is the optimum nonlinearity which ignores this latter term.

REFERENCES

1. James H. Higbie, "Adaptive Nonlinear Suppression of Interference," Proc. IEEE Military Communications Conference, paper 23.3, MILCOM 88, San Diego, CA, pages 381-389, 23-26 October 1988.
2. James H. Higbie, "Estimating the Phase of a Weak Signal in the Presence of a Strong Jammer," Internal Memorandum F3B-86-103, Applied Physics Lab, Johns Hopkins University, Laurel, MD, 12 May 1986.
3. I. S. Gradshteyn and I. M. Ryzhik, Table of Integrals, Series and Products, Academic Press, Inc., New York, NY, 1980.

Technical Report 8631
6 October 1989

**Determination of Noise Field Directionality
Directly From Spatial Correlation for Linear,
Planar, and Volumetric Arrays**

A. H. Nuttall
ABSTRACT

The spatial correlation between two points of an array is given by a two-dimensional integral in terms of the noise field directionality. Depending on the dimensionality of the array, this integral equation can be partially solved to yield explicit expressions for the noise field directionality in terms of a multidimensional Fourier transform. In particular, for a linear array, a one-dimensional collapsed field distribution can be determined; for a planar array, the sum of symmetrically-arriving rays can be solved for; and for a volumetric array, the complete field can be found. The effects of finite length and discrete arrays on the estimate of the noise field directionality are also considered.

Approved for public release; distribution is unlimited.

TABLE OF CONTENTS

	Page
LIST OF ILLUSTRATIONS	ii
LIST OF SYMBOLS	ii
INTRODUCTION	1
CHARACTERIZATION OF NOISE FIELD	5
LINEAR ARRAY	9
Solution of Integral Equation	10
Example	12
Discrete Infinite-Length Array	13
Discrete Finite-Length Array	15
PLANAR ARRAY	17
Solution of Integral Equation	18
Behavior Near Plane of Array	20
Discrete Infinite-Length Array	21
Discrete Finite-Length Array	24
VOLUMETRIC ARRAY	25
Solution of Integral Equation	25
Simultaneous Equations	27
Angular Representations	29
SUMMARY	33
APPENDIX A. ALTERNATIVE LOCATION OF LINEAR ARRAY	35
APPENDIX B. ALTERNATIVE LOCATION OF PLANAR ARRAY	37
APPENDIX C. EXAMPLE FOR VOLUMETRIC ARRAY	39
REFERENCES	43

LIST OF ILLUSTRATIONS

Figure		Page
1	Coordinate System	5
2	Window Function Q^2	28

LIST OF SYMBOLS

θ	polar angle, figure 1
ϕ	azimuthal angle, figure 1
f	temporal-frequency
$N_f(\theta, \phi)$	noise field directionality, (1)
τ_1	time of arrival at location x_1, y_1, z_1 , (2)
c	speed of propagation, (2)
$H_1(f)$	transfer function, (3)
λ	wavelength = c/f , (3)
x, y, z	separation distances, (5)
$G_f(x, y, z)$	spatial correlation at temporal-frequency f , (6)
$G_f(z)$	spatial correlation for linear array, (7)
$\bar{N}_f(\theta)$	integrated noise field directionality, (8)
δ	delta function, (9)
Δ	spacing in z , (12)
M	size of fast Fourier transform, (13), (14), (29), (30)
\otimes	convolution, (15a)
$w(z)$	weighting, (15b)
$W(u)$	window, (15c)

$G_f(x,y)$	spatial correlation for planar array, (16)
$\tilde{N}_f(\theta,\phi)$	sum of symmetrically-arriving rays, (17)
$I(u,v)$	two-dimensional Fourier transform of $G_f(x,y)$, (18)
$\arg(z)$	argument of complex number z , (21)
C_1	circle of radius 1 at origin, (23)
F	auxiliary function, (24)
Δ_x, Δ_y	spacings in x,y , (28)
N	size of fast Fourier transform, (29),(30)
$I(u,v,w)$	three-dimensional Fourier transform of $G_f(x,y,z)$, (36)
$q(z)$	weighting in z , (36)
$Q(t)$	Fourier transform of $q(z)$, (37)
s	auxiliary function, (42)
F_1, F_2	auxiliary functions, (44)
w_1, w_2	two distinct values of w , (46),(47)
$Q_n(\pm)$	abbreviated notation, (48)
D	denominator, (49)
L_z	effective length of weighting $q(z)$, figure 2
$I(\pm)$	abbreviated notation, (55)
θ'	complementary angle = $\pi - \theta$, (56)
$I'(\pm)$	abbreviated notation, (57)

DETERMINATION OF NOISE FIELD DIRECTIONALITY DIRECTLY FROM
SPATIAL CORRELATION FOR LINEAR, PLANAR, AND VOLUMETRIC ARRAYS

INTRODUCTION

When an array is located in a homogeneous stationary noise field, measurement of the crosscorrelations between all pairs of separated elements, at each temporal-frequency of interest, is the most general second-order statistical information that can be extracted. These spatial correlations depend upon the directionality of the surrounding noise field, which is the primary quantity of interest here. Instead of beamforming the element outputs, for example, and trying to suppress the inherent sidelobes by proper weighting procedures, we want to avoid any preconceived notions about data processing and go directly from the spatial correlation to the noise field directionality in as direct and simple a manner as possible.

However, because the noise field directionality is a two-dimensional function of polar and azimuthal angles, some inherent loss or condensation of information takes place with a linear array and, to a much lesser extent, with a planar array. Nevertheless, we want to preserve and extract the maximum amount of information about the noise field directionality, consistent with the dimensionality of the array employed, and to minimize the amount of data processing required.

We begin by assuming the array to be an infinite continuous line in the one-dimensional case, and solve the integral equation for the integrated (or collapsed) noise field directionality, at each temporal-frequency, in terms of the spatial correlation along the line. Then, we discretize the line, so as to be an equi-spaced array, and determine the effect that this limitation has upon the estimated directionality. Finally, we investigate the smoothing that is caused by the practical requirement that any physical array must have finite length. Thus, the facts that the spatial correlation will never be available on a continuum, nor for infinite separations, are included in the analysis.

A similar procedure is pursued for the two-dimensional case, where the planar array is presumed to have equal spacings Δ_x and Δ_y in the x and y dimensions, respectively. Again, the aliasing effects are considered, as well as the limitation of having to employ a finite-size planar array. Finally, in the three-dimensional case, where the problem is overdetermined, a plausible and efficient procedure for collapsing the surplus information is presented, although it is recognized that an unlimited number of alternatives exist.

Although it was stated that the noise field directionality is of interest, this does not preclude the presence of plane-wave arrivals, that is, additive signals or interferences in the background. In fact, the examples are specifically of that type, for these can be considered as the fundamental building blocks of a general noise field.

Some related results on this problem of restoring the noise field directionality from the spatial correlation are given in [1,2,3,4], but limited to the line array. Specifically, [1] gave a least squares approach, starting from a discrete finite-length array. However, ill-conditioning of the simultaneous linear equations for the noise field directionality precluded its use for more than approximately ten elements. This ill-conditioning is circumvented here by deferring the discretization until after the integral equation is solved; this procedure for the line array was first given in [4].

CHARACTERIZATION OF NOISE FIELD

Let $N_f(\theta, \phi)$ be the intensity of the homogeneous stationary noise field at temporal-frequency f , arriving from direction θ, ϕ , where $0 \leq \theta \leq \pi$, $-\pi < \phi \leq \pi$; see figure 1. The amount of power received in solid angle $d\theta d\phi \sin\theta$ about θ, ϕ is

$$d\theta d\phi \sin\theta N_f(\theta, \phi). \quad (1)$$

We call $N_f(\theta, \phi)$ the noise field directionality; the product $\sin\theta N_f(\theta, \phi)$ could be called the plane-wave density.

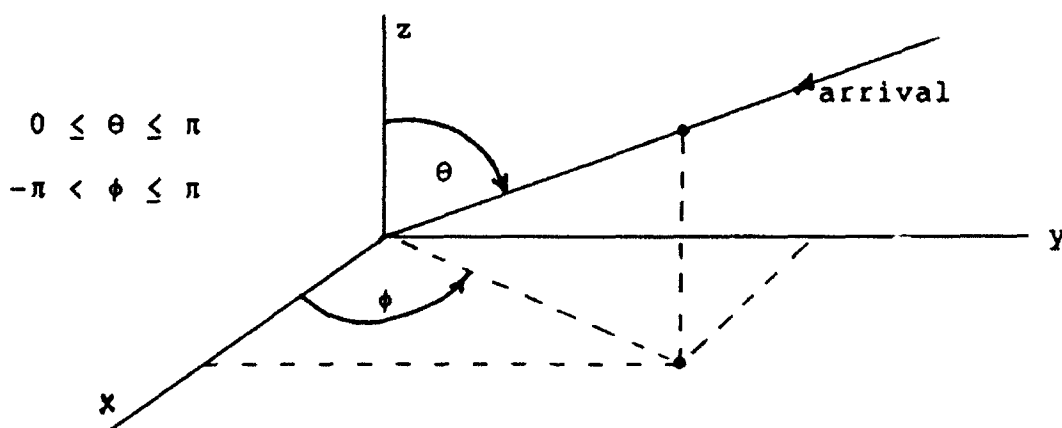


Figure 1. Coordinate System

Consider general field point x_1, y_1, z_1 . Then if the time of arrival at the origin, of the component from direction θ, ϕ , is zero, then the time of arrival at x_1, y_1, z_1 is

$$\tau_1 = -\frac{1}{c} (x_1 \sin\theta \cos\phi + y_1 \sin\theta \sin\phi + z_1 \cos\theta), \quad (2)$$

where c is the speed of propagation. Therefore, the transfer function at x_1, y_1, z_1 applied to the arrival from direction θ, ϕ is

$$H_1(f) = \exp(-i2\pi f\tau_1) =$$

$$= \exp\left[i\frac{2\pi}{\lambda} (x_1 \sin\theta \cos\phi + y_1 \sin\theta \sin\phi + z_1 \cos\theta)\right], \quad (3)$$

where wavelength $\lambda = c/f$.

The elemental contribution to the crosscorrelation between this arrival at x_1, y_1, z_1 and x_2, y_2, z_2 , at temporal-frequency f , is then

$$d\theta d\phi \sin\theta N_f(\theta, \phi) H_1(f) H_2^*(f) = d\theta d\phi \sin\theta \times$$

$$\times N_f(\theta, \phi) \exp\left[i\frac{2\pi}{\lambda} (x \sin\theta \cos\phi + y \sin\theta \sin\phi + z \cos\theta)\right], \quad (4)$$

where separations

$$x = x_1 - x_2,$$

$$y = y_1 - y_2,$$

$$z = z_1 - z_2. \quad (5)$$

If the arrivals from different directions are uncorrelated, the spatial correlation (at frequency f) between two points separated by x, y, z is then given by integrating over all angular space,

$$G_f(x, y, z) = \int_0^\pi d\theta \int_{-\pi}^\pi d\phi \sin\theta N_f(\theta, \phi) \times$$

$$\times \exp\left[i\frac{2\pi}{\lambda} (x \sin\theta \cos\phi + y \sin\theta \sin\phi + z \cos\theta)\right]. \quad (6)$$

The problem of interest is: given spatial correlation $G_f(x, y, z)$ versus x, y, z (or restricted slices of $G_f(x, y, z)$), solve for noise field directionality $N_f(\theta, \phi)$ (or smoothed versions of

$N_f(\theta, \phi)$). That is, invert integral equation (6) for noise field directionality $N_f(\theta, \phi)$ or for whatever can be determined. There are three cases that must be distinguished, namely, linear, planar, and volumetric arrays.

LINEAR ARRAY

It is most convenient mathematically to locate the line array along the z axis, that is, $x = y = 0$. Then the exponential in (6) is independent of ϕ , and (6) reduces to*

$$\begin{aligned}
 G_f(z) &= \int_0^\pi d\theta \int_{-\pi}^\pi d\phi \sin\theta N_f(\theta, \phi) \exp\left(i\frac{2\pi}{\lambda} z \cos\theta\right) = \\
 &= \int_0^\pi d\theta \sin\theta \bar{N}_f(\theta) \exp\left(i\frac{2\pi}{\lambda} z \cos\theta\right), \quad (7)
 \end{aligned}$$

where

$$\bar{N}_f(\theta) = \int_{-\pi}^\pi d\phi N_f(\theta, \phi) \quad \text{for } 0 \leq \theta \leq \pi \quad (8)$$

is the integrated or averaged noise field directionality, and $G_f(z)$ is the one-dimensional spatial correlation at separation z along the line, both functions evaluated at frequency f . $G_f(z)$ is the only second-order function that can be measured (or estimated) from the line array, and $\bar{N}_f(\theta)$ is the only field function that can be determined. There is no possibility of undoing the integration of (8); this is a mathematical representation of the inherent conical symmetry of response of

*The case where the line array is located on the x axis is treated in appendix A.

a linear array. It is also one reason for choosing the line array to lie along the $\theta = 0$ axis, since all the two-dimensional field information is conveniently collapsed into a one-dimensional function of θ alone. See appendix A for the problems associated with choosing a different coordinate system.

SOLUTION OF INTEGRAL EQUATION

To solve integral equation (7) for noise field directionality $\bar{N}_f(\theta)$, consider the following:

$$\begin{aligned} & \int_{-\infty}^{+\infty} dz \exp\left(-i\frac{2\pi}{\lambda} u z\right) G_f(z) = \\ &= \int_0^{\pi} d\theta \sin\theta \bar{N}_f(\theta) \int_{-\infty}^{+\infty} dz \exp\left(-i\frac{2\pi}{\lambda} z (u - \cos\theta)\right) = \\ &= \int_0^{\pi} d\theta \sin\theta \bar{N}_f(\theta) \lambda \delta(u - \cos\theta), \end{aligned} \quad (9)$$

where δ is the delta function. Now let $t = \cos\theta$, which is a one-to-one transformation for $0 \leq \theta \leq \pi$, to get

$$\begin{aligned} & \int_{-\infty}^{+\infty} dz \exp\left(-i\frac{2\pi}{\lambda} u z\right) G_f(z) = \lambda \int_{-1}^1 dt \bar{N}_f(\arccos(t)) \delta(u - t) = \\ &= \begin{cases} \lambda \bar{N}_f(\arccos(u)) & \text{for } |u| < 1 \\ 0 & \text{for } |u| > 1 \end{cases}, \end{aligned} \quad (10)$$

where \arccos is the principal value inverse cosine function.

That is,

$$\bar{N}_f(\arccos(u)) = \frac{1}{\lambda} \int_{-\infty}^{+\infty} dz \exp\left(-i\frac{2\pi}{\lambda} u z\right) G_f(z) \quad \text{for } |u| < 1, \quad (11a)$$

or

$$\bar{N}_f(\theta) = \frac{1}{\lambda} \int_{-\infty}^{+\infty} dz \exp\left(-i\frac{2\pi}{\lambda} \cos\theta z\right) G_f(z) \quad \text{for } 0 \leq \theta \leq \pi. \quad (11b)$$

Compare (11b) with starting point (7).

Thus, given the spatial correlation $G_f(z)$ for all possible separations z along the line array, the integrated noise field directionality \bar{N}_f is available via a single one-dimensional Fourier transform.

EXAMPLE

An example is informative at this point. Let

$$\bar{N}_f(\theta) = \delta(\theta - \theta_0), \quad 0 < \theta_0 < \pi.$$

Then the spatial correlation is, from (7),

$$G_f(z) = \sin\theta_0 \exp\left(i\frac{2\pi}{\lambda} z \cos\theta_0\right).$$

Observe that as $\theta_0 \rightarrow 0$ or π , that is, endfire of the line array, the strength of this quantity decays to zero, due to the $\sin\theta$ term in the area element in (1). Substitution of correlation $G_f(z)$ into (11b) yields noise field directionality

$$\bar{N}_f(\theta) = \sin\theta_0 \delta(\cos\theta - \cos\theta_0) \quad \text{for } 0 \leq \theta \leq \pi.$$

Now the delta function here is located at $\theta = \theta_0$ and has area $1/\sin\theta_0$. Thus, $\bar{N}_f(\theta)$ is $\delta(\theta - \theta_0)$, as it should be; however, the trigonometric form shows $\bar{N}_f(\theta)$ as the product of two terms, the first of which tends to zero as $\theta_0 \rightarrow 0$ or π , and the second of which has an area that tends to infinity as $\theta_0 \rightarrow 0$ or π . This behavior will re-occur in the following investigations.

We have employed the following useful property above: if $g(x)$ has an isolated zero at x_0 , then in the neighborhood of x_0 ,

$$\delta(g(x)) = \delta(g'(x_0)(x-x_0)) = \frac{1}{|g'(x_0)|} \delta(x - x_0).$$

That is, the area of the delta function at x_0 is equal to the reciprocal absolute slope of the argument at x_0 , if nonzero.

DISCRETE INFINITE-LENGTH ARRAY

If samples of spatial correlation $G_f(z)$ at increment Δ in z are available, an approximation to (11a) is afforded, for $|u| < 1$, by

$$\bar{N}_f(\arccos(u)) \approx \frac{\Delta}{\lambda} \sum_{n=-\infty}^{+\infty} \exp\left(-i \frac{2\pi}{\lambda} u \Delta n\right) G_f(\Delta n), \quad (12)$$

the right-hand side of which has period λ/Δ in u . Since the integrated noise field directionality in (11a) is defined on an interval of length 2, that is, $-1 < u < 1$, aliasing will occur in approximation (12) unless $\Delta < \lambda/2$. Thus, the spacing Δ , between samples of $G_f(z)$, must be less than a half-wavelength at the temporal-frequency f of interest. This is presumed true henceforth.

Now if u is restricted to the values

$$u_m = \frac{m}{M} \frac{\lambda}{\Delta} \quad \text{for} \quad -\frac{M}{2} \leq m \leq \frac{M}{2} - 1, \quad (13)$$

which cover a full period, there follows, for $\left|\frac{m}{M} \frac{\lambda}{\Delta}\right| \leq 1$,

$$\bar{N}_f\left(\arccos\left(\frac{m}{M} \frac{\lambda}{\Delta}\right)\right) \approx \frac{\Delta}{\lambda} \sum_{n=-\infty}^{+\infty} \exp(-i 2\pi m n / M) G_f(\Delta n). \quad (14a)$$

The sum on the right-hand side can be accomplished via an M -point fast Fourier transform when collapsing is employed [5; page 5]. The resultant angles at which $\bar{N}_f(\theta)$ is available are

$$\theta_m = \arccos\left(\frac{m}{M} \frac{\lambda}{\Delta}\right), \quad \text{or} \quad \cos \theta_m = \frac{m}{M} \frac{\lambda}{\Delta} \quad \text{for} \quad -\frac{M}{2} \leq m \leq \frac{M}{2} - 1, \quad (14b)$$

provided that $\frac{|m|}{M} \frac{\lambda}{\Delta} \leq 1$. These values are equally spaced in $\cos\theta$ space.

The right-hand side of (12) can be rewritten in the form
[5; pages 3-4]

$$\begin{aligned} & \frac{1}{\lambda} \int_{-\infty}^{+\infty} dz \exp\left(-i \frac{2\pi}{\lambda} u z\right) G_f(z) \Delta \sum_{n=-\infty}^{+\infty} \delta(z - \Delta n) = \\ & = \bar{N}_f(\arccos(u)) \otimes \sum_{n=-\infty}^{+\infty} \delta\left(u - \frac{n\lambda}{\Delta}\right) = \sum_{n=-\infty}^{+\infty} \bar{N}_f\left(\arccos\left(u - \frac{n\lambda}{\Delta}\right)\right), \quad (15a) \end{aligned}$$

where \otimes denotes convolution. The separation of these aliased lobes (for $n \neq 0$) is λ/Δ on the u scale; then, since the extent of $\bar{N}_f(\arccos(u))$ is 2 on the u scale, overlapped aliasing lobes do not occur if $\Delta < \lambda/2$. This is a mathematical back-up to the claim under (12).

DISCRETE FINITE-LENGTH ARRAY

The effect of a finite-length array can easily be incorporated by modifying (15a), so as to include weighting $w(z)$. Then, we have, for the estimated noise field directionality,

$$\begin{aligned} \frac{1}{\lambda} \int_{-\infty}^{+\infty} dz \exp\left(-i \frac{2\pi}{\lambda} u z\right) G_f(z) \Delta \sum_{n=-\infty}^{+\infty} \delta(z - \Delta n) w(z) = \\ = \bar{N}_f(\arccos(u)) \otimes \sum_{n=-\infty}^{+\infty} W\left(u - \frac{n\lambda}{\Delta}\right), \end{aligned} \quad (15b)$$

where window

$$W(u) = \frac{1}{\lambda} \int_{-\infty}^{+\infty} dz \exp\left(-i \frac{2\pi}{\lambda} u z\right) w(z). \quad (15c)$$

Thus, not only is the noise field directionality aliased at separations λ/Δ in u , but, in addition, it is smoothed by window W . Sampling, per se, does not distort the estimated directionality, if done finely enough, that is, $\Delta < \lambda/2$. However, the finite length of the array always causes smearing, with a window width of the order of λ/L_z , where L_z is the effective length of weighting $w(z)$.

PLANAR ARRAY

It is now most advantageous mathematically to locate the planar array in the x, y plane, that is, at $z = 0$. Then the exponential in (6) is independent of $\cos\theta$, and (6) reduces to

$$G_f(x, y) = \int_0^\pi d\theta \int_{-\pi}^\pi d\phi \sin\theta N_f(\theta, \phi) \exp\left(i\frac{2\pi}{\lambda} \sin\theta (x \cos\phi + y \sin\phi)\right) =$$

$$= \int_0^{\pi/2} d\theta \int_{-\pi}^\pi d\phi \sin\theta \tilde{N}_f(\theta, \phi) \exp\left(i\frac{2\pi}{\lambda} \sin\theta (x \cos\phi + y \sin\phi)\right), \quad (16)$$

where

$$\tilde{N}_f(\theta, \phi) = N_f(\theta, \phi) + N_f(\pi - \theta, \phi)$$

$$\text{for } 0 \leq \theta \leq \pi/2, \quad -\pi < \phi \leq \pi. \quad (17)$$

\tilde{N}_f is the sum of the elemental components in symmetrically-arriving rays on opposite sides of the planar array; recall that $\theta = \pi/2$ now corresponds to the plane of the array. Spatial correlation $G_f(x, y)$ is the only function that can be measured (or estimated) from the planar array, and $\tilde{N}_f(\theta, \phi)$ is the only field directionality function that can be determined. There is no possibility of undoing the summation of (17); this is a mathematical representation of the inherent two-sided symmetric response of a planar array. It is also one reason for choosing the planar array to lie along the $\theta = \pi/2$ plane, since the totality of the two-dimensional field information is conveniently collapsed into a one-sided function of θ , that is, $0 \leq \theta \leq \pi/2$.

SOLUTION OF INTEGRAL EQUATION

Consider the two-dimensional Fourier transform of (16),

$$\begin{aligned}
 I(u, v) &= \iint_{-\infty}^{+\infty} dx \, dy \exp\left(-i\frac{2\pi}{\lambda} (ux + vy)\right) G_f(x, y) = \\
 &= \int_0^{\pi/2} d\theta \int_{-\pi}^{\pi} d\phi \sin\theta \tilde{N}_f(\theta, \phi) \lambda^2 \delta(u - \sin\theta \cos\phi) \delta(v - \sin\theta \sin\phi).
 \end{aligned}
 \tag{18}$$

Let

$$\alpha = \sin\theta \cos\phi, \quad \beta = \sin\theta \sin\phi \quad \text{for } 0 \leq \theta \leq \pi/2, \quad -\pi < \phi \leq \pi. \tag{19}$$

These relations can be inverted by using

$$\alpha + i\beta = \sin\theta \exp(i\phi), \tag{20}$$

to give

$$\sin\theta = |\alpha + i\beta| = (\alpha^2 + \beta^2)^{1/2}, \quad \phi = \arg(\alpha + i\beta). \tag{21}$$

Thus, (19) is a one-to-one two-dimensional transformation in the ranges $0 \leq \theta \leq \pi/2$, $-\pi < \phi \leq \pi$ allowed in (18). From (19) and (21), the Jacobian is

$$\begin{aligned}
 \frac{\partial(\alpha, \beta)}{\partial(\theta, \phi)} &= \begin{vmatrix} \cos\theta \cos\phi & -\sin\theta \sin\phi \\ \cos\theta \sin\phi & \sin\theta \cos\phi \end{vmatrix} = \\
 &= \sin\theta \cos\theta = (\alpha^2 + \beta^2)^{1/2} (1 - \alpha^2 - \beta^2)^{1/2}.
 \end{aligned}
 \tag{22}$$

Substitution of these results in (18) yields

$$I(u,v) = \lambda^2 \iint_{C_1} d\alpha d\beta F(\alpha, \beta) (1 - \alpha^2 - \beta^2)^{-\frac{1}{2}} \delta(u-\alpha) \delta(v-\beta) =$$

$$= \begin{cases} \lambda^2 F(u,v) (1 - u^2 - v^2)^{-\frac{1}{2}} & \text{for } u^2 + v^2 < 1 \\ 0 & \text{otherwise} \end{cases}, \quad (23)$$

where C_1 is a circle of radius 1 located at the origin, and

$$F(\alpha, \beta) = \tilde{N}_f(\arcsin(|\alpha + i\beta|), \arg(\alpha + i\beta)). \quad (24)$$

Here, \arcsin is the principal value inverse sine function. From (23), (24), and (18), the noise field directionality is

$$\tilde{N}_f(\arcsin(|u + iv|), \arg(u + iv)) =$$

$$= \frac{(1 - u^2 - v^2)^{\frac{1}{2}}}{\lambda^2} \iint_{-\infty}^{+\infty} dx dy \exp\left(-i\frac{2\pi}{\lambda} (ux + vy)\right) G_f(x, y)$$

$$\text{for } u^2 + v^2 < 1. \quad (25)$$

An alternative form is available by letting

$$u = \sin\theta \cos\phi, \quad v = \sin\theta \sin\phi \quad \text{for } 0 \leq \theta \leq \pi/2, \quad -\pi < \phi \leq \pi, \quad (26)$$

namely

$$\tilde{N}_f(\theta, \phi) = \frac{\cos\theta}{\lambda^2} \iint_{-\infty}^{+\infty} dx dy \exp\left(-i\frac{2\pi}{\lambda} \sin\theta (x \cos\phi + y \sin\phi)\right) G_f(x, y)$$

$$\text{for } 0 \leq \theta \leq \pi/2, \quad -\pi < \phi \leq \pi. \quad (27)$$

It is interesting to compare this form with starting result (16). An alternative, when the planar array lies in the $y = 0$ plane, is given in appendix B.

BEHAVIOR NEAR PLANE OF ARRAY

At first sight, the presence of the $\cos\theta$ term in (27) would appear to be a problem for $\theta = \pi/2$, which is the plane of the array. However, the following example illustrates what is happening; let

$$\tilde{N}_f(\theta, \phi) = \delta(\theta - \theta_0) \delta(\phi - \phi_0) \quad \text{for } 0 < \theta_0 < \pi/2, -\pi < \phi_0 \leq \pi.$$

Then (16) yields spatial correlation

$$G_f(x, y) = \sin\theta_0 \exp\left(i\frac{2\pi}{\lambda} \sin\theta_0 (x \cos\phi_0 + y \sin\phi_0)\right).$$

The strength of this quantity tends to zero as $\theta_0 \rightarrow 0$. Substitution of this $G_f(x, y)$ into (27) yields noise field directionality

$$\begin{aligned} \tilde{N}_f(\theta, \phi) = \sin\theta_0 \cos\theta \delta(\sin\theta \cos\phi - \sin\theta_0 \cos\phi_0) \times \\ \times \delta(\sin\theta \sin\phi - \sin\theta_0 \sin\phi_0). \end{aligned}$$

By use of the property

$$\delta(ax + by) \delta(cx + dy) = \frac{\delta(x) \delta(y)}{|ad - bc|},$$

it may be shown that $\tilde{N}_f(\theta, \phi)$ is $\delta(\theta - \theta_0) \delta(\phi - \phi_0)$, as expected; however, the trigonometric form shows \tilde{N}_f as the product of two terms, the first of which tends to 0 as $\theta_0 \rightarrow 0$ or $\pi/2$, and the second of which has impulses with area which tends to infinity as $\theta_0 \rightarrow 0$ or $\pi/2$. Thus, the $\sin\theta_0$ and $\cos\theta$ terms are not a problem since they are compensated by multiplicative terms; however, they may lead to inaccuracies in numerical computation.

DISCRETE INFINITE-LENGTH ARRAY

The form in (25) gives the noise field directionality sum \tilde{N}_f , defined in (17), as a double Fourier transform of the two-dimensional spatial correlation function $G_f(x, y)$. If samples of $G_f(x, y)$ at increments Δ_x in x and Δ_y in y , respectively, are available, an approximation to (25) is afforded, for $u^2 + v^2 < 1$, by

$$\tilde{N}_f(\arcsin(|u + iv|), \arg(u + iv)) \approx \frac{(1 - u^2 - v^2)^{\frac{1}{2}}}{\lambda^2} \Delta_x \Delta_y \times \\ \times \sum_{k=-\infty}^{+\infty} \sum_{j=-\infty}^{+\infty} \exp\left(-i \frac{2\pi}{\lambda} (u \Delta_x k + v \Delta_y j)\right) G_f(\Delta_x k, \Delta_y j). \quad (28)$$

The summation on the right-hand side of (28) has periods λ/Δ_x in u , and λ/Δ_y in v . Since the sum \tilde{N}_f is defined within the circle $u^2 + v^2 < 1$, overlapped aliasing lobes will occur in (28) unless $\Delta_x < \lambda/2$ and $\Delta_y < \lambda/2$; that is, the spacings between samples of $G_f(x, y)$ must be less than a half-wavelength at the temporal-frequency f of interest. We presume this to be true henceforth.

Now if we restrict u and v in (28) to the values

$$u_m = \frac{m}{M} \frac{\lambda}{\Delta_x} \quad \text{for} \quad -\frac{M}{2} \leq m \leq \frac{M}{2} - 1, \\ v_n = \frac{n}{N} \frac{\lambda}{\Delta_y} \quad \text{for} \quad -\frac{N}{2} \leq n \leq \frac{N}{2} - 1, \quad (29)$$

both of which cover full periods in u and v , respectively, there follows

$$\tilde{N}_f(\arcsin(|u_m + iv_n|), \arg(u_m + iv_n)) \approx \frac{(1 - u_m^2 - v_n^2)^{\frac{1}{2}}}{\lambda^2} \times \\ \times \Delta_x \Delta_y \sum_{k=-\infty}^{+\infty} \sum_{j=-\infty}^{+\infty} \exp(-i2\pi mk/M - i2\pi nj/N) G_f(\Delta_x k, \Delta_y j), \quad (30)$$

provided that

$$|u_m + iv_n| = \left| \frac{m}{M} \frac{\lambda}{\Delta_x} + i \frac{n}{N} \frac{\lambda}{\Delta_y} \right| \leq 1. \quad (31)$$

The double sum in (30) can be accomplished as an $M \times N$ two-dimensional fast Fourier transform, when collapsing is employed [5; page 5]. The resultant angles at which noise field directionality $\tilde{N}_f(\theta, \phi)$ is available are

$$0 \leq \theta_{mn} = \arcsin \left| \frac{m}{M} \frac{\lambda}{\Delta_x} + i \frac{n}{N} \frac{\lambda}{\Delta_y} \right| \leq \frac{\pi}{2}, \\ -\pi < \phi_{mn} = \arg \left(\frac{m}{M} \frac{\lambda}{\Delta_x} + i \frac{n}{N} \frac{\lambda}{\Delta_y} \right) \leq \pi, \quad (32)$$

or

$$\sin \theta_{mn} = \left| \frac{m}{M} \frac{\lambda}{\Delta_x} + i \frac{n}{N} \frac{\lambda}{\Delta_y} \right| = \\ = \left[\left(\frac{m}{M} \frac{\lambda}{\Delta_x} \right)^2 + \left(\frac{n}{N} \frac{\lambda}{\Delta_y} \right)^2 \right]^{\frac{1}{2}}, \quad (33a)$$

where

$$-\frac{M}{2} \leq m \leq \frac{M}{2} - 1, \quad -\frac{N}{2} \leq n \leq \frac{N}{2} - 1, \quad (33b)$$

but remembering that (31) must remain true.

The right-hand side of (28) can be re-written in the form
[5; pages 3-4]

$$\begin{aligned}
 & \frac{(1 - u^2 - v^2)^{\frac{1}{2}}}{\lambda^2} \iint_{-\infty}^{+\infty} dx \, dy \exp\left(-i\frac{2\pi}{\lambda} (ux + vy)\right) G_f(x, y) \times \\
 & \times \Delta_x \sum_{k=-\infty}^{+\infty} \delta(x - \Delta_x k) \Delta_y \sum_{j=-\infty}^{+\infty} \delta(y - \Delta_y j) = \\
 & = \tilde{N}_f(\arcsin(|u + iv|), \arg(u + iv)) \otimes \\
 & \otimes \sum_{k=-\infty}^{+\infty} \delta\left(u - \frac{k\lambda}{\Delta_x}\right) \otimes \sum_{j=-\infty}^{+\infty} \delta\left(v - \frac{j\lambda}{\Delta_y}\right). \quad (34a)
 \end{aligned}$$

The separations of the aliased lobes (for $(k, j) \neq (0, 0)$) are λ/Δ_x on the u scale and λ/Δ_y on the v scale. Then, since the extent of the noise field directionality \tilde{N}_f is $u^2 + v^2 < 1$, overlapped aliasing lobes do not occur if $\Delta_x < \lambda/2$ and $\Delta_y < \lambda/2$. This is a quantitative restatement of the claims made in the sequel to (28).

DISCRETE FINITE-LENGTH ARRAY

The effect of finite lengths in the x and y directions can be incorporated by modifying (34a) so as to include weighting $w(x,y)$. Then, we have, for the estimated noise field directionality,

$$\begin{aligned} & \frac{(1 - u^2 - v^2)^{\frac{1}{2}}}{\lambda^2} \iint_{-\infty}^{+\infty} dx \, dy \exp\left(-i\frac{2\pi}{\lambda} (ux + vy)\right) G_f(x,y) \times \\ & \times \Delta_x \sum_{k=-\infty}^{+\infty} \delta(x - \Delta_x k) \Delta_y \sum_{j=-\infty}^{+\infty} \delta(y - \Delta_y j) w(x,y) = \\ & = \tilde{N}_f(\arcsin(|u + iv|), \arg(u + iv)) \otimes^{uv} \sum_{k=-\infty}^{+\infty} \sum_{j=-\infty}^{+\infty} W\left(u - \frac{k\lambda}{\Delta_x}, v - \frac{j\lambda}{\Delta_y}\right), \end{aligned} \quad (34b)$$

where window

$$W(u,v) = \frac{1}{\lambda^2} \iint_{-\infty}^{+\infty} dx \, dy \exp\left(-i\frac{2\pi}{\lambda} (ux + vy)\right) w(x,y). \quad (34c)$$

Thus, not only is the noise field directionality aliased at separations λ/Δ_x in u and λ/Δ_y in v , but, in addition, it is smoothed by window W . Sampling alone does not distort the estimated directionality if done with $\Delta_x < \lambda/2$ and $\Delta_y < \lambda/2$; see (34a). However, the finite lengths of the array always smears, with window widths of the order of λ/L_x in u and λ/L_y in v , where L_x and L_y are the effective lengths of weighting $w(x,y)$ in x and y , respectively.

VOLUMETRIC ARRAY

We now have the full version (6):

$$G_f(x, y, z) = \int_0^\pi d\theta \int_{-\pi}^\pi d\phi \sin\theta N_f(\theta, \phi) \times \\ \times \exp\left(i\frac{2\pi}{\lambda} (x \sin\theta \cos\phi + y \sin\theta \sin\phi + z \cos\theta)\right). \quad (35)$$

However, since noise field directionality N_f is a function of two variables, while spatial correlation G_f has three arguments, some of the information in G_f is superfluous and must be reduced or collapsed in some fashion.

SOLUTION OF INTEGRAL EQUATION

We begin by defining triple Fourier transform

$$I(u, v, w) = \int_{-\infty}^{+\infty} \int_{-\infty}^{+\infty} \int_{-\infty}^{+\infty} dx dy dz q(z) \exp\left(-i\frac{2\pi}{\lambda} (ux + vy + wz)\right) G_f(x, y, z) = \\ = \int_0^\pi d\theta \int_{-\pi}^\pi d\phi \sin\theta N_f(\theta, \phi) \lambda^2 \delta(u - \sin\theta \cos\phi) \delta(v - \sin\theta \sin\phi) \times \\ \times Q(w - \cos\theta), \quad (36)$$

where we use a weighting $q(z)$ on the z variable, and define

$$Q(t) = \int_{-\infty}^{+\infty} dz \exp(-i2\pi tz/\lambda) q(z). \quad (37)$$

(If $q(z) = 1$ for all z , then $Q(t) = \lambda \delta(t)$.)

We now break the right-hand side of (36) into two parts according to

$$\int_0^{\pi} d\theta \int_{-\pi}^{\pi} d\phi = \int_0^{\pi/2} d\theta \int_{-\pi}^{\pi} d\phi + \int_{\pi/2}^{\pi} d\theta \int_{-\pi}^{\pi} d\phi, \quad (38)$$

and in each region, we make the change of variable used in (19) and the sequel, namely

$$\alpha = \sin\theta \cos\phi, \quad \beta = \sin\theta \sin\phi. \quad (39)$$

Then $\phi = \arg(\alpha + i\beta)$, while

$$\theta = \begin{cases} \arcsin(|\alpha + i\beta|) & \text{for } 0 \leq \theta \leq \pi/2 \\ \pi - \arcsin(|\alpha + i\beta|) & \text{for } \pi/2 \leq \theta \leq \pi \end{cases} \quad (40)$$

and

$$\cos\theta = \begin{cases} (1 - \alpha^2 - \beta^2)^{1/2} & \text{for } 0 \leq \theta \leq \pi/2 \\ -(1 - \alpha^2 - \beta^2)^{1/2} & \text{for } \pi/2 \leq \theta \leq \pi \end{cases}. \quad (41)$$

Define, for future use,

$$s(\alpha, \beta) = (1 - \alpha^2 - \beta^2)^{1/2} \quad \text{for } \alpha^2 + \beta^2 \leq 1. \quad (42)$$

Using these results in (36), there follows

$$\begin{aligned} I(u, v, w) = & \lambda^2 \iint_{C_1} d\alpha d\beta s(\alpha, \beta)^{-1} F_1(\alpha, \beta) \delta(u - \alpha) \delta(v - \beta) Q(w - s(\alpha, \beta)) \\ & + \lambda^2 \iint_{C_1} d\alpha d\beta s(\alpha, \beta)^{-1} F_2(\alpha, \beta) \delta(u - \alpha) \delta(v - \beta) Q(w + s(\alpha, \beta)), \end{aligned} \quad (43)$$

where C_1 is a circle of radius 1 located at the origin, and

$$\left. \begin{aligned} F_1(\alpha, \beta) &= N_f(\arcsin(|\alpha + i\beta|), \arg(\alpha + i\beta)) \\ F_2(\alpha, \beta) &= N_f(\pi - \arcsin(|\alpha + i\beta|), \arg(\alpha + i\beta)) \end{aligned} \right\} \text{for } |\alpha + i\beta| \leq 1. \quad (44)$$

Evaluating the integrals in (43), we have

$$I(u, v, w) = \lambda^2 s(u, v)^{-1} \left[F_1(u, v) Q(w - s(u, v)) + F_2(u, v) Q(w + s(u, v)) \right] \quad \text{for } u^2 + v^2 < 1. \quad (45)$$

SIMULTANEOUS EQUATIONS

If we evaluate the triple Fourier transform in (36) at two different values of w , we have

$$\frac{s(u, v)}{\lambda^2} I(u, v, w_1) = F_1(u, v) Q(w_1 - s(u, v)) + F_2(u, v) Q(w_1 + s(u, v)) \quad (46)$$

and

$$\frac{s(u, v)}{\lambda^2} I(u, v, w_2) = F_1(u, v) Q(w_2 - s(u, v)) + F_2(u, v) Q(w_2 + s(u, v)). \quad (47)$$

Also, if we define

$$\begin{aligned} Q_n(+) &= Q(w_n + s(u, v)) , \\ Q_n(-) &= Q(w_n - s(u, v)) , \end{aligned} \quad (48)$$

and denominator

$$D = Q_1(-) Q_2(+) - Q_1(+) Q_2(-), \quad (49)$$

the solutions to (46) and (47) are

$$\left. \begin{aligned} F_1(u,v) &= \frac{s(u,v)}{\lambda^2 D} \left(Q_2(+) I(u,v,w_1) - Q_1(+) I(u,v,w_2) \right) \\ F_2(u,v) &= \frac{s(u,v)}{\lambda^2 D} \left(Q_1(-) I(u,v,w_2) - Q_2(-) I(u,v,w_1) \right) \end{aligned} \right\} \begin{aligned} &\text{for} \\ &u^2 + v^2 < 1, \end{aligned} \quad (50)$$

provided that $D \neq 0$. Function s is defined in (42).

There is a great deal of leeway in these solutions. Namely, $Q(t)$ in (37) is arbitrary, and the values w_1 and w_2 are arbitrary as well; the only restriction is that D in (49) not be zero. In the special case where weighting $q(z)$ in (36) is real and even, then $Q(t)$ in (37) is also real and even; we presume this to be the case henceforth. If we then choose $w_2 = -w_1$, (49) becomes

$$D = Q^2(w_1 - s(u,v)) - Q^2(w_1 + s(u,v)). \quad (51)$$

If the effective length of weighting $q(z)$ is L_z , a representative plot of $Q^2(t)$ is displayed in figure 2. For small s , a good location for w_1 is at the point where $Q^2(t)$ has its maximum slope. For larger s , a value for w_1 near s would guarantee a large value for D in (51).

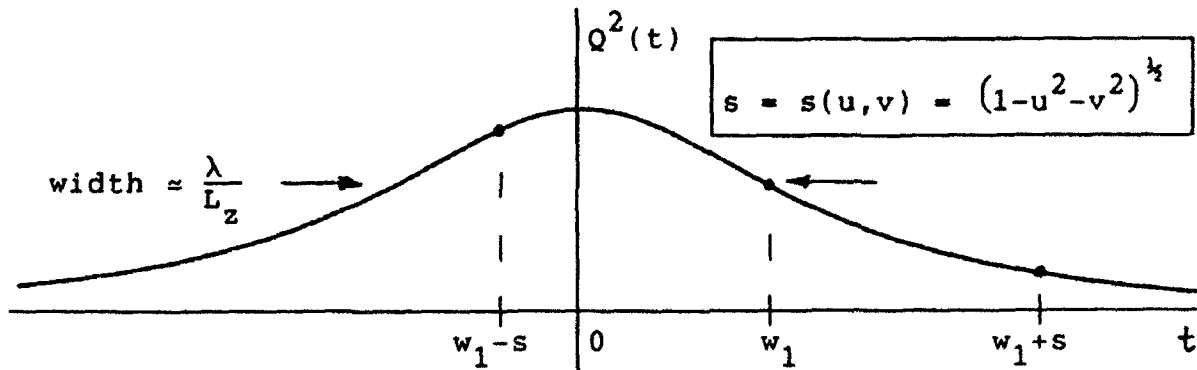


Figure 2. Window Function Q^2

ANGULAR REPRESENTATIONS

If we make the substitutions

$$u = \sin\theta \cos\phi, \quad v = \sin\theta \sin\phi \quad \text{for } 0 \leq \theta \leq \pi/2, \quad -\pi < \phi \leq \pi, \quad (52)$$

then (42), (44), and (51) yield

$$\left. \begin{aligned} s(\sin\theta \cos\phi, \sin\theta \sin\phi) &= \cos\theta \\ F_1(\sin\theta \cos\phi, \sin\theta \sin\phi) &= N_f(\theta, \phi) \\ F_2(\sin\theta \cos\phi, \sin\theta \sin\phi) &= N_f(\pi - \theta, \phi) \\ D &= Q^2(w_1 - \cos\theta) - Q^2(w_1 + \cos\theta) \end{aligned} \right\} \quad \begin{array}{l} \text{for} \\ 0 \leq \theta \leq \pi/2, \quad -\pi < \phi \leq \pi. \end{array} \quad (53)$$

Then (50) becomes

$$N_f(\theta, \phi) = \frac{\cos\theta}{\lambda^2} \frac{Q(w_1 - \cos\theta) I(+) - Q(w_1 + \cos\theta) I(-)}{Q^2(w_1 - \cos\theta) - Q^2(w_1 + \cos\theta)}, \quad (54a)$$

$$N_f(\pi - \theta, \phi) = \frac{\cos\theta}{\lambda^2} \frac{Q(w_1 - \cos\theta) I(-) - Q(w_1 + \cos\theta) I(+)}{Q^2(w_1 - \cos\theta) - Q^2(w_1 + \cos\theta)}, \quad (54b)$$

$$\text{for } 0 \leq \theta \leq \pi/2, \quad -\pi < \phi \leq \pi,$$

where we define

$$\begin{aligned} I(\pm) &= I(\sin\theta \cos\phi, \sin\theta \sin\phi, \pm w_1) = \int_{-\infty}^{+\infty} \int \int dx \, dy \, dz \, q(z) \times \\ &\times \exp\left(-i \frac{2\pi}{\lambda} (x \sin\theta \cos\phi + y \sin\theta \sin\phi \pm z w_1)\right) G_f(x, y, z), \quad (55) \end{aligned}$$

upon use of (36). We repeat that these results for the noise field directionality apply only for $Q(t)$ real and even; otherwise, $Q(t)$ and w_1 are arbitrary.

An alternative form to (54b) is available, if desired, by the substitution $\theta' = \pi - \theta$, namely

$$N_f(\theta', \phi) = \frac{\cos \theta'}{\lambda^2} \frac{Q(w_1 + \cos \theta') I'(-) - Q(w_1 - \cos \theta') I'(+)}{Q^2(w_1 - \cos \theta') - Q^2(w_1 + \cos \theta')}$$

for $\pi/2 \leq \theta' \leq \pi, -\pi < \phi \leq \pi,$ (56)

where

$$I'(\pm) = I(\sin \theta' \cos \phi, \sin \theta' \sin \phi, \pm w_1). \quad (57)$$

The most extensive calculation required here is that given by (55); rewriting it differently,

$$I(u, v, \pm w_1) = \int_{-\infty}^{+\infty} dx \int_{-\infty}^{+\infty} dy \exp\left(-i \frac{2\pi}{\lambda} (ux + vy)\right) \times$$

$$\times \int_{-\infty}^{+\infty} dz \exp\left(-i \frac{2\pi}{\lambda} (\pm w_1)z\right) q(z) G_f(x, y, z). \quad (58)$$

The innermost integral, the Fourier transform on z , only needs to be accomplished for the two values $\pm w_1$, whereas the outer integrals must be done for ranges of u and v . This is the collapsing operation alluded to under (35). On the other hand, the inner integral must be repeated for every x, y value of

interest; nevertheless, (58) is not as difficult as a three-dimensional Fourier transform.

An example of this procedure for the volumetric array is carried out in appendix C; it illustrates the care that must be taken with respect to the θ variable in (54).

SUMMARY

The noise field directionality for the cases of one-, two-, and three-dimensional arrays have been solved for, explicitly, in terms of the appropriate spatial correlation available in each case. In the one-dimensional case, only the polar directionality can be determined, while in the two-dimensional case, the sum of symmetrically arriving rays on both sides of the planar array can be evaluated. For the three-dimensional case, all ambiguity can be eliminated, but the overdetermined nature of the problem requires some collapsing of information and leaves many options to consider. For example, one could let the volumetric array be a thin-shelled sphere; however, the resulting two-dimensional integral equation for the noise field directionality cannot be solved explicitly. The attractive feature of large stacked planar arrays is that it permits the use of Fourier transforms and, therefore, an explicit expression for the noise field directionality in terms of the three-dimensional spatial correlation. Also, Fourier transforms are efficiently evaluated by the use of fast Fourier transforms.

In this investigation, we have presumed exact knowledge of the spatial correlation $G_f(z)$ or $G_f(x,y)$ or $G_f(x,y,z)$, depending on the dimensionality of the array employed. In practice, G_f must be estimated from measurements made from a physical array; in this case, maximum advantage should be taken of the stationarity and homogeneity of the noise field. Thus, for a line array of equi-spaced elements, $G_f(n\Delta)$ should be estimated

from all the available pairs of elements that have separation $n\Delta$ in space and over the total available observation time that data have been recorded on all elements.

A comparison [6] is underway between the methods of this report and the Fourier series method given in [4], at least for the line array. Results are similar, but not identical; in particular, the aliasing of the Fourier series method is more severe than for the Fourier integral approach.

APPENDIX A. ALTERNATIVE LOCATION OF LINEAR ARRAY

If we locate the line array along the x axis, that is, $y = z = 0$, then (6) reduces to

$$\begin{aligned} G_f(x) &= \int_0^{\pi} d\theta \int_{-\pi}^{\pi} d\phi \sin\theta N_f(\theta, \phi) \exp\left(i\frac{2\pi}{\lambda} x \sin\theta \cos\phi\right) = \\ &= \int_0^{\pi/2} d\theta \int_0^{\pi} d\phi \sin\theta \check{N}_f(\theta, \phi) \exp\left(i\frac{2\pi}{\lambda} x \sin\theta \cos\phi\right), \quad (A-1) \end{aligned}$$

where

$$\check{N}_f(\theta, \phi) = N_f(\theta, \phi) + N_f(\pi - \theta, \phi) + N_f(\theta, -\phi) + N_f(\pi - \theta, -\phi) \quad (A-2)$$

for $0 \leq \theta \leq \pi/2$, $0 \leq \phi \leq \pi$. Therefore, Fourier transform

$$\begin{aligned} I(u) &= \int_{-\infty}^{+\infty} dx \exp\left(-i\frac{2\pi}{\lambda} u x\right) G_f(x) = \\ &= \int_0^{\pi/2} d\theta \int_0^{\pi} d\phi \sin\theta \check{N}_f(\theta, \phi) \lambda \delta(u - \sin\theta \cos\phi). \quad (A-3) \end{aligned}$$

Now let

$$s = \sin\theta, \quad t = \cos\phi, \quad (A-4)$$

which are one-to-one transformations in the ranges allowed in integral (A-3). Then

$$I(u) = \lambda \int_0^1 \frac{ds}{(1-s^2)^{\frac{1}{2}}} \int_{-1}^1 \frac{s dt}{(1-t^2)^{\frac{1}{2}}} \vec{N}_f(\arcsin(s), \arccos(t)) \delta(u-ts). \quad (A-5)$$

The innermost integral on t yields

$$\left\{ \begin{array}{ll} \frac{\vec{N}_f(\arcsin(s), \arccos(u/s))}{(1-u^2/s^2)^{\frac{1}{2}}} & \text{for } |u| < s \\ 0 & \text{for } |u| > s \end{array} \right\}, \quad (A-6)$$

thereby giving

$$I(u) = \lambda \int_{|u|}^1 \frac{ds s}{(1-s^2)^{\frac{1}{2}} (s^2-u^2)^{\frac{1}{2}}} \vec{N}_f(\arcsin(s), \arccos(u/s)) \quad \text{for } |u| < 1. \quad (A-7)$$

This integral equation for noise field directionality \vec{N}_f is more general than Abel's integral equation, because limit u is also involved in one of the arguments of \vec{N}_f . We have been unable to simplify (A-7) and extract any simple descriptor of the noise field directionality analogous to (8). Placing the linear array along the y axis, instead, encounters the same problem.

APPENDIX B. ALTERNATIVE LOCATION OF PLANAR ARRAY

Suppose the planar array lies in the x, z plane, that is, $y = 0$. Then (6) becomes

$$\begin{aligned} G_f(x, z) &= \int_0^\pi d\theta \int_{-\pi}^\pi d\phi \sin\theta N_f(\theta, \phi) \exp\left(i\frac{2\pi}{\lambda}(x \sin\theta \cos\phi + z \cos\theta)\right) = \\ &= \int_0^\pi d\theta \int_0^\pi d\phi \sin\theta \underline{N}_f(\theta, \phi) \exp\left(i\frac{2\pi}{\lambda}(x \sin\theta \cos\phi + z \cos\theta)\right), \quad (B-1) \end{aligned}$$

where

$$\underline{N}_f(\theta, \phi) = N_f(\theta, \phi) + N_f(\theta, -\phi) \quad \text{for } 0 \leq \theta \leq \pi, 0 \leq \phi \leq \pi. \quad (B-2)$$

Then

$$\begin{aligned} I(u, v) &= \int_{-\infty}^{+\infty} dx \int_{-\infty}^{+\infty} dz \exp\left(-i\frac{2\pi}{\lambda}(ux + vz)\right) G_f(x, z) = \\ &= \int_0^\pi d\theta \int_0^\pi d\phi \sin\theta \underline{N}_f(\theta, \phi) \lambda^2 \delta(u - \sin\theta \cos\phi) \delta(v - \cos\theta). \quad (B-3) \end{aligned}$$

Now let

$$s = \sin\theta \cos\phi, \quad t = \cos\theta, \quad (B-4)$$

for which the Jacobian is

$$\frac{\partial(s, t)}{\partial(\theta, \phi)} = \sin^2\theta \sin\phi = (1 - t^2)^{\frac{1}{2}} (1 - s^2 - t^2)^{\frac{1}{2}}. \quad (B-5)$$

Then

$$I(u,v) = \lambda^2 \iint_{C_1} ds dt \frac{\underline{N}_f \left(\arccos(t), \arccos \left(s(1-t^2)^{-\frac{1}{2}} \right) \right)}{(1-s^2-t^2)^{\frac{1}{2}}} \delta(u-s) \delta(v-t) =$$

$$= \begin{cases} \frac{\lambda^2}{(1-u^2-v^2)^{\frac{1}{2}}} \underline{N}_f \left(\arccos(v), \arccos \left(\frac{u}{(1-v^2)^{\frac{1}{2}}} \right) \right) & \text{for } u^2 + v^2 < 1 \\ 0 & \text{otherwise} \end{cases}.$$

(B-6)

Thus, we have the explicit representation for the noise field directionality,

$$\underline{N}_f \left(\arccos(v), \arccos \left(\frac{u}{(1-v^2)^{\frac{1}{2}}} \right) \right) = \frac{(1-u^2-v^2)^{\frac{1}{2}}}{\lambda^2} \iint_{-\infty}^{+\infty} dx dz \times$$

$$\times \exp \left(-i \frac{2\pi}{\lambda} (ux + vz) \right) G_f(x, z) \quad \text{for } u^2 + v^2 < 1. \quad (B-7)$$

If we now let

$$u = \sin\theta \cos\phi, \quad v = \cos\theta, \quad (B-8)$$

this becomes

$$\underline{N}_f(\theta, \phi) = \frac{\sin\theta \sin\phi}{\lambda^2} \iint_{-\infty}^{+\infty} dx dz \exp \left(-i \frac{2\pi}{\lambda} (x \sin\theta \cos\phi + z \cos\theta) \right) \times$$

$$\times G_f(x, z) \quad \text{for } 0 \leq \theta \leq \pi, 0 \leq \phi \leq \pi. \quad (B-9)$$

This is a viable alternative to (27). Compare with starting result (B-1).

APPENDIX C. EXAMPLE FOR VOLUMETRIC ARRAY

Let the noise field directionality be given by

$$N_f(\theta, \phi) = \delta(\theta - \theta_0) \delta(\phi - \phi_0), \quad 0 < \theta_0 < \pi, \quad -\pi < \phi_0 \leq \pi. \quad (C-1)$$

Notice that arrival angle θ_0 can range over an interval of length π . We distinguish two cases:

$$A: \quad 0 < \theta_0 < \pi/2,$$

$$B: \quad \pi/2 < \theta_0 < \pi. \quad (C-2)$$

From (35), the three-dimensional spatial correlation is

$$G_f(x, y, z) = \sin\theta_0 \exp\left(i\frac{2\pi}{\lambda} (x \sin\theta_0 \cos\phi_0 + y \sin\theta_0 \sin\phi_0 + z \cos\theta_0)\right). \quad (C-3)$$

The problem addressed here is the reestablishment of (C-1) by means of the solution procedure given in (54)-(57). Recall that $Q(t)$ is real and even.

First, substituting (C-3) in (55), there follows

$$I(\pm) = \sin\theta_0 \lambda^2 \delta(\sin\theta \cos\phi - \sin\theta_0 \cos\phi_0) \times \\ \times \delta(\sin\theta \sin\phi - \sin\theta_0 \sin\phi_0) Q(\pm w_1 - \cos\theta_0). \quad (C-4)$$

Now, when we recall that θ is limited to $(0, \pi/2)$ in (54), the delta functions in (C-4) are located at

$$A: \quad \theta = \theta_0, \quad \phi = \phi_0,$$

$$\text{or} \quad B: \quad \theta = \pi - \theta_0, \quad \phi = \phi_0. \quad (C-5)$$

By means of the two-dimensional transformation employed in (19)-(22), we find that

$$\begin{aligned} \text{A: } I(\pm) &= \frac{\lambda^2}{\cos\theta_0} \delta(\theta - \theta_0) \delta(\phi - \phi_0) Q(w_1 \mp \cos\theta_0) , \\ \text{B: } I(\pm) &= \frac{\lambda^2}{|\cos\theta_0|} \delta(\theta - \pi + \theta_0) \delta(\phi - \phi_0) Q(w_1 \mp \cos\theta_0) . \end{aligned} \quad (\text{C-6})$$

Substitution of (C-6) in the numerator of (54a) yields

$$\begin{aligned} \text{A: } \cos\theta \frac{\lambda^2}{\cos\theta_0} \delta(\theta - \theta_0) \delta(\phi - \phi_0) C(\theta, \theta_0) , \\ \text{B: } \cos\theta \frac{\lambda^2}{|\cos\theta_0|} \delta(\theta - \pi + \theta_0) \delta(\phi - \phi_0) C(\theta, \theta_0) , \end{aligned} \quad (\text{C-7})$$

where

$$C(\theta, \theta_0) = Q(w_1 - \cos\theta) Q(w_1 - \cos\theta_0) - Q(w_1 + \cos\theta) Q(w_1 + \cos\theta_0). \quad (\text{C-8})$$

But since

$$\begin{aligned} C(\theta_0, \theta_0) &= Q^2(w_1 - \cos\theta_0) - Q^2(w_1 + \cos\theta_0) , \\ C(\pi - \theta_0, \theta_0) &= 0, \end{aligned} \quad (\text{C-9})$$

we find that

$$N_f(\theta, \phi) = \left\{ \begin{array}{ll} \delta(\theta - \theta_0) \delta(\phi - \phi_0) & \text{for case A} \\ 0 & \text{for case B} \end{array} \right\} . \quad (\text{C-10})$$

On the other hand, substitution of (C-6) in the numerator of (54b) yields

$$A: \cos\theta \frac{\lambda^2}{\cos\theta_0} \delta(\theta - \theta_0) \delta(\phi - \phi_0) D(\theta, \theta_0) ,$$

$$B: \cos\theta \frac{\lambda^2}{|\cos\theta_0|} \delta(\theta - \pi + \theta_0) \delta(\phi - \phi_0) D(\theta, \theta_0) , \quad (C-11)$$

where

$$D(\theta, \theta_0) = Q(w_1 - \cos\theta) Q(w_1 + \cos\theta_0) - Q(w_1 + \cos\theta) Q(w_1 - \cos\theta_0). \quad (C-12)$$

But since

$$D(\theta_0, \theta_0) = 0 ,$$

$$D(\pi - \theta_0, \theta_0) = Q^2(w_1 + \cos\theta_0) - Q^2(w_1 - \cos\theta_0) , \quad (C-13)$$

we find that

$$N_f(\pi - \theta, \phi) = \left\{ \begin{array}{ll} 0 & \text{for case A} \\ \delta(\theta - \pi + \theta_0) \delta(\phi - \phi_0) & \text{for case B} \end{array} \right\} . \quad (C-14)$$

This last case could be written in a form similar to (56) as

$$N_f(\theta', \phi) = \delta(\theta' - \theta_0) \delta(\phi - \phi_0) \quad \text{for } \pi/2 < \theta' < \pi. \quad (C-15)$$

In any event, (C-10) and (C-14) confirm starting result (C-1) for the noise field directionality.

REFERENCES

1. A. H. Nuttall, **Estimation of Noise Directionality Spectrum**, NUSC Technical Memorandum TC-211-71, Naval Underwater Systems Center, New London, CT, 29 October 1971; also NUSC Technical Report 4345, 1 September 1972.
2. A. H. Nuttall, **Estimation of Noise Directionality Spectrum; Extensions and Generalizations**, NUSC Technical Memorandum TC-6-73, Naval Underwater Systems Center, New London, CT, 7 May 1973.
3. N. Yen, **Ambient Sea Noise Directionality: Measurement and Processing**, NUSC Technical Report 5545, Naval Underwater Systems Center, New London, CT, 28 February 1977.
4. J. H. Wilson, "Signal Detection and Localization Using the Fourier Series Method (FSM) and Cross-Sensor Data," **Journal of the Acoustical Society of America**, volume 73, number 5, pages 1648-1656, May 1983.
5. A. H. Nuttall, **Alias-Free Wigner Distribution Function and Complex Ambiguity Function for Discrete-Time Samples**, NUSC Technical Report 8533, Naval Underwater Systems Center, New London, CT, 14 April 1989.
6. A. H. Nuttall, **Estimation of Noise Field Directionality; Comparison with Fourier Series Method**, NUSC Technical Report 8599, Naval Underwater Systems Center, New London, CT, 15 October 1989.

Technical Report 8599
15 October 1989

**Estimation of Noise Field Directionality;
Comparison with Fourier Series Method**

**A. H. Nuttall
ABSTRACT**

For a line array immersed in a stationary homogeneous noise field, the noise field directionality, at any temporal-frequency of interest, is estimated without any a priori assumptions about the field and without the limitations of ill-conditioning. The key to this development is the deferment of the inherent discretization associated with an array until after the integral equation for the noise field directionality has been solved in terms of the observed spatial correlation.

Comparison with the Fourier series method reveals nearly identical results, except that the Fourier series method has some inaccurate low-order Fourier coefficients. Also, no Bessel function evaluations are required for the new method proposed here; instead, one FFT suffices for approximate evaluation of the field directionality. However, neither procedure has the superresolution capability of some of the recent eigen-decomposition approaches.

Approved for public release; distribution is unlimited.

TABLE OF CONTENTS

	Page
LIST OF ILLUSTRATIONS	ii
LIST OF TABLES	ii
LIST OF SYMBOLS	iii
INTRODUCTION	1
NOISE FIELD CHARACTERIZATION	3
LINE ARRAY	7
Integrated Directionality Function	8
Equispaced Line Array	9
FOURIER INTEGRAL METHOD	11
Infinitely-Long Discrete Array	13
Finite-Length Discrete Array	16
Approximate Field	18
Discussion	20
FOURIER SERIES METHOD	23
Fourier Series Expansion	24
Example	27
Disallowed Component	28
Discrete Array	31
Resolution Capability	37
Discussion	38
GRAPHICAL RESULTS	39
SUMMARY	51
APPENDIX A. EXAMPLE OF FOURIER SERIES METHOD	53
APPENDIX B. NUMERICAL INVESTIGATION OF (58)	55
REFERENCES	61

LIST OF ILLUSTRATIONS

Figure	Page
1. Angular Geometry	3
2. Geometry of Line Array	7
3. Approximation $B_b(u)$	14
4. Aliasing of Disallowed Component	15
5. Weighting Function $w(p)$	16
6. Summation $R(\theta)$ in (40)	28
7. Reconstructed Field $R(\theta)$ for $u_0 > 1$	29
8. Bessel Functions $J_k(x)$	32
9. Weighted Functions $J_k(x)/x$	34
10. Coefficients for Five Separated Arrivals	43
11. Directionality for Five Separated Arrivals	44
12. Coefficients for Five Close Arrivals	45
13. Directionality for Five Close Arrivals	46
14. Coefficients for Three Arrivals	47
15. Directionality for Three Arrivals	48
16. Directionality for Flat Weighting	49
17. Directionality for Hann Weighting	50

LIST OF TABLES

1. Cosine Series Coefficients	40
B-1. Values of $\frac{\pi}{2} \tilde{a}_1$	57
B-2. Values of $\frac{\pi}{2} \tilde{a}_2$	58
B-3. Values of $\frac{\pi}{2} \tilde{a}_{10}$	59

LIST OF SYMBOLS

θ	polar angle, figures 1 and 2
ϕ	azimuthal angle, figure 1
f	temporal-frequency
$N(f, \theta, \phi)$	noise field directionality at frequency f , (1)
M	number of receiving elements
$G(f)$	cross-spectral matrix of size $M \times M$
$\tau_k(\theta, \phi)$	wavefront time delay to k -th element, (2)
$H_k(f, \theta, \phi)$	transfer function to k -th element, (2)
$G_{kj}(f)$	cross-spectrum between elements k and j , (4)
d_k	distance of k -th element from reference point, (5)
c	speed of propagation, (5)
$\bar{N}(f, \theta)$	integrated (averaged) directionality, (8)
d	element spacing, (9)
f_0	design frequency, (11), (12)
α	$\pi f / f_0$, (11)
u	bearing, $\cos \theta$, (11)
λ_0	design wavelength, c / f_0 , (12)
$C(p)$	spatial correlation function, (13), (15)
$B(u)$	directionality function, (14)
δ	delta function, (18)
$B_b(u)$	approximation to $B(u)$, (20)
\otimes	convolution, (21)
λ	wavelength, c / f , (21)
$B_c(u)$	approximation to $B(u)$, (25)
w_n	weights used for approximate field, (25)

LIST OF SYMBOLS (cont'd)

$w(p)$	continuous weighting function, (27), figure 5
$W(u)$	window function, (30)
$B_a(u)$	approximation to $B(u)$, (32)
K	size of discrete Fourier transform, (33)
Δ_x	sampling increment in x , (34), (59)
$A(\theta)$	noise field directionality, (37), (39)
a_q	Fourier series coefficient, (40)
$R(\theta)$	right-hand side of (40)
$J_q(x)$	Bessel function, (41)
sub r	real part, (43)
sub i	imaginary part, (44)
θ_o	plane-wave arrival angle, (49)
u_o	$\cos\theta_o$, (50)
\tilde{a}_q	approximate Fourier coefficient, (58)
q'	critical q value, (63)
L	length of array, $(M-1)d$, (64)
Δ_θ	resolution in θ , (65)

ESTIMATION OF NOISE FIELD DIRECTIONALITY;
COMPARISON WITH FOURIER SERIES METHOD

INTRODUCTION

The possibility of estimating the directionality of a stationary homogeneous noise field, directly from the element outputs of a line array, was investigated in [1,2,3] and found feasible only for small array sizes, due to ill-conditioning of the solutions of the fundamental least-squares equations relating the observed discrete spatial correlations to the impingent field. In addition, the possibility of incorporating a priori information about the field directionality and allowing for additive uncorrelated noises at the elements were considered in [2].

Recently, the ill-conditioning associated with these approaches was circumvented in [4] by employing a Fourier series method for the unknown field. However, this method requires numerous Bessel function evaluations and can have inaccurate low-order expansion coefficients, leading to bias in the estimated field directionality. Here, we will eliminate both of these drawbacks.

NOISE FIELD CHARACTERIZATION

Consider a (wide-sense) stationary homogeneous noise field characterized by directionality $N(f, \theta, \phi)$ that measures the power density spectrum at temporal-frequency f , due to noise arrivals from direction (θ, ϕ) . See figure 1. This characterization presumes that noise arrivals from different directions are uncorrelated and thereby precludes multipath arrivals, for example.

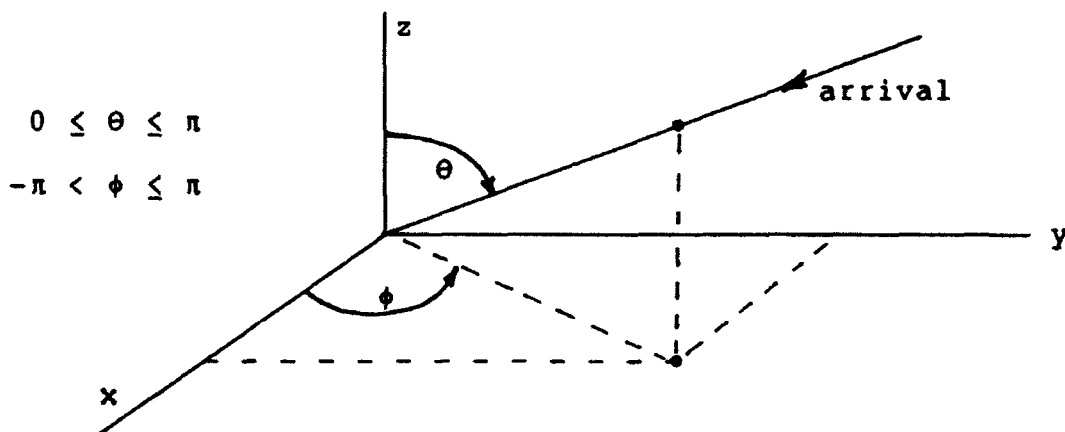


Figure 1. Angular Geometry

Suppose a collection of M receiving elements with arbitrary, but known, locations is immersed in this field. The largest amount of second-order information that can be extracted from these element outputs is the set of joint probability density functions between elements. However, in so far as estimating $N(f, \theta, \phi)$ is concerned, there is no need to retain anything more about the element outputs than the (Hermitian) matrix $G(f)$ of their cross-spectral functions $G_{kj}(f)$, $1 \leq k, j \leq M$.

In order to relate $G_{kj}(f)$ to noise field directionality $N(f, \theta, \phi)$, consider the power density spectrum of the elemental contribution due to solid angle $d\theta d\phi \sin\theta$ centered at (θ, ϕ) , namely

$$d\theta d\phi \sin\theta N(f, \theta, \phi). \quad (1)$$

In addition, let $\tau_k(\theta, \phi)$ be the time taken for a noise arrival from direction (θ, ϕ) to reach sensor k of a receiving array. Consequently, the transfer function applied to this arrival in reaching the k -th sensor is

$$\exp[-i2\pi f \tau_k(\theta, \phi)] \equiv H_k(f, \theta, \phi). \quad (2)$$

Then the cross-spectrum of the outputs of omnidirectional sensors k and j , owing to the elemental contribution (1), is

$$\begin{aligned} d\theta d\phi \sin\theta N(f, \theta, \phi) H_k(f, \theta, \phi) H_j^*(f, \theta, \phi) = \\ = d\theta d\phi \sin\theta N(f, \theta, \phi) \exp[-i2\pi f \{\tau_k(\theta, \phi) - \tau_j(\theta, \phi)\}]. \end{aligned} \quad (3)$$

Assuming that the noise arrivals from different directions are uncorrelated, the cross-spectrum $G_{kj}(f)$ of the outputs of sensors k and j is given by the sum of components (3) over all angular space:

$$G_{kj}(f) = \int_0^\pi d\theta \int_{-\pi}^\pi d\phi \sin\theta N(f, \theta, \phi) \exp[-i2\pi f \{\tau_k(\theta, \phi) - \tau_j(\theta, \phi)\}]. \quad (4)$$

This result holds for $1 \leq k, j \leq M$, where M is the number of sensors in the receiving array. $N(f, \theta, \phi)$ is called the noise field directionality at temporal-frequency f . The product

$\sin\theta N(f, \theta, \phi)$ could be called the plane-wave density.

Equation (4), for all k, j , constitutes the totality of information about $N(f, \theta, \phi)$ from the available elements. The problem is to estimate $N(f, \theta, \phi)$ from measurements of $\{G_{kj}(f)\}$. It should be noted that not all $\{G_{kj}(f)\}$ contain independent information. Thus, $G_{kk}(f) = G_{11}(f)$ for all k , and $G_{kj}(f) = G_{jk}^*(f)$ for all k, j . Also, for example, if elements 1,2 and 3,4 have $\tau_1 - \tau_2 = \tau_3 - \tau_4$ for all θ, ϕ , (4) indicates that $G_{12}(f) = G_{34}(f)$; this is due to the homogeneity of the noise field.

Array processing techniques, whether they are standard delay and add, weighted, or optimum (adaptive), result in a preprocessing of noise field directionality $N(f, \theta, \phi)$. Attempts to then estimate $N(f, \theta, \phi)$ from these processed quantities must, in some sense, undo what the array process has already done. But why should array processing be used on the elements at all, when we are interested in estimating the noise field directionality? An "optimum" estimation technique should accept matrix $G(f)$ as its input and emit an estimate of $N(f, \theta, \phi)$ as its output. This is the goal of this investigation.

LINE ARRAY

In this report, we will address only the case where the receiving array lies entirely on a single line in space. In figure 1, let θ be measured with respect to the location of the line. That is, let the line array lie along the $\theta = 0$ axis, namely the z-axis. See figure 2. Then if d_k is the distance (measured downward) of the k-th element from some reference point on the line, we have delay

$$\tau_k(\theta, \phi) = \frac{d_k}{c} \cos \theta \quad \text{for } 1 \leq k \leq M. \quad (5)$$

The values $\theta = 0$ and π correspond to endfire of the line array, and c is the speed of propagation.

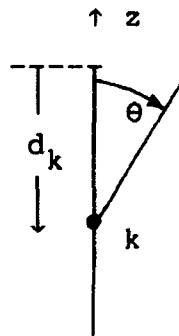


Figure 2. Geometry of Line Array

INTEGRATED DIRECTIONALITY FUNCTION

It follows from (4) and (5) that cross-spectrum

$$G_{kj}(f) = \int_0^{\pi} d\theta \int_{-\pi}^{\pi} d\phi \sin\theta N(f, \theta, \phi) \exp\left[-i2\pi f \frac{d_k - d_j}{c} \cos\theta\right] = \quad (6)$$

$$= \int_0^{\pi} d\theta \sin\theta \exp\left[-i2\pi f \frac{d_k - d_j}{c} \cos\theta\right] \bar{N}(f, \theta) \quad \text{for } 1 \leq k, j \leq M, \quad (7)$$

where we define integrated (or collapsed or averaged) noise directionality

$$\bar{N}(f, \theta) = \int_{-\pi}^{\pi} d\phi N(f, \theta, \phi). \quad (8)$$

Notice that $N(f, \theta, \phi)$ is defined in terms of a coordinate system centered on the line. According to (7), the only quantity that can be estimated about the noise field directionality is the integrated function $\bar{N}(f, \theta)$ in (8); this is a manifestation of the inherent conical symmetry of a line array response. The problem is to invert the measurements $\{G_{kj}(f)\}$ in (7) and solve for the quantity $\bar{N}(f, \theta)$, if possible.

EQUISPACED LINE ARRAY

For an equispaced line array, figure 2 can be specialized to

$$d_k = k d \quad \text{for } 1 \leq k \leq M, \quad (9)$$

where d is the element spacing. Then, (7) becomes

$$\begin{aligned} G_{kj}(f) &= \int_0^\pi d\theta \sin\theta \exp[-i\alpha(k-j) \cos\theta] \bar{N}(f, \theta) = \\ &= \int_{-1}^1 du \exp[-i\alpha(k-j)u] \bar{N}(f, \arccos(u)), \end{aligned} \quad (10)$$

where \arccos is the principal value inverse cosine function and

$$\alpha = \pi \frac{f}{f_0}, \quad f_0 = \frac{c}{2d}, \quad u = \cos\theta. \quad (11)$$

The quantity f_0 is the (design) frequency at which spacing d would be a half-wavelength:

$$\lambda_0 = \frac{c}{f_0} = 2 d. \quad (12)$$

Also, $u = 0$ corresponds to broadside of the line array.

At this point, a change of notation is very convenient. We suppress the explicit appearance of frequency f (it still appears through α in (11)) and express (10) as a spatial correlation

$$C(k-j) = \int_{-1}^1 du \exp(-i\alpha(k-j)u) B(u), \quad (13)$$

where we recognize that the only dependence on k, j is through their difference and define the noise directionality function

$$B(u) = \begin{cases} \bar{N}(f, \arccos(u)) & \text{for } -1 < u < 1 \\ 0 & \text{for } |u| > 1 \end{cases}. \quad (14)$$

Finally, we modify spatial correlation (13) to

$$C(p) = \int_{-1}^1 du \exp(-i\alpha p u) B(u). \quad (15)$$

This can be considered as an integral equation for noise field directionality $B(u)$, where α is known, and spatial correlation $C(p) = C^*(-p)$ is available only for integer p satisfying $|p| < M$; this was the approach considered in [1; section 2.3].

FOURIER INTEGRAL METHOD

Suppose that spatial correlation $C(p)$ in (15) were available for all continuous p , not just the integers $|p| < M$. Then multiplying (15) by $\exp(i\alpha pu')$ and integrating over all p , we have, using (11),

$$\begin{aligned} \int_{-\infty}^{+\infty} dp \exp(i\alpha pu') C(p) &= \int_{-\infty}^{+\infty} dp \exp(i\alpha pu') \int_{-1}^1 du \exp(-i\alpha pu) B(u) = \\ &= \int_{-1}^1 du B(u) \frac{2\pi}{\alpha} \delta(u-u') = \begin{cases} \frac{2f_0}{f} B(u') & \text{if } -1 < u' < 1 \\ 0 & \text{otherwise} \end{cases}. \end{aligned} \quad (16)$$

That is,

$$B(u) = \frac{f}{2f_0} \int_{-\infty}^{+\infty} dp \exp(i\alpha pu) C(p) \quad \text{for } -1 < u < 1. \quad (17)$$

This is an explicit integral relationship for the (integrated) noise field directionality $B(u)$ at bearing u , in terms of spatial correlation $C(p)$ at separation p . We will call this the Fourier integral method for the determination of the noise field directionality.

As an example, if the field is composed of a single plane-wave arrival,

$$B(u) = \delta(u-u_0), \quad |u_0| < 1, \quad (18)$$

then (15) gives spatial correlation

$$C(p) = \exp(-i\alpha p u_0) \quad \text{for all } p, \quad (19)$$

and (17) restores directionality (18). We should also note that the highest rate of variation of spatial correlation $C(p)$ is $\exp(\pm i\alpha p)$, obtained when $u_0 \rightarrow \pm 1$. If we insert a higher variation for $C(p)$ into solution (17), such as (19) with $|u_0| > 1$, we get nonzero values for directionality $B(u)$ outside the allowed $(-1,1)$ range of u , namely $\delta(u-u_0)$. Since this is disallowed according to (14), noisy estimates of spatial correlation $C(p)$ require some preprocessing prior to insertion into (17); alternatively, nonzero values of $B(u)$ for $|u| > 1$ might be ignored, but this is not an attractive approach.

INFINITELY-LONG DISCRETE ARRAY

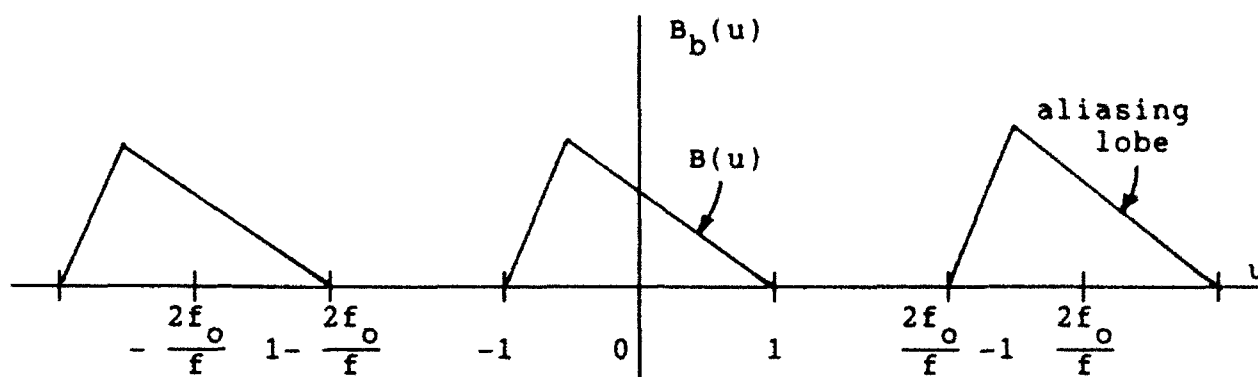
Equation (17) gives the impression that spatial correlation $C(p)$ is required for all continuous p . But since (13) indicates that $C(p)$ will only be available for integer p , we consider that case first; in fact, we consider spatial correlation $C(p)$ to be known for all integer p , which corresponds physically to an infinitely-long equispaced line array. The corresponding trapezoidal approximation to integral (17) for the noise field directionality is denoted as

$$B_b(u) = \frac{f}{2f_0} \sum_{n=-\infty}^{+\infty} \exp(i\alpha n u) C(n) \quad \text{for all } u. \quad (20)$$

But this can be developed according to

$$\begin{aligned} B_b(u) &= \frac{f}{2f_0} \int_{-\infty}^{+\infty} dp \exp(i\alpha p u) C(p) \sum_{n=-\infty}^{+\infty} \delta(p-n) = \\ &= B(u) \oplus \sum_{n=-\infty}^{+\infty} \delta\left(u - n \frac{2\pi}{\alpha}\right) = \sum_{n=-\infty}^{+\infty} B\left(u - n \frac{2\pi}{\alpha}\right) = \\ &= \sum_{n=-\infty}^{+\infty} B\left(u - n \frac{2f_0}{f}\right) \quad \text{for all } u, \end{aligned} \quad (21)$$

where \oplus denotes convolution, and we used (11). Function $B_b(u)$ has period $2f_0/f$ in u ; if we define $\lambda = c/f$, this period is λ/d , where we used (12).

Figure 3. Approximation $B_b(u)$

The plot of approximation $B_b(u)$ to the noise field directionality in figure 3 reveals aliasing lobes separated by $2f_o/f$ on the u -axis. If $f < f_o$, that is, if the array is being used below its design frequency, then these lobes do not overlap, and we have

$$B_b(u) = B(u) \quad \text{for } -1 < u < 1. \quad (22)$$

Thus, exact recovery of the noise field directionality $B(u)$ is possible from knowledge of spatial correlation $C(p)$ at integer p , provided that

$$f < f_o, \quad \text{that is, } d < \lambda/2; \quad (23)$$

here, we used $\lambda = c/f$ and (12). The element spacing must be less than a half-wavelength at the temporal-frequency f of interest in order to avoid aliasing. The discrete nature of the array does not, in itself, prevent recovery of the field; it is the finite length of a physical array that causes problems.

If spatial correlation $C(p)$ contains a component with too high a rate of variation, as, for example, (19) again with $|u_o| > 1$, we get $B(u) = \delta(u - u_o)$ as before. However, a plot of the corresponding $B_b(u)$ in figure 4 (for $u_o > 1$) reveals an aliased component within the fundamental range $(-1,1)$. We would be led to believe that the noise field directionality has a component

$$\delta(u - u_1) = \delta\left(u - u_o + \frac{2f_o}{f}\right), \quad (24)$$

which is incorrect. Thus, the discrete nature of an array can be a problem if the measured spatial correlation $C(p)$ contains disallowed components, which show up as aliased components inside the fundamental range $(-1,1)$ of u . This problem exists even if the array has infinite length.

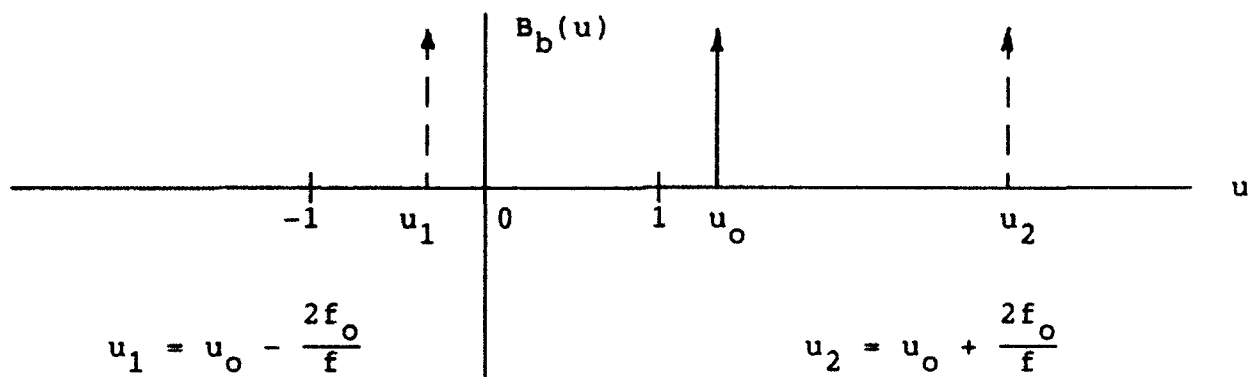


Figure 4. Aliasing of Disallowed Component

FINITE-LENGTH DISCRETE ARRAY

The approximate noise field directionality for a finite array of M elements is a modification of (20):

$$B_c(u) = \frac{f}{2f_0} \sum_{n=-\infty}^{+\infty} \exp(i\alpha_n u) C(n) w_n \quad \text{for all } u, \quad (25)$$

where weights

$$w_n = 0 \quad \text{for } |n| \geq M. \quad (26)$$

We consider that weights $\{w_n\}$ are samples of a continuous function $w(p)$; that is,

$$w_n = w(n), \quad (27)$$

where function w satisfies

$$w(p) = 0 \quad \text{for } |p| \geq M. \quad (28)$$

See figure 5. It then follows immediately from (25) and (20) that

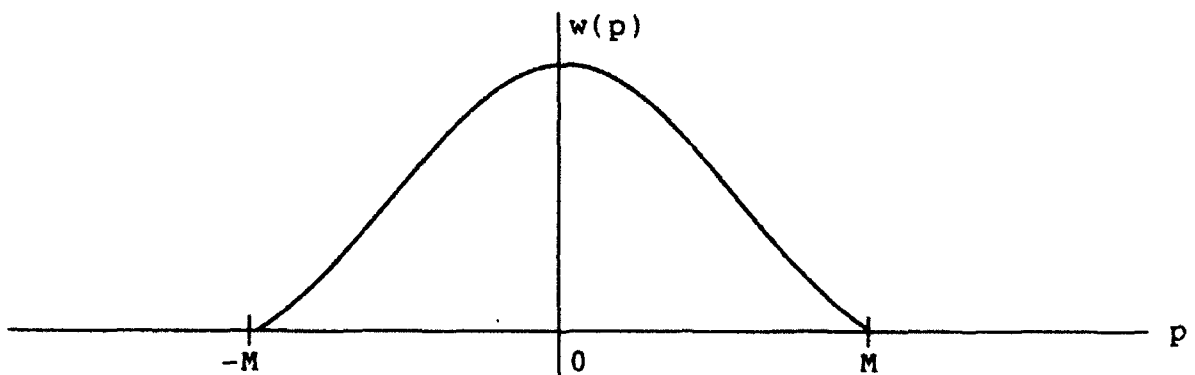


Figure 5. Weighting Function $w(p)$

$$B_c(u) = B_b(u) \otimes W(u), \quad (29)$$

where window

$$W(u) = \frac{f}{2f_0} \int_{-\infty}^{+\infty} dp \exp(i\alpha up) w(p). \quad (30)$$

(For the case of no weighting, that is, $w(p) = 1$ for all p , then $W(u) = \delta(u)$, and (29) reduces to (21).) The window $W(u)$ has

$$\text{effective width } \frac{1}{M} \frac{2f_0}{f} \text{ in } u. \quad (31)$$

(For flat weighting, that is, $w(p) = 1$ for $|p| < M$, the effective width is half of (31); however, the sidelobes of $W(u)$ are then significant.)

Although the aliasing of $B_b(u)$ in figure 3 can be controlled through satisfaction of (23), the convolution result in (29) reveals that the true noise field directionality $B(u)$ will be smeared by window $W(u)$. This is a result of the finite length, (26), of the array. Also, (29) and (31) reveal that approximation $B_c(u)$ has no superresolution capabilities; in fact, the smaller that f is chosen below design frequency f_0 , the more smeared $B_c(u)$ becomes. Thus, there is good reason to operate near the design frequency, that is, maximize f/f_0 , in order to minimize the width in (31); however, there is the conflicting requirement depicted in figure 3 and (29), which points to smaller values of f/f_0 . A compromise is in order.

If spatial correlation $C(p)$ contains a disallowed component such as (19) with $|u_0| > 1$, (29) and figure 4 indicate the presence of a smeared and aliased component within the fundamental range $(-1,1)$. Thus, such disallowed components should be preprocessed out of spatial correlation $C(p)$ before submission into approximation (25).

APPROXIMATE FIELD

The approximate noise field directionality that we will consider at length, here, is obtained by setting $w_n = 1$ for $|n| < M$ in (25):

$$B_a(u) = \frac{f}{2f_0} \sum_{n=1-M}^{M-1} \exp(i\alpha u n) C(n) \quad \text{for } -1 < u < 1. \quad (32)$$

This is a sampled box-car approximation to the exact integral result for $B(u)$ in (17). $B_a(u)$ has period $2f_0/f$ in u . If $|C(n)|$ for $|n| \geq M$ is substantially smaller than $C(0)$, (32) could give a good approximation to $B(u)$. If not, then one of the super-resolution techniques, such as maximum entropy, could be used to effectively extrapolate spatial correlation $C(n)$ out to $n = \pm\infty$ and the transform carried out analytically in closed form.

Approximations (32) and (25) have the same form as [1; (41) & (42)], if weighting $\hat{w}(f,u)$ there is independent of u . Also, if $f = f_0$, (32) reduces identically to [1; (47) or (51)].

However, we do not solve any ill-conditioned equations here, when $f < f_0$; on the other hand, we have not minimized any error measure either.

The actual numerical evaluation of approximation $B_a(u)$ is best done by specializing to the particular argument values

$$B_a\left(\frac{k}{K} \frac{2f_0}{f}\right) = \frac{f}{2f_0} \sum_{n=1-M}^{M-1} \exp(i2\pi kn/K) C(n) =$$

$$= \frac{f}{2f_0} \left[C(0) + 2 \operatorname{Re} \left\{ \sum_{n=1}^{M-1} \exp(-i2\pi kn/K) C^*(n) \right\} \right], \quad (33)$$

which can be accomplished by a discrete Fourier transform. The K values of k , that are swept out, cover an interval of length $2f_0/f$ in u , which is broader than the length 2 interval required, when $f < f_0$. See figure 3.

The $\exp(ix)$ function in (32) is being sampled at increment

$$\Delta_x = \alpha u = \pi \frac{f}{f_0} u. \quad (34)$$

So, if $f < f_0$ and $|u| < 1$, then $|\Delta_x| < \pi$, meaning that $\exp(ix)$ has at least two samples per period. This is well known to be the requirement for avoidance of overlapped aliasing lobes and is corroborated by figure 3. This sampling rate interpretation will be very important later when we discuss the Fourier series method [4].

Similarly, the spatial correlation $C(p)$ in (17) is being sampled at increment $\Delta_p = 1$. But since the sampling increment of $\exp(-ix)$ in (19), for basic elemental example (18), is

$$\Delta_x = \alpha u_0 = \pi \frac{f}{f_0} u_0, \quad (35)$$

we again have $|\Delta_x| < \pi$ if $f < f_0$ and $|u_0| < 1$. Thus, at least two samples per period are taken of spatial correlation $C(p)$, as well, even if values of u_0 near ± 1 occur.

DISCUSSION

It can be seen from (34) and (35) that the most troublesome cases will be when frequency f is near f_0 and u_0 is near ± 1 , that is, when the array is employed at its design frequency and when arrivals come in near endfire. Since arrivals come in of their own accord, no control is had of u_0 , except to turn the line array. And although one could choose $f < f_0$ in order to alleviate aliasing, losses in resolution will then occur, as (31) indicates. Thus, a trade-off is in order in regards to choice of f/f_0 ; perhaps, values somewhat less than 1 are a reasonable compromise, as was done in [1; figures 3,4,5]. Of course, a larger number of elements, M , always helps in improving resolution, as shown by (31); this is now a viable alternative, since there is no ill-conditioning as there was in [1].

The reason that we have been able to circumvent the ill-conditioning is that we have deferred the inherent sampling of (15), with increment $\Delta_p = 1$, until after we solved the integral equation for noise field directionality $B(u)$ in explicit form (17). So, instead of facing up to the discrete issue, as explicitly posed in (13), we have put it off as long as possible, and have then addressed it in the various forms (20), (25), and (32), which are reasonable approximations to the ideal continuous result (17). This procedure of temporarily ignoring the discrete sampling associated with a line array was first presented in [4; section 3] in connection with a cosine series expansion for the field distribution; this latter procedure is fully developed in the next section.

FOURIER SERIES METHOD

In order to derive this method, we return to a combination of (14) and (15):

$$\begin{aligned} C(p) &= \int_{-1}^1 du \exp(-i\alpha p u) \bar{N}(f, \arccos(u)) = \\ &= \int_0^\pi d\theta \exp(-i\alpha p \cos\theta) \sin\theta \bar{N}(f, \theta) . \end{aligned} \quad (36)$$

This equation relates the measured spatial correlation $C(p)$, at integer separations p , to the integrated noise field directionality $\bar{N}(f, \theta)$ (see(8)). We again suppress the f dependence and define plane-wave density

$$A(\theta) = \sin\theta \bar{N}(f, \theta) \quad \text{for } 0 < \theta < \pi , \quad (37)$$

to obtain

$$C(p) = \int_0^\pi d\theta \exp(-i\alpha p \cos\theta) A(\theta) . \quad (38)$$

As in (15) and the sequel, spatial correlation $C(p)$ is known only for integer p satisfying $|p| < M$. Function $A(\theta)$ is the unknown field function that must be estimated. It is related to the B function of the preceding section according to

$$A(\theta) = \sin\theta B(\cos\theta) \quad \text{for } 0 < \theta < \pi . \quad (39)$$

See (37) and (14).

FOURIER SERIES EXPANSION

We expand $A(\theta)$ in a cosine series according to

$$A(\theta) = \sum_{q=0}^{+\infty} a_q \cos(q\theta) \quad \text{for } 0 < \theta < \pi. \quad (40)$$

This basis is a complete set on interval $(0, \pi)$. See [5; page 92]. If we substitute (40) into (38), and interchange operations, we get

$$\begin{aligned} C(p) &= \sum_{q=0}^{+\infty} a_q \int_0^{\pi} d\theta \exp(-i\alpha p \cos\theta) \cos(q\theta) = \\ &= \pi \sum_{q=0}^{+\infty} a_q (-i)^q J_q(\alpha p), \end{aligned} \quad (41)$$

where we used [6; 9.1.21]. As a special case,

$$C(0) = \pi a_0, \quad (42)$$

which allows explicit determination of a_0 .

Equation (41) constitutes an infinite set of complex simultaneous linear equations for coefficients $(a_q)_0^{\infty}$. If we split this equation into its real and imaginary parts, we have

$$\frac{1}{\pi} C_r(p) = \sum_{\substack{q=0 \\ q \text{ even}}}^{+\infty} a_q (-i)^q J_q(\alpha p) = \sum_{k=0}^{+\infty} a_{2k} (-1)^k J_{2k}(\alpha p), \quad (43)$$

$$\frac{1}{\pi} C_i(p) = \sum_{\substack{q=1 \\ q \text{ odd}}}^{+\infty} a_q (-i)^{q+1} J_q(\alpha p) = \sum_{k=1}^{+\infty} a_{2k-1} (-1)^k J_{2k-1}(\alpha p). \quad (44)$$

We now have two infinite sets of real simultaneous linear equations, one for the even coefficients, the other for the odd coefficients, in cosine expansion (40).

Since spatial correlation $C(p)$ in (38) is only known for a finite number of discrete p values, namely integer $|p| < M$, there is no hope of solving for the infinite number of unknowns $\{a_q\}$ in (43) and (44). What we shall do, for the time being, is to ignore this limitation and pretend that $C(p)$ is known for all continuous $p \geq 0$. (Of course, $C(p)$ is then also known for $p < 0$, according to $C(-p) = C^*(p)$ from (15), since field $B(u)$ is real.) This procedure was first propounded for the line array in [4].

We multiply both sides of (43) by $J_{2m}(\alpha p)/p$ and integrate over p , to obtain

$$\begin{aligned} \frac{1}{\pi} \int_0^{+\infty} dp \frac{J_{2m}(\alpha p)}{p} C_r(p) &= \sum_{k=0}^{+\infty} a_{2k} (-1)^k \int_0^{+\infty} dp \frac{J_{2m}(\alpha p)}{p} J_{2k}(\alpha p) = \\ &= \frac{a_{2m} (-1)^m}{2(2m)} \quad \text{for } m \geq 1; \end{aligned} \quad (45)$$

here, we used [6; 11.4.6]. In a similar fashion, from (44),

$$\begin{aligned} \frac{1}{\pi} \int_0^{+\infty} dp \frac{J_{2m-1}(\alpha p)}{p} C_i(p) &= \sum_{k=1}^{+\infty} a_{2k-1} (-1)^k \int_0^{+\infty} dp \frac{J_{2m-1}(\alpha p)}{p} J_{2k-1}(\alpha p) \\ &= \frac{a_{2m-1} (-1)^m}{2(2m-1)} \quad \text{for } m \geq 1. \end{aligned} \quad (46)$$

Combining (42), (45), and (46), we have

$$\begin{aligned} a_0 &= \frac{1}{\pi} C(0) = \frac{1}{\pi} C_r(0), \\ \left. \begin{aligned} a_{2m} &= \frac{2}{\pi} (-1)^m 2m \int_0^{+\infty} dp \frac{J_{2m}(\alpha p)}{p} C_r(p) \\ a_{2m-1} &= \frac{2}{\pi} (-1)^m (2m-1) \int_0^{+\infty} dp \frac{J_{2m-1}(\alpha p)}{p} C_i(p) \end{aligned} \right\} \quad \text{for } m \geq 1. \end{aligned} \quad (47)$$

Convergence of the first integral at $p = 0$ is guaranteed since $J_{2m}(\alpha p)/p \rightarrow 0$ as $p \rightarrow 0$, because $2m \geq 2$. The second integral also converges at $p = 0$, since $J_{2m-1}(\alpha p) C_i(p)/p \rightarrow 0$ as $p \rightarrow 0$, because $2m-1 \geq 1$ and $C_i(0) = 0$. Thus, both integrands in (47) approach zero at the origin.

We now have explicit integral relations for the coefficients $\{a_q\}$ in the cosine series expansion of $A(\theta)$ in (40). They are exact results for $\{a_q\}$, presuming that spatial correlation $C(p)$ is available for all continuous $p \geq 0$. They agree with [4; (13)-(15)].

EXAMPLE

Consider the same single plane-wave arrival given in (18):

$$B(u) = \delta(u - u_0) , \quad |u_0| < 1. \quad (48)$$

Then (39) yields

$$A(\theta) = \sin\theta \delta(\cos\theta - u_0) = \delta(\theta - \theta_0) \quad \text{for } 0 < \theta < \pi , \quad (49)$$

where $\theta_0 = \arccos(u_0)$, $0 < \theta_0 < \pi$. Substitution in (38) gives spatial correlation

$$C(p) = \exp(-i\alpha p \cos\theta_0) = \exp(-i\alpha p u_0) , \quad (50)$$

as in (19). When this result is used in (47), the coefficients are found to be (see appendix A)

$$a_0 = \frac{1}{\pi} ,$$

$$a_q = \frac{2}{\pi} \cos(q \theta_0) \quad \text{for } q \geq 1 , \quad (51)$$

independent of α . Then the summation on the right-hand side of (40) becomes (appendix A)

$$R(\theta) = \sum_{m=-\infty}^{+\infty} \left[\delta(\theta - \theta_0 - m2\pi) + \delta(\theta + \theta_0 - m2\pi) \right] \quad \text{for all } \theta. \quad (52)$$

The plot of this function in figure 6 reveals that the only impulse component lying in the allowed range of θ , namely $(0, \pi)$, is that at $\theta = \theta_0$. Therefore,

$$A(\theta) = \delta(\theta - \theta_0) \quad \text{for } 0 < \theta < \pi, \quad (53)$$

as desired. Thus, the use of all the exact coefficients $\{a_q\}$ in (51) restores field distribution $A(\theta)$ precisely.

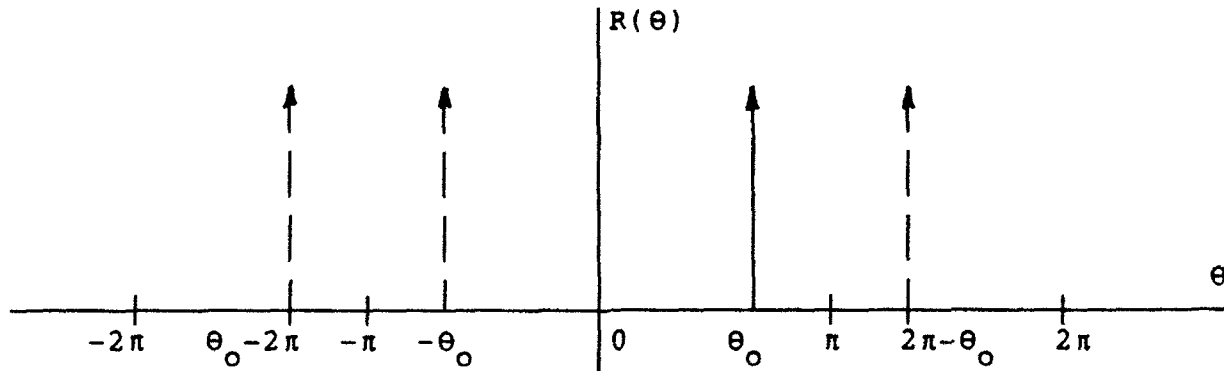


Figure 6. Summation $R(\theta)$ in (40)

DISALLOWED COMPONENT

The highest rate of variation of spatial correlation $C(p)$ in (50) is $\exp(\pm i\alpha p)$, just as in (19) and the sequel. If we insert a higher variation for $C(p)$ into integral solution (47) for the coefficients, namely

$$C(p) = \exp(-i\alpha p u_0) , \quad u_0 > 1 , \quad (54)$$

we obtain [7; 6.693 1&2]

$$a_0 = \frac{1}{\pi} ,$$

$$a_q = \frac{2}{\pi} Q^q \quad \text{for } q \geq 1 , \quad (55a)$$

where

$$Q = \frac{1}{u_0 + \sqrt{u_0^2 - 1}} = u_0 - \sqrt{u_0^2 - 1} , \quad (55b)$$

independent of α . Use of these coefficients in summation (40) gives reconstructed field (right-hand side of (40))

$$R(\theta) = \frac{1}{\pi} \frac{\sqrt{u_0^2 - 1}}{u_0 - \cos\theta} . \quad (56)$$

A plot of this function in figure 7 reveals that it is spread out over the entire $(0, \pi)$ interval; this is in contrast to the Fourier integral method in (19) which correctly restored a zero field in the fundamental interval, namely

$$B(u) = \delta(u - u_0) , \quad u_0 > 1 , \quad (57)$$

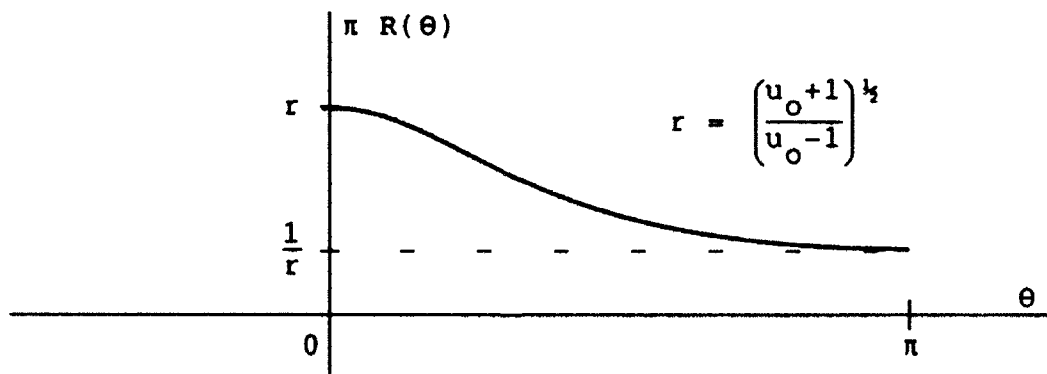


Figure 7. Reconstructed Field $R(\theta)$ for $u_0 > 1$

for this example. Thus, the Fourier series method gives nonzero field values for $0 < \theta < \pi$, even when all the coefficients $\{a_q\}$ are determined exactly by the integrals in (47). The use of noisy estimates for $C(p)$ in (47) is therefore more debilitating for the Fourier series method than for the Fourier integral method, and some preprocessing (that is, low-pass filtering) of the available spatial correlation $C(p)$ values is required prior to insertion into (47). If this is not done, a spurious background will be yielded from the Fourier series method in the fundamental range $0 < \theta < \pi$, due to "spillover" from disallowed components of $C(p)$.

Substitution of the reconstructed field $R(\theta)$ of (56) and figure 7 into the right-hand side of (38) does not restore the spatial correlation (54) for this example with $u_0 > 1$. This is expected, since the coefficients $\{a_q\}$ in (55) decay with q , preventing summation (40) for $A(\theta)$ from retaining the arbitrarily narrow behavior required versus θ , namely the delta function in (49).

DISCRETE ARRAY

For an equispaced line array of M elements, (13) indicates that spatial correlation $C(p)$ will be available only for integer $|p| < M$. We therefore adopt, as approximations to the exact integral results in (47), the forms

$$\left. \begin{aligned} \tilde{a}_{2m} &= \frac{2}{\pi} (-1)^m 2m \sum_{n=1}^{M-1} \frac{J_{2m}(\alpha n)}{n} C_r(n) \\ \tilde{a}_{2m-1} &= \frac{2}{\pi} (-1)^m (2m-1) \sum_{n=1}^{M-1} \frac{J_{2m-1}(\alpha n)}{n} C_i(n) \end{aligned} \right\} \text{ for } m \geq 1, \quad (58)$$

along with $\tilde{a}_0 = a_0 = C_r(0)/\pi$; see [4; (16)-(18)]. These are explicit finite sums for the approximate coefficients $\{\tilde{a}_q\}$, to be used in the cosine series (40) in place of the exact, but unknown, $\{a_q\}$. (The terms for $n = 0$ in the summands of (58) are zero by virtue of the discussion under (47).)

Several potential problems exist with approximations (58). First, the increment in the $J_k(x)$ Bessel functions in (58) is

$$\Delta_x = \alpha = \pi \frac{f}{f_0}. \quad (59)$$

For the design frequency $f = f_0$, (that is, $d = \lambda/2$), this increment is π , which is rather large. The plots of $J_k(x)$ in figure 8, for $0 < x < 20\pi$ and selected k values between 1 and 35, reveal that the low-order Bessel functions are very poorly sampled at values $x_n = n\pi$, especially for small n . For example,

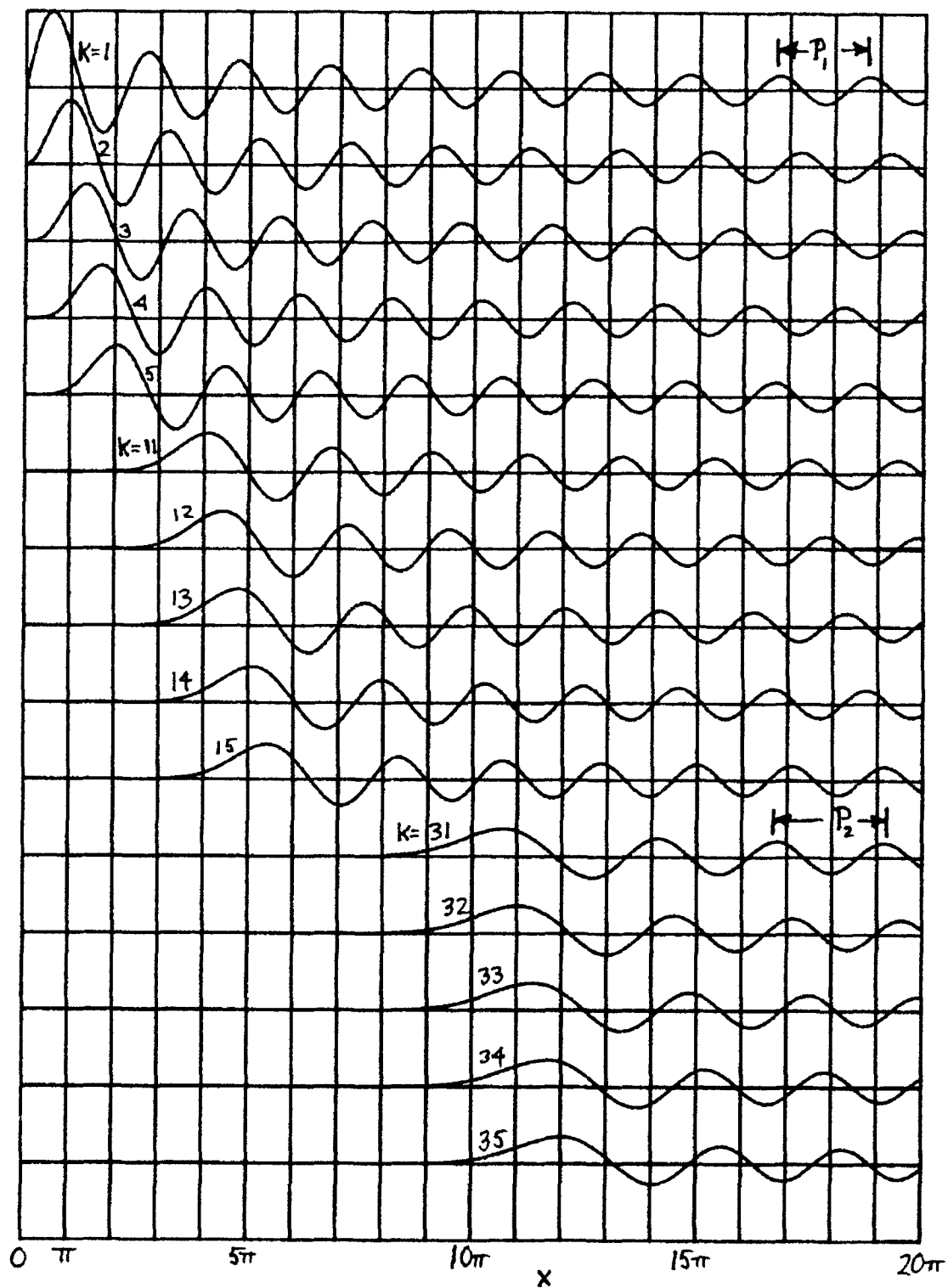


Figure 8. Bessel Functions $J_k(x)$

the peaks of $J_1(x)$ at x near $.6\pi$ and 1.7π are badly represented by samples at $x = \pi$ and 2π . (The curves in figure 8 are scaled relative to the largest value of $J_1(x)$ at x near $.6\pi$.)

Of more relevance are the plots of weighted functions $J_k(x)/x$ in figure 9, because this is the actual integrand in (47). (The curves in figure 9 are scaled individually for plotting appearances, so that each has the same peak value.) We again observe that the low-order weighted functions are poorly represented by samples taken at $x_n = n\pi$.

For larger arguments x , the "period" P_1 of $J_1(x)$, indicated on figure 8, is approximately 2π ; thus, we are getting just 2 samples per period at $\Delta_x = \pi$, which is barely adequate for $J_1(x)$ at large argument values. For the higher-order weighted Bessel functions, the initial peaks (near $x = k+2$) are well represented by samples at $\Delta_x = \pi$. In addition, the period P_2 in figures 8 and 9 is greater than 2π , for larger arguments; thus, we are getting more than 2 samples per period of the higher-order Bessel functions. Of course, eventually, for large enough x , all the $J_k(x)$ have period 2π . (See [6; 9.2.1].)

These sampling considerations indicate that the low-order coefficients \tilde{a}_q will likely be inaccurate, especially when f is near f_0 , while the higher-order coefficients will not be badly affected by this particular feature. A numerical investigation of these effects is undertaken in appendix B. In particular, coefficients \tilde{a}_1 , \tilde{a}_2 , \tilde{a}_{10} are computed for a variety of values of

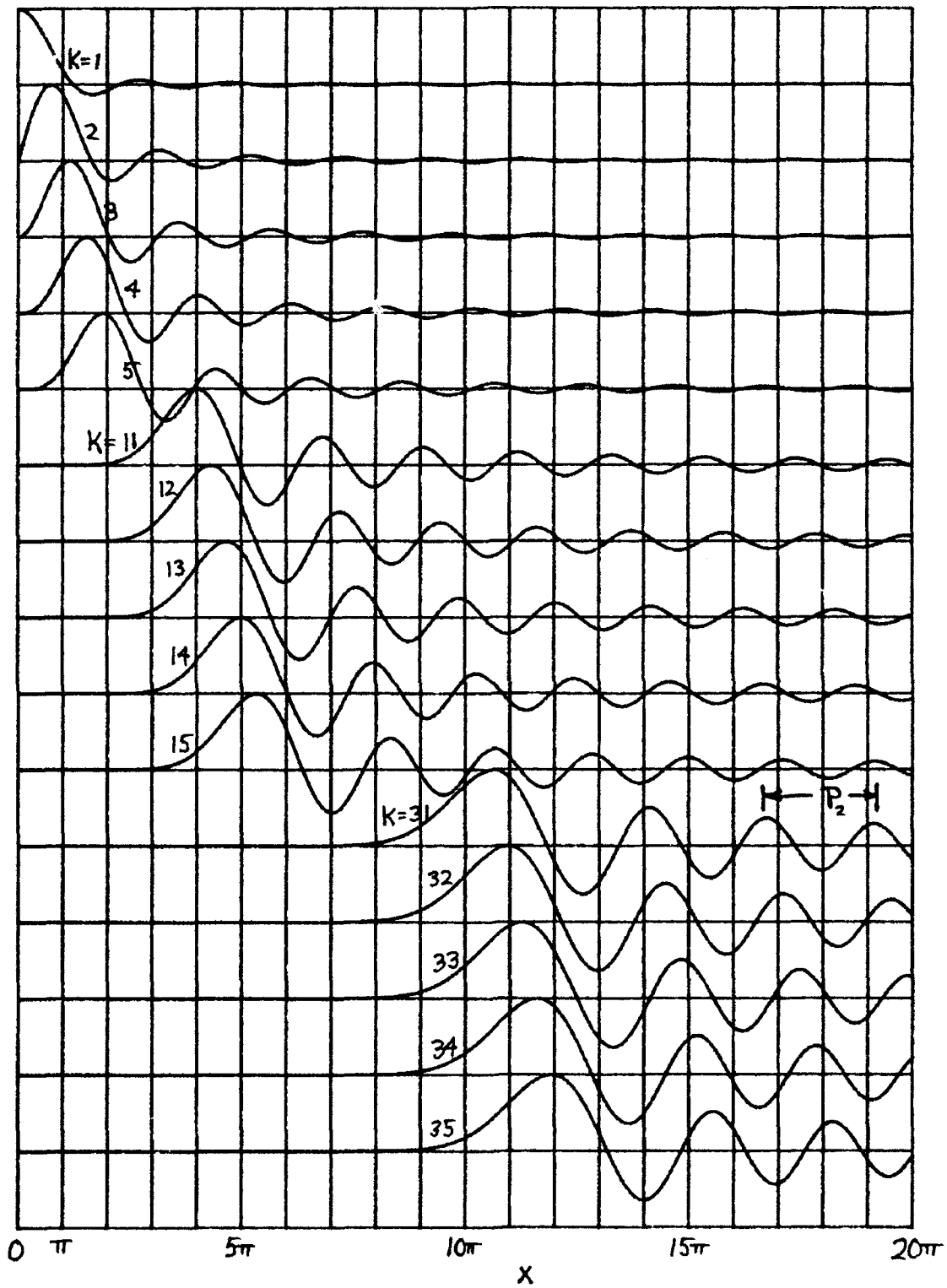


Figure 9. Weighted Functions $J_k(x)/x$

$u_0(\cos\theta_0)$, $\alpha(\pi f/f_0)$, M , and compared with the exact values a_1 , a_2 , a_{10} . The results quantitatively confirm the above expectations.

The second problem with approximations (58) is that the increment in the samples of spatial correlation $C(p)$ is $\Delta_p = 1$. The discussion surrounding (35) is directly relevant again and should be reviewed. Arrivals near endfire, $\theta_0 \sim 0$ or π , will be most severely affected.

A third problem with (58) is that M is not infinite; therefore, the summands may not have decayed sufficiently to terminate the summation at $M-1$, with negligible error. As seen earlier, for plane-wave arrival (48)-(50), spatial correlation $C(p)$ does not decay at all with p , and since [6; 9.2.1]

$$\frac{J_k(x)}{x} \propto \frac{1}{x^{3/2}} \quad \text{as } x \rightarrow +\infty, \quad (60)$$

the integrands of (47) can decay very slowly with p .

Furthermore, if α in (11) is less than π , $J_{2m}(\alpha n)$ and $J_{2m-1}(\alpha n)$ in (58) may not yet have even reached their substantial range of values by the time n reaches $M-1$. To develop this point, observe from figure 8 that

$$J_k(x) \approx 0 \quad \text{for } |x| < k - 2\pi. \quad (61)$$

Therefore

$$J_{2m}(\alpha n) \approx 0 \quad \text{for } 2m > \alpha n + 2\pi. \quad (62)$$

So, for example, if $M = 64$ and $f = f_0$, then $\alpha = \pi$, $\max n = M-1 = 63$, and (62) indicates that the Bessel function is essentially zero for $2m > 204$. Thus, approximate coefficients \tilde{a}_q , determined from (58), will be substantially zero for $q > 200$; this is the limit that was unknown in [4; under (5b) and bottom of page 1651].

As another example, if $M = 64$ and $f = f_0/2$, then (62) indicates that the approximate coefficients \tilde{a}_q for $q > 105$ will be substantially zero; this is verified by [4; figure 3]. Thus, figures 8 and 9, with (62), give a quantitative indication of when the Fourier series method will collapse, in terms of the loss of the higher-order coefficients and the attendant degraded resolution.

RESOLUTION CAPABILITY

The general situation is as follows: approximate coefficient \tilde{a}_q in (58) involves $J_q(\alpha n)$ for $n = 1$ to $M-1$. Reference to (61) therefore indicates that if

$$q > \alpha n_{\max} + 2\pi = \alpha(M-1) + 2\pi = q', \quad (63)$$

then $\tilde{a}_q \approx 0$. Thus, summation (40) for field $A(\theta)$ will have zero terms for $q > q'$. For the same plane-wave example considered in (48)-(53), this would result in a resolution capability of the order of (appendix A, especially (A-9) and (A-10))

$$\frac{\pi}{q' + \frac{1}{2}} \approx \frac{\pi}{\alpha(M-1)} = \frac{\lambda}{2d(M-1)} = \frac{\lambda}{2L} \quad (64)$$

at broadside, where we used (63), (11), and defined L as the length of the line array. However, the coefficients $\{\tilde{a}_q\}$ deteriorate before q reaches q' , typically for $q > q'3/4$. This results in a resolution of the order of

$$\Delta_\theta \approx \frac{4}{3} \frac{\lambda}{2L} = \frac{2}{3} \frac{\lambda}{L}. \quad (65)$$

This is somewhat sharper than the standard quoted result of λ/L , but not significantly so. Thus, the Fourier series method has slightly better resolution than standard beamforming, which corroborates several of the results in [4].

DISCUSSION

It was demonstrated in (51)-(53), that for the plane-wave arrival of (48)-(50), use of all the exact coefficients $\{a_q\}$ in the Fourier series method restored the field $A(\theta)$ precisely for all θ . However, when we discretize the array and must resort to approximations $\{\tilde{a}_q\}$ in (58), this restoration capability is lost, even if the array is infinitely long; see the tabular results in appendix B for $M = 100, 1000, 10000, 100000$. This result for the Fourier series method is distinctly different from that for the Fourier integral method, as a review of (21) and figure 3 reveals. In both methods, we are presuming that $f < f_0$, that is, that the array is used at or below its design frequency. Thus, sampling (in space) is more detrimental to the Fourier series method than to the Fourier integral method; this is related to the fact that the latter employs a (single) Fourier transform in (17), whereas the former uses (numerous) Bessel transforms in (47).

The summation on q in (40) for field $A(\theta)$ cannot be carried out to ∞ . However, when employed with approximate coefficients $\{\tilde{a}_q\}$, it should be carried out at least to the limit q' given in (63), after which $\{\tilde{a}_q\}$ are essentially zero; this will maximally preserve the resolution capability of the Fourier series method. This procedure was not employed in [4; figures 1,4,6]; thus, some inherent resolution of the Fourier series method was lost in those examples.

GRAPHICAL RESULTS

We shall re-do the examples given in [4], where the Fourier series method was introduced, but now using more coefficients and comparing the results with the Fourier integral method presented here. The first example is that of five plane-waves with arrival angles $54^\circ, 57^\circ, 60^\circ, 63^\circ, 66^\circ$, as given in [4; figures 1 and 2]. (Angle 90° corresponds to broadside of the line array.) The two arrivals at 57° and 63° each have twice the common power of the other three arrivals. The exact cosine series coefficients $\{a_q\}$ for $0 \leq q \leq 250$ are plotted in figure 10A, and are listed numerically in table 1 for $0 \leq q \leq 30$. We have normalized the total power so that the origin value of the spatial correlation is $C(0) = \pi$; then $a_0 = \tilde{a}_0 = 1$.

For a line array with $M = 64$ elements, employed at its design frequency, $f = f_0$, the approximate coefficients $\{\tilde{a}_q\}$, as determined via (58), are given in figure* 10B and table 1. A comparison of the numerical results in table 1 shows a very large discrepancy between a_1 and \tilde{a}_1 and between a_2 and \tilde{a}_2 . However, this discrepancy decreases to about 5% for $q = 3$ and 4, and is much smaller for $q > 4$. Comparison of the plots in figure 10 reveals that \tilde{a}_q is substantially zero for $q > 205$, in agreement with (62) and the sequel, and that \tilde{a}_q and a_q are very similar for $2 < q < 175$.

*This figure is not in complete agreement with [4; figure 2].

Table 1. Cosine Series Coefficients

q	a_q	\tilde{a}_q
0	1.0000	1.0000
1	.9977	.4837
2	-.9906	-.4407
3	-1.9580	-2.0569
4	-.9628	-.9130
5	.9423	.9265
6	1.8349	1.8428
7	.8887	.8868
8	-.8561	-.8535
9	-1.6399	-1.6395
10	-.7806	-.7784
11	.7383	.7390
12	1.3869	1.3895
13	.6463	.6471
14	-.5974	-.5942
15	-1.0938	-1.0933
16	-.4954	-.4916
17	.4431	.4433
18	.7809	.7852
19	.3379	.3376
20	-.2857	-.2810
21	-.4687	-.4697
22	-.1841	-.1793
23	.1353	.1335
24	.1766	.1811
25	.0433	.0406
26	-.0007	.0031
27	.0790	.0754
28	.0769	.0794
29	-.1114	-.1157
30	-.2857	-.2851

For these same parameter values, the reconstructed field distribution, via the Fourier integral method of (32), is depicted in figure 11A, while that for the Fourier series method of (58), (40), and (63), using approximate coefficients $\{\tilde{a}_q\}$, is displayed in figure 11B. This latter figure is an improvement over [4; figure 1] for two reasons: 250 coefficients $\{\tilde{a}_q\}$ were used instead of 140, and the angular sampling increment was

previously insufficient to track the detailed behavior of the field distribution. The two parts of figure 11 are very similar, except for the drift in the Fourier series method near $\theta = \pi$, due mainly to inaccurate low-order coefficients \tilde{a}_1 and \tilde{a}_2 .

Both plots yield some negative values for the reconstructed field distribution, due to sidelobes from the plane-wave components. These can be suppressed at the cost of decreased resolution. See (25)-(31) for the Fourier integral method. As for the Fourier series method, if approximations (58) (to exact results (47)) used a taper, instead of box-car weighting out to $p = M-1$, a similar control of sidelobes is achievable.

If all the parameter values above are kept unchanged, except that the arrival angles are squeezed closer together, namely $56^\circ, 58^\circ, 60^\circ, 62^\circ, 64^\circ$, we then have the example considered in [4; figures 4 and 5]. The exact and approximate cosine series coefficients are given in figures 12A and 12B, respectively. The field distribution for the Fourier integral method is plotted in figure 13A, while that for the Fourier series method is plotted in figure 13B. All five plane-waves are resolved by both procedures; in fact, the only essential difference is the slight drift in figure 13B near $\theta = \pi$, due to poor values of \tilde{a}_1 and \tilde{a}_2 . Figure 13B is a significant improvement over [4; figure 4], again due to additional coefficients and finer angular sampling in θ .

The third example of the Fourier series method, from [4; figure 6], corresponds to three plane-waves with arrivals closer to endfire, namely $27^\circ, 30^\circ, 33^\circ$. The power level of the

33° arrival is one-half of the common power level of the other two arrivals; all other parameters are unchanged. The exact and approximate coefficients are given in the two parts of figure 14; the approximation appears to deteriorate for $q > 100$. The field distribution for the Fourier integral method is depicted in figure 15A, while that for the Fourier series method is plotted in figure 15B. The major discrepancy is again the drift in the latter plot near $\theta = \pi$; this is in spite of the seemingly poor results for coefficients $\{\tilde{a}_q\}$ in figure 14B.

The final example considered here is that given in [1; page 15], namely

$$B(u) = \begin{cases} 0 & \text{for } -1 < u < 0 \\ 2u & \text{for } 0 < u < 1 \end{cases} . \quad (66)$$

However, those earlier results were limited to $M \leq 12$ due to ill-conditioning. The spatial correlation follows from (15) as

$$C(p) = \frac{2}{\alpha^2 p^2} \left[\exp(-i\alpha p) (1 + i\alpha p) - 1 \right] . \quad (67)$$

The reconstructed field distribution via the Fourier integral method, for $M = 64$ elements, is presented in figures 16A and 16B for flat weighting (32), with $f/f_0 = 1$ and .5, respectively. The corresponding plots for Hann weighting, (25) and figure 5, are depicted in figure 17. The familiar tradeoff between resolution and sidelobes is quite evident. Perhaps a plot of both results, with and without weighting, would yield important information not available from either plot alone.

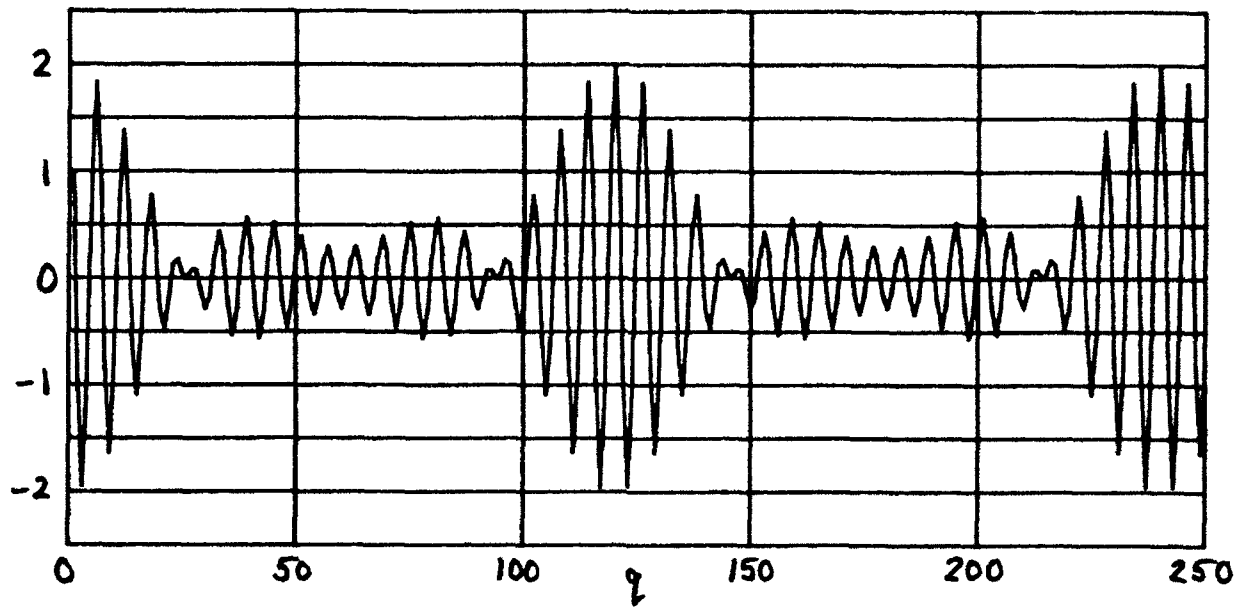


Figure 10A. Coefficients a_q

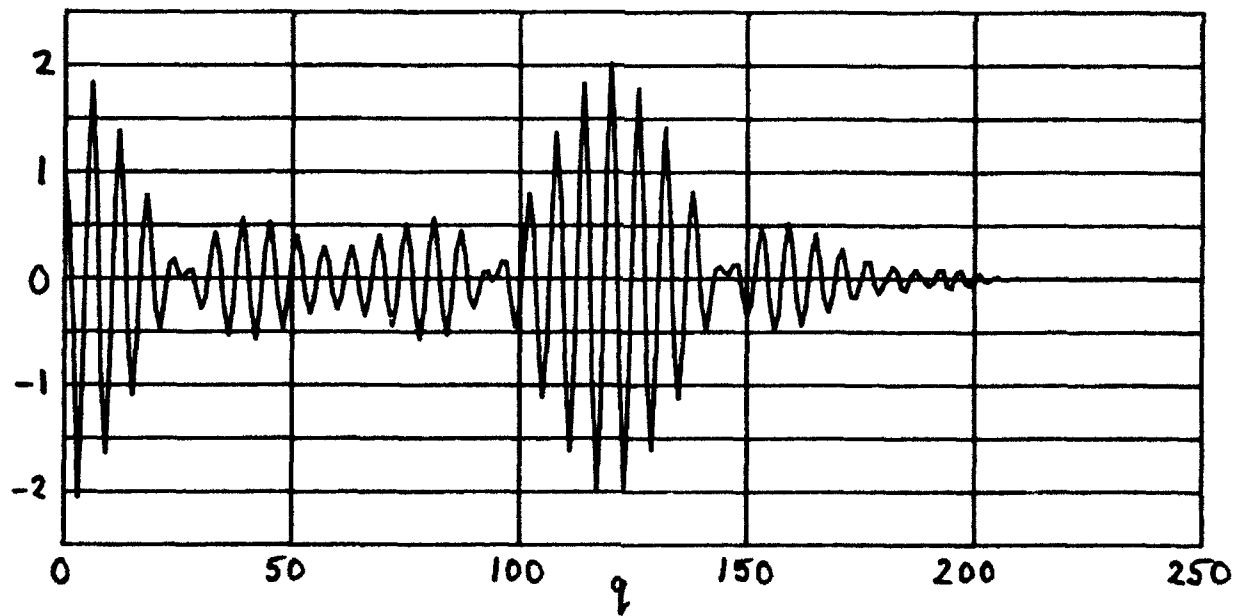


Figure 10B. Coefficients \tilde{a}_q

Figure 10. Coefficients for Five Separated Arrivals

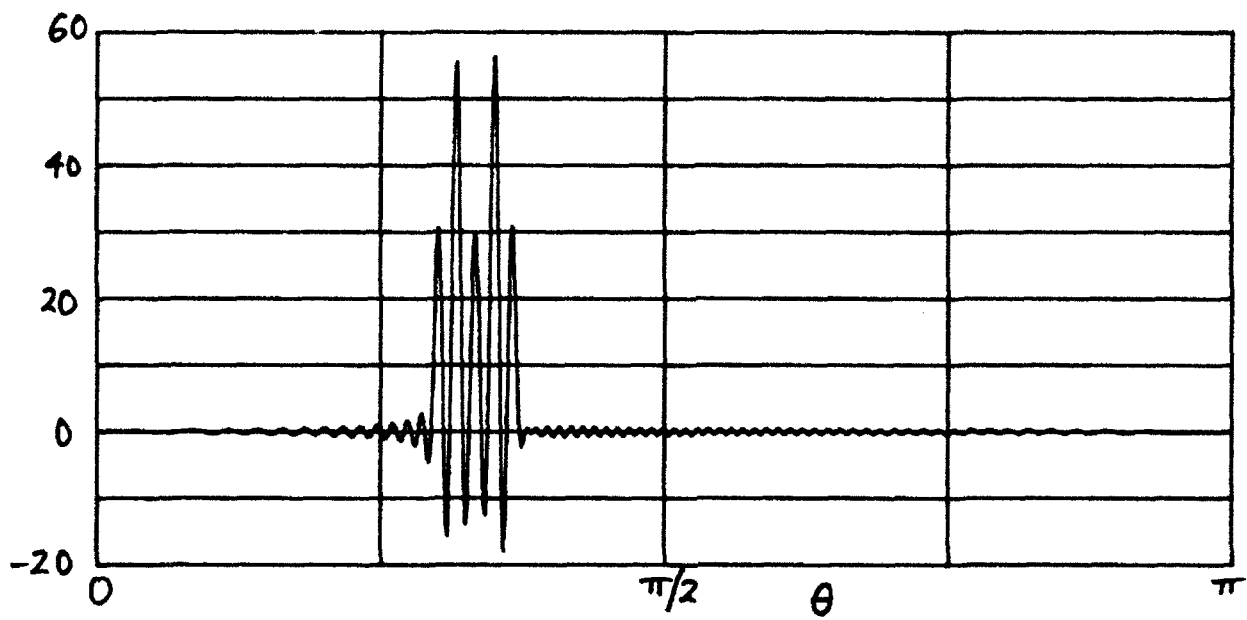


Figure 11A. Fourier Integral Method

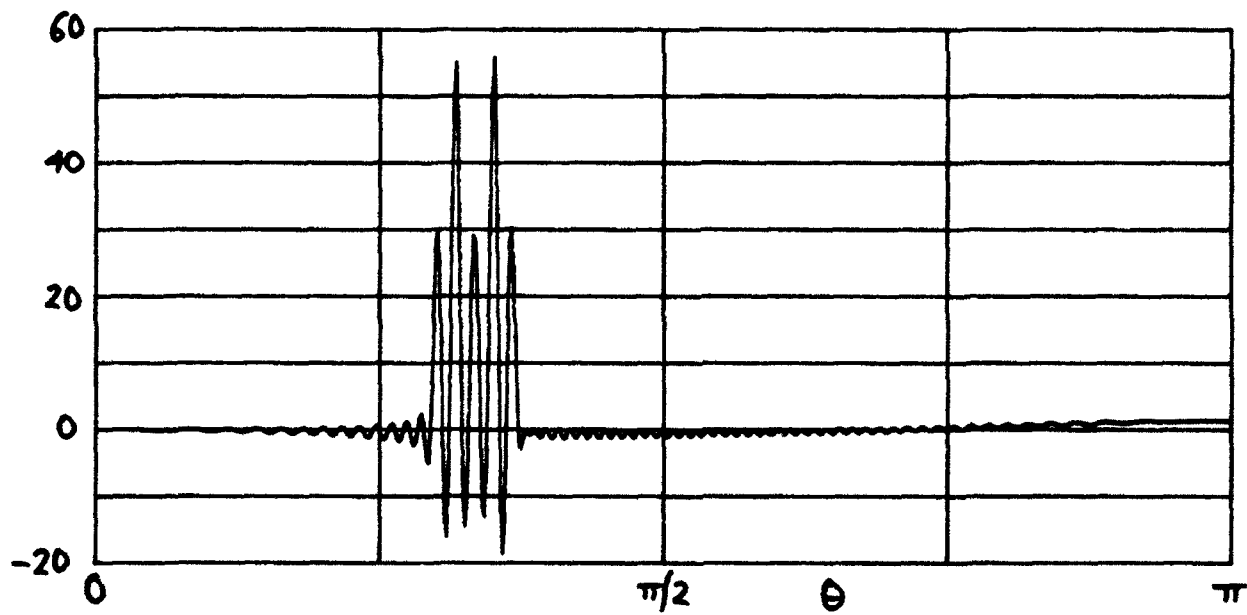


Figure 11B. Fourier Series Method

Figure 11. Directionality for Five Separated Arrivals

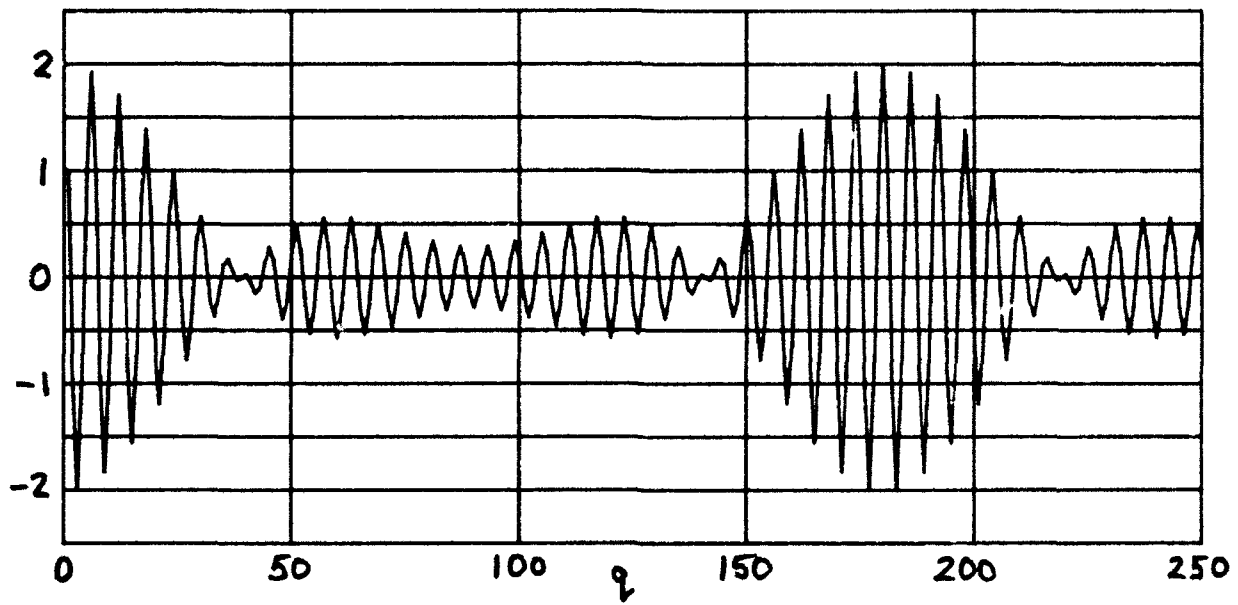


Figure 12A. Coefficients a_q

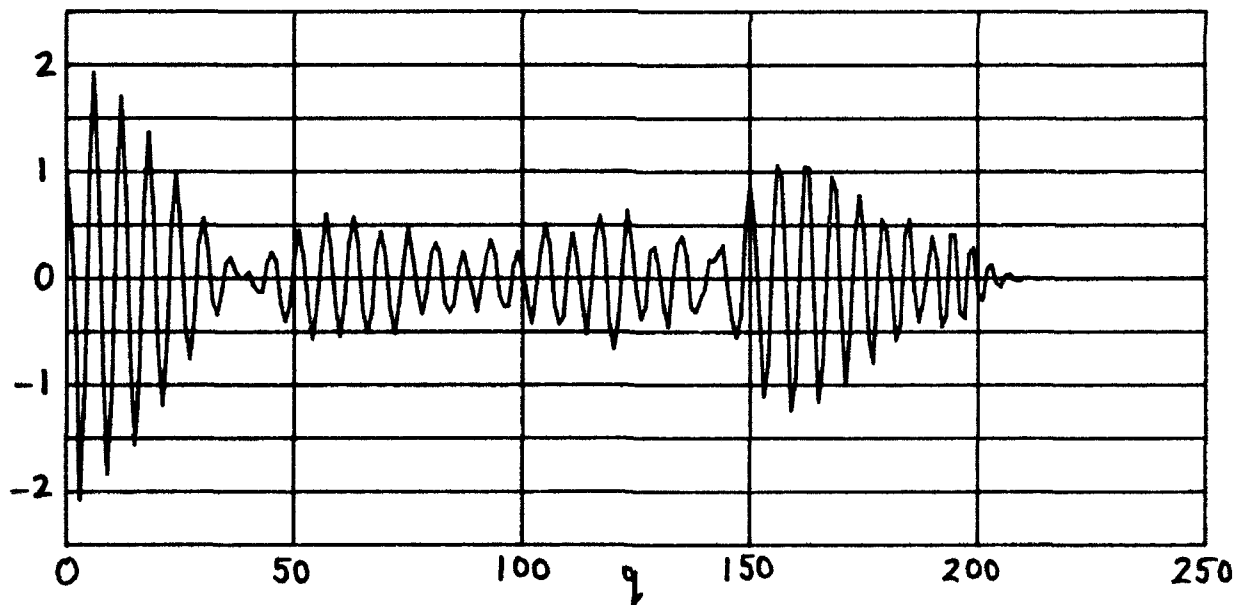


Figure 12B. Coefficients \tilde{a}_q

Figure 12. Coefficients for Five Close Arrivals

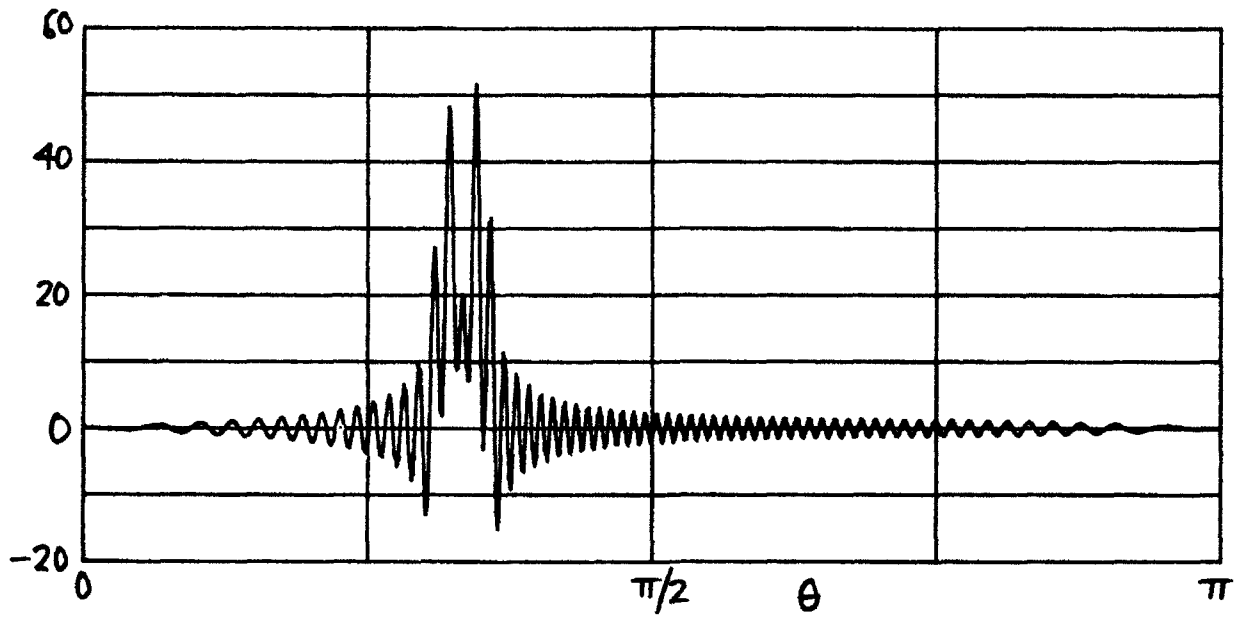


Figure 13A. Fourier Integral Method

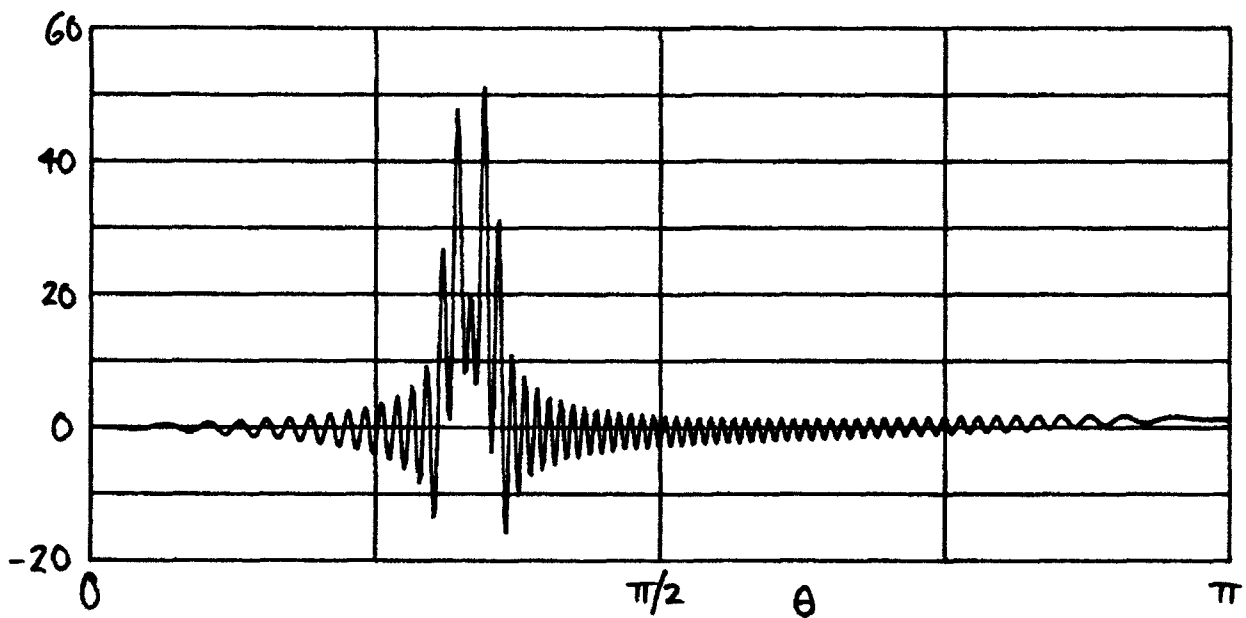


Figure 13B. Fourier Series Method

Figure 13. Directionality for Five Close Arrivals

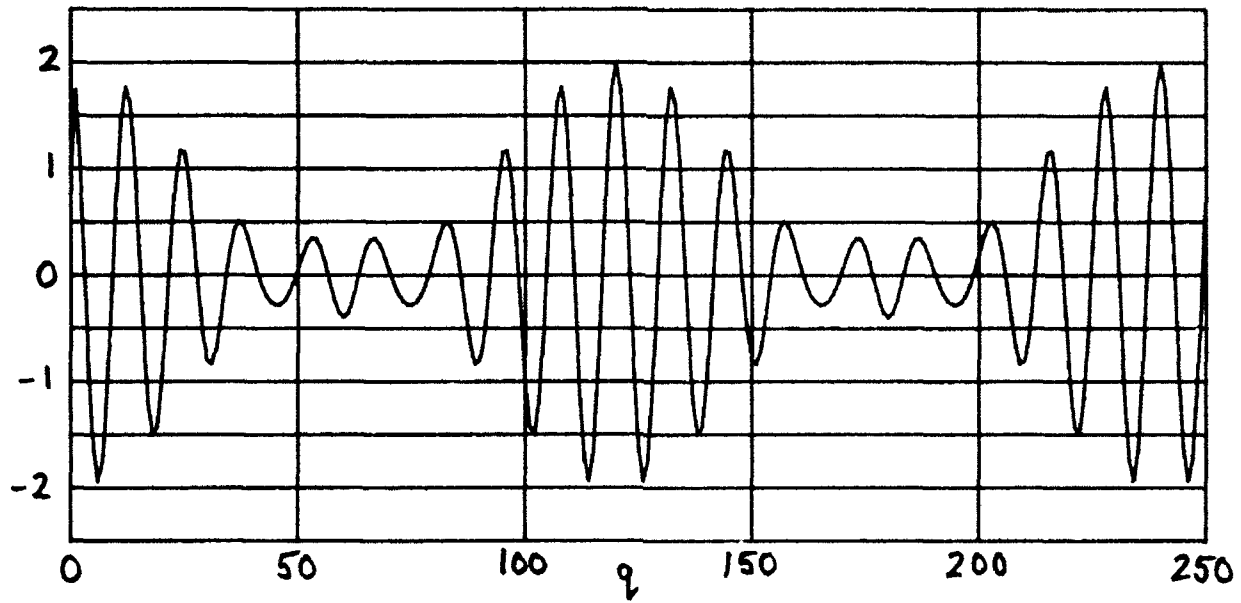


Figure 14A. Coefficients a_q

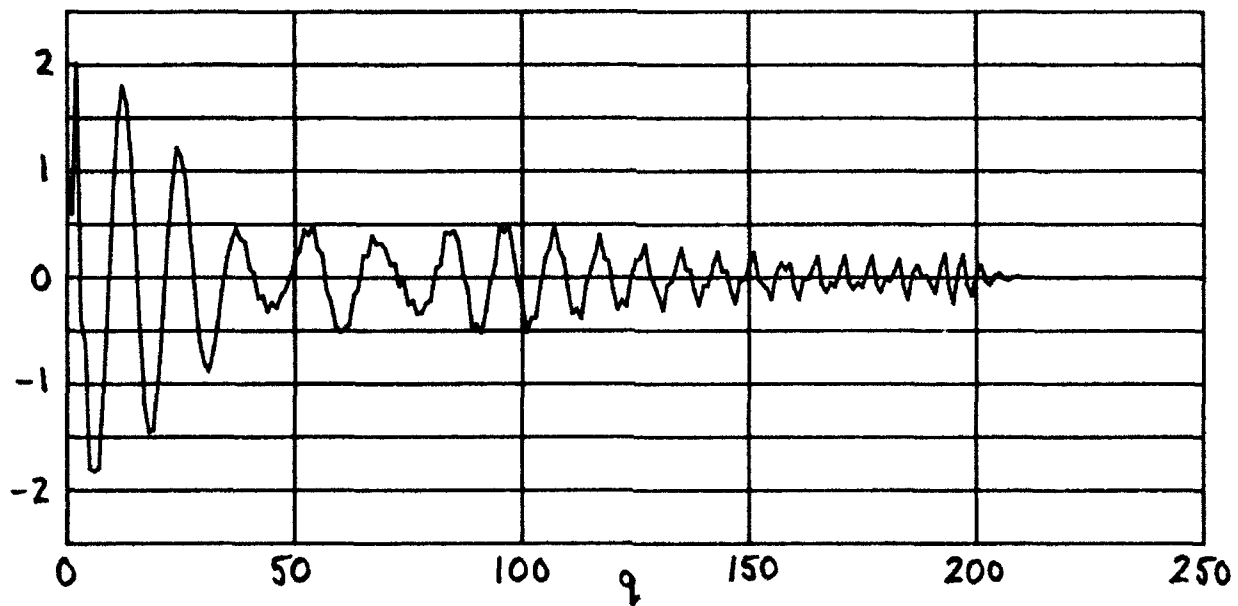


Figure 14B. Coefficients \tilde{a}_q

Figure 14. Coefficients for Three Arrivals

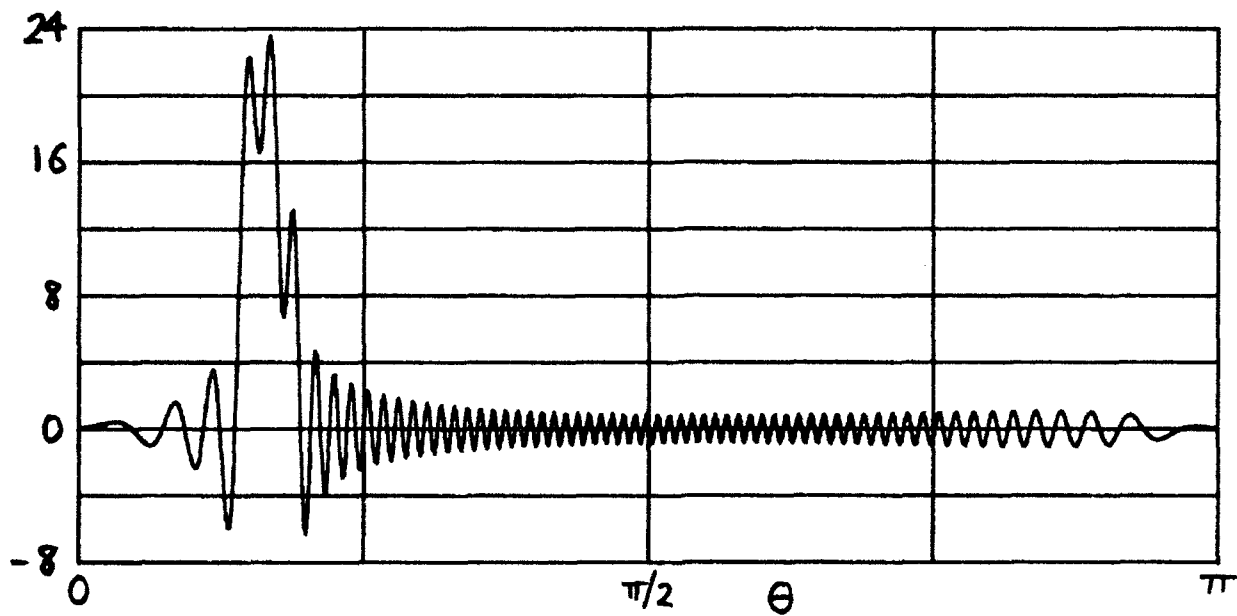


Figure 15A. Fourier Integral Method

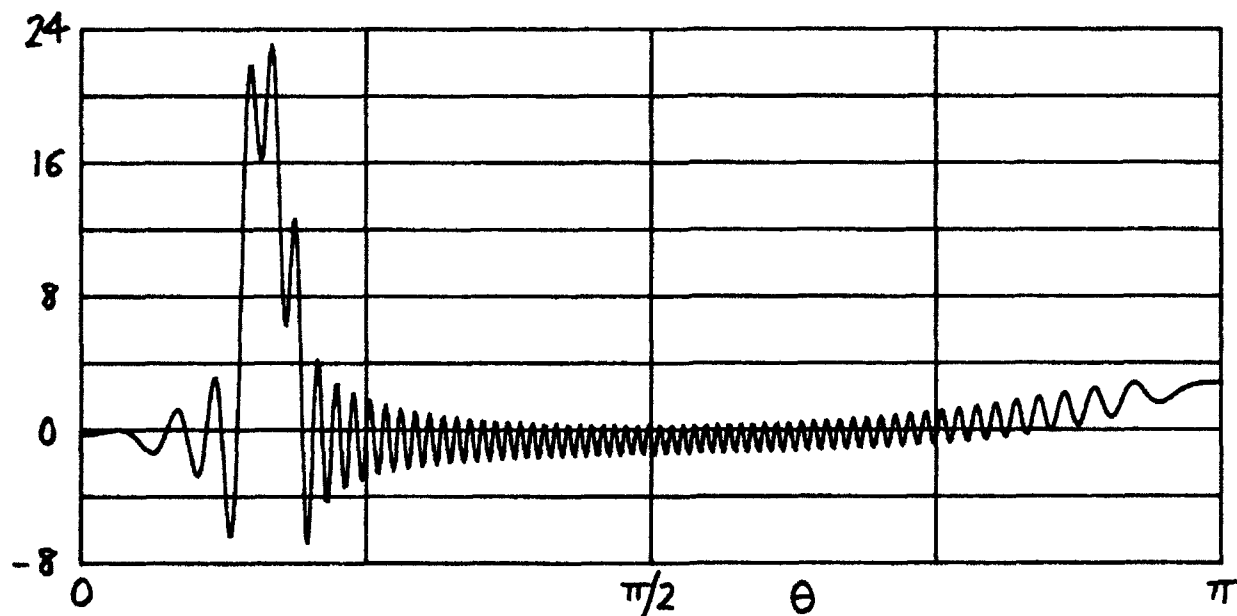


Figure 15B. Fourier Series Method

Figure 15. Directionality for Three Arrivals

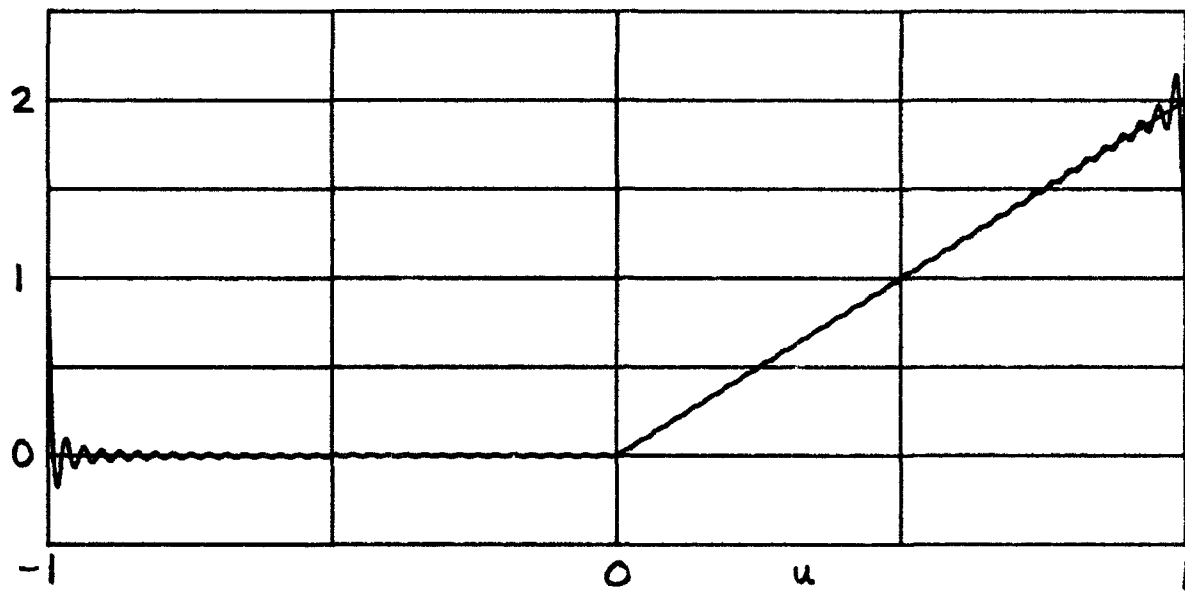


Figure 16A. $f/f_0 = 1$

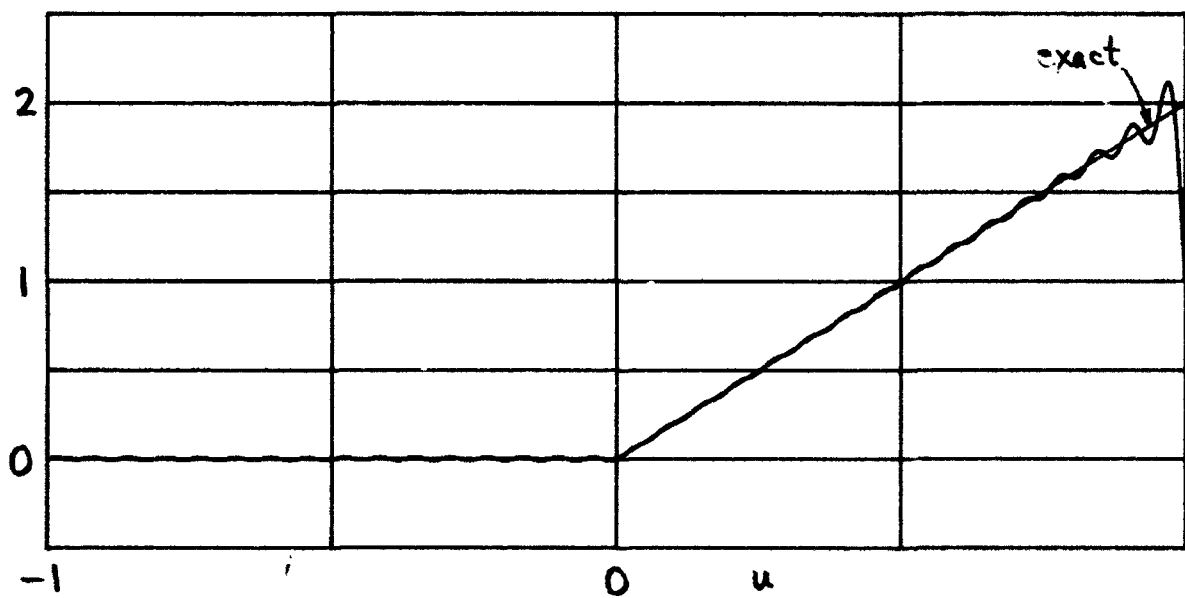


Figure 16B. $f/f_0 = .5$

Figure 16. Directionality for Flat Weighting

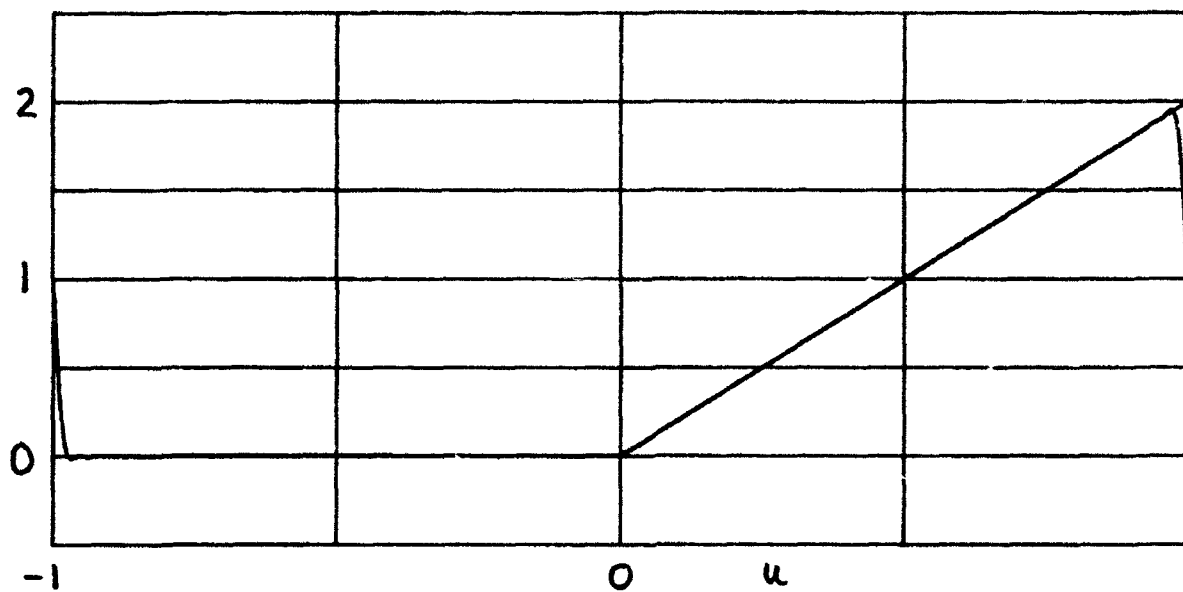


Figure 17A. $f/f_0 = 1$

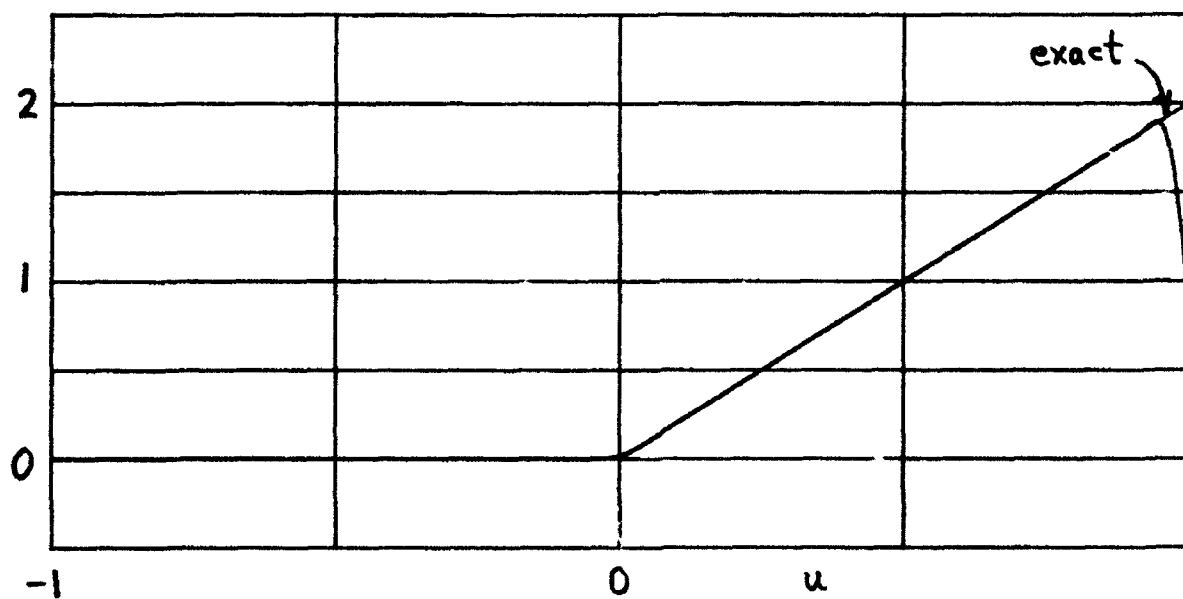


Figure 17B. $f/f_0 = .5$

Figure 17. Directionality for Hann Weighting

SUMMARY

The Fourier integral method and the Fourier series method have very similar performance; the major difference is the slow drift in the background level of the noise field directionality for the Fourier series method due to inaccurate low-order cosine series expansion coefficients. There is a rather large difference, however, in terms of the amount of computation, since the Fourier integral method can employ a fast Fourier transform to good advantage, while the Fourier series method requires numerous Bessel function evaluations.

Use of the array somewhat below its design frequency eases the aliasing problems associated with both methods; but there is a tradeoff connected with this approach, namely, a loss of resolution. Similarly, weighting can be used to suppress sidelobes, but again, only at the expense of resolution.

It has been presumed throughout this report that the spatial correlation is known exactly, for all required argument values, without any random error. In practice, the spatial correlation must be estimated from a finite observation time on random processes. This limitation will further degrade the performance of both techniques considered here; which one will suffer most, and by how much, is unknown.

Extension of the Fourier integral method to two- and three-dimensional arrays have been undertaken in [9]. The effects of finite array length and discrete sampling on the estimate of the full noise field directionality have also been considered.

APPENDIX A. EXAMPLE OF FOURIER SERIES METHOD

The single plane-wave arrival was given in (48); it yields spatial correlation (50):

$$C(p) = \exp(-i\alpha p \cos\theta_0); \quad 0 < \theta_0 < \pi. \quad (A-1)$$

Substitution in (47) yields coefficients [7; 6.693 2&1]

$$\left. \begin{aligned} a_{2m} &= \frac{2}{\pi} (-1)^m \cos(2m\beta) \\ a_{2m-1} &= \frac{2}{\pi} (-1)^{m-1} \sin[(2m-1)\beta] \end{aligned} \right\} \text{ for } m \geq 1, \quad (A-2)$$

where

$$\beta = \arcsin(\cos\theta_0) = \frac{\pi}{2} - \theta_0 \quad (A-3)$$

Although spatial correlation $C(p)$ depends on α , coefficients $\{a_q\}$ do not. Also, observe that

$$\begin{aligned} \cos(2m\beta) &= \cos(m\pi - 2m\theta_0) = (-1)^m \cos(2m\theta_0), \\ \sin[(2m-1)\beta] &= \sin\left[(2m-1)\left(\frac{\pi}{2} - \theta_0\right)\right] = (-1)^{m-1} \cos[(2m-1)\theta_0], \end{aligned} \quad (A-4)$$

giving

$$a_q = \frac{2}{\pi} \cos(q \theta_0) \quad \text{for } q \geq 1. \quad (A-5)$$

When these coefficients, along with $a_0 = 1/\pi$, are substituted in the right-hand side of (40), we obtain (letting θ be arbitrary)

$$\begin{aligned}
 R(\theta) &= \frac{1}{\pi} + \frac{2}{\pi} \sum_{q=1}^{+\infty} \cos(q\theta_0) \cos(q\theta) = \\
 &= \frac{1}{\pi} + \frac{1}{\pi} \sum_{q=1}^{+\infty} [\cos(q(\theta-\theta_0)) + \cos(q(\theta+\theta_0))]. \quad (A-6)
 \end{aligned}$$

But [8; page 28]

$$\frac{1}{2\pi} + \frac{1}{\pi} \sum_{q=1}^{+\infty} \cos(qt) = \frac{1}{2\pi} \sum_{q=-\infty}^{+\infty} \cos(qt) = \sum_{m=-\infty}^{+\infty} \delta(t-m2\pi), \quad (A-7)$$

giving

$$R(\theta) = \sum_{m=-\infty}^{+\infty} [\delta(\theta - \theta_0 - m2\pi) + \delta(\theta + \theta_0 - m2\pi)] \quad \text{for all } \theta. \quad (A-8)$$

This function is discussed in (52) and the sequel.

For future reference, if the sum in (A-7) were terminated at q' , we have

$$\frac{1}{2\pi} + \frac{1}{\pi} \sum_{q=1}^{q'} \cos(qt) = \frac{1}{2\pi} \frac{\sin[(2q'+1)t/2]}{\sin(t/2)}. \quad (A-9)$$

The first zero crossing of this function is at

$$t_0 = \frac{\pi}{q' + \frac{1}{2}}. \quad (A-10)$$

This is approximately the resolution of waveform (A-9).

APPENDIX B. NUMERICAL INVESTIGATION OF (58)

For the single plane-wave arrival given in (48)-(50), the spatial correlation is

$$C(p) = \exp(-i\alpha p u_0) , \quad \alpha = \pi f/f_0 , \quad |u_0| < 1. \quad (B-1)$$

Substitution in (58) gives approximate coefficients

$$\begin{aligned} \frac{\pi}{2} \tilde{a}_1 &= \sum_{n=1}^{M-1} \frac{J_1(\alpha n)}{n} \sin(\alpha n u_0) , \\ \frac{\pi}{2} \tilde{a}_2 &= -2 \sum_{n=1}^{M-1} \frac{J_2(\alpha n)}{n} \cos(\alpha n u_0) , \\ \frac{\pi}{2} \tilde{a}_{10} &= -10 \sum_{n=1}^{M-1} \frac{J_{10}(\alpha n)}{n} \cos(\alpha n u_0) . \end{aligned} \quad (B-2)$$

The exact coefficients are given by (51) as

$$\frac{\pi}{2} a_q = \cos(q\theta_0) = \cos(q \arccos(u_0)) \quad \text{for } q \geq 1 , \quad (B-3)$$

and are independent of α .

Numerical values of approximations (B-2) are given in tables B-1, B-2, B-3, respectively, for several values of u_0 , α , and for $M = 100, 1000, 10000, 100000$. The exact values, from (B-3), are listed in the right-most column for comparison purposes.

Several observations can be made from these tables. Except for $u_0 = 1$, the sums in (B-2) for $M = 100$ are not too different from what they would have been for $M = \infty$. Part of this is due to the fact that $M = 100$ is considerably larger than the biggest coefficient order, 10, that we considered here.

The values of the approximate coefficients \tilde{a}_1 and \tilde{a}_2 are poor for $\alpha = \pi$, that is, for frequency f equal to design frequency f_0 , even for a large number of elements M , independent of arrival angle u_0 . However, if α is decreased, so that f is well below the design frequency f_0 , $d < \lambda/2$, then \tilde{a}_1 and \tilde{a}_2 are rather close to a_1 and a_2 , respectively. However, the loss in resolution is unlikely to be tolerable in this case.

By contrast, the values of \tilde{a}_{10} in table B-3 are good approximations to a_{10} , with two exceptions:

$$u_0 = 1, \quad \alpha = \pi, \quad \text{all } M ;$$

$$u_0 = 1, \quad \text{all } \alpha, \quad M = 100 . \quad (B-4)$$

That is, endfire arrivals will cause the most problems, as is expected physically.

Table B-1. Values of $\frac{\pi}{2} \tilde{a}_1$

u_0	α	$\frac{\pi}{2} \tilde{a}_1$ for:				$\frac{\pi}{2} a_1$
		M=100	M=1000	M=10000	M=100000	
0	all	0	0	0	0	0
.25	π	.129232	.129164	.129166	.129166	.25
.25	.75 π	.187050	.187166	.187169	.187169	.25
.25	.5 π	.223371	.223390	.223387	.223387	.25
.25	.25 π	.244032	.243504	.243520	.243520	.25
.5	π	.243202	.243356	.243361	.243361	.5
.5	.75 π	.371340	.371278	.371273	.371273	.5
.5	.5 π	.446531	.446295	.446302	.446302	.5
.5	.25 π	.487704	.487032	.487014	.487014	.5
.75	π	.312112	.311716	.311728	.311728	.75
.75	.75 π	.548651	.548352	.548355	.548355	.75
.75	.5 π	.668571	.668247	.668229	.668230	.75
.75	.25 π	.730345	.730503	.730458	.730456	.75
1	π	0	0	0	0	1
1	.75 π	.675038	.700277	.708228	.710741	1
1	.5 π	.843507	.874322	.884057	.887135	1
1	.25 π	.910216	.953689	.967453	.971806	1

Table B-2. Values of $\frac{\pi}{2} \tilde{a}_2$

u_0	α	$\frac{\pi}{2} \tilde{a}_2$ for:				$\frac{\pi}{2} a_2$
		M=100	M=1000	M=10000	M=100000	
0	π	-.774782	-.774469	-.774460	-.774459	-1
0	$.75\pi$	-.877975	-.878516	-.878500	-.878500	-1
0	$.5\pi$	-.948405	-.947527	-.947499	-.947498	-1
0	$.25\pi$	-.984898	-.987151	-.987084	-.987082	-1
.25	π	-.638731	-.639064	-.639054	-.639054	-.875
.25	$.75\pi$	-.751196	-.750903	-.750906	-.750907	-.875
.25	$.5\pi$	-.822242	-.822027	-.822058	-.822057	-.875
.25	$.25\pi$	-.860117	-.862071	-.862055	-.862057	-.875
.5	π	-.226752	-.226437	-.226428	-.226427	-.5
.5	$.75\pi$	-.367826	-.367496	-.367515	-.367515	-.5
.5	$.5\pi$	-.444596	-.445729	-.445695	-.445694	-.5
.5	$.25\pi$	-.485886	-.486894	-.486983	-.486980	-.5
.75	π	.497761	.497414	.497424	.497425	.125
.75	$.75\pi$.275027	.273883	.273906	.273905	.125
.75	$.5\pi$.182765	.181761	.181708	.181709	.125
.75	$.25\pi$.136903	.138239	.138154	.138149	.125
1	π	1.992866	2.080480	2.108031	2.116738	1
1	$.75\pi$	1.105007	1.155646	1.171553	1.176580	1
1	$.5\pi$.969535	1.031886	1.051378	1.057535	1
1	$.25\pi$.884033	.973009	1.000600	1.009308	1

Table B-3. Values of $\frac{\pi}{2} \tilde{a}_{10}$

u_0	α	$\frac{\pi}{2} \tilde{a}_{10}$ for:				$\frac{\pi}{2} a_{10}$
		M=100	M=1000	M=10000	M=100000	
0	π	-1.001835	-1.000047	-.999998	-.999996	-1
0	$.75\pi$	-.997211	-1.000083	-1.000002	-1.000000	-1
0	$.5\pi$	-1.004328	-1.000142	-1.000004	-1.000000	-1
0	$.25\pi$	-.993657	-1.000337	-1.000013	-1.000003	-1
.25	π	.818745	.816853	.816903	.816904	.816895
.25	$.75\pi$.815431	.816916	.816897	.816895	.816895
.25	$.5\pi$.815723	.817043	.816890	.816894	.816895
.25	$.25\pi$.823767	.816816	.816904	.816892	.816895
.5	π	-.501787	-.499985	-.499935	-.499934	-.5
.5	$.75\pi$	-.501841	-.499903	-.500002	-.499999	-.5
.5	$.5\pi$	-.495030	-.500171	-.500005	-.500000	-.5
.5	$.25\pi$	-.492036	-.499587	-.500016	-.500003	-.5
.75	π	.589326	.587351	.587401	.587402	.586426
.75	$.75\pi$.592357	.586315	.586433	.586429	.586426
.75	$.5\pi$.593192	.586680	.586418	.586426	.586426
.75	$.25\pi$.593387	.586898	.586445	.586423	.586426
1	π	1.329489	1.797572	1.936303	1.979867	1
1	$.75\pi$.606719	.882941	.963235	.988393	1
1	$.5\pi$.504084	.856082	.954934	.985763	1
1	$.25\pi$.252087	.794347	.936197	.979862	1

REFERENCES

1. A. H. Nuttall, **Estimation of Noise Directionality Spectrum**, NUSC Technical Memorandum TC-211-71, Naval Underwater Systems Center, New London, CT, 29 October 1971; also NUSC Technical Report 4345, 1 September 1972.
2. A. H. Nuttall, **Estimation of Noise Directionality Spectrum; Extensions and Generalizations**, NUSC Technical Memorandum TC-6-73, Naval Underwater Systems Center, New London, CT, 7 May 1973.
3. N. Yen, **Ambient Sea Noise Directionality: Measurement and Processing**, NUSC Technical Report 5545, Naval Underwater Systems Center, New London, CT, 28 February 1977.
4. J. H. Wilson, "Signal Detection and Localization Using the Fourier Series Method (FSM) and Cross-Sensor Data," **Journal of the Acoustical Society of America**, volume 73, number 5, pages 1648-1656, May 1983.
5. F. B. Hildebrand, **Methods of Applied Mathematics**, Prentice-Hall, Inc., New York, NY, 1954.
6. **Handbook of Mathematical Functions**, U. S. Department of Commerce, National Bureau of Standards, Applied Mathematics Series No. 55, U. S. Government Printing Office, Washington, DC, June 1964.
7. I. S. Gradshteyn and I. M. Ryzhik, **Table of Integrals, Series and Products**, Academic Press, Inc., New York, NY, 1980.
8. P. M. Woodward, **Probability and Information Theory, with Applications to Radar**, Pergamon Press, Inc., New York, NY, 1957.

REFERENCES (cont'd)

9. A. H. Nuttall, **Determination of Noise Field Directionality Directly from Spatial Correlation for Linear, Planar, and Volumetric Arrays**, NUSC Technical Report 8631, Naval Underwater Systems Center, New London, CT, 6 October 1989.

SUBJECT MATTER INDEX

Alias-Free, 8533
Aliasing, 8225, 8533, 8599
Ambiguity Function, 8225, 8533
Amplitude Modulation, 8611
Area Mismatch, 8317
Array Processing, 8631, 8599
Breakpoint, 8595
Characteristic Function, 8595
Combiner, 8595
Complex Envelope, 8611
Cross Wigner, 8225
Dead Zone, 8595
Deflection, 8611
Detection Probability, 8595
Diamond Gating Function, 8533
Discrete-Time Samples, 8533
Diversity, 8595
Effective Area, 8225, 8317
Equi-Spaced Line Array, 8599
Exceedance Distribution, 8595
False Alarm Probability, 8595
Fast Fourier Transform, 8533, 8631, 8599
Filtering, 8225
Fourier Integral Method, 8631
Fourier Series Method, 8631, 8599
Frequency Modulation, 8225, 8317
Ill conditioning, 8599
Instantaneous Spectrum, 8225
Integral Equation, 8631, 8599
Interference, 8225
Interpolation, 8533
Interspersed Aliasing, 8533
Linear Array, 8631, 8599
Marginals, 8225, 8317
Matched Filters, 8595
Memoryless, 8595, 8611
Moments, 8225, 8317, 8611
Multiple Channels, 8595
Narrowband, 8225, 8611
Noise Behavior, 8225, 8611
Noise Field Directionality, 8631, 8599
Nonlinearities, 8595, 8611
Operating Characteristics, 8595
Optimum Nonlinearity, 8611
Optimum Wigner Distribution, 8317
Phase Differences, 8611
Phase Modulation, 8611
Planar Array, 8631
Reconstruction, 8533
Sampling, 8225, 8533
Short-Term Spectrum, 8225, 8317
Smoothing, 8225, 8317, 8599

Spatial Correlation, 8631, 8599
Spectral Correlation, 8533
Spread, 8225, 8317
Spurious Signal, 8611
Super Resolution, 8599
Temporal Averaging, 8225
Temporal Correlation Function, 8533
Two-Dimensional Convolution, 8317
Two-Frequency Domain, 8533
Volumetric Array, 8631
Weighting, 8225, 8317, 8631
Wigner Distribution, 8225, 8317, 8533